Installing and Understanding Group-13 X-type Metallo-ligands

Liam Patrick Griffin

Thesis submitted for the Degree of Doctor of Philosophy

October 2024

Abstract

This thesis describes synthetic, spectroscopic and computational efforts to access and understand metal complexes of the trielyl ligands, *i.e.* X-type ligands for the form EX_2^-, where E is a group 13 element in the +1 oxidation state. In particular, this thesis focusses on understanding aluminyl ligands (E = Al). Such compounds receive much attention in the current literature, as the electropositive nature of aluminium renders aluminyl ligands highly electron donating. Such properties are best understood through comparison with lighter and heavier congeners (and also other related ligands from across the Periodic Table), and so this thesis additionally explores boryl complexes, and series of isostructural compounds bearing aluminyl, gallyl and indyl metallo-ligands (E = Al, Ga and In respectively).

Chapter 1 introduces the group 13 elements, and discusses their use as ligands to metal centres. Ligand modes which involve low valent metal centres (L- and X- type ligation) receive the most attention, with a particular focus on the X-type ligands (trielyls). Aluminyl ligands are tackled last, with a discussion of all metal-aluminyl complexes reported to date.

Chapters 2-6 take the form of papers. Chapters 4 and 6 are published papers, chapter 2 is a submitted manuscript, and chapters 3 and 5 are draft manuscripts presented in publication format. In all cases, I am the first author, having conducted a significant majority (or in some cases all) of the synthesis, crystallographic and spectroscopic characterisation, sample preparation, computational analysis, and preparation of the manuscript text and supplementary information. A declaration to this effect can be found at the end of each chapter, signed by myself and my supervisor Prof. Simon Aldridge.

Chapter 2 details the synthesis of a zinc boryl complex, with the goal of comparing its reactivity to that of its reported aluminyl congener. Both the synthesis and onward chemistry of this species are dominated by B–O bond formation, which is further exploited to access a zinc(I) compound bearing a Zn–Zn bond without the need for alkali metal reductions.

Chapter 3 makes use of the aforementioned zinc boryl and aluminyl complexes, as well as a family of related Zn–X compounds. These are studied by X-ray spectroscopy in order to probe and compare the ligand properties of these X ligands, via the electronic structure they induce at the zinc centre. These data are rationalised in terms of common models of chemical bonding, and also compared to parameters generated by computational analysis of the compounds studied. In this way, computational techniques are evaluated against experimental data, identifying which techniques most effectively capture the measured trends for potential extrapolation of this analysis to other X-type ligands.

Chapter 4 describes the convenient synthesis of sources of the indium trielyl congener (indyl anion) via indium(I) precursors, and applies them in the synthesis of isostructural series of linear d^{10} metal complexes bearing aluminyl, gallyl and indyl ligands. Spectroscopic and structural probes inherent within these molecules are then used to evaluate the *trans* influence of these trielyl ligands.

Chapter 5 investigates the reactivity of aluminyl, gallyl and indyl anions with $Fe(CO)_5$ in order to access iron-trielyl complexes of the form $[Fe(CO)_4EX_2]^-$ (E = Al, Ga, In). In the aluminium case, undesired products due to redox processes and Al–O bond formation are observed, with tuning of the counterion required to access the target motif. More facile access to Fe–E bonded products is observed for the heavier congeners, and a range of techniques (IR, Mössbauer, crystallography, computational analysis) are used to compare the behaviour of the trielyl ligands in the resulting complexes.

Chapter 6 discusses the synthesis and reactivity of a bis(aluminyl) magnesium compound. Whilst the relatively covalent Al–Mg bonds serve to curtail the reactivity of the aluminyl anion, this species is nonetheless able to activate small molecule substrates such as the kinetically inert gas SF_6. Despite a thermal reactivity profile consistent with the more expected Al(I)–Mg(II)–Al(I) description of this trimetallic compound, photolytic reactivity (which both eliminates magnesium metal and yields products associated with radical intermediates) indicates that this species can also act as a Al(II)–

Mg(0)–Al(II) synthon. Such unusual reactivity highlights the effect that a strongly electron donating aluminyl ligand can have on the reactivity of a metal complex.

Finally, chapter 7 draws on the results of the previous chapters to offer overall conclusions from this work, and suggest areas where future study might be particularly fruitful. The research presented in this thesis has generated a range of data quantifying the donor properties of the aluminyl metallo-ligand, as compared to its group 13 congeners and other X-type ligands from across the Periodic Table. These data have demonstrated its extremely σ-donating nature, and the unusual effects this can have on the electronic structure of a metal centre. The possibility of accessing isostructural series presented by this thesis has allowed for the chemistry of group 13 ligands based on the metals aluminium, gallium and indium to be evaluated without complications arising from differing supporting ligands, showing a decrease in donor-strength as the group is descended. Additionally, this thesis has helped to establish design principles for the synthesis of metal aluminyl complexes. These include both co-ligand choice to ensure the stability of the complex, and methodological considerations for preventing unwanted reactivity when installing aluminyl ligands.

Acknowledgements

I am extremely grateful to my supervisor Prof. Simon Aldridge. My time under his supervision during both my Masters and D.Phil has been highly enjoyable and rewarding. His endless support, enthusiasm and excitement for research, as well as his advice and mentorship, have been invaluable.

I am also very thankful for all the members of the Aldridge group who have made my time so enjoyable and memorable, and who have taught me so much. In particular, I would like to thank Joe Boronski for his friendship and support, Aggy for his computational and crystallographic expertise, and Job, Caitilin, Aisling, Lewis, Marcel, Matthias, Matt Roy, Alexa, Malte and Max among many others for being friends as well as colleagues and for making the CRL such a great place to work. I also thank my Masters students Jonathon, Charlotte and James for their hard work and dedication to their projects.

I am grateful to my collaborators Prof. Mike Neidig, Dr. Will Myers, Prof. Kevin Lovelock, Frances Tower-Tompkins, all the beamline scientists at I20 and B07 and especially Lewis Parker and Alexis Bauer for their all of their help and expertise. This thesis is greatly improved for their involvement.

Thanks also go to Dr. Moritz Malishewski and his whole research group for hosting my placement at the FU Berlin. I had an amazing time and learnt a lot. I'm grateful to Amina for putting up with my mumbling in the lab, and to Jan for helping me explore more of Germany.

Thank you to the whole 2021 CDT cohort for helping me survive the taught course, especially Kam, Fran, Matt and Charlie, and to Maitane and Alexa for their work behind the scenes.

I'm grateful to everyone in crystallography, NMR and CRL facilities who keep the pumps, instruments and building running for us.

Finally, I must thank my friends and family, in particular Mum, Tom and Frances, who's support made all of this possible and worthwhile.

Abbreviations

The following abbreviations are used throughout this thesis

Ar = general aryl group

br. = broad

CAAC= Cyclic-alkyl amino carbene

Cp = cyclopentadiene

Cp* = permethylcyclopentadiene

d = doublet

DAB = Diazabutadiene

DFT = Density Functional Theory

Dipp = 2,6-diisopropylphenyl

DiPEP = 2,6-CH(Et)2-phenyl

DMAP = 4-dimethylaminopyridine

Et = ethyl

h = hour(s)

HOMO = Highest Occupied Molecular Orbital

i = ipso

IR = Infra-Red

^{i}Pr = isopropyl

LUMO = Lowest Unoccupied Molecular Orbital

m = multiplet

m = meta

Me = methyl

Mes = mesityl, 2,4,6-trimethylphenyl

Nacnac = $[(NArCMe)_2CH]^-$

NBO = Natural Bonding Orbitals

NHC = N-heterocyclic carbenes

NMR = Nuclear Magnetic Resonance

NON = NON = 4,5-bis(2,6-diisopropylanilido)-2,7-di-tert-butyl -9,9-dimethylxanthene

o = ortho

OMO = Occupied Molecular Orbital

p = para

Ph = phenyl

QT-AIM = Quantum Theory of Atoms In Molecules

pin = pinacol

ppm = parts per million

R = general aliphatic group

rt = room temperature

s = singlet

sept = septet

t = triplet

^{t}Bu = tert-butyl

THF = tetrahydrofuran

TMS = trimethylsilyl

UMO = Unoccupied Molecular Orbital

UV-Vis = Ultraviolet-Visible spectroscopy

VT = Variable temperature

Table of contents

Introduction

In this introduction, I will discuss the fundamental properties of the group 13 elements (the 'triels'), in order to contextualise the chemistry discussed thereafter. I will then discuss their use as ligands (Z, L and X-type) at other metal centres, looking first to the most well-developed chemistry (that of boron) before discussing the heavier congeners, with emphasis on the chemistry of the most abundant and electropositive element in the series, aluminium. For reasons of brevity, only species in which a direct σ-bonding interaction is present between triel and metal centres will be discussed, excluding such ligand motifs where the triel element is included as a component in a π-complex such as borole complexes and their heavier congeners.

The Z-type coordination mode is considered briefly, before a more detailed treatment of the low valent coordination modes, *i.e.* L- and X-type ligands. L-type coordination is described second, followed by X-type; the primary focus of this work. Boryl ligands, the most ubiquitous trielyl donor, are detailed first, providing context to the remaining congeners, which are then treated in ascending order, with the exception of aluminyl fragments. These are discussed last, due to the central role that aluminyl metallo-ligands play in this work, and also the diverse reactivity exemplified.

Group 13 chemistry

The group 13 elements, boron, aluminium, gallium, indium and thallium, are all (with the exception of semi-metal boron) metallic main group elements and all are classically characterised by predominantly electrophilic behaviour. This results from a combination of their preferred oxidation states and the inert pair effect. For the lighter elements, the group oxidation state (+3) is preferred, since the high charge density of these small 3+ cations leads to strong bonding, more than compensating for the second and third ionization enthalpies.[1] The resulting valence electronic structure (ns^0 np^0) leads to trivalent compounds bearing a vacant p-orbital. This vacant site allows for the donation of additional electron density to the triel centre, resulting in highly Lewis acidic behaviour.[1] These properties are borne out both in the solid-state chemistry of these elements (aluminium oxide Al_2O_3 features six-coordinate aluminium centres in order to maximise coulombic interactions between ions) and their solution phase uses ($AlCl_3$ accepts electron density into its aluminium centred vacant p-orbital during use as a common Lewis-acid catalyst for Friedel-Crafts chemistry).[2,3]

For the heaviest element thallium, the +1 (n-2) oxidation state becomes increasingly favoured. However, these additional valence electrons are located in the increasingly core-like, non-directional s-orbital, and so do not lead to significant nucleophilicity. This results in a large, redox-stable 1+ cation.[4] This general behaviour again plays into the common applications of these elements, with thallium being a classic (albeit outdated, due to its biotoxicity) choice of cation for salt metathesis chemistry as a result of the insolubility of its halide salts, the by-products of such reactions.[5] The chemistry of gallium and indium is intermediate. Gallium displays fairly thermodynamically flexible redox chemistry (vide infra), and the indium(III) state still plays a key role in ionic species such as halides and oxides where coulombic interactions are maximised, despite indium(I) species being readily accessible under suitable conditions.[6]

Typical behaviour and uses

Boron, the only non-metal of the group, is found in nature as in various minerals such as borax ($Na_2[B_4O_5(OH)_4]\cdot 8H_2O$). Its propensity to form strong and highly covalent bonds, especially with other relatively light elements, dominates its major applications, such as in polymer cross-linking.[7] Being electron deficient, boron finds use as a hole dopant in semiconducting materials, and BN species have received significant research for their contrasting electronic and physical properties as compared to isoelectronic all-carbon analogues.[8] The electrophilicity of common boron compounds leads to unusual bonding scenarios. Indeed borane (B_2H_6) was the first species to which the three-centre two-electron bonding model was applied.[9] This electron deficient bonding mode can be further generalised to higher order borane species of the type $(B_nH_m)^{x-}$, the structures of which can be predicted by simple rules based on an understanding of this bonding behaviour.[10]

Aluminium, the lightest group 13 metal and the most abundant metal in the earth's crust, is a highly oxophillic element owing to the incredible charge density of the favoured 3+ oxidation state (second only to diagonally related beryllium in its 2+ state).[1] Indeed, the corrosion resistance of the widely used metallic material is due to the highly stable native coating of aluminium oxide found on the surface. The low density of aluminium and its abundance makes it a favourable component of alloys for specialist applications.[11] Aluminium's more electropositive nature leads to significantly more ionic bonding than for boron, which is utilized for example in the polymerization catalyst activator methyl aluminium oxide (MAO), which acts as a source of highly reactive $Al(CH_3)_2^+$ fragments.[12]

Gallium is the main metallic element of group 13 for which meaningful redox flexibility is observed. Oxidation of gallium with iodine is sensitive to stoichiometry, with solutions corresponding to gallium(I) and gallium(III) iodide being easily prepared at room temperature.[13] By contrast, the equivalent reaction with aluminium yields aluminium(III) iodide regardless of stoichiometry, with the synthesis of aluminium(I) halides requiring metal vapour synthesis methods and low temperature

storage to prevent highly exergonic disproportionation to the corresponding trihalide and aluminium metal.[14,15]

Indium is significantly less abundant than the lighter group 13 elements, and finds its primary modern utility as a component in transparent conducting materials such as indium tin oxide (ITO), and in the synthesis of indium phosphide quantum dots for display technologies as an alternative to the toxic cadmium sulphide forbears.[16] Despite the increased stability of indium in the +1 oxidation state, its stable oxides and halides are still the trivalent species, with maximization of strong ionic interactions the primary thermodynamic driving force.

For thallium, the +1 oxidation state dominates, with the trihalides being unstable to disproportionation at only slightly elevated temperatures, and the triiodide existing as a Tl(I) salt of the trinuclear mono-anion I_3^-.[17] In its organometallic chemistry, thallium typically participates in chemistry resembling that of the alkali metal cations, with its remaining lone pair of electrons sufficiently stabilized in a non-directional and core-like 6s orbital as to be unavailable for participation in interactions with other atoms.[1]

Group 13-centred ligands

Whilst not as ubiquitous as ligands based on C-donors (CO, carbocycles), N-donors (N_2, amides) or O-donors (aryloxides, alkoxides), boron-based ligands and their heavier congeners are nonetheless important motifs in inorganic chemistry. Whilst Z-type examples that exploit the underlying electron deficiency of group 13 are known, it is the low-valent ligand fragments which have had the most transformative impact, in particular for boron. As detailed below, the borylation and highly flexible onward functionalisation of C–H bonds, achieved via transition metal boryl complexes, has had a very significant impact on organic synthesis. Indeed, many powerful transformations have been unlocked or improved by the inclusion of a group 13 centred ligand, in research conducted by a great many research groups over the past half century. These efforts are summarized below, taking each ligand class in turn.

Z-type ligands

Z-type ligand behaviour is common for compounds of the group 13 elements, due to their intrinsically electron deficient nature.[1] Accordingly, there exists a wealth of literature detailing structurally authenticated adducts between electron rich metal centres and EX_3 species.[18] More recent efforts to utilize such linkages to fine tune the chemical properties of the electron rich metal have typically involved the use of frameworks which hold a group 13 element in the coordination sphere of a transition metal. The resulting polarization induced by Lewis acidic Z-ligand in turn renders the typically electron donating transition metal itself more Lewis acidic. This increases the ambiphilic character of the transition metal, leading to stronger interactions with substrate molecules (which generally act as both σ-donors and π-acceptors) and allowing for bond activation *trans* to the electrophilic group 13 metal, as demonstrated by compounds **1-4** (Figure 1).[19]

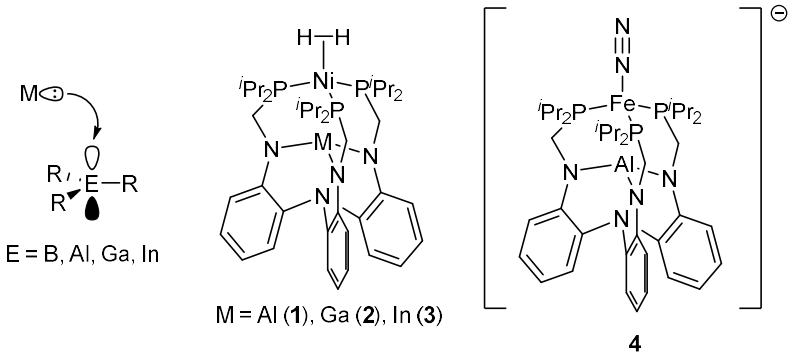

Figure 1: Left, Orbital diagram of a Lewis acidic ER_3 system demonstrating the Z-type ligand binding mode. Right, two classes of bimetallic species in which a group 13 element held in close proximity to a transition metal acts as a Z-type ligand, influencing the properties of the transition metal centre (nickel binds dihydrogen, terminal iron-N_2 complex is highly nucleophilic at the distal nitrogen atom).

L-type ligands

Moving to low-oxidation state species, *i.e.* those featuring a group 13 element in oxidation state +1, the additional electron density present at the triel centre permits additional modes of ligation, i.e. as donors rather than acceptors. Neutral E(I) species, either with or without an additional stabilizing Lewis base, are able to act as L-type donors, termed trielenes.

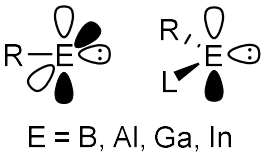

Figure 2: Schematic orbital diagrams for one coordinate (left) and base stabilized (right) free trielenes, detailing an available lone pair and either one or two vacant orthogonal p-orbitals

Borylenes

Borylene ligands are known with various R groups, including C, N and Si donors, and with or without external stabilising Lewis bases.[20] Free borylenes generated *in situ* are highly reactive, and attempts to isolate such species typically lead to decomposition or more interesting onward reactivity, such as the reduction of dinitrogen.[21] Metal complexation therefore serves as a means of stabilization of these highly reactive fragments. Noteworthy examples of borylene complexes include the first terminal examples reported by the groups of Cowley (**5**) and Braunschweig (**6**) in 1998 (Figure 3).[22] [23] Two further seminal studies involved the isolation of complexes bearing the borylene BF in both bridging (**7**) and terminal (**8**) coordination modes.[24,25] This diatomic molecule is isolobal with the archetypal L-type ligand CO (and N_2) and structural and spectroscopic parameters associated with these compounds reveal it to be an extremely strongly σ-donating and π-accepting ligand.

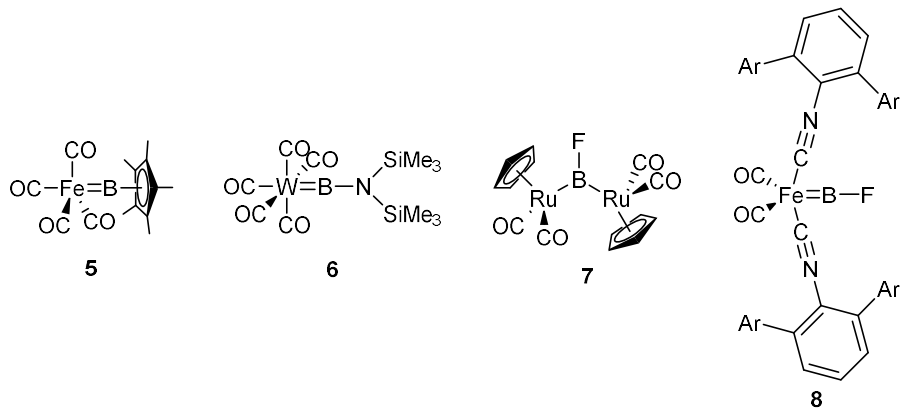

*Figure 3: Noteworthy metal-borylene complexes. From left to right; the first two metal borylene species to be reported in 1998 (**5** and **6**), a bridging borylene complex (**7**) featuring the CO-isolobal fragment BF, a terminal complex (**8**) also featuring the BF fragment. Ar = 2,4,6-triisopropylphenyl.*

Aluminylenes

The first aluminium(I) species to be isolated was reported by Schnöckel and co-workers in 1991. $[AlCp^*]_4$ (**9**) is a tetramer of alumylene units which adopts a cluster of tetrahedral geometry which has been shown to monomerise in solution at high temperature.[26] Initially prepared utilising the metastable Al(I) species AlCl in a salt metathesis reaction (and later by alkali metal reduction of Cp^*AlCl_2), it was subsequently shown that this species can also be accessed via a remarkable C–H reductive elimination at the Al(III) species Cp^*_2AlH.[27] A wide range of metal complexes of this fragment have been prepared with transition metals such as iron, cobalt and nickel, and f-block metals such as uranium.[28]

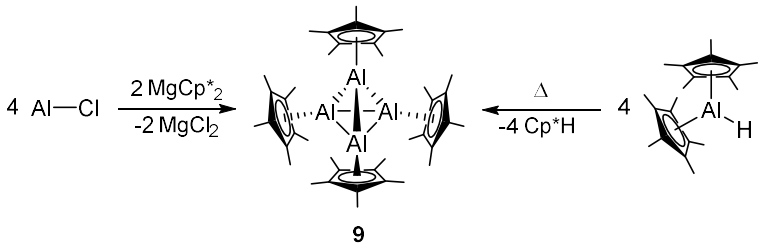

9

*1: Salt metathesis and reductive elimination routes to the first Al(I) species $[Cp^*Al]_4$ (**9**).*

Variation of the substitution pattern of the cyclopentadienyl ligand has since permitted the isolation of monomeric derivatives in the case of both the Cp^{3t} (**10**) and $Cp^{5\prime}$ (**11**) ligands.[29] For the latter, it was possible to prepare the donor-acceptor adduct with $LiCp^5$, an alkali metal aluminylene complex and the first hetero dimetallocene (**12**). Dispersion interactions between the many C-H bonds of the bulky ligands contribute significantly to adduct stabilization.

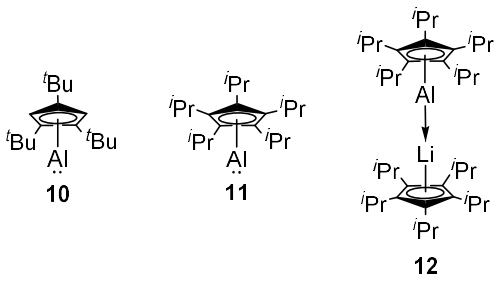

*Figure 4: Left, Monomeric aluminylenes **10** and **11** based on substituted Cp derivatives. Right, Coordination of a monomeric aluminylene to Cp^5Li, yielding hetero-dimetallocene **12**.*

The first monomeric aluminylene to be isolated was the cyclic, donor stabilised species {HC(MeCDippN)$_2$}Al ((Nacnac)Al, **13**).[31] The donor properties of this species have been thoroughly explored through the synthesis, and spectroscopic and structural analysis, of a range of d-metal carbonyl complexes. The onward chemistry of these bimetallic systems includes remarkable reactivity, such as C-H activation processes in the case of a bis-aluminylene palladium(0) species.[32,33] XPS studies on the electronic structure of **13** have been conducted and align well with a description as a Al(I) centre.[34] However, such spectroscopic studies have yet to be extended to its metal complexes in order to better understand their electronic structure.

One-coordinate 'free' aluminylenes have more recently been isolated, making use of highly sterically intimidating ligands such as terphenyl (**14**) and carbazoyl (**15**) derived donors (Figure 5).[35] These one-coordinate aluminium species have also been utilized as L-type donors, despite the highly encumbered metal centres. Investigation of these ligands has shown that they have highly flexible ligand properties, behaving ambiphilically in isolation (due to σ-donation by the available lone pair and π-acidity via vacant p-orbitals, **17**), or as pure σ-donors upon coordination of additional Lewis base moieties (which themselves occupy the available p-orbital sites, **18**).[36]

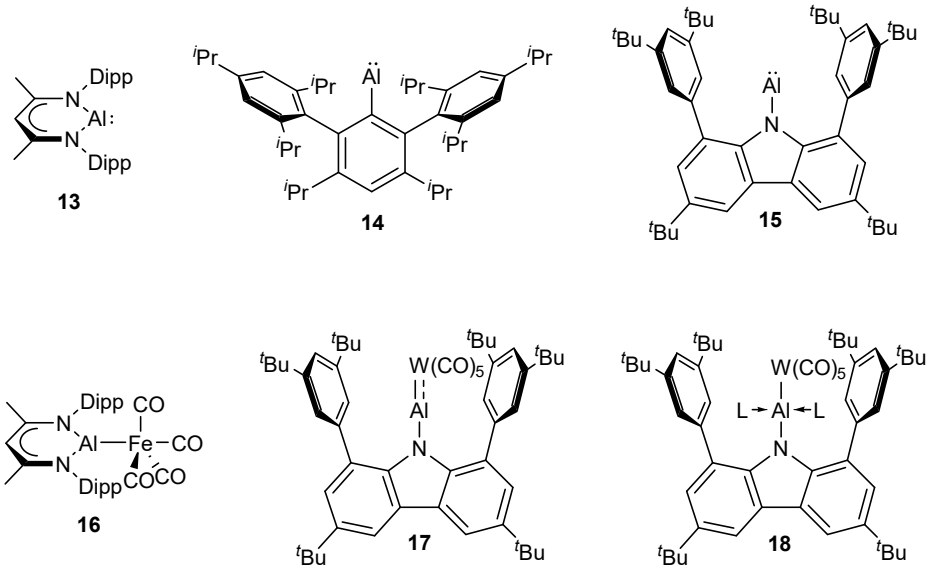

Figure 5: Top, Base stabilised and one coordinate free aluminylenes. Bottom, metal complexes of one and two coordinate aluminylenes, displaying the flexible ligand behaviour of one coordinate aluminylenes.

Gallylenes

Gallylene species are also well established, with the 1+ oxidation state for gallium being much more easily accessible than for aluminium.[37] GaCp*, which is a liquid at room temperature and adopts a hexameric structure in the solid state, has been used to synthesise complexes in which gallium acts as an L-donor centre, for example at metal carbonyl moieties such as iron, cobalt and chromium carbonyls.[28] The increased stability of the Ga(I) oxidation state means that simple diatomic halides such as GaI may be installed at an appropriate metal centre, albeit displaying weaker bonding interactions than both of the valence isoelectronic analogues BF and CO (the latter of which is able to displace the metalloligand).[38] This complex (**19**) was the first example of the coordination of a simple EX (E = group 13 element, X = halide) diatomic to a metal centre.

The gallium congener of (Nacnac)Al (**13**) is accessible, and indeed more stable and synthetically higher-yielding that its aluminium congener. Gallylene complexes of both copper and nickel bearing this metalloligand are known.[39,40] Finally, gallylene complexes have been isolated through co-reduction routes between gallium(III) halides and early transition metal halides such as titanocene and

zirconocene dichloride, yielding formally titanium and zirconium species in the 2+ oxidation state stabilised by gallylene (or indylene) coordination (**20** and **21**, Figure 6).[41]

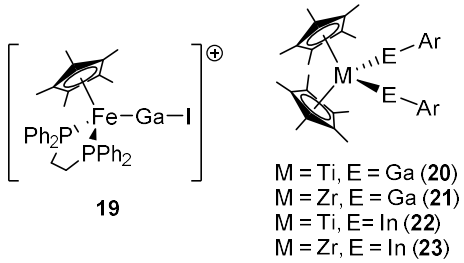

Figure 6: Noteworthy gallylene complexes. Left, An iodogallylene complex, the first example of an EX (E = triel, X = halide) fragment coordinated to a transition metal. Right, Titanium and zirconium bis-gallylenes (and indylenes) synthesised by co-reduction of metal precursors.

Indylenes

In the case of indium, the +1 oxidation state becomes sufficiently stabilized that InCp (with only hydrogen substituents on the C_5 ring) is easily prepared, existing as a somewhat volatile solid, with a coordination polymer structure in the solid state. Many metal complexes of this motif have been prepared, and comparisons with the lighter congeners indicate a marked decrease in donor strength as the lone pair becomes more diffuse and stabilized in an increasingly core-like 5s orbital. As for gallium, co-reduction has also proved to be a successful route for the installation of indylene ligands, with the analogous Zr and Ti complexes reported (see **22** and **23**, above)

Numerous other neutral indium(I) species in bearing various ligands (N-heterocyclic imides, N-heterocyclic olefins, N-heterocyclic boryloxy) in a variety of aggregation states (tetrahedral clusters, ligand-bridged dimers) have been reported.[42,43] However, the chemistry of metal complexes of such fragments is less well explored, likely due to the lower donor strengths compared to the lighter congeners.

Thallium(I) complexes are by far the most abundant class for this heavy group 13 metal. As for indium, TlCp is also stable and adopts as coordination polymer structure in the solid state, although this

material is significantly less volatile than the indium congener due to larger number of coulombic interactions possible between the larger cation and the anionic Cp units. However, none of the compounds reported display L-type ligation of a metal, due to the highly stabilized s-based lone pair being essentially unavailable for nucleophilic donation.

X-type ligands

Moving to the final ligation mode – anionic X-type ligands – these are known as trielyl species. These X_2E^- anions are isoelectronic with singlet carbenes, bearing an element-centred lone pair and a p-based vacant orbital.

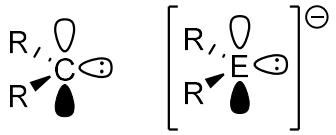

Figure 7: Schematic orbital diagram of a carbene (left) and valence isoelectronic trielyl anion (right).

Boryls

X-type ligands are again by far the most well established for the lightest triel element. Boryl ligands are a common motif in inorganic chemistry. Not only does the formal negative charge on boron and its lower electronegativity compared to carbon make them stronger σ-donors than N-heterocyclic carbenes, but a wide range of methods by which metal boryl complexes can be accessed also contributes to their relative abundance.[44]

The covalent nature of the bonding of the small non-metal boron leads to a wealth of compounds featuring B–B, B–X and B–H bonds which are stable in the absence of significant steric or kinetic stabilization. A number of metal boryl complexes have been accessed through oxidative addition of these bonds to a low-oxidation state transition metal fragment.[45] Pioneering work by Hartwig and Marder (amongst others) to the isolation or detection of boryl complexes of various metals such iron, manganese, tungsten, rhenium, iridium and ruthenium through photolytically induced CO

displacement followed by oxidative addition at the so-generated vacant site.[46-49] Remarkably, many such species have the capacity for onward activation of the C–H bonds of aromatic and aliphatic hydrocarbons, yielding borylated products derived from unactivated starting materials. Such reactions can even be conducted catalytically in metal, and the versatility of the borylated products for onward transformations (in particular C–C bond forming cross coupling reactions) has transformed our ability to functionalize unactivated C–H positions of organic molecules, once considered a 'Holy Grail' of the field.[50]

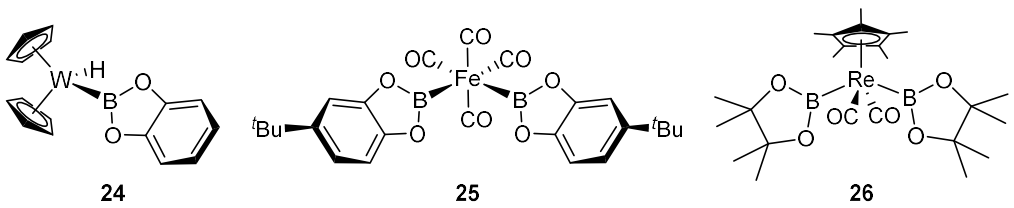

*Figure 8: A selection of early transition metal mono- and bis-boryl complexes generated by oxidative addition of B-H (**24**) or B-B (**25**, **26**) bonds.*

The generation of boryl species by diborane disproportionation is also an available route.[51] Typically utilizing coinage metal alkoxides, in which the M-O bond is relatively weak, B-O bond extrusion and boryl installation is driven by the extremely high B-O bond enthalpy (see compound **27**, Scheme 2).[52] Such complexes show diverse reactivity and have been utilized for, amongst other things the catalytic reduction of CO_2.[53, 54] The strongly donating boryl fragment can lead to nucleophilic behaviour for the generally electrophilic metal gold.[52] Remarkable work by Hill et al showed that this could be extended to the more oxophilic group 2 metals utilizing a magnesium alkyl complex and driven thermodynamically by B–C bond formation.[55]

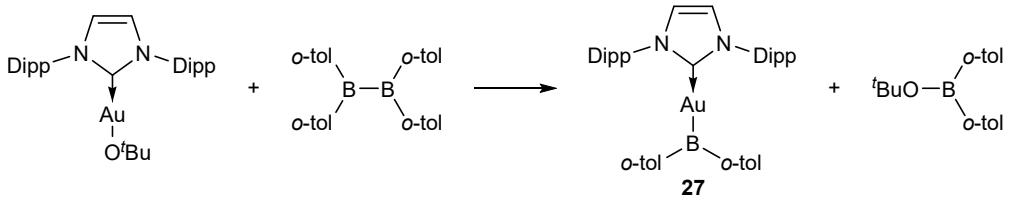

*Scheme 2: Installation of a boryl ligand at a gold centre via diborane(4) disproportionation, yielding gold boryl **27**.*

Installation of boryl ligand fragments at more oxophillic metal centres where oxidative addition chemistry is not typically accessible (groups 1, 2 12, as well as the f-block elements) remained a significant challenge until the report by Yamashita and co-workers of the boryl-lithium species **29** (Figure 9)[56] Accessed by low temperature reduction of a bromo-borane precursor (**28**) with lithium metal in the presence of catalytic naphthalene, this species demonstrates nucleophilic behaviour in its reactions with both organic and metal-centred substrates alike.[57] Access to this reagent as a simple lithium salt permitted the development of metal boryl chemistry for a wide range of new metals, with boryl complexes accessed via this starting material now known for all blocks of the Periodic Table. [58-64]

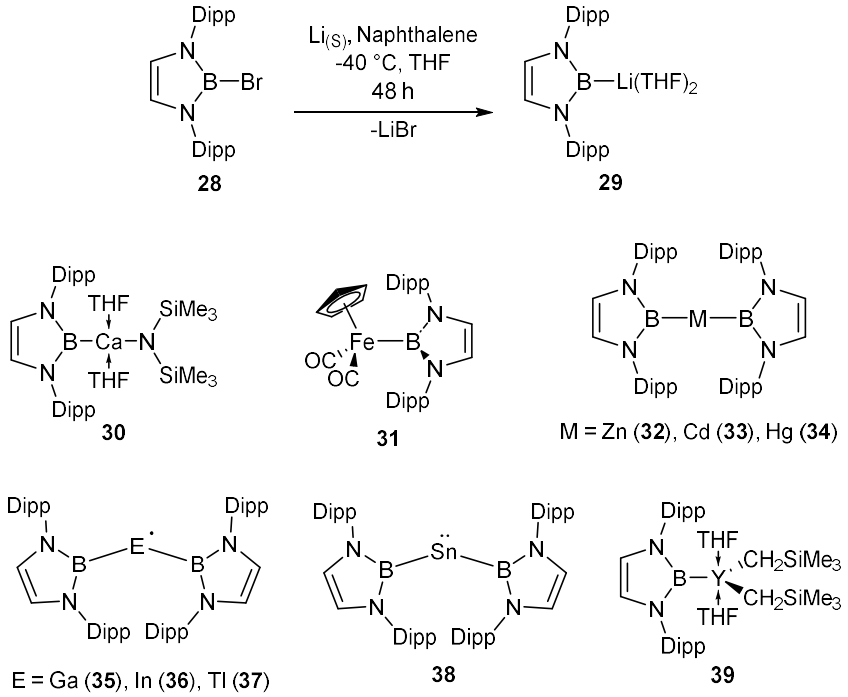

Figure 9: Top, the synthesis of the diazabutadiene supported boryl-lithium reagent. Bottom, Metal-boryl complexes from every group of the periodic table synthesised from this nucleophilic boryl precursor.

Gallyls

The synthesis and chemistry of metal gallyl complexes is well developed, given that the isolation of an alkali metal gallyl salt predates the report of boryl-lithium. Initial reports utilizing diazabutadiene-stabilized digallane(4) starting materials gave low yields,[65] but subsequent approaches exploiting halide precursors (such as **40**) allowed synthetically useful quantities to be accessed.[66]

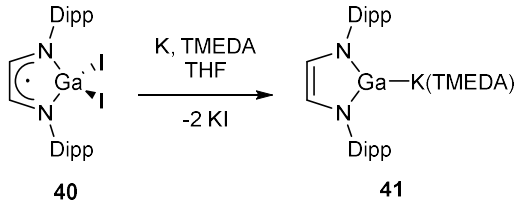

40 **41**

Scheme 3; A high yielding route to access a diazabutadiene stabilized potassium gallyl reagent.

The various diazabutadiene-supported gallyl anions have been demonstrated to be highly versatile as metallo-ligands, and have been coordinated to metals from all blocks of the Periodic Table.[44, 67-71] This broad utility is due to a fine balance of properties which render the gallium centre nucleophilic but not highly reducing. Its bonding is consequently well understood, involving polar-covalent interactions with metals, and almost pure σ-donation, with π-backdonation not typically present despite the availability of the vacant Ga 4p orbital. This is likely due to poor overlap resulting from diffuse orbitals and energetic mismatch. These studies have indicated that the *trans* influence of this metalloligand is comparable to that of tertiary phosphines, i.e. strong, but less so that a boryl or NHC ligand. This combined with the relatively covalent bonding character and the steric stabilization provided by the flanking groups explains the high stability observed for metal complexes of this metallo-ligand.

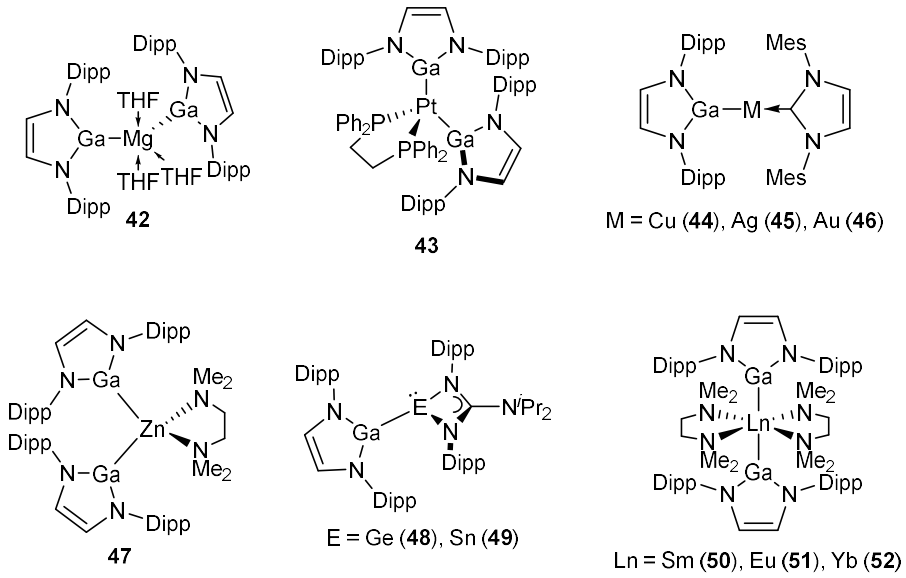

Figure 10: A range of diazabutadiene stabilised gallyl complexes featuring metals from every block of the periodic table.

Only recently was a gallyl anion reported with a significantly different ligand framework. The NON gallyl bears the same framework as the first reported aluminyl anion (**58**), and has been installed at both coinage metal centres and the alkaline earth metal beryllium, yielding complexes with significantly reduced reactivities compared to the aluminium congeners (vide infra).[72-74] Subsequently, gallyl anions have been isolated via salt metathesis of a boryloxy ligand with the Ga(I) precursor GaCp*, although no metal complexes of this acyclic metalloligand have yet been reported.[42]

Metal gallyl complexes have also been accessed via attack by transition metal nucleophiles on suitable Ga(III) precursors, yielding species with more diverse supporting frameworks at gallium.[75] Additionally, the remarkable dimethyl gallyl fragment can be installed at a tungsten centre, via the reaction between $GaMe_3$ and a corresponding metal hydride, eliminating methane as a by-product.[28]

Indyls

Remarkably, given the high stability of indium in the +1 oxidation state, an alkali metal salt of an indyl anion (**53** and **54**) was only recently reported in 2018 by Coles and co-workers, and its synthesis was conducted by a reductive route via an indium(III) halide precursors.[76] Prior to this, early metal indyl complexes were synthesised via a range of methods, including salt metathesis using a nucleophilic transition metal fragment,[77, 78] alkane extrusion between an indium (III) alkyl species and a platinum hydride,[75] and oxidative addition routes, involving M-X bond insertion both by low valent transition metals such as ruthenium,[79] and also by the In(I) species (Nacnac)In.[80]

The first indyl anion was reported both as a separated-ion-pair potassium salt, and also as the contact-ion-pair with a lithium cation, a species which bears a direct In-Li bond. This reagent has subsequently been used to generate metal-indyl complexes of both zinc and cadmium (**55** and **56**) , with the zinc congener exhibiting onward reactivity with a range of organic azides.[81]

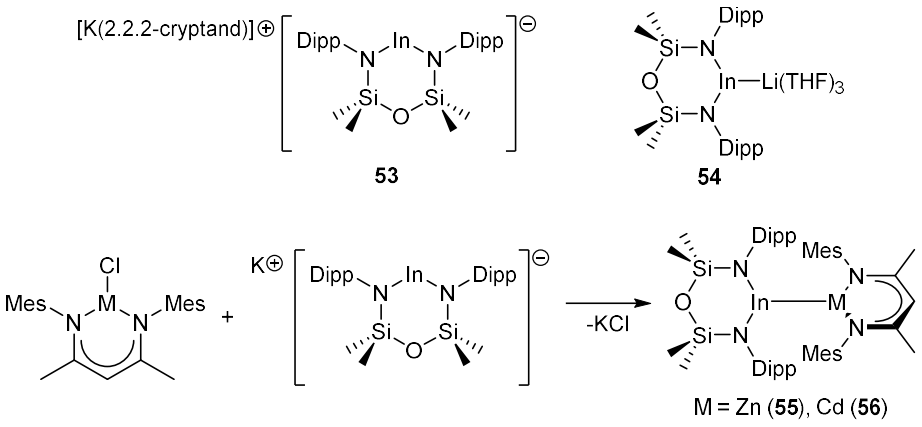

*Figure 11: Top, The first reported indyl anion as its potassium separated ion pair salt (**53**) and lithium contact ion pair salt (**54**). Bottom, the application of this reagent in the synthesis of species containing In-Zn (**55**) and In-Cd (**56**) bonds.*

An acyclic bis-boryloxy indyl compound, generated as a potassium salt by analogous means to the aforementioned gallium congener (i.e. from InCp) has been recently reported, but its use as a ligand is as yet also unexplored.[42]

Thallyls

Whilst a broad spectrum of Tl-M bonds have been structurally characterised, all feature Lewis acidic Thallium(I) or (III) centres coordinated by nucleophilic metal centres. No evidence has been reported for nucleophilicity of any thallium centre, even in the case of the single reported thallyl anion (**57**), which was isolated as a contact ion pair with a potassium(18-crown-6) counterion via reduction of the corresponding bis-boryl thallium radical **37**.[61]

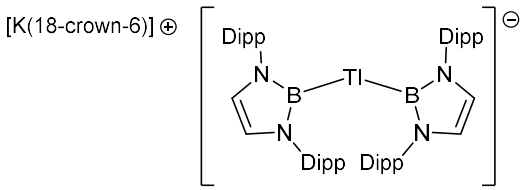

57

Figure 12: The only reported thallyl anion.

Aluminyls

The last in the series of trielyl ions to be isolated was an alkali metal salt of an aluminyl anion. Until this point, the only unsupported metal aluminyl species known were accessed either through salt metathesis by a nucleophilic transition metal fragment with an aluminium (III) halide species [82-85] or by the oxidative addition of a M–X bond at an aluminylene such as **13** or **15**.[36, 86] Supported examples (i.e. those in which a ligand bridges the aluminium and transition metal centres, holding the M–Al together) of aluminyls bonded to rhodium (accessed by co-reduction),[87] iridium (via Al–H bond oxidative addition),[88] nickel (Al–C bond oxidative addition)[89] and palladium (Al–Cl bond oxidative addition)[90] have also been reported. Similar to boron, access to a broader range of metal aluminyl species was more readily afforded by the synthesis of an aluminyl anion reagent. The first such example (**58**) was reported by the Aldridge and co-workers in 2018.[72] Based on a xanthene backbone framework and kinetically and thermodynamically stabilised by bulky amido-aryl groups, this species adopts a dimeric structure in the solid state and arene solution in which potassium-arene contacts bridge the two anionic units. Since this initial report, a number of related complexes have

subsequently been reported, featuring a range of supporting ligand frameworks. Cyclic and acyclic bis-amide supported species are reported, as well as alkyl, alkyl-amido and (acyclic) boryloxy supported species.[91-100] The full list of reported aluminyl anions is shown in figure 13, below.

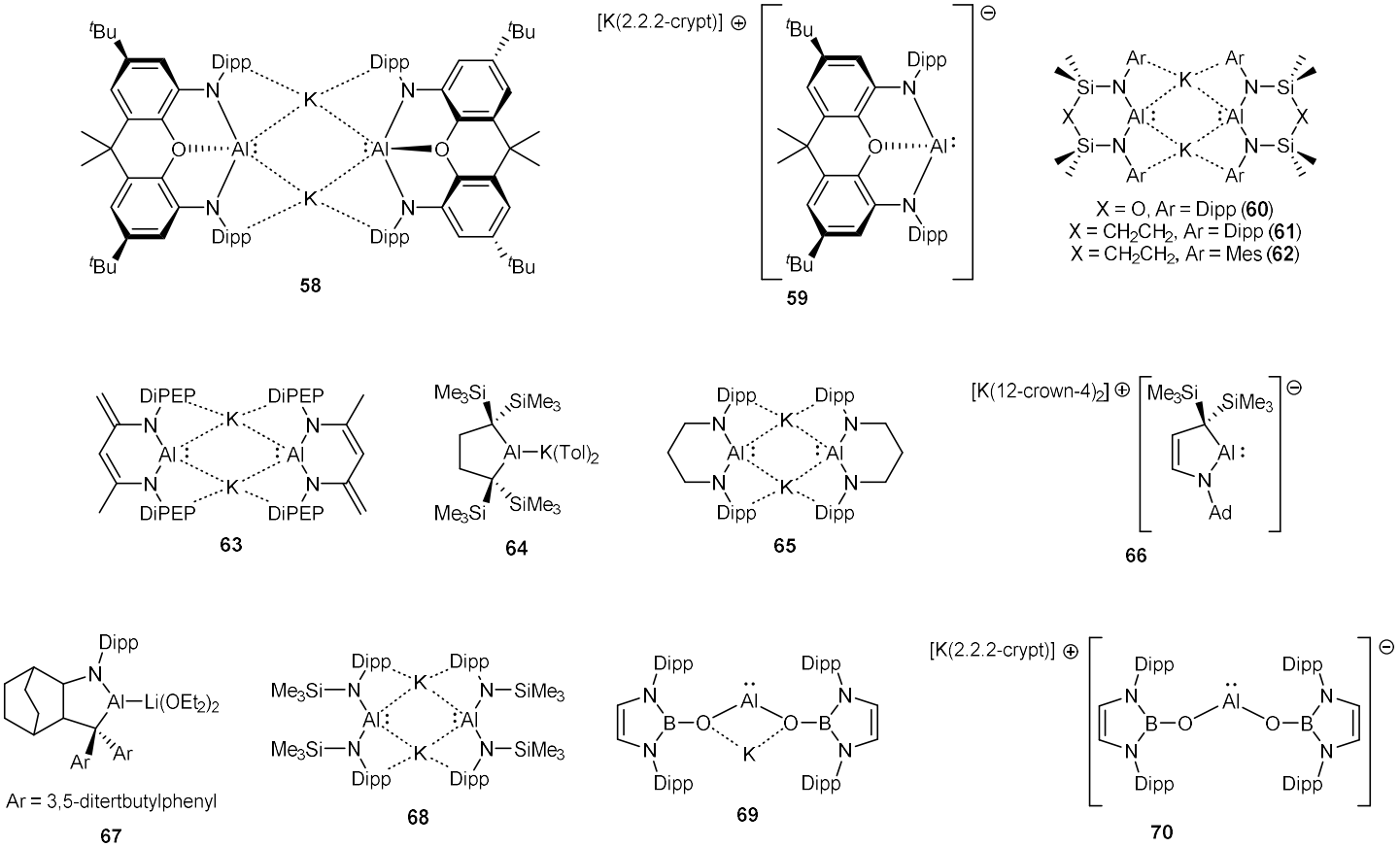

Figure 13 All known aluminyl anion species, pictured as the alkali metal salt with which they were first reported.

With the exception of **63**, which is synthesised by backbone deprotonation of (Nacnac)Al, and **69** and **70** which utilise the low valent starting material $[Cp^*Al]_4$ as their Al(I) source, all aluminyl species have been synthesised via alkali metal reductions, either of aluminum halides or Al-Al bonded dialane(4) species. The latter route is surprising, given that for related boron species this reduction is known to populate an E–E π-bonding orbital, strengthening the interaction rather than leaving to bond cleavage. This key difference between these group 13 elements likely results from poorer π-overlap of aluminium p-orbitals due to their diffuse nature, as well as influences of ligand choices which may partially occupy the atomic orbitals with additional σ- or π- donor interactions.

Notwithstanding their potential as ligands, it bears mention that these species are highly reactive, capable of activating a broad range of substrates such as H–H, C–H and C–C single bonds, multiple bonds such as those found in CO, CO_2, alkenes alkynes and heteroalenes, as well as halogenated species such as fluoroalkanes and SF_6.[91, 101] Such reactions are typically driven by oxidation of the thermodynamically disfavoured aluminium(I) centre, and the formation of strong Al–E bonds. Therefore, ancillary ligand sets present in transition metal substrates must be carefully designed or chosen in order to avoid unwanted and unproductive reactions.

Crucially, significant evidence has been presented in the literature for the dependence of the reactivity observed for aluminyl compounds on both the availability and identity of the alkali metal counterion, for example in the mode of benzene activation and rate of H_2 splitting.[102, 103] Such observations imply significant bimetallic character to the observed reactivity, and provide additional motivation for the synthesis of species in which a direct Al-M linkage is present for a wide variety of metals, in order to access the onward reaction chemistry therein.

Significantly fewer metal aluminyl complexes are reported as compared to the more abundant examples of boryls and gallyls. This is presumably due to both the short period for which nucleophilic aluminyl reagents have been known in the literature, and also synthetic difficulties associated with the incredibly reactive and reducing nature of these anions as mentioned above. Additionally, those species that are reported have been shown to undergo a variety of remarkable onward chemical transformations. For this reason, all of the metals for which aluminyl-ligated complexes have been reported to date are each discussed below in turn.

As already discussed, much attention has been given to the effect on small molecule reactivity of the identity of the alkali metal counterion. Salts of the full group 1 series have been isolated for the aluminyl anion **60**, as separated ion pairs, their solvated contact ion pairs, and contact-ion-bridged dimeric forms.[102, 104, 105] Kinetic studies on the activation of H_2 and Si–H bonds have revealed that, although a counterion effect is present, its magnitude in this particular instance is small. More

significant however is the extent of structural distortion observed in the contact-ion-pair dimers as the group is traversed away from potassium. Descending the group leads to increased Al–M interaction, which is accompanied by 'slipping' of the two aluminyl units relative to each other to minimise the distance of this contact (**71**). In contrast, reduced interaction is seen between aluminium and the heavier alkali metals (**72**), with the aluminyl units twisting relative to the other to accommodate the large size of these cations between the flanking arenes.

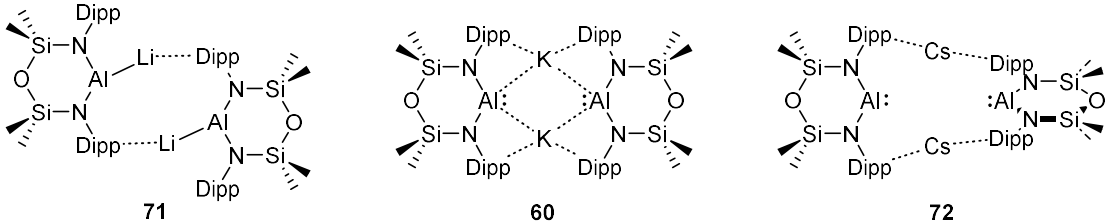

Figure 14: Representative examples of the complete series of alkali metal aluminyl contact-ion-pair dimers. Smaller cations lead to more direct Al-M interactions, and consequently 'slipped' structures, whilst larger metals lead to minimal Al-M interaction, and a relative twisting of the two aluminyl units to accommodate the cations between the flanking arenes.

More significant differences in reactivity are observed upon moving to alkaline earth metal aluminyl systems. These are reported so far for the elements beryllium, magnesium and calcium.[72, 73, 93, 98, 106, 107] Different ancillary ligands are utilized at the alkaline-earth centre in each case, with Cp analogues known for beryllium (**73**) and magnesium (**74**), and Nacnac analogues for magnesium (**75**) and calcium (**76**) . Comparing like for like pairs, both computational and reactivity studies demonstrate that covalency in the Al–Ae bond decreases dramatically as the group is descended, as would be expected based on the increasingly diffuse orbitals of the Ae element. Analogously, as electronegativity decreases down the group and the ionic character increases, greater anionic charge resides on the aluminium centre. This has a marked influence on reactivity. For example, in reactions with carbodiimide substrates, **73** reacts in a manner consistent with nucleophilicity at beryllium. However, the equivalent reaction of **74** appears to operate via a mechanism in which initial attack at the electrophilic carbon centre is by aluminium. Correspondingly, **76** is significantly more reactive as compared to **75**, the former being both unstable in donor solvents (activating THF via C-O bond

insertion by aluminium), and capable of the 2-electron reduction of cyclooctatetraene to yield a bimetallic inverse sandwich complex.

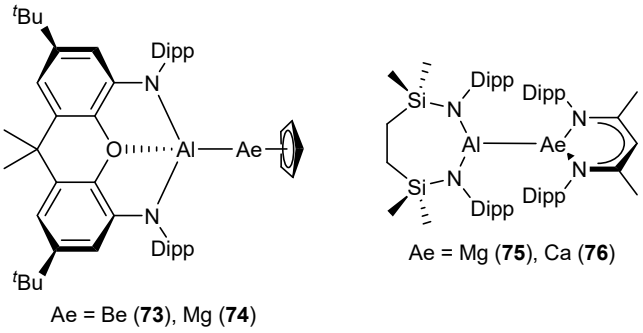

Figure 15: Representative examples of the known alkaline-earth aluminyl complexes.

Moving to transition metal aluminyl complexes, Yamashita an co-workers have reported examples for scandium (**77**), yttrium (**78**) and vanadium (**79**).[95, 108, 109] Both group 3 species are accessed by salt metathesis routes involving potassium aluminyl reagents **64** and **65**, and the scandium compound shows complex onward reactivity with benzene in the presence of alkyl bromides, which appears to derive from the ability of the Lewis acidic scandium centre to bind and activate arene substrates. In the yttrium case, computational investigations have shown a significant decrease in the HOMO-LUMO energy gap for the complex as compared to a boryl congener (**39**), due to stronger σ-donation raising the HOMO energy, and more effective π-overlap based on orbital size match, lowering the LUMO.[59] Experimentally, this change is indicated by UV/vis absorption in the visible region for this d^0 species for the aluminyl complex (which is not present in the boryl case, where absorption lies in the UV region). The synthesis of vanadium aluminyl **79** can either be achieved via salt metathesis between a potassium aluminyl and vanadium chloride precursor, or via photolytic activation of the corresponding dialane(4) with vanadocene. This alternative synthesis (which draws parallels with early boryl chemistry and is known in the absence of light for the gallyl congener), combined with the facile metal-metal bond insertion chemistry of the heterobimetallic species, opens up the possibility for catalytic aluminylation of alkene substrates, a remarkable overall transformation. Inspection of the vanadium

pre-edge energy by XAS was also used to probe the bonding, leading to the description of **79** as a partially reduced V(III) centre featuring a polar covalent V–Al bond, as supported by DFT calculations.

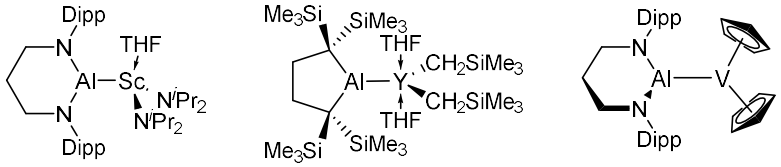

77 78 79

Figure 16: Early-transition metal aluminyl complexes.

Moving to the right within the d-block, a significant gap exists in which no metal aluminyl species synthesised via nucleophilic introduction of the aluminium fragment has been reported. Recent reports tackle the synthesis of palladium aluminyl complexes, in which palladium (0) centres bearing one, two or three aluminyl ligands have been reported.[110] In the case of tris-aluminyl ligation, a smaller aluminyl species than for mono- or bis-ligation was found to be necessary. This species rendered the palladium (0) centre sufficiently electron rich that oxidative addition of B–B bonds at the palladium centre could be induced, a reaction which computationally has been shown to be challenging for this metal.[111]

The first covalent metal-aluminyl linkage reported via nucleophilic installation of aluminium was that of the gold aluminyl **82**.[112] This remarkable species was shown to feature a metal-metal bond highly polarised towards the gold centre. This was demonstrated through the reaction of this species with CO_2 and a carbodiimide, with the mode of insertion indicating nucleophilicity at the gold centre. This reactivity is highly unusual for this electropositive metal, the typical catalytic applications of which depend on its electrophilic character.[113] This report serves as an excellent example of the strongly sigma-donating properties of the aluminyl metallo-ligand.

This chemistry has since been extended to the other members of the coinage metal series for aluminyl metalloligands **58** and **61**.[74, 114, 115] These studies indicate that both the rate and outcome of onward reactivity with heteroallenes depends heavily depends on the coinage metal identity, with copper

yielding immediate conversion to carbonate products in reactions with CO_2. Increasingly slow conversion as the group is descended permits the isolation of metallocarbene intermediates in the case of silver, and ultimately inhibits conversion beyond this point in the case of gold. These observations are consistent with a decrease in M–O and an increase in M–C bond dissociation enthalpies as the coinage metal triad is descended, which both destabilised the intermediate species and increases the favourability of the final product for the lighter elements.

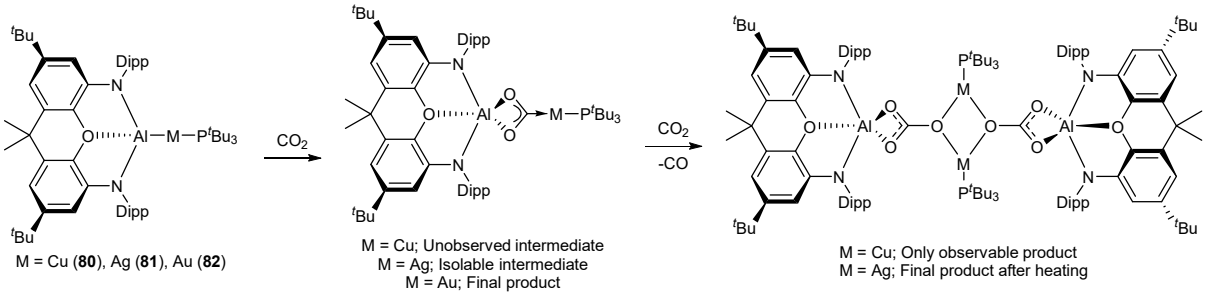

*Scheme 4: A complete series of isostructural coinage metal aluminyl complexes **80**-**82**, and their divergent reactivity with CO_2.*

Group 12 aluminyl complexes have thus far been limited to zinc, with two similar species having been reported, accessed by analogous salt metathesis reactions between either **58** or **60** and a Nacnac-stabilized zinc iodide.[116, 107] Both react analogously with CO_2 to yield metallocarbene complexes of zinc (e.g. **85**) , implying initial nucleophilic attack on the carbon atom by the group 12 centre as a result of the incredibly strong electron donation of the aluminyl ligand. No subsequent conversion to a carbonate product (via initial loss of CO and a presumed bridging oxo-species) was observed, unlike in the case of the lighter coinage metal complexes. This is in striking contrast to the diagonally related magnesium congeners of both systems, which undergo not only onward conversion to carbonate species, but also a ligand redistribution process to yield $Nacnac_2Mg$ and magnesium bis-metallo-carbonate complex **86**. Here, a clear preference for maximising Coulombic interactions in the case of magnesium, versus more covalent bonding behaviour in the case of zinc, is demonstrated.

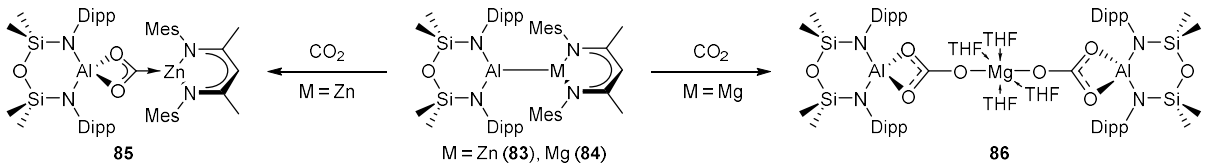

*Scheme 5: Isostructural, diagonally related zinc and magnesium aluminy complexes **83** and **84**, which display divergent reactivity with CO_2.*

Only one f-element aluminyl complex has been reported to date. Accessed via salt metathesis between a simple samarium diiodide THF solvate and the corresponding potassium aluminyl salt, the Al–Sm–Al arrangement of **87** is roughly linear.[117] The metal-metal bond lengths exceed the sum of the respective covalent radii, indicating predominantly ionic bond character as is typical of lanthanide chemistry. The exotic bonding orbital manifold (in which HOMO and HOMO-1 bonding orbitals are largely aluminium based with small samarium s and f contributions, and two of six samarium f-based SOMOs mix with aluminium AOs) yields unprecedented reactivity with unsaturated small molecule substrates. Carbodiimide insertion into both Al–Sm bonds (through nucleophilic attack by the aluminium centre) precedes the reductive coupling of a further two substrate molecules to form a new C-C bond in a tetradentate bis-amidinate ligand which bridges two samarium centres. In reactions with ethene, the initially formed product of simple cycloaddition (**88**) at each aluminium centre rearranges under mild conditions to a doubly anionic Al_2C_4 heterocycle, in a reaction facilitated (as supported by DFT calculations) by the highly Lewis acidic samarium(II) centre.

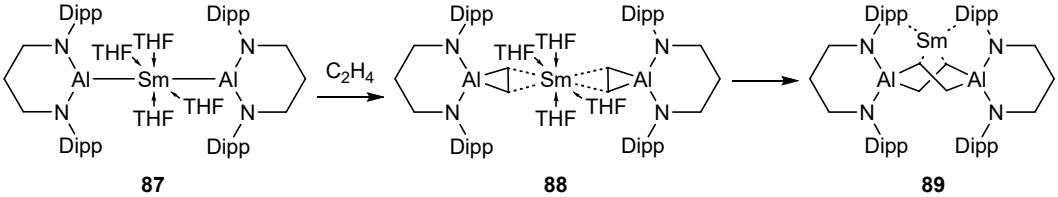

Scheme 6: The reactivity of bis-aluminyl samarium, the only reported f-block aluminyl complex, with ethene, and subsequent Sm^{2+} mediated alkyl-relay based rearrangement.

Outlook

It is clear from the above survey that the installation of trielyl metallo-ligands has significant and diverse effects on the electronic structure and onward chemistry of a given metal centre. Additionally, whilst boryl and gally ligated species are fairly well developed (and those of indium typically display more limited reactivity), the chemistry of the aluminyl congeners is far less developed, both in terms of the range of metals for which complexes have been reported, the understanding of the resulting electronic structure, and onward reactivity. This deficiency, especially in terms of our understanding of the underlying donor properties primarily results from the recent isolation of aluminyl anions and their high inherent reactivity. Nonetheless it requires addressing in the literature, especially given the striking and unusual transformations known for the examples reported so far.

In this thesis, efforts to not only synthesise, but also probe in detail the electronic structure of metal aluminyl complexes is discussed. Choices of transition metal fragment are made both on the basis of stabilizing the so-generated complexes, but also with the goal of accessing 'probe-rich' final products which spectroscopically inform on the ligand properties of the aluminyl moiety. Additionally, congeners throughout group 13 are also targeted, in order to provide greater insight and establish trends through comparison of these spectroscopic parameters, as well as via associated quantum chemical calculations.

Chapter 2 details the synthesis of a Nacnac-supported zinc-boryl species, to provides a means of comparison to the reported aluminyl congener. Due to undesired product formation when using a direct salt-metathesis approach with the boryl-lithium reagent **29**, diborane(4) disproportionation is instead investigated, utilizing the formation of strong B-O bonds (as well as alkali metal halide lattice enthalpy) as the driving force. This B-O bond extrusion methodology is extended further, and leveraged in the onward conversion of this zinc-boryl species into a Zn–Zn bonded zinc(I) compound and a boron ether, thereby accessing a bona fide low valent zinc complex with a diborane(4) acting as the formal reductant.

Chapter 3 describes the use of XAS measurements to probe the electronic structure of a series of isostructural NacnacZnX species (X = methyl, silyl, boryl, aluminyl, berylyl, boryloxy), as well as a Zn–Zn bonded zinc(I) reference species. The data collected has been used to investigate the donor strengths of these highly electron-releasing main-group ligand fragments. Additionally, the experimentally determined trends are compared to parameters generated by common computational techniques, in order to benchmark these methods in their ability to accurately describe the exotic electronic structures of the compounds studied.

Chapter 4 begins by extending the NON ligand system used to stabilise aluminyl **58** and its gallium congener to the heavier group 13 metal indium, using indium(I) precursors to circumvent the need for a reductive step. With this reagent in hand, isostructural series of linear d^{10} species of the type (NON)EAgP^tBu_3 and (NON)EHgB{$(NDippCH)_2$} are prepared as probes of the *trans* effects of the corresponding trielyls. DFT calculations have been carried out in order to rationalise the structural and spectroscopic data gathered.

Chapter 5 turns to the classic organometallic fragment [$Fe(CO)_4$] as an information-rich probe (SC-XRD, IR, Mössbauer) of ligand donor properties. Synthetic efforts to access species of the type [(NON)E$Fe(CO)_4$]$^-$ are detailed. Owing to its reducing power and oxophilicity, reactions of the aluminyl anion with $Fe(CO)_5$ lead initially to Al-O bond formation, and reaction tuning based on potassium cation availability is required to access the desired Fe–Al motif. In the case of the heavier congeners, such considerations are unnecessary, and the target species are accessed straightforwardly. With an essentially isostructural series in hand, spectroscopic measurements and DFT calculations are used in tandem to interrogate the trends in metallo-ligand properties down group 13.

Chapter 6 details the synthesis and reactivity of a bis-aluminyl magnesium reagent which was initially targeted as a more covalent aluminyl source for more selective transfer of the metallo-ligand fragment (by analogy with Grignard chemistry). Reactivity of {(NON)Al}$_2$Mg with various metal halide substrates yielded only the (NON)AlX reduction products. Turning to the small molecule activation chemistry of

this unusual trimetallic species, reductive defluorination of SF_6 yielded a fluxional metal fluoride species formally containing a solubilized MgF_2 fragment. DFT calculations indicated a high degree of electron density on the magnesium centre, despite reactions with the carbon electrophile MeI confirming aluminium centred nucleophilicity. However, in photolytically activated reactions with cyclooctadiene (COD), magnesium(0) metal was eliminated from the molecule, and the formal transfer of (NON)Al(II) radical fragments to the COD substrate was observed. *In situ* EPR measurements confirmed the intermediacy of electron-unpaired species, and the overall transannular cyclisation of COD to tetrahydropentalene species is commonly viewed as a probe reaction for radical chemistry in the organic literature. This unusual reactivity demonstrates the striking impact an extremely electron donating ligand such as an aluminyl can have on the chemistry of a metal complex, as well as the differences between the thermal and photolytic reactivity pathways available to such trimetallic species.

References

[1] A. J. Downs, *Chemistry of aluminium, gallium, indium and thallium*, Springer Science & Business Media, **1993**.
[2] I. Levin, D. Brandon, *Journal of the American Ceramic Society* **1998**, *81*, 1995-2012.
[3] R. Sunke, S. B. Nallapati, J. S. Kumar, K. Shiva Kumar, M. Pal, *Organic & Biomolecular Chemistry* **2017**, *15*, 4042-4057.
[4] A. Lennartson, *Nature Chemistry* **2015**, *7*, 610-610.
[5] J. Fujihara, N. Nishimoto, *Current Research in Toxicology* **2024**, *6*, 100157.
[6] A. J. Downs, *Coordination Chemistry Reviews* **1999**, *189*, 59-100.
[7] X. Zhang, Y. Zhao, S. Wang, X. Jing, *Materials Chemistry Frontiers* **2021**, *5*, 5534-5548.
[8] J. Wang, L. Zhang, L. Wang, W. Lei, Z.-S. Wu, *ENERGY & ENVIRONMENTAL MATERIALS* **2022**, *5*, 10-44.
[9] P. Laszlo, *Angewandte Chemie International Edition* **2000**, *39*, 2071-2072.
[10] R. W. Rudolph, *Accounts of Chemical Research* **1976**, *9*, 446-452.
[11] X. You, Z. Xing, S. Jiang, Y. Zhu, Y. Lin, H. Qiu, R. Nie, J. Yang, D. Hui, W. Chen, Y. Chen, *Developments in the Built Environment* **2024**, *17*, 100319.
[12] L. Luo, J. M. Younker, A. V. Zabula, *Science* **2024**, *384*, 1424-1428.
[13] M. L. H. Green, P. Mountford, G. J. Smout, S. R. Speel, *Polyhedron* **1990**, *9*, 2763-2765.
[14] M. Mocker, C. Robl, H. Schnöckel, *Angewandte Chemie International Edition in English* **1994**, *33*, 1754-1755.
[15] C. Klemp, M. Bruns, J. Gauss, U. Häussermann, G. Stösser, L. van Wüllen, M. Jansen, H. Schnöckel, *Journal of the American Chemical Society* **2001**, *123*, 9099-9106.
[16] G. Almeida, R. F. Ubbink, M. Stam, I. du Fossé, A. J. Houtepen, *Nature Reviews Materials* **2023**, *8*, 742-758.
[17] K. F. Tebbe, U. Georgy, *Acta Crystallographica Section C* **1986**, *42*, 1675-1678.
[18] E. I. Davydova, T. N. Sevastianova, A. Y. Timoshkin, *Coordination Chemistry Reviews* **2015**, *297-298*, 91-126.
[19] R. C. Cammarota, L. J. Clouston, C. C. Lu, *Coordination Chemistry Reviews* **2017**, *334*, 100-111.
[20] H. Braunschweig, R. D. Dewhurst, V. H. Gessner, *Chemical Society Reviews* **2013**, *42*, 3197-3208.
[21] M.-A. Légaré, G. Bélanger-Chabot, R. D. Dewhurst, E. Welz, I. Krummenacher, B. Engels, H. Braunschweig, *Science* **2018**, *359*, 896-900.
[22] H. Braunschweig, C. Kollann, U. Englert, *Angewandte Chemie International Edition* **1998**, *37*, 3179-3180.
[23] A. H. Cowley, V. Lomelí, A. Voigt, *Journal of the American Chemical Society* **1998**, *120*, 6401-6402.
[24] D. Vidovic, S. Aldridge, *Angewandte Chemie International Edition* **2009**, *48*, 3669-3672.
[25] M. J. Drance, J. D. Sears, A. M. Mrse, C. E. Moore, A. L. Rheingold, M. L. Neidig, J. S. Figueroa, *Science* **2019**, *363*, 1203-1205.
[26] C. Dohmeier, C. Robl, M. Tacke, H. Schnöckel, *Angewandte Chemie International Edition in English* **1991**, *30*, 564-565.
[27] C. Ganesamoorthy, S. Loerke, C. Gemel, P. Jerabek, M. Winter, G. Frenking, R. A. Fischer, *Chemical Communications* **2013**, *49*, 2858-2860.
[28] R. A. Fischer, J. Weiß, *Angewandte Chemie International Edition* **1999**, *38*, 2830-2850.
[29] A. Hofmann, T. Tröster, T. Kupfer, H. Braunschweig, *Chemical Science* **2019**, *10*, 3421-3428.
[30] I.-A. Bischoff, S. Danés, P. Thoni, B. Morgenstern, D. M. Andrada, C. Müller, J. Lambert, E. C. J. Gießelmann, M. Zimmer, A. Schäfer, *Nature Chemistry* **2024**, *16*, 1093-1100.
[31] C. Cui, H. W. Roesky, H.-G. Schmidt, M. Noltemeyer, H. Hao, F. Cimpoesu, *Angewandte Chemie International Edition* **2000**, *39*, 4274-4276.

[32] T. N. Hooper, M. Garçon, A. J. P. White, M. R. Crimmin, *Chemical Science* **2018**, *9*, 5435-5440.
[33] R. Y. Kong, M. R. Crimmin, *Dalton Transactions* **2021**, *50*, 7810-7817.
[34] A. B. Altman, C. D. Pemmaraju, C. Camp, J. Arnold, S. G. Minasian, D. Prendergast, D. K. Shuh, T. Tyliszczak, *Journal of the American Chemical Society* **2015**, *137*, 10304-10316.
[35] X. Zhang, Y. Mei, L. L. Liu, *Chemistry – A European Journal* **2022**, *28*, e202202102.
[36] X. Zhang, L. L. Liu, *Angewandte Chemie International Edition* **2021**, *60*, 27062-27069.
[37] P. Jutzi, B. Neumann, G. Reumann, H.-G. Stammler, *Organometallics* **1998**, *17*, 1305-1314.
[38] H.-J. Himmel, G. Linti, *Angewandte Chemie International Edition* **2008**, *47*, 6326-6328.
[39] G. Prabusankar, S. Gonzalez-Gallardo, A. Doddi, C. Gemel, M. Winter, R. A. Fischer, *European Journal of Inorganic Chemistry* **2010**, *2010*, 4415-4418.
[40] U. Chakraborty, B. Mühldorf, N. J. C. van Velzen, B. de Bruin, S. Harder, R. Wolf, *Inorganic Chemistry* **2016**, *55*, 3075-3078.
[41] X.-J. Yang, Y. Wang, B. Quillian, P. Wei, Z. Chen, P. v. R. Schleyer, G. H. Robinson, *Organometallics* **2006**, *25*, 925-929.
[42] D. Sarkar, P. Vasko, T. Gluharev, L. P. Griffin, C. Bogle, J. Struijs, J. Tang, A. F. Roper, A. E. Crumpton, S. Aldridge, *Angewandte Chemie International Edition* **2024**, *63*, e202407427.
[43] S. R. Baird, E. Hupf, I. C. Watson, M. J. Ferguson, E. Rivard, *Chemical Communications* **2023**, *59*, 2903-2906.
[44] M. Asay, C. Jones, M. Driess, *Chem. Rev.* **2011**, *111*, 354-396.
[45] I. A. I. Mkhalid, J. H. Barnard, T. B. Marder, J. M. Murphy, J. F. Hartwig, *Chem. Rev.* **2010**, *110*, 890-931.
[46] J. F. Hartwig, K. S. Cook, M. Hapke, C. D. Incarvito, Y. Fan, C. E. Webster, M. B. Hall, *Journal of the American Chemical Society* **2005**, *127*, 2538-2552.
[47] K. M. Waltz, J. F. Hartwig, *Science* **1997**, *277*, 211-213.
[48] X. He, J. F. Hartwig, *Organometallics* **1996**, *15*, 400-407.
[49] J. Hu, M. Ferger, Z. Shi, T. B. Marder, *Chemical Society Reviews* **2021**, *50*, 13129-13188.
[50] aI. F. Yu, J. W. Wilson, J. F. Hartwig, *Chem. Rev.* **2023**, *123*, 11619-11663; bN. Miyaura, K. Yamada, A. Suzuki, *Tetrahedron Letters* **1979**, *20*, 3437-3440.
[51] E. C. Neeve, S. J. Geier, I. A. I. Mkhalid, S. A. Westcott, T. B. Marder, *Chem. Rev.* **2016**, *116*, 9091-9161.
[52] A. Suzuki, X. Guo, Z. Lin, M. Yamashita, *Chemical Science* **2021**, *12*, 917-928.
[53] T. M. Horsley Downie, R. S. C. Charman, J. W. Hall, M. F. Mahon, J. P. Lowe, D. J. Liptrot, *Dalton Transactions* **2021**, *50*, 16336-16342.
[54] A. Suzuki, L. Wu, Z. Lin, M. Yamashita, *Angewandte Chemie International Edition* **2021**, *60*, 21007-21013.
[55] A.-F. Pécharman, A. L. Colebatch, M. S. Hill, C. L. McMullin, M. F. Mahon, C. Weetman, *Nature Communications* **2017**, *8*, 15022.
[56] Y. Segawa, M. Yamashita, K. Nozaki, *Science* **2006**, *314*, 113-115.
[57] Y. Segawa, Y. Suzuki, M. Yamashita, K. Nozaki, *Journal of the American Chemical Society* **2008**, *130*, 16069-16079.
[58] A. V. Protchenko, P. Vasko, M. Á. Fuentes, J. Hicks, D. Vidovic, S. Aldridge, *Angewandte Chemie International Edition* **2021**, *60*, 2064-2068.
[59] L. M. A. Saleh, K. H. Birjkumar, A. V. Protchenko, A. D. Schwarz, S. Aldridge, C. Jones, N. Kaltsoyannis, P. Mountford, *Journal of the American Chemical Society* **2011**, *133*, 3836-3839.
[60] A. V. Protchenko, D. Dange, A. D. Schwarz, C. Y. Tang, N. Phillips, P. Mountford, C. Jones, S. Aldridge, *Chemical Communications* **2014**, *50*, 3841-3844.
[61] A. V. Protchenko, D. Dange, J. R. Harmer, C. Y. Tang, A. D. Schwarz, M. J. Kelly, N. Phillips, R. Tirfoin, K. H. Birjkumar, C. Jones, N. Kaltsoyannis, P. Mountford, S. Aldridge, *Nature Chemistry* **2014**, *6*, 315-319.
[62] R. Frank, J. Howell, R. Tirfoin, D. Dange, C. Jones, D. M. P. Mingos, S. Aldridge, *Journal of the American Chemical Society* **2014**, *136*, 15730-15741.

[63] T. Kajiwara, T. Terabayashi, M. Yamashita, K. Nozaki, *Angewandte Chemie International Edition* **2008**, *47*, 6606-6610.
[64] A. V. Protchenko, J. I. Bates, L. M. A. Saleh, M. P. Blake, A. D. Schwarz, E. L. Kolychev, A. L. Thompson, C. Jones, P. Mountford, S. Aldridge, *Journal of the American Chemical Society* **2016**, *138*, 4555-4564.
[65] E. S. Schmidt, A. Jockisch, H. Schmidbaur, *Journal of the American Chemical Society* **1999**, *121*, 9758-9759.
[66] R. J. Baker, R. D. Farley, C. Jones, M. Kloth, D. M. Murphy, *Journal of the Chemical Society, Dalton Transactions* **2002**, 3844-3850.
[67] O. Bonello, C. Jones, A. Stasch, W. D. Woodul, *Organometallics* **2010**, *29*, 4914-4922.
[68] S. P. Green, C. Jones, D. P. Mills, A. Stasch, *Organometallics* **2007**, *26*, 3424-3430.
[69] C. Jones, D. P. Mills, R. P. Rose, A. Stasch, *Dalton Transactions* **2008**, 4395-4408.
[70] S. P. Green, C. Jones, K.-A. Lippert, D. P. Mills, A. Stasch, *Inorganic Chemistry* **2006**, *45*, 7242-7251.
[71] C. Jones, A. Stasch, W. D. Woodul, *Chemical Communications* **2009**, 113-115.
[72] J. Hicks, P. Vasko, J. M. Goicoechea, S. Aldridge, *Nature* **2018**, *557*, 92-95.
[73] J. T. Boronski, L. P. Griffin, C. Conder, A. E. Crumpton, L. L. Wales, S. Aldridge, *Chemical Science* **2024**.
[74] C. McManus, J. Hicks, X. Cui, L. Zhao, G. Frenking, J. M. Goicoechea, S. Aldridge, *Chemical Science* **2021**, *12*, 13458-13468.
[75] R. A. Fischer, J. Behm, *Journal of Organometallic Chemistry* **1991**, *413*, C10-C14.
[76] R. J. Schwamm, M. D. Anker, M. Lein, M. P. Coles, C. M. Fitchett, *Angewandte Chemie International Edition* **2018**, *57*, 5885-5887.
[77] C. Jones, S. Aldridge, T. Gans-Eichler, A. Stasch, *Dalton Transactions* **2006**, 5357-5361.
[78] L. M. Clarkson, K. McCrudden, N. C. Norman, L. J. Farrugia, *Polyhedron* **1990**, *9*, 2533-2547.
[79] I. M. Riddlestone, N. A. Rajabi, S. A. Macgregor, M. F. Mahon, M. K. Whittlesey, *Chemistry – A European Journal* **2018**, *24*, 1732-1738.
[80] M. S. Hill, P. B. Hitchcock, R. Pongtavornpinyo, *Dalton Transactions* **2008**, 2854-2860.
[81] M. D. Anker, Y. Altaf, M. Lein, M. P. Coles, *Dalton Transactions* **2019**, *48*, 16588-16594.
[82] B. N. Anand, I. Krossing, H. Nöth, *Inorganic Chemistry* **1997**, *36*, 1979-1981.
[83] F. Kallmeier, A. J. R. Matthews, G. R. Nelmes, N. R. Lawson, J. Hicks, *Dalton Transactions* **2024**, *53*, 12450-12454.
[84] R. A. Fischer, T. Priermeier, *Organometallics* **1994**, *13*, 4306-4314.
[85] I. M. Riddlestone, J. Urbano, N. Phillips, M. J. Kelly, D. Vidovic, J. I. Bates, R. Taylor, S. Aldridge, *Dalton Transactions* **2013**, *42*, 249-258.
[86] T. Chu, I. Korobkov, G. I. Nikonov, *Journal of the American Chemical Society* **2014**, *136*, 9195-9202.
[87] N. Hara, T. Saito, K. Semba, N. Kuriakose, H. Zheng, S. Sakaki, Y. Nakao, *Journal of the American Chemical Society* **2018**, *140*, 7070-7073.
[88] S. Morisako, S. Watanabe, S. Ikemoto, S. Muratsugu, M. Tada, M. Yamashita, *Angewandte Chemie International Edition* **2019**, *58*, 15031-15035.
[89] B. J. Graziano, M. V. Vollmer, C. C. Lu, *Angewandte Chemie International Edition* **2021**, *60*, 15087-15094.
[90] J. Takaya, N. Iwasawa, *Journal of the American Chemical Society* **2017**, *139*, 6074-6077.
[91] J. Hicks, P. Vasko, J. M. Goicoechea, S. Aldridge, *Angewandte Chemie International Edition* **2021**, *60*, 1702-1713.
[92] R. J. Schwamm, M. D. Anker, M. Lein, M. P. Coles, *Angewandte Chemie International Edition* **2019**, *58*, 1489-1493.
[93] R. J. Schwamm, M. P. Coles, M. S. Hill, M. F. Mahon, C. L. McMullin, N. A. Rajabi, A. S. S. Wilson, *Angewandte Chemie International Edition* **2020**, *59*, 3928-3932.
[94] S. Kurumada, S. Takamori, M. Yamashita, *Nature Chemistry* **2020**, *12*, 36-39.

[95] G. Feng, K. L. Chan, Z. Lin, M. Yamashita, *Journal of the American Chemical Society* **2022**, *144*, 22662-22668.
[96] K. Koshino, R. Kinjo, *Journal of the American Chemical Society* **2020**, *142*, 9057-9062.
[97] C. Yan, R. Kinjo, *Angewandte Chemie International Edition* **2022**, *61*, e202211800.
[98] R. A. Jackson, A. J. R. Matthews, P. Vasko, M. F. Mahon, J. Hicks, D. J. Liptrot, *Chemical Communications* **2023**, *59*, 5277-5280.
[99] S. Grams, J. Mai, J. Langer, S. Harder, *Organometallics* **2022**, *41*, 2862-2867.
[100] D. Sarkar, P. Vasko, A. F. Roper, A. E. Crumpton, M. M. D. Roy, L. P. Griffin, C. Bogle, S. Aldridge, *Journal of the American Chemical Society* **2024**, *146*, 11792-11800.
[101] M. P. Coles, M. J. Evans, *Chemical Communications* **2023**, *59*, 503-519.
[102] M. J. Evans, M. D. Anker, M. G. Gardiner, C. L. McMullin, M. P. Coles, *Inorganic Chemistry* **2021**, *60*, 18423-18431.
[103] J. Hicks, P. Vasko, J. M. Goicoechea, S. Aldridge, *Journal of the American Chemical Society* **2019**, *141*, 11000-11003.
[104] T. X. Gentner, M. J. Evans, A. R. Kennedy, S. E. Neale, C. L. McMullin, M. P. Coles, R. E. Mulvey, *Chemical Communications* **2022**, *58*, 1390-1393.
[105] G. M. Ballmann, M. J. Evans, T. X. Gentner, A. R. Kennedy, J. R. Fulton, M. P. Coles, R. E. Mulvey, *Inorganic Chemistry* **2022**, *61*, 19838-19846.
[106] J. T. Boronski, L. R. Thomas-Hargreaves, M. A. Ellwanger, A. E. Crumpton, J. Hicks, D. F. Bekiş, S. Aldridge, M. R. Buchner, *Journal of the American Chemical Society* **2023**, *145*, 4408-4413.
[107] M. J. Evans, G. H. Iliffe, S. E. Neale, C. L. McMullin, J. R. Fulton, M. D. Anker, M. P. Coles, *Chemical Communications* **2022**, *58*, 10091-10094.
[108] K. Sugita, M. Yamashita, *Chemistry – A European Journal* **2020**, *26*, 4520-4523.
[109] P. Zatsepin, T. Moriyama, C. Chen, S. Muratsugu, M. Tada, M. Yamashita, *Journal of the American Chemical Society* **2024**, *146*, 3492-3497.
[110] C. Yan, K. Koshino, L. Zhu, R. Kinjo, *Nature Synthesis* **2024**, *3*, 858-866.
[111] S. Sakaki, T. Kikuno, *Inorganic Chemistry* **1997**, *36*, 226-229.
[112] J. Hicks, A. Mansikkamäki, P. Vasko, J. M. Goicoechea, S. Aldridge, *Nature Chemistry* **2019**, *11*, 237-241.
[113] A. S. K. Hashmi, *Chem. Rev.* **2007**, *107*, 3180-3211.
[114] C. McManus, A. E. Crumpton, S. Aldridge, *Chemical Communications* **2022**, *58*, 8274-8277.
[115] H.-Y. Liu, R. J. Schwamm, M. S. Hill, M. F. Mahon, C. L. McMullin, N. A. Rajabi, *Angewandte Chemie International Edition* **2021**, *60*, 14390-14393.
[116] M. M. D. Roy, J. Hicks, P. Vasko, A. Heilmann, A.-M. Baston, J. M. Goicoechea, S. Aldridge, *Angewandte Chemie International Edition* **2021**, *60*, 22301-22306.
[117] G. Feng, K. L. Chan, Z. Lin, M. Yamashita, *Journal of the American Chemical Society* **2024**, *146*, 7204-7209.

Synthesis and reactivity of a zinc-boryl complex

Introduction

Given that interest in group ligands has primarily arisen due to the widespread and highly impactful utility of boryl ligands, and that our understanding of group 13 ligands in general draws on analogies with the lightest congener, it is useful to synthesise boryl analogues of existing any heavy trielyl-metal complexes. This enables us to better understand the similarities and differences between these ligands for E = B, Al, Ga, In and Tl, as well as identify design principles that may aid the development of metallo-ligands with more desirable properties.

In this chapter, a zinc boryl species was targeted, in order to facilitate comparison between itself and the previously reported zinc aluminyl species (Nacnac^{Mes})ZnAl(NON). In practice, installation of a boryl ligand is non-trivial, and salt metathesis methods utilizing the boryl lithium reagent Li(THF)$_2$[B{(NDippCH)$_2$}] were unsuitable due to formation of the corresponding bis-boryl zinc species and Li(Nacnac^{Mes}) . Alternative methods of zinc borylation were therefore considered, with diborane-4 disproportionation via B-O bond formation yielding the desired result in the form of the isolable zinc complex (Nacnac^{Mes})ZnBpin. This species was structurally and spectroscopically characterised as its DMAP adduct, and reactivity studies with CO_2 were carried out to compare the outcomes of such reactions with those observed for (Nacnac^{Mes})ZnAl(NON), *i.e.* CO_2 insertion via nucleophilic attack by zinc. A different outcome was observed for the boryl analogue, which may be due to differing steric effects of the supporting ligand frameworks. Close inspection of *in situ* spectroscopic data revealed that a reductive side reaction was also at play, which was subsequently exploited to yield overall conversion of two equivalents of (Nacnac^{Mes})ZnI to the zinc(I) species [(Nacnac^{Mes})Zn]$_2$ under mild conditions which utilized B_2pin_2 as the overall reductant.

Zinc borylation and reduction by a diborane(4) species via B-O bond formation

Liam P. Griffin,[a] Simon Aldridge*[a]

[a] Mr. L. P. Griffin, S. Aldridge
Inorganic Chemistry Laboratory, Department of Chemistry
University of Oxford
South Parks Road, Oxford, OX1 3QR (UK)
E-mail: simon.aldridge@chem.ox.ac.uk

Abstract

We report a convenient synthesis of the zinc-boryl complex (Nacnac^{Mes})ZnBpin under mild conditions via formal disproportionation of bis(pinacolato)diboron(4), aided thermodynamically by B–O bond formation. This species can be isolated both base-free and as the DMAP adduct (Nacnac^{Mes})Zn(DMAP)Bpin and crystallographically characterised in the latter form. Onward reactivity of the base free zinc boryl complex with CO_2 occurs reductively, yielding further B–O bonds as well as CO gas. The strength of this driving force can then be harnessed in the reaction between (Nacnac^{Mes})ZnBpin and a Zn–O bonded species (Nacnac^{Mes})ZnOB{(NDippCH)$_2$}, which yields the metal-metal bonded dimer [(Nacnac^{Mes})Zn]$_2$, the overall formation of which utilizes a diboron(4) species as the stoichiometric reductant of Zn(II) to Zn(I).

Introduction

The boryl functional group, BX_2, is an important motif in organic chemistry, enabling powerful and wide-ranging reactivity, for example in cross-coupling chemistry, leading to the formation of C–C and C–X bonds.[1] Of considerable additional value is the fact that unactivated C–H bonds at both aromatic and aliphatic carbon centres can be borylated, often catalytically, allowing for the introduction of molecular complexity at otherwise hard to activate positions.[2,3] Such catalytic processes typically proceed via metal-boryl complexes generated *in situ*, and in a number of cases the competence of such species as catalytic intermediates has been explicitly demonstrated.[2,4]

Beyond organic synthesis, the boryl anion, $[BX_2]^-$ is also of significant interest in its own right. Featuring a formally anionic B(I) centre, these systems act as X-type ligands, and exert a marked influence on the electronic structure and reactivity of the metal centre to which they are bound, based on their strongly σ-donating and *trans*-labilising properties.[5] Installation of such ligands is typically achieved by oxidative addition of B–H or B–B bonds at low-valent metal centres,[6] or by salt metathesis, for example using an isolable boryl anion equivalent, and being facilitated by the landmark synthesis of $(THF)_2Li\{B(NDippCH)_2\}$ (**I**) by Yamashita, Nozaki *et al.* in 2006.[7-11] While the latter approach has been widely utilized in the synthesis of metal boryl complexes from across the Periodic Table, these anions typically require harsh alkali metal reductants, are challenging to store and handle, and (in the case of metathesis at redox-active metals) can lead to side-reactions caused by their strongly reducing nature.[12] For main group systems, installation of a boryl ligand by oxidative addition is also not trivial, as access to low-valent metal precursors is generally less facile than for their transition metal counterparts.

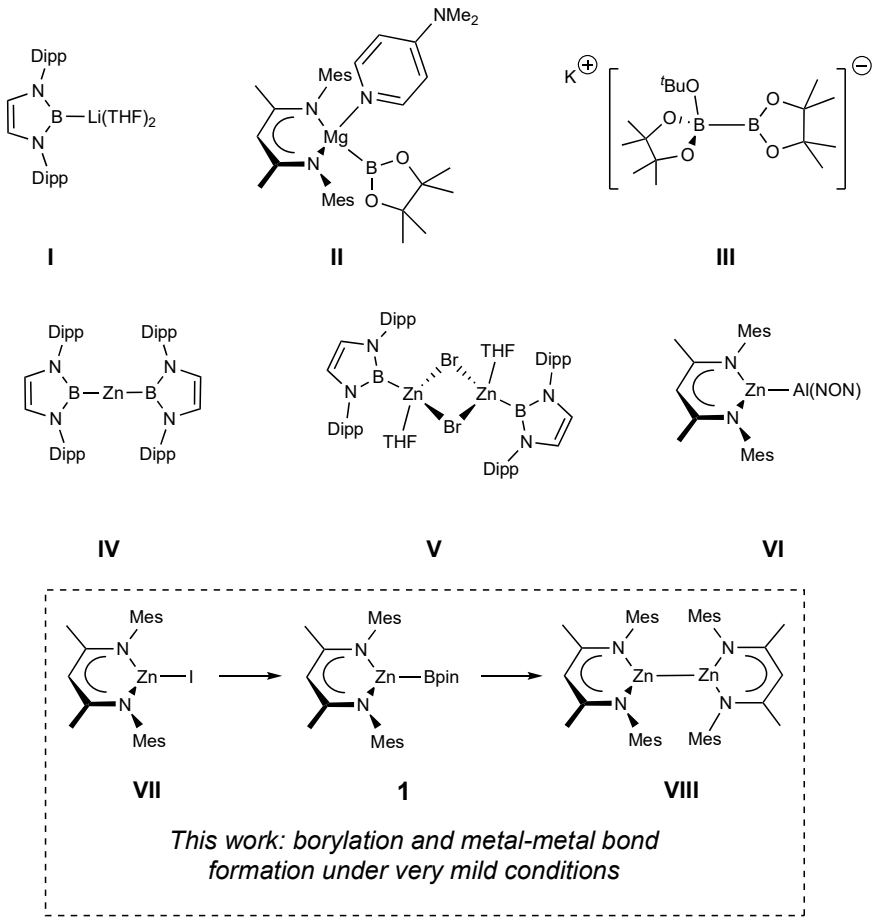

Figure 1; Boryl and related compounds of relevance to the current study.

In seminal work, Hill *et al.* demonstrated that a DMAP-stabilized magnesium boryl reagent (**II**) could be synthesised by the formal disproportionation of bis(pinacolato)diboron(4), via a reaction with an alkylmagnesium reagent.[13] More broadly, borylation reactions relying on sp^2-sp^3 diborane reagents have found widespread application in organic chemistry, with species such as K[^{t}BuOB$_2$pin$_2$] (**III**) allowing the gentle introduction of a (nucleophilic) pinacolato boryl fragment at a carbon electrophile, driven thermodynamically by B–O bond formation and the lattice enthalpy of the potassium halide salt.[14]

This report prompted us to investigate whether the introduction of a boryl fragment via diborane(4) disproportionation could be accomplished at other main group metals, and whether simple metal halides could serve as alternative precursors, rather than the metal alkyl species used in Hill's studies.

In these endeavours we targeted a β-diketiminate (Nacnac) supported zinc boryl complex (**1**), since such species are relatively rare in the literature (see Figure 1 for representative examples of zinc boryl complexes, **IV**/**V**), and well-characterized examples would permit direct comparison with established magnesium boryl chemistry, and also with heavier zinc aluminyl species (e.g. **VI**). Additionally, we reasoned that the installation of a Zn–B linkage might provide a platform for convenient access to low oxidation state zinc complexes bearing homometallic bonds through the extrusion of B–O bonds in reactions between Zn–B and Zn–OR precursors. Such species (e.g. **VIII**), originating with Carmona's seminal report of decamethyldizincocene, Cp*ZnZnCp*, offer useful insights into fundamental questions of structure and bonding, with multiple examples now known for zinc and also magnesium and (most recently) beryllium.[15-17] Typically, such species are accessed through the use of (very strong) alkali metal reductants, which are often unpredictable and technically challenging. Overall reductive processes in which a more stable, commercially available reductant could be used (e.g. the diboron(4) species B_2pin_2) could open up a range of 'soft' metal-metal bond forming reactions, driven by B–O bond formation. Accordingly, we also report that the combination of zinc boryl and zinc boryloxy complexes leads to elimination of a B–O–B moiety and Zn–Zn bond formation; the preceding formation of both zinc compounds from the same (Nacnac)ZnI precursor (**VII**), then offers an overall route to Zn(I) from Zn(II) using a diboron(4) reagent as the net reductant.[4,18-22]

Results as Discussion

(i) Syntheses of zinc boryl complexes from B_2pin_2

In targeting a complex of type **1**, the reactions of $(THF)_2Li\{B(NDippCH)_2\}$ (**I**) with Nacnac-ligated zinc halides were initially trialled, but these yielded the previously reported zinc bis(boryl) species $Zn\{B(NDippCH)_2\}_2$ (**IV**) and the lithiated Nacnac ligand, presumably due to the thermodynamic stability of the homoleptic product.[4] As such, 'soft' introduction of the boryl ligand by diborane disproportionation was examined instead. Pre-mixing KO^{t}Bu and B_2pin_2 in benzene, followed by heating to 80 °C for 1 h, with occasional sonication yielded a homogeneous suspension. Subsequent addition of the zinc iodide precursor (Nacnac^{Mes})ZnI (**VII**),[24] and heating to 80 °C for 16 h leads to clean and complete conversion of the zinc starting material to one new solution-phase species, as well as one equivalent of ^{t}BuOBpin (as identified by ^{1}H and ^{11}B NMR spectroscopy).[24] The new species gives rise to a relatively broad low-field ^{11}B NMR resonance at 38.7 ppm, which remains unchanged between ^{1}H coupled and decoupled spectra. The ^{1}H NMR spectrum is consistent with a 1:1 ratio of pinacolate and Nacnac signals, as well as a symmetrical environment for both fragments, suggesting the formation of zinc boryl complex **1** (Scheme 1). **1** is both highly soluble and highly sensitive, and single crystals suitable for X-ray crystallographic analysis could not be obtained in our hands. Spectroscopic data are, however, consistent with its characterisation as (Nacnac^{Mes})ZnBpin, and *in situ* generated solutions (which are stable for several days in a rigorously air- and moisture-free environment, even at temperatures up to 80 °C) were used for onward reactivity, as discussed below. Interestingly, no reaction was observed under equivalent conditions with the bulkier Dipp-substituted β-diketiminate zinc iodide precursor, (Nacnac^{Dipp})ZnI, presumably on steric grounds.

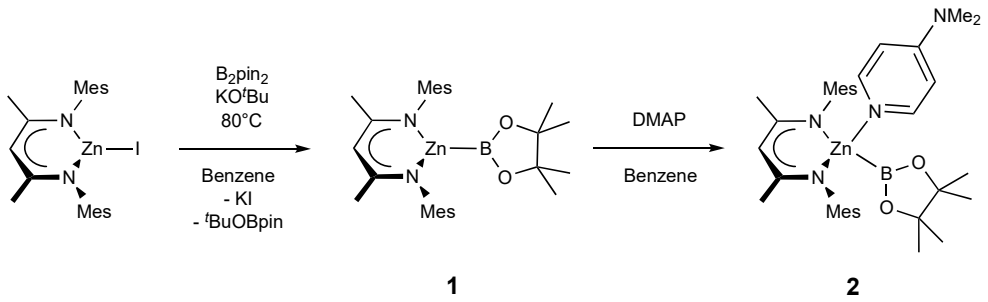

1 **2**

*Scheme 1; Synthesis of base-free zinc-boryl species (Nacnac^{Mes})ZnBpin (**1**), and subsequent DMAP coordination.*

Addition of the strong donor *N*,*N*-dimethylaminopyridine (DMAP) to an *in situ* generated solution of (Nacnac^{Mes})ZnBpin (**1**) leads to the formation of a new species as shown by ^{1}H NMR monitoring, which features a 1:1:1 ratio of Nacnac, DMAP and pinacolate resonances, as well as a further downfield shifted (broad) ^{11}B NMR resonance at 41.3 ppm (Scheme 1). This adduct (**2**) is highly crystalline, and single colourless needles could be obtained from hexane. Crystallographic studies show that the pinacolato-boryl fragment had indeed been installed at the zinc centre under relatively mild conditions via diborane disproportionation. However, relative to base-free **1**, DMAP complex (Nacnac^{Mes})Zn(DMAP)Bpin (**2**) is thermally labile, showing significant decomposition after only a few hours at 80 °C.

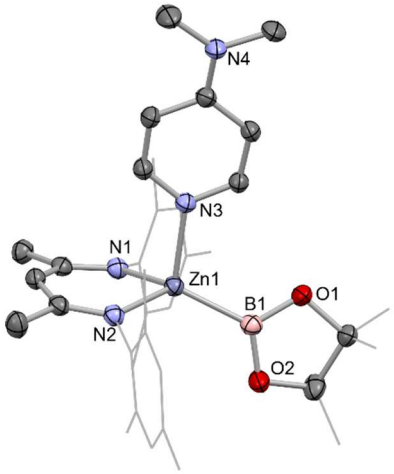

Figure 2; Molecular structure of (Nacnac^{Mes})Zn(DMAP)Bpin, as determined by single crystal X-ray crystallography. Hydrogen atoms omitted and some residues displayed as wireframe for clarity. Two crystallographically independent molecules are present in the asymmetric unit, with only one discussed here due to high similarity between the geometrical parameters Key bond lengths (Å) and bond angles (°): Zn1–B1 2.085(2) Zn1–N1 2.028(1), Zn1–N2 1.025(1), Zn1–N3 2.119(1), B1–Zn1–N3 118.1(7), N1–Zn1–N2 93.86(6).

The asymmetric unit of **2** features two crystallographically independent molecules; the geometric parameters for each are very similar and only one is discussed here. The Zn–B bond length (2.085(2) Å) is the longest example featuring a 4-coordinate zinc centre (range: 2.062(2)-2.079(2) Å), with the remaining 2-coordinate species spanning a wider range which encompasses that of **2** (2.052(3)–2.139(2) Å).[4,18-21] It can also be put into context by comparison with the sum of the respective covalent radii (2.06 Å).[25] The zinc centre adopts a distorted tetrahedral geometry, closely resembling that of magnesium analogue **II**;[13] the Mg–B bond length (while significantly longer) is also in excess of the sum of respective covalent radii (2.324(2), *cf.* 2.26 Å). The most significant structural difference is in the angle between the Bpin and DMAP ligands (∠B1–Zn1–N3 = 111.81(7); ∠B1–Mg1–N3 = 104.50(7) °), likely due to increased steric repulsion at the smaller metal centre.

*(ii) Onward reactivity of zinc boryl complexes **1** and **2** proceeding via B–O bond formation*

Zinc boryl complexes have previously been shown to act as sources of the boryl fragment in (Pd-catalysed) C–B bond forming reactions,[4] and (simplistically) we expected both **1** and **2** to evidence nucleophilic reactivity at the boryl centre based on the relative electronegativities of Zn (1.65) and B (2.04).[26] In both cases, this can be confirmed experimentally by reactivity studies using MeI as a simple electrophilic probe. These yield the known species pinacolato(methyl)borane, and either the zinc iodide starting material (Nacnac^{Mes})ZnI (**VII**) or its DMAP adduct (Nacnac^{Mes})Zn(DMAP)I (**3**), which has been characterised crystallographically (Fig S1). These results further support our characterisation of (Nacnac^{Mes})ZnBpin.[13,27] We additionally wished to compare the reactivity of **1** with its heavier analogue Nacnac^{Mes}ZnAl(NON) (**VI**). **VI** inserts CO_2 into the metal-metal bond to yield the zinc-carbene complex Nacnac^{Mes}ZnCO_2Al(NON), featuring Zn–C and Al–O bonds, in line with the high oxophilicity of aluminium and the extremely strong electron donating properties of the aluminyl fragment.[22] Exposure of a solution of **1** to an atmosphere of CO_2 gas yielded no reaction at room temperature. However, at higher temperatures, conversion to a new species could be seen to occur slowly. Crystallographic analysis reveals that this product is the dimeric boryloxy species [(Nacnac^{Mes})ZnOBpin]$_2$ (**4**), in which each of the assimilated oxygen atoms bridges two zinc and one boron centres. Overall, one molecule of CO_2 has been reduced to CO per zinc boryl unit. This difference in reactivity between boron and aluminium is likely, at least in part, steric in nature, with dimerization presumably facilitated by the small size of the pinacolato boryloxy fragment.[28-30]

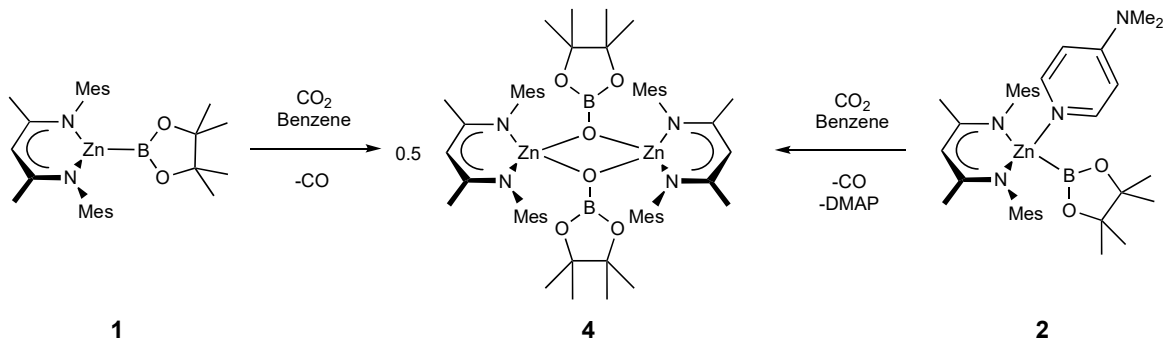

1 **4** **2**

*Scheme 2; Reaction of **1** with CO_2 to yield dimeric boryloxy complex **4**.*

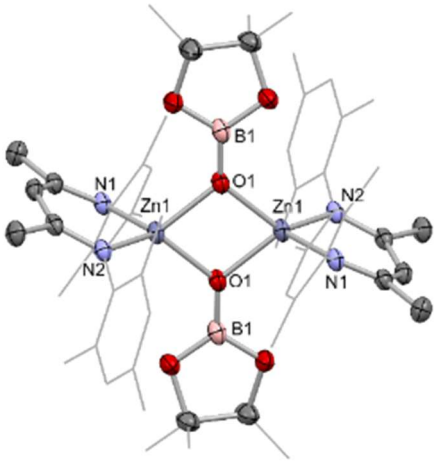

*Figure 3; Molecular structure of **4**, as determined by single crystal X-ray crystallography. Hydrogen atoms omitted and some residues displayed as wireframe for clarity. Key bond lengths (Å) and bond angles (°): Zn1–O1 1.963(1), Zn1–O1' 2.012(1), Zn1–N1 1.966(1), Zn1–N2 1.972(1), B1–O1 1.331(2), B1–O2 1.401(8), B2–O3 1.36(1), O1–Zn1–O1' 80.78(4), N1–Zn1–N1 97.70(5).*

Given the well-known thermodynamic driver associated with the formation of B–O bonds,[31] we hypothesised that under suitable reaction conditions species **1** might react with a zinc–alkoxide/boryloxide such as **4** to extrude (in this case) $O(Bpin)_2$ and yield the metal-metal bonded Zn(I) species $[(Nacnac^{Mes})Zn]_2$ (**VIII**). Intriguingly, close inspection of the ^1H NMR spectra obtained *in situ* for the reaction between **1** and CO_2 reveals that **VIII** is formed in trace quantities. We postulate that it results from a side reaction between as-yet-unreacted zinc boryl complex **1** and the boryloxy product **4** under the relatively harsh reaction conditions employed.[32]

Reasoning that this metal-metal bond forming reaction might proceed more cleanly in the case of a *monomeric* zinc boryloxy species, a complex of this type was targeted, utilizing the bulky N-heterocyclic boryloxy ligand $\{(HCDippN)_2\}BO–$.[33] Accordingly, the reaction of the protio-ligand $\{(HCDippN)_2\}BOH$ with $(Nacnac^{Mes})ZnMe$ cleanly generates the target complex with concomitant release of methane gas.[34] $(Nacnac^{Mes})ZnOB\{(NDippCH)_2\}$ (**5**) has been characterised by multinuclear NMR and by X-ray crystallography, with the latter revealing a monomeric state of aggregation in the solid state. NMR-scale reactions between zinc iodide complex **VII** and the potassiated boryloxy ligand $KOB\{(NDippCH)_2\}$ lead to identical product spectra.

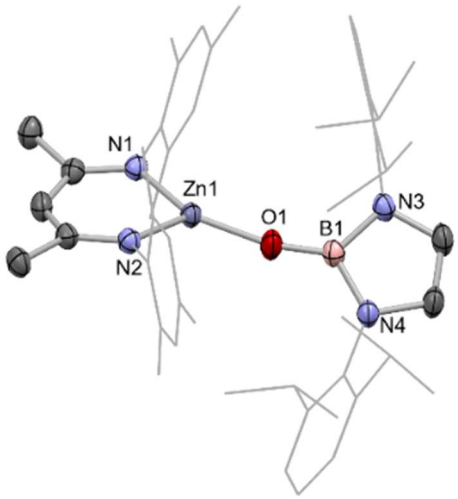

*Figure 4; Molecular structure of **5**, as determined by X-ray crystallography. Hydrogen atoms omitted and some residues displayed as wireframe for clarity. Key bond lengths (Å) and bond angles (°): Zn1–N1 1.930(1), Zn1–N2 1.942(1), Zn1–O1 1.790(1), B1–O1 1.322(2), B1–N3 1.454(2), B1–N4 1.452(2), N1–Zn1–N2 100.40(5), N1–Zn1–O1 139.57(5), N2–Zn1–O1 119.60(5), Zn1–O1–B1 164.6(1).*

With **5** in hand, we examined its reaction with **1**, which (at 80 °C) can be shown by *in situ* NMR monitoring to yield [(Nacnac^{Mes})Zn]$_2$ (**VIII**) as the major Nacnac-containing species, together with the by-product {(HCDippN)$_2$}BOBpin (**6**), which was characterised spectroscopically. Further confirmation of the identity of the dizinc product was provided by crystallographic analysis (see ESI).

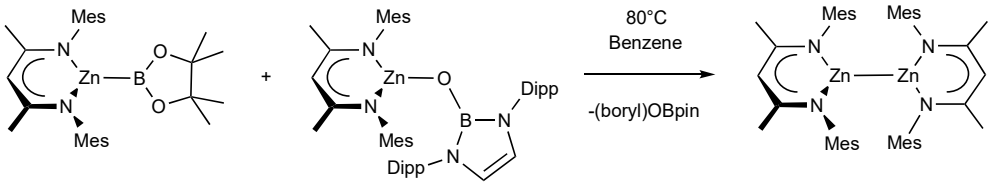

*Scheme 3; Synthesis of [(Nacnac^{Mes})Zn]$_2$ (**VII**) via metathesis, driven thermodynamically by B-O bond formation.*

Overall, this reaction represents a reduction by bis(pinacolato)diboron(4) of two Zn(II) centres to two Zn(I) centres in two mild steps which avoid the use of harsh alkali metal reductants. The driving force for each step is the formation of strong B–O bonds. Calculated Gibbs energies indicate that this metal-metal bond forming step is exergonic to the tune of 31.3 kcal mol^{-1}. We were further interested to see whether B–O bond formation alone is sufficient to drive the whole process, and equivalent

calculations were carried out on the reaction between bis(pinacolato)diboron(4) and two equivalents of (Nacnac^{Mes})ZnOB{(NDippCH)$_2$} (**5**) to yield [(Nacnac^{Mes})Zn]$_2$ (**VII**) and {(HCDippN)$_2$}BOBpin (**6**). These indicate that this process is in principle even more strongly favourable (-41.8 kcal mol^{-1}), likely due to the formation of two B–O linkages in a single step. However, experimentally no reaction was observed even at 80 °C, implying that initial installation of the zinc–boryl linkage from **5** and B_2pin_2 alone is not kinetically facile.

Conclusions

In conclusion, we have demonstrated that by exploiting the formation of strong B–O single bonds, a zinc boryl species can be synthesized under mild conditions, and its onward reduction to Zn(I) can also be promoted using the same driving forces, circumventing the need for alkali metal reductants and instead favouring convenient diboron(4) reagents. In more general terms, this reduction chemistry offers analogies between diboron(4) species and more recently developed Mg–Mg bonded Mg(I) species, in that both can act as mild molecular reductants, albeit with the difference that Mg–Hal versus B–O bond-based driving forces mean that their substrate scopes differ significantly (and complementarily).[16] Work is currently ongoing in our laboratory to extend this chemistry towards the synthesis of new heterobimetallic bonds featuring zinc using B–O bond formation as a thermodynamic driving force.

Acknowledgements

We thank the EPSRC Centre for Doctoral Training in Inorganic Chemistry for Future Manufacturing (OxICFM; EP/023828/1; studentship to LPG), Drs J Boronski, M. Dietz and A. Crumpton for helpful discussions and the Oxford ARC for computational resources.

References

[1] N. Miyaura, K. Yamada, A. Suzuki, *Tet. Lett.* **1979**, *20*, 3437-3440.

[2] I. A. I. Mkhalid, J. H. Barnard, T. B. Marder, J. M. Murphy, J. F. Hartwig, *Chem. Rev.* **2010**, *110*, 890-931.

[3] I. F. Yu, J. W. Wilson, J. F. Hartwig, *Chem. Rev.* **2023**, *123*, 11619-11663.

[4] J. Campos, S. Aldridge, *Angew. Chem. Int. Ed.* **2015**, *54*, 14159-14163.

[5] G. J. Irvine, M. J. G. Lesley, T. B. Marder, N. C. Norman, C. R. Rice, E. G. Robins, W. R. Roper, G. R. Whittell, L. J. Wright, *Chem. Rev.* **1998**, *98*, 2685-2722.

[6] J. F. Hartwig, K. S. Cook, M. Hapke, C. D. Incarvito, Y. Fan, C. E. Webster, M. B. Hall, *J. Am. Chem. Soc.* **2005**, *127*, 2538-2552.

[7] A. V. Protchenko, D. Dange, A. D. Schwarz, C. Y. Tang, N. Phillips, P. Mountford, C. Jones, S. Aldridge, *Chem. Commun.* **2014**, *50*, 3841-3844.

[8] L. M. A. Saleh, K. H. Birjkumar, A. V. Protchenko, A. D. Schwarz, S. Aldridge, C. Jones, N. Kaltsoyannis, P. Mountford, *J. Am. Chem. Soc.* **2011**, *133*, 3836-3839.

[9] E. C. Neeve, S. J. Geier, I. A. I. Mkhalid, S. A. Westcott, T. B. Marder, *Chem. Rev.* **2016**, *116*, 9091-9161.

[10] Y. Segawa, Y. Suzuki, M. Yamashita, K. Nozaki, *J. Am. Chem. Soc.* **2008**, *130*, 16069-16079.

[11] Y. Segawa, M. Yamashita, K. Nozaki, *Science* **2006**, *314*, 113-115.

[12] R. Frank, J. Howell, R. Tirfoin, D. Dange, C. Jones, D. M. P Mingos, S. Aldridge, *J. Am. Chem. Soc.* **2015**, *136*, 15730-15741.

[13] A.-F. Pécharman, A. L. Colebatch, M. S. Hill, C. L. McMullin, M. F. Mahon, C. Weetman, *Nature Commun.* **2017**, *8*, 15022.

[14] R. D. Dewhurst, E. C. Neeve, H. Braunschweig, T. B. Marder, *Chem. Commun.* **2015**, *51*, 9594-9607.

[15] I. Resa, E. Carmona, E. Gutierrez-Puebla, A. Monge, *Science* **2004**, *305*, 1136-1138.

[16] S. P. Green, C. Jones, A. Stasch, *Science* **2007**, *318*, 1754-1757.

[17] J. T. Boronski, A. E. Crumpton, L. L. Wales, S. Aldridge, *Science* **2023**, *380*, 1147-1149.

[18] S.-S. Asami, M. Okamoto, K. Suzuki, M. Yamashita, *Angew. Chem. Int. Ed.* **2016**, *55*, 12827-12831.

[19] N. A. Phillips, R. Y. Kong, A. J. P. White, M. R. Crimmin, *Angew. Chem. Int. Ed.* **2021**, *60*, 12013-12019.

[20] T. Kajiwara, T. Terabayashi, M. Yamashita, K. Nozaki, *Angew. Chem. Int. Ed.* **2008**, *47*, 6606-6610.

[21] W. Lu, H. Hu, Y. Li, R. Ganguly, R. Kinjo, *J. Am. Chem. Soc.* **2016**, *138*, 6650-6661.

[22] M. M. D. Roy, J. Hicks, P. Vasko, A. Heilmann, A.-M. Baston, J. M. Goicoechea, S. Aldridge, *Angew. Chem. Int. Ed.* **2021**, *60*, 22301-22306.

[23] S. Schulz, T. Eisenmann, U. Westphal, S. Schmidt, U. Flörke, *Z. Anorg. Allg. Chem.* **2009**, *635*, 216-220.

[24] J. Bykowski, J. Sinclair, J. Trach, M. J. Ferguson, E. Rivard, *Dalton Trans.* **2023**, *52*, 1602-1607.

[25] B. Cordero, V. Gómez, A. E. Platero-Prats, M. Revés, J. Echeverría, E. Cremades, F. Barragán, S. Alvarez, *Dalton Trans.* **2008**, 2832-2838.

[26] L. Pauling, *J. Am. Chem. Soc.* **1932**, *54*, 3570-3582.

[27] A. Bismuto, S. P. Thomas, M. J. Cowley, *Angew. Chem. Int. Ed.* **2016**, *55*, 15356-15359.

[28] D. D. L. Jones, A. J. R. Matthews, C. Jones, *Dalton Trans.* **2019**, *48*, 5785-5792.

[29] J. Li, M. Luo, X. Sheng, H. Hua, W. Yao, S. A. Pullarkat, L. Xu, M. Ma, *Org. Chem. Front.* **2018**, *5*, 3538-3547.

[30] Y. Yang, M. D. Anker, J. Fang, M. F. Mahon, L. Maron, C. Weetman, M. S. Hill, *Chem. Sci.* **2017**, *8*, 3529-3537.

[31] A. J. Downs, H.-J. Himmel in *The Chemistry of the Group 13 Metals Aluminium, Gallium, Indium and Thallium: Chemical Patterns and Peculiarities* (Eds. S. Aldridge, A. J. Downs), Wiley, Chichester, **2011**, pp 1-74.

[32] S. Schulz, D. Schuchmann, U. Westphal, M. Bolte, *Organometallics* **2009**, *28*, 1590-1592.

[33] Y. K. Loh, L. Ying, M. Ángeles Fuentes, D. C. H. Do, S. Aldridge, *Angew. Chem. Int. Ed.* **2019**, *58*, 4847-4851.

[34] J. Prust, A. Stasch, W. Zheng, H. W. Roesky, E. Alexopoulos, I. Usón, D. Böhler, T. Schuchardt, *Organometallics* **2001**, *20*, 3825-3828.

Supporting information

General considerations

All manipulations were carried out using standard Schlenk line or dry-box techniques under an atmosphere of argon or dinitrogen. Solvents were degassed by sparging with argon and dried by passing through a column of the appropriate drying agent. Toluene and hexane were purified using an MBraun SPS-800 and stored over a potassium mirror. THF and Et_2O were purified using an MBraun SPS-800 and stored over activated molecular sieves. NMR spectra were measured in benzene-d_6 (which was dried over potassium, with the solvent then being distilled under reduced pressure), or THF-d_8 (dried by storing over activated molecular sieves and degassed by three freeze pump thaw cycles) and stored under argon in Teflon valve ampoules. NMR samples were prepared under argon in 5 mm Wilmad 507-PP tubes fitted with J. Young Teflon valves. ^{1}H, ^{13}C{^{1}H}, ^{31}P and ^{11}B NMR spectra were recorded on Bruker Avance III HD nanobay 400 MHz or Bruker Avance III 500 MHz spectrometer at ambient temperature and referenced internally to residual protio-solvent (^{1}H) or solvent (^{13}C) resonances and are reported relative to tetramethylsilane or Et_2OBF_3 (δ = 0 ppm. Assignments were confirmed using two-dimensional ^{1}H-^{1}H and ^{13}C-^{1}H NMR correlation experiments. Chemical shifts are quoted in (ppm) and coupling constants in Hz. Elemental analyses were carried out by London Metropolitan University. B_2pin_2, HOBpin, DMAP, CO_2 and KO^{t}Bu were used as received. MeI was degassed and stored over molecular sieves. (Nacnac^{Mes})ZnI,[s1] (Nacnac^{Mes})ZnMe,[s2] {(HCDippN)$_2$}BOH[s3] were prepared according to literature procedures.

X-ray crystallographic details

Single-crystal X-ray diffraction data for compounds (Nacnac^{Mes})Zn(DMAP)Bpin, (Nacnac^{Mes})Zn(DMAP)I, [(Nacnac^{Mes})ZnOBpin]$_2$, (Nacnac^{Mes})ZnOB{(NDippCH)$_2$} and [(Nacnac^{Mes})Zn]$_2$ were collected on an Oxford Diffraction/Agilent SuperNova diffractometer equipped with a 135 mm Atlas CCD area detector or a Rigaku XtaLAB Synergy-DW VHF equip with a PhotonJet-R dual wavelength rotating anode and HyPix-Arc 150° detector. Crystals were selected under Paratone-N oil, mounted on MiTeGen Micromount loops and quench-cooled using an Oxford Cryosystems open flow N2 cooling device.[s4] Data were collected at 150 K using mirror monochromated Cu Kα radiation (λ = 1.5418 Å; Oxford Diffraction Supernova) or Mo Kα radiation (λ = 0.71073 Å; Oxford Diffraction Supernova). Data collected were processed using the CrysAlisPro package, including unit cell parameter refinement and inter-frame scaling (which was carried out using SCALE3 ABSPACK within CrysAlisPro).[s5] Equivalent reflections were merged and diffraction patterns processed with the CrysAlisPro suite.[s5] Structures were solved ab initio from the integrated intensities using SHELXT[s6] and refined on F2 using SHELXL[s7] with the graphical interface OLEX2.[s8] Selected crystallographic data are summarised in Table s1.

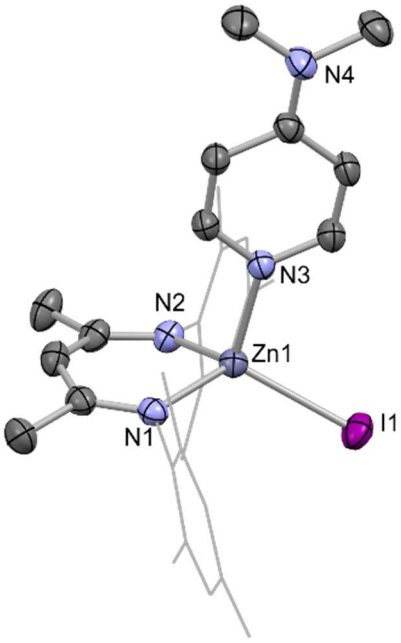

Fig S1. *Molecular structure of (Nacnac^{Mes})Zn(DMAP)I, as determined by single crystal X-ray crystallography. Hydrogen atoms omitted and some residues displayed as wireframe for clarity. Key bond lengths (Å) and bond angles (°): Zn1-N1 2.000(2), Zn1-N2 1.989(2), Zn1-N3 2.047(2), Zn1-I1 2.5572(5), N1-Zn1-N1 96.88(7), N3-Zn1-I1 106.46(5).*

	(Nacnac^{Mes})Zn(DMAP)Bpin	**(Nacnac^{Mes})Zn(DMAP)I**	**[(Nacnac^{Mes})ZnOBpin]$_2$**	**(Nacnac^{Mes})ZnOB{(NDippCH)$_2$}**	**[(Nacnac^{Mes})Zn]$_2$**
Formula	$C_{36}H_{51}BN_4O_2Zn$	$C_{30}H_{39}IN_4Zn(C_6H_{14})$	$C_{58}H_{82}B_2N_4O_6Zn_2$	$C_{49}H_{65}BN_4OZn$	$C_{46}H_{58}N_4Zn_2$
Fw (g mol^{-1})	647.98	734.09	1083.63	802.23	797.70
Crystal system	Monoclinic	Monoclinic	Monoclinic	Monoclinic	Orthorhombic
Space group	P 1 2_1/c 1	P 1 2_1/n 1	P 1 2_1/n 1	P 1 2_1/c 1	P b c a
a (Å)	13.88904(6)	8.60930(10)	14.94854(6)	16.1404(2)	21.7767(2)
b (Å)	26.07802(12)	29.1368(3)	11.80920(5)	15.15920(10)	10.91670(10)
c (Å)	2016258(9)	14.2475(2)	16.28848(6)	19.0592(2)	36.1028(4)
α (°)	90	90	90	90	90
β (°)	92.9187(4)	91.3760(10)	91.3130(4)	101.4280(10)	90
γ (°)	90	90	90	90	90
V (Å^{-3})	7293.39(5)	3572.92(7)	2874.654(19)	4570.87(8)	8582.71(15)
Z	8	4	2	4	8
ρ_{calc} (g cm^{-3})	1.180	1.365	1.252	1.166	1.235
Radiation, λ (Å)	1.54184	1.54184	1.54184	1.54184	1.54184
Absorption	Multi-scan	Multi-scan	Multi-scan	Multi-scan	Multi-scan
μ (mm^{-1})	1.196	7.943	1.423	1.030	1.626
Reflections collected	325188	79811	100530	103585	130609
Independent reflections	15080	7460	5915	9545	8834
$R_{(int)}$	0.0730	0.0466	0.0397	0.0488	0.0747
Parameters	821	335	414	542	485
R_1 (all data/I>2σ(I))	0.0386	0.0250	0.0316	0.0319	0.0803
ωR_2 (all data/I >2σ(I))	0.1124	0.0622	0.0864	0.0921	0.1829
GooF	1.079	1.039	1.095	1.033	1.162
T (K)	100.00(10)	149.98(16)	100.00(10)	149.98(11)	100.00(10)

Table s1: X-ray crystallographic details

Synthesis of novel compounds

(Nacnac^{Mes})ZnBpin

To an NMR tube fitted with a J-Youngs valve was added KO^{t}Bu (0.004 g, 0.04 mmol) and B_2pin_2 (0.01 g, 0.04 mmol) and C_6D_6 (0.5 ml). The suspension was heated to 80 °C for 1 h with occasional ultrasonication to yield a homogeneous mixture. To this was added (Nacnac^{Mes})ZnI (0.02 g, 0.038 mmol) before further heating at 80 °C for 12 h. The resulting solution was filtered to remove precipitated KI and the product was characterised by multinuclear NMR spectroscopy. This indicated quantitative conversion. Also present were signals corresponding to the by-product ^{t}BuOBpin.[s9]

(Nacnac^{Mes})ZnBpin

^{1}H NMR (500 MHz, benzene-d_6, 298 K): δ_H 1.02 (12 H, s, {OC(C*H*$_3$)$_2$}$_2$), 1.64 (6 H, s, Nacnac-C*H*$_3$), 2.17 (6 H, s, *p*-C*H*$_3$), 2.20 (12 H, s, *o*-C*H*$_3$), 4.99 (1 H, s, C*H*), 6.82 (4 H, s, Ar-*H*) ppm.

^{13}C{^{1}H} NMR (101 MHz, benzene-d_6): δ_C 19.0 (*o*-*C*H$_3$), 21.0 (*p*-*C*H$_3$), 22.6 (Nacnac-*C*H$_3$), 25.2, ({OC(*C*H$_3$)-$_2$}$_2$), 83.1 (O*C*(CH$_3$)$_2$), 96.1 (Nacnac-*C*H), 129.3 (Ar-*C*H), 131.2 (Ar-*C*CH$_3$), 133.4 (Ar-*C*CH$_3$), 146.1 (Ar-*C*N), 166.4 (Nacnac-*C*N) ppm.

^{11}B NMR (128 MHz, benzene-d_6, 298 K): δ_B 38.8 (br) ppm

^{t}BuOBpin

^{1}H NMR (500 MHz, benzene-d_6, 298 K): δ_H 1.06 (12 H, s, {OC(C*H*$_3$)$_2$}$_2$), 1.38 (9 H, s, C(C*H*$_3$)$_3$) ppm.

^{13}C{^{1}H} NMR (101 MHz, benzene-d_6): δ_C 24.6 ({OC(*C*H$_3$)$_2$}$_2$), 30.3 (C(*C*H$_3$)$_3$, 73.5 (*C*(CH$_3$)$_3$), 81.76 (O*C*(CH$_3$)$_2$) ppm.

^{11}B NMR (128 MHz, benzene-d_6, 298 K): δ_B 21.7 ppm

(Nacnac^{Mes})Zn(DMAP)Bpin

To an *in situ* generated C_6D_6 solution of (Nacnac^{Mes})ZnBpin (0.1 mmol, 0.7 mL) was added DMAP (0.012 g, 0.1 mmol). The sample was solicited briefly to aid dissolution of the DMAP, at which point NMR spectroscopy indicated that conversion was complete. Removal of volatiles *in vacuo*, extraction into hexane and filtration yielded a colourless solution. Single crystals suitable for X-ray crystallographic analysis were obtained by slow evaporation of the hexane solution. Yield 0.047 g (73 %).

^{1}H NMR (500 MHz, benzene-d_6, 298 K): δ_H 0.97 (12 H, s, {OC(C*H*$_3$)$_2$}$_2$), 1.81 (6 H, s, Nacnac-C*H*$_3$), 2.13 (6 H, s, N(C*H*$_3$)$_2$), 2.18 (6 H, s, *p*-C*H*$_3$), 2.27 (12 H, s, *o*-C*H*$_3$), 5.00 (1 H, s, C*H*), 6.02 (2 H, d, $^3J_{HH}$ = 6.24 Hz, DMAP-*m*-C*H*), 6.84 (4 H, s, Ar-*H*), 8.64 (2 H, d, $^3J_{HH}$ = 6.24 Hz, DMAP-*o*-C*H)* ppm.

^{13}C{^{1}H} NMR (101 MHz, benzene-d_6): δ_C 19.2 (*o*-*C*H$_3$), 21.0 (*p*-*C*H$_3$), 23.1 (Nacnac-*C*H$_3$), 25.7, ({OC(*C*H$_3$)-$_2$}$_2$), 38.2 (N(*C*H$_3$)$_2$), 80.3 (O*C*(CH$_3$)$_2$), 93.7 (Nacnac-*C*H), 106.6 (DMAP-m-*C*H), 129.2 (Ar-*C*CH$_3$), 131.7 (Ar-*C*H), 132.3 (Ar-*C*CH$_3$), 147.6 (Ar-*C*N), 150.5 (DMAP-*o*-*C*H), 154.4 (DMAP-*p*-*C*N), 165.2 (Nacnac-*C*N) ppm.

^{11}B NMR (128 MHz, benzene-d_6, 298 K): δ_B 42.2 (br.) ppm

Elemental Microanalysis – Expected for $C_{36}H_{51}BN_4O_2Zn$: C 66.73, H 7.93, N 8.65 %. Found: C 67.04, H 8.00, N 8.27 %.

Reaction of (Nacnac^{Mes})ZnBpin and MeI

To an *in situ* generated C_6D_6 solution of (Nacnac^{Mes})ZnBpin (0.038 mmol, 0.5 mL) was added MeI (0.02 mL, excess). Immediate reaction yielded the known species (Nacnac^{Mes})ZnI and MeBpin, as determined by *in situ* NMR spectroscopy.

Reaction of (Nacnac^{Mes})Zn(DMAP)Bpin and MeI

To a solution of (Nacnac^{Mes})Zn(DMAP)Bpin (0.01 g, 0.015 mmol) in C_6D_6 (0.5 mL) was added MeI (0.02 mL, excess). Immediate reaction yielded the known species MeBpin, as well as a new species. Removal of volatiles, extraction into hexane and filtration yielded a colourless solution, from which colourless single crystals could be obtained when left to stand. Single crystal crystallographic measurements showed that this new species was (Nacnac^{Mes})Zn(DMAP)I, for which an alternative synthesis was conducted by analogy to the reported chloride analogue, yielding a clean sample for collection of characterising data.[s10]

(Nacnac^{Mes})Zn(DMAP)I

^{1}H NMR (500 MHz, benzene-d_6, 298 K): δ_H 1.63 (6 H, s (br.), *o*-C*H*$_3$), 1.65 (6 H, s, Nacnac-C*H*$_3$), 2.18 (6 H, s, *p*-C*H*$_3$), 2.21 (6 H, s (br.), *o*-C*H*$_3$), 3.05 (6 H, s, N(C*H*$_3$)$_2$), 4.84 (1 H, s, C*H*), 6.66 (2 H, s, Ar-*H*), 6.67 (2 H, br., DMAP-*m*-C*H*), 6.79 (2 H, s, Ar-*H*), 8.20 (2 H, d (br.), $^3J_{HH}$ = 4.86 Hz, DMAP-*o*-C*H)* ppm.

^{13}C{^{1}H} NMR (101 MHz, benzene-d_6): δ_C 18.9, 20.1 (*o*-*C*H$_3$), 21.1 (*p*-*C*H$_3$), 23.8 (Nacnac-*C*H$_3$), 39.2 (N(*C*H$_3$)$_2$), 93.9 (Nacnac-*C*H), 107.5 (DMAP-*m*-*C*H), 129.4, 130.0 (Ar-*C*H), 132.0, 33.1, 133.7 (Ar-*C*CH$_3$), 146.3 (Ar-*C*N), 149.6 (DMAP-*o*-*C*H), 156.6 (DMAP-*p*-*C*N), 167.9 (Nacnac-*C*N) ppm.

Reaction of (Nacnac^{Mes})ZnBpin with CO_2

An *in situ* generated C_6D_6 solution of (Nacnac^{Mes})ZnBpin (0.5 mmol, 0.6 mL) was degassed by three freeze-pump-thaw cycles before the addition of one atmosphere of CO_2. Heating to 80 °C for 16 h led to the formation of one predominant species by *in situ* NMR. Removal of volatiles, extraction into hexane and filtration yielded a colourless solution, from which colourless single crystals could be obtained when left to stand. These crystals were suitable for X-ray crystallographic measurements. The minor species observed by NMR exactly matches the signals of the known species [(Nacnac^{Mes})Zn]$_2$. An alternative direct synthesis of [(Nacnac^{Mes})ZnOBpin]$_2$ is given below.

[(Nacnac^{Mes})ZnOBpin]$_2$

To a mixture of (Nacnac^{Mes})ZnMe (0.02 g, 0.048 mmol) and HOBpin (0.007 g, 0.049 mmol) was added benzene (0.5 mL), leading to immediate bubbling of the solution, which ceased after one minute. The resulting solution was left to stand, resulting in the formation of large colourless crystals of [(Nacnac^{Mes})ZnOBpin]$_2$. The supernatant solution was decanted, and the crystals were washed with hexane (0.5 mL), before removal of all remaining volatiles *in vacuo*.

^{1}H NMR (500 MHz, THF-d$_8$, 298 K): δ_H 1.01 (12 H, s, {OC(C*H*$_3$)$_2$}$_2$), 1.37 (6 H, s, Nacnac-C*H*$_3$), 1.78 (12 H, s, *o*-C*H*$_3$), 2.37 (6 H, s, *p*-C*H*$_3$), 4.69 (1 H, s, C*H*), 6.72 (4 H, s, Ar-*H*) ppm.

^{13}C{^{1}H} NMR (101 MHz, THF-d$_8$): δ_C 18.8 (*o*-*C*H$_3$), 21.4 (*p*-*C*H$_3$), 23.3 (Nacnac-*C*H$_3$), 25.4 ({OC(*C*H$_3$)$_2$}$_2$), 81.8 (O*C*(CH$_3$)$_2$), 95.0 (Nacnac-*C*H), 130.0 (Ar-*C*H), 132.9 (Ar-*C*CH$_3$), 133.1 (Ar-*C*CH$_3$), 146.5 (Ar-*C*N), 168.1 (Nacnac-*C*N) ppm.

^{11}B NMR (128 MHz, THF-d$_8$, 298 K): δ_B 22.6 ppm

(Nacnac^{Mes})ZnOB{(NDippCH)$_2$}

To a mixture of (Nacnac^{Mes})ZnMe (0.2 g, 0.48 mmol) and {(HCDippN)$_2$}BOH (0.195 g, 0.48 mmol) in a J-Young ampoule was added toluene (5 mL) before stirring at 80 °C for 16 h, during which gas evolution could be observed. Evaporation of volatiles *in vacuo* yielded a sticky solid. Extraction into hexane (5 mL), filtration and removal of solvent *in vacuo* afforded an off-white powder. Single crystals could be obtained by recrystallisation of a portion of this material by slow evaporation from hexane. These crystals were suitable for single crystal X-ray crystallographic measurements. Yield 0.311 g (80 %).

^{1}H NMR (500 MHz, benzene-d$_6$, 298 K): δ_H 1.00 (12 H, d, $^3J_{HH}$ = 6.91 Hz, CH(C*H*$_3$)$_2$), 1.21 (12 H, d, $^3J_{HH}$ = 6.91 Hz, CH(C*H*$_3$)$_2$), 1.36 (6 H, s, Nacnac-C*H*$_3$), 1.78 (12 H, s, *o*-C*H*$_3$), 2.24 (6 H, s, *p*-C*H*$_3$), 3.37 (4 H, sept., $^3J_{HH}$ = 7.01 Hz, C*H*(CH$_3$)$_2$) 4.73 (1 H, s, C*H*), 5.90 (2 H, s, {DippNC*H*}$_2$) 6.65 (4 H, s, Ar-*H*), 7.11 (4 H, d (br.), $^3J_{HH}$ = 7.57 Hz, Ar-*m*-*H*), 7.21 (2 H, d (br.), $^3J_{HH}$ = 7.57 Hz, Ar-*p*-*H*) ppm.

$^{13}C\{^1H\}$ NMR (101 MHz, benzene-d_6): δ_C 18.1 (*o*-CH_3), 21.1 (*p*-CH_3), 23.0 (Nacnac-CH_3), 23.7 (CH(CH_3)$_2$), 23.9 (CH(CH_3)$_2$), 28.7 ($CH(CH_3)_2$), 95.6 (Nacnac-*C*H), 115.6 ({DippN*C*H}$_2$), 123.3 (Dipp-*m*-*C*H), 129.9 (Mes-*m*-*C*H), 131.0 (Mes-CCH_3), 133.9 (Mes-CCH_3), 141.1 (Dipp-*C*N), 143.9 (Mes-*C*N), 146.6 (Dipp-$CCH(CH_3)_2$), 170.0 (Nacnac-*C*N) ppm.

^{11}B NMR (128 MHz, benzene-d_6, 298 K): δ_B 21.5 ppm

Elemental Microanalysis – Expected for $C_{49}H_{65}BN_4OZn$: C 73.36, H 8.17, N 6.98 %. Found: C 73.72, H 8.00, N 6.63 %.

Reaction of (Nacnac^{Mes})ZnBpin and (Nacnac^{Mes})ZnOB{(NDippCH)$_2$}

To an *in situ* generated C_6D_6 solution of (Nacnac^{Mes})ZnBpin (0.38 mmol, 0.5 mL) was added (Nacnac^{Mes})ZnOB{(NDippCH)$_2$} (0.03 g, 0.037 mmol), before heating to 80 °C for 12 h. NMR spectroscopy indicates clean conversion to the known species [(Nacnac^{Mes})Zn]$_2$ and one new species, which gives rise to signals consistent with the proposed complex {(HCDippN)$_2$}BOBpin.[s1] Attempts at crystallisation yielded only crystals of [(Nacnac^{Mes})Zn]$_2$, as well as a stickly gel-like substance assigned to the {(HCNDipp)$_2$}BOBpin by-product.

{(HCDippN)$_2$}BOBpin

^1H NMR (500 MHz, benzene-d_6, 298 K): δ_H 0.69 (12 H, s, {OCC*H*$_3$}$_2$), 1.25 (12 H, d, $^3J_{HH}$ = 7.00 Hz, CH(C*H*$_3$)$_2$), 1.39 (12 H, d, $^3J_{HH}$ = 7.00 Hz, CH(C*H*$_3$)$_2$), 3.40 (4 H, sept., $^3J_{HH}$ = 7.00 Hz, C*H*(CH_3)$_2$), 6.01 (2 H, s, {DippNC*H*}$_2$), 7.15 (4 H, br., Ar-*m*-*H*), 7.20 (2 H, m, Ar-*p*-*H*) ppm.

24.3 ({OC(*C*H$_3$)$_2$}$_2$), 24.5 (CH(*C*H$_3$)$_2$), 24.8 (CH(*C*H$_3$)$_2$), 30.3 (*C*H(CH_3)$_2$), 82.2 (O*C*(CH_3)$_2$), 117.0 ({DippN*C*H}$_2$), 123.7, 129.3, 138.0 (Ar-*C*), 146.9 (Ar-*C*N) ppm.

^{11}B NMR (128 MHz, benzene-d_6, 298 K): δ_B 20.78, 21.71 ppm

NMR Spectra of novel compounds

(Nacnac^{Mes})ZnBpin

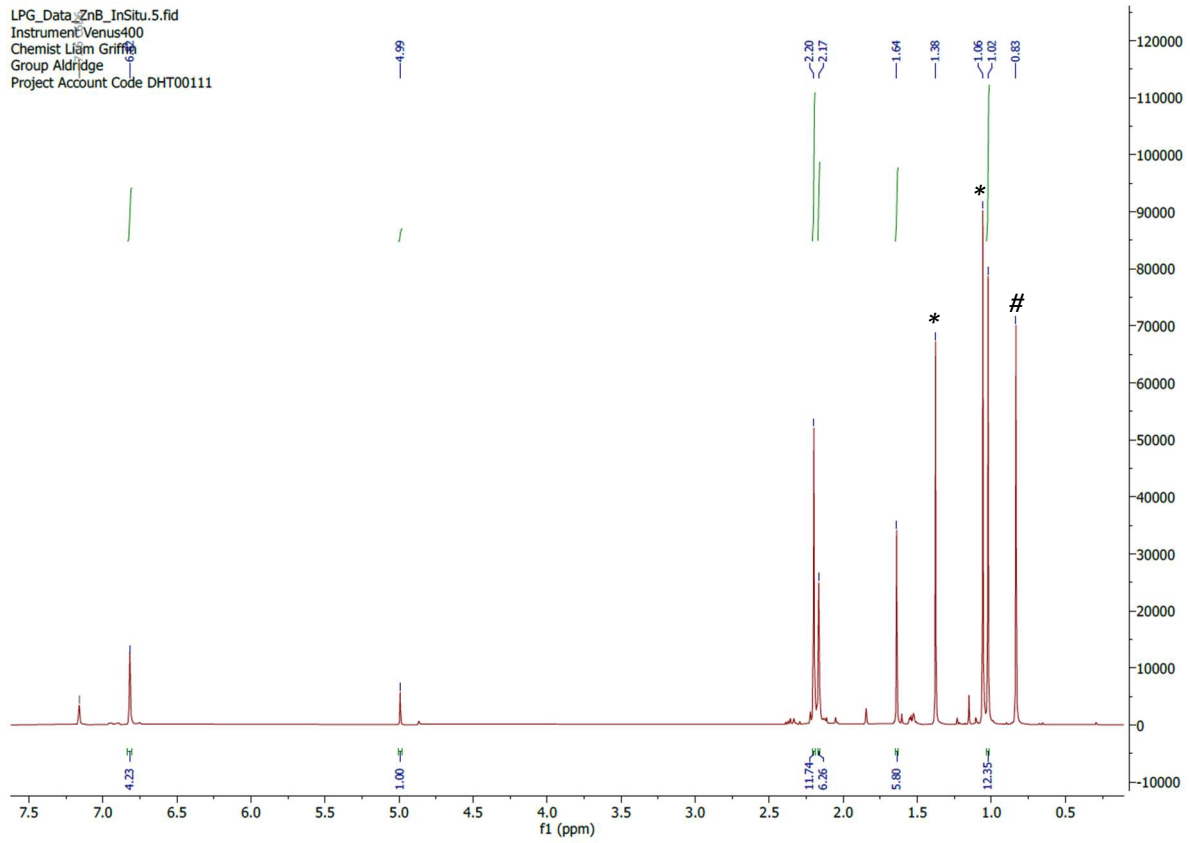

Fig S2. *In situ ^{1}H NMR of (Nacnac^{Mes})ZnBpin. ^{t}BuOBPin by-product marked * and residual B_2pin_2 marked #.*

(Nacnac^{Mes})Zn(DMAP)Bpin

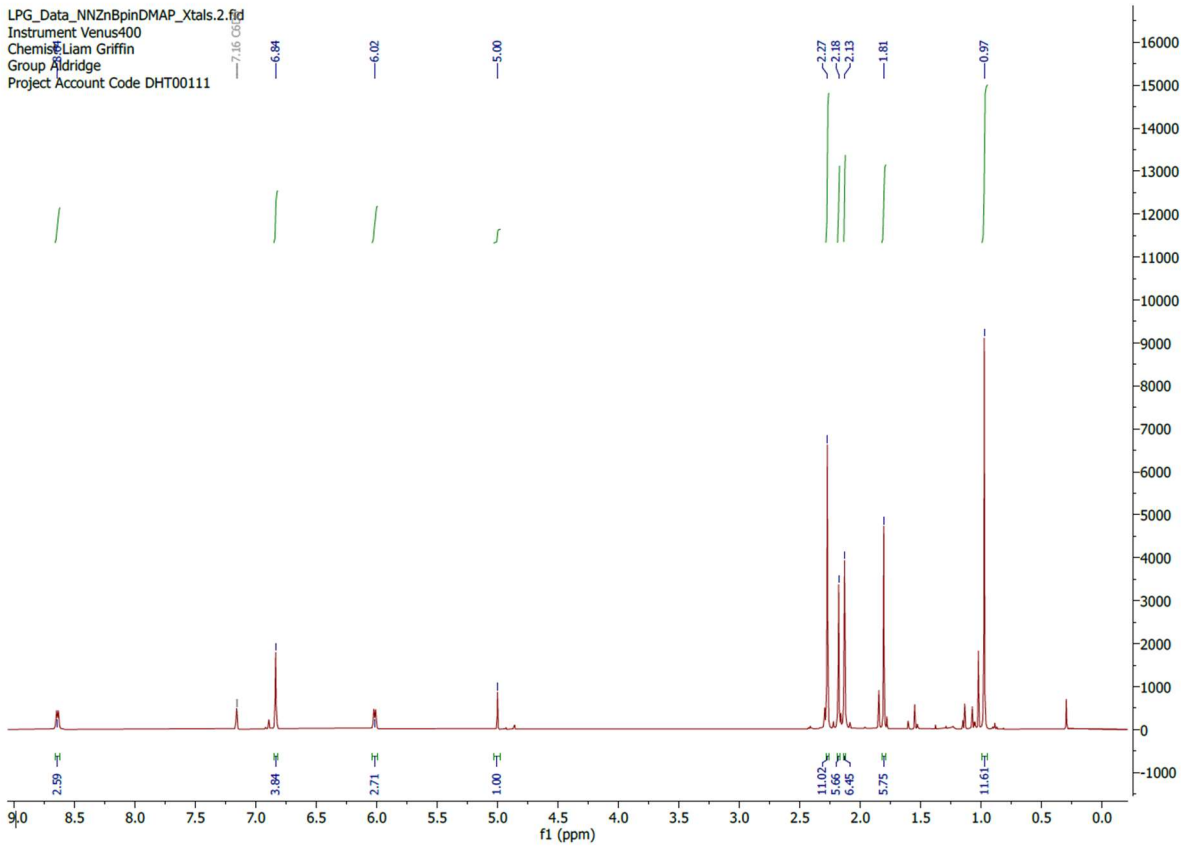

Fig S3. *^{1}H NMR of (Nacnac^{Mes})Zn(DMAP)Bpin.*

(Nacnac^{Mes})Zn(DMAP)I

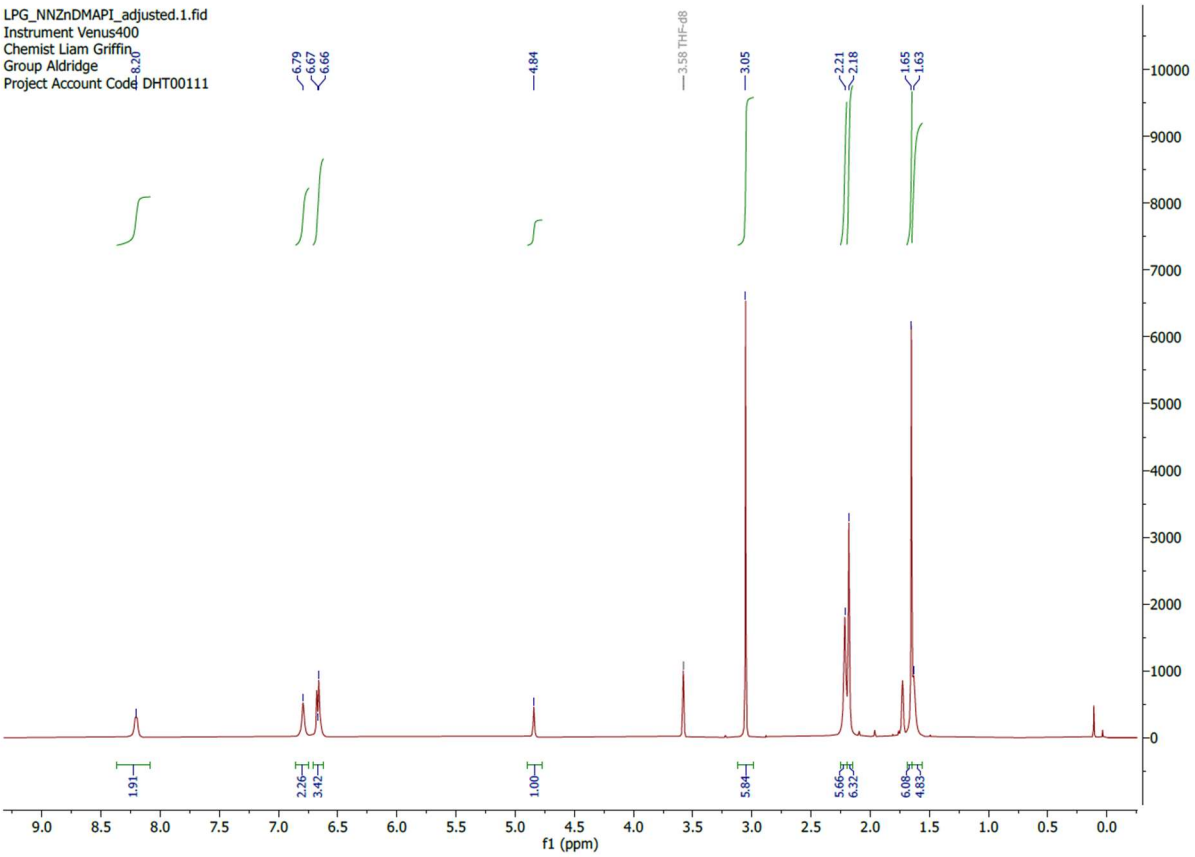

Fig S4. *^{1}H NMR of (Nacnac^{Mes})Zn(DMAP)I.*

[(Nacnac^{Mes})ZnOBpin]$_2$

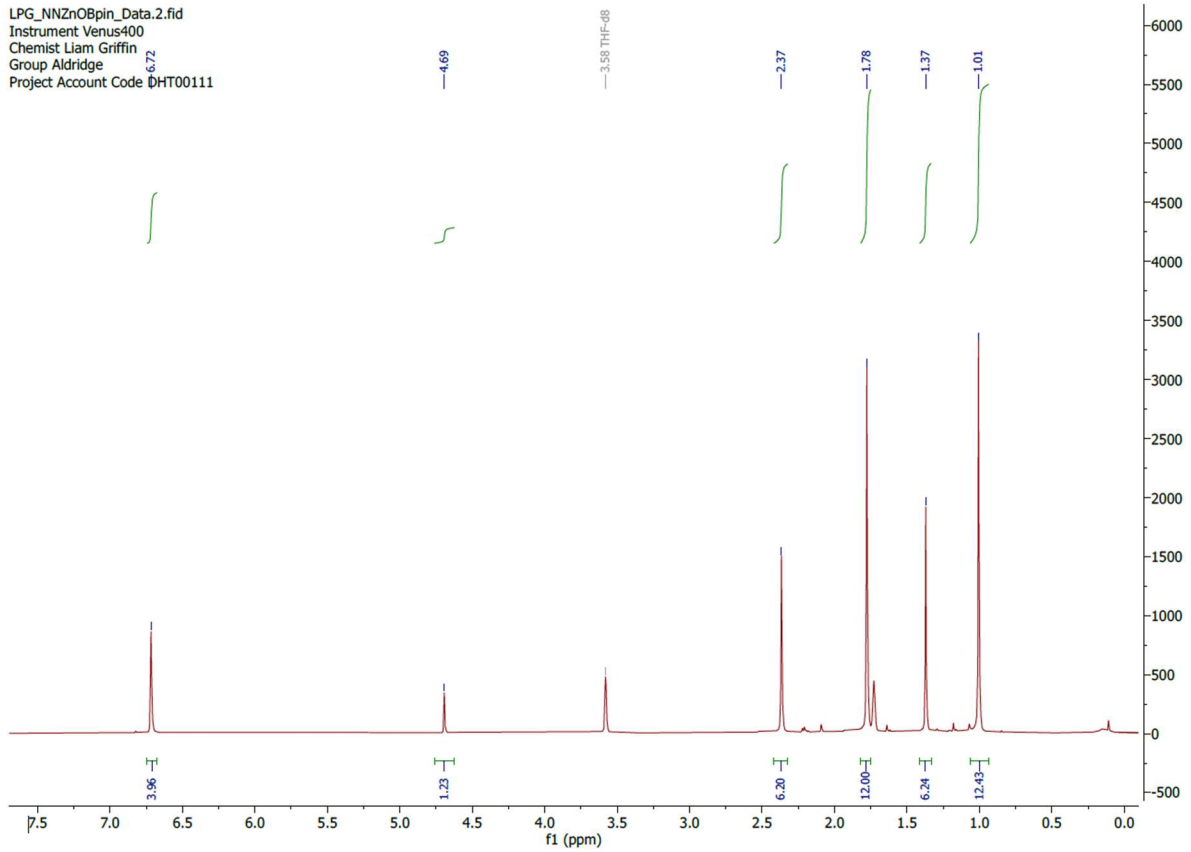

Fig S5. *^{1}H NMR of [(Nacnac^{Mes})ZnOBpin]$_2$.*

(Nacnac^{Mes})ZnOB{(NDippCH)$_2$}

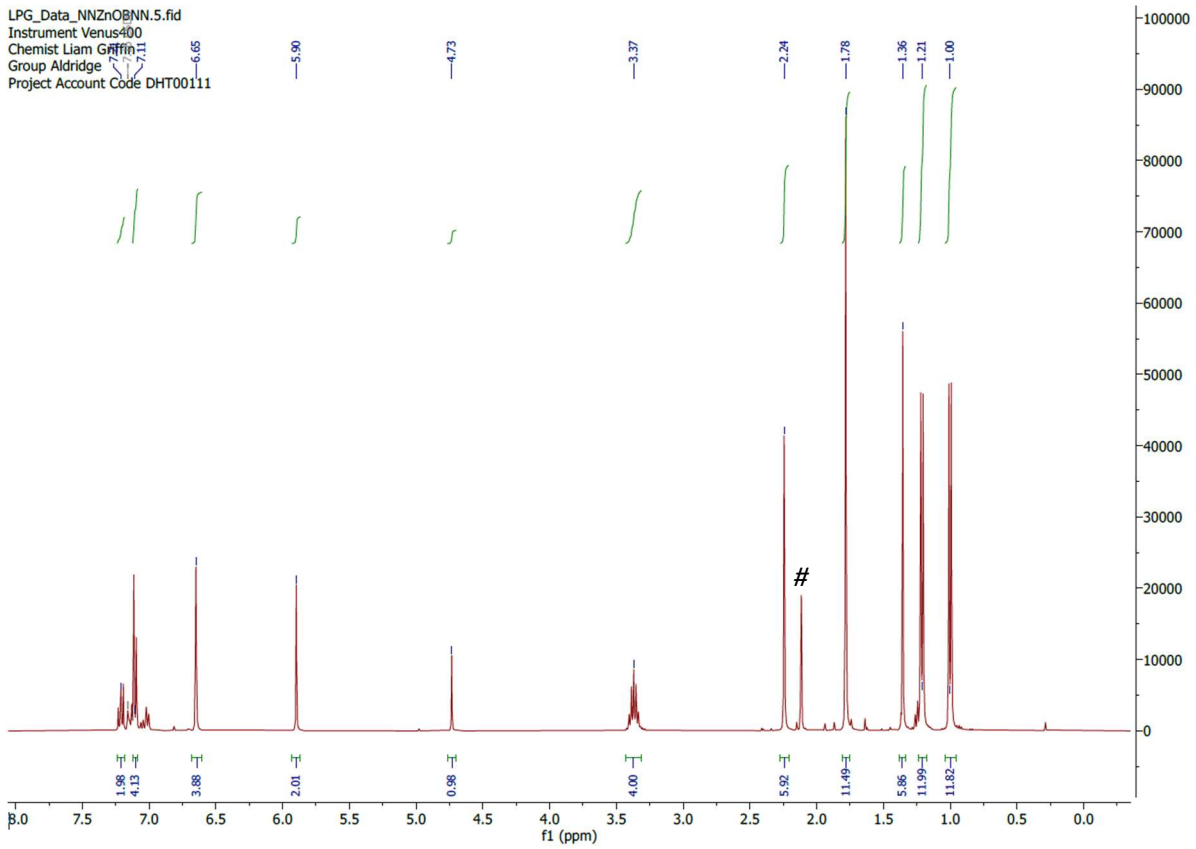

Fig S6. *In situ ^{1}H NMR of (Nacnac^{Mes})ZnOB{(NDippCH)$_2$}. Residual toluene marked #.*

{(HCDippN)$_2$}BOBpin

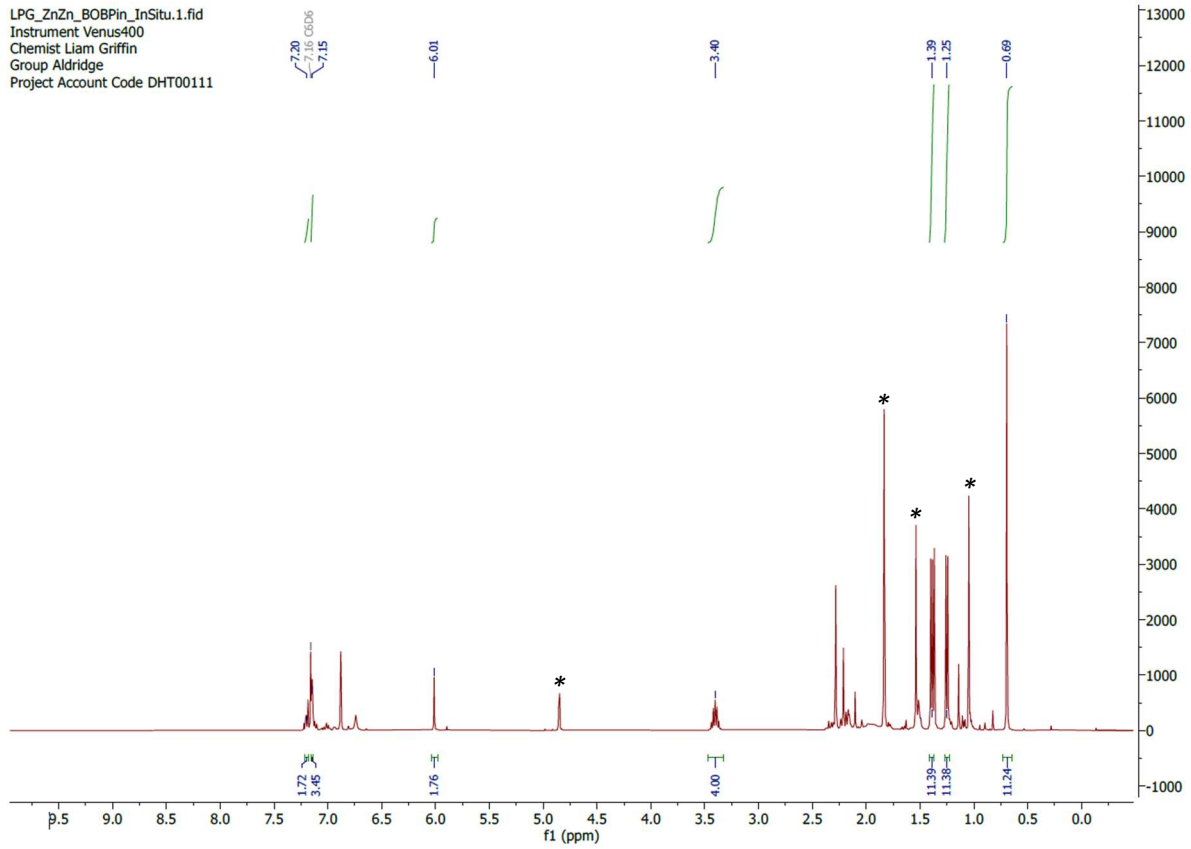

Fig S7. *In situ ^{1}H NMR of {(HCDippN)$_2$}BOBpin. Diagnostic signals of [(Nacnac^{Mes})Zn]$_2$ are marked *.*

Computational details

Gas phase geometry optimizations and frequency analyses were carried out using the ORCA (5.0.4) software package,[s11, s12] using the R2-Scan-3C method.[s13] The optimized structures were confirmed to be minima on the potential energy surface by the absence of imaginary frequencies. Single point calculations were performed using the ωB97X-D4 functional and Def2-TZVP basis set.[s14-s16] Natural bonding orbital (NBO) analyses were carried out using the NBO 7.0 program.[s17, s18] Atoms in molecules (AIM) analyses were conducted using Multiwfn software package.[s19] AIM bonding classifications have been made in accordance with the literature precedent.[s20] All iso-surfaces have been rendered at 0.05, unless otherwise stated.

(Nacnac^{Mes})ZnBpin

LUMO

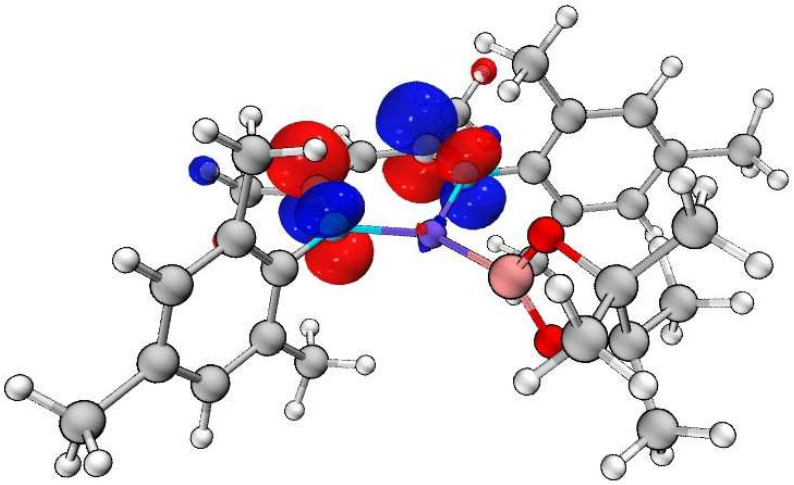

Fig S8. *Ligand based LUMO of (Nacnac^{Mes})ZnBpin, E = 1.2292 eV.*

HOMO

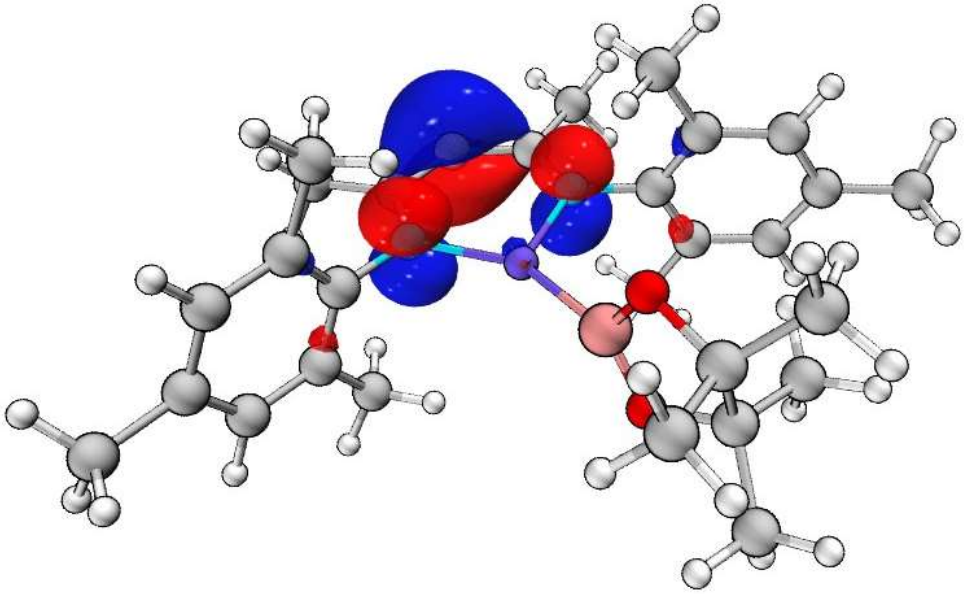

Fig S9. *Ligand based HOMO of (Nacnac^{Mes})ZnBpin, E = -7.8818 eV.*

Zn-B bonding contributions

HOMO-2

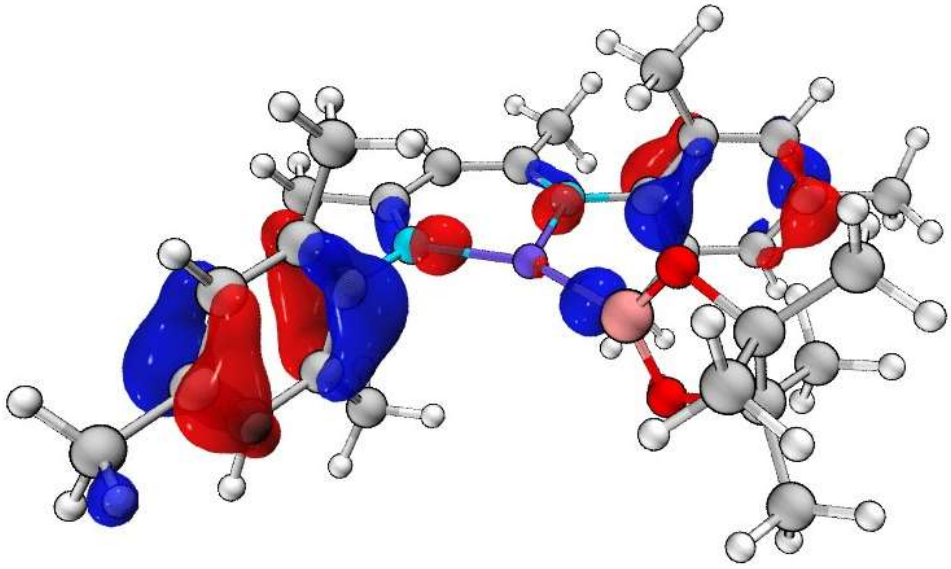

Fig S10. *HOMO-2 of (Nacnac^{Mes})ZnBpin, featuring a small region of electron density between B and Zn, E = -8.6125 eV.*

HOMO-3

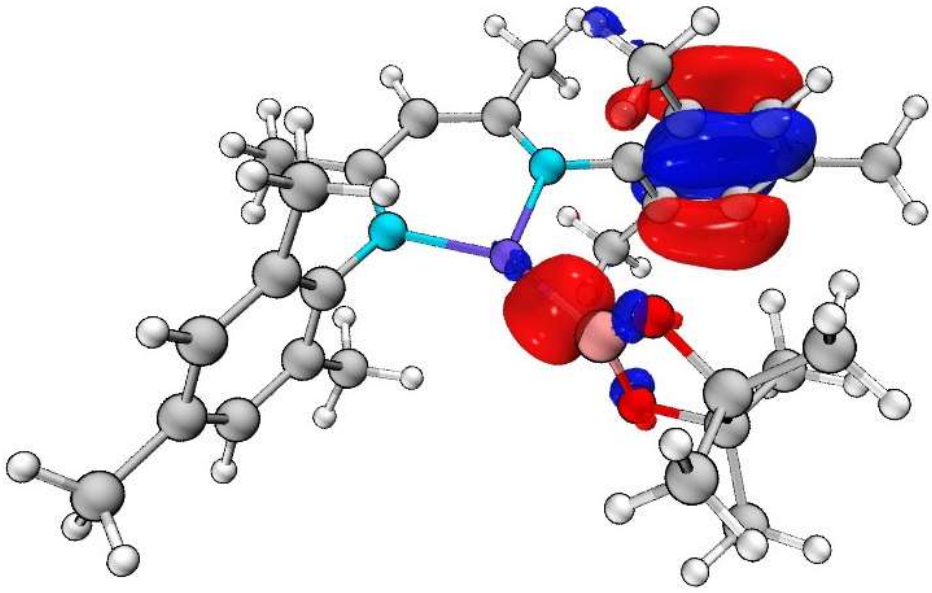

Fig S11. *HOMO-3 of (Nacnac^{Mes})ZnBpin, featuring a significant region of electron density between B and Zn, E = -8.8903 eV.*

HOMO-4

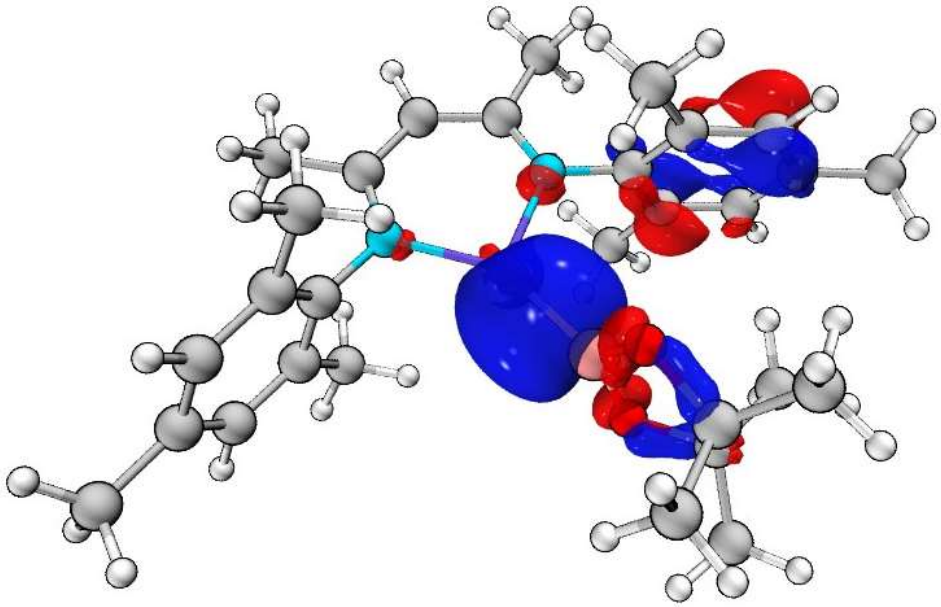

Fig S12. *HOMO-4 of (Nacnac^{Mes})ZnBpin, featuring the most significant region of electron density between B and Zn, E = -8.9182 eV.*

NBO analysis

One conventional NBO was located for the Zn-B interaction.

1.96172 electrons

21.75% (0.4664 electrons) Zn: s 96.5%, p 2.4%, d 1.1%

78.25% (0.8846 electrons) B: s 47.6%, p 52.4%

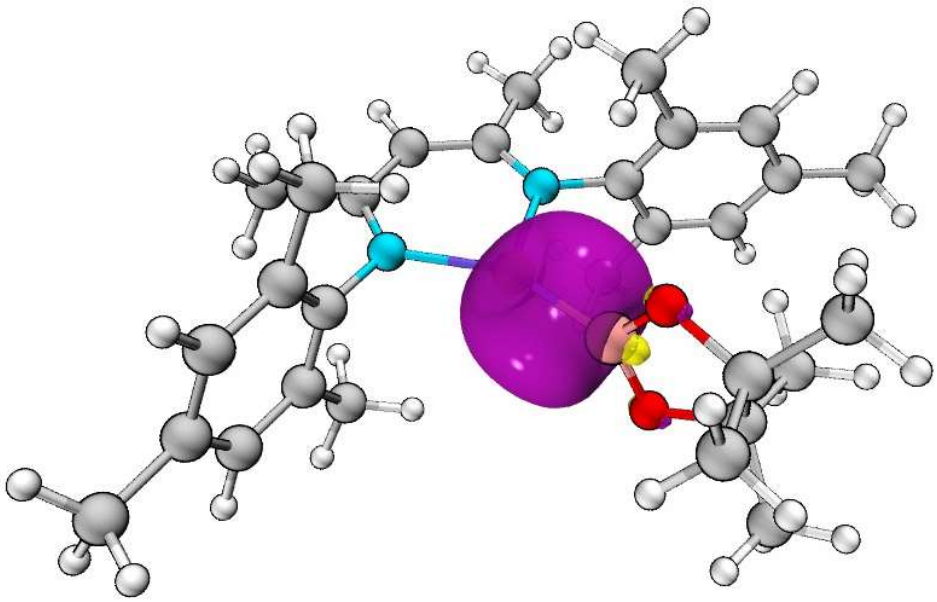

Fig S13. *NBO corresponding to the Zn-B bonding interaction in (Nacnac^{Mes})ZnBpin.*

WBI: 0.592

NPA charges

Zn: 1.47012 e

B: 0.46825 e

Bader charges

Zn: 0.879 e

B: 1.352 e

QTAIM

ρ	0.1001319145E+00
$\nabla^2\rho$	0.5864727743E-01
G(r)	0.5672856343E-01
K(r)	0.4206674407E-01
V(r)	-0.9879530750E-01
E(r)	-0.4206674407E-01
ELF	0.5441836390E+00
ε	0.084374

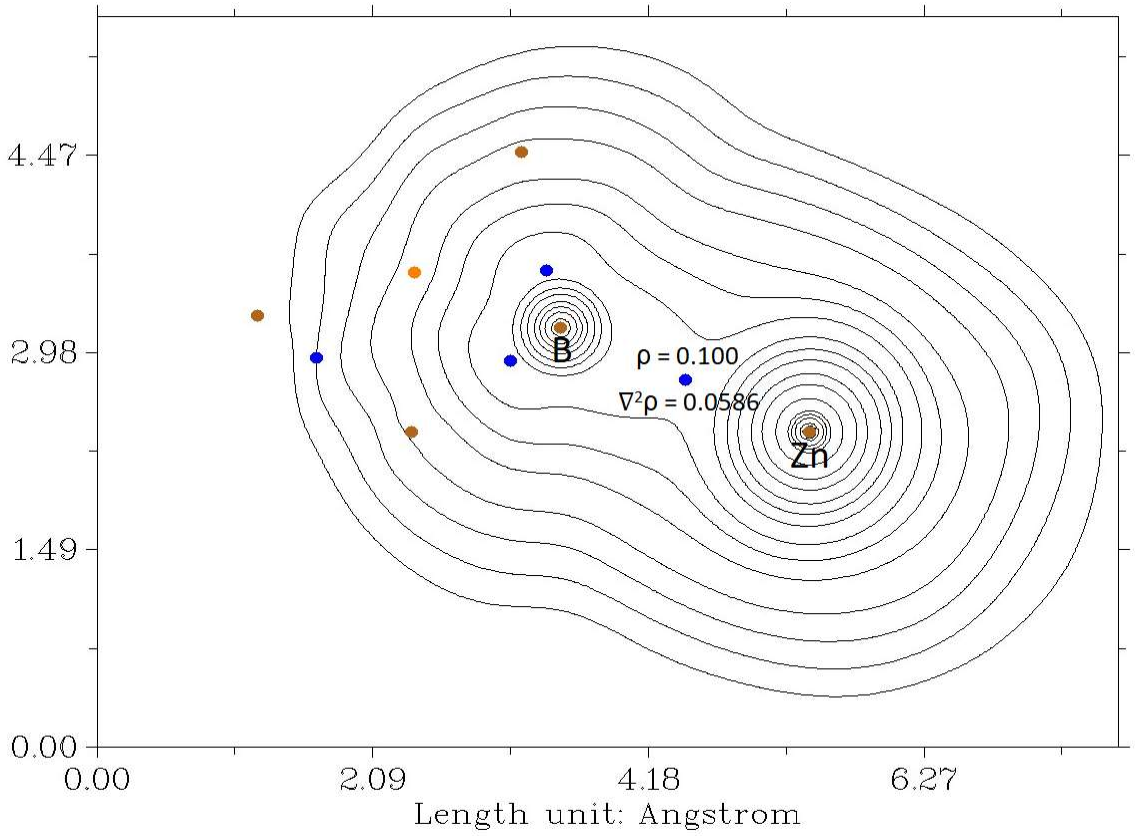

Fig S14. *Contour plot of electron density in the region around the Zn-B bond in (Nacnac^{Mes})ZnBpin.*

(Nacnac^{Mes})Zn(DMAP)Bpin

LUMO

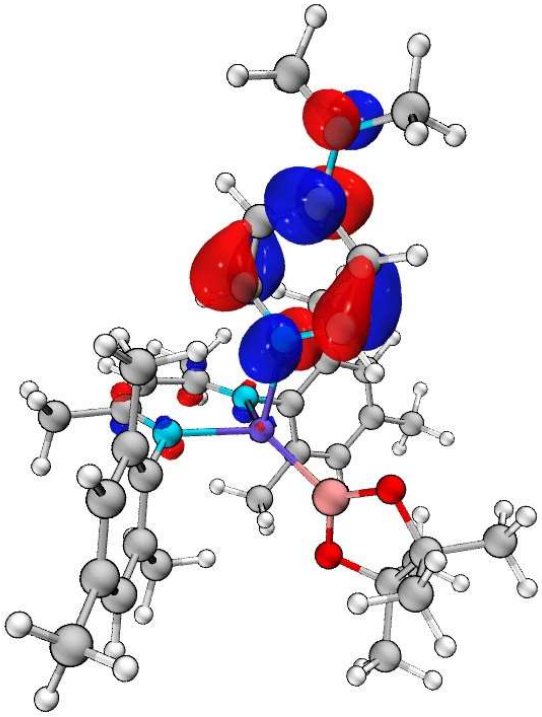

Fig S15. *DMAP-based LUMO of (Nacnac^{Mes})Zn(DMAP)Bpin, E = 1.3777 eV*

HOMO

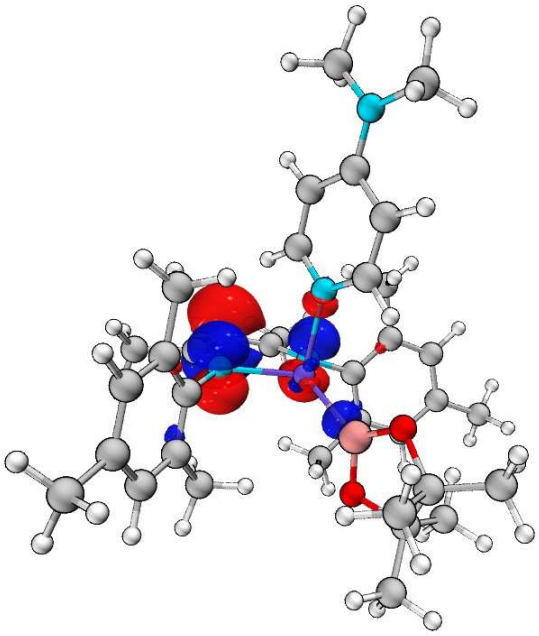

Fig S16. *Primarily ligand-based HOMO of (Nacnac^{Mes})Zn(DMAP)Bpin, with a small amount of electron density between B and Zn, E = -7.1873 eV.*

Zn-B bonding contributions

HOMO-2

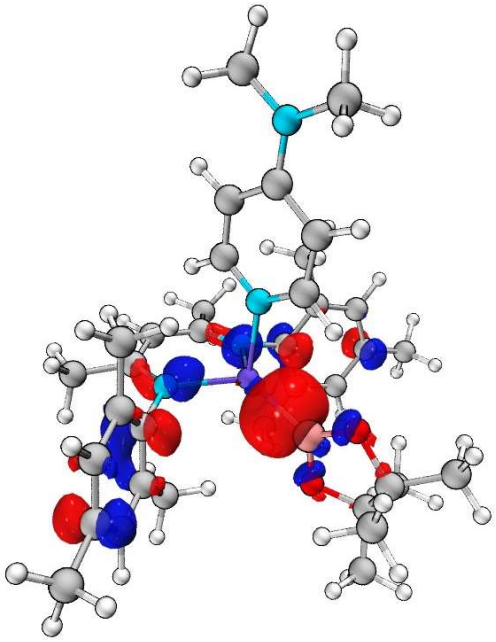

Fig S17. *HOMO-2 of (Nacnac^{Mes})Zn(DMAP)Bpin, featuring a significant contribution to Zn-B σ-bonding, E = -8.1452 eV.*

HOMO-3

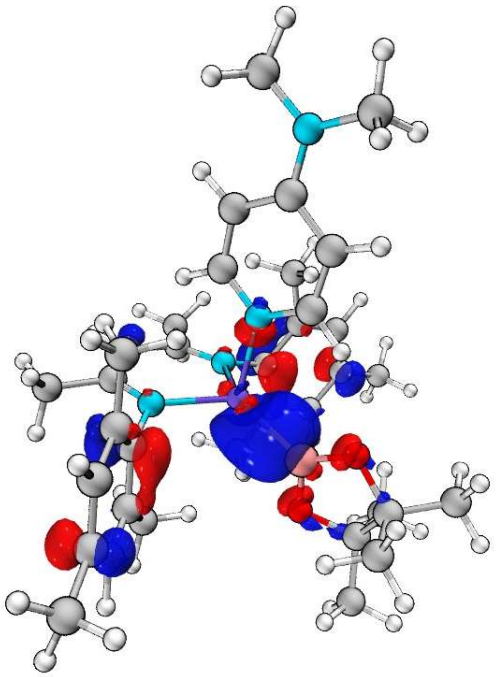

Fig S18. *HOMO-3 of (Nacnac^{Mes})Zn(DMAP)Bpin, featuring a significant contribution to Zn-B σ-bonding, E = -8.2358 eV.*

NBO analysis

No NBO was located for the Zn-B bonding interaction. This is instead described as a second-order perturbation interaction between a B-based lone pair and a Zn based vacant orbital, with an overall stabilization energy of 232.81 kcal/mol.

B-based lone pair – 1.64650 electrons: s 49.3%, p 50.67%

Zn vacant orbital – 0.44130 electrons: s 98.7%, p 1.0%, d 0.3%

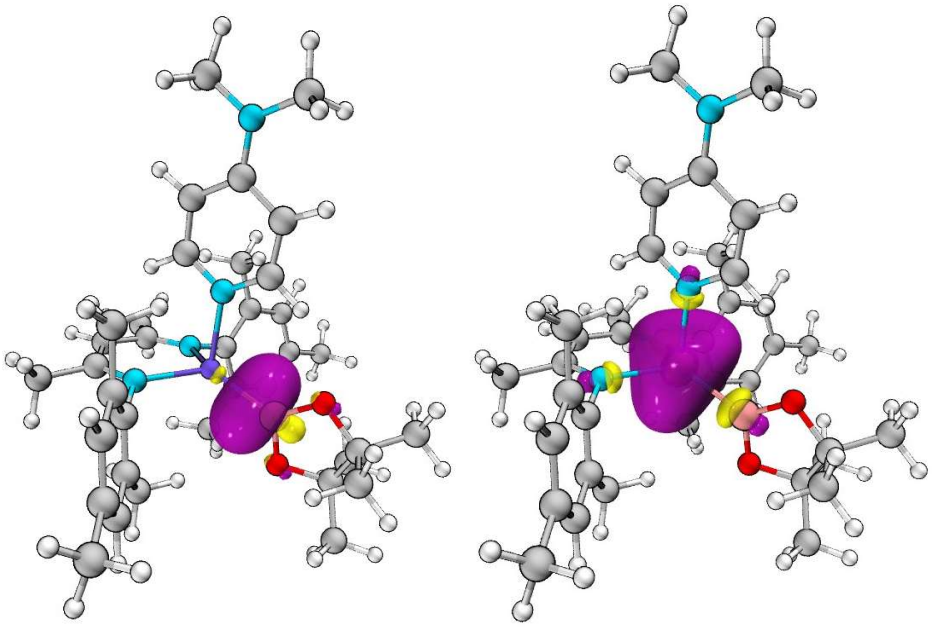

Fig S19. *NBO orbitals calculated to interact by Second Order Perturbation Theory, leading to a Zn-B σ-bonding interaction. Left, B-based lone pair, Right, Zn-based vacant orbital.*

WBI: 0.496

NPA charges

Zn: 1.56613 e

B: 0.41854 e

Bader charges

Zn: 0.975 e

B: 1.272 e

QTAIM

ρ	0.9544211041E-01
$\nabla^2\rho$	0.9014936624E-01
G(r)	0.6015711525E-01
K(r)	0.3761977370E-01
V(r)	-0.9777688895E-01
E(r)	-0.3761977370E-01
ELF	0.4750102996E+00
ε	0.058560

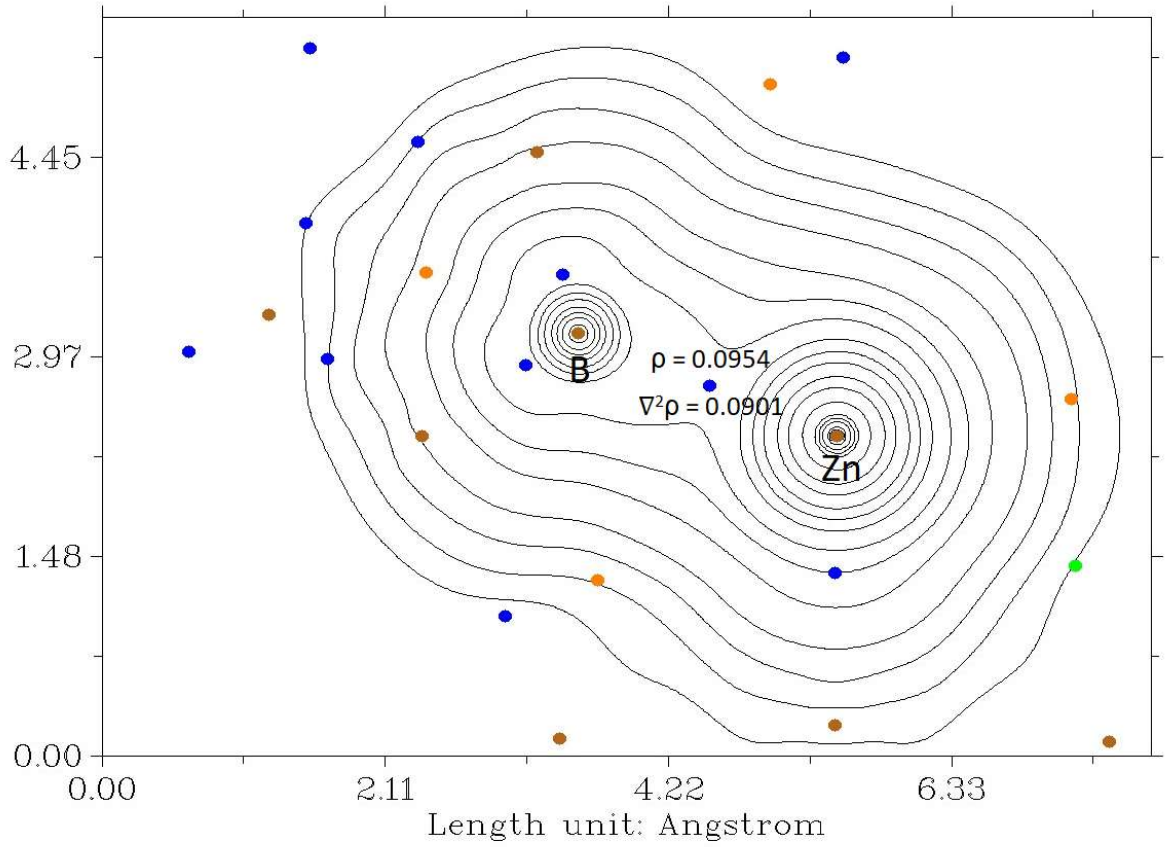

Fig S20. *Contour plot of electron density in the region around the Zn-B bond in (Nacnac^{Mes})Zn(DMAP)Bpin.*

Computational analysis

In an attempt to rationalize the significantly reduced stability brought about by DMAP coordination in **2**, the impact of the L-donor on the nature of the Zn-B bond was probed via DFT calculations carried out on both the DMAP-complexed and base-free species. Both species converged to acceptable geometries, with metrical parameters that were consistent between the two species, and in the case of **2**, between the calculated geometry and the crystallographic data (N1–Zn1 2.026, N2–Zn1 2.034, N3–Zn1 2.151, B1–Zn1 2.067 Å, N1–Zn1–N2 93.1, B1–Zn1–N1 111.1 °).

An orbital analysis shows that in the case of DMAP adduct **2**, the HOMO-2 and HOMO-3 contain significant Zn–B sigma bond contributions, while the LUMO is predominantly π* in nature and localised on the DMAP ring. At 8.57 eV, the HOMO-LUMO gap is very large. The WBI for the Zn–B bond is found to be 0.496, consistent with the idea of a weak single bond. In the case of base-free system **1**, the HOMO-LUMO gap is larger, at 9.11 eV. However, both the frontier orbitals are ligand based, with no significant contribution to the Zn–B bonding. These are found lower in the orbital manifold, with the HOMO-4 exhibiting the most significant Zn–B σ-bonding character. The WBI for the Zn-B bond in this case was calculated to be 0.592, i.e. notably higher than in the DMAP coordinated case. This is consistent with the calculated structures, which predicts a shorter Zn–B bond length for **1** (2.041 Å) compared to **2** (2.067 Å).

In order to better inspect the Zn-B bonding interactions, natural bond orbital (NBO) analyses were undertaken. Here, a conventional NBO was located for the Zn-B bond only in the case of **1**. The bond is strongly polarized towards the boron centre (78.3%), and is almost entirely s based at zinc (96.5%), with a relatively even s/p split at boron (47.6% s, 52.4% p). By contrast, for **2**, no NBO was located for the Zn–B interaction. Instead, this interaction is described as a second order perturbation, in which the boron centred lone pair donates into a zinc s-based vacant orbital, with an overall stabilization energy of 232.8 kcal mol^{-1}. This difference in the descriptions of the two Zn–B interactions, along with

the differing WBIs speaks to a weaker and more labile Zn–B bond in the DMAP coordinated case as a result of a more crowded zinc centre, resulting in the observed decrease in stability.

The more polarized ionic nature in **2** is also borne out in the Bader charges calculated for the two systems, which return a higher positive charge at zinc (0.975, cf. 0.880) and a lower charge at boron (1.272, cf. 1.352). In a broader context, both species feature a relatively low charge at zinc, in line with the highly σ-donating nature of the boryl ligand.

Finally, Quantum Theory of Atoms in Molecules (QTAIM) analysis was undertaken to further compare the Zn–B bonding in **1** and **2**. In both cases a Bond Critical Point (BCP) could be located along the bond path between zinc and boron. In both cases, the parameters (a low electron density and small positive Laplacian of electron density) are consistent with ionic bonding. The most significant difference is observed between the two values of the Laplacian, in which a more positive value for the DMAP-coordinated species is consistent with a more ionic bond, and therefore a more labile linkage.[s20]

	(Nacnac^{Mes})ZnBpin (**1**)	(Nacnac^{Mes})Zn(DMAP)Bpin (**2**)
ρ	0.1001	0.09544
$\nabla^2\rho$	0.05865	0.09015

Table S2. *Key QTAIM parameters (in a.u.) relating to the BCPs of the Zn-B bonding interactions for the two zinc-boryl species **1** and **2**.*

Optimised XYZ coordinates

Nacnac^{Mes}ZnBpin: -3195.348038663298 E_h	**Nacnac^{Mes}Zn(DMAP)Bpin: -3577.947517146553 E_h**
Zn -1.00569597992652 8.36829931809950 15.63429840251350	Zn -1.26553191673102 9.20671671871936 15.25186422618441
O 0.23312213009687 8.82138844931929 12.91695432176124	O 0.62814103947869 8.95479881441431 12.82191992819689
O 0.52007541007981 6.66428836442517 13.61985128564829	O 0.36528032194073 6.96907404899294 13.91345855822676
N -1.00132060882704 8.98680513854936 17.48706083474262	N -1.06392003773432 9.37679795263189 17.26035161109705
N -2.98397560074018 8.17560082294936 15.52626010096209	N -3.23414404414391 8.70999275545253 15.38177745620870
C -3.82584362761764 8.48661489253424 16.50201497363231	N -1.52908695091188 11.29520777089302 14.80891942924737
C 0.27947824933209 9.24194269732946 18.05966785395151	N -2.16731187117123 15.32451903815807 13.87917139410685
C -3.46404433021647 7.68090421113294 14.28142371969911	C -3.94417620553340 8.76278782690625 16.49763279302369
C -2.09955684484563 9.18168116580471 18.21976143433770	C 0.27484094683242 9.36954430087198 17.74286749969442
C 0.86515508562621 10.50775852417875 17.91062008689743	C -1.95655840408870 14.01361082010496 14.18365343195196
C -3.40577565560078 8.95756409529206 17.75964034207281	C -0.88916569858478 11.88352962182920 13.78554778262874
H -4.19559568496607 9.17288776875349 18.46873064547313	H -0.21024017985852 11.24411579905140 13.22309972612208
C 0.96903761986552 8.20356947631389 18.70082616086399	C -3.78508436822343 8.11529808565273 14.21250446333112
C -5.31030102528431 8.34069367031991 16.26740517725800	C -2.07306614194328 9.33398643407010 18.11815566495661
H -5.62208463098462 8.94142523664205 15.40560004437338	C -2.62225873772952 13.38259550188070 15.26002643524619
H -5.88284359683960 8.65155586413264 17.14269733518252	H -3.32436641605613 13.91701385445641 15.88781789729889
H -5.56550887310249 7.30293616430865 16.02633832431562	C 0.96190396124200 10.57013083073125 17.98277179435226
C 0.98883870833172 8.15462424257073 11.85552865940697	C -3.42170439523415 9.15629630439873 17.74741536416273
C -3.64647705186926 8.56705293370207 13.20887074662354	H -4.13427310476222 9.17767826726401 18.56327070485789
C 2.12870611863673 10.72821612053757 18.45538848032458	C -1.06287572691330 13.20884228336104 13.44077689278275
H 2.58266030170770 11.71221954637801 18.35024483314607	H -0.50613343476579 13.60418008719275 12.60032389318660
C 2.82588523452401 9.72211164650550 19.12392416834940	C 0.92749093711957 8.13556286555375 17.90783189838368
C -3.35937440624044 10.03143294109755 13.38047222482478	C -5.39411309526736 8.33131165259412 16.46894299648225
H -2.28290962635983 10.18931165992444 13.53062775621891	H -5.93710563272217 8.81330884468875 15.64963077116276

H -3.86960279493573 10.45249679558921 14.25332004757756	H -5.89260034311823 8.55574714577229 17.41366491507839
H -3.66177085846881 10.59461133397619 12.49374523406720	H -5.46121237817722 7.25153965165966 16.28917057075596
C 2.23170623746087 8.46600218474290 19.23138906501148	C 1.58355134526437 8.03202607580994 12.21378632870030
H 2.76606100526013 7.66423628153838 19.73788484041198	C -4.44027254136962 8.89624037930226 13.24751893985695
C -3.63946841055333 6.29994085257612 14.10533858610848	C 2.28936571473082 10.51310303253106 18.40768077141137
C 4.20210410669543 9.97759265939289 19.67750303863014	H 2.81686115071809 11.44528859973450 18.60557961334156
H 4.96499938477502 9.86933477596887 18.89661662063115	C 2.95665978459078 9.30245705695284 18.58263909446783
H 4.44673722145007 9.27179505412282 20.47645313837126	C -2.37849293749274 12.05155286502302 15.52227636220139
H 4.28795363921820 10.99223159360665 20.07871758419871	H -2.88659594640651 11.54957684709012 16.34509156086150
C -1.94189946723816 9.67975989421774 19.63715538683082	C -4.62801498089666 10.37564179980695 13.44120480757852
H -1.33342618185558 8.98590239961452 20.22745636879637	H -3.70263750322077 10.91804092198689 13.21372369902822
H -2.91203616060652 9.79933243346003 20.12135277569335	H -4.88977574184495 10.62660707342213 14.47351062815040
H -1.41468466011727 10.63992671532522 19.65507029765383	H -5.41195195163585 10.75545499486912 12.77948052294114
C 0.73778903605291 6.64510792256562 12.17264868152541	C 2.25672910223635 8.12466342147698 18.32747464060057
C 0.14709628785161 11.59027223124144 17.15500716485876	H 2.75662789845649 7.16645827216380 18.45911827102763
H 0.71435088699354 12.52422152384613 17.17935720872944	C -3.59329956680569 6.73860137821030 13.99626623571138
H -0.85367516445567 11.78192751575098 17.55761340447506	C 4.40052328980350 9.27151602350944 19.00753852808011
H 0.00837957513403 11.30265187491263 16.10435787225475	H 5.06778056102759 9.40307054960300 18.14645297948997
C 0.36244534525873 6.83121960931995 18.78743644526742	H 4.65638973484680 8.31750011118451 19.47794618528025
H 1.00078531357699 6.15846248631201 19.36579675140064	H 4.62452415983883 10.07339319295949 19.71836318544659
H 0.23327981850129 6.40125201527618 17.78547917198924	C -1.78036775358060 9.42858535426770 19.59986331680805
H -0.63186491435181 6.84660215836907 19.24738622244431	H -1.23584728915769 8.53650968096788 19.93179473401442
C -4.06062734999684 8.05480853953977 11.97976339516872	H -2.70102361673284 9.50827558032556 20.18051609835974
H -4.21032914424376 8.74183593281979 11.14847199228339	H -1.13459612917668 10.28328716634244 19.82528793196243
C -3.32804713498226 5.34782570386731 15.22523578652070	C 1.01824420291861 6.64545667544002 12.64990854737005

H -3.59362019477010 4.32362007682671 14.95098716579851	C 0.29685408016528 11.90255007379514 17.77160084144748
H -3.85143537262757 5.60608696496562 16.15209415423432	H 0.84133776096735 12.69313953123065 18.29619177363537
H -2.25462285626204 5.37161412988234 15.45576953485031	H -0.74148686290990 11.90481546524815 18.11653792148049
B 0.07304448756951 7.92702078893298 13.95840084221468	H 0.27161936037104 12.15998355275500 16.70593242501789
C -4.05920697301049 5.83025511932885 12.86182836852453	C 0.20509405092519 6.85200925603445 17.61176184284935
H -4.20118919368124 4.75946534422299 12.72531708326651	H 0.79927361377384 5.99024480228407 17.92810452289015
C 2.44717334875777 8.57193069660631 12.02548239821174	H 0.01734794849685 6.75997120906963 16.53455978936514
H 2.50886617339186 9.66350991338173 11.98765709434612	H -0.77026754797415 6.80633318455014 18.10831062515848
H 3.07651032636746 8.16148502024486 11.22885191362045	C -4.90624690336926 8.28152217699090 12.08453199526003
H 2.83878400900518 8.24260417030653 12.99255647722442	H -5.42408197584109 8.88818079176188 11.34295010284350
C 0.45080207650664 8.62408617740779 10.51437488118228	C -3.06898833414687 16.12657773421233 14.69214581236577
H -0.63061134178426 8.48404400542419 10.44969500250764	H -4.09002972229802 15.72140727711195 14.68063267801040
H 0.92828452643038 8.07644501509085 9.69388056646429	H -3.10671973706630 17.14095584464822 14.29280121583255
H 0.66704568073475 9.68894959713337 10.38562408499210	H -2.73323848037799 16.18485568020135 15.73735042490094
C -4.27870160251624 6.69111208084301 11.78765328700445	C -1.43828710185272 15.94562152516713 12.78379448954290
C 1.90288007569518 5.72087170226832 11.86398665901859	H -0.35227017840812 15.92587552602433 12.95340972673260
H 2.79574565993803 5.99527596060713 12.42946067267719	H -1.74733405685107 16.98769161124066 12.69197701308686
H 2.14065537036363 5.74717890579368 10.79440644423122	H -1.64654038513497 15.44660099962431 11.82762526362192
H 1.63379180553312 4.69358449202173 12.12732160136328	C -2.86025101937157 5.90466533755352 15.00767228455904
C -4.68118532347664 6.15632897055789 10.43970265670045	H -2.96012537451184 4.84021856635251 14.77684799241215
H -5.28049991822012 6.88387713391947 9.88410960345592	H -3.22395857253546 6.07728595690756 16.02621205258793
H -5.26214419480631 5.23405474856243 10.53358303092309	H -1.79234011027148 6.15558879139963 15.00229128997870
H -3.79661350826854 5.92678277334761 9.83177579487694	B 0.02293614467769 8.31688073157744 13.90249638014754
C -0.55189104368806 6.10996662259340 11.55342687561135	C -4.07049392323907 6.16684336336941 12.81828022478338
H -0.77000315874329 5.13040721296623 11.98944954521262	H -3.92390723837612 5.09986678666656 12.65705766606767

H -0.45902216422676 5.99436058083086 10.46809608281842 H -1.39884362541463 6.76814635717840 11.77174318518715	C 2.94706431838104 8.34223713327858 12.82935413523168 H 3.18149606839142 9.39666932443945 12.65454558016698 H 3.73963788651468 7.73319722110851 12.38139653934403 H 2.93458780514179 8.17239302505781 13.91030001957622 C 1.61176475786661 8.27158563620232 10.71382409595862 H 0.61181576734759 8.20996263023565 10.27937439068170 H 2.25794707262806 7.53764391007084 10.21841480393719 H 2.01331742101697 9.26903019344319 10.50891488744611 C -4.72688105162236 6.92096580235294 11.84699739467886 C 2.06579937863317 5.57326565862179 12.89774287110351 H 2.75942553626272 5.86814565564713 13.68784724709862 H 2.63534225683707 5.37111996747664 11.98332952819973 H 1.57421570015284 4.64494545124974 13.20461443469272 C -5.20277806972058 6.28810629909843 10.56660443856796 H -6.07423123527803 6.81240194524293 10.16255650428035 H -5.47509404860167 5.23908696135406 10.71820044633717 H -4.41893669050920 6.31485290508029 9.79908627097158 C -0.07368688426667 6.12145755048355 11.71739243415303 H -0.56546565474143 5.26989732448132 12.19789883418369 H 0.33820099594650 5.78887568306445 10.75842225620661 H -0.83594087427613 6.88566261595050 11.53541945118655
Nacnac^{Mes}ZnOB{(NDippCH)$_2$}: -4007.029880121355 E_h	**[Nacnac^{Mes}Zn]$_2$: -5567.498683630937 E_h**
Zn 1.77209368059339 8.07311725809021 15.09667972475072 O 1.36650550644669 8.30270856516209 13.34274955456828 N 3.61564948723860 7.80273374126823 15.68911459300305	Zn 2.64300758150056 2.28642526406573 5.81276762161217 N 2.03342380440939 1.57602673351300 7.56362145273025 N 4.28670080060830 3.10904935583277 6.56783267122283

N 0.82016550544546 7.62751184508411 16.71614580906611	C 2.70897416462438 1.67859941902235 8.70442870141882
N -0.01990301896639 10.00950916287920 12.06662725842504	C 3.94024553125163 2.34354443838709 8.82638673099562
N 1.28556264005621 8.56357797229134 10.86541686442202	H 4.37672084552565 2.34657191654596 9.81766159109818
C 4.69001897398264 7.94824184130176 14.75962943057442	C 4.66485202361652 3.03267332750375 7.83901991374136
C 5.51515992922284 9.08146830864706 14.80962973594603	C 2.13005561952597 1.05592540414187 9.95411131806192
C 1.49197808428461 7.26148499284366 17.81424249839451	H 1.17311887914037 1.52193025438396 10.21333119795595
C 3.86720329345713 7.31729339118173 16.90203945706116	H 2.81202195356203 1.16013572819544 10.79944608353056
C -0.75423942721806 10.73291543767099 13.04317901783591	H 1.91963833745642 -0.00713668493024 9.79376302073310
C 4.87702005432260 6.96195722069282 13.78052830224434	C 5.93912825588554 3.72353676939099 8.26615742428139
C -0.60775639293589 7.59650064149891 16.75924920628608	H 6.79873470277744 3.33606905547675 7.70835352787102
C -1.31662306328746 8.76434727189238 17.06268246041562	H 6.12149538210506 3.59199463851847 9.33386573292856
C 2.88504888430707 7.12585638269352 17.89098868138104	H 5.88743733837717 4.79523813248032 8.04419088187690
H 3.25806796598992 6.77854170036045 18.84623406512002	C 0.75100526755024 0.96229862150509 7.55151677895013
C 5.27650494980375 10.16843909914266 15.82106079840106	C -0.38704078500299 1.73549717494756 7.82443894541841
H 4.21590483169879 10.43242473453470 15.87629222814001	C -1.63821846008401 1.12075605779301 7.78408271562769
H 5.84341412043759 11.06637740538387 15.56152537920866	H -2.52083069566166 1.71730174377987 8.00786778908926
H 5.57546894438557 9.86926717318692 16.83337432328468	C -1.78686158101102 -0.22310080307772 7.44798450273359
C 5.27588502102586 6.89636462914789 17.24649101398751	C -0.64113733292457 -0.95868030911241 7.14362438650270
H 5.61864914838416 6.13456862342055 16.53693268794416	H -0.73785736205911 -2.00749955953545 6.86713704609573
H 5.32587052360669 6.48687568061776 18.25613988782268	C 0.62950127763432 -0.38746599659674 7.18587633390518
H 5.98161612315752 7.72803808877052 17.16611072164149	C -0.25485132269176 3.20278707600893 8.11752645100502
C 2.29151579363558 7.65811094634765 10.43600795097646	H -1.22051172590050 3.63062156785431 8.39908847567480
C -0.17718080761309 10.26287161711502 10.69307882349267	H 0.09825004418182 3.73872510907657 7.22596875051890
H -0.85340264636654 11.02568815488026 10.33288573811368	H 0.46707749446374 3.40429402400823 8.91620906318229
C 6.56415583701451 9.17908738598511 13.89575646710691	C -3.14948891510594 -0.85691189132425 7.36752407232035

H 7.20950758896698 10.05546846987835 13.92959258210126	H -3.89436595413214 -0.26926000674546 7.91182246896004
C 3.49843947740264 8.16478680932075 9.91307957864631	H -3.14394393134557 -1.86978167461516 7.78300024180326
C 0.70658060124963 6.94157968977419 19.06426566996504	H -3.48583999944737 -0.93573327141008 6.32580827489071
H 0.03210283138662 7.76541473393862 19.32000090069417	C 1.85454683375523 -1.18809343441223 6.84517964143024
H 1.37416118575120 6.75124450935122 19.90539317958655	H 1.58773429990710 -2.20914908924743 6.55984669690580
H 0.07084678611829 6.06224280902954 18.91346272296993	H 2.55720814287599 -1.23545396360887 7.68527318317116
C -1.27642164579708 6.39303405089054 16.49051387007683	H 2.40245133375378 -0.72762517537680 6.01261075188564
C 5.93346353455527 7.10348130989805 12.88349808327244	C 5.07051709151048 3.83672464025954 5.63152583517302
H 6.07281696913556 6.34488105711096 12.11637564007251	C 6.08758290536050 3.18478903654028 4.92020566239216
C 0.59951931996091 9.41227955653025 9.98611466011858	C 6.82143780952144 3.91433845158846 3.98454780804288
H 0.70158521255100 9.32527091685278 8.91296570042303	H 7.61973243034716 3.41275767528615 3.44053328912960
C -2.70762730190231 8.69571976780864 17.14692785334080	C 6.54576680802702 5.25242487435780 3.71451056000005
H -3.26300462928344 9.60051601636510 17.38593804280635	C 5.50228823294939 5.86566937881855 4.40910224417845
C -2.06669445263916 10.32629303560555 13.34900076951729	H 5.26293241076176 6.90778421186094 4.20260075649991
C 2.06752092917377 6.27362908696819 10.56005518981009	C 4.75583685640362 5.17955378902641 5.36518338834799
C -0.17101215306035 11.85672528392986 13.65501504406458	C 6.35029141725758 1.72219625069917 5.13802831239190
C 3.75842387316118 9.66213232464734 9.89215800083883	H 7.24596348394262 1.40450513283513 4.59798753797512
H 2.82292856466026 10.16357735571861 9.61935519843585	H 5.50836280712801 1.12399732639511 4.76342464050072
C 3.06827190875428 5.40226055061084 10.12684888215428	H 6.46978725572009 1.47468014250371 6.19814366725302
H 2.92135878775355 4.32972010101117 10.20629880076456	C 7.31775135510692 6.00914464309914 2.66744193675499
C 3.95411314278257 5.77963910863267 13.70312713367153	H 7.59263477638493 7.00940240262806 3.01820629783925
H 3.86781746173416 5.26243521050568 14.66598400376226	H 6.72000924739296 6.13832210178552 1.75625376090953
H 4.30083703607981 5.06838518580404 12.94972043267317	H 8.23495025156669 5.48153785435853 2.39056914745999
H 2.94659216317115 6.10110648663425 13.40680225446494	C 3.62800746699279 5.85076419398473 6.09775383657129
C -3.39775732249191 7.50466703483411 16.93189330053000	H 3.50236086824563 6.88235720884236 5.75808970048299

C 4.46581936594266 7.25439971531786 9.48571263460324	H 3.79337156319259 5.86235855769464 7.18149752777189
H 5.40336381642570 7.61628398037640 9.07500364708017	H 2.68096260805946 5.31844036658531 5.93833657601635
C -2.66474247219893 6.36458263759720 16.59929187578624	Zn 1.76519431368122 2.28717101252798 3.64876826035315
H -3.18960297373295 5.43231726142043 16.39813171062026	N 2.37419994823698 1.57697205515855 1.89769353832478
C 6.79334709761805 8.19880908689507 12.93121993061535	N 0.12195156070401 3.11149821054290 2.89387480884532
C 4.25350144256477 5.88572152457404 9.58810438421271	C 1.69845920707474 1.68004918179999 0.75700890738855
H 5.01719581578589 5.19127732198192 9.24764094901641	C 0.46776836747360 2.34606267282164 0.63521243888033
C 0.74910115129283 5.75684031231684 11.11089294770564	H 0.03125820876965 2.34958538578776 -0.35604494010298
H 0.48454245068384 6.38841581522578 11.96775275694785	C -0.25615547022863 3.03580912466208 1.62265635102767
C -2.67279690569914 9.12349660139833 12.64904880979682	C 2.27650718580546 1.05668123818491 -0.49274471911502
H -2.24778794615910 9.08411116531873 11.63871799340595	H 3.23408979123103 1.52129220030094 -0.75203772155826
B 0.91767548346090 8.90713307594080 12.23878374175500	H 1.59461827745930 1.16181391467458 -1.33802682525712
C -2.27569658519296 7.82909450821320 13.37354098382239	H 2.48540450566906 -0.00668434541298 -0.33238382402917
H -1.18851836529513 7.73163616350687 13.45671390238629	C -1.52957629491427 3.72825783669441 1.19551818686079
H -2.66097918897686 6.95344435541312 12.83692990103138	H -2.38974298991020 3.34160940515699 1.75302390986627
H -2.68935387090205 7.82294633459427 14.38613136146491	H -1.71189882326501 3.59728915360086 0.12773193460580
C 0.81345903004320 4.31477658285622 11.61907864246420	H -1.47666646468820 4.79982062743029 1.41786684686409
H 0.94193373417456 3.59738518597792 10.80008983762849	C 3.65625364788277 0.96245644419438 1.90924235331614
H -0.12539145553646 4.06245472246749 12.12389954939622	C 4.79459870257808 1.73486786198635 1.63527524814513
H 1.63226876553790 4.16911811039522 12.33239467923955	C 6.04539385300444 1.11931817643541 1.67473617991175
C -0.58692308315431 10.05518374859213 17.29462680677016	H 6.92823077741457 1.71523191555917 1.45015222962222
H 0.19322427050255 9.95350199107229 18.05759855936460	C 6.19343713997782 -0.22459081786530 2.01094875744069
H -1.27839180964261 10.84271031699713 17.60197073063119	C 5.04748720956212 -0.95934989190514 2.31638408904221
H -0.09520235838538 10.39469841256519 16.37376404519366	H 5.14372285569336 -2.00818130014993 2.59299672238013
C -4.90038162800373 7.45964875753917 16.98914223428702	C 3.77717505802639 -0.38730862008662 2.27504019477214

H -5.30138500334102 8.27571005885600 17.59692259093909	C 4.66307656526918 3.20215387160735 1.34183885593770
H -5.25621357547604 6.51284258986791 17.40699182871699	H 5.62900318996933 3.62960404023356 1.06061001873421
H -5.33014369931980 7.55409403097139 15.98352317833097	H 4.30967927599896 3.73839405708088 2.23307903765257
C -2.77045002539485 11.04270802530881 14.31759933342557	H 3.94160829613819 3.40372677751863 0.54274170800459
H -3.78146312050653 10.74591414355507 14.57918930185187	C 7.55572779113322 -0.85923974812023 2.09044541168041
C -0.50721881919855 5.17159476736260 16.07071678336314	H 8.30072892630636 -0.27169232323390 1.54620969359847
H -1.17717657837363 4.31968994243826 15.93033800741539	H 7.54943968401241 -1.87184346622382 1.67431898571697
H 0.26046712462375 4.89036267422421 16.80041600254391	H 7.89244015227471 -0.93891672951081 3.13197652275406
H 0.01635382116123 5.35017022124383 15.12165654763733	C 2.55188350959424 -1.18717376905265 2.61663506669449
C 1.23375188661575 12.29761969730995 13.28897258866543	H 2.81832466647753 -2.20821209833961 2.90237701231767
H 1.46325358625114 11.86786687955432 12.30703151071396	H 1.84892296471288 -1.23463878239003 1.77679202913092
C 4.14019986782764 10.15118531170080 11.29876689735639	H 2.00446398485892 -0.72604377074607 3.44915345509268
H 3.39092622670136 9.86232472171439 12.04158103026599	C -0.66120627518957 3.83974171652599 3.83025741403968
H 4.23801157751387 11.24360327127860 11.31139634097495	C -1.67949371551395 3.18880009318333 4.54087983227117
H 5.09401261262317 9.71411437969078 11.60937467291683	C -2.41306271538729 3.91897391731733 5.47618515071468
C -0.91329589666709 12.54754609325839 14.61555536372044	H -3.21235783860178 3.41829461948730 6.01957880829103
H -0.48559922319707 13.41860221152663 15.10431401537396	C -2.13603933251655 5.25677647728553 5.74662159029350
C 4.81740391836010 10.09342524936681 8.87624112716375	C -1.09145546809394 5.86890509546024 5.05284277279724
H 5.81874495050685 9.74736123534991 9.15815061144486	H -0.85107904137040 6.91074411456807 5.25950298467141
H 4.85736207356555 11.18668121907239 8.82726936356248	C -0.34510146083453 5.18206404849751 4.09711242413416
H 4.59585527598027 9.71467359728650 7.87263023070392	C -1.94392672849585 1.72663241022340 4.32225526859590
C -2.19897394693483 12.14226037720955 14.94661781593183	H -2.83938110057453 1.40947523831211 4.86296747444796
H -2.76476704680747 12.69273669167171 15.69392942128826	H -1.10222328380920 1.12728057142489 4.69547138054394
C 7.89378810776611 8.35558848801834 11.91785251765525	H -2.06484258679408 1.48004574739432 3.26207077699211
H 7.54096385304162 8.92556162964884 11.04800597858413	C -2.90765648713404 6.01381224290894 6.79371325097285

H 8.23964317485524 7.38434864277351 11.55241599637056 H 8.75058249590890 8.89330061897517 12.33504167801856 C 2.25295619163431 11.73479912980944 14.28965883718382 H 2.04584568772915 12.10378941399017 15.30217689292425 H 3.27333297093790 12.02771369213324 14.01680825984477 H 2.21369021533195 10.63905588485738 14.30227467485301 C -0.36772372824453 5.89679049477568 10.06387533497799 H -0.48317251072023 6.93542252000634 9.74253856367856 H -1.32471907324905 5.55993276736850 10.47940303588602 H -0.14217363635615 5.28437190826925 9.18271899534775 C -4.19484572827726 9.20595049318874 12.51119247638568 H -4.69627506231178 9.10943407204559 13.48132721837126 H -4.55401899391795 8.38679663151796 11.87935918570378 H -4.50962636490736 10.15189216522061 12.05766954858662 C 1.37399690208347 13.81930908002849 13.17806101355828 H 0.60881178139301 14.24108577210339 12.51854413272241 H 2.35791681048499 14.07334044361921 12.76913631929695 H 1.29113332786567 14.31168533953158 14.15340298613594	H -3.16880104868542 7.01971075119276 6.44878988823193 H -2.31553883347948 6.12925331110818 7.71045864240975 H -3.83262686725161 5.49419796512397 7.05969781480762 C 0.78375763006949 5.85225243689384 3.36518915024743 H 0.91061334735144 6.88350402113528 3.70544332986449 H 0.61865639979668 5.86465403012965 2.28140964011874 H 1.73011333753537 5.31867749931471 3.52452875483176
{(HCDippN)$_2$}BOBpin: -1634.929067902274 E_h	**B$_2$pin$_2$: -823.230375444391 E_h**
N -0.27767672420927 9.42334436577732 12.03597161894040 N 1.05407548357170 8.22094710087637 10.62463590420619 C -0.89793908864084 10.01437076174841 13.17183385162329 C 2.03918285628917 7.37591528596370 10.03297344001831 C -0.54052258376547 9.80678823130487 10.71140455350665 H -1.27453139924964 10.56413597293417 10.47660534266072 C 3.31935417084815 7.89890552438230 9.78303549152910	B 2.99647900353390 7.63231442239154 4.06880138345847 O 1.71731978187177 7.17740910901088 3.85202156783805 O 3.59569910721975 8.10143587688927 2.92390221534774 C 1.50439144922485 7.14191401881129 2.40628823254165 C 2.56648832135963 8.16966958057668 1.88799062955685 C 0.05974267529106 7.51005098666192 2.11445723968233 C 1.78790264588254 5.70905948314124 1.96121330065336

C 0.24836159190121 9.09325738938099 9.87503711887983	C 2.05588252001086 9.60860061230225 1.88087759079686
H 0.30910242207340 9.12819814238430 8.79662364614057	C 3.19563902120082 7.82407300652325 0.54909582098991
C -2.24180091904982 9.71523298427296 13.45954408182512	H -0.10860356145079 7.57132546294021 1.03361458915338
C 1.70865565492961 6.04569690665699 9.72964400163563	H -0.21099139528627 8.46551595705514 2.56770262587917
C -0.13569569223634 10.85772078099751 14.00087555150896	H -0.60255900134467 6.73985554225316 2.52050423568369
C 3.66418047355870 9.32927259015195 10.15588224582716	H 1.58783061136296 5.57601225250869 0.89322545029313
H 2.72667225063541 9.89559564002169 10.20510778535828	H 1.13905123461885 5.03116748285422 2.52307290965889
C 2.70318525471720 5.22944404247613 9.18750101465614	H 2.82701503234689 5.43084605015237 2.16206963559285
H 2.47865556537268 4.19308556996301 8.95210625022234	H 1.32180638018239 9.76912273747494 1.08480944191630
C 4.28030373543085 7.04813471986027 9.23573695330397	H 2.90229460511230 10.28082822999508 1.71402205398941
H 5.28052117388928 7.42217609066823 9.03804973871230	H 1.59849279220583 9.86867531643926 2.84029917313629
C 3.97677174431658 5.72446319261221 8.94391803474320	H 2.43239906454102 7.79329890066217 -0.23626624699273
H 4.73856149730736 5.07509775572343 8.52138591882470	H 3.70648996351157 6.85986035997933 0.58133419270878
C 0.32808191748939 5.49088630107379 10.02512426561503	H 3.92930546761676 8.59039091538860 0.28231339114695
H -0.34995047530986 6.34179075635485 10.15760900566340	B 3.75515838328411 7.61768442312303 5.59104708386602
C -3.07947771916563 8.83238050400592 12.55353684805544	O 5.03431617004404 8.07259389668102 5.80782679451489
H -2.42812127725678 8.44344998928776 11.76395387729665	O 3.15594054949252 7.14855940099526 6.73594597200860
B 0.74320249395657 8.41037755333230 12.01093729487811	C 5.24724503085427 8.10808816453954 7.25356007271885
C -3.66051098456920 7.62496869616465 13.29875032102023	C 4.18515214413024 7.08032812415630 7.77185693554083
H -2.85683660886606 7.03086300828283 13.74049943517413	C 6.69189533013489 7.73995625594299 7.54539010757866
H -4.22508925547413 6.99170972149974 12.60502082871517	C 4.96372884619389 9.54094118390420 7.69863672682009
H -4.34489874138905 7.93362884971411 14.09724045171924	C 4.69576323521996 5.64139896094510 7.77896779675303
C 0.34572659276120 4.69837698639444 11.34176903529595	C 3.55600097439349 7.42592069916558 9.11075254458754
H 1.00814087072109 3.82888246153467 11.25660875141802	H 6.86024223165445 7.67868135271049 8.62623262880590
H -0.66009794213644 4.34185045795120 11.59205745787653	H 6.96263276493435 6.78449273681250 7.09214367295325

H 0.70716915397828 5.31848014261426 12.16769194264242 C -2.80596925563966 10.26444262107796 14.61044886116454 H -3.84234896392283 10.04596248508724 14.85489062493070 C 1.28548054364669 11.26840627998264 13.65627092325660 H 1.57555032366145 10.75063383711345 12.73555213666610 C 4.30816222811118 9.37027074655575 11.55144261361346 H 3.66035806509453 8.91157072807682 12.30497419442841 H 4.51063820196659 10.40580065046590 11.84998547887850 H 5.25871547659314 8.82380241389997 11.54859551822005 C -0.74028206818962 11.37009033247475 15.15117381226526 H -0.17038437296873 12.02101332160834 15.80930365492193 C 4.56217636176267 10.01888992679359 9.12388721894623 H 5.57111454555915 9.59257647372857 9.10976449922550 H 4.66387350005949 11.08115450828855 9.37042150481447 H 4.14538458094499 9.93926867093296 8.11452048274983 C -2.06089495068698 11.07431249791927 15.45826414447513 H -2.51521694973932 11.48474732800939 16.35597073921612 C 2.28836997897480 10.87413116267311 14.74737115735774 H 2.05867566944093 11.36910888330626 15.69820091767124 H 3.30118364354111 11.17073199258351 14.45315805041331 H 2.29016662891271 9.79361527137177 14.91878563491658 C -0.22382237184823 4.63266244240774 8.88145050393301 H -0.19229409315399 5.17144772677035 7.92892830101040 H -1.26436750086180 4.35986705258475 9.08785143994608 H 0.33902178556442 3.70054732505809 8.76275047441895	H 7.35419400983545 8.51015454127284 7.13934360649596 H 5.16380084814770 9.67398797201758 8.76662464383819 H 5.61257759787193 10.21883610231875 7.13677757157077 H 3.92461539722164 9.81915118868052 7.49778115063802 H 5.42984059750986 5.48087858734135 8.57503518155547 H 3.84935375376542 4.96916803046555 7.94582319691846 H 5.15315313922848 5.38132715442136 6.81954550450191 H 4.31924131128947 7.45669663055966 9.89611416807490 H 3.04514646309679 8.39013150518658 9.07851566701614 H 2.82233750268491 6.65959978474801 9.37753454021103

C -4.19316948428417 9.64998289611272 11.88196740425694 H -4.90141525212988 10.03395072268023 12.62508710835871 H -4.75139083214933 9.02796755033480 11.17343309920074 H -3.78452320442236 10.50827656805932 11.33857370529514 C 1.35108241238437 12.77591824702027 13.36879029024302 H 0.64201664433717 13.05742718776992 12.58359886882024 H 2.35835873391564 13.05623320450504 13.04086570818634 H 1.11327772609229 13.36206288758572 14.26376735231792 B 0.90335569856757 7.38630455623714 14.27032403539840 O 1.73853987493220 7.15621492355490 15.33795776122884 O -0.42158617369412 7.11584470946919 14.53216784621564 C 0.87640059412919 6.94732572037502 16.49556170228996 C -0.46291356034347 6.45804384858192 15.83515412717292 C 1.53439329781554 5.93856252325247 17.41978843231342 C 0.73169636613592 8.29987095896571 17.18854018370363 C -0.48535633729384 4.95627659553280 15.56614948728269 C -1.71882567136203 6.89256036930128 16.57100204193672 H 0.86800659306538 5.69245794811792 18.25369625750051 H 1.79323411333670 5.01896524817905 16.89116568309152 H 2.45306238760673 6.36545129688448 17.83306051255255 H 0.15865655580651 8.21361031869512 18.11706224130179 H 1.72906516406354 8.67900513183243 17.43071332602787 H 0.23725912406757 9.02869981227190 16.53776626171865 H -0.58521281932554 4.38462858284413 16.49427865268786 H -1.34173099964111 4.72688373859880 14.92488781573178	

H 0.42385664430839 4.63250106733777 15.04955479559924 H -1.69824164149406 6.52719477213115 17.60361822784869 H -1.81775764332178 7.98058440218253 16.57806461509044 H -2.60249275675242 6.47287560650410 16.08173144872267 O 1.38360794639730 7.80643544994263 13.07083606096923	

References for SI

s1 S. Schulz, T. Eisenmann, U. Westphal, S. Schmidt, U. Flörke, *Zeitschrift für anorganische und allgemeine Chemie* **2009**, *635*, 216-220.

s2 J. Prust, A. Stasch, W. Zheng, H. W. Roesky, E. Alexopoulos, I. Usón, D. Böhler, T. Schuchardt, *Organometallics* **2001**, *20*, 3825-3828.

s3 Y. K. Loh, L. Ying, M. Ángeles Fuentes, D. C. H. Do, S. Aldridge, *Angewandte Chemie International Edition* **2019**, *58*, 4847-4851.

s4 J. Cosier, A. M. Glazer, *Journal of Applied Crystallography* **1986**, *19*, 105-107.

s5 A. Technologies, **2011**.

s6 G. Sheldrick, *Acta Crystallographica Section A* **2015**, *71*, 3-8.

s7 G. Sheldrick, *Acta Crystallographica Section C* **2015**, *71*, 3-8.

s8 O. V. Dolomanov, L. J. Bourhis, R. J. Gildea, J. A. K. Howard, H. Puschmann, *Journal of Applied Crystallography* **2009**, *42*, 339-341.

s9 J. Bykowski, J. Sinclair, J. Trach, M. J. Ferguson, E. Rivard, *Dalton Transactions* **2023**, *52*, 1602-1607.

s10 G. Bendt, S. Schulz, J. Spielmann, S. Schmidt, D. Bläser, C. Wölper, *European Journal of Inorganic Chemistry* **2012**, *2012*, 3725-3731.

s11 F. Neese, *WIREs Computational Molecular Science* **2012**, *2*, 73-78.

s12 F. Neese, *WIREs Computational Molecular Science* **2022**, *12*, e1606.

s13 S. Grimme, A. Hansen, S. Ehlert, J.-M. Mewes, *The Journal of Chemical Physics* **2021**, *154*, 064103.

s14 J.-D. Chai, M. Head-Gordon, *Physical Chemistry Chemical Physics* **2008**, *10*, 6615-6620.

s15 E. Caldeweyher, C. Bannwarth, S. Grimme, *The Journal of Chemical Physics* **2017**, *147*, 034112.

s16 F. Weigend, R. Ahlrichs, *Physical Chemistry Chemical Physics* **2005**, *7*, 3297-3305.

s17 J. K. B. E. D. Glendening, A. E. Reed, J. E. Carpenter, J. A. Bohmann, C. M. Morales, P. Karafiloglou, C. R. Landis, F. Weinhold, **2018**.

s18 E. D. Glendening, C. R. Landis, F. Weinhold, *Journal of Computational Chemistry* **2019**, *40*, 2234-2241.

s19 T. Lu, F. Chen, *Journal of Computational Chemistry* **2012**, *33*, 580-592.

s20 R. Bianchi, G. Gervasio, D. Marabello, *Inorganic Chemistry* **2000**, *39*, 2360-2366.

Conclusions and outlook

Future work in this area should attempt to generalize the powerful bond-forming methodologies described here. Alternative metal halide precursors could be readily screened to establish the viability of this procedure with, for example, the isostructural heavier group 12 congeners, or other abundant 3d metals.

Additionally, the use of B–O extrusion as a metal-metal bond forming reaction could be generalised to other systems in which a (Nacnac^{Mes})Zn 'zincyl' fragment is installed at a range of other metal centres for which cleavable M–O bonds can be accessed. One potentially fruitful line of investigation in this area may be the synthesis of coinage metal-zinc bonded species (which are unknown beyond copper) given the low M–O bond strengths for this triad.

Statement of Authorship for joint/multi-authored papers for PGR thesis

To appear at the end of each thesis chapter submitted as an article/paper

The statement shall describe the candidate's and co-authors' independent research contributions in the thesis publications. For each publication there should exist a complete statement that is to be filled out and signed by the candidate and supervisor **(only required where there isn't already a statement of contribution within the paper itself).**

Title of Paper	**Zinc borylation and reduction by a diborane(4) species via B-O bond formation**
Publication Status	□Published □ Accepted for Publication √Submitted for Publication □Unpublished and unsubmitted work written in a manuscript style
Publication Details	Liam P. Griffin and Simon Aldridge; Zinc borylation and reduction by a diborane(4) species via B-O bond formation.

Student Confirmation

Student Name:	Liam P. Griffin		
Contribution to the Paper	Performed all synthetic, spectroscopic and crystallographic work, as well as all quantum chemical calculations. Analysed and interpreted data. Wrote the manuscript and prepared the supporting information.		
Signature	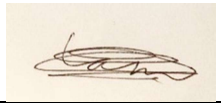	Date	19/09/2024

Supervisor Confirmation

By signing the Statement of Authorship, you are certifying that the candidate made a substantial contribution to the publication, and that the description described above is accurate.

Supervisor name and title: Professor Simon Aldridge		
Supervisor comments: I can confirm that Mr Griffin made a substantial contribution to the work described in this chapter, and that the above description is accurate.		
Signature 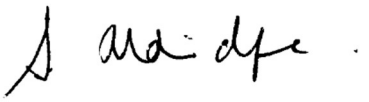	Date	20 September 2024

Probing main group-centred ligand properties via X-ray spectroscopy

Introduction

In order for the ligand properties of aluminyl (and other trielyl) ligands to be properly understood, comparative studies of their ligand properties are required, both within group 13 and to other X-ligands in other areas of the Periodic Table. Finding ways in which meaningful comparative data can be generated between aluminyl and boryl ligands, and common ligands such as a simple methyl group or O-donor ligand, will give significant insights as we are able to rationalize the properties of these exotic ligands in relation to more well understood fragments.

Taking further advantage of the (Nacnac^{Ar})ZnX molecular platform, which was shown in chapter 2 to be highly flexible in the X-ligands it can support, we sought to investigate this class of compounds by other means. In a collaboration with the Lovelock group at the University of Reading, X-ray spectroscopic techniques were used at the Diamond Light Source to probe the electronic structure at zinc for a family of these compounds, where X = BeCp, Al(NON), Si(TMS)$_3$, Zn(Nacnac^{Mes}), OB{(NDippCH)$_2$}, Bpin and Me. The data so generated proved to be highly information rich, and was interpreted in terms of how the electronic structure was affected by the X-ligand, thereby providing information on the donor properties at play.

These complexes proved to be highly suitable for such an application. The Nacnac supporting ligand ensured monomeric complexes and three coordinate zinc centres, so spectra were directly comparable without any differences due to geometric effects. Additionally, the d^{10} zinc centre avoided any complications to the spectra as a result of pre-edge effects. The resulting data was compared both to simple models of bonding and ligand design, as well as computationally generated parameters for the complexes under investigation.

Quantifying X-ligand donor properties via X-ray spectroscopy of (Nacnac^{Ar})ZnX species

Liam P. Griffin,[a] Lewis Parker,[b] Frances Tower-Tompkins,[b] Shusaku Hayama,[c] Kevin R. J. Lovelock*,[b] Josef T. Boronski*,[a] Simon Aldridge*[a]

[a] Mr. L. P. Griffin, Dr. J. T. Boronski, Prof. S. Aldridge
Inorganic Chemistry Laboratory, Department of Chemistry
University of Oxford
South Parks Road, Oxford, OX1 3QR (UK)
E-mail: simon.aldridge@chem.ox.ac.uk, josef.boronski@chem.ox.ac.uk
[b] Mr L. Parker, Miss F. Tower-Tompkins, Prof. K. R. J. Lovelock
Chemistry and Pharmacy Building
University of Reading
Pepper Ln, Reading RG6 6DX
Email: k.r.j.lovelock@reading.ac.uk
[c] Dr. S. Hayama
Diamond light source
Harwell Science and Innovation Campus
Fermi Ave, Didcot OX11 0DE
Email: shusaku.hayama@diamond.ac.uk

Abstract

X-ray spectroscopic measurements have been performed at the Diamond Light Source on a family of compounds of the form (Nacnac^{Ar})ZnX, (X = AlNON, BeCp, Si(TMS)$_3$, Me, Zn(Nacnac^{Mes}), Bpin and OB{(NDippCH)$_2$}). The resulting data regarding the electronic centre have been interpreted in terms of the donor properties of the X-type ligands, providing a new and unambiguous approach to evaluate such properties. The resulting trends have been compared to existing theories of chemical bonding, as well as computationally generated parameters, allowing these to be benchmarked based on experimentally generated data.

Introduction

The chemical behaviour of a metal centre is heavily influenced by the electronic structure induced by its supporting ligand set.[1] Indeed, ligand design, encompassing both steric and electronic properties, has been widely employed to allow for the isolation of complexes featuring metals in novel oxidation states, or which display unique reactivity. In order to assist these efforts, numerous experimental and computational strategies have been developed in order to quantify and compare certain ligand properties, such as σ-donor strength.[2-4]

One example of such a method is the Tolman electronic parameter (TEP), which establishes the donor strength of an L-type ligand by measurement of the A_1 carbonyl stretching mode of a complex of the form $Ni(CO)_3L$.[5] However, such approaches may be flawed if they rely on indirect probes (i.e., those based on ancillary ligands such as carbonyl ligand stretching frequency) in order to gauge the donor properties of a particular ligand. In this example for instance, the TEP is a function of both the σ-donor and π-acceptor properties of L, with the deconvolution of these two contributions presenting a non-trivial task. Hence, both theorists and experimentalists have made extensive efforts to develop more comprehensive, universal systems for the evaluation of ligand properties.[6]

In recent decades, a versatile class of exotic ligands featuring electropositive main group donor atoms has emerged.[7-11]These may behave as supporting ancillary ligands or as reactive sites, which act co-operatively with the metal to which they are coordinated, in order to facilitate chemical transformations. In particular, anionic boryl and aluminyl systems (of the form $[EX_2]^-$, where E = B, Al) have attracted much attention due to their potent σ-donor properties and their isoelectronic relationship with carbenes.[12] The electron donating/reducing nature of these ligands has been shown to induce novel reactivity from the metal centres to which they are coordinated. For example, these ligands have been used to induce nucleophilic reactivity in a range of typically electrophilic metals from across the Periodic Table. Additionally, the *trans* labilising effect of these ligands can serve to speed up pre-catalyst activation, *e.g.* in borylation chemistry.

In the more established boron case, the interest in these systems extends to their applicability in catalytic processes, most significantly C–H borylation.[13] Attempts to extend this synthetically powerful methodology to the highly abundant element aluminium are a current topic of much research.[14] However, in order for this "next generation" of ligands to find wider application, a comprehensive understanding of their electronic properties is necessary, and the relative σ-donor strengths of electropositive, main group-centred X-type ligands must be assessed. Whilst such analysis has previously been carried out computationally for a variety of systems, these results have not been validated though direct physical measurements of their respective electron releasing characteristics.[12] Crucially, this knowledge could allow for the determination of the most suitable ligand for a particular synthetic application, making it important from both fundamental and applied perspectives.

To this end, we have investigated the use of X-ray spectroscopic measurements to probe the electronic structure of a metal centre, providing direct experimental data quantifying the electron richness and frontier orbital structure induced by its ligand set.[15] Thus, we believe this experimental technique is able to circumvent many of the pitfalls that plague indirect measures of ligand σ-donor strength and thereby offer an unambiguous approach to investigate an emerging class of main group donor ligands.

In order to permit meaningful comparisons that eliminate secondary effects such as coordination geometry and ancillary ligand identity, we desired a modular molecular platform which allowed for the electronic effects of numerous X-type ligands to be screened at the same reporter metal ion. To this end, we pursued complexes of the synthetically versatile (Nacnac^{Ar})Zn moiety. Species of the type (Nacnac^{Ar})ZnX can be generated for a wide range of common and exotic X-type ligands (boryl, aluminyl, methyl, silyl, beryllyl, boryloxy) by routes including salt metathesis, reduction and methanolysis.[11, 16-18] Additionally, the availability of the Zn–Zn bonded species [(Nacnac^{Mes})Zn]$_2$ provides an ideal reference species in the form of a compound bearing a *bona fide* zinc(I) centre, which permits an assessment of the validity of formal oxidation state descriptions based on Pauling

electronegativities of a range of compounds.[19, 20] Comparability between measured spectra is also ensured through the use of this molecular platform; in addition to the geometric constraints enforced by the chelating β-diketiminate framework and the sterically bulky Dipp/Mes substituents which ensure a tricoordinate zinc centre, such species also feature a d^{10} metal ion, avoiding any complications arising from pre-edge features.[15]

In addition to allowing for comparisons between the donor strengths of different X-type ligands, the data collected provide a set of experimentally generated parameters, against which those generated by computational methods can be validated. This benchmarking of calculated parameters (for a range of both common and unusual bonding combinations) offers the potential for a scale of donor properties to be extrapolated beyond the compounds measured in this study, *e.g.* by computational methods.

Results and Discussion

Sample selection, synthesis and measurement

A range of (Nacnac^{Ar})ZnX species reported in the literature were prepared, as well as a novel zinc silyl species (Nacnac^{Mes})ZnSi(TMS)$_3$. This species, bearing the hypersilyl ligand, was prepared by simple salt metathesis between the potassium salt of the hypersilyl anion and (Nacnac^{Mes})ZnI (procedure and characterising data described in the supporting information). The full list of zinc complexes is given below (figure 1), along with acronyms used in the data discussion for clarity.

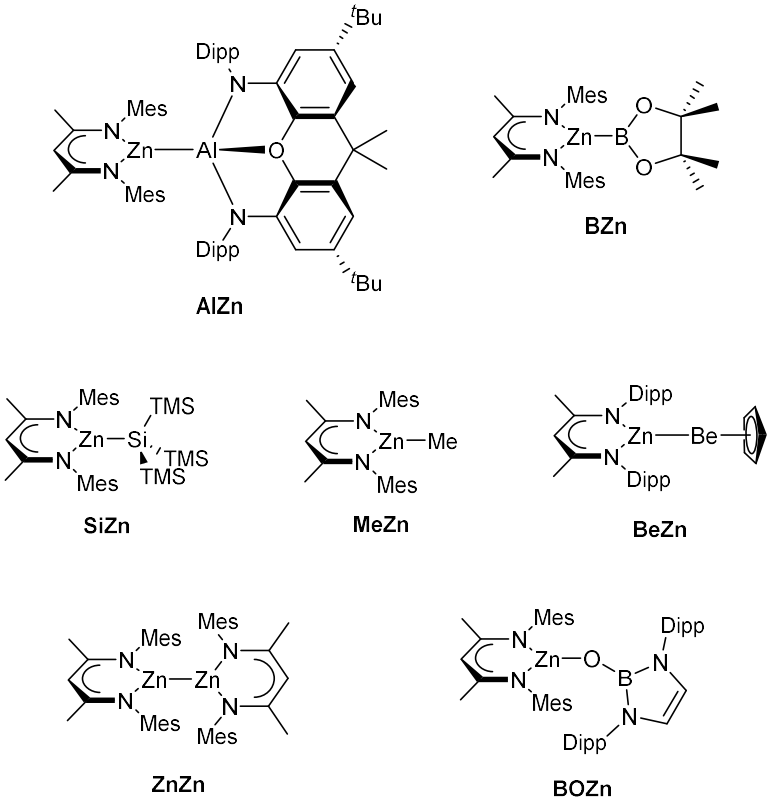

Figure 4: Zinc β-diketiminate compounds investigated in this study.

Spectroscopic measurements were carried out at the Diamond Light Source synchrotron facility on the I20 beamline in conjunction with the Lovelock group from the University of Reading. Preparation of toluene solutions of all compounds was carried out immediately before measurement. Data processing, computational structure optimisation and spectra simulation were conducted by the Lovelock group. Subsequent computational analyses (NBO, QT-AIM, Bader charge analysis) and data interpretation were conducted by the Aldridge group. Further details are available in the supporting information.

Data analysis

Samples of all seven compounds were measured using zinc 1s high energy resolution fluorescence detection-X-ray absorption near edge structure (HERFD-XANES), zinc 1s non resonant valence to core-X-ray emission spectroscopy (NRVtC-XES), and zinc 1s resonant valence to core-X-ray emission spectroscopy (RVtC-XES). These methods directly probe the energies of p-based atomic orbitals, *i.e.* the orbitals most involved in Zn–X bonding interactions. Each technique is discussed in turn, before comparison is made with computational data.

(i) HERFD-XANES

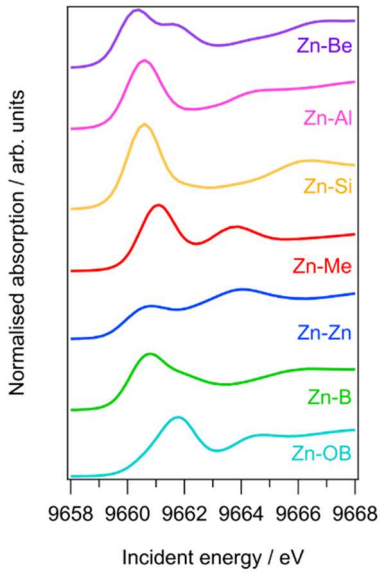

Figure 5: HERFD-XANES spectra of compounds ***BeZn, AlZn, SiZn, MeZn, ZnZn, BZn*** *and* ***BOZn****.*

Zn 1s HERFD-XANES probes the promotion energy of a Zn 1s electron into the zinc-specific unoccupied molecular orbitals (UMOs).[21] The Zn K-edge (leftmost peak) provides a measure of the electron richness at zinc, with a lower incident photon energy indicating that less energy is required to ionise that electron, *i.e.* the electron is less stabilised. By this measure, lower incident energy indicates a more electron rich, Lewis basic zinc centre, and therefore a more strongly sigma donating X-ligand. To the right of the edge energy (the EXAFS region) are features generated by the interaction of the ionised electron with nearby atoms, which provides structural information. This region is not

analysed in this study. Comparing the edge positions, here we observe (figure 2) that **BeZn** features the most electron rich zinc centre, consistent with beryllium being the most electropositive (χ = 1.57) of the donor atoms studied. As expected, the oxy-bound species **BOZn** leads to the most Lewis acidic zinc centre as a result of the strong electron withdrawing effect of this electronegative (χ = 3.44) O-donor ligand. Interestingly, **AlZn** and **SiZn** yield spectra with almost identical peak maxima positions, implying equivalently strong σ-donation, despite significant differences in the elemental electronegativities (χ = 1.61, 1.90 for Al and Si respectively). Likely features of the supporting ligand framework at the X-type ligand donor-atom centre (*i.e.* an electron withdrawing bis-amide ligand at aluminium versus an electron donating TMS groups at silicon) is having a significant influence. Remarkably, the boryl ligated species **BZn** leads to an incident energy equal to that of the symmetric species **ZnZn**, again despite significant electronegativity differences (χ = 2.04, 1.65 for B and Zn respectively), presumably due to the possibility for closer approach of the smaller boryl ligand. The methyl substituted species **MeZn** leads to values intermediate between **BZn** and **BOZn**, aligning well with the electronegativity of carbon (χ = 2.55) as compared to boron and oxygen.

Based on these data, one could tentatively assign a formal oxidation at zinc based on electron richness versus **ZnZn**, which would yield values greater than 1 for **BZn**, **MeZn** and **BOZn**, and values less than 1 for **BeZn**, **AlZn** and **SiZn**. This is in line with Pauling electronegativities in all cases except for **SiZn**, which would predict the opposite formal assignment.

The form of these spectra is also informative, will all seven indicating that the three-coordinate geometry at the metal centre (based on either crystallographic data or a calculated structure) is retained in solution in all cases.[15]

(ii) Non-resonant Valence to Core-XES

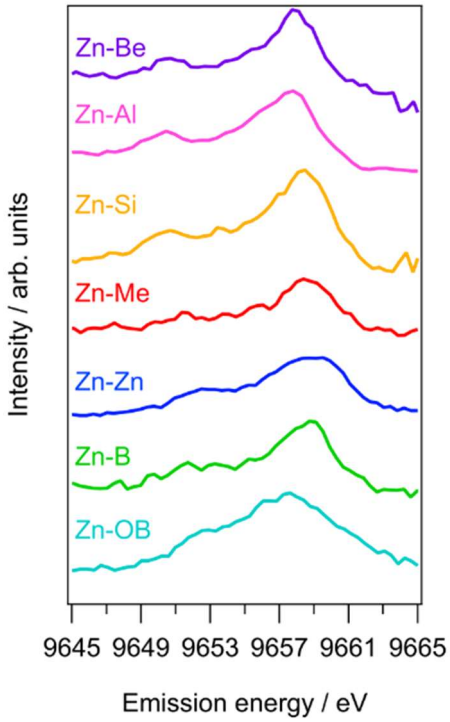

*Figure 6: VtC-XES spectra of compounds **BeZn**, **AlZn**, **SiZn**, **MeZn**, **ZnZn**, **BZn** and **BOZn**.*

Non Resonant Valence to Core X-ray Emission Spectra were also measured for all seven compounds.[21] For these measurements, the refilling of the Zn 1s core hole by a Zn 4p valence electron is probed, meaning that the peak maxima positions relate to zinc p-based Occupied Molecular Orbitals (OMOs), and are reported as emission energy, meaning that a higher value relates to an orbital that is closer in energy to an unbound electron, *i.e.* less stabilised by bonding interactions with the X-ligand fragment. Here, **ZnZn** gives the highest value, followed by a decrease in the order **BZn** > **MeZn** > **SiZn** > **BeZn** > **AlZn** > **BOZn**. Consistent with expectations, the strongly σ-withdrawing O-donor ligand leads to the most stabilized zinc 4p OMO.

This trend appears to consist of two series, namely:

(a) **BZn** > **MeZn** > **BOZn** for the second-row non-metal donor ligands. This is the expected trend for these formally zinc(II) compounds based on increasing bond polarization and therefore greater

electron withdrawal across the row. As the donor atom becomes more electronegative, the zinc 4p OMOs become more stabilised.

(b) **SiZn** > **BeZn** > **AlZn** for the remaining species. Here the bond polarity is switched, with zinc being the most electronegative centre. Therefore, Zn 4p destabilisation decreases as the difference in electronegativity increases and reduced covalency leads to less efficient orbital overlap.

(iii) VtC-RXES

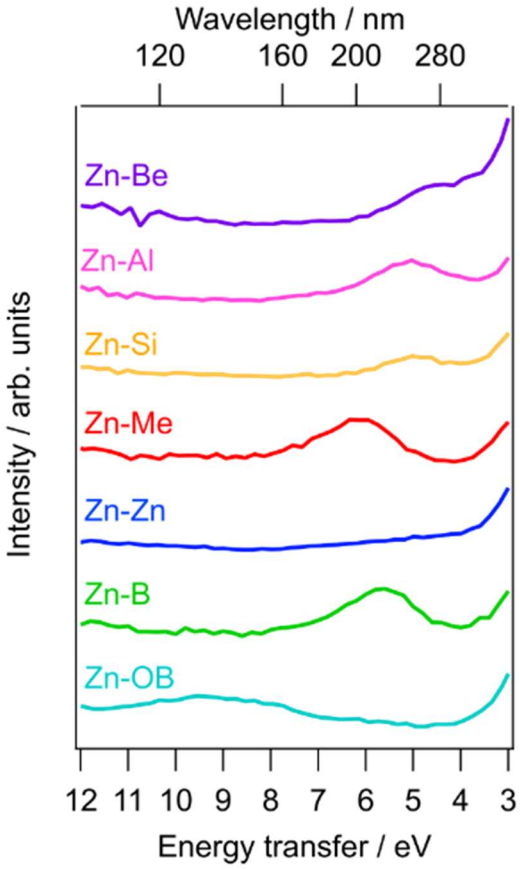

*Figure 7: Resonant VtC-XES spectra of compounds **BeZn**, **AlZn**, **SiZn**, **MeZn**, **ZnZn**, **BZn** and **BOZn**.*

Finally, resonant XES was measured for all compounds, expressed as energy transfer (energy transfer = emission energy – incident energy) with the elastic peak shifted to 0 eV to correct for deviations in the alignment of the detector. These data provide information on the zinc-specific occupied to unoccupied frontier orbital gap, effectively probing the Zn 4p OMO – Zn 4p UMO

transition.[22] This would be expected to be smallest for destabilizing, strongly electron donating X-ligands, which lead to more Lewis basic zinc centres, and largest for stabilizing, electron with drawing ligands which generate Lewis acidic zinc centres. Accordingly, we see a trend which closely mirrors that determined by HERFD-XANES (**BeZn** < **SiZn** ~ **AlZn** < **BZn** < **MeZn** < **BOZn**), *i.e.* the ligands which are the most σ-donating (and yield the most electron rich zinc centre) also lead to the smallest OMO-UMO gaps. No value could be measured in the case of **ZnZn**, likely due to very small p-orbital non-degeneracy in this symmetric homo-metallic compound, meaning that the small RXES peak is hidden by the elastic peak.

Computational analysis

Calculated molecular geometries were generated without restraints for all seven species.[23, 24] These gave geometrical parameters that closely align with the crystallographic data (where available). Simulated spectra for all optimised species as calculated by DFT (Non-resonant VtC-XES) and TD-DFT (HERFD-XANES) capture the trend in the experimental data to a reasonable degree, helping to validate the calculated geometric and electronic structures (see ESI). Attempts to simulate Resonant VtC-XES did not effectively capture the trend in the measured data, likely due to approximations made about the nature of the final state of the measured transitions during the calculations. A higher level of theory (such as Restricted Active Space Second Order Perturbation Theory – RASPT2) is likely required to properly simulate these transitions and their resulting spectra.[25]

Natural Bonding Orbital analysis was performed on all compounds to more closely study the composition of the Zn–X interaction.[26, 27] An NBO was located for this linkage in all species with the exception of the highly ionic Zn–O bond found in **BOZn** (which is instead described by second order perturbation interactions between O-centred lone pairs and a Zn-centred vacant orbitals).

The full orbital breakdowns are listed in the supporting information. Most significantly, the zinc orbital contribution to the bonding decreases in the order **BeZn** > **ZnZn** > **AlZn** > **BZn** > **SiZn** >

MeZn. This does not closely replicate any of the trends in the above data, (although it is similar the HERFD-XANES trend seen with the exception of **ZnZn** and **SiZn**) suggesting that such a metric does not represent a good way of comparing the diverse electronic structures in the above compounds. This trend does however exactly replicate that seen in the Wiberg Bond Indices (see below).

The charges at zinc as determined by Natural Population Analysis are also given in Table 1. These increase from +0.87 to +1.47 in the order **ZnZn** < **BeZn** < **AlZn** < **BZn** < **SiZn** < **MeZn** < **BOZn**. This trend approximates that determined by HERFD-XANES with the exceptions of **ZnZn** and **SiZn**, thereby providing reasonable agreement with the experimentally determined measure of electron richness.

		AlZn	**BZn**	**BeZn**	**BOZn**	**ZnZn**	**SiZn**	**MeZn**
WBI		0.7470	0.6525	0.8334	0.2253	0.7705	0.5568	0.5182
NPA Charges	Zn	1.259	1.382	0.9156	1.649	0.8741	1.430	1.470
	E	1.000	0.3919	0.8618	-1.200	0.8741	-0.9104	-1.232
ρ		0.06323	0.1034	0.06400	0.1291	0.06509	0.07392	0.1181
$\nabla^2\rho$		-0.04093	0.01444	-0.01771	0.6925	0.02026	-0.03044	0.1784

*Table 1: Calculated parameters for compounds **BeZn**, **AlZn**, **SiZn**, **MeZn**, **ZnZn**, **BZn** and **BOZn**.*

Hoping to access a description of the bonding which more closely replicates experiment, QT-AIM topological analyses were conducted to inspect the character of the Zn–X interactions.[28] All such bonds generated a Bond Critical Point (BCP), and the associated parameters are listed in Table 1; contour plots of the respective bonding regions are provided in the supporting information. Based on literature precedent, the bonding descriptors for each system are polar covalent (**AlZn**, **BeZn**, **SiZn**), metallic (**ZnZn**) and dative (**BZn**, **MeZn**, **BOZn**).[29]

For the three first row non-metal ligated systems, the Laplacian of the electron density at the BCP becomes larger in the order **BZn** < **MeZn** < **BOZn**, in line with a more polarised linkage, and consistent with the results of the VtC-XES measurements. Aside from this, few parallels can be drawn between these parameters and the measured data, suggesting that this topological analysis is providing a description of the bonding which does not closely relate to the electronic structure measured by X-ray spectroscopic data, perhaps due to the p-selectivity inherent to the measurements

which is not captured by this computational method. Additionally, the species studied may be too diverse for topological comparisons to be meaningful beyond the simple first row cases discussed above.

Finally, a Bader charge analysis was performed on all compounds to investigate whether this method would align more closely with the calculated data. Here we see a zinc charge increasing in the order **BeZn** < **AlZn** < **ZnZn** < **SiZn** < **BZn** < **MeZn** < **BOZn**, a series which very closely replicates that determined by HERFD-XANES measurements, with only the silyl-ligated system out of place (by one position). This basin-based analysis therefore appears to yield a relative charge distribution very close to that which has been experimentally determined.[28]

	AlZn	**BZn**	**BeZn**	**BOZn**	**ZnZn**	**SiZn**	**MeZn**
Zn	0.1659	0.8633	0.001625	1.309	0.6338	0.8156	1.038
Nacnac	-0.6080	-0.5970	-0.6860	-0.5381	-0.6338	-0.5669	-0.5911
X-ligand	0.4421	-0.2663	0.6844	-0.7705	N/A	-0.2487	-0.4471

*Table 2: Bader charge analysis for compounds **BeZn**, **AlZn**, **SiZn**, **MeZn**, **ZnZn**, **BZn** and **BOZn**.*

Conclusions

We report extensive X-ray spectroscopic analysis of a series of complexes with the general form (Nacnac^{Mes})ZnX. These data have been interpreted in the context of directly measuring the σ-donor properties of the X-type ligands investigated, thereby generating a trend in terms of increasing donor strength: boryloxy < methyl < boryl ≈ zincyl < silyl ≈ aluminyl < beryllyl. These data have also been compared to computational metrics generated for the complete family of compounds, with the best agreement found for density and basin-based approaches. As a whole, this study proved a novel means of probing ligand donor properties, especially of exotic 'next generation' ligands such as boryl and aluminyl ligands.

Acknowledgements

We thank the EPSRC Centre for Doctoral Training in Inorganic Chemistry for Future Manufacturing (OxICFM, EP/S023828/1, studentship to L.P.G.). Oxford Advanced Research Computing and ARCHER are thanked for computational resources. The Diamond Light Source is thanked to access to beamline facilities.

References

[1] R. J. Lundgren, M. Stradiotto, in *Ligand Design in Metal Chemistry*, **2016**, pp. 1-14.
[2] A. Gómez-Suárez, D. J. Nelson, S. P. Nolan, *Chemical Communications* **2017**, *53*, 2650-2660.
[3] L. Maser, C. Schneider, L. Vondung, L. Alig, R. Langer, *Journal of the American Chemical Society* **2019**, *141*, 7596-7604.
[4] G. Comas-Vilà, P. Salvador, *ChemPhysChem* **2024**, *25*, e202400582.
[5] C. A. Tolman, *Chem. Rev.* **1977**, *77*, 313-348.
[6] H. P. Stevens, J. Olsen, J. K. Kirkland, D. H. Ess, *Organometallics* **2024**, *43*, 40-47.
[7] I. A. I. Mkhalid, J. H. Barnard, T. B. Marder, J. M. Murphy, J. F. Hartwig, *Chem. Rev.* **2010**, *110*, 890-931.
[8] J. Hicks, P. Vasko, J. M. Goicoechea, S. Aldridge, *Nature* **2018**, *557*, 92-95.
[9] J. Hicks, A. Mansikkamäki, P. Vasko, J. M. Goicoechea, S. Aldridge, *Nature Chemistry* **2019**, *11*, 237-241.
[10] J. Campos, S. Aldridge, *Angewandte Chemie International Edition* **2015**, *54*, 14159-14163.
[11] J. T. Boronski, A. E. Crumpton, L. L. Wales, S. Aldridge, *Science* **2023**, *380*, 1147-1149.
[12] J. Hicks, P. Vasko, J. M. Goicoechea, S. Aldridge, *Angewandte Chemie International Edition* **2021**, *60*, 1702-1713.
[13] I. F. Yu, J. W. Wilson, J. F. Hartwig, *Chem. Rev.* **2023**, *123*, 11619-11663.
[14] J. Hicks, P. Vasko, J. M. Goicoechea, S. Aldridge, *Journal of the American Chemical Society* **2019**, *141*, 11000-11003.
[15] M. L. Baker, M. W. Mara, J. J. Yan, K. O. Hodgson, B. Hedman, E. I. Solomon, *Coordination Chemistry Reviews* **2017**, *345*, 182-208.
[16] M. M. D. Roy, J. Hicks, P. Vasko, A. Heilmann, A.-M. Baston, J. M. Goicoechea, S. Aldridge, *Angewandte Chemie International Edition* **2021**, *60*, 22301-22306.
[17] J. Prust, A. Stasch, W. Zheng, H. W. Roesky, E. Alexopoulos, I. Usón, D. Böhler, T. Schuchardt, *Organometallics* **2001**, *20*, 3825-3828.
[18] S. Schulz, T. Eisenmann, U. Westphal, S. Schmidt, U. Flörke, *Zeitschrift für anorganische und allgemeine Chemie* **2009**, *635*, 216-220.
[19] S. Schulz, D. Schuchmann, U. Westphal, M. Bolte, *Organometallics* **2009**, *28*, 1590-1592.
[20] L. Pauling, *Journal of the American Chemical Society* **1932**, *54*, 3570-3582.
[21] M. Bauer, *Physical Chemistry Chemical Physics* **2014**, *16*, 13827-13837.
[22] L. J. P. Ament, M. van Veenendaal, T. P. Devereaux, J. P. Hill, J. van den Brink, *Reviews of Modern Physics* **2011**, *83*, 705-767.
[23] F. Neese, *WIREs Computational Molecular Science* **2012**, *2*, 73-78.
[24] F. Neese, *WIREs Computational Molecular Science* **2022**, *12*, e1606.
[25] V. Sauri, L. Serrano-Andrés, A. R. M. Shahi, L. Gagliardi, S. Vancoillie, K. Pierloot, *Journal of Chemical Theory and Computation* **2011**, *7*, 153-168.
[26] J. K. B. E. D. Glendening, A. E. Reed, J. E. Carpenter, J. A. Bohmann, C. M. Morales, P. Karafiloglou, C. R. Landis, F. Weinhold, **2018**.
[27] E. D. Glendening, C. R. Landis, F. Weinhold, *Journal of Computational Chemistry* **2019**, *40*, 2234-2241.
[28] T. Lu, F. Chen, *Journal of Computational Chemistry* **2012**, *33*, 580-592.
[29] R. Bianchi, G. Gervasio, D. Marabello, *Inorganic Chemistry* **2000**, *39*, 2360-2366.

Supporting information

Synthetic considerations

All manipulations were carried out using standard Schlenk line or dry-box techniques under an atmosphere of argon or dinitrogen. Solvents were degassed by sparging with argon and dried by passing through a column of the appropriate drying agent. Toluene and hexane were purified using an MBraun SPS-800 and stored over a potassium mirror. NMR spectra were measured in benzene-d_6 (which was dried over potassium, with the solvent then being distilled under reduced pressure), stored under argon in Teflon valve ampoules. NMR samples were prepared under argon in 5 mm Wilmad 507-PP tubes fitted with J. Young Teflon valves. ^{1}H, ^{13}C{^{1}H} and ^{29}Si NMR spectra were measured on Bruker Avance III HD nanobay 400 MHz or Bruker Avance III 500 MHz spectrometer at ambient temperature and referenced internally to residual protio-solvent (^{1}H) or solvent (^{13}C) resonances and are reported relative to tetramethylsilane (δ = 0 ppm. Assignments were confirmed using two-dimensional ^{1}H-^{1}H, ^{1}H-^{29}Si and ^{13}C-^{1}H NMR correlation experiments. Chemical shifts are quoted in δ (ppm) and coupling constants in Hz. Elemental analyses were carried out by London Metropolitan University. (Nacnac^{Mes})ZnI,[s1] (Nacnac^{Mes})ZnMe,[s2] (Nacnac^{Mes})ZnOB{(NDippCH)$_2$}, [(Nacnac^{Mes})Zn]$_2$, (Nacnac^{Mes})ZnBpin, (Nacnac^{Mes})ZnAl(NON),[s3] (Nacnac^{Mes})ZnBeCp[s4] and KSi(TMS)$_3$[s5] were prepared according to literature procedures.

Synthesis of (Nacnac^{Mes})ZnSi(TMS)$_3$

To a Schlenk flack containing a mixture of (Nacnac^{Mes})ZnI (300 mg, 0.57 mmol) and (THF)$_2$KSi(TMS)$_3$ (244 mg, 0.57 mmol) was added toluene (10 mL), and the resulting mixture stirred at room temperature for 16 h. Removal of volatiles *in vacuo*, extraction into hexane (2x 5 mL) and filtration yielded a clear, pale yellow solution. Concentration *in vacuo* and storage at –30 °C yielded large quantities of colourless single crystals suitable for single crystal X-ray diffraction experiments, which confirmed the identity of the product as (Nacnac^{Mes})ZnSi(TMS)$_3$. Yield (311 mg, 86 %). EA: Calculated for $C_{32}H_{56}N_2Si_4Zn$ C 59.45, H 8.73, N 4.33 %, found C 59.21, H 8.80, N 4.13 %.

^{1}H NMR (500 MHz, benzene-d$_6$, 298 K): δ_H 0.14 (s, 27H, Si(C*H*$_3$)$_3$), 1.50 (s, 6H, Nacnac-C*H*$_3$), 2.14 (s, 12H, *o*-C*H*$_3$), 2.19 (s, 6H, *p*-C*H*$_3$), 5.02 (s, 1H, C*H*), 6.82 (s, 4H, Ar*H*) ppm.

^{13}C{^{1}H} NMR (101 MHz, benzene-d$_6$, 298 K): δ_C 4.5 (Si(*C*H$_3$)$_3$), 19.4 (*o*-*C*H$_3$), 21.0 (*p*-*C*H$_3$), 23.4 (Nacnac-*C*H$_3$), 97.4 (*C*H), 130.1 (*p*-*C*CH$_3$), 131.4 (*m*-*C*H), 134.5 (*o*-*C*CH$_3$), 146.7 (*i*-*C*N), 167.5 (Nacnac-*C*N) ppm.

^{29}Si NMR (99.4 MHz, benzene-d$_6$, 298 K): δ_{Si} -7.6, 49.5 ppm.

NMR data

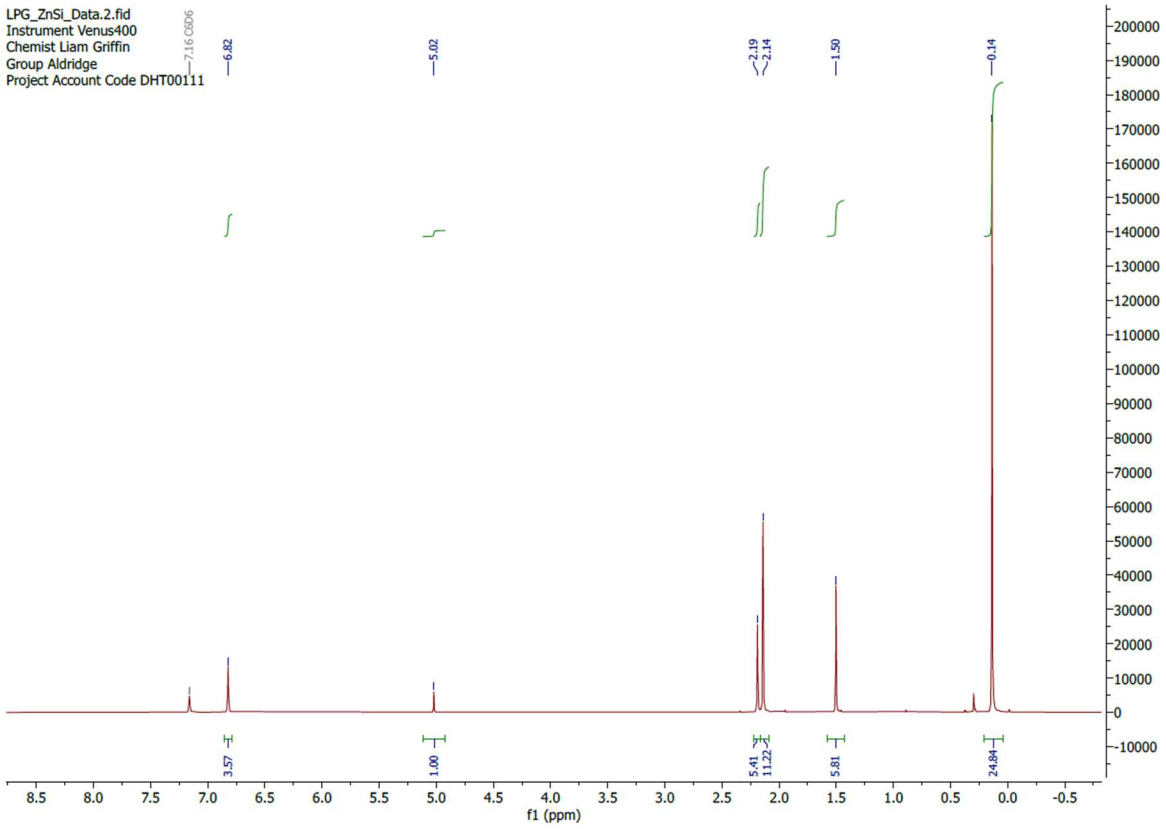

Fig s1: ^{1}H NMR spectrum of **(Nacnac^{Mes})ZnSi(TMS)$_3$**

X-ray crystallographic details

Single-crystal X-ray diffraction data for ($Nacnac^{Mes}$)ZnSi$(TMS)_3$ were collected on an Oxford Diffraction/Agilent SuperNova diffractometer equipped with a 135 mm Atlas CCD area detector. Crystals were selected under Paratone-N oil, mounted on MiTeGen Micromount loops and quench-cooled using an Oxford Cryosystems open flow N2 cooling device.[s6] Data were collected at 150 K using mirror monochromated Cu Kα radiation (λ = 1.5418 Å; Oxford Diffraction Supernova). Data collected were processed using the CrysAlisPro package, including unit cell parameter refinement and inter-frame scaling (which was carried out using SCALE3 ABSPACK within CrysAlisPro).[s7] Equivalent reflections were merged and diffraction patterns processed with the CrysAlisPro suite.[s7] Structures were solved ab initio from the integrated intensities using SHELXT[s8] and refined on F^2 using SHELXL[s9] with the graphical interface OLEX2.[s10] Selected crystallographic data are summarised in Table s1.

	(Nacnac^{Mes})ZnSi(TMS)$_3$
Formula	$C_{32}H_{56}N_2Si_4Zn$
Fw (g mol^{-1})	646.51
Crystal system	Orthorhombic
Space group	P 2_1 2_1 2_1
a (Å)	13.4115(3)
b (Å)	17.5166(4)
c (Å)	48.5318(9)
α (°)	90
β (°)	90
γ (°)	90
V (Å^{-3})	11401.3(4)
Z	12
ρ_{calc} (g cm^{-3})	1.130
Radiation, λ (Å)	1.54184
Absorption	Multi-scan
μ (mm^{-1})	2.255
Reflections collected	45204
Independent reflections	21799
$R_{(int)}$	0.0458
Parameters	1188
R_1 (all data/I>2σ(I))	0.0427
ωR_2 (all data/I >2σ(I))	0.0942
GooF	1.020
T (K)	150.01(10)

Table s1: X-ray crystallographic details

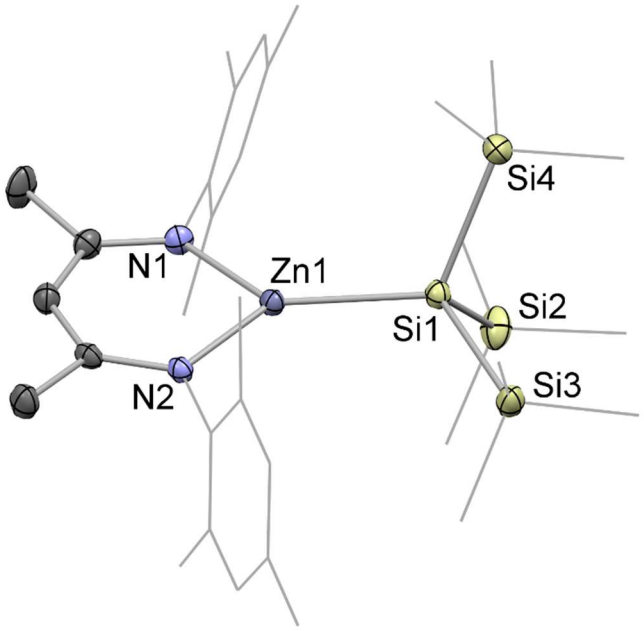

Figure s2: Molecular structure of **(Nacnac^{Mes})ZnSi(TMS)$_3$** as determined by X-ray diffraction. Three crystallographically independent molecules present in the asymmetric unit. Due to their similar geometric parameters, only one is shown and discussed. Hydrogens omitted and some residues shown as wireframe for clarity. Key bond lengths (Å) and bond angles (°): Zn1–Si1 2.384(1), Zn1–N1 1.982(4), Zn1–N2 1.977(4), Si1–Zn1–N1 131.7(1), Si1–Zn1–N2 132.7(1), N1–Zn1–N2 95.6(2).

X-ray Spectroscopic Details

All compounds were transported to the Diamond Light Source as dry powders sealed in NMR tubes fitted with J. Young valves. Samples were prepared as dilute (~5 millimolar) solutions in dry toluene and loaded into plastic sample capsules in a nitrogen filled glovebox at the synchrotron facility. The capsules were sealed before being transferred to the I20 beamline and placed in a sample holder. Samples were studied using a combination of Zn 1s HERFD-XANES, Zn 1s Valence to Core-XES and resonant Valence to Core-XES.[s11, s12] Frequent XANES spectra were measured for comparison, allowing any beam damage or decomposition to be detected. Beam flux was optimised based on signal intensity and the propensity of a sample towards damage. All samples were referenced to zinc foil, and multiple samples were measured on more than one visit to ensure replicability. RVtC-XES spectra were additionally shifted relative to the elastic peak to allow for direct comparison between samples.

X-ray spectroscopy data

Peak maximum listed for each technique.

	XAS / eV	XES / eV	RXES / eV
BeZn	9660.3	9658.2	4.75
AlZn	6660.6	9657.8	5.03
SiZn	9660.6	9658.5	5.02
BZn	9660.8	9658.9	5.60
MeZn	9661.1	9658.7	6.14
ZnZn	9660.8	9659.1	-
BOZn	9661.7	9658	9.34 (broad)

Table s2: X-ray spectroscopic data

No RXES peak could be measured for **ZnZn**, likely due to overlap with the elastic peak, since very little loss of p-orbital degeneracy would be expected for this homo-metallically bonded complex.

Computational details

Gas phase geometry optimizations, frequency analyses and single point calculations were carried out using the ORCA software package using the ωB97X-D3BJ functional and the ZORA-def2-QZVPP basis set and the CPCM(Toluene) solvation correction.[s13-s16] The optimised structures were confirmed to be minima on the potential energy surface by the absence of imaginary frequencies.

Zn 1s HERFD-XANES and NRVtC-XES spectra were calculated in ORCA using TDDDFT and ground state DFT respectively.[s14, s15]

Natural bonding orbital (NBO) analyses were carried out using the NBO 7.0 program.[s17, s18] Atoms in molecules (AIM) analyses were conducted using Multiwfn software package.[s19] AIM bonding classifications have been made in accordance with the literature precedent.[s20]

Simulated spectra

HERFD-XANES

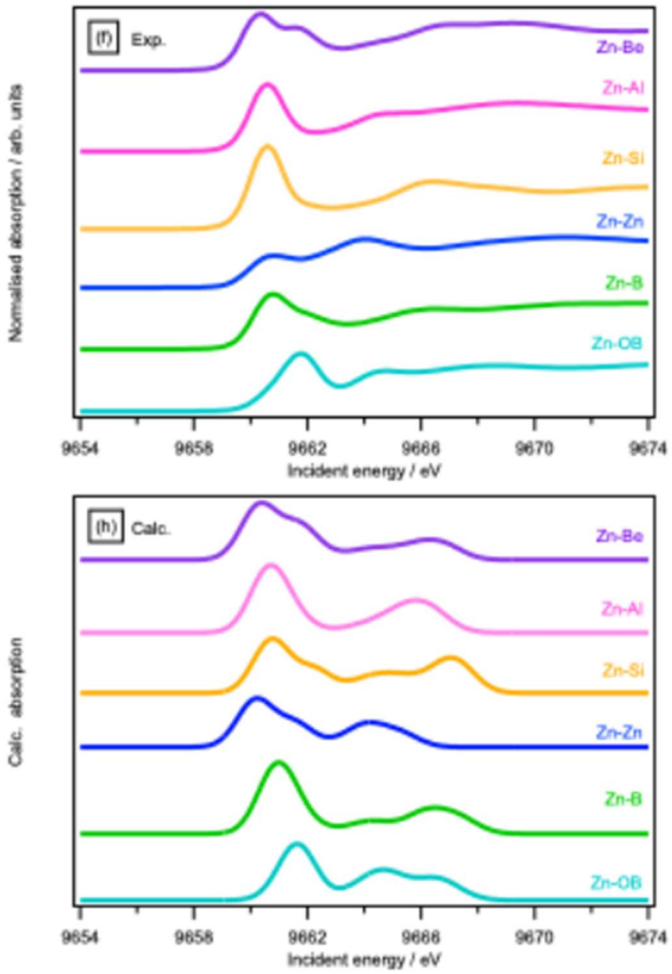

Figure s3: Experimental (top) and simulated (bottom) HERFD-XANES spectra.

Non-resonant VtC-XES

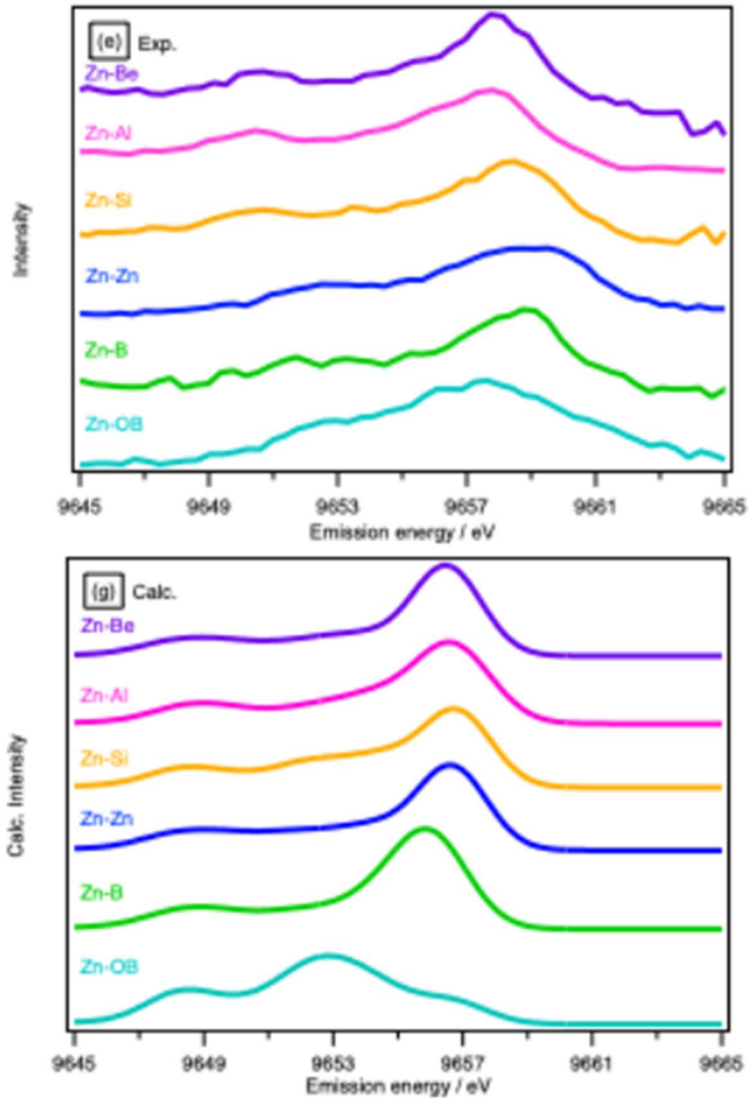

Figure s4: Experimental (top) and simulated (bottom) NRVtC-XES spectra.

Bader charge analysis

	ZnAl	ZnB	ZnBe	ZnOB	ZnZn	ZnSi	ZnMe
Zn	0.165897	0.8633	0.001625	1.308583	0.6338	0.815647	1.03829
$Nacnac^{Ar}$	-0.60799	-0.5970	-0.6860	-053809	-0.6338	-0.56691	-0.59117
X-ligand	0.442097	-0.2663	0.6844	-0.77049	N/A	-0.24874	-0.44712

QTAIM and NBO parameters of Zn–X bonds

		ZnAl	ZnB	ZnBe	ZnOB	ZnZn	ZnSi	ZnMe
ρ		0.06323	0.10344	0.06400	0.1291	0.06509	0.07392	0.01181
$\nabla^2\rho$		-0.04093	0.01444	-0.01771	0.6925	0.02026	-0.03044	0.1784
WBI		0.7470	0.6525	0.8334	0.2253	0.7705	0.5568	0.5182
NPA Charges	Zn	1.25923	1.38202	0.91563	1.64863	0.87406	1.43048	1.46987
	E	1.00048	0.39187	0.86181	-1.19881	0.87406	-0.91038	-1.23209

Electron density contour plots

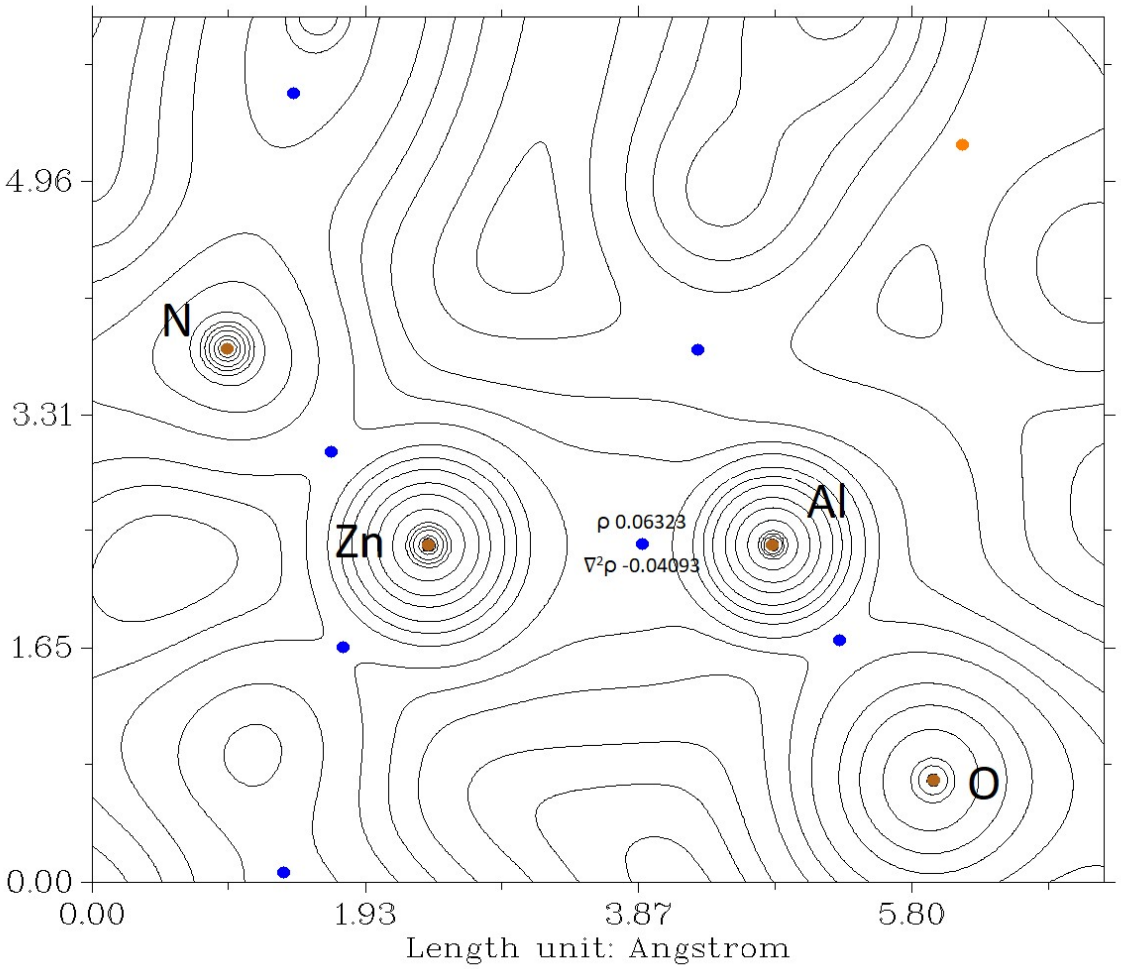

Figure s5: QTAIM electron density contour plot for the Zn–Al bond region of **AlZn**

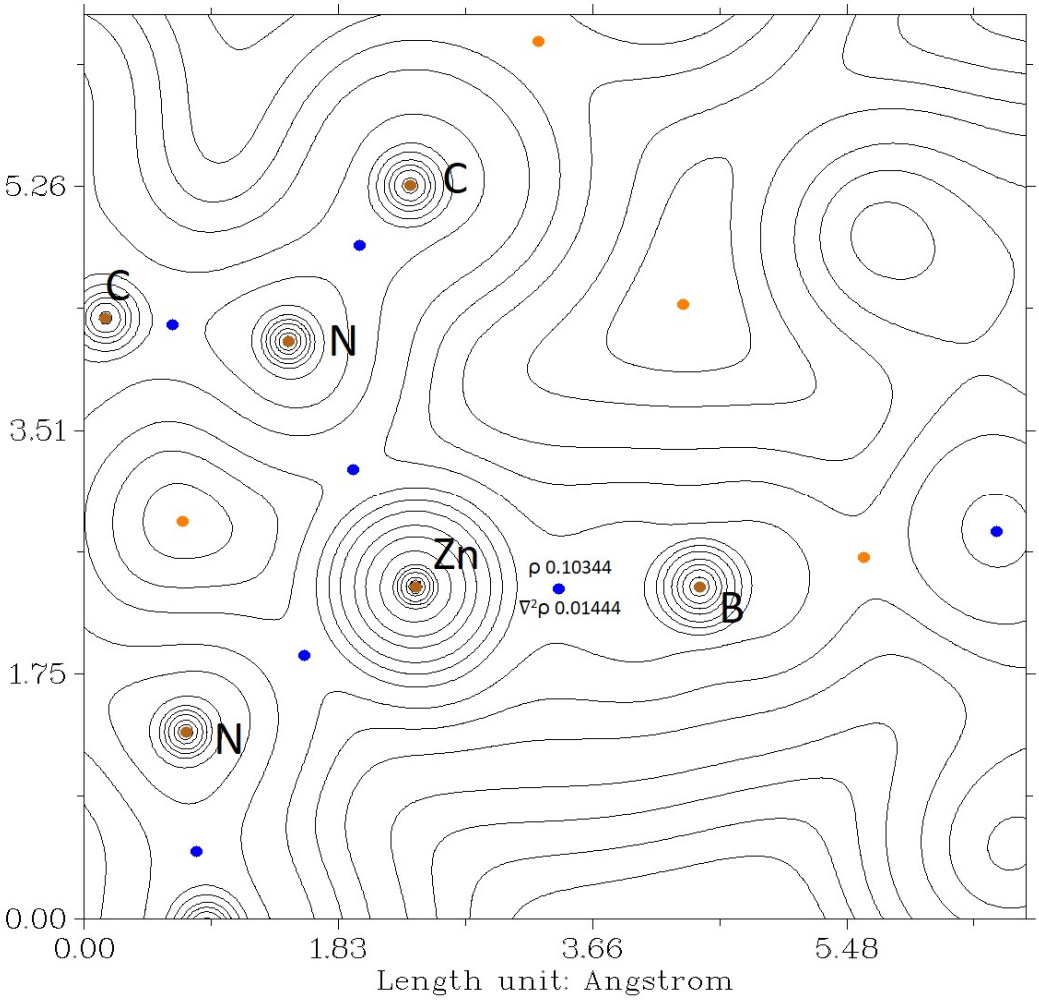

Figure s6: QTAIM electron density contour plot for the Zn–B bond region of **BZn**

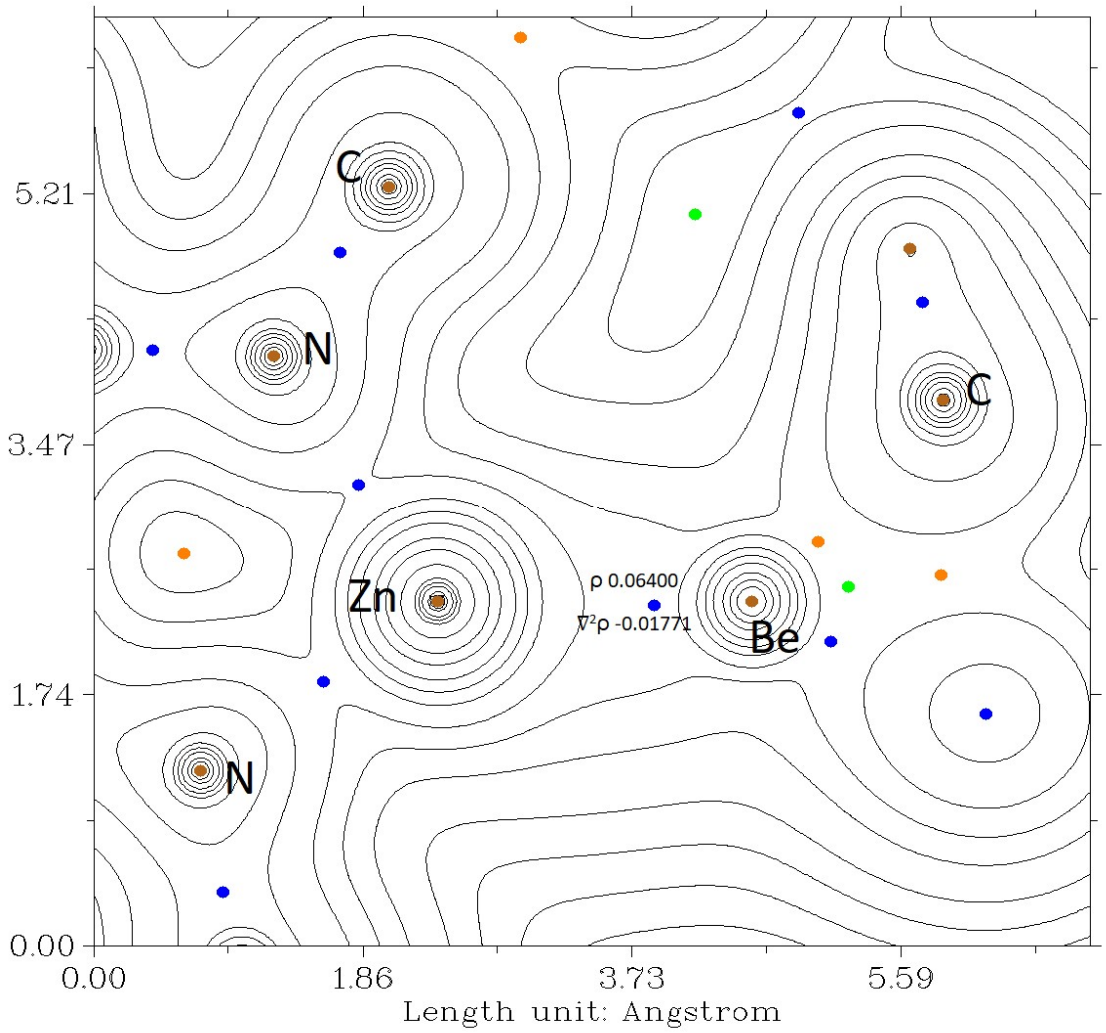

Figure s7: QTAIM electron density contour plot for the Zn–Be bond region of **BeZn**

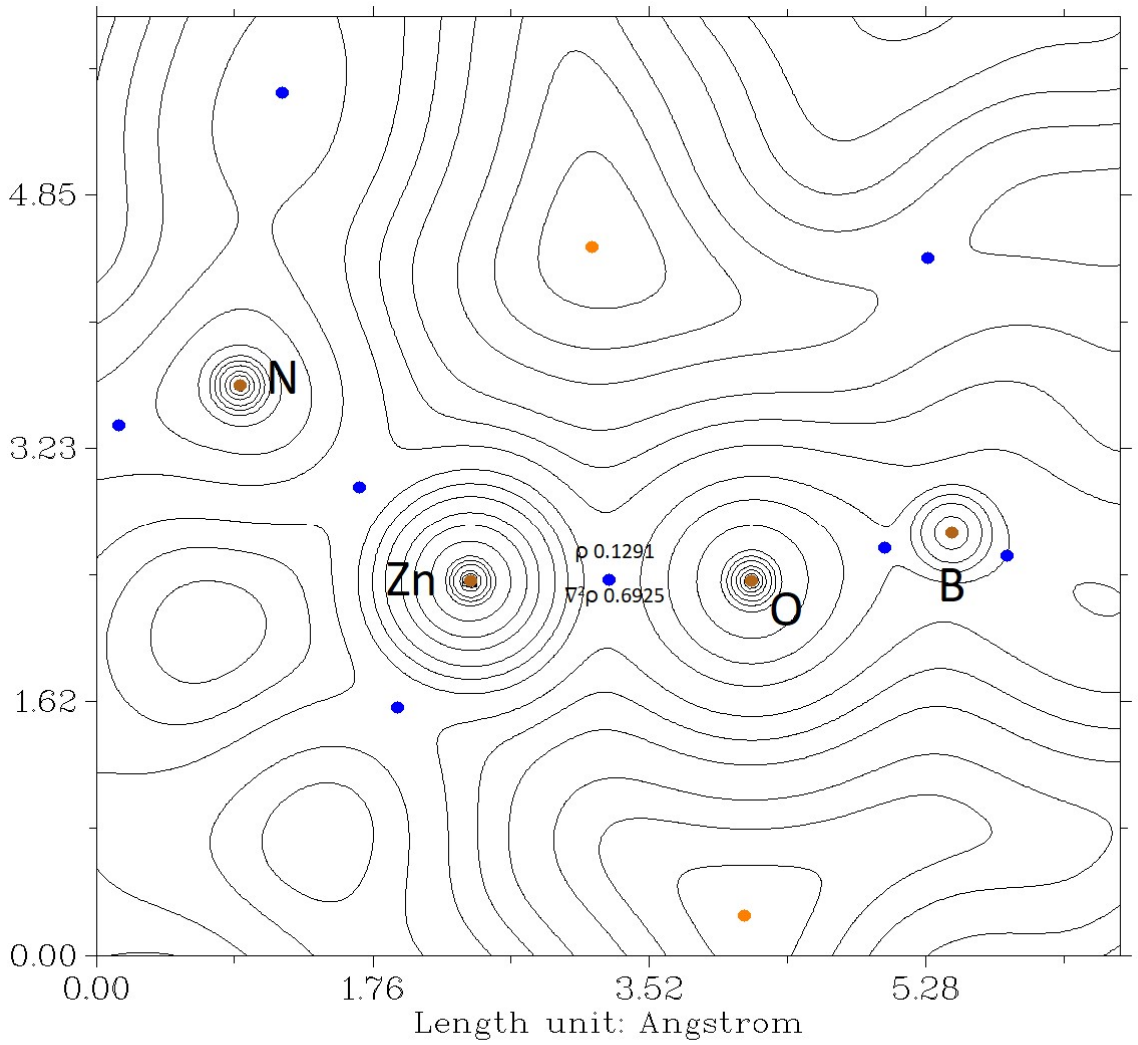

Figure s8: QTAIM electron density contour plot for the Zn–O bond region of **BOZn**

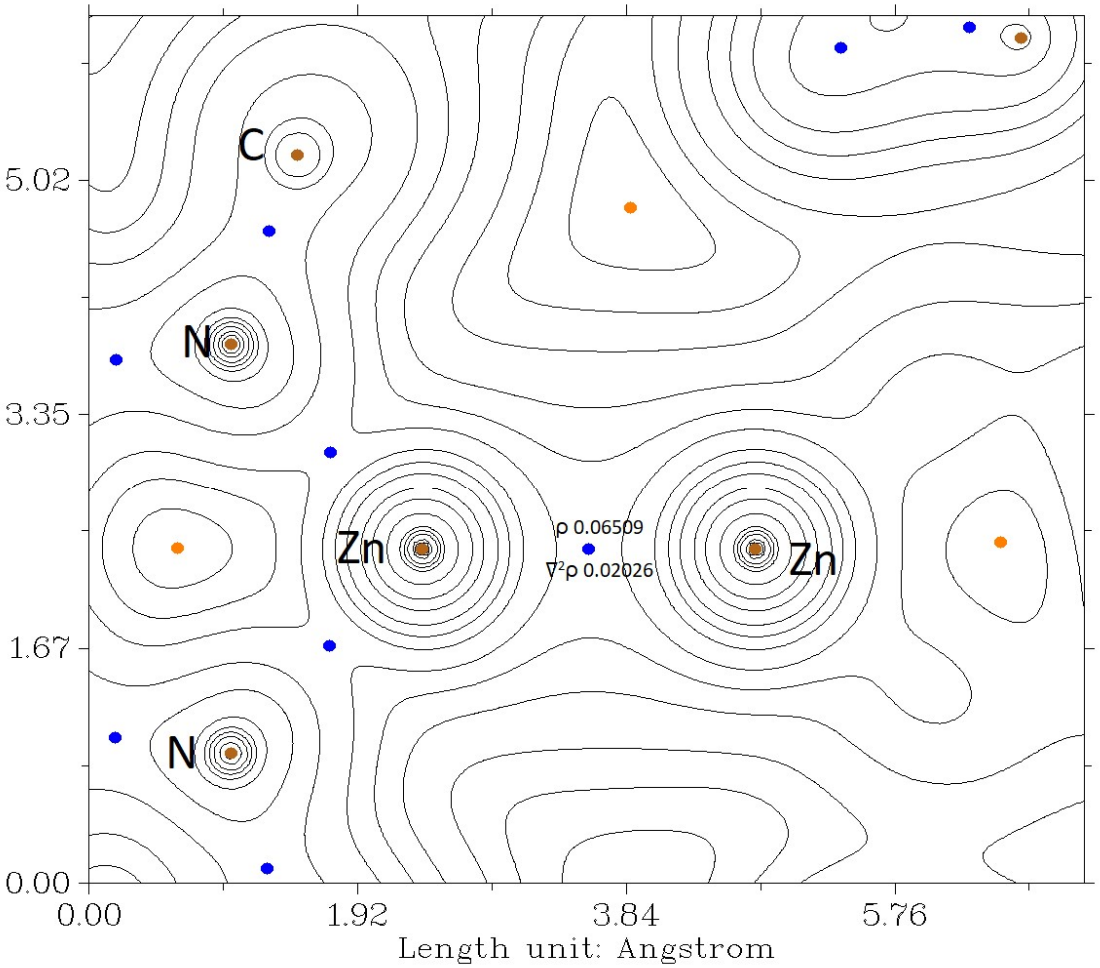

Figure s9: QTAIM electron density contour plot for the Zn–Zn bond region of **ZnZn**

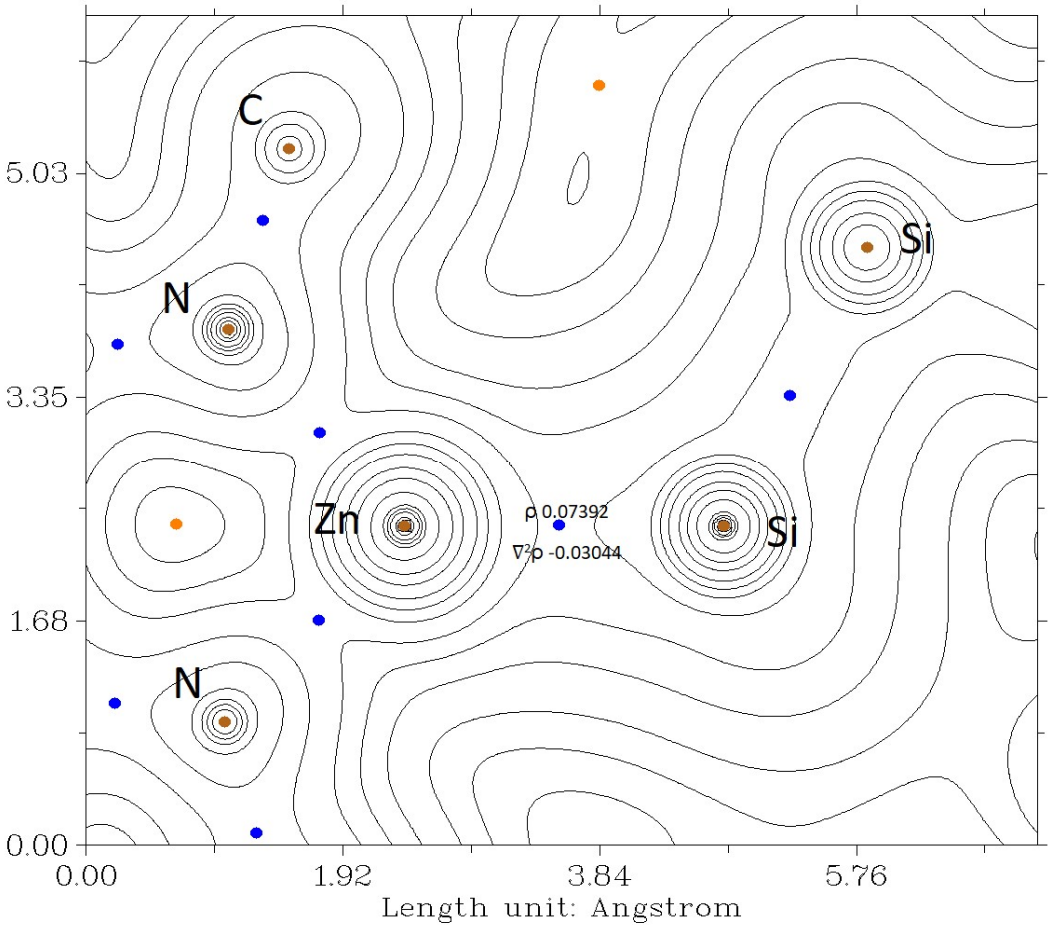

Figure s10: QTAIM electron density contour plot for the Zn–Si bond region of **SiZn**

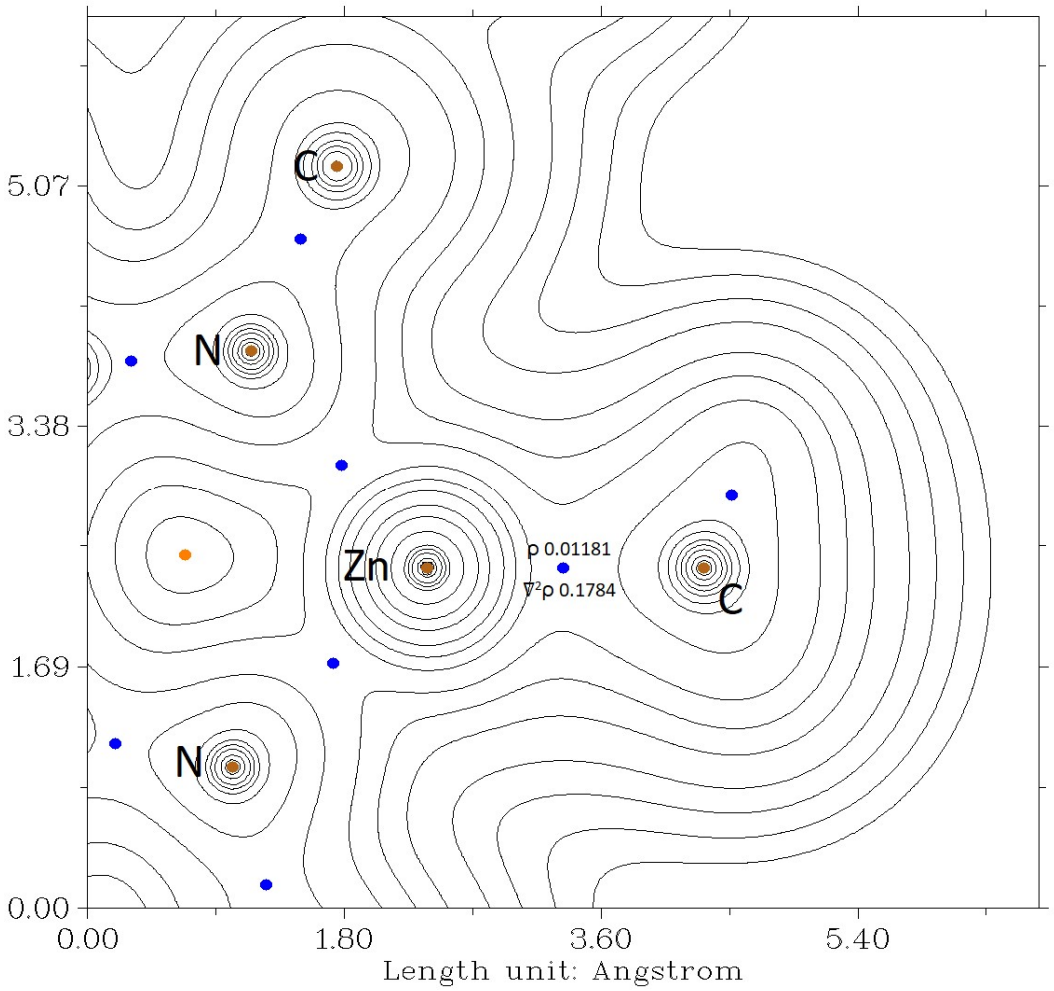

Figure s11: QTAIM electron density contour plot for the Zn–C bond region of **MeZn**

Zn–X NBO analysis

ZnAl

1.95420 e

Zn: 0.5700 e (32.5%), s 95.9%, p 3.1%, d 1.0%

Al: 0.8216 e (67.5%), s 58.3%, p 41.3%, d 0.4%

ZnB

1.95965 e

Zn: 0.5067 e (25.7%), s 96.2%, p 1.8%, d 2.0%

B: 0.8621 e (74.3%), s 48.0%, p 52.0%

ZnBe

1.94039 e

Zn: 0.7197 e (51.8%), s 94.7%, p 3.7%, d 1.6%

Be: 0.6943 e (48.2%) s 92.6%, p 7.4%

ZnMe

1.98968 e

Zn: 0.4380 e (19.2%), s 95.8%, p 1.9%, d 2.3%

C: 0.8990 e (80.8%), s 17.1%, p 82.9%

ZnSi

1.96110 e

Zn: 0.4645 e (21.6%), s 95.9%, p 2.8%, d 1.3%

Si: 0.8856 e (78.4%), s 24.0%, p 75.7%, d 0.3%

ZnZn

1.95473 e

Zn: 0.7071 (50.0%), s 93.4%, p 5.1%, d 1.5%

Zn: 0.7071 (50.0%), s 93.4%, p 5.1%, d 1.5%

No conventional NBO is located for the Zn–O bond of ZnOB. This is represented as second order perturbation interactions between an O-centred lone pairs, and vacant Zn-centred valence orbital.

XYZ coordinates of calculated structures

ZnAl	ZnB
Zn -1.97402 -0.46587 1.05700	Zn -1.005696 8.368299 15.634298
Al 0.01097 -0.00802 -0.28027	O 0.233122 8.821388 12.916954
O 1.86638 0.20512 0.47864	O 0.520075 6.664288 13.619851
N 0.34217 1.77912 -0.85141	N -1.001321 8.986805 17.487061
N 0.82018 -1.61571 -0.97450	N -2.983976 8.175601 15.526260
N -3.89769 -0.82999 0.67152	C -3.825844 8.486615 16.502015
N -2.08695 -0.98044 2.98720	C 0.279478 9.241943 18.059668
C 2.47303 1.39428 0.07993	C -3.464044 7.680904 14.281424
C 1.63412 2.23764 -0.65116	C -2.099557 9.181681 18.219761
C 2.20839 3.44058 -1.07714	C 0.865155 10.507759 17.910620
H 1.58404 4.13883 -1.63772	C -3.405776 8.957564 17.759640
C 3.55787 3.73211 -0.81441	H -4.195596 9.172888 18.468731
C 4.34734 2.80966 -0.11098	C 0.969038 8.203569 18.700826
H 5.39797 3.02290 0.07350	C -5.310301 8.340694 16.267405
C 3.80690 1.60236 0.35432	H -5.622085 8.941425 15.405600
C 4.53318 0.50550 1.14479	H -5.882844 8.651556 17.142697
C 4.02685 -0.83093 0.59008	H -5.565509 7.302936 16.026338
C 4.79202 -1.96221 0.29047	C 0.988839 8.154624 11.855529
H 5.85432 -1.96920 0.53424	C -3.646477 8.567053 13.208871
C 4.21637 -3.07573 -0.34878	C 2.128706 10.728216 18.455388
C 2.87652 -3.03184 -0.75223	H 2.582660 11.712220 18.350245
H 2.44143 -3.83998 -1.33747	C 2.825885 9.722112 19.123924
C 2.08360 -1.89745 -0.49991	C -3.359374 10.031433 13.380472
C 2.68536 -0.90246 0.27003	H -2.282910 10.189312 13.530628
C 5.09498 -4.29793 -0.63802	H -3.869603 10.452497 14.253320
C 6.27931 -3.87695 -1.52006	H -3.661771 10.594611 12.493745
H 6.90784 -3.11911 -1.03000	C 2.231706 8.466002 19.231389
H 5.92465 -3.45336 -2.47227	H 2.766061 7.664236 19.737885
H 6.91792 -4.74576 -1.74686	C -3.639468 6.299941 14.105339
C 5.61461 -4.86577 0.69049	C 4.202104 9.977593 19.677503
H 6.25196 -5.74673 0.51154	H 4.964999 9.869335 18.896617
H 4.77810 -5.17308 1.33696	H 4.446737 9.271795 20.476453
H 6.21065 -4.12537 1.24415	H 4.287954 10.992232 20.078718
C 4.32892 -5.40344 -1.36576	C -1.941899 9.679760 19.637155
H 3.95485 -5.06735 -2.34461	H -1.333426 8.985902 20.227456
H 3.47140 -5.76245 -0.77687	H -2.912036 9.799332 20.121353
H 4.99419 -6.26262 -1.54107	H -1.414685 10.639927 19.655070
C 6.04645 0.62778 1.02025	C 0.737789 6.645108 12.172649
H 6.54703 -0.15903 1.60280	C 0.147096 11.590272 17.155007
H 6.38988 1.59265 1.42022	H 0.714351 12.524222 17.179357
H 6.37413 0.54773 -0.02641	H -0.853675 11.781928 17.557613
C 4.12544 0.62637 2.62626	H 0.008380 11.302652 16.104358
H 3.03597 0.54987 2.74969	C 0.362445 6.831220 18.787436
H 4.44752 1.59795 3.03149	H 1.000785 6.158462 19.365797
H 4.59559 -0.17536 3.21678	H 0.233280 6.401252 17.785479
C 4.13528 5.05140 -1.34125	H -0.631865 6.846602 19.247386
C 4.03008 5.06841 -2.87342	C -4.060627 8.054809 11.979763
H 2.98637 4.98676 -3.21051	H -4.210329 8.741836 11.148472
H 4.59036 4.22882 -3.31273	C -3.328047 5.347826 15.225236

H 4.44243 6.00674 -3.27814	H -3.593620 4.323620 14.950987
C 3.33895 6.22794 -0.75961	H -3.851435 5.606087 16.152094
H 3.39732 6.23587 0.33967	H -2.254623 5.371614 15.455770
H 2.27615 6.18146 -1.03893	B 0.073044 7.927021 13.958401
H 3.74009 7.18460 -1.13073	C -4.059207 5.830255 12.861828
C 5.60469 5.23435 -0.95947	H -4.201189 4.759465 12.725317
H 5.97296 6.19496 -1.35076	C 2.447173 8.571931 12.025482
H 6.23951 4.44040 -1.38127	H 2.508866 9.663510 11.987657
H 5.74431 5.24437 0.13232	H 3.076510 8.161485 11.228852
C -0.68512 2.74739 -0.99648	H 2.838784 8.242604 12.992556
C -0.97721 3.63304 0.06851	C 0.450802 8.624086 10.514375
C -2.00825 4.56286 -0.09241	H -0.630611 8.484044 10.449695
H -2.23982 5.24842 0.72724	H 0.928285 8.076445 9.693881
C -2.75758 4.61675 -1.26170	H 0.667046 9.688950 10.385624
H -3.56561 5.34524 -1.36508	C -4.278702 6.691112 11.787653
C -2.47409 3.73436 -2.29771	C 1.902880 5.720872 11.863987
H -3.06688 3.77353 -3.21336	H 2.795746 5.995276 12.429461
C -1.43700 2.80433 -2.18979	H 2.140655 5.747179 10.794406
C -1.15152 1.82593 -3.30662	H 1.633792 4.693584 12.127322
H -0.07639 1.59107 -3.24733	C -4.681185 6.156329 10.439703
C -1.94331 0.54419 -3.06273	H -5.280500 6.883877 9.884110
H -1.72100 0.09484 -2.07808	H -5.262144 5.234055 10.533583
H -1.75132 -0.22498 -3.82379	H -3.796614 5.926783 9.831776
H -3.01993 0.75911 -3.04956	C -0.551891 6.109967 11.553427
C -1.43843 2.38121 -4.69728	H -0.770003 5.130407 11.989450
H -2.51719 2.53015 -4.86470	H -0.459022 5.994361 10.468096
H -1.08788 1.67974 -5.46827	H -1.398844 6.768146 11.771743
H -0.93420 3.34597 -4.85932	
C -0.25081 3.56960 1.39899	
H 0.53965 2.81238 1.32140	
C -1.19165 3.10575 2.50576	
H -2.03621 3.79916 2.64572	
H -0.65696 3.01360 3.46264	
H -1.60546 2.11391 2.26965	
C 0.42677 4.89080 1.75455	
H 1.13065 5.19781 0.96832	
H 0.99080 4.79212 2.69530	
H -0.30723 5.70116 1.89085	
C 0.21743 -2.54827 -1.85986	
C 0.28593 -2.31880 -3.25800	
C -0.35889 -3.21558 -4.11385	
H -0.32759 -3.04793 -5.19159	
C -1.03620 -4.32768 -3.62139	
H -1.53594 -5.01324 -4.31012	
C -1.05863 -4.56918 -2.25512	
H -1.57273 -5.45402 -1.87045	
C -0.43147 -3.69831 -1.35741	
C -0.43248 -4.02934 0.12134	
H 0.17014 -3.25813 0.61490	
C 0.23540 -5.37569 0.40058	
H -0.33554 -6.21122 -0.03520	

H 0.30373 -5.55162 1.48578 H 1.25430 -5.41166 -0.01047 C -1.83047 -3.98449 0.73226 H -2.30796 -3.00365 0.59682 H -1.79273 -4.18794 1.81329 H -2.49601 -4.73422 0.27498 C 1.08053 -1.15087 -3.81843 H 0.90277 -0.29282 -3.14919 C 0.67232 -0.74536 -5.23109 H 0.99103 -1.49473 -5.97319 H 1.15889 0.20336 -5.50318 H -0.41325 -0.61071 -5.33644 C 2.58715 -1.42843 -3.79969 H 2.96579 -1.62152 -2.78937 H 3.13731 -0.56577 -4.20730 H 2.82298 -2.30689 -4.42235 C -4.46560 -0.28241 -0.50947 C -4.84002 1.07299 -0.52078 C -5.41473 1.60474 -1.67759 H -5.69925 2.66089 -1.68238 C -5.63001 0.83007 -2.81868 C -5.22546 -0.50679 -2.78694 H -5.35443 -1.12679 -3.67936 C -4.62313 -1.07464 -1.66220 C -4.09497 -2.47626 -1.71076 H -4.39543 -2.97970 -2.63950 H -4.42882 -3.08983 -0.86101 H -2.99323 -2.47618 -1.67951 C -6.20957 1.43252 -4.06560 H -6.86762 2.28321 -3.83635 H -6.78923 0.69544 -4.64045 H -5.41068 1.80656 -4.72910 C -4.60163 1.93401 0.68304 H -5.04789 2.92858 0.55280 H -3.52133 2.08525 0.84410 H -5.00696 1.48223 1.60165 C -6.12238 -1.72586 1.15158 H -6.62741 -0.75127 1.06348 H -6.63440 -2.32116 1.91668 H -6.23721 -2.21752 0.17508 C -4.67247 -1.51778 1.50234 C -4.23382 -2.05506 2.72863 H -4.95171 -2.69008 3.24639 C -3.06238 -1.75877 3.44473 C -2.93384 -2.35309 4.82375 H -1.94037 -2.80827 4.95152 H -3.70431 -3.11390 4.99878 H -3.02386 -1.58211 5.60308 C -1.12290 -0.46394 3.88693 C -1.48114 0.59379 4.74434 C -0.50832 1.13944 5.58766	

H -0.78958 1.96780 6.24532 C 0.80719 0.67644 5.59988 C 1.13688 -0.37260 4.73655 H 2.16005 -0.75964 4.72834 C 0.19994 -0.94903 3.87950 C 0.58323 -2.07193 2.96926 H 0.06842 -3.00925 3.23595 H 1.66594 -2.25453 2.97846 H 0.28376 -1.84514 1.93515 C 1.84864 1.28869 6.49137 H 1.42239 2.07663 7.12812 H 2.66307 1.73801 5.90003 H 2.30794 0.53412 7.14957 C -2.87613 1.14749 4.73707 H -3.57716 0.51272 5.30431 H -3.27408 1.20830 3.71395 H -2.90322 2.15004 5.18548	
ZnBe	**ZnMe**
Zn 2.81407 7.90019 3.00368 Be 0.92723 7.00162 3.60670 N 4.13422 9.36831 3.40301 N 3.96291 7.20105 1.46324 C 5.26715 9.58958 2.75182 C 5.71973 8.82344 1.66760 H 6.66197 9.13091 1.24064 C 5.11460 7.70884 1.06563 C 6.14605 10.73746 3.18997 H 7.04044 10.80415 2.57517 H 6.44245 10.61711 4.23340 H 5.60362 11.68252 3.12850 C 5.83720 7.06989 -0.09615 H 5.20582 7.07096 -0.98652 H 6.06539 6.02522 0.12336 H 6.76417 7.59223 -0.32120 C 3.75642 10.19963 4.49677 C 4.11060 9.82518 5.80476 C 3.65066 10.59973 6.86759 H 3.91225 10.32275 7.88103 C 2.85951 11.71766 6.65045 H 2.51074 12.30837 7.48819 C 2.51456 12.07396 5.35516 H 1.89167 12.94419 5.19202 C 2.95197 11.32894 4.26244 C 4.93462 8.57704 6.06765 H 5.34546 8.24727 5.11367 C 6.11468 8.83373 7.01052 H 6.72882 7.93510 7.10074 H 5.78042 9.10473 8.01397 H 6.74813 9.64241 6.64113 C 4.04249 7.44429 6.59513 H 3.22410 7.23933 5.90271	Zn -0.606311 1.480976 -0.000000 N -1.859159 2.978850 -0.000001 N -1.923539 0.035078 0.000000 C 1.352480 1.400862 -0.000002 H 1.811439 2.393731 0.000005 H 1.727162 0.868378 -0.879857 H 1.727164 0.868364 0.879843 C -3.168490 2.803620 -0.000000 C -3.223540 0.264730 -0.000000 C -3.802494 1.547660 -0.000001 C -4.075152 4.012881 0.000000 H -5.121262 3.714446 -0.000001 H -3.888081 4.633759 -0.879195 H -3.888082 4.633757 0.879197 C -4.181059 -0.904591 -0.000000 H -5.213512 -0.561893 0.000001 H -4.020433 -1.532857 0.879195 H -4.020434 -1.532856 -0.879196 H -4.883186 1.571130 -0.000001 C -1.327117 4.337320 -0.000000 C -1.447148 -1.343811 0.000001 H -0.357245 -1.336636 0.000001 H -1.779054 -1.895593 -0.885339 H -1.779054 -1.895592 0.885341 H -0.238502 4.286241 0.000000 H -1.636476 4.902037 0.885318 H -1.636476 4.902037 -0.885319

H 3.60571 7.71295 7.56005 H 4.61962 6.52585 6.72645 C 2.52013 11.70314 2.85550 H 3.15073 11.14985 2.15984 C 2.70182 13.19368 2.55246 H 2.46970 13.39672 1.50478 H 3.72804 13.51445 2.74150 H 2.04128 13.81523 3.16020 C 1.07096 11.26165 2.60466 H 0.77527 11.46917 1.57344 H 0.38525 11.79239 3.26965 H 0.95195 10.19211 2.78721 C 3.38295 6.06682 0.83550 C 3.64409 4.78323 1.34869 C 2.92407 3.70302 0.84349 H 3.10682 2.71058 1.23599 C 1.97502 3.87605 -0.15357 H 1.42101 3.02593 -0.53139 C 1.74883 5.14266 -0.67226 H 1.01702 5.27084 -1.45998 C 2.44589 6.25133 -0.19731 C 4.66521 4.57312 2.45326 H 5.23488 5.49674 2.55283 C 5.65855 3.45349 2.12405 H 5.16970 2.47814 2.08109 H 6.43412 3.39867 2.89102 H 6.14340 3.62452 1.16110 C 3.97757 4.32146 3.80103 H 3.31996 5.15156 4.06019 H 4.71663 4.20729 4.59748 H 3.37384 3.41110 3.76475 C 2.17162 7.63076 -0.77080 H 2.94279 8.30161 -0.39292 C 2.25354 7.65095 -2.30115 H 1.46113 7.05340 -2.75631 H 3.20935 7.25732 -2.65199 H 2.14909 8.67283 -2.67214 C 0.82285 8.17549 -0.28429 H 0.64853 9.18125 -0.67368 H 0.79405 8.21989 0.80471 H 0.00226 7.53529 -0.61797 C -0.89511 7.27682 4.14446 C -0.81927 6.67493 2.86403 C -0.07731 5.47572 2.98324 C 0.30192 5.33333 4.33930 C -0.20088 6.44594 5.05795 H -1.33782 8.23275 4.36985 H -1.18890 7.09754 1.94514 H 0.23309 4.84089 2.16930 H 0.93385 4.55798 4.73821 H -0.02305 6.66052 6.09860	

ZnOB				ZnSi			
Zn	1.767827	7.870657	14.935359	Zn	13.294418	17.551633	32.875441
O	1.446914	8.358328	13.242829	Si	13.027261	17.630633	30.509031
N	3.590489	7.512900	15.501030	Si	10.953574	16.713639	29.883941
N	0.801488	7.347361	16.521965	Si	14.657965	16.399917	29.357856
N	-0.072566	9.892894	11.947839	Si	13.051938	19.761703	29.499084
N	1.173936	8.390920	10.778200	N	13.398089	18.982915	34.240156
C	4.733000	8.073638	14.829062	N	13.400771	16.046957	34.168814
C	5.235360	9.303353	15.271062	C	13.411500	16.230882	35.485482
C	1.439979	6.687329	17.487417	C	12.307734	21.075973	33.565078
C	3.806814	6.771311	16.581932	C	12.429778	22.394973	33.146734
C	-0.762141	10.610530	12.966158	H	11.639479	22.893198	32.977067
C	5.320928	7.406634	13.752269	C	13.678389	12.033904	32.810409
C	-0.583644	7.679651	16.728581	C	13.398089	17.474560	36.112998
C	-0.923110	8.923463	17.262120	H	13.376295	17.449687	37.062522
C	2.795167	6.342458	17.455285	C	13.410159	18.749769	35.549543
H	3.071912	5.726736	18.123666	C	14.740580	14.102615	33.515576
C	4.561221	10.055249	16.387086	C	13.489287	14.687669	33.697085
H	3.679452	10.361692	16.088633	C	14.735215	20.951605	33.655347
H	5.108442	10.828899	16.637098	C	14.822390	12.785366	33.080731
H	4.456680	9.464919	17.162305	H	15.677185	12.387109	32.964400
C	5.224690	6.382478	16.953504	C	13.474534	20.354289	33.817929
H	5.661105	5.963175	16.182693	C	13.647542	23.009806	32.968137
H	5.204588	5.749748	17.701617	C	12.326510	13.957227	33.442293
H	5.724805	7.183248	17.216332	C	15.983826	20.166862	33.939258
C	2.136238	7.443622	10.333397	H	15.987568	19.888050	34.878785
C	-0.338646	10.027962	10.581298	H	16.768372	20.727463	33.762166
H	-0.947102	10.650824	10.201451	H	16.010890	19.375444	33.362943
C	6.372459	9.823010	14.657007	C	14.795567	22.282867	33.242827
H	6.721503	10.654644	14.955273	H	15.643147	22.700936	33.148433
C	3.327585	7.904007	9.749605	C	13.457099	19.909368	36.515326
C	0.674673	6.307743	18.742242	H	14.243402	20.462156	36.324742
H	0.330144	7.118124	19.172436	H	13.511483	19.569020	37.432723
H	1.273116	5.838899	19.360707	H	12.645677	20.450210	36.415399
H	-0.073355	5.721264	18.503831	C	12.441849	12.639979	33.004051
C	-1.573876	6.756304	16.380547	H	11.651375	12.140896	32.832491
C	6.460348	7.959793	13.174642	C	10.448900	17.204805	28.128061
H	6.876958	7.504607	12.452384	H	10.370147	18.180724	28.072006
C	0.392597	9.147819	9.891023	H	9.586339	16.795021	27.909134
H	0.384831	9.049633	8.946214	H	11.128581	16.895549	27.493896
C	-2.274747	9.220129	17.442768	C	13.171434	19.676397	27.613138
H	-2.514156	10.059372	17.818039	H	14.037200	19.294272	27.357861
C	-2.042115	10.167730	13.353609	H	13.089973	20.578747	27.239638
C	1.895517	6.075201	10.506199	H	12.449963	19.112187	27.265262
C	-0.125768	11.699871	13.566016	C	13.741423	24.444415	32.504658
C	3.628703	9.393701	9.686836	H	14.434569	24.908290	33.018367
H	2.753253	9.877189	9.682016	H	12.878970	24.888846	32.643168
C	2.853578	5.170197	10.046452	H	13.970532	24.464927	31.552367
H	2.702685	4.238058	10.150712	C	9.599952	17.344937	31.033660
C	4.731010	6.126136	13.226016	H	9.830603	17.127223	31.960860
H	4.669696	5.471804	13.953000	H	8.748281	16.919880	30.800416

H	5.303278	5.771107	12.514219
H	3.835614	6.301816	12.868343
C	-3.274217	8.336650	17.094922
C	4.254214	6.963379	9.301627
H	5.060638	7.255830	8.893290
C	-2.910052	7.107846	16.573339
H	-3.589235	6.485849	16.340083
C	7.007344	9.154792	13.620192
C	4.011238	5.603295	9.445660
H	4.646076	4.971717	9.128413
C	0.615148	5.577070	11.144728
H	0.184587	6.355692	11.601206
C	-2.728895	9.048526	12.578334
H	-2.470080	9.158673	11.618729
B	0.906231	8.834024	12.134465
C	-2.231838	7.676316	13.016224
H	-1.251953	7.674224	13.034345
H	-2.548282	6.997274	12.384459
H	-2.575455	7.474789	13.911640
C	0.855647	4.510620	12.193872
H	1.209638	3.703969	11.764537
H	0.010913	4.297800	12.642897
H	1.501750	4.840424	12.852744
C	0.134388	9.928215	17.624724
H	0.780953	9.516279	18.235007
H	-0.283622	10.698696	18.062951
H	0.595179	10.224956	16.812217
C	-4.736194	8.702897	17.262493
H	-4.820180	9.413636	17.931883
H	-5.238529	7.914952	17.557752
H	-5.094503	9.016707	16.406029
C	-2.627628	10.799262	14.441611
H	-3.480832	10.511647	14.744659
C	-1.214694	5.412289	15.802173
H	-2.032618	4.897468	15.639570
H	-0.643396	4.927028	16.433471
H	-0.734520	5.538050	14.957178
C	1.208961	12.207704	13.047422
H	1.349323	11.934111	12.095869
C	4.376606	9.819523	10.933442
H	3.856132	9.573823	11.726689
H	4.510761	10.790121	10.918534
H	5.246946	9.369826	10.961781
C	-0.774964	12.298204	14.650468
H	-0.370073	13.035411	15.092132
C	4.382995	9.798452	8.423417
H	5.283122	9.411316	8.442135
H	4.448474	10.775372	8.380711
H	3.901923	9.468633	7.635849
C	-1.997337	11.829330	15.085930
H	-2.407884	12.227426	15.844467
H	9.516626	18.316968	30.937615
C	11.489632	20.725641	29.898501
H	10.716298	20.270542	29.504665
H	11.560740	21.629743	29.528397
H	11.378384	20.777490	30.870593
C	15.997237	14.882103	33.798031
H	16.016510	15.686098	33.237052
H	16.779007	14.326372	33.598614
H	16.014498	15.143609	34.742605
C	13.455758	15.020485	36.399821
H	12.655588	14.474054	36.256167
H	13.485223	15.318092	37.333378
H	14.254882	14.490012	36.200646
C	10.963901	20.434866	33.787354
H	10.256042	21.083102	33.585850
H	10.888381	20.150028	34.721882
H	10.871053	19.657093	33.199488
C	13.789704	10.597543	32.361004
H	14.255177	10.559620	31.499759
H	12.892542	10.214315	32.264669
H	14.293346	10.084674	33.027540
C	10.974630	14.559798	33.715527
H	10.898413	14.771083	34.669468
H	10.275583	13.919794	33.465928
H	10.870369	15.379575	33.189588
C	14.843848	14.654388	30.013521
H	15.136715	14.686951	30.948146
H	15.510078	14.174695	29.478701
H	13.982763	14.191214	29.956302
C	10.963901	14.826050	29.929076
H	11.568237	14.485738	29.237012
H	10.057512	14.490432	29.764990
H	11.270086	14.521839	30.808909
C	14.240331	16.216868	27.518016
H	13.331018	15.863226	27.423088
H	14.875848	15.600196	27.098459
H	14.297356	17.092225	27.081278
C	16.320454	17.225824	29.517526
H	16.314379	18.072156	29.023084
H	17.014204	16.638580	29.150237
H	16.509154	17.401761	30.463071
C	14.538066	20.772936	30.031478
H	14.469681	20.977179	30.987457
H	14.564487	21.609634	29.520438
H	15.358085	20.263098	29.864092

C	8.253373	9.733116	12.990257
H	8.041999	10.599767	12.584237
H	8.584698	9.121321	12.300094
H	8.941256	9.853571	13.677675
C	2.364628	11.776576	13.904896
H	2.268109	12.161680	14.800928
H	3.202912	12.088204	13.504069
H	2.376942	10.798808	13.969178
C	-0.350838	5.076816	10.091474
H	-0.536743	5.794559	9.450947
H	-1.186388	4.797250	10.520696
H	0.045455	4.313611	9.620872
C	-4.246892	9.086424	12.634191
H	-4.545106	8.905151	13.549166
H	-4.612699	8.406504	12.029999
H	-4.561677	9.972313	12.356717
C	1.270753	13.572032	12.445509
H	1.056313	14.240628	13.127789
H	0.624226	13.634291	11.711202
H	2.173472	13.735296	12.099363

ZnZn

Zn	2.675860	2.301487	5.823516
N	1.971775	1.743525	7.615396
N	4.472390	2.810784	6.541403
C	2.714963	1.660460	8.723069
C	4.051568	2.054809	8.802351
H	4.474881	1.904621	9.638687
C	4.859992	2.648010	7.803477
C	2.092132	1.141094	10.013147
H	1.385717	1.754433	10.304729
H	2.780212	1.081523	10.707760
H	1.708153	0.252551	9.856286
C	6.231484	3.117873	8.256461
H	6.921631	2.670664	7.723817
H	6.355929	2.897205	9.203489
H	6.300402	4.087803	8.134416
C	0.568753	1.407909	7.703949
C	-0.364450	2.402172	8.031672
C	-1.716761	2.057326	8.109818
H	-2.350910	2.726041	8.342554
C	-2.162588	0.770239	7.859485
C	-1.214031	-0.198013	7.524004
H	-1.507554	-1.086557	7.354844
C	0.144215	0.088938	7.427125
C	0.066807	3.838608	8.253623
H	-0.724988	4.406638	8.350123
H	0.595398	4.143180	7.485404
H	0.611376	3.894824	9.067254
C	-3.643490	0.444691	7.924386
H	-4.126066	1.198149	8.323633
H	-3.777946	-0.356592	8.473114

H	-3.981503	0.281078	7.019931
C	1.145184	-0.973286	7.036961
H	0.672783	-1.809809	6.840176
H	1.772872	-1.118440	7.774905
H	1.637681	-0.682140	6.240359
C	5.427551	3.410698	5.618973
C	6.386231	2.597668	5.006100
C	7.297933	3.203455	4.140246
H	7.965411	2.665630	3.727565
C	7.268208	4.553470	3.860773
C	6.288838	5.336294	4.470239
H	6.261816	6.269307	4.289538
C	5.345685	4.781689	5.338175
C	6.437385	1.108372	5.264002
H	7.195080	0.719057	4.779608
H	5.604901	0.694725	4.955580
H	6.546245	0.947276	6.225222
C	8.291369	5.171843	2.896904
H	9.062012	4.571929	2.809865
H	8.589879	6.036893	3.248847
H	7.876911	5.301055	2.018940
C	4.265330	5.645900	5.975456
H	4.395276	6.580591	5.708661
H	4.323860	5.574582	6.949921
H	3.384789	5.340490	5.676494
Zn	1.732291	2.301487	3.637308
N	2.436376	1.743525	1.845428
N	-0.064239	2.810784	2.919421
C	1.693188	1.660460	0.737755
C	0.356582	2.054809	0.658473
H	-0.066730	1.904621	-0.177863
C	-0.451841	2.648010	1.657347
C	2.316019	1.141094	-0.552323
H	3.022433	1.754433	-0.843905
H	1.627939	1.081523	-1.246937
H	2.699998	0.252551	-0.395462
C	-1.823333	3.117873	1.204363
H	-2.513480	2.670664	1.737007
H	-1.947778	2.897205	0.257334
H	-1.892251	4.087803	1.326408
C	3.839397	1.407909	1.756875
C	4.772601	2.402172	1.429152
C	6.124912	2.057326	1.351006
H	6.759060	2.726041	1.118269
C	6.570739	0.770239	1.601339
C	5.622182	-0.198013	1.936820
H	5.915705	-1.086557	2.105979
C	4.263936	0.088938	2.033699
C	4.341343	3.838608	1.207201
H	5.133138	4.406638	1.110701
H	3.812752	4.143180	1.975420

H	3.796774	3.894824	0.393570
C	8.051641	0.444691	1.536438
H	8.534216	1.198149	1.137191
H	8.186097	-0.356592	0.987710
H	8.389653	0.281078	2.440893
C	3.262966	-0.973286	2.423863
H	3.735367	-1.809809	2.620648
H	2.635279	-1.118440	1.685919
H	2.770469	-0.682140	3.220464
C	-1.019400	3.410698	3.841851
C	-1.978080	2.597668	4.454724
C	-2.889782	3.203455	5.320578
H	-3.557261	2.665630	5.733259
C	-2.860057	4.553470	5.600051
C	-1.880687	5.336294	4.990585
H	-1.853665	6.269307	5.171286
C	-0.937534	4.781689	4.122649
C	-2.029234	1.108372	4.196821
H	-2.786929	0.719057	4.681216
H	-1.196750	0.694725	4.505244
H	-2.138094	0.947276	3.235602
C	-3.883218	5.171843	6.563920
H	-4.653861	4.571929	6.650959
H	-4.181728	6.036893	6.211977
H	-3.468761	5.301055	7.441884
C	0.142820	5.645900	3.485368
H	0.012874	6.580591	3.752163
H	0.084290	5.574582	2.510903
H	1.023362	5.340490	3.784330

References for supporting information

s1 S. Schulz, T. Eisenmann, U. Westphal, S. Schmidt, U. Flörke, *Zeitschrift für anorganische und allgemeine Chemie* **2009**, *635*, 216-220.

s2 J. Prust, A. Stasch, W. Zheng, H. W. Roesky, E. Alexopoulos, I. Usón, D. Böhler, T. Schuchardt, *Organometallics* **2001**, *20*, 3825-3828.

s3 M. M. D. Roy, J. Hicks, P. Vasko, A. Heilmann, A.-M. Baston, J. M. Goicoechea, S. Aldridge, *Angewandte Chemie International Edition* **2021**, *60*, 22301-22306.

s4 J. T. Boronski, A. E. Crumpton, L. L. Wales, S. Aldridge, *Science* **2023**, *380*, 1147-1149.

s5 K. W. Klinkhammer, *Chemistry – A European Journal* **1997**, *3*, 1418-1431.

s6 J. Cosier, A. M. Glazer, *Journal of Applied Crystallography* **1986**, *19*, 105-107.

s7 A. Technologies, **2011**.

s8 G. Sheldrick, *Acta Crystallographica Section A* **2015**, *71*, 3-8.

s9 G. Sheldrick, *Acta Crystallographica Section C* **2015**, *71*, 3-8.

s10 O. V. Dolomanov, L. J. Bourhis, R. J. Gildea, J. A. K. Howard, H. Puschmann, *Journal of Applied Crystallography* **2009**, *42*, 339-341.

s11 M. Bauer, *Physical Chemistry Chemical Physics* **2014**, *16*, 13827-13837.

s12 L. J. P. Ament, M. van Veenendaal, T. P. Devereaux, J. P. Hill, J. van den Brink, *Reviews of Modern Physics* **2011**, *83*, 705-767.

s13 J.-D. Chai, M. Head-Gordon, *Physical Chemistry Chemical Physics* **2008**, *10*, 6615-6620.

s14 F. Neese, *WIREs Computational Molecular Science* **2012**, *2*, 73-78.

s15 F. Neese, *WIREs Computational Molecular Science* **2022**, *12*, e1606.

s16 E. Caldeweyher, C. Bannwarth, S. Grimme, *The Journal of Chemical Physics* **2017**, *147*, 034112.

s17 J. K. B. E. D. Glendening, A. E. Reed, J. E. Carpenter, J. A. Bohmann, C. M. Morales, P. Karafiloglou, C. R. Landis, F. Weinhold, **2018**.

s18 E. D. Glendening, C. R. Landis, F. Weinhold, *Journal of Computational Chemistry* **2019**, *40*, 2234-2241.

s19 T. Lu, F. Chen, *Journal of Computational Chemistry* **2012**, *33*, 580-592.

s20 R. Bianchi, G. Gervasio, D. Marabello, *Inorganic Chemistry* **2000**, *39*, 2360-2366.

Conclusions and outlook

The data generated in this study offers a means of comparing the ligand properties of highly disparate X-ligands, ranging from low oxidation state aluminium and beryllium, to a simple methyl group or bulky O-donor ligand. This demonstrates both the chemical versatility and also the spectroscopic utility of the (Nacnac^{Ar})Zn unit. Such studies allow us to better rationalise the ligand properties of more unusual ligands, through comparison with simpler, more common and well understood motifs.

The comparison of measured spectra to computationally generated parameters allows us to extrapolate to ligand systems which haven't been measured in this study through methods that give the best agreement to the experimental data. Here it is shown that TD-DFT based predictive methods as well as basin-based analyses yield the closest agreement with experiment. By this method, the data accessed here by (non-trivial) synchrotron based spectroscopic methods can provide insight more generally into the ligand properties of other X-type ligands by pure computational investigations.

Future work could well include using such computational methods to analyse ligand motifs such as the heavier trielyls which were not included in this study due to the time limited nature of beamline access. Additionally, in work already underway, analysis into the effect on a given ligand of coordination to a range of different metals can be explored by analogous spectroscopic methods. To this end, we have investigated the aluminium-centred electronic structure of a range of metal aluminyl complexes, with data analysis currently underway. We hope that this will improve our understanding of how aluminyl ligands engage in bonding with metal centres from across the Periodic Table.

Statement of Authorship for joint/multi-authored papers for PGR thesis

To appear at the end of each thesis chapter submitted as an article/paper

The statement shall describe the candidate's and co-authors' independent research contributions in the thesis publications. For each publication there should exist a complete statement that is to be filled out and signed by the candidate and supervisor **(only required where there isn't already a statement of contribution within the paper itself).**

Title of Paper	Quantifying X-ligand donor properties via X-ray spectroscopy of (Nacnac^{Ar})ZnX species
Publication Status	□Published □ Accepted for Publication □Submitted for Publication √Unpublished and unsubmitted work written in a manuscript style
Publication Details	Liam P. Griffin, Lewis Parker, Frances Tower-Tompkins, Shusaku Hayama, Kevin R. J. Lovelock* Josef T. Boronski* Simon Aldridge*

Student Confirmation

Student Name:	Liam P. Griffin		
Contribution to the Paper	Synthesised all samples, and performed all crystallographic and spectroscopic characterization of novel compounds. Prepared samples X-ray spectroscopic analysis. Performed a significant portion of the quantum chemical calculations. Analysed and interpreted all experimental and computational data. Wrote the manuscript and prepared the SI.		
Signature	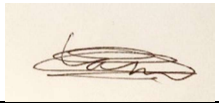	Date	7 October 2024

Supervisor Confirmation

By signing the Statement of Authorship, you are certifying that the candidate made a substantial contribution to the publication, and that the description described above is accurate.

Supervisor name and title: Professor Simon Aldridge			
Supervisor comments: I can confirm that the candidate made a substantial contribution to the work described in this chapter, as outlined above.			
Signature	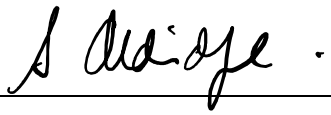	Date	8 October 2024

Probing the *trans* influence of trielyl ligands via analysis of linear d^{10} complexes

Introduction

In this chapter, the *trans* influence of aluminyl, gallyl and indyl metallo-ligands is probed experimentally. Taking stock of the results described in chapter 2, isostructural series, in which the supporting ligand framework of the group 13 element remains consistent, were targeted. To this end, the synthesis of an NON indyl source is conducted via the In(I) precursor InCp. The resulting coordination polymer, as well as TMEDA and 18-crown-6 coordinated analogues are reported and characterised, and utilised to complete the series of reported aluminium and gallium silver phosphine complexes, which offer the highly sensitive $^{1}J_{AgP}$ coupling constant as an experimental measure of the trans influence. This approach was then extended to boryl mercury systems, which also allow for comparisons both to bis(boryl) mercury systems, and between supporting ligand systems in the case of gallyl ligands.

These investigations allow us to parameterise experimentally the donor strength of these exotic ligands via a number of spectroscopic handles. Additionally, due to the isostructural nature of the complexes, this study permits analysis of fundamental bonding trends within group 13 independent of supporting ligand set.

Mercury-Group 13 Metal Covalent Bonds: A Systematic Comparison of Aluminyl, Gallyl and Indyl Metallo-ligands

Liam P. Griffin, Mathias A. Ellwanger, Agamemnon E. Crumpton, Matthew M. D. Roy, Andreas Heilmann, Simon Aldridge*

[*] L. P. Griffin, Dr. M. A. Ellwanger, A. E. Crumpton, Dr. M. M. D. Roy, Dr. A. Heilmann, Prof. S. Aldridge
Inorganic Chemistry Laboratory, Department of Chemistry,
University of Oxford
South Parks Road, Oxford, OX1 3QR (UK)
E-mail: simon.aldridge@chem.ox.ac.uk

Abstract

Bimetallic compounds containing direct metal-group 13 element bonds have been shown to display unprecedented patterns of cooperative reactivity towards small molecules, which can be influenced by the identity of the group 13 element. In this context, we present here a systematic appraisal of group 13 metallo-ligands of the type $[(NON)E]^-$ (NON = 4,5-bis(2,6-di*iso*propylanilido)-2,7-di-tert-butyl-9,9-dimethylxanthene) for E = Al, Ga and In, through a comparison of structural and spectroscopic parameters associated with the *trans* L or X ligands in linear d^{10} complexes of the types LM{E(NON)} and XM'{E(NON)}. These studies are facilitated by convenient syntheses (from the In(I) precursor, InCp) of the potassium indyl species $[\{K(NON)In\}\cdot KCp]_n$ (**1**) and $[(18\text{-crown-}6)_2K_2Cp][(NON)In]$ (**1'**), and lead to the first structural characterisation of Ag–In and Hg–E (E = Al, In) covalent bonds. The resulting structural, spectroscopic and quantum chemical probes of Ag/Hg complexes are consistent with markedly stronger σ-donor capabilities of the aluminyl ligand, $[(NON)Al]^-$, over its gallium and indium counterparts.

Introduction

Bimetallic compounds featuring metals of different electronic character have received significant recent attention, not least due to their potential for the activation of small molecules in cooperative fashion. Systems featuring direct metal-metal bonds have featured heavily in such studies, with the proximity of the two metal centres, and the electronic perturbation brought about by the covalent interaction, helping to enable novel patterns of reactivity not accessible to either metal in isolation.[1] One class of bimetallic compound of this sort are systems featuring a late *d*-block metal (M) and a group 13 element (E) such as aluminium - with the combination of electron-rich and electron-deficient metal centres allowing for the activation of kinetically inert substrates, such as C–H and C–F bonds, and CO_2.[2-4]

The study and use of 'metallo-ligands' featuring Group 13 metal centres has been greatly accelerated in recent years due to the development of nucleophilic sources of the $[EX_2]^-$ unit (typically as group 1 metal salts),[5] which allow access to M-Group 13 linkages via metathesis chemistry. Historically, anionic gallyl and boryl reagents were the first to be accessed (Figure 1);[6,7] since then $[BX_2]^-$ and $[GaX_2]^-$ ligands have been widely installed at metal centres from across the Periodic Table, with metal boryl complexes, for example, showing widespread synthetic utility in C–H borylation chemistry.[8] Subsequently, both thallyl and indyl systems were accessed by our group and the group of Coles, respectively,[9,10] with the most electropositive Group 13 element aluminium predictably being the last to yield tractable systems of the type $[EX_2]^-$.[11,12] As such, aluminyl and indyl metallo-ligands have been much less widely applied than their boryl and gallyl equivalents;[2,13,14] to our knowledge, no examples of covalently bound metal thallyl complexes currently exist.

While a number of supporting ligand frameworks have been employed to stabilize anionic E(I) systems, systematic comparison of their behaviour as metallo-ligands as a function of the Group 13 metal (*i.e.* E = Al, Ga, In) has proved difficult due to the absence of a contiguous set of identically-supported systems. With this in mind, we sought a convenient source of the $[(NON)In]^-$ anion (NON =

4,5-bis(2,6-di*iso*propylanilido)-2,7-di-tert-butyl-9,9-dimethylxanthene), so that its chemistry as a metallo-ligand could be systematically compared with that of its previously reported aluminium and gallium congeners.[11a] These studies are reported here.

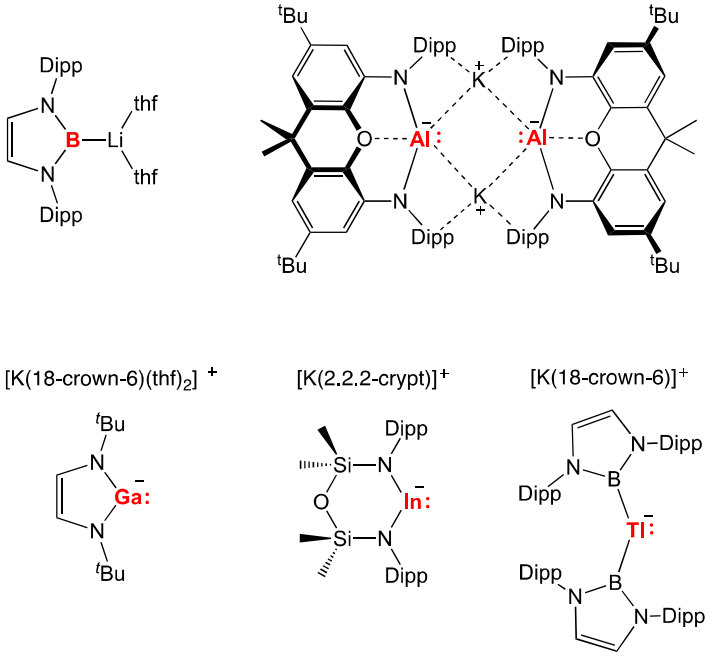

Figure 1; Early examples of trielyl anions relevant to the current study.

Results and Discussion

In contrast to previously reported methodologies for the synthesis of group 13 systems of the type $[EX_2]^-$ (which largely rely on the reduction of E(III) halide precursors),[11g] we hypothesised that the more readily available nature of E(I) precursors might offer an alternative metathesis approach for the heavier group 13 metals. With this in mind, we examined InCp as a convenient In(I) source,[15] aiming to use the reaction with K_2[NON] to access the potassium salt of the indyl anion, $[K\{(NON)In\}]_n$, and precipitate the sparingly soluble KCp by-product. In practice, this reaction proceeds rapidly, leading to the formation of a bright yellow solution, followed by immediate precipitation of a yellow microcrystalline material. Some of the crystalline material was of sufficient quality for single crystal X-ray diffraction studies, although due to relatively rapid crystallisation, the data obtained can only be used to establish connectivity. The structure of $[\{K(NON)In\}\cdot KCp]_n$, **1** (Figure 2), confirms that In(I) has been assimilated by the NON framework via substitution of the cyclopentadienyl ligand. However, the KCp co-product, rather than precipitating out of the benzene reaction solvent, has been retained, resulting in a coordination polymer in which $[(NON)In]^-$ fragments are bridged by potassium arene interactions involving both the Cp and NON fragments.

1 is resolutely insoluble in compatible solvents (but can act as a viable source of the $[(NON)In]^-$ unit *in situ*, see below). With the aim of generating a more tractable derivative, however, two equivalents of 18-crown-6 were added, leading to the formation of a related species **1'**, featuring discrete $[(18\text{-crown-6})K(\mu_2\text{-}\eta^5,\eta^5\text{-}C_5H_5)K(18\text{-crown-6})]^+$ and $[(NON)In]^-$ ions.[10] Crystallization from *ortho*-difluorobenzene yielded single crystals suitable for X-ray crystallography (Figure 2), and **1'** could also be characterised in solution by multinuclear NMR spectroscopy. The KCp by-product is again retained, this time in the form of the crown ether inverse-sandwich cation $[(18\text{-crown-6})K(\mu_2\text{-}\eta^5,\eta^5\text{-}C_5H_5)K(18\text{-crown-6})]^+$. No close K···In contacts are observed in the solid state.

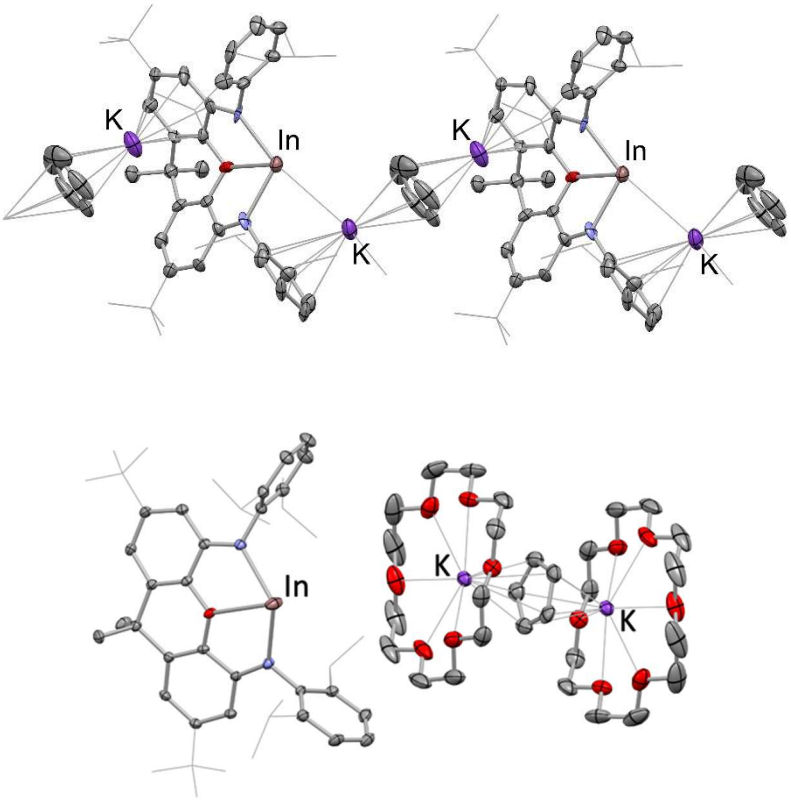

*Figure 2; Molecular structures of [{K(NON)In}·KCp]$_n$ (**1**; upper), and [(18-crown-6)K(μ_2-η^5,η^5-C_5H_5)K(18-crown-6)][(NON)In] (**1'**, lower) in the solid state as determined by X-ray crystallography. Hydrogen atoms and solvent molecules omitted, and selected groups shown in wireframe format for clarity; thermal ellipsoids set at the 40 % level. Key bond lengths (Å) and angles (°): (for **1'**) In–N 2.342(4), 2.388(3); In–O 2.564(3); 120.7(1).*

With a complete set of NON-stabilised aluminyl, gallyl and indyl systems in hand, complexation studies were targeted to give systematic insight into their electronic structure, and (in particular) to probe their relative capabilities as σ-donor metallo-ligands. With a view to minimising the complicating influence of steric factors, we targeted linear d^{10} metal complexes of the types LAgE(NON) and XHgE(NON). In the former case, the aluminyl and gallyl complexes (^{t}Bu$_3$P)AgAl(NON) and (^{t}Bu$_3$P)AgGa(NON) have previously been reported by us,[2l] and so (^{t}Bu$_3$P)AgIn(NON) was targeted for initial comparison, via the bond length and coupling constant associated with the Ag–P bond *trans* to the indyl ligand. Accordingly, the reaction of (^{t}Bu$_3$P)AgI with **1** in toluene leads to the immediate formation of a bright yellow solution, and a colourless precipitate. Single crystals of the product were obtained from hexane solution, and X-ray crystallography was exploited to confirm the identity of the

silver indyl complex **2** (Figure 3 and Table 1). As such, this chemistry not only delivers the first example of a silver–indium covalent bond,[16] but also, confirms that KCp inclusion species **1** is able to react as a functional source of the indyl anion [(NON)In]$^-$.

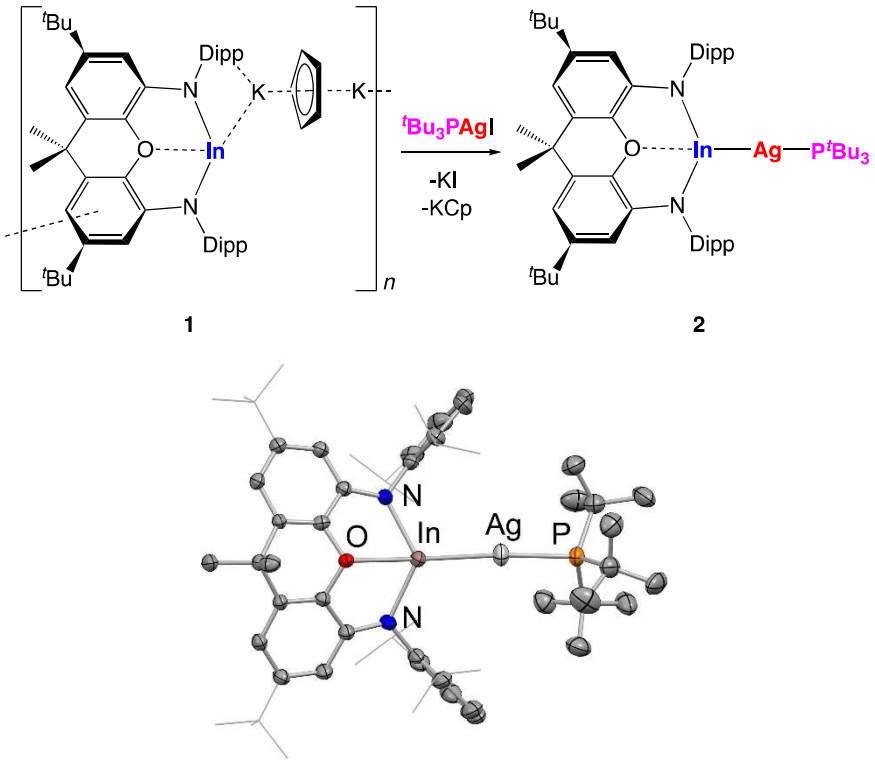

*Figure 3; (upper) Synthesis and (lower) molecular structure of (^{t}Bu$_3$P)AgIn(NON), **2**, in the solid state as determined by X-ray crystallography. Hydrogen atoms and solvent molecules omitted, and selected groups shown in wireframe format for clarity; thermal ellipsoids set at the 40 % level. Key bond lengths (Å) and angles (°): Ag–P 2.408(1), Ag–In 2.584(1), P–Ag–In 172.8(1).*

M	*d*(Ag-P)/Å	δ_P/ppm	$^1J_{Ag\text{-}P}$/Hz
Al[2l]	-	58.9	161 (broad)[a]
Ga[2l]	2.4335(6)	65.4	278, 322
In	2.408(1)	68.5	334, 385

Table 1; NMR parameters and bond lengths for silver complexes (^{t}Bu$_3$P)AgM(NON) (M = Al, Ga, In). [a] Not resolved into ^{107}Ag and ^{109}Ag components due to quadrupolar broadening (^{27}Al; I = 5/2).

The structure of **2** features a near linear P–Ag–In skeleton (172.8(1)°) in common with its gallyl counterpart;[2l] the P–Ag bond *trans* to the metallo-ligand is somewhat shorter for the indyl compound (2.408(1) vs 2.4335(6) Å), implying that the heavier trielyl ligand has a weaker *trans* influence. Consistently, the $^1J_{AgP}$ coupling constants measured for **2** in benzene-d$_6$ solution (334 and 385 Hz for

the ^{107}Ag and ^{109}Ag isotopes, respectively) are larger than those measured for (^{t}Bu$_3$P)AgGa(NON) (278 and 322 Hz).[2l] For additional context, the corresponding $^{1}J_{AgP}$ coupling constant measured for (^{t}Bu$_3$P)AgAl(NON) is *much* lower (161 Hz) and is not resolved into ^{107}Ag/^{109}Ag components, presumably due to the quadrupolar nature of ^{27}Al. In addition, the ^{31}P NMR spectrum of the aluminyl complex in benzene-d_6 solution features 'free' ^{t}Bu$_3$P in equilibrium with the complex itself, consistent with the very high *trans* labilising ability of the [(NON)Al]$^-$ donor.[2l] As such, we have been unable to crystallise (^{t}Bu$_3$P)AgAl(NON) from hydrocarbon solution. With this in mind, we turned instead to mercury(II) systems of the type XHgE(NON), hypothesizing that the X-ligand would be less labile, and would therefore allow us to structurally characterise (for the first time) a complete series of otherwise identical aluminyl, gallyl and indyl complexes.

While a number of supporting Hg–X systems were examined, most promising results were obtained for the borylmercury systems {(HCDippN)$_2$}BHgE(NON) (hitherto abbreviated as (boryl)HgE(NON)), for which (i) the bromide-bridged precursor [(boryl)Hg(μ-Br)]$_2$, is readily available;[17] and (ii) benchmarking of the [(NON)E]$^-$ ligands against other supporting group 13 ligand frameworks is also possible, by comparison with the known compounds (boryl)$_2$Hg and (boryl)Hg{Ga(NDippCH)$_2$}.[17]

Gallyl complex (boryl)HgGa(NON) is the most straightforward to synthesise and isolate (Scheme 1 and Figure 4). Addition of [(boryl)Hg(μ-Br)]$_2$ to a solution of K$_2$[(NON)Ga]$_2$ in benzene-d_6 leads to clean conversion to a new highly symmetrical species, (as judged by the presence of two Dipp CH_3 and one Dipp CH signals for the NON backbone in the ^{1}H NMR spectrum). Crystallisation from hexane yields a pale-yellow crystalline material in 62 % yield, which is stable at room temperature (in an inert atmosphere) and can be characterised by multinuclear NMR spectroscopy and elemental microanalysis. Moreover, X-ray diffraction could be employed to confirm the structure of the mercury gallyl product, (boryl)HgGa(NON), **4** (Figure 4 and Table 2). This compound offers direct comparison

on another level with the diazabutadiene-supported gallyl complex (boryl)Hg {Ga(NDippCH)$_2$},[17] which was previously reported by us, and which also features the expected linear Ga–Hg–B skeleton.

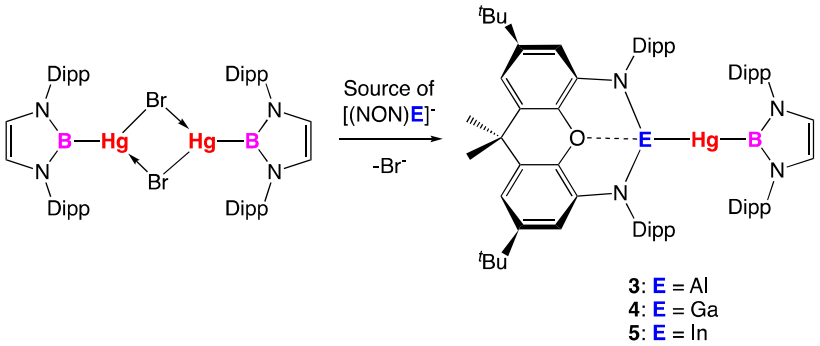

*Scheme 1; Syntheses of (boryl)HgE(NON) complexes (E = Al (**3**), Ga (**4**), In (**5**)) from [(boryl)Hg(μ-Br)]$_2$.*

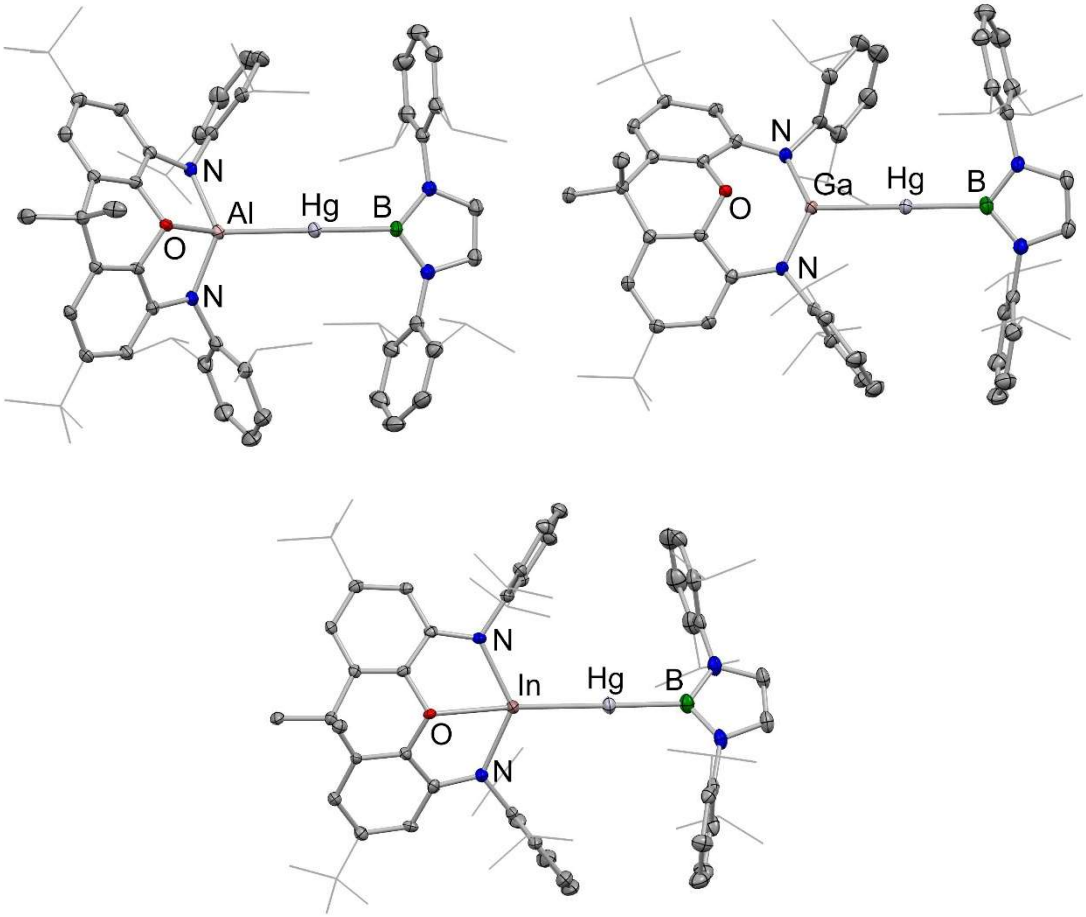

*Figure 4; Molecular structures of **3** (upper), **4** (centre) and **5** (lower) in the solid state as determined by X-ray crystallography. Hydrogen atoms and solvent molecules omitted, and selected groups shown in wireframe format for clarity; thermal ellipsoids set at the 40 % level. For key geometric data see Table 2.*

The indium congener, (boryl)HgIn(NON) (**5**) can be synthesized in similar fashion from (boryl)Hg(μ-Br)]$_2$ and *in situ* generated **1**, with accompanying precipitation of KBr and KCp. ^{1}H NMR spectroscopy is consistent with a molecular structure in solution similar to that of **4**, and single crystals could also be obtained from hexane, although in lower yields (ca. 34 %) due to slow decomposition of the product to indium metal. X-ray diffraction confirms the formation of complex **5** (Figure 4 and Table 2), which features the first example of an unsupported covalent bond between indium and mercury.

Finally, in the case of the more highly reducing aluminyl anion, the analogous synthetic approach is not as straightforward. Addition of [(boryl)BHg(μ-Br)]$_2$ to a solution of K$_2$[(NON)Al]$_2$ at room temperature leads to a complex ^{1}H NMR spectrum in which (boryl)$_2$Hg (**6**) can be observed as

well as a major new species, the signals of which decrease steadily over the course of 1 h at room temperature. Use of the less reducing bis(aluminyl)-magnesium compound, Mg{Al(NON)}$_2$,[18] as the aluminyl source results in a cleaner product mixture (as judged by *in situ* ^{1}H NMR), with fewer unidentified side products, but decomposition of the major species still proceeds at room temperature. Reaction in a concentrated toluene solution at room temperature followed by immediate filtration and storage at 243 K, however, leads to the formation of single crystalline material, allowing for its investigation by X-ray crystallography. The solid-state structure determined confirms the formation of (boryl)HgAl(NON) (**3**; Figure 4 and Table 2), a mercury aluminyl complex, and the first structurally authenticated species containing a Hg–Al bond.

	M/E	*d*(Hg-B) (Å)	*d*(Hg-E) (Å)	r_{cov}(E) (Å)[19]	∠(B-Hg-M) (°)	δ_B (ppm)
3	Al	2.222(3)	2.594(1)	1.21	175.2(1)	75.7
4	Ga	2.181(4)	2.554(1)	1.22	179.5(1)	60.0
5	In	2.199(7)	2.709(1)	1.42	178.0(2)	54.4
6[17]	B	2.150(3)	2.151(3)	0.84	179.0(1)	68.6
7[17]	Ga	2.116(5)	2.476(1)	1.22	179.1(1)	56.4

*Table 2; Structural parameters for mercury complexes (boryl)HgM(NON) (M = Al (**3**), Ga (**4**), In(**5**)) and related compounds.*

Structurally, complexes **3** - **5** feature very similar close-to-linear coordination geometries at the central metal centre, consistent with expectations for divalent mercury. The Hg–B bond lengths associated with the boryl group *trans* to the Al-, Ga- or In-based metallo-ligand are consistent with the hypothesis that the aluminyl ligand is a stronger σ-donor that its gallyl counterpart: the bond length is significantly longer for the aluminium donor (2.222(3) vs 2.181(4) Å). Unfortunately, the quality of the X-ray data in the case of indyl complex **5** renders any related analysis statistically insignificant. Interestingly, comparison of the structural data measured for the gallyl systems **4** and (boryl)Hg{Ga(NDippCH)$_2$} (**7**) reveals a markedly longer *trans* Hg–B bond in the case of **4** (2.181(4) vs. 2.116(5) Å) suggesting that the NON-ligand frame-work confers stronger donor properties on the group 13 donor than its diazabutadiene-derived analogue.

With a view to better understanding the structural properties of compounds **3**-**5** we also examined their electronic structures through a variety of quantum chemical techniques – carried out in each case on related model systems (**3***-**5***) in which the backbone ^{t}Bu groups of the NON ligands were replaced by Me for computational efficiency (see ESI for computational details). The geometries of the fully optimized structures agree closely with those measured crystallographically in the solid state, especially with respect to the Hg–B and Hg–E bond lengths. Quantum Theory of Atoms in Molecules (QT-AIM) and Electron Localization Function (ELF) methods were found to be the most informative probes of electronic structure; key data for model compounds **3***-**5*** are listed in Table 3 and shown pictorially (in the case of aluminyl compound **3***) in Figure 5.

	Bond	$\rho(r)$ (e Å^{-3})	$\nabla^2\rho(r)$ (e Å^{-5})	WBI	Occupancy of ELF basin (e$^-$)
3*	Hg–B	0.100	-0.030	0.365	1.959 (37.6% Hg; 59.5% B)
	Hg-Al	0.059	0.013	0.545	1.862 (75.5% Hg; 21.8% Al)
4*	Hg–B	0.105	-0.054	0.466	1.939 (41.6% Hg; 55.9% B)
	Hg–Ga	0.069	0.004	0.516	1.919 (44.6% Hg; 54.1% Ga)
5*	Hg–B	0.105	-0.068	0.429	1.883 (44.0% Hg; 53.8% B)
	Hg–In	0.056	0.032	0.490	1.756 (40.8% Hg; 57.9% In)

*Table 3; Selected (calculated) parameters relating to the Hg–E and Hg–B bonds in model mercury complexes **3*-5***.*

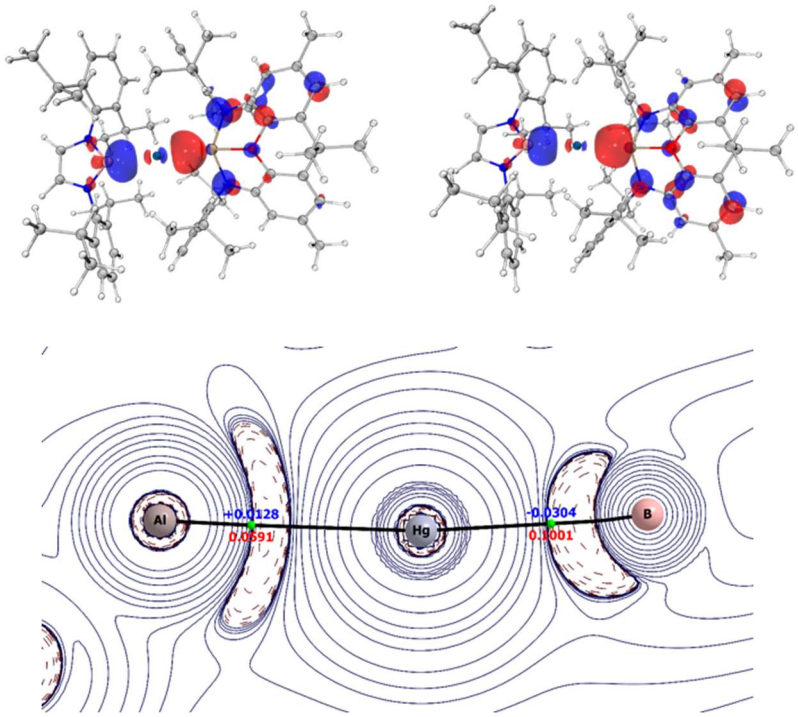

Figure 5; Analysis of bonding in model mercury aluminyl complex 3: (upper) HOMO and HOMO-3 of 3*; (lower) Contour plot of the Laplacian of the electron density in the plane of the Al–Hg–B moiety from QT-AIM analysis: Bond Critical Points (BCPs) are shown in green, along with the electron density [ρ(r)] and Laplacian of the electron density [$\nabla^2\rho(r)$] at the Hg–Al and Hg–B bond critical points.*

In each of **3***-**5*** the HOMO and HOMO-3 are identified as σ-bonding orbitals extending across the whole of the E–Hg–B unit, with the HOMO-3 becoming the more dominant bonding component from Al to Ga to In. QT-AIM methods were also used to probe the nature of both Hg–B and Hg–E bonds. Conventional bond paths and Bond Critical Points (BCPs) were located for all Hg–E/Hg–B linkages (Figure 5). Analysis of both the electron density at the critical point ρ(*r*) and its Laplacian $\nabla^2\rho(r)$, together with the associated kinetic and potential energy densities at the BCPs classify the Hg–B bonds as (polar) covalent and the Hg–E bonds as metallic (Table 3).[20] Comparisons of (i) the values of ρ(*r*) for the Hg–B bonds (0.100, 0.105, 0.105 e $Å^{-3}$, for **3***, **4*** and **5***, respectively); (ii) the Wiberg Bond Indices (WBIs) for the Hg–B bonds (0.365, 0.466 and 0.429) and (iii) the Bader charges at mercury (-0.44, -0.06 and -0.01) and all imply that the aluminyl ligand in **3*** is the strongest σ-donor of the three metallo-ligands. ELF calculations were also used to analyse the electron density in the regions between the Hg and E/B nuclei, and provide further corroboration that the $[(NON)Al]^-$ system is the strongest

σ-donor of the three. As such, the Hg–B bond is more polarized towards boron, and the Hg–E bond *significantly* more polarized towards mercury in the case of (model) aluminyl complex **3*** (i.e. for E = Al; Table 3).

Conclusion

Facile syntheses of sources of the indyl anion $[(NON)In]^-$ are reported, and their utility in the construction of In–Ag and In–Hg covalent bonds has been demonstrated. In both cases the corresponding aluminium and gallium congeners have also been synthesised, thereby providing two complete series showcasing the three metallo-ligands $[(NON)E]^-$ (E = Al, Ga, In) in which the supporting ligand scaffold is unchanged. Crystallographic, spectroscopic and quantum chemical comparisons of these complexes provide insight into how the geometric and electronic structure of these ligands varies as group 13 is descended, and also allows for comparison with metallo-ligands featuring alternative supporting frameworks. In this regard the NON-supported systems are thought to be stronger σ-donors than their diazabutadiene-derived analogues, with $[(NON)Al]^-$ offering the most potent σ-donation - consistent with aluminium's position as the most electropositive metal of Group 13.[21]

Acknowledgements

We thank the EPSRC Centre for Doctoral Training in Inorganic Chemistry for Future Manufacturing (OxICFM, EP/S023828/1, studentships to L.P.G. and A.E.C.), the Leverhulme Trust (studentship to A.H.) and the Alexander von Humboldt Foundation for funding (Feodor Lynen postdoctoral research fellowship to M. A. E.).

References

[1] For reviews of bimetallics in small molecule activation see, for example: (a) B. G. Cooper, J. W. Napoline, C. M. Thomas, *Catal. Rev.: Sci. Eng.* **2012**, *54*, 1-40; (b) N. P. Mankad, *Chem.–Eur. J*. **2016**, *22*, 5822-5829; (c) J. Takaya, *Chem. Sci.* **2021**, *12*, 1964-1981; (d) M. T. Whited, *Dalton Trans.* **2021**, *50*, 16443-16450.

[2] Examples of transition metal-aluminium bimetallics featuring an X-type group 13 ligand: (a) R. A. Fischer, T. Priermeier, *Organometallics,* **1994**, *13*, 4306-4314; (b) B. N. Anand, I. Krossing, H. Nöth, *Inorg. Chem.* **1997**, 3*6*, 1979-1981; (c) I. M. Riddlestone, J. Urbano, N. D. Phillips, M. J. Kelly, D. Vidovic, J. I. Bates, R. Taylor, S. Aldridge, *Dalton Trans*. **2013**, *42*, 249–258; (d) J. Takaya, N. Iwasawa, *J. Am. Chem. Soc.* **2017**, *139*, 6074-6077; (e) N. Hara, T. Saito, K. Semba, N. Kuriakose, H. Zheng, S. Sakaki, Y. Nakao, *J. Am. Chem. Soc.* **2018**, *140*, 7070-7073; (f) J. Hicks, A. Mansikkamäki, P. Vasko, J. M. Goicoechea, S. Aldridge, *Nature Chem.* **2019**, *11*, 237-241; (g) S. Morisako, S. Watanabe, S. Ikemoto, S. Muratsugu, M. Tada, M. Yamashita, *Angew. Chem. Int. Ed.* **2019**, *58*, 15031-15035; (h) K. Sugita, M. Yamashita, *Chem.-Eur. J.* **2020**, *26*, 4520-4523; (i) I. Fujii, K. Semba, Q.-Z. Li, S. Sakaki, Y. Nakao, *J. Am. Chem. Soc.* **2020**, *142*, 11647;(j) R. Seki, N. Hara, T. Saito, Y. Nakao, *J. Am. Chem. Soc.* **2021**, *143*, 6388-6394; (k) H. Y. Liu, R. J. Schwamm, M. S. Hill, M. F. Mahon, C. F. McMullin, N. A. Rajabi, *Angew. Chem. Int. Ed.* **2021**, 60, 14390-14393; (l) C. McManus, J Hicks, X. Cui, L. Zhao, G. Frenking, J. M. Goicoechea, S. Aldridge, *Chem. Sci.* **2021**, *12*, 13458-13468; (m) B. J. Graziano, M. V. Vollmer, C. C. Lu, *Angew. Chem. Int. Ed.* **2021**, *60*, 15087-15094; (n) M. M. D. Roy, J. Hicks, P. Vasko, A. Heilmann, A.-M. Baston, J. M. Goicoechea, S. Aldridge, *Angew. Chem. Int. Ed.* **2021**, *60*, 22301-22306; (o) M. J. Evans, G. H. Iliffe, S. E. Neale, C. L. McMullin, J. R. Fulton, M. D. Anker, M. P. Coles, *Chem. Commun.* **2022**, 58, 10091-10094; (p) C. McManus, A. E. Crumpton, S. Aldridge, *Chem. Commun*. **2022**, *58*, 8274-8277.

[3] Transition metal-aluminium bimetallics featuring a L-type group 13 ligand have a longer historical precedent. For a review of early work in this area see: R. A. Fischer, J. Weiß, *Angew. Chem. Int. Ed*. **1999**, *38*, 2830-2850.

[4] For a review of transition metal-aluminium bimetallics featuring a Z-type group 13 ligand see: R. C. Cammarota, L. J. Clouston, C. C. Lu, *Coord. Chem. Rev*. **2017**, *334*, 100-111.

[5] See for example, M. Assay, C. Jones, M. Driess, *Chem. Rev*. **2011**, *111*, 354-396.

[6] Ga: (a) E. S. Schmidt, A. Jockisch, H. Schmidbaur, *J. Am. Chem. Soc.* **1999**, *121*, 9758-9759. See also (b) R. J. Baker, R. D. Farley, C. Jones, M. Kloth, D. M. Murphy, *J. Chem. Soc., Dalton Trans.* **2002**, 3844-3850; (c) I. L. Fedushkin, A. N. Lukoyanov, G. K. Fukin, S. Y. Ketkov, M. Hummert, H. Schumann, *Chem.-Eur. J.* **2008**, 14, 8465-8468.

[7] B: (a) Y. Segawa, M. Yamashita, K. Nozaki, *Science* **2006**, *314*, 113-115. See also (b) Y. Segawa, Y. Suzuki, M. Yamashita, K. Nozaki, *J. Am. Chem. Soc*. **2008**, *130*, 16069-16079; (c) W. Lu, H. Hu, Y. Li, R. Ganguly, R. Kinjo, *J. Am. Chem. Soc*. **2016**, *138*, 6650-6661; (d) A.-F. Pécharman, A. L. Colebatch, M. S. Hill, C. L. McMullin, M. F. Mahon, C. Weetman, *Nat. Commun.* **2017**, *8*, 15022; (e) L. Weber, *Eur. J. Inorg. Chem.* **2017**, 3461-3488.

[8] (a) I. A. I. Mkhalid, J. H. Barnard, T. B. Marder, J. M. Murphy, J. F. Hartwig, *Chem. Rev.* **2010**, *110*, 890-931; (b) I. F. Yu, J. W. Wilson, J. F. Hartwig, *Chem. Rev.* **2023**, *123*, 11619-11663.

[9] Tl: A. V. Protchenko, D. Dange, J. R. Harmer, C. Y. Tang, A. D. Schwarz, M. J. Kelly, N. Phillips, R. Tirfoin, K. H. Birjkumar, C. Jones, N. Kaltsoyannis, P. Mountford, S. Aldridge, *Nature Chem*. **2014**, *6*, 315-319.

[10] In: R. J. Schwamm, M. D. Anker, M. Lein, M. P. Coles, C. M. Fitchett, *Angew. Chem. Int. Ed*. **2018**, *57*, 5885-5887.

[11] Al: (a) J. Hicks, P.Vasko, J. M. Goicoechea, S. Aldridge, *Nature* **2018**, *557*, 92-95. See also: (b) R. J. Schwamm, M. D. Anker, M. Lein, M. P. Coles, *Angew. Chem. Int. Ed.* **2019**, *58*, 1489-1493; (c) J. Hicks, P. Vasko, J. M. Goicoechea, S. Aldridge, J. *Am. Chem. Soc.* **2019**, *141*, 11000-11003; (d) S. Kurumada, S. Takamori, M. Yamashita, *Nature Chem*. **2020**, *12*, 36-39; (e) R. J. Schwamm, M. P. Coles, M. S. Hill, M. F. Mahon, C. L. McMullin, N. A. Rajabi, A. S. S. Wilson, *Angew. Chem. Int. Ed*. **2020**, *59*, 3928-3932; (f) K. Koshino, R. Kinjo, J. Am. Chem. Soc. **2020**, *142*, 9057-9062; (g) S. Grams, J. Eyselein, J. Langer, C. Färber, S. Harder, *Angew. Chem. Int. Ed*. **2020**, *59*, 15982-15986; (h) S. Grams, J. Mai, J. Langer, S. Harder, *Organometallics* **2022**, *41*, 2862–2867; (i) G. Feng, K. L. Chan, Z. Lin, M. Yamashita, *J. Am. Chem. Soc*. **2022**, *144*, 22662–22668; (j) C. Yan, R. Kinjo, *Angew. Chem. Int. Ed*. **2022**, *61*, e202211800; (k) R. A. Jackson, A. J. R. Matthews, P. Vasko, M. F. Mahon, J. Hicks, D. Liptrot, *Chem. Commun*. **2023**, *59*, 5277-5280; (l) D. Sarkar, P. Vasko, A. F. Roper, M. M. D. Roy, A. E. Crumpton, L. P. Griffin, C. Bogle, S. Aldridge, submitted manuscript (copy supplied for review).

[12] For recent reviews of aluminyl and related chemistry, see for example: (a) K. Hobson, C. J. Carmalt, C. Bakewell, *Chem. Sci.* **2020**, *11*, 6942–6956; (b) J. Hicks, P. Vasko, J. M. Goicoechea, S. Aldridge, *Angew. Chem. Int. Ed*. **2021**, *60*, 1702-1711; (c) M. P. Coles, M. J. Evans, Chem. Commun. **2023**, *59*, 503–519.

[13] (a) G. J. Irvine, M. J. G. Lesley, T. B. Norman, N. C. Norman, C. R. Rice, E. G. Robins, W. R. Roper, G. R. Whittell, L. J. Wright, *Chem. Rev.* **1998**, *98*, 2685-2722; (b) H. Braunschweig, R. D. Dewhurst, A. Schneider, *Chem. Rev.* **2010**, 110, 3924-3957.

[14] For a review of the coordination chemistry of gallyl systems, see for example: R. J. Baker, C. Jones, *Coord. Chem. Rev*. **2005**, *249*, 1857-1869.

[15] E. O. Fischer, H. P. Hofmann, *Angew. Chem.* **1957**, *69*, 639-640.

[16] For an example of an In/Ag donor/acceptor interaction see: M. Lichtenthaler, F. Stahl, D. Kratzert, L. Heidinger, E. Schleicher, J. Hamann, D. Himmel, S. Weber, I. Krossing, *Nature Commun.* **2015**, *6*, 8288.

[17] A.V. Protchenko, D. Dange, A.D. Schwarz, C.Y. Tang, N. Phillips, P. Mountford, C. Jones, S. Aldridge, *Chem. Commun.* **2014**, *50*, 3841-3844.

[18] L. P. Griffin, M. Ellwanger, J. Clarke, A. F. Roper, A. Heilmann, S. Aldridge, submitted manuscript. Copy available for review at ChemRxiv (DOI: 10.26434/chemrxiv-2022-s63x6).

[19] B. Cordero, V. Gómez, A. E. Platero-Prats, M. Revés, J. Echeverría, E. Cremades, F. Barragán, S. Alvarez, Dalton Trans. (2008) 2832-2838.

[20] R. Bianchi, G. Gervasio, D. Marabello, *Inorg. Chem.* **2000**, *39*, 2360-2366.

[21] Deposition numbers 2334028-2334034 contain the supplementary crystallographic data for this paper. These data are provided free of charge by the joint Cambridge Crystallographic Data Centre and Fachinformationszentrum Karlsruhe Access Structures service.

[22] C. A. Cruz, D. J. H. Emslie, L. E. Harrington, J. F. Britten, C. M. Robertson, *Organometallics* **2007**, *26*, 692-701.

[23] R. G. Goel, A. L. Beauchamp, *Inorg. Chem*. **1983**, *22*, 395-400.

[24] J. Cosier, A.M. Glazer, *J. Appl. Cryst*. **1986**, *19*, 105-107.

[25] CrysAlisPro v.1.171.42.70a, Agilent Technologies, 2011.

[26] G.M. Sheldrick, *Acta Crystallogr.* **2015**, *A71*, 3-8.

[27] G.M. Sheldrick, *Acta Crystallogr.* **2015**, *C71*, 3-8.

[28] O. V. Dolomanov, L. J. Bourhis, R. J. Gildea, J. A. K. Howard, H. Puschmann, *J. Appl. Cryst*. **2009**, *42*, 339-341.

[29] Y. Zhao, D. G. Truhlar, *Theor. Chem. Acc*. **2008**, *120*, 215-241.

[30] F. Weigend, R. Ahlrichs, *Phys. Chem. Chem. Phys*. **2005**, *7*, 3297-3305.

[31] S. Grimme, J. Antony, S. Ehrlich, H. Krieg, J. Chem. Phys. **2010**, *132*, 154104.

[32] Gaussian 16, Revision C.01, M. J. Frisch, G. W. Trucks, H. B. Schlegel, G. E. Scuseria, M. A. Robb, J. R. Cheeseman, G. Scalmani, V. Barone, G. A. Petersson, H. Nakatsuji, X. Li, M. Caricato, A. V. Marenich, J. Bloino, B. G. Janesko, R. Gomperts, B. Mennucci, H. P. Hratchian, J. V. Ortiz, A. F. Izmaylov, J. L. Sonnenberg, D. Williams-Young, F. Ding, F. Lipparini, F. Egidi, J. Goings, B. Peng, A. Petrone, T. Henderson, D. Ranasinghe, V. G. Zakrzewski, J. Gao, N. Rega, G. Zheng, W. Liang, M. Hada, M. Ehara, K. Toyota, R. Fukuda, J. Hasegawa, M. Ishida, T. Nakajima, Y. Honda, O. Kitao, H. Nakai, T. Vreven, K. Throssell, J. A. Montgomery, Jr., J. E. Peralta, F. Ogliaro, M. J. Bearpark, J. J. Heyd, E. N. Brothers, K. N. Kudin, V. N. Staroverov, T. A. Keith, R. Kobayashi, J. Normand, K. Raghavachari, A. P. Rendell, J. C. Burant, S. S. Iyengar, J. Tomasi, M. Cossi, J. M. Millam, M. Klene, C. Adamo, R. Cammi, J. W. Ochterski, R. L. Martin, K. Morokuma, O. Farkas, J. B. Foresman, D. J. Fox, Gaussian, Inc., Wallingford CT, 2016.

[33] E. van Lenthe, J. G. Snijders, E. J. Baerends, *J. Chem. Phys*. **1996**, *105*, 6505-6516.

[34] J. D. Rolfes, F. Neese, D. A. Pantazis, *J. Comput. Chem*. **2020**, *41*, 1842-1849.

[35] D. A. Pantazis, F. Neese, *J. Chem. Theory Comput*. **2009**, *5*, 2229-2238.

[36] D. A. Pantazis, X. Y. Chen, C. R. Landis, F. Neese, *J. Chem. Theory Comput*. **2008**, *4*, 908-911.

[37] D. A. Pantazis, F. Neese, *Theor. Chem. Acc*. **2012**, *131*, 1292.

[38] D. A. Pantazis, F. Neese, *J. Chem. Theory Comput*. **2011**, *7*, 677-684.

[39] F. Weigend, *Phys. Chem. Chem. Phys*. **2006**, *8*, 1057-1065.

[40] F. Neese, F. Wennmohs, U. Becker, C. Riplinger, *J. Chem. Phys*. **2020**, *152*, 224108.

[41] NBO 7.0. E. D. Glendening, J, K. Badenhoop, A. E. Reed, J. E. Carpenter, J. A. Bohmann, C. M. Morales, P. Karafiloglou, C. R. Landis, F. Weinhold, Theoretical Chemistry Institute, University of Wisconsin, Madison (2018).

[42] AIMAll (Version 19.10.12), T. A. Keith, TK Gristmill Software, Overland Park KS, USA, 2019 (aim.tkgristmill.com)

[43] T. Lu, F. Chen, *J. Comput. Chem.* **2012**, *33*, 580-592.

[44] B. Silvi, A. Savin, *Nature* **1994**, *371*, 683-686.

[45] E. F. Pettersen, T. D. Goddard, C. C. Huang, G. S. Couch, D. M. Greenblatt, E. C. Meng, T. E. Ferrin, *J. Comput. Chem*. **2004**, *25*, 1605-1612.

[46] R. Bianchi, G. Gervasio, D. Marabello, *Inorg. Chem*. **2000**, *39*, 2360-2366.

Supporting information

General considerations

All manipulations were carried out using standard Schlenk line or dry-box techniques under an atmosphere of argon or dinitrogen. Solvents were degassed by sparging with argon and dried by passing through a column of the appropriate drying agent. Toluene was purified using an MBraun SPS-800 and stored over a potassium mirror. NMR spectra were measured in benzene-d_6 (which was dried over potassium, with the solvent then being distilled under reduced pressure), thf-d_8 or dichloromethane-d_2 (dried by storing over activated molecular sieves and degassed by three freeze pump thaw cycles) and stored under argon in Teflon valve ampoules. NMR samples were prepared under argon in 5 mm Wilmad 507-PP tubes fitted with J. Young Teflon valves. ^{1}H, ^{13}C{^{1}H}, ^{31}P and ^{11}B NMR spectra were recorded on Bruker Avance III HD nanobay 400 MHz or Bruker Avance III 500 MHz spectrometer at ambient temperature and referenced internally to residual protio-solvent (^{1}H) or solvent (^{13}C) resonances and are reported relative to tetramethylsilane (□ = 0 ppm). Assignments were confirmed using two-dimensional ^{1}H-^{1}H and ^{13}C-^{1}H NMR correlation experiments. Chemical shifts are quoted in □ (ppm) and coupling constants in Hz. Elemental analyses were carried out by London Metropolitan University or Elemental Microanalysis Ltd. H_2NON,[s1] $K_2[NON]$,[s2], $K_2[Al(NON)]_2$,[s2] $K_2[Ga(NON)]_2$,[s2] $^{t}Bu_3PAgI$,[s3] $[(boryl)HgBr]_2$ (boryl = {$(HCDippN)_2$}B),[s4] and $Mg[Al(NON)]_2$[s5] were synthesized according to the literature procedure. InCp was sublimed before use and stored in the dark. 18-crown-6 was recrystallized from acetonitrile before drying under vacuum. TMEDA was distilled and stored over molecular sieves under argon in a Teflon valve ampoule.

X-ray crystallographic details

Single-crystal X-ray diffraction data for compounds **1, 1', 1.TMEDA$_2$, 2, 3, 4,and 5** were collected on an Oxford Diffraction/Agilent SuperNova diffractometer equipped with a 135 mm Atlas CCD area detector or a Rigaku XtaLAB Synergy-DW VHF equip with a PhotonJet-R dual wavelength rotating anode and HyPix-Arc 150° detector. Crystals were selected under Paratone-N oil, mounted on MiTeGen Micromount loops and quench-cooled using an Oxford Cryosystems open flow N2 cooling device.[s6] Data were collected at 150 K using mirror monochromated Cu Kα radiation (λ = 1.5418 Å; Oxford Diffraction Supernova) or Mo Kα radiation (λ = 0.71073 Å; Oxford Diffraction Supernova). Data collected were processed using the CrysAlisPro package, including unit cell parameter refinement and inter-frame scaling (which was carried out using SCALE3 ABSPACK within CrysAlisPro).[s7] Equivalent reflections were merged and diffraction patterns processed with the CrysAlisPro suite.[s7] Structures were solved ab initio from the integrated intensities using SHELXT[s8] and refined on F2 using SHELXL[s9] with the graphical interface OLEX2.[s10] Selected crystallographic data are summarised in Table s1 and full details are given in the supplementary deposited CIF files (CCDC 2334028-2334034). These data can be obtained free of charge from the Cambridge Crystallographic Data Centre via http://www.ccdc.cam.ac.uk/ data_request/cif.

	1	**1'**	**2**	**3**	**4**	**5**	**1''**
Formula	$C_{52}H_{67}InK_2N_2O$	$C_{47}H_{62}InN_2O$, $C_{29}H_{53}K_2O_{12}$, $(C_6H_4F_2)$	$C_{59}H_{89}AgInN_2OP$, $2(C_6H_6)$	$C_{73}H_{98}AlBHgN_4O$, C_7H_8	$C_{73}H_{98}GaHgN_4O$, C_6H_{14}	$C_{73}H_{98}BHgInN_4O$	$C_{59}H_{94}InKN_6O$, C_7H_8
Fw (g mol^{-1})	929.09	1571.80	1252.19	1378.06	1414.84	1373.77	1149.45
Crystal system	monoclinic	triclinic	triclinic	monoclinic	triclinic	monoclinic	orthorhombic
Space group	P 2_1/n	P -1	P 1	P 2_1/c	P 1	P 2_1/c	P 2_1 2_1 2_1
***a* (Å)**	12.2765(4)	13.7358(6)	13.0060(4)	13.7202(1)	12.0043(1)	13.7482(3)	12.5909(1)
***b* (Å)**	13.9672(6)	15.3298(5)	14.1458(4)	25.3643(1)	13.7383(1)	44.2145(9)	22.2710(3)
***c* (Å)**	28.8458(11)	23.2750(9)	20.0581(5)	20.7147(1)	22.6001(2)	11.9933(2)	23.5709(3)
***α* (°)**	90	73.209(3)	89.309(2)	90	92.6730(10)	90	90
***β* (°)**	97.231(4)	89.373(4)	74.027(2)	90.7320(10)	96.6790(10)	91.126(2)	90
***γ* (°)**	90	65.674(4)	73.595(3)	90	90.8850(10)	90	90
***V* (Å^{-3})**	4906.8(3)	4242.5(3)	3394.75(18)	7208.20(7)	3697.04(5)	7289.0(2)	6609.56(13)
Z	4	2	2	4	2	4	4
ρ_{calc} (g cm^{-3})	1.258	1.230	1.225	1.270	1.271	1.252	1.155
Radiation, λ (Å)	1.54184	1.54184	1.54184	1.54184	1.54184	1.54184	1.54184
Absorption	multi-scan	multi-scan	gaussian	gaussian	gaussian	gaussian	multi-scan
μ (mm^{-1})	5.639	3.608	5.549	4.291	4.447	6.556	3.737
Reflections collected	22128	48640	77324	88691	73443	46022	31325
Independent reflections	10163	17245	13845	15003	15270	14870	13731
$R_{(int)}$	0.2003	0.0699	0.0842	0.0576	0.0329	0.0934	0.0522
Parameters	539	980	781	818	845	752	671
R_1 (all data/I >2σ(I))	0.1102	0.0656	0.0441	0.0370	0.0326	0.0488	0.0501
ωR_2 (all data/I >2σ(I))	0.2756	0.1737	0.1147	0.1003	0.0796	0.1062	0.1287
GooF	0.884	1.056	1.058	1.052	1.164	0.963	1.041
***T* (K)**	150.01(10)	150.00(10)	195.00(10)	150.01(11)	150.01(18)	100.0(5)	150.01(10)
CCDC ref.	2334028	2334032	2334034	2334029	2334031	2334033	2334030

Table s1: X-ray crystallographic details

Syntheses of novel compounds

1, [{K(NON)In}·KCp]$_n$

To an NMR tube fitted with a J-Youngs valve was added K_2[NON] (20 mg, 0.027 mmol) and InCp (5 mg, 0.028 mmol), along with 0.5 mL of C_6D_6. A dark solution was rapidly formed, accompanied by the precipitation of microcrystalline yellow material. Some of this material was suitable for single crystal X-ray diffraction measurements, although the resulting data was of low quality. The material was found to be soluble in THF, allowing multinuclear NMR measurements to be made.

^{1}H NMR (500 MHz, THF-d_8, 298 K): δ_H 1.01 (d, $^3J_{HH}$ = 6.7 Hz, 12H, CH(CH_3)$_2$), 1.10 (s, 18H, C(*CH$_3$*)$_3$), 1.11 (d, $^3J_{HH}$ = 6.7 Hz, 12H, CH(CH_3)$_2$), 1.59 (s, 6H, XA-C(CH_3)$_2$), 3.55 (sept, $^3J_{HH}$ = 6.9 Hz, 4H, C*H*(CH$_3$)$_2$), 5.61 (d, $^4J_{HH}$ = 2.0 Hz, 2H, XA-o-C*H*), 5.72 (s, 5H, C_5H_5), 6.11 (d, $^4J_{HH}$ = 2.0 Hz, 2H, XA-*p*-C*H*), 7.81 (t, 2H, $^3J_{HH}$ = 7.6 Hz Dipp-*p*-C*H*), 7.02 (d, 4H, $^3J_{HH}$ = 7.5 Hz Dipp-*o*-C*H*) ppm.

^{13}C{^{1}H} NMR (101 MHz, benzene-d_6): δ_C 148.8, 146.8, 146.3, 145.2, 141.4, 131.3, 129.3, 125.7, 123.4, 122.5, 107.5, 105.8, 101.8, 58.2, 46.0, 36.2, 35.0, 32.3, 30.1, 28.4, 26.2, 25.3 ppm.

1', [(18-crown-6)KCpK(18-crown-6)][(NON)In]

A mixture of K_2[NON] (300 mg, 0.400 mmol), InCp (77 mg, 0.428 mmol) and 18-crown-6 (217 mg, 0.822 mmol) in toluene (5 mL) was sonicated for 5 min, leading to the formation of a grey suspension. Volatiles were removed *in vacuo*, and the residue redissolved in *ortho*-difluorobenzene (5 mL). The resulting dark solution was filtered and concentrated *in vacuo*. Storage at -30 °C yielded yellow single crystals suitable for X-ray crystallography. Isolation of this crystalline material yielded 310 mg (58 %) of **1**'.

^{1}H NMR (500 MHz, dichloromethane-d_2, 298 K): δ_H 0.98 (d, $^3J_{HH}$ = 6.8 Hz, 6H, CH(CH_3)$_2$), 1.04 (d, $^3J_{HH}$ = 6.8 Hz, 6H, CH(CH_3)$_2$), 1.11 (s, 18H, C(*CH$_3$*)$_3$), 1.18 (d, $^3J_{HH}$ = 5.8 Hz, 6H, CH(CH_3)$_2$), 1.20 (d, $^3J_{HH}$ = 6.1 Hz,

6H, CH(CH_3)$_2$), 1.64 (s, 3H, C(CH_3)$_2$), 1.72 (s, 3H, C(CH_3)$_2$), 3.57 (br s, 52H, overlapping CH(CH$_3$)$_2$ and OCH_2CH_2O), 5.73 (d, $^4J_{HH}$ = 2.1 Hz, 2H, XA-o-CH), 5.76 (s, 5H, C$_5H_5$), 7.14–7.25 (m, 6H, ArH) ppm.

^{13}C{^{1}H} NMR (101 MHz, dichloromethane-d$_2$, 298 K): δ_C 148.7, 147.6, 145.8, 145.7, 144.8, 139.0, 133.5, 132.5, 131.8, 124.1, 123.6, 123.4, 108.8, 102.6, 70.5, 36.8, 34.9, 31.9, 27.9, 27.6, 25.7, 25.0 ppm.

2, (^{t}Bu$_3$P)AgIn(NON)

To an *in situ* generated suspension of **1** (0.027 mmol) in benzene-d$_6$ (0.5 mL) in an NMR tube fitted with a J-Young valve was added (^{t}Bu$_3$P)AgI (13 mg, 0.030 mmol). The resulting suspension was filtered, yielding a bright yellow solution, which was dried *in vacuo*. Extraction into hexane (0.5 mL), filtration and slow evaporation led to the formation of yellow crystals suitable for single crystal X-ray diffraction. Isolation yielded 23 mg of yellow crystalline material (77 %). The product in hexane solution appears to show light sensitivity, so slow evaporation was carried out in ambered glassware.

^{1}H NMR (500 MHz, benzene-d$_6$, 298 K): δ_H 0.83 (d, $^3J_{HP}$ = 13.1 Hz, 27H P(C(CH_3)$_3$)$_3$), 1.29 (t, $^3J_{HH}$ = 7.0 Hz 24H, CH(CH_3)$_2$), 1.37 (s, 18H, C(CH_3)$_3$), 1.74 (s, 6H, XA-C(CH_3)$_2$), 3.76 (sept, $^3J_{HH}$ = 6.9 Hz, 4H, CH(CH$_3$)$_2$), 6.43 (d, $^4J_{HH}$ = 2.1 Hz 2H, XA-o-CH), 6.79 (d, $^4J_{HH}$ = 2.1 Hz 2H, XA-p-CH), 7.13 (t, $^3J_{HH}$ = 7.9 Hz, 2H, Ar-p-H), 7.26 (d, $^3J_{HH}$ = 7.9 Hz, 2H, Ar-m-H) ppm.

^{13}C{^{1}H} NMR (101 MHz, benzene-d$_6$, 298 K): δ_C 147.7, 146.2, 143.9, 143.2, 139.8, 131.1, 124.3, 123.1, 108.1, 104.7, 36.7, 36.6, 36.1, 34.7, 31.8, 31.7, 31.6, 29.6, 27.9, 25.9, 25.2 ppm.

^{31}P NMR (162 MHz, benzene-d$_6$, 298 K): δ_P 68.5 (d, $^1J_{AgP}$ = 334, 385) ppm.

Elemental analysis: calc. (for $C_{59}H_{91}AgInN_2OP$) C 64.66 %, H 8.19 %, 2.56 %; meas. C 64.97 %, H 7.81 %, N 2.45 %.

3, (boryl)HgAl(NON)

Method A: A solution of $K_2[(NON)Al]_2$ (50 mg, 0.339 mmol) in toluene (2 mL) was cooled to -78 °C and added to a solution of $[(boryl)HgBr]_2$ (0.42 mg, 0.0636 mmol of monomer) in toluene (1 mL) also at -78 °C, and the reaction mixture stirred for 10 min. Filtration and concentration of the resulting pale yellow solution, and storage at -30 °C resulted in the formation of highly temperature sensitive crystals of compound **3** suitable for single crystal X-ray diffraction, as well as some mercury metal.

Method B: To a vial in a nitrogen-filled glovebox was added $Mg[(NON)Al]_2$ (20 mg, 0.014 mmol), $[(boryl)HgBr]_2$ (19 mg, 0.029 mmol of monomer) and benzene-d_6 (0.5 mL). The reaction mixture was shaken before being immediately filtered into an NMR tube fitted with a J-Youngs valve for multinuclear NMR measurements. ^{1}H and ^{11}B NMR spectra both show the formation of a new species, as well as a significant amount of $(boryl)_2Hg$, which increased over time. ^{13}C NMR data was highly complex due to the presence of these several species in constantly changing amounts, and significant broadening at low temperature meant that the best data was measured at room temperature. Carrying out this reaction using $K_2[(NON)Al]_2$ led to a higher proportion of the decomposition products.

^{1}H NMR (500 MHz, benzene-d_6, 298 K): δ_H 1.11 (dd, 12H, $^3J_{HH}$ = 6.5 and 7.6 Hz, boryl CH(CH_3)$_2$), 1.14 (s 18H, C(CH_3)$_3$), 1.18 (dd, 12H, $^3J_{HH}$ = 4.9 and 5.3 Hz, boryl C(*CH$_3$*)$_3$), 1.21 (s, 12H, NON C(*CH$_3$*)$_3$), 1.23 (br s, 6H, NON C(*CH$_3$*)$_3$), 1.37 (d, 6H, $^3J_{HH}$ = 6.4 Hz, NON C(*CH$_3$*)$_3$), 1.50 (s, 6H, XA-C(CH_3)$_2$), 3.20 (sept, $^3J_{HH}$ = 7.0 Hz, 4H, boryl C*H*(CH$_3$)$_2$), 3.56 (sept, $^3J_{HH}$ = 7.0 Hz, 4H, NON C*H*(CH$_3$)$_2$), 6.28 (s, 2H, (NC*H*)$_2$), 6.38 (m, 2H, XA-o-C*H*), 6.77 (m, 2H, XA-p-C*H*), 7.12–7.30 (m, 12H, Ar*H*) ppm.

^{11}B NMR (128 MHz, benzene-d_6, 298 K): δ_B 75.7 (br) ppm.

4, (boryl)HgGa(NON)

To an NMR tube fitted with a J-Youngs valve was added $[(boryl)HgBr]_2$ (18 mg, 0.027 mmol of monomer), $K_2[(NON)Ga]_2$ (22 mg, 0.014 mmol) and benzene-d_6 (0.5 mL). The resulting pale-yellow solution was dried *in vacuo*, and the residue extracted in to hexane (0.5 mL) and filtered. After concentration by slow evaporation, yellow crystals suitable for single crystal X-ray diffraction were obtained. Spectroscopic conversion was essentially quantitative. Isolation yielded 22 mg of crystalline pale-yellow material (62 %).

^{1}H NMR (500 MHz, benzene-d_6, 298 K): δ_H 1.03 (br d, 24H, CH(C*H*$_3$)$_2$), 1.10 (br t, 24H, CH(C*H*$_3$)$_2$), 1.19 (s, 18H, C(*CH*$_3$)$_3$), 1.60 (s, 6H, XA-C(C*H*$_3$)$_2$), 3.01 (sept, $^3J_{HH}$ = 6.9 Hz, 4H, C*H*(CH$_3$)$_2$), 3.50 (sept, $^3J_{HH}$ = 6.8 Hz, 4H, C*H*(CH$_3$)$_2$), 6.09 (s, 2H, (NC*H*)$_2$), 6.14 (br d, 2H, XA-o-C*H*), 6.74 (br d, 2H, XA-p-C*H*), 7.03–7.23 (m, 12H, Ar*H*) ppm.

^{13}C{^{1}H} NMR (101 MHz, benzene-d_6): δ_c 149.0, 147.5, 142.5, 140.7, 133.7, 127.9, 126.5, 124.5, 110.7, 107.1, 37.5, 35.1, 31.8, 29.5, 27.3, 25.6, 25.5 ppm.

^{11}B NMR (128 MHz, benzene-d_6, 298 K): δ_B 60.0 (br) ppm.

^{31}P NMR (162 MHz, benzene-d_6, 298 K): δ_P 68.5 (d, $^1J_{AgP}$ = 334, 385) ppm.

Elemental analysis: calc. (for $C_{59}H_{91}AgInN_2OP$) C 64.66 %, H 8.19 %, 2.56 %; meas. C 64.97 %, H 7.81 %, N 2.45 %.

5, (boryl)HgIn(NON)

To an *in situ* prepared suspension of compound **1** (0.027 mmol) in C_6D_6 (0.5 mL) in an NMR tube fitted with a J-Youngs valve was added $[(boryl)HgBr]_2$ (17 mg, 0.026 mmol of monomer). The resulting suspension was filtered, yielding a bright yellow solution, which was dried *in vacuo*. Extraction into hexane (0.5 mL), filtration and concentration *in vacuo* led to the formation of yellow crystals suitable for single crystal X-ray diffraction. Spectroscopic conversion was essentially quantitative. Crystallization yielded 12 mg of material (34 %). Elemental analysis was precluded by the decomposition of compound **5** to metal at room temperature.

^{1}H NMR (500 MHz, benzene-d_6, 298 K): δ_H 0.91 (d, $^3J_{HH}$ = 6.9 Hz, 12H, CH(CH_3)$_2$), 0.98 (d, $^3J_{HH}$ = 6.9 Hz, 12H, CH(CH_3)$_2$), 1.11 (d, $^3J_{HH}$ = 7.0 Hz, 12H, CH(CH_3)$_2$), 1.14 (d, $^3J_{HH}$ = 6.7 Hz, 12H, CH(CH_3)$_2$), 1.26 (s, 18H, C(*CH*$_3$)$_3$), 1.62 (s, 6H, XA-C(CH_3)$_2$), 2.95 (sept, $^3J_{HH}$ = 6.8 Hz, 4H, C*H*(CH$_3$)$_2$), 3.49 (sept., $^3J_{HH}$ = 6.8 Hz, 4H, C*H*(CH$_3$)$_2$), 6.05 (s, 2H, (NC*H*)$_2$), 6.18 (br d, 2H, XA-o-C*H*), 6.74 (br d, 2H, XA-p-C*H*), 7.01–7.25 (m, 12H, Ar*H*) ppm.

^{13}C{^{1}H} NMR (101 MHz, benzene-d_6, 298 K): δ_c 148.0, 147.3, 146.0, 143.4, 142.0, 141.4, 139.4, 134.0, 124.1, 123.8, 110.1, 106.8, 37.0, 32.3, 29.0, 28.4, 25.7, 25.0 ppm.

^{11}B NMR (128 MHz, benzene-d_6, 298 K): δ_B 54.4 (br) ppm.

1'', (NON)InK(TMEDA)$_2$

To an *in situ* prepared suspension of compound **1** (0.027 mmol) in C_6D_6 (0.5 mL) in an NMR tube fitted with a J-Youngs valve was added TMEDA (0.02 mL, 0.133 mmol). The resulting solution was suitable for measurement by NMR. Pumping to dryness *in vacuo*, redissolution in a minimum volume of toluene, and storage at -30 °C, yielded a small quantity of single crystals suitable for X-ray diffraction.

^{1}H NMR (500 MHz, benzene-d_6, 298 K): δ_H 1.31 (d, $^3J_{HH}$ = 6.9 Hz, 12H, CH(CH_3)$_2$), 1.35 (d, $^3J_{HH}$ = 6.9 Hz, 12H, CH(CH_3)$_2$), 1.41 (s, 18H, C(*CH*$_3$)$_3$), 1.81 (s, 6H, XA-C(CH_3)$_2$), 2.05 (s, 18H, N(CH_3)$_2$), 2.24 (s, 8H, NCH_2),

3.79 (sept., $^{3}J_{HH}$ = 6.8 Hz, 4H, C*H*$(CH_3)_2$), 5.84 (s, 5H, C_5H_5), 6.24 (d, $^{4}J_{HH}$ = 2.1 Hz, 2H, XA-o-C*H*), 6.62 (d, $^{4}J_{HH}$ = 2.1 Hz, 2H, XA-*p*-C*H*), 7.10 (t, 2H, $^{3}J_{HH}$ = 7.5 Hz Dipp-*p*-C*H*), 7.33 (d, 4H, $^{3}J_{HH}$ = 7.5 Hz Dipp-*o*-C*H*) ppm.

$^{13}C\{^{1}H\}$ NMR (101 MHz, benzene d_6, 298 K): δ_c 148.8, 146.8, 146.3, 145.2, 141.4, 131.3, 129.3, 125.7, 123.4, 122.5, 107.5, 105.8, 101.8, 58.2, 46.0, 36.2, 35.1, 32.3, 30.1, 28.4, 26.2, 25.3 ppm.

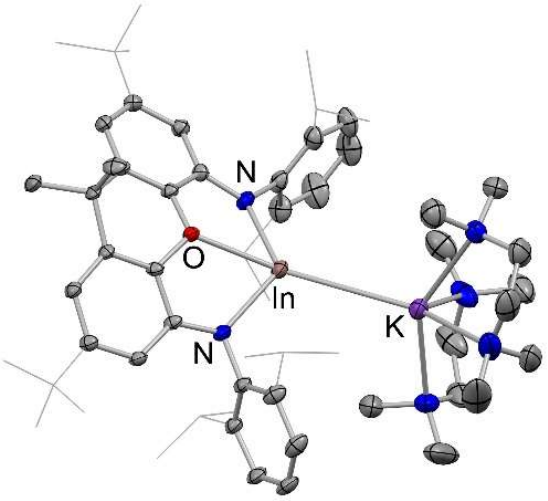

Figure s1: Molecular structure of **1''**, (NON)InK(TMEDA)$_2$, in the solid state as determined by X-ray crystallography. Hydrogen atoms and solvent molecules omitted, and selected groups shown in wireframe format for clarity; thermal ellipsoids set at the 40 % level. Key bond lengths (Å) and angles (°): K···In 3.740(1); In–N 2.311(4), 2.319(4); In–O 2.518(3); K–N 2.832(7), 2.851(7), 2.853(5), 2.911(8).

NMR spectra of novel compounds

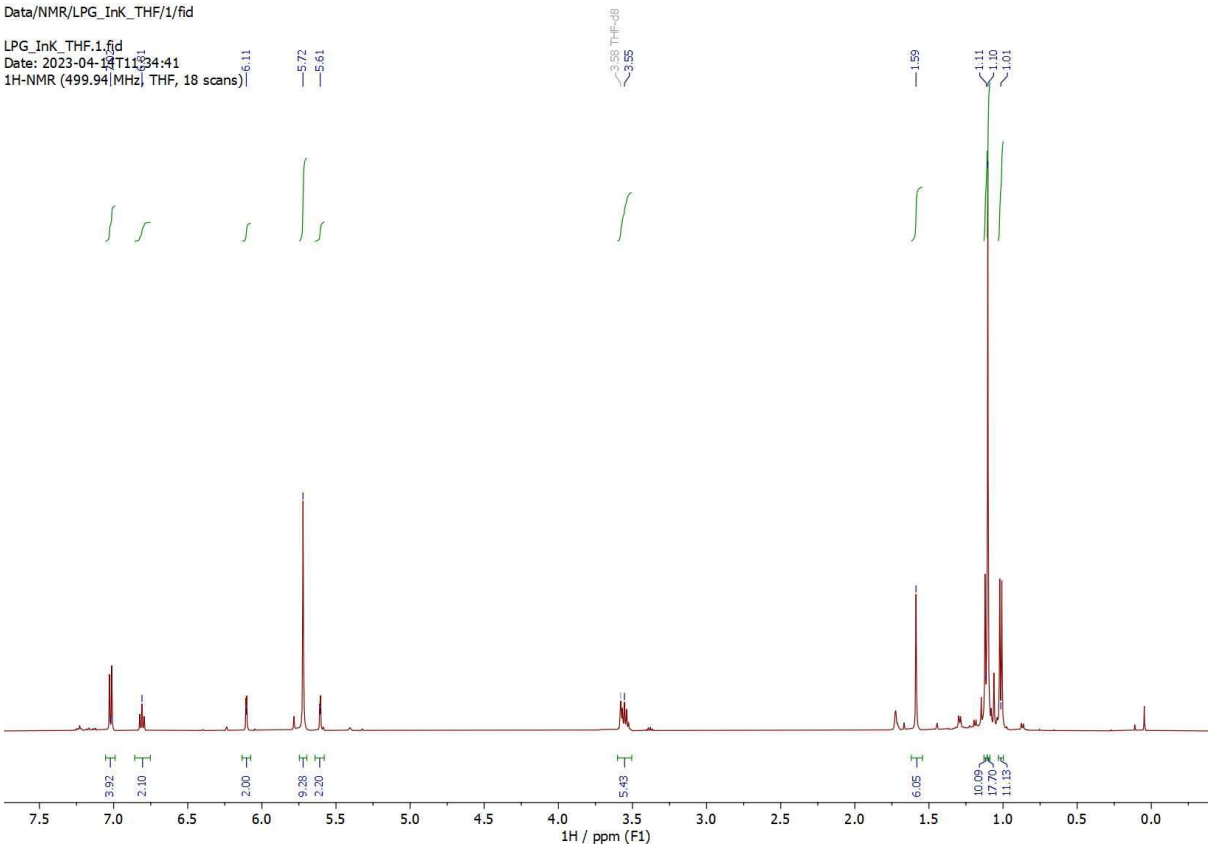

Figure s2: ^{1}H NMR spectrum of compound **1** in THF-d_8

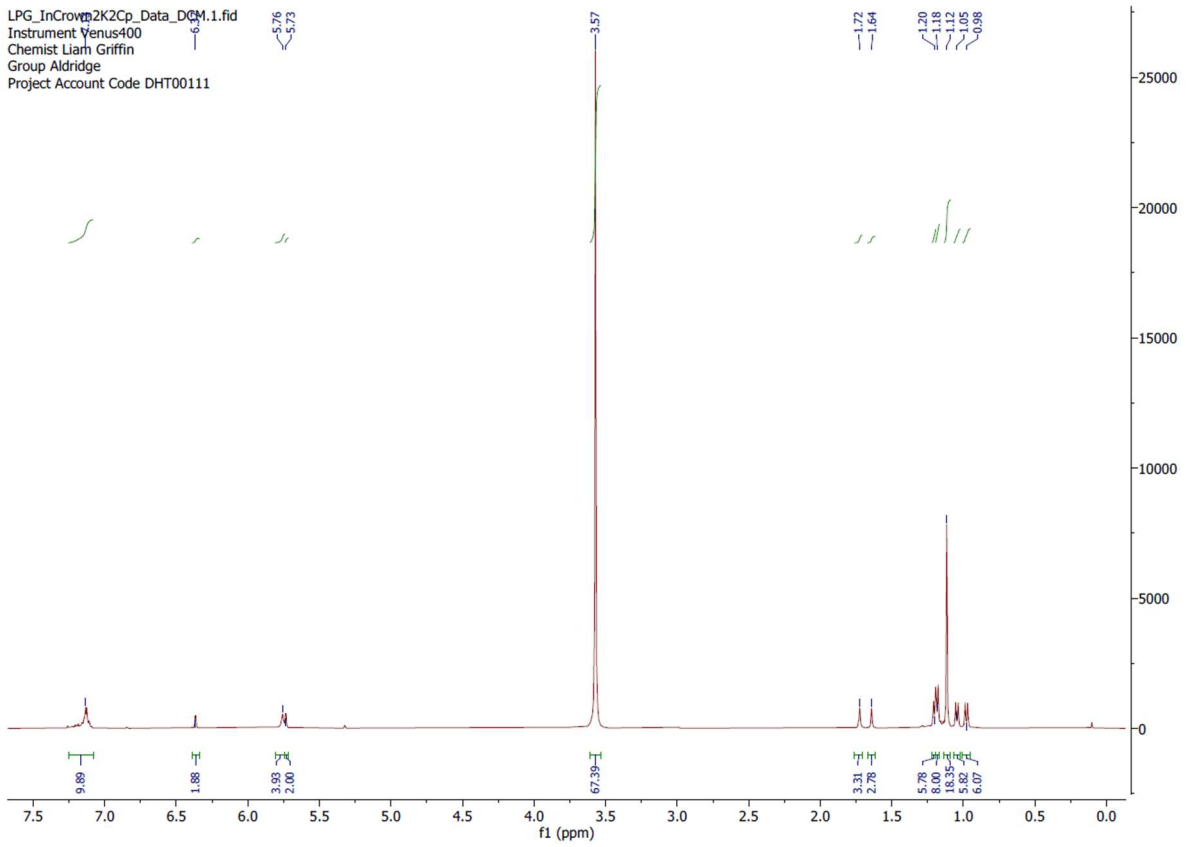

Figure s3: ^{1}H NMR spectrum of compound **1'** in dichloromethane-d_2

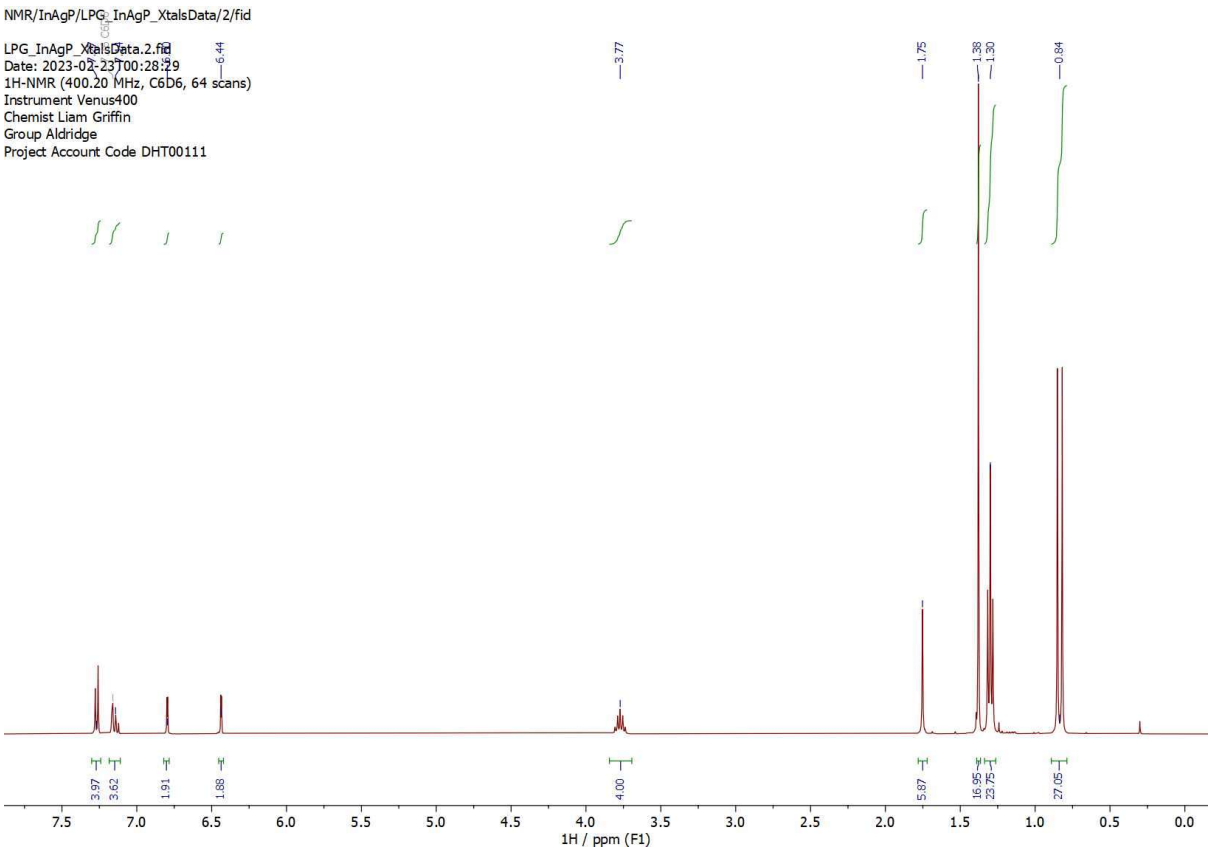

Figure s4: ^{1}H NMR spectrum of compound **2** in benzene-d_6

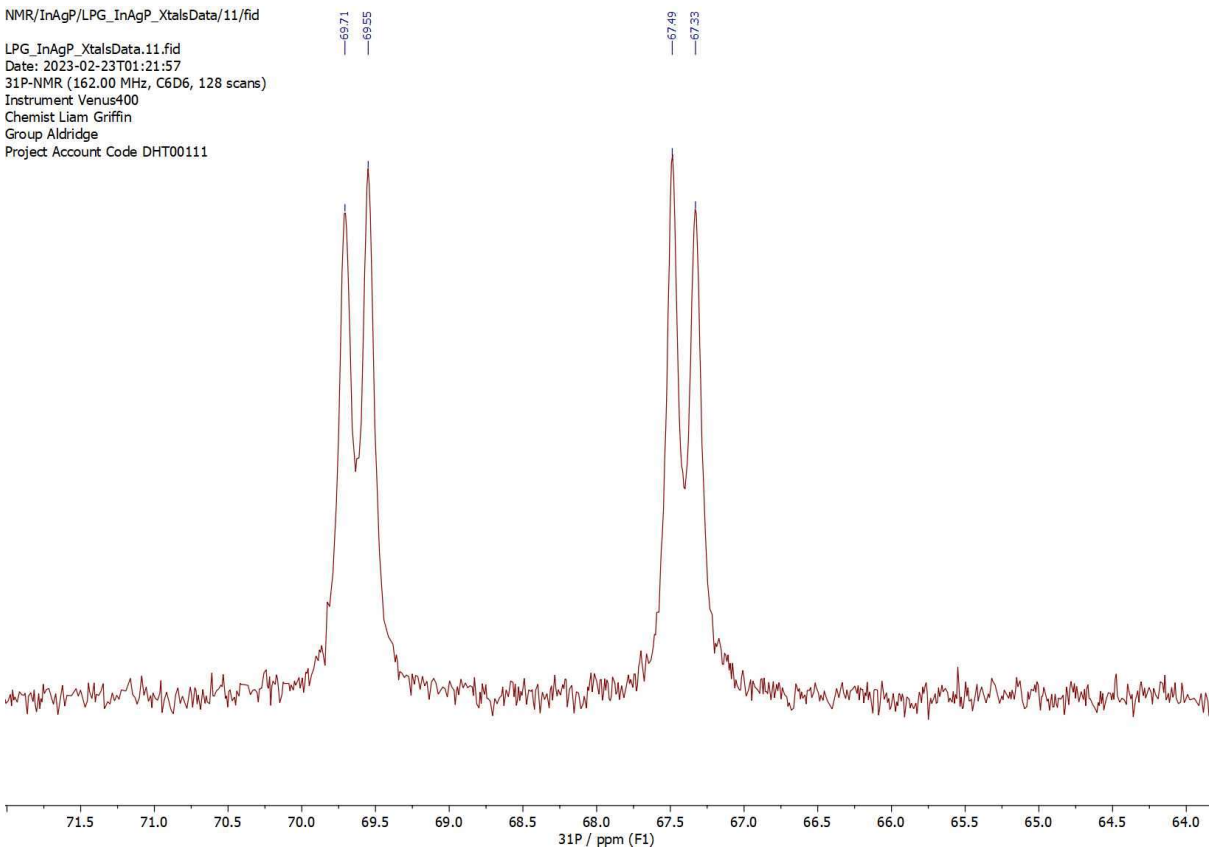

Figure s5: ^{31}P NMR spectrum of compound **2** in benzene-d_6

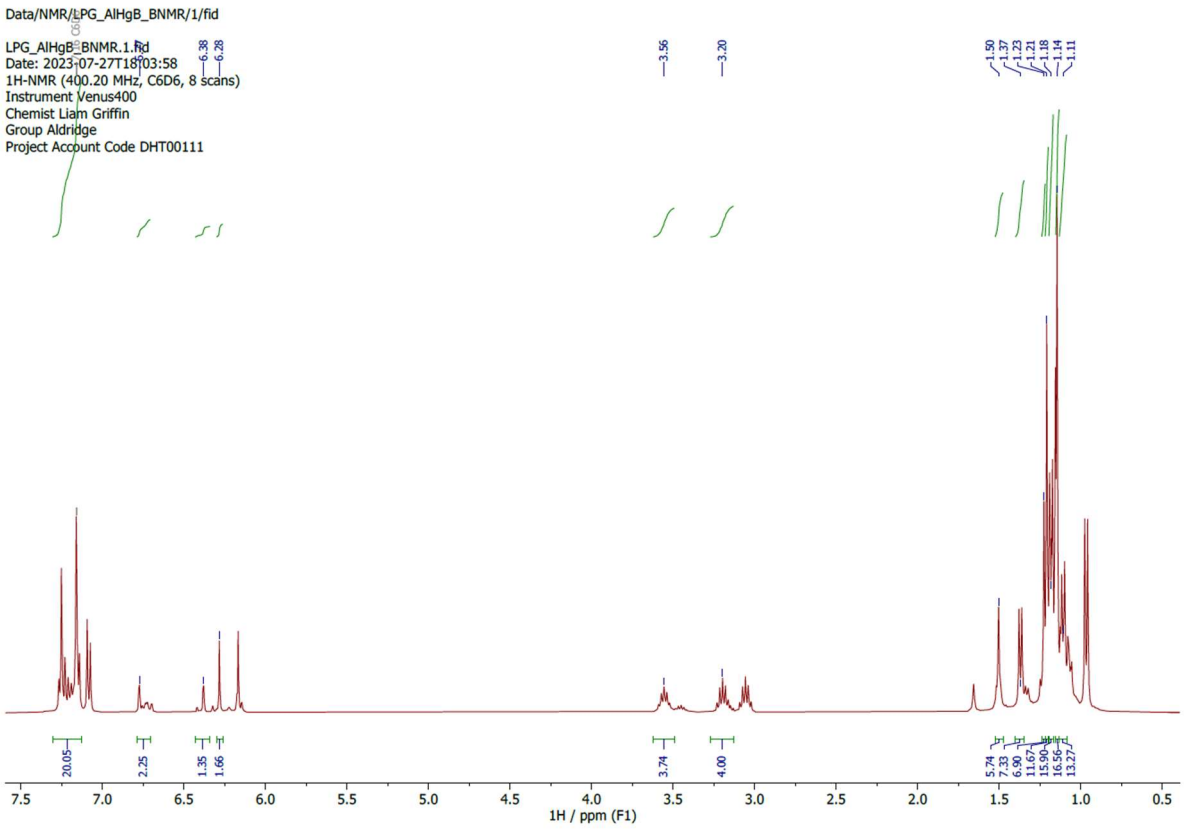

Figure s6: ^{1}H NMR spectrum of compound **3** in benzene-d_6

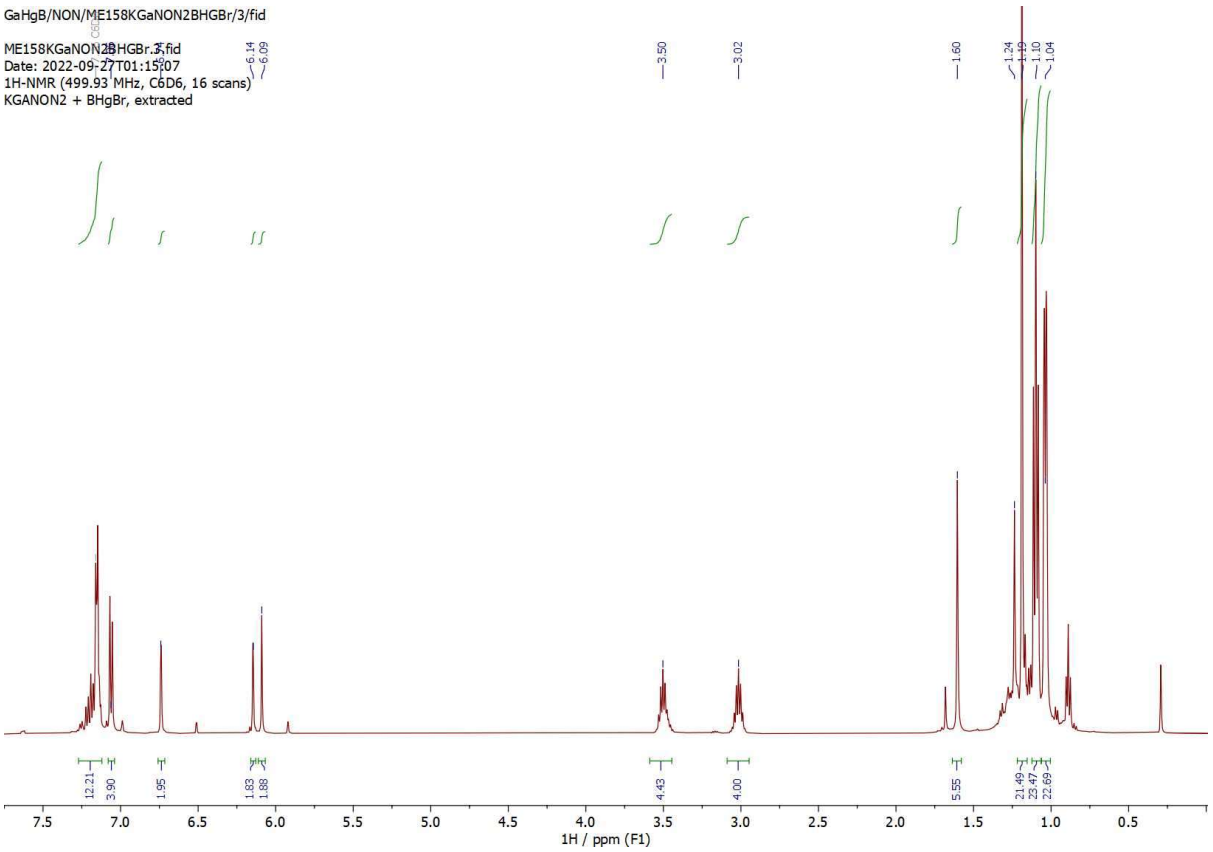

Figure s7: ^{1}H NMR spectrum of compound **4** in benzene-d_6

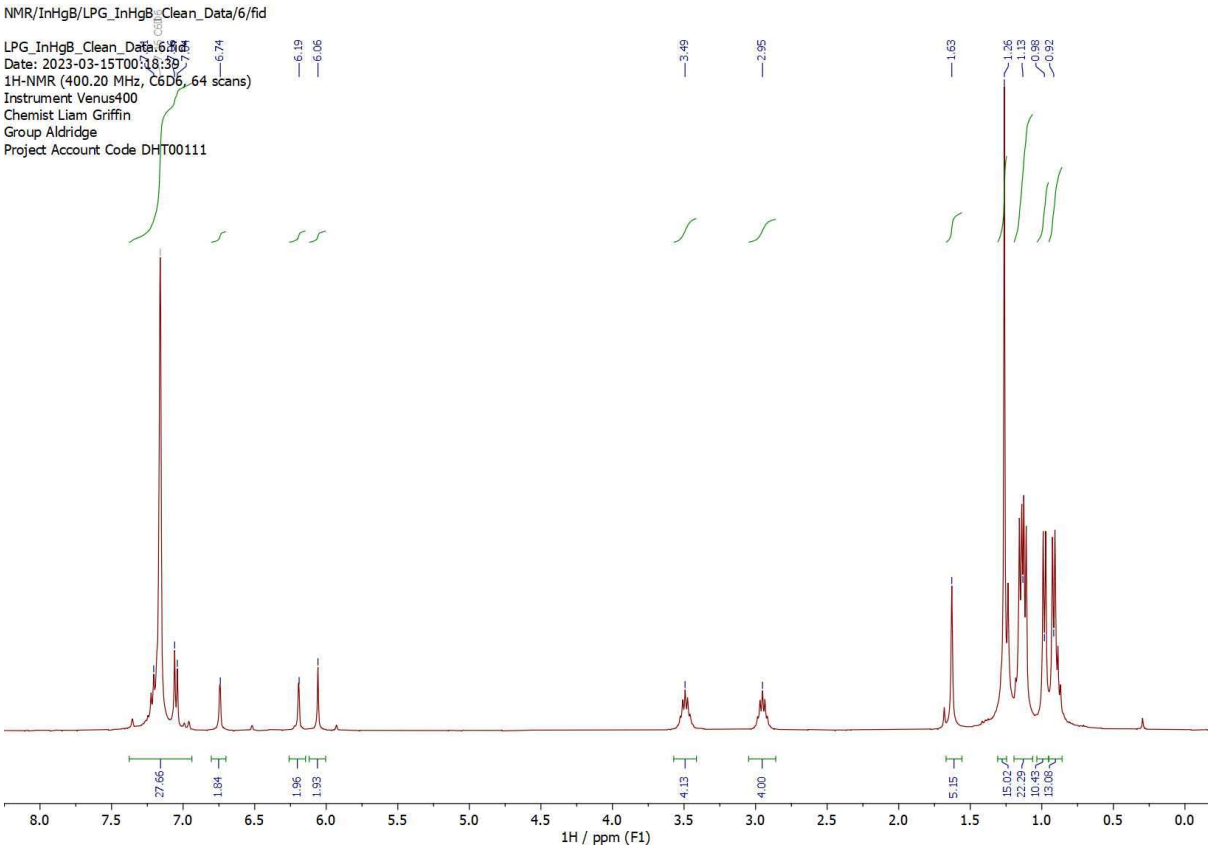

Figure s8: ^{1}H NMR spectrum of compound **5** in in benzene-d_6

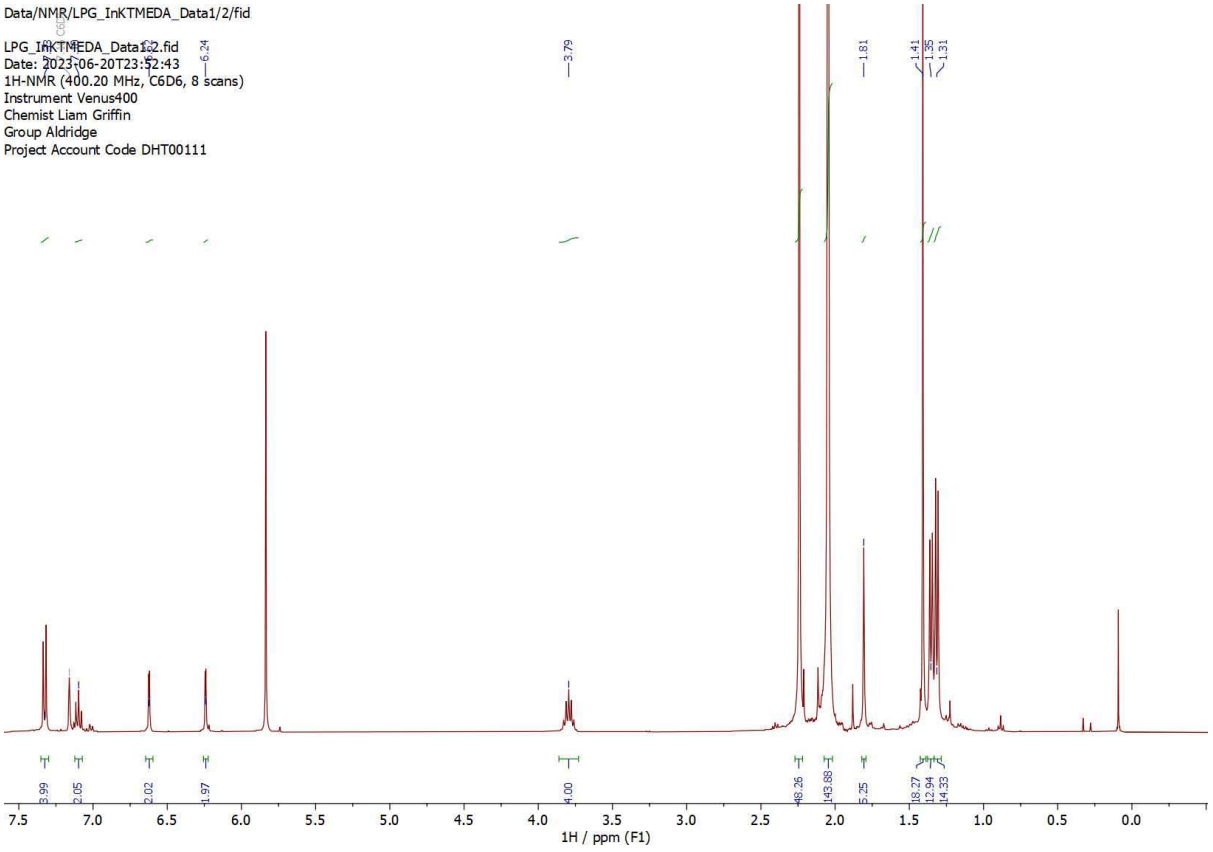

Figure s9: ^{1}H NMR spectrum of compound **5** in in benzene-d_6, in the presence of excess TMEDA

Computational details

Gas phase geometry optimizations and frequency analyses were carried out using the Gaussian 16 software package, using the M06-2X functional and the def2-SVP basis set with D3 empirical dispersion correction.[S11-14] The optimized structures were confirmed to be minima on the potential energy surface by the absence of imaginary frequencies. Single point calculations were performed using the zeroth order regular approximation (ZORA, to account for the heavy elements Hg and In) in conjunction with the M06-2X functional; D3 empirical dispersion correction; the SARC-ZORA-TZVP basis set for Hg and In and the recontracted ZORA-def2-TZVP basis set for all other elements using the ORCA (5.0.4) software package. [S14-22] Natural bonding orbital (NBO) analyses were carried out using the NBO 7.0 program.[S23] Atoms in molecules (AIM) analyses were conducted using Multiwfn software package, with figures generated using the AIMAll software package.[S24,25] Electron localization function (ELF) analysis was performed with Multiwfn software package, with figures generated using UCSF Chimera.[S26,S27] Multiple bisynaptic basins located for each of the Hg-M bonds is due to improper clustering, despite the selection of a suitably fine grid. Plotting these basins in real space shows that they are in close proximity. All are listed below for completeness, and summed in the main text for clarity. AIM bonding classifications have been made in accordance with the literature precedent.[S28] To reduce the computational burden, the -^{t}Bu substituents of the (**NON**) ligand were replaced by –CH_3 (**NON***). All iso-surfaces have been rendered at 0.05, unless otherwise stated.

Molecular Orbitals

3*

The HOMO and HOMO-3 show σ bonding interactions between B, Hg and Al, whilst the LUMO and LUMO+1 are vacant π-symmetry orbitals.

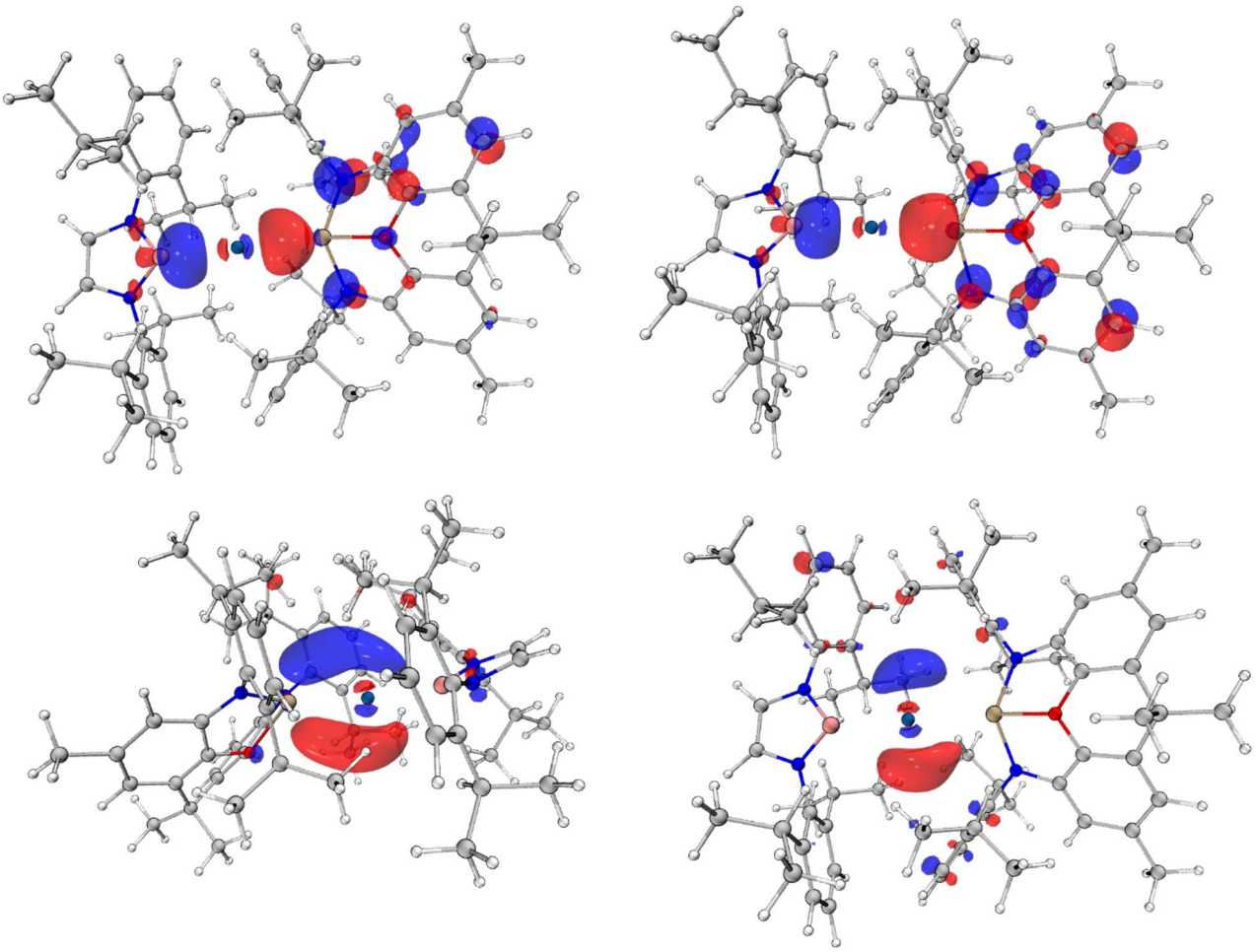

Figure s10: MOs of compound **3***, top right, HOMO; top left, HOMO-3, bottom left, LUMO; bottom right, LUMO+1

4*

The HOMO and HOMO-3 show σ bonding interactions between B, Hg and Ga, whilst the LUMO and LUMO+1 are vacant π-symmetry orbitals.

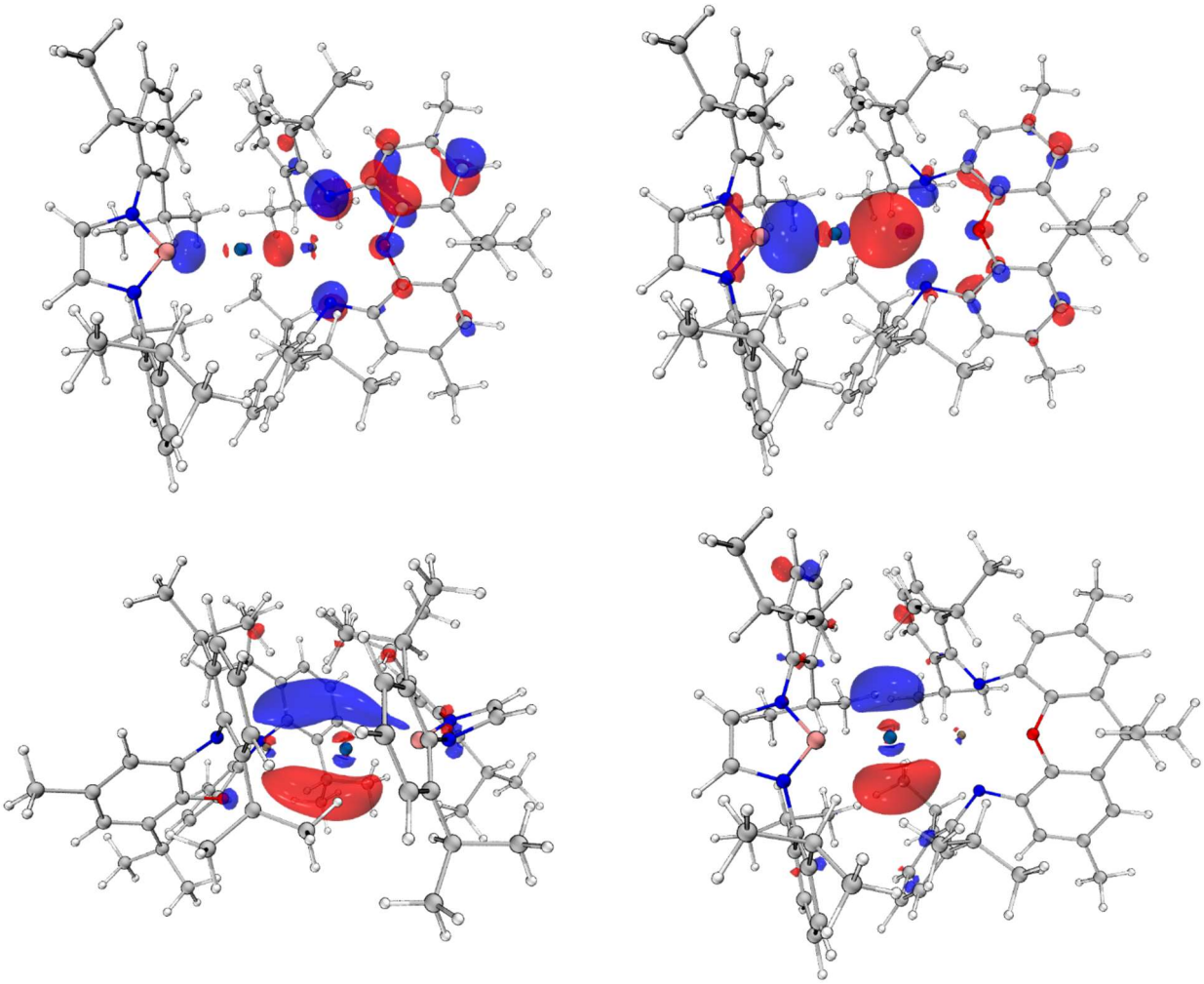

Figure s11: MOs of compound **4'**. top right, HOMO; top left, HOMO-3, bottom left, LUMO; bottom right, LUMO+1

5*

The HOMO and HOMO-3 show σ bonding interactions between B, Hg and In, whilst the LUMO and LUMO+1 are vacant π-symmetry orbitals. The HOMO is of decreasing bonding character down the series.

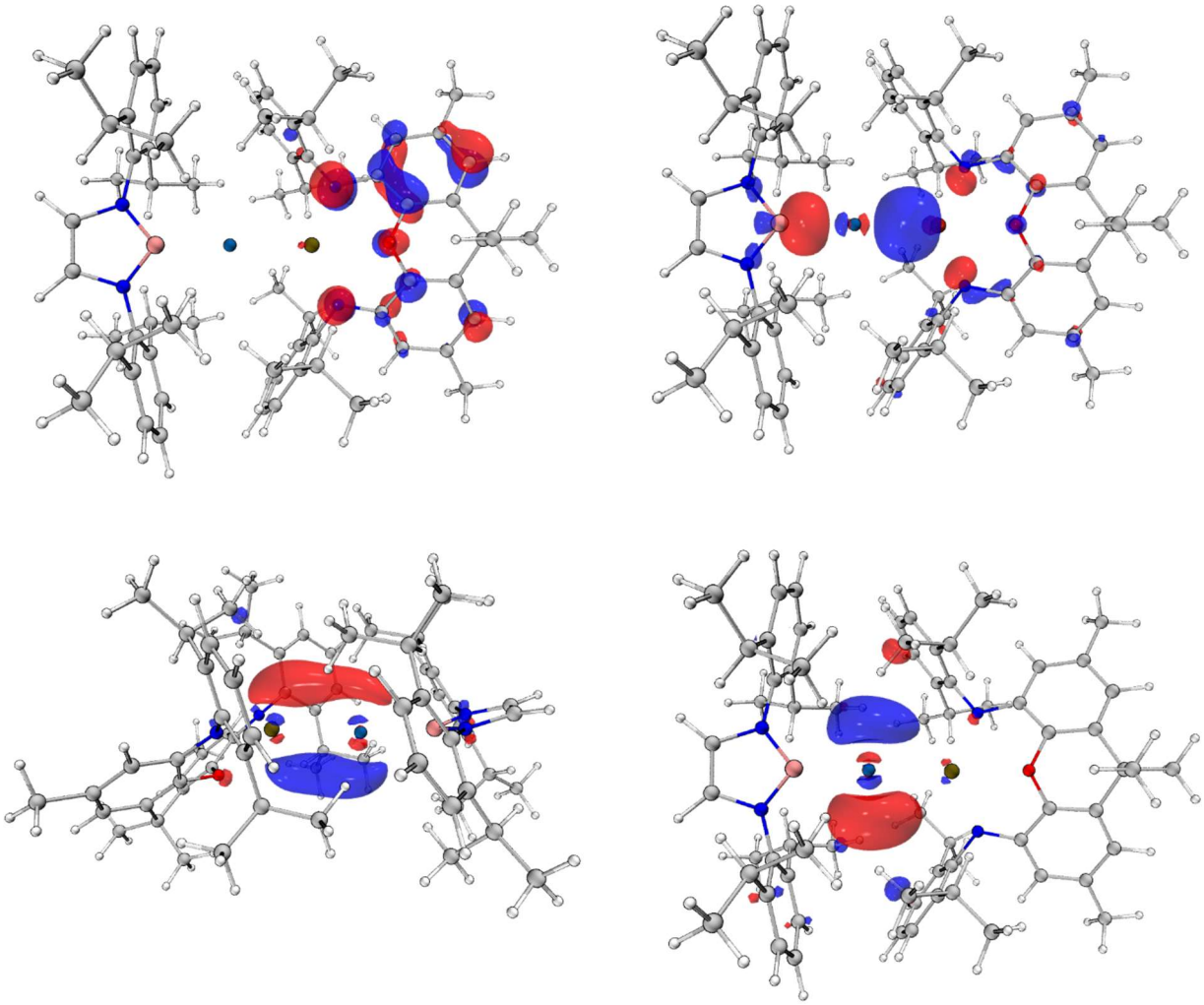

Figure s12: MOs of compound **5***, top right, HOMO; top left, HOMO-3, bottom left, LUMO; bottom right, LUMO+1

Natural Bonding Orbitals and Natural Population Analysis

3*

NBO analysis returns one bonding orbital between Hg and B, and an Al centred lone pair. The interaction between the aluminium fragment and the B-Hg fragment is detected through one 3c-4e hyperbonding interaction between the Hg-B bond and the Al lone pair, and one donor-acceptor interaction between the Al lone pair and the Hg-B antibonding orbital (as detected by Second Order Perturbation Theory (SOPT) analysis).

Hg-B bond

128. Occupancy 1.95971 e

(44%) Hg s (93%) d (7%)

(56%) B s (40%) p (60%)

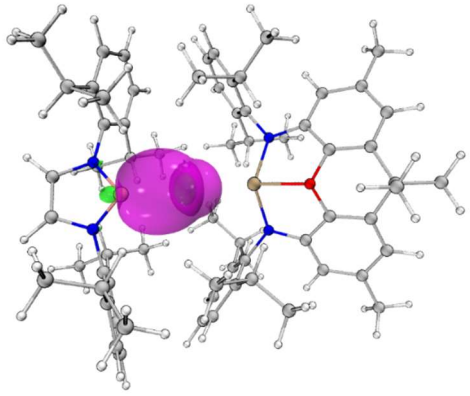

Hg-B antibond

317. Occupancy 0.81121 e

(56%) Hg s (93%) d (7%)

(44.04%) B s (40%) p (60%)

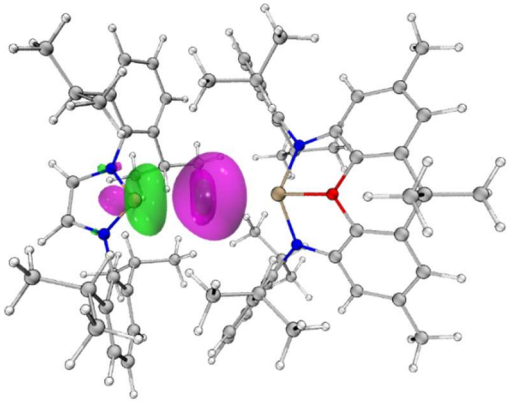

Al centred lone pair

118. Occupancy 1.13827 e

Al s(69%) p (31%)

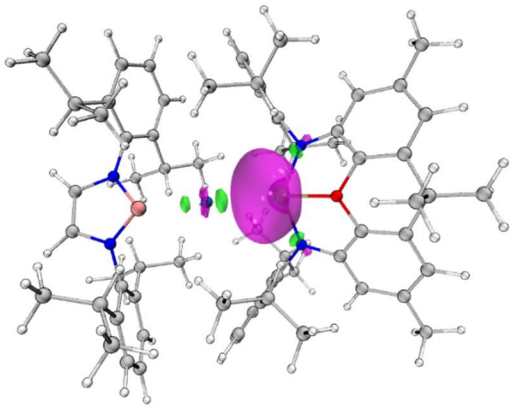

Figure s13: NBO orbitals for compound **3***

3c-4e interaction: %B-Hg/%Hg-Al: 39.0/61.0

SOPT interaction energy: 488.57 kJ/mol

NPA charges

Hg: 0.68324, Al: 1.25379, B: 0.22775

NPA orbital occupancies

Hg [core]6s(1.37)5d(9.92)6p(0.01)

Al [core]3s(0.86)3p(0.86)3d(0.01)4d(0.01)

B [core]2s(0.91)2p(1.81)3s(0.01)3p(0.03)

Wiberg Bond Indicies

Hg-B: 0.3653

Hg-Al: 0.5454

Al-B: 0.3552

4*

NBO analysis returns one bonding orbital between Hg and Ga, and a B centred lone pair. The interaction between the aluminium fragment and the Ga-Hg fragment is detected through one 3c-4e hyperbonding interaction between the Ga-Hg bond and the B lone pair, and one donor-acceptor interaction between the B lone pair and the Ga-Hg antibonding orbital (as detected by Second Order Perturbation Theory (SOPT) analysis).

Hg-Ga bonding orbital

138. Occupancy 1.95976 e

(43.54%) Hg s (94%) p (1%) d (5%)

(56.46%) Ga s (66%) p (34%)

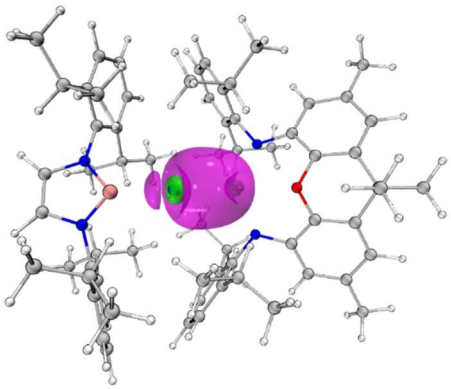

Hg-Ga antibonding orbital

327. Occupancy 0.56676

(56.46%) Hg s (94%) p (1%) d (5%)

(43.54%) Ga s (66%) p (34%)

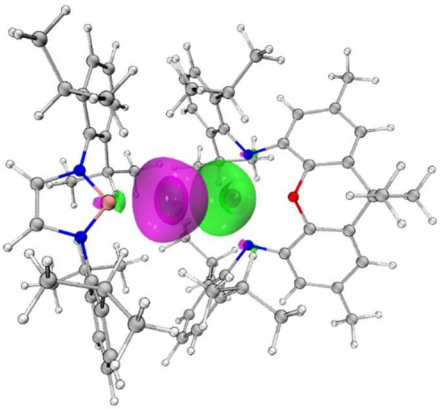

B lone pair

137. Occupancy 1.38337

B s (33%) p (67%)

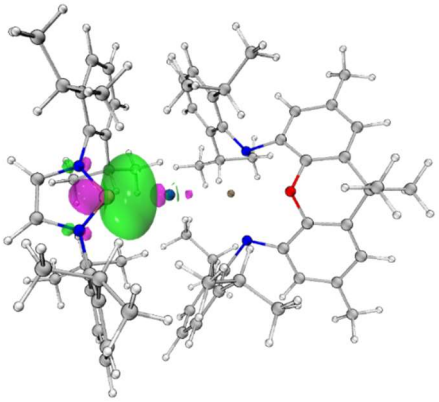

Figure s14: NBO orbitals for compound **4***

3c-4e interaction: %Ga-Hg/%Hg-B : 52.8/47.2

SOPT interaction energy: 276.81 kJ/mol

Natural Population Analysis

NPA charges

Hg: 0.82990, Ga: 1.03479, B: 0.27203

NPA occupancies

Hg [core]6s(1.21)5d(9.93)6p(0.02)

Ga [core]4s(1.09)4p(0.85)5s(0.01)4d(0.01)5p(0.01)

B [core]2s(0.86)2p(1.83)3s(0.01)3p(0.02)

Wiberg Bond Indicies

Hg-Ga: 0.5157

Hg-B: 0.4660

B-Ga: 0.2918

5*

NBO analysis returns one bonding orbital between Hg and In, and a B centred lone pair. The interaction between the aluminium fragment and the In-Hg fragment is detected through one 3c-4e hyperbonding interaction between the In-Hg bond and the B lone pair, and one donor-acceptor interaction between the B lone pair and the In-Hg antibonding orbital (as detected by Second Order Perturbation Theory (SOPT) analysis).

In-Hg bonding orbital

146. Occupancy 1.95273

(48.44%) Hg s (94%) p (1%) d (5%)

(51.56%) In s (83%) p (17%)

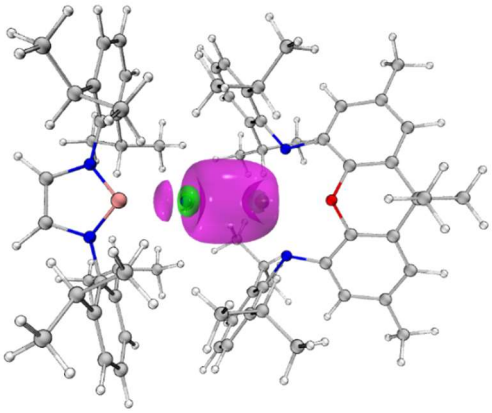

In-Hg antibonding orbital

335. Occupancy 0.61173

(51.56%) Hg s (94%) p (1%) d (5%)

(48.44%) In s (83%) p (17%)

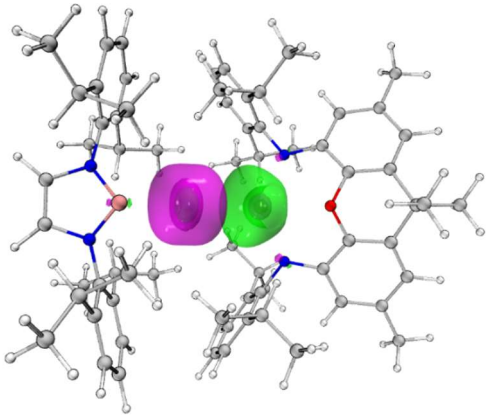

B Lone Pair

145. Occupancy 1.36890

B s (30%) p (70%)

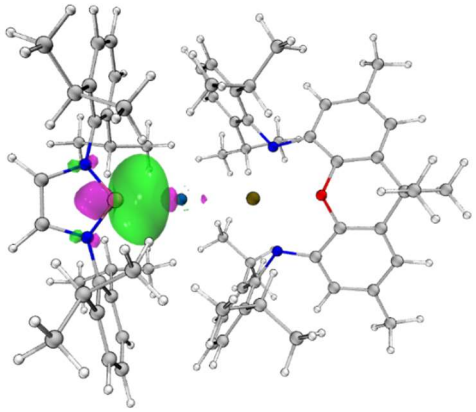

Figure s15: NBO orbitals for compound **5***

3c-4e interaction: %In-Hg/%Hg-B : 54.0/46.0

SOPT interaction energy: 292.71 kJ/mol

Natural Population Analysis

NPA charges

Hg: 0.73206, In: 1.27135, B: 0.23180

NPA occupancies

Hg [core]6s(1.30)5d(9.94)6p(0.02)6d(0.01)

In [core]5s(1.21)5p(0.47)5d(0.01)6p(0.04)

B [core]2s(0.85)2p(1.87)3s(0.01)3p(0.03)

Wiberg Bond Indicies

Hg-In: 0.4904

Hg-B: 0.4294

In-B: 0.3222

QTAIM

3*

Bader charges

Hg: -0.442454

Al: 2.254431

B: 1.377814

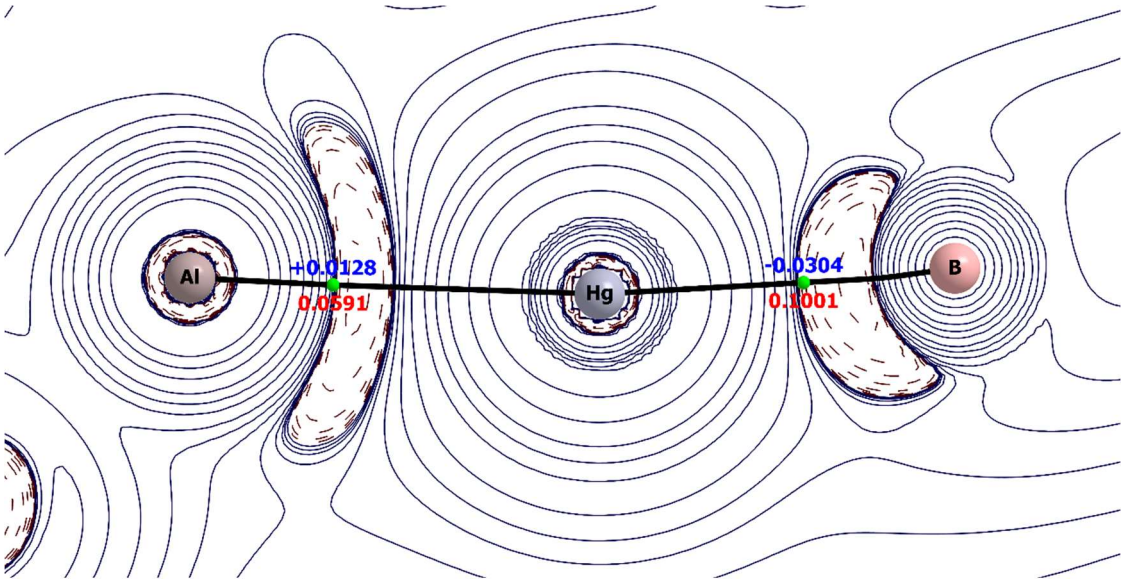

Figure s16: QTAIM contour plot of the Laplacian of electron density of compound **3***, in the Al-Hg-B plane. Electron density (red) and Laplacian of electron density (blue) at the bond critical points listed.

4*

Bader charges

Hg: -0.057637

Ga: 1.404890

B: 1.448442

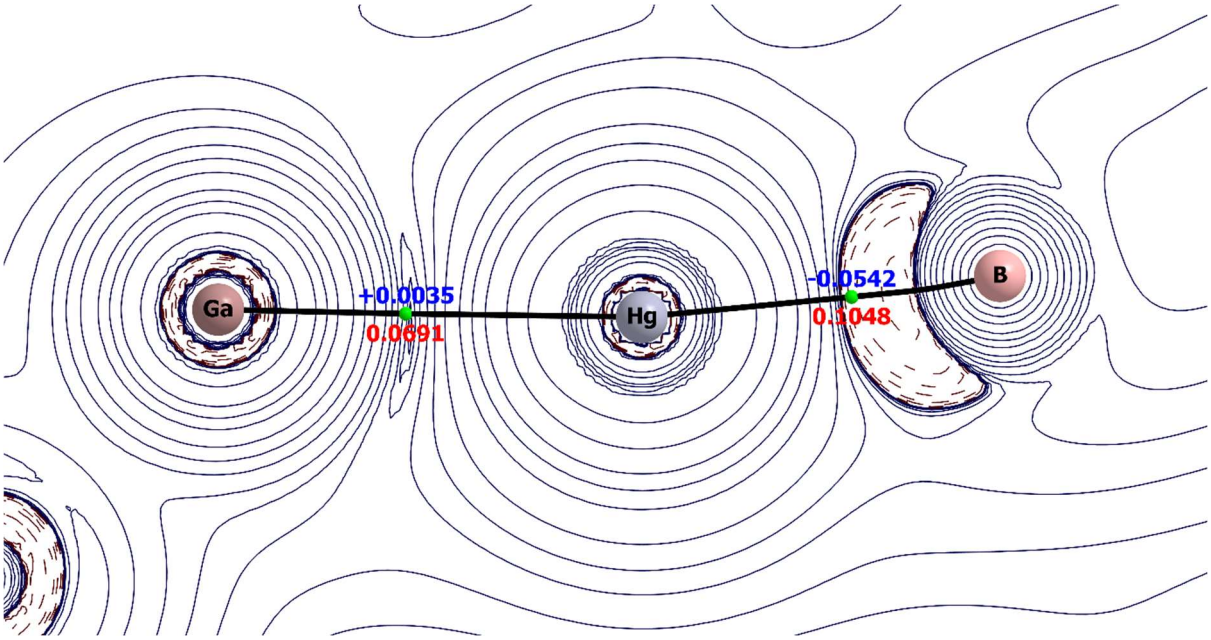

Figure s17: QTAIM contour plot of the Laplacian of electron density of compound **4***, in the Ga-Hg-B plane. Electron density (red) and Laplacian of electron density (blue) at the bond critical points listed.

5*

Bader charges

Hg: -0.014862

In: 1.286239

B: 1.503211

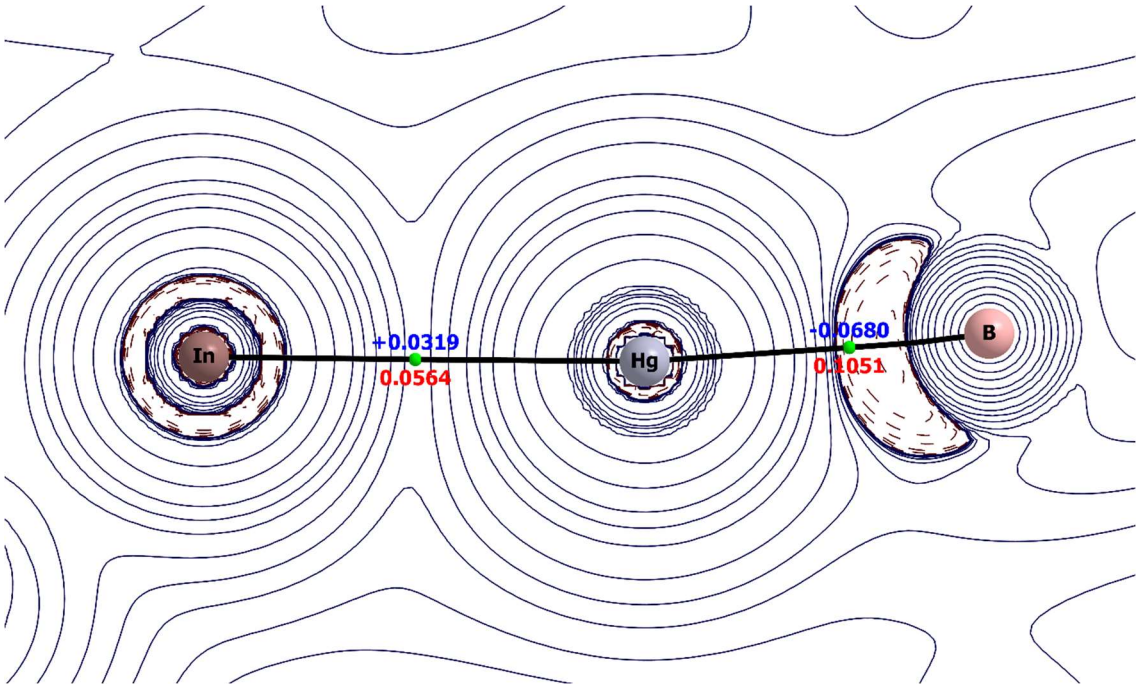

Figure s18: QTAIM contour plot of the Laplacian of electron density of compound **5'**, in the In-Hg-B plane. Electron density (red) and Laplacian of electron density (blue) at the bond critical points listed.

Complex	Bond	ρ(r)	∇²ρ(r)	G(r)	K(r)	V(r)	E(r)	ELF	Class
3*	AlHg	0.5901572678E-01	0.1415850683E-01	0.2683255564E-01	0.2329292893E-01	-0.5012548457E-01	-0.2329292893E-01	0.4779758264E+00	Metallic
	BHg	0.1001367122E+00	-0.3211625649E-01	0.3852730112E-01	0.4655636524E-01	-0.8508366636E-01	-0.4655636524E-01	0.7213185367E+00	Polar covalent
4*	GaHg	0.6906456204E-01	0.3528075062E-02	0.2622778557E-01	0.2534576680E-01	-0.5157355237E-01	-0.2534576680E-01	0.6181133751E+00	Metallic
	BHg	0.1048197990E+00	-0.5417162951E-01	0.3822542752E-01	0.5176833490E-01	-0.8999376243E-01	-0.5176833490E-01	0.7538206245E+00	Polar covalent
5*	InHg	0.5637426006E-01	0.3187703267E-01	0.2398241579E-01	0.1601315762E-01	-0.3999557342E-01	-0.1601315762E-01	0.4959276228E+00	Metallic
	BHg	0.1050598895E+00	-0.6797418668E-01	0.3626842407E-01	0.5326197074E-01	-0.8953039482E-01	-0.5326197074E-01	0.7741332756E+00	Polar covalent

Table s2: QT-AIM parameters associated with the Hg–B and Hg–E bonds of model complexes **3***, **4*** and **5***

Electron Localisation Function

3*

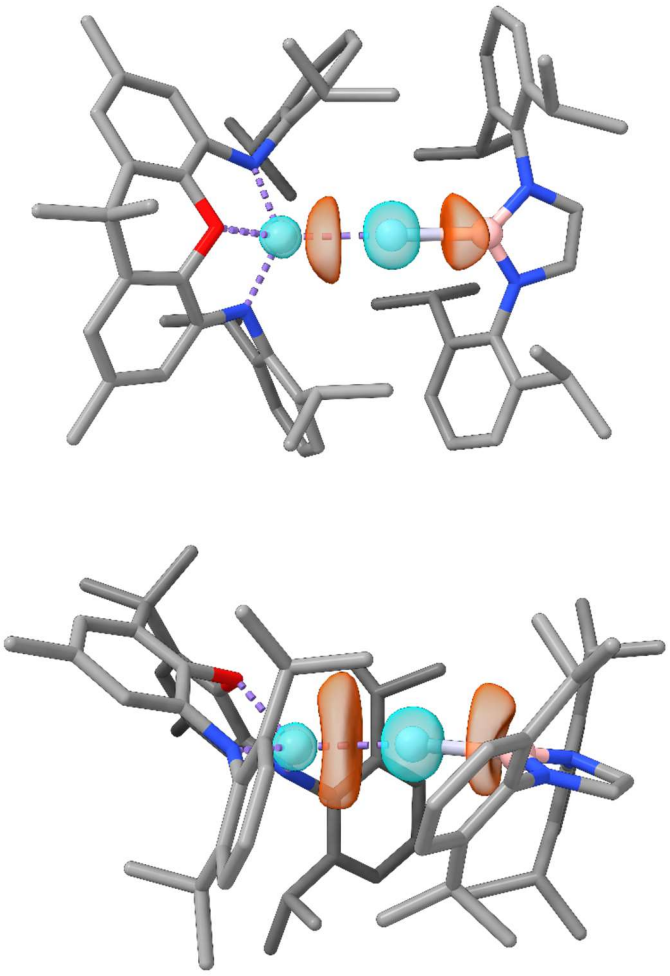

Figure s19: ELF isosurfaces (0.05) for basins associated with B, Hg and Al. Core basins shown in blue, bonding basins in orange.

	Total	B	Hg	Al
V(BHg)	**1.9589**	**1.1661 (59.5 %)**	**0.73669 (37.6 %)**	**-**
V(AlHg)1	1.0129	-	0.76354	0.22277
V(AlHg)2	0.8491	-	0.64278	0.18356
Sum V(AlHg)	**1.8620**	**-**	**1.40632 (75.5 %)**	**0.40633 (21.8 %)**

Table s3: Populations of relevant ELF basins for model complex **3***

4*

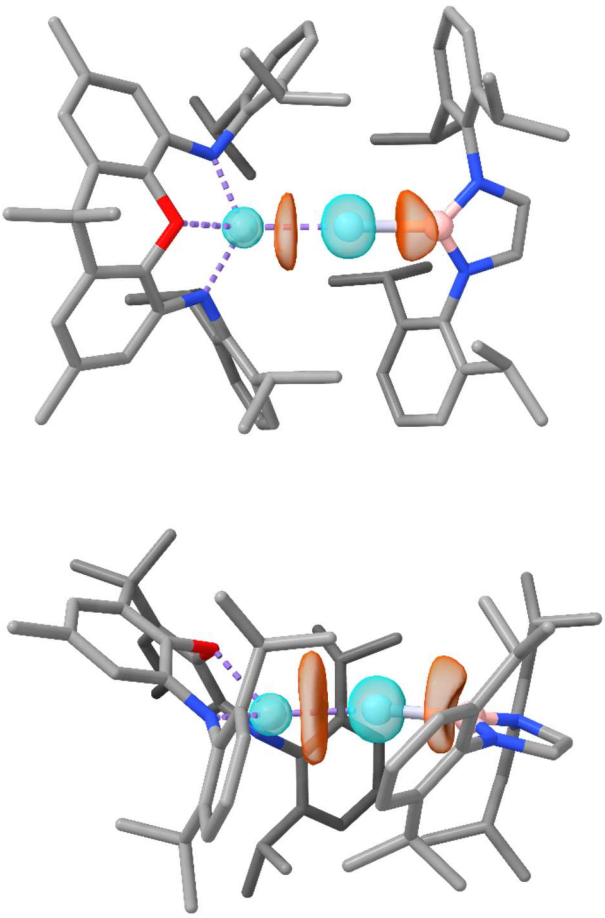

Figure s20: ELF isosurfaces (0.05) for basins associated with B, Hg and Ga. Core basins shown in blue, bonding basins in orange.

	Total	**B**	**Hg**	**Ga**
V(BHg)	**1.9388**	**1.08376 (55.9 %)**	**0.80577 (41.6 %)**	**-**
V(GaHg)1	0.0315	-	0.01556	0.01551
V(GaHg)2	0.7768	-	0.33761	0.42897
V(GaHg)3	1.1110	-	0.50345	0.59438
Sum V(GaHg)	**1.9193**	**-**	**0.85662 (44.6 %)**	**1.03886 (54.1 %)**

Table s4: Populations of relevant ELF basins for model complex **4***

5*

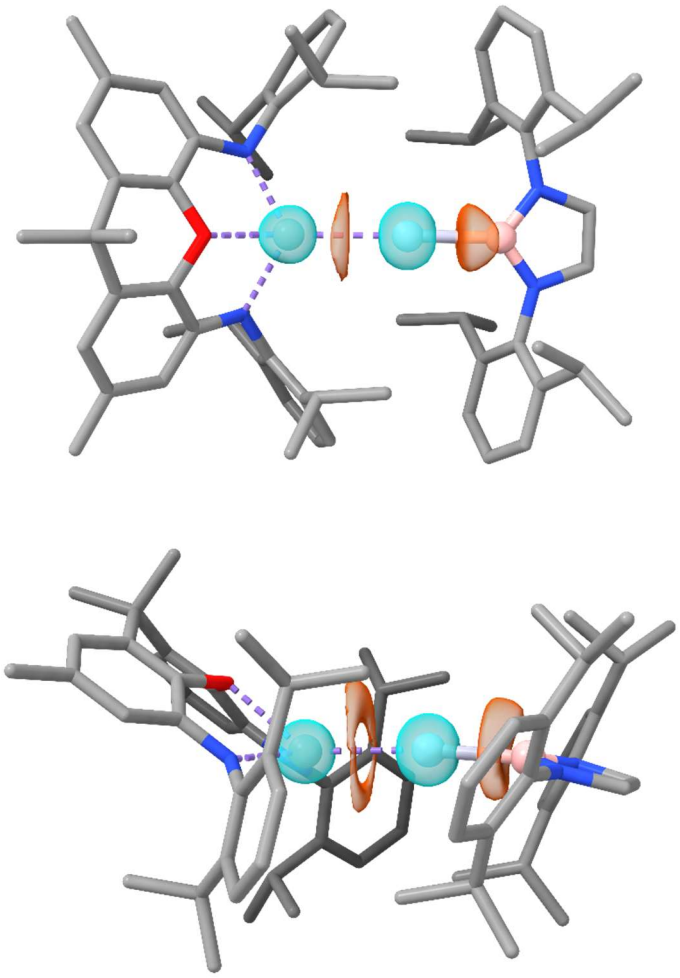

Figure s21: ELF isosurfaces (0.05) for basins associated with B, Hg and In. Core basins shown in blue, bonding basins in orange.

	Total	**B**	**Hg**	**In**
V(BHg)	**1.8830**	**1.01220 (53.8 %)**	**0.82822 (44.0 %)**	**-**
V(InHg)1	1.0153	-	0.41789	0.58469
V(InHg)2	0.7410	-	0.29901	0.43210
Sum V(InHg)	**1.7563**	**-**	**0.71690 (40.8%)**	**1.01679 (57.9 %)**

Table s5: Populations of relevant ELF basins for model complex **5***

XYZ coordinates

3‘				**4‘**			
Hg	0.989019	0.119087	-0.413446	Hg	1.120390	0.108720	-0.420740
Al	-1.518686	-0.082465	0.059029	Ga	-1.394320	-0.049250	0.094110
O	-3.098963	-0.486630	-1.156737	O	-3.096820	-0.463470	-1.219480
N	-2.489482	1.514903	0.296159	N	-2.477150	1.550520	0.308370
N	-1.915648	-1.819200	0.671466	N	-1.935710	-1.820250	0.684860
N	4.267710	-0.661803	-0.661755	N	4.347200	-0.695750	-0.643330
N	3.885977	1.528382	-0.253637	N	3.985020	1.499970	-0.234760
C	-5.238734	0.364155	-1.836020	C	-5.222940	0.420780	-1.854970
C	-6.128833	1.444390	-1.795789	C	-6.108860	1.502270	-1.802250
H	-7.105697	1.370936	-2.273777	H	-7.088730	1.437530	-2.275480
C	-5.782332	2.623035	-1.119741	C	-5.752470	2.672770	-1.117270
C	-4.570847	2.721405	-0.420287	C	-4.540490	2.752260	-0.419150
H	-4.339511	3.619109	0.156862	H	-4.303090	3.642260	0.167560
C	-3.668184	1.648404	-0.418602	C	-3.642200	1.672570	-0.423860
C	-4.023943	0.558373	-1.212251	C	-4.000120	0.592790	-1.234760
C	-3.712263	-1.703145	-0.845059	C	-3.714480	-1.660150	-0.875040
C	-3.065918	-2.409775	0.166053	C	-3.090030	-2.370000	0.150600
C	-3.642415	-3.635569	0.522059	C	-3.693450	-3.583520	0.512100
H	-3.156302	-4.254245	1.279687	H	-3.223380	-4.201200	1.280720
C	-4.831601	-4.058357	-0.088429	C	-4.885270	-3.994380	-0.097610
C	-5.472928	-3.254414	-1.043577	C	-5.509980	-3.186190	-1.060270
H	-6.420791	-3.586189	-1.468049	H	-6.464710	-3.501710	-1.481970
C	-4.913171	-2.033702	-1.438362	C	-4.924190	-1.981860	-1.462180
C	-5.488013	-1.023336	-2.437894	C	-5.486150	-0.963030	-2.461860
C	-4.700910	-1.144071	-3.757676	C	-4.701770	-1.090030	-3.782650
H	-5.062959	-0.399089	-4.480611	H	-5.056470	-0.339410	-4.503540
H	-4.831624	-2.150547	-4.180549	H	-4.845640	-2.093870	-4.207800
H	-3.628247	-0.974434	-3.590167	H	-3.627380	-0.933420	-3.615700
C	-6.969662	-1.266458	-2.695703	C	-6.970170	-1.189140	-2.721820
H	-7.552726	-1.189044	-1.767330	H	-7.553400	-1.107470	-1.793870
H	-7.122304	-2.265333	-3.126800	H	-7.133680	-2.185340	-3.155350
H	-7.355982	-0.533843	-3.417447	H	-7.347740	-0.450320	-3.441990
C	-1.972765	2.726475	0.828554	C	-1.943030	2.758250	0.823920
C	-1.446030	3.689064	-0.055142	C	-1.390120	3.701340	-0.065570
C	-1.072922	4.933611	0.454653	C	-0.991500	4.942070	0.434270
H	-0.670505	5.688655	-0.224063	H	-0.573310	5.683060	-0.250560
C	-1.185128	5.209571	1.812446	C	-1.096470	5.230660	1.790140
H	-0.884822	6.185245	2.199217	H	-0.776760	6.203270	2.169160
C	-1.650444	4.229471	2.686183	C	-1.577430	4.265260	2.672130
H	-1.704482	4.448130	3.752588	H	-1.622810	4.491270	3.737530
C	-2.058080	2.979461	2.211434	C	-2.012870	3.021400	2.206590
C	-1.268921	3.395774	-1.531741	C	-1.205080	3.385550	-1.536330
H	-1.605841	2.367120	-1.715860	H	-1.546610	2.355720	-1.706520
C	0.208125	3.468353	-1.918358	C	0.275690	3.447430	-1.913670
H	0.359638	3.070574	-2.932482	H	0.435880	3.026590	-2.917280
H	0.840670	2.897056	-1.219321	H	0.902860	2.893570	-1.195150
H	0.577712	4.504909	-1.899355	H	0.646990	4.483700	-1.915870
C	-2.114849	4.323361	-2.405960	C	-2.043610	4.301810	-2.429190
H	-1.815314	5.373192	-2.264023	H	-1.745210	5.353320	-2.296820
H	-3.182440	4.231142	-2.162556	H	-3.112560	4.211250	-2.191300
H	-1.980061	4.075619	-3.469051	H	-1.901340	4.041050	-3.488200
C	-2.609427	1.909903	3.137298	C	-2.579460	1.966830	3.139770
H	-2.189408	0.947543	2.800436	H	-2.187100	0.994270	2.799090
C	-2.203537	2.112975	4.593190	C	-2.154090	2.161290	4.591170
H	-2.670389	3.015807	5.014671	H	-2.594860	3.075000	5.017340
H	-1.112634	2.204982	4.701730	H	-1.060190	2.227650	4.688550
H	-2.542611	1.261537	5.200577	H	-2.506590	1.318310	5.202780

C	-4.132895	1.803710	3.018768
H	-4.513631	1.019260	3.689822
H	-4.443314	1.559518	1.995759
H	-4.601518	2.758821	3.302497
C	-0.922993	-2.749566	1.090699
C	-0.167491	-3.428669	0.110207
C	0.761930	-4.384552	0.528029
H	1.375606	-4.898975	-0.213069
C	0.908227	-4.697708	1.874785
H	1.626598	-5.461047	2.178552
C	0.154698	-4.025722	2.832644
H	0.286591	-4.265455	3.889004
C	-0.751079	-3.031359	2.457713
C	-0.382114	-3.192045	-1.374986
H	-0.952364	-2.259785	-1.496256
C	0.939164	-3.028942	-2.122083
H	1.594088	-2.285313	-1.643364
H	0.760396	-2.721032	-3.163228
H	1.501762	-3.973739	-2.141291
C	-1.212615	-4.318898	-1.999762
H	-0.680639	-5.278062	-1.902271
H	-1.376080	-4.123792	-3.070182
H	-2.191582	-4.416189	-1.512497
C	-1.482269	-2.191517	3.482033
H	-2.413662	-1.842307	3.011424
C	-0.616325	-0.967089	3.786234
H	-1.119039	-0.268790	4.468996
H	-0.359436	-0.423776	2.861853
H	0.331434	-1.284395	4.247692
C	-1.836933	-2.942362	4.760875
H	-0.937608	-3.214574	5.333621
H	-2.394836	-3.863831	4.540692
H	-2.457876	-2.309186	5.410731
C	5.479853	-0.029648	-0.370655
H	6.413692	-0.585465	-0.335031
C	5.252690	1.283972	-0.139356
H	5.957719	2.075883	0.103045
C	4.171193	-2.070872	-0.481846
C	4.212461	-2.938624	-1.586185
C	4.181522	-4.313222	-1.337024
H	4.206678	-5.014420	-2.171515
C	4.109473	-4.804033	-0.034182
H	4.087442	-5.881624	0.138460
C	4.041095	-3.926821	1.042383
H	3.955217	-4.315810	2.059050
C	4.064253	-2.545613	0.836602
C	4.277379	-2.368145	-2.992068
H	3.577139	-1.516043	-3.013642
C	3.860855	-3.364108	-4.070882
H	3.799319	-2.855424	-5.043029
H	2.884033	-3.818377	-3.859795
H	4.601663	-4.172152	-4.170821
C	5.677217	-1.827688	-3.306016
H	6.419684	-2.636420	-3.225826
H	5.964291	-1.021010	-2.621533
H	5.711104	-1.430899	-4.331391
C	3.943836	-1.587249	2.007599
H	4.085080	-0.565310	1.633371
C	2.545951	-1.661238	2.619573
H	2.387451	-2.619193	3.135415

C	-4.105710	1.896960	3.032870
H	-4.500270	1.120130	3.704740
H	-4.427240	1.662190	2.011040
H	-4.549370	2.862410	3.321880
C	-0.956910	-2.767140	1.089420
C	-0.203990	-3.445590	0.105750
C	0.716320	-4.412930	0.517770
H	1.323030	-4.930460	-0.226850
C	0.864190	-4.731940	1.862960
H	1.574580	-5.504570	2.162190
C	0.122310	-4.053360	2.825600
H	0.256550	-4.296470	3.880900
C	-0.776990	-3.051420	2.456110
C	-0.406470	-3.186540	-1.377110
H	-0.955420	-2.240220	-1.489310
C	0.923290	-3.045960	-2.115620
H	1.602240	-2.338760	-1.614190
H	0.759130	-2.703600	-3.148410
H	1.455970	-4.007440	-2.160440
C	-1.261400	-4.284170	-2.020530
H	-0.753980	-5.257460	-1.932110
H	-1.414990	-4.071500	-3.089050
H	-2.244760	-4.361950	-1.538670
C	-1.499360	-2.207160	3.483260
H	-2.436730	-1.865450	3.019570
C	-0.637520	-0.975490	3.771020
H	-1.139880	-0.273160	4.450210
H	-0.388680	-0.437570	2.841030
H	0.315010	-1.283350	4.229260
C	-1.835250	-2.949910	4.771790
H	-0.927970	-3.213770	5.336010
H	-2.391220	-3.875560	4.564880
H	-2.451710	-2.315040	5.424170
C	5.561570	-0.079350	-0.330010
H	6.488120	-0.646350	-0.283080
C	5.346580	1.237330	-0.098570
H	6.057320	2.020460	0.155190
C	4.212510	-2.103650	-0.475230
C	4.234660	-2.961550	-1.587480
C	4.158280	-4.336530	-1.351050
H	4.168270	-5.030850	-2.191500
C	4.057850	-4.835740	-0.053420
H	4.000040	-5.913510	0.109520
C	4.002170	-3.966320	1.030070
H	3.888670	-4.361210	2.041620
C	4.069870	-2.584760	0.837250
C	4.323770	-2.379750	-2.987140
H	3.649740	-1.506560	-3.003360
C	3.878300	-3.351520	-4.076120
H	3.837280	-2.832890	-5.044020
H	2.885710	-3.773530	-3.871070
H	4.591320	-4.183550	-4.180580
C	5.741050	-1.879890	-3.288950
H	6.456830	-2.713150	-3.218580
H	6.051720	-1.093670	-2.590780
H	5.791590	-1.468680	-4.307870
C	3.951430	-1.634400	2.014960
H	4.113350	-0.611140	1.651990
C	2.545550	-1.693610	2.611810
H	2.368110	-2.652370	3.119850

H	1.756969	-1.580575	1.851586
H	2.403075	-0.850095	3.349705
C	5.026071	-1.829442	3.058474
H	4.936556	-1.096423	3.873725
H	6.027896	-1.732628	2.616531
H	4.940961	-2.834124	3.499630
C	3.310512	2.798627	0.012212
C	3.513647	3.846030	-0.903767
C	2.947286	5.091195	-0.617866
H	3.097241	5.924626	-1.304381
C	2.168065	5.271854	0.519195
H	1.709107	6.241749	0.718626
C	1.959476	4.218144	1.403188
H	1.332899	4.374373	2.279908
C	2.544468	2.969947	1.183163
C	4.263937	3.587430	-2.198989
H	5.104885	2.917428	-1.971665
C	3.356046	2.855892	-3.194163
H	2.538117	3.519710	-3.510844
H	2.914217	1.954903	-2.744501
H	3.924045	2.556016	-4.087133
C	4.837580	4.851792	-2.831042
H	5.469642	4.587697	-3.690423
H	5.446820	5.422422	-2.115537
H	4.039276	5.510991	-3.204002
C	2.446647	1.871987	2.229908
H	2.398969	0.904410	1.713414
C	1.203505	1.973169	3.105924
H	1.208254	2.880325	3.729924
H	1.152362	1.108793	3.783759
H	0.287721	1.992357	2.495389
C	3.725246	1.846537	3.073124
H	4.611740	1.690692	2.441640
H	3.682666	1.030984	3.811333
H	3.846030	2.797824	3.613369
B	3.196747	0.302223	-0.577696
C	-5.414260	-5.396388	0.286578
H	-4.858910	-6.210546	-0.203718
H	-5.354424	-5.564407	1.370508
H	-6.465590	-5.474630	-0.018957
C	-6.718352	3.803518	-1.122869
H	-6.336347	4.597073	-1.783391
H	-7.718006	3.521493	-1.477434
H	-6.814805	4.233217	-0.116223

H	1.763840	-1.600080	1.837500
H	2.405350	-0.884990	3.345270
C	5.017940	-1.902910	3.075620
H	4.928760	-1.178400	3.898420
H	6.026100	-1.814950	2.646510
H	4.913610	-2.911550	3.503240
C	3.408890	2.772380	0.025250
C	3.615400	3.814690	-0.895080
C	3.043250	5.059690	-0.620510
H	3.195670	5.889530	-1.310850
C	2.254840	5.243820	0.509550
H	1.791480	6.213220	0.700530
C	2.039460	4.193380	1.395750
H	1.401130	4.351450	2.263610
C	2.628990	2.945320	1.186820
C	4.368630	3.548910	-2.186660
H	5.198110	2.865070	-1.957980
C	3.450290	2.835360	-3.185420
H	2.637690	3.510050	-3.493070
H	2.999880	1.935640	-2.741530
H	4.011540	2.536320	-4.082870
C	4.963500	4.806560	-2.812590
H	5.597370	4.535660	-3.668460
H	5.575800	5.367140	-2.091830
H	4.176900	5.477420	-3.189370
C	2.508700	1.848170	2.232230
H	2.471080	0.879780	1.716740
C	1.245500	1.952320	3.079500
H	1.244880	2.852780	3.712960
H	1.168010	1.081270	3.746160
H	0.344080	1.990140	2.448080
C	3.768870	1.816750	3.102130
H	4.667270	1.655480	2.488890
H	3.706130	1.001730	3.839490
H	3.883890	2.767540	3.644340
B	3.296090	0.283560	-0.575700
C	-5.491920	-5.319640	0.284990
H	-4.984320	-6.143730	-0.239560
H	-5.392050	-5.505170	1.363020
H	-6.557220	-5.361570	0.023160
C	-6.678700	3.861090	-1.111760
H	-6.323780	4.631310	-1.813980
H	-7.695840	3.576820	-1.411120
H	-6.725360	4.321760	-0.115450

5‘

Hg	1.431070	-0.004310	-0.230620
In	-1.329070	-0.011320	0.082860
O	-3.287610	-0.051040	-1.246130
N	-2.376430	1.880030	0.337150
N	-2.319410	-1.919050	0.373610
N	4.496850	-1.102380	-0.186140
N	4.460660	1.165580	-0.108020
C	-5.231400	1.175580	-1.896610
C	-5.943770	2.380770	-1.843440
H	-6.900360	2.480080	-2.356600
C	-5.435200	3.469070	-1.126130
C	-4.236740	3.348460	-0.411260
H	-3.874030	4.190510	0.183220
C	-3.508910	2.143780	-0.400530

C	-4.026940	1.122190	-1.218270
C	-4.041300	-1.208660	-1.124550
C	-3.510810	-2.188380	-0.265450
C	-4.273070	-3.364490	-0.145860
H	-3.905060	-4.170440	0.493500
C	-5.497230	-3.507640	-0.812010
C	-5.994150	-2.471160	-1.610160
H	-6.962680	-2.590560	-2.096190
C	-5.257060	-1.291650	-1.779190
C	-5.660140	-0.091780	-2.645120
C	-4.874530	-0.165260	-3.972140
H	-5.116090	0.703930	-4.601670
H	-5.136420	-1.085510	-4.515040
H	-3.791480	-0.168540	-3.785720
C	-7.156670	-0.090010	-2.947210
H	-7.752300	-0.036910	-2.024740
H	-7.437310	-0.999520	-3.496000
H	-7.417650	0.765930	-3.584660
C	-1.699310	2.976300	0.925650
C	-0.905150	3.828960	0.122630
C	-0.267740	4.922710	0.717810
H	0.344830	5.584330	0.100160
C	-0.399430	5.176220	2.077850
H	0.093050	6.041460	2.526340
C	-1.149060	4.311090	2.871190
H	-1.225150	4.504590	3.941770
C	-1.797660	3.201900	2.320790
C	-0.722540	3.589570	-1.366870
H	-1.224960	2.644560	-1.618920
C	0.758540	3.448260	-1.732840
H	0.868240	3.118820	-2.777230
H	1.277030	2.722970	-1.081790
H	1.295960	4.402900	-1.623190
C	-1.379490	4.694820	-2.201490
H	-0.915820	5.670680	-1.987770
H	-2.454390	4.767220	-1.985210
H	-1.257500	4.490700	-3.275800
C	-2.624870	2.269170	3.191850
H	-2.486460	1.251350	2.792540
C	-2.185950	2.261460	4.655320
H	-2.409080	3.219350	5.149260
H	-1.107780	2.065950	4.757790
H	-2.732560	1.483970	5.208670
C	-4.119920	2.591200	3.085460
H	-4.708080	1.900790	3.708950
H	-4.476740	2.507650	2.050980
H	-4.312190	3.618000	3.435000
C	-1.612640	-3.020270	0.918300
C	-0.792760	-3.814290	0.082790
C	-0.122430	-4.910590	0.636870
H	0.513380	-5.526460	-0.003530
C	-0.258580	-5.230920	1.983080
H	0.259300	-6.099170	2.395840
C	-1.054930	-4.436720	2.804970
H	-1.152560	-4.687800	3.862800
C	-1.733160	-3.327910	2.293130
C	-0.648190	-3.523460	-1.400830
H	-1.092390	-2.534970	-1.588480
C	0.818020	-3.472250	-1.838180
H	1.427230	-2.832490	-1.175540

H	0.897510	-3.085810	-2.865540
H	1.282040	-4.470330	-1.823220
C	-1.430710	-4.539810	-2.241120
H	-1.037350	-5.555940	-2.079620
H	-1.341720	-4.306410	-3.312830
H	-2.496650	-4.535750	-1.973340
C	-2.554860	-2.427260	3.196440
H	-3.305730	-1.935160	2.561560
C	-1.650610	-1.340350	3.788860
H	-2.226140	-0.624720	4.394090
H	-1.125790	-0.775660	2.998440
H	-0.876720	-1.793840	4.428490
C	-3.291630	-3.177310	4.305660
H	-2.596500	-3.600000	5.047000
H	-3.896280	-3.999100	3.895950
H	-3.963210	-2.492390	4.843350
C	5.787860	-0.633320	0.054070
H	6.627680	-1.313900	0.173960
C	5.766060	0.721920	0.100440
H	6.584350	1.419040	0.265950
C	4.183660	-2.493730	-0.183430
C	4.475020	-3.264180	-1.328690
C	4.178610	-4.628170	-1.297150
H	4.399190	-5.249000	-2.166340
C	3.593700	-5.208580	-0.172790
H	3.362810	-6.275590	-0.169370
C	3.302020	-4.431270	0.940980
H	2.836730	-4.889870	1.816340
C	3.603230	-3.063960	0.964110
C	5.029190	-2.603050	-2.580850
H	5.666480	-1.765740	-2.260720
C	3.879750	-2.015800	-3.409800
H	4.267190	-1.467970	-4.281940
H	3.270050	-1.323460	-2.809890
H	3.223980	-2.822880	-3.771390
C	5.885020	-3.536790	-3.435820
H	5.278110	-4.322960	-3.909580
H	6.672010	-4.023340	-2.841850
H	6.365770	-2.968580	-4.244860
C	3.335880	-2.258480	2.224000
H	3.557580	-1.205330	2.002890
C	1.871610	-2.351410	2.662860
H	1.623820	-3.357080	3.034420
H	1.173520	-2.147110	1.832250
H	1.667330	-1.635510	3.473830
C	4.277270	-2.691050	3.353270
H	4.104040	-2.082740	4.253570
H	5.329550	-2.576500	3.056170
H	4.111680	-3.746360	3.619660
C	4.110320	2.546490	-0.035310
C	4.424650	3.389960	-1.122210
C	4.104940	4.745160	-1.018660
H	4.345340	5.420960	-1.840200
C	3.470920	5.247280	0.116630
H	3.222920	6.308670	0.177260
C	3.150010	4.397920	1.167790
H	2.643210	4.794690	2.049950
C	3.473890	3.036360	1.119850
C	5.026030	2.814990	-2.395320
H	5.681590	1.979910	-2.108470

C	3.911660	2.241420	-3.280160
H	3.239470	3.048130	-3.611130
H	3.311000	1.499520	-2.732640
H	4.333050	1.754340	-4.172410
C	5.871010	3.818130	-3.179300
H	6.385030	3.308870	-4.006900
H	6.630890	4.293790	-2.542680
H	5.250940	4.611390	-3.623250
C	3.167600	2.154040	2.318180
H	3.369690	1.113180	2.030870
C	1.697080	2.252880	2.735910
H	1.473590	3.224190	3.201900
H	1.448790	1.468240	3.467880
H	1.014150	2.157640	1.874090
C	4.099300	2.487680	3.488180
H	5.153350	2.362240	3.201820
H	3.893080	1.829650	4.345680
H	3.956970	3.528940	3.816390
B	3.607830	0.021660	-0.279240
C	-6.271740	-4.793390	-0.660850
H	-5.772060	-5.616850	-1.193900
H	-6.348780	-5.087890	0.395520
H	-7.287810	-4.697920	-1.065610
C	-6.174000	4.784010	-1.103540
H	-5.615640	5.556220	-1.654870
H	-7.166770	4.693060	-1.563320
H	-6.303710	5.147840	-0.074110

References for Supporting Information

s1. C. A. Cruz, D. J. H. Emslie, L. E. Harrington, J. F. Britten, C. M. Robertson, *Organometallics* 2007, 26, 692.

s2. J. Hicks, P. Vasko, J. M. Goicoechea, S. Aldridge, *Nature* 2018, 557, 92.

s3. R. G. Goel, A. L. Beauchamp, *Inorg. Chem*. 1983, 22, 395.

s4. A. V. Protchenko, D. Dange, A. D. Schwarz, C. Y. Tang, N. Phillips, P. Mountford, C. Jones, S. Aldridge, Chem. Commun. 2014, 50, 3841.

s5. L. P. Griffin, M. A. Ellwanger, J. Clark, A. F. Roper, A. Heilmann, S. Aldridge, *ChemRxiv*, DOI: 10.26434/chemrxiv-2022-s63x6.

s6. J. Cosier, A.M. Glazer, *J. Appl. Cryst*. 1986, 19, 105.

s7. CrysAlisPro v.1.171.42.70a, Agilent Technologies, 2011.

s8. G.M. Sheldrick, *Acta Crystallogr.* 2015, A71, 3.

s9. G.M. Sheldrick, *Acta Crystallogr.* 2015, C71, 3.

s10. O. V. Dolomanov, L. J. Bourhis, R. J. Gildea, J. A. K. Howard, H. Puschmann, *J. Appl. Cryst*. 2009, 42, 339.

S11. Y. Zhao, D. G. Truhlar, *Theor. Chem. Acc*. 2008, 120, 215.

S12. F. Weigend, R. Ahlrichs, *Phys. Chem. Chem. Phys*. 2005, 7, 3297.

S13. S. Grimme, J. Antony, S. Ehrlich, H. Krieg, *J. Chem. Phys*. 2010, 132, 154104.

S14. Gaussian 16, Revision C.01, M. J. Frisch, G. W. Trucks, H. B. Schlegel, G. E. Scuseria, M. A. Robb, J. R. Cheeseman, G. Scalmani, V. Barone, G. A. Petersson, H. Nakatsuji, X. Li, M. Caricato, A. V. Marenich, J. Bloino, B. G. Janesko, R. Gomperts, B. Mennucci, H. P. Hratchian, J. V. Ortiz, A. F. Izmaylov, J. L. Sonnenberg, D. Williams-Young, F. Ding, F. Lipparini, F. Egidi, J. Goings, B. Peng, A. Petrone, T. Henderson, D. Ranasinghe, V. G. Zakrzewski, J. Gao, N. Rega, G. Zheng, W. Liang, M. Hada, M. Ehara, K. Toyota, R. Fukuda, J. Hasegawa, M. Ishida, T. Nakajima, Y. Honda, O. Kitao, H. Nakai, T. Vreven, K. Throssell, J. A. Montgomery, Jr., J. E. Peralta, F. Ogliaro, M. J. Bearpark, J. J. Heyd, E. N. Brothers, K. N. Kudin, V. N. Staroverov, T. A. Keith, R. Kobayashi, J. Normand, K. Raghavachari, A. P. Rendell, J. C. Burant, S. S. Iyengar, J. Tomasi, M. Cossi, J. M. Millam, M. Klene, C. Adamo, R. Cammi, J. W. Ochterski, R. L. Martin, K. Morokuma, O. Farkas, J. B. Foresman, D. J. Fox, Gaussian, Inc., Wallingford CT, 2016.

S15. E. van Lenthe, J. G. Snijders, E. J. Baerends, *J. Chem. Phys*. 1996, 105, 6505.

S16. J. D. Rolfes, F. Neese, D. A. Pantazis, *J. Comput. Chem*. 2020, 41, 1842.

S17. D. A. Pantazis, F. Neese, *J. Chem. Theory Comput*. 2009, 5, 2229

S18. D. A. Pantazis, X. Y. Chen, C. R. Landis, F. Neese, *J. Chem. Theory Comput*. 2008, 4, 908.

S19. D. A. Pantazis, F. Neese, *Theor. Chem. Acc*. 2012, 131, 1292.

S20. D. A. Pantazis, F. Neese, *J. Chem. Theory Comput*. 2011, 7, 677.

S21. F. Weigend, *Phys. Chem. Chem. Phys*. 2006, 8, 1057.

S22. F. Neese, F. Wennmohs, U. Becker, C. Riplinger, *J. Chem. Phys*. 2020, 152, 224108.

S23. NBO 7.0. E. D. Glendening, J, K. Badenhoop, A. E. Reed, J. E. Carpenter, J. A. Bohmann, C. M. Morales, P. Karafiloglou, C. R. Landis, F. Weinhold, Theoretical Chemistry Institute, University of Wisconsin, Madison (2018).

S24. AIMAll (Version 19.10.12), T. A. Keith, TK Gristmill Software, Overland Park KS, USA, 2019 (aim.tkgristmill.com)

S25. L. Tian, C. Feiwu, *J. Comput. Chem.* 2012, 33, 580.

S26. B. Silvi, A. Savin, Nature 1994, 371, 683.

S27. E. F. Pettersen, T. D. Goddard, C. C. Huang, G. S. Couch, D. M. Greenblatt, E. C. Meng, T. E. Ferrin, *J. Comput. Chem*. 2004, 25, 1605.

S28. R. Bianchi, G. Gervasio, D. Marabello, Inorg. Chem. 2000, 39, 2360.

Conclusions and Outlook

Future work in this area could include the use of these systems classes, in particular the highly sensitive and spectroscopically convenient silver phosphine systems, as a more general probe for ligand donicity. The synthesis and measurement of a library of $XAgP^tBu_3$ systems where X is a range of exotic 1- ligand fragments (highly electron donating/withdrawing for example) would allow for trends in bonding character to be assessed across the Periodic Table, and provide a set of benchmarks for novel ligand systems.

This work also allows certain design principles to be established for the installation of extremely electron donating ligand species such as an aluminyl anion. It is clear that the identity and nature of the ligand *trans* to the aluminyl ligand is of central importance to the stability and tractability of the so-generated metal complex. In the examples above, the use of a L-donor phosphine ligand *trans* to the aluminyl precluded crystallization, due to dissociation as a result of the extreme lability induced. Choosing instead an X-type ligand (and therefore a divalent metal cation) permitted crystallization. However, in this case the resulting electron richness of the mercury complex rendered it unstable at room temperature. These data suggest that a strongly bound ligand which can additionally stabilize an electron rich metal centre would be suitable, such as a strongly σ-donating and π-acidic carbonyl or CAAC moiety.

Statement of Authorship for joint/multi-authored papers for PGR thesis

To appear at the end of each thesis chapter submitted as an article/paper

The statement shall describe the candidate's and co-authors' independent research contributions in the thesis publications. For each publication there should exist a complete statement that is to be filled out and signed by the candidate and supervisor **(only required where there isn't already a statement of contribution within the paper itself).**

Title of Paper	**Mercury-Group 13 Metal Covalent Bonds: A Systematic Comparison of Aluminyl, Gallyl and Indyl Metallo-ligands**
Publication Status	√Published □ Accepted for Publication □Submitted for Publication □Unpublished and unsubmitted work written in a manuscript style
Publication Details	Liam P. Griffin, Dr. Mathias A. Ellwanger, Agamemnon E. Crumpton, Dr. Matthew M. D. Roy, Dr. Andreas Heilmann, Prof. Simon Aldridge; Mercury-Group 13 Metal Covalent Bonds: A Systematic Comparison of Aluminyl, Gallyl and Indyl Metallo-ligands; *Angew. Chem. Int. Ed.*, 2024, 63, e202404527, doi.org/10.1002/anie.202404527

Student Confirmation

Student Name:	Liam P. Griffin		
Contribution to the Paper	Performed a high majority of the synthetic work. Performed spectroscopic analysis on all reported compounds. Performed quantum chemical calculations. Analysed and interpreted all data. Wrote the manuscript and prepared the supporting information.		
Signature	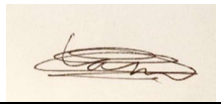	Date	19/09/2024

Supervisor Confirmation

By signing the Statement of Authorship, you are certifying that the candidate made a substantial contribution to the publication, and that the description described above is accurate.

Supervisor name and title: Professor Simon Aldridge		
Supervisor comments: I can confirm that Mr Griffin made a substantial contribution to the work described in this chapter, and that the above description is accurate.		
Signature 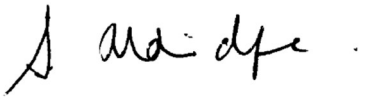	Date	20 September 2024

Probing trielyl ligand properties via the $Fe(CO)_4$ fragment

Introduction

With an increasing appreciation of how best to access metal-trielyl species to allow studies which inform on the trielyl ligand properties, we turned to a classic organometallic probe, *i.e.* the iron carbonyl fragment. This is a potentially highly informative avenue, given the possibility for structural, IR, Mossbauer, NMR and computational analyses of any species synthesised. Additionally, based on information obtained from chapter 4, the use of carbonyl co-ligands for a metal-aluminyl complex increases the likelihood of product stability, based on their strong σ-donor behaviour (which prevents dissociative decomposition routes), and their π-acidity, which relieves the iron centre of excess electron density. However, the use of these oxygen containing supporting ligands also presents challenges, especially in the case of the aluminyl congener, which typically behaves in a highly reductive and oxophilic manner, risking the possibility of unwanted modes of reactivity. Indeed, preliminary studies investigating the possibility of salt metathesis reactions with $Cp^*Fe(CO)_2I$ yielded only reduced products, and the $Fe(CO)_5$ chemistry reported herein was highly sensitive to the availability of the potassium counterion. Tuning reactivity by controlling this parameter ultimately allowed access to the target motifs $[Fe(CO)_4EX_2]^-$ (E = Al, Ga, In), which were much more readily accessed for the heavier congeners, and spectroscopic data could be obtained. This study therefore not only provided a wealth of data on the complexation of these ligands to $Fe(CO)_4$, but also serves as a methodological study for the installation of such ligands at more challenging redox active metal centres.

Synthesis and analysis of iron-trielyl complexes

Liam P. Griffin, Alexis K. Bauer, Agamemnon E. Crumpton, Mathias A. Ellwanger, Andreas Heilmann, Anja Weisner, Michael L. Neidig, Simon Aldridge*

[*] L. P. Griffin, A. K. Bauer, Dr. A. E. Crumpton, Dr. M. A. Ellwanger, A. E. Crumpton, Dr. A. Heilmann, Dr. A Weisner, Prof. S. Aldridge
Inorganic Chemistry Laboratory, Department of Chemistry,
University of Oxford
South Parks Road, Oxford, OX1 3QR (UK)
E-mail: simon.aldridge@chem.ox.ac.uk

Abstract

The reactivity of group 13 centred anions of the form $(NON)E^-$ (NON = 4,5-bis(2,6-diisopropylanilido)-2,7-di-*tert*-butyl-9,9-dimethylxanthene, E = Al, Ga, In) towards $Fe(CO)_5$ has been investigated. In the case of aluminium, the reaction outcome and product structure are highly sensitive to the availability of the potassium counterion, with sequestration by 18-crown-6 necessary to yield a species with a direct, unsupported Al–Fe bond. The use of cryptand or no sequestering agent leads to a specie with bridging carbonyl ligands, or isocarbonyl ligation of aluminium, respectively. Owing to their lower oxophilicity, the heavier congeners gallium and indium more straightforwardly deliver E–Fe bonded adducts, and the series is closely interrogated by structural and computational analysis, as well as IR and Mössbauer spectroscopy, all of which indicate a dramatic shift in bond polarity and electron richness at iron as the group is descended, consistent with established trends of diminishing donor strength of heavier trielyl ligands.

Introduction

The synthesis of metal complexes bearing the heavier group 13 analogues of boryl ligands (i.e. EX_2^-, where E = Al – Tl) has been an significant target for synthetic chemists in recent years.[1-4] Metal boryl complexes have shown great utility in the C–H functionalization/borylation of unactivated alkane and arene substrates, in part due to the combination of strong sigma donor capabilities and (albeit modest) Lewis acidic properties of the boryl moiety.[5] The synthesis of heavier trielyl complexes not only offers fundamental insight into these metallo-ligands in comparison with their boron analogues but also promises new small molecule transformations enabled across the metal-metal bonds of transition metal-triel bimetallics.

In the case of aluminium, its low electronegativity and high oxophilicity, partnered with the strongly reducing nature of Al(I) suggest that metal complexes featuring the aluminyl ligand might possess unusual electronic properties (and reactivity profiles) as a result of the close proximity of highly electron rich and electron deficient metal centres.[6] This scenario is amply demonstrated by the gold aluminyl complex $^tBu_3PAuAl(NON)$ through the formation of Au–C and Al–O bonds, in a process involving the gold centre formally acting as a nucleophile.[7] Given that trielyl ligands are now available for all of the group 13 metals (E = Al – Tl), a fundamental understanding of electronic structure as a function of E offers a mechanism through which to tune such reactivity.[8-11]

Early examples of complexes bearing aluminyl ligands were either synthesised by reduction or Al–X oxidative addition at heterobimetallic species bearing bridging ligands to generate supported M–Al bonds or, for transition metals for which suitably nucleophilic precursors exist (typically containing π-acceptor ancillary ligands, such as carbonyls), via salt metathesis at an electrophilic Al(III) halide. By far the most common example of this approach involves the use of the $[CpFe(CO)_2]^-$ anion, due to its relative ease of synthesis and handling.[12-14] Approaches that make use of low valent aluminium precursors have also been known for several years, with the oxidative addition of M–X

bonds at charge neutral Al(I) centre such as ($Nacnac^{Dipp}$)Al ($Nacnac^{Dipp}$ = $HC(MeCDippN)_2$; Dipp = 2,6-$C_6H_3{}^iPr_2$) yielding metal aluminyl species for metals such as beryllium and copper. [15, 16]

Since the first report of a potassium aluminyl species in 2018, the range of accessible metal aluminyl complexes has increased greatly; isolable nucleophilic precursors of the type $[AlX_2]^-$ can (in theory) be combined with a wide range of metal electrophiles, and this approach has been used to synthesise complexes featuring metals from groups 1, 2, 3, 5, 10, 11 and 12 (as well as the rare earth metal samarium).[8, 17-28] Unsurprisingly, aluminyl species were the last of the group 13 element trieyl derivatives for which a simple alkali metal salt could be accessed, owing to the same elemental properties which make their application as ligands so interesting. In our laboratory, having access to a common series of aluminyl, gallyl and indyl metalloligands, we have been interested in probing trends in the properties of these systems for a common supporting scaffold at the group 13 metal. As part of these studies, we turned to the iron carbonyl fragment $[Fe(CO)_4]$, as a classic organometallic probe-group, to deliver data on the properties of these metalloligands through IR and Mossbauer spectroscopies, X-ray crystallography and quantum chemical calculations. These studies are reported here.

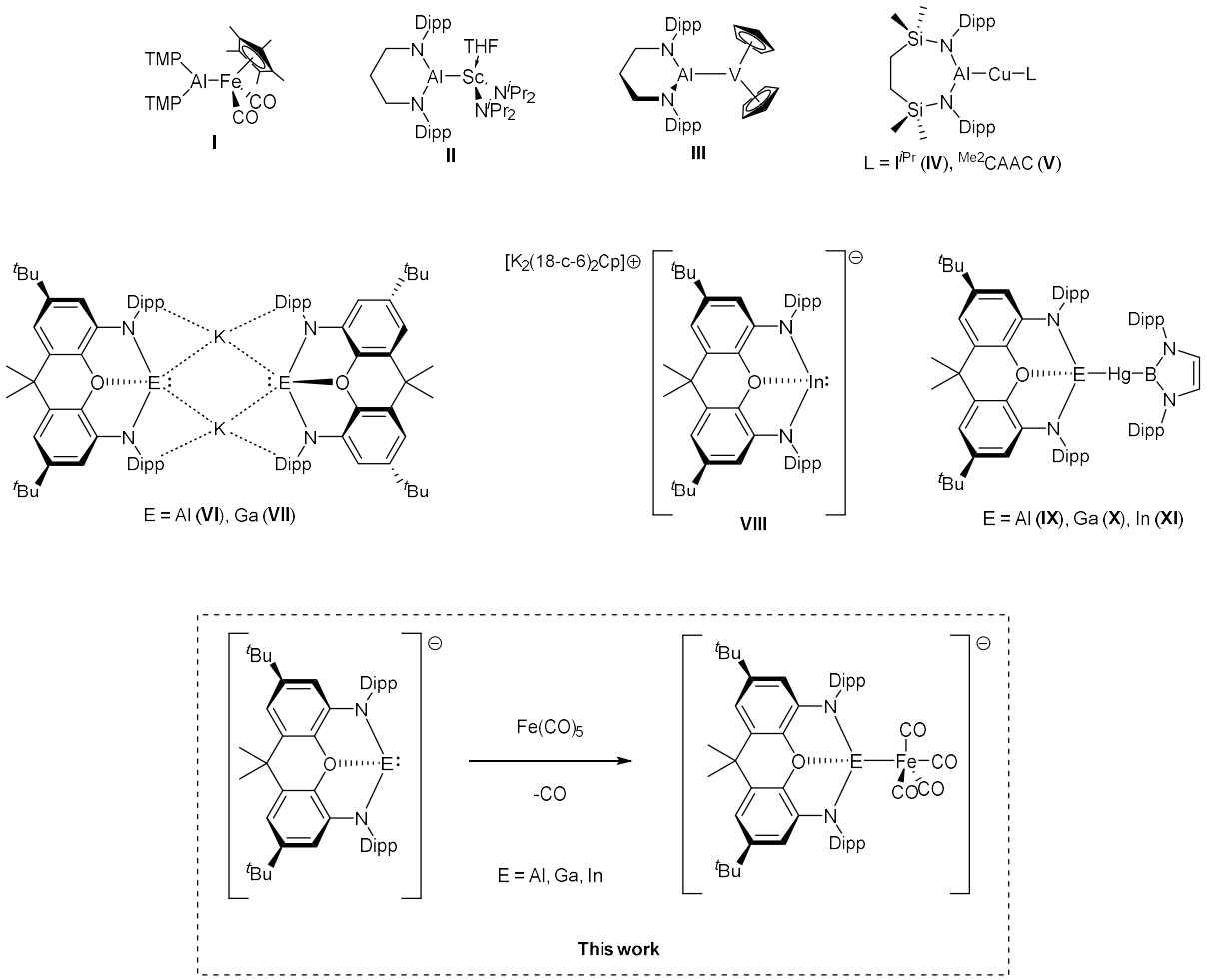

*Figure 8: (upper row) Iron aluminyl species **1** synthesised by salt metathesis between a nucleophilic iron precursor and an aluminium electrophile and 3d metal aluminyl species **II, III, IV,** and **V** synthesised via nucleophilic aluminium. (middle row) Sources of the series of aluminium, gallium and indium (I) anions stabilized by a common xanthene ligand framework, and an isostructural series of mercury(boryl) trielyl complexes generated via these reagents. (bottom row) This work, accessing an essentially isostructural series of iron carbonyl complexes of trielyl ligands.*

Results and discussion

Syntheses and structures of aluminyl complexes of iron

Seeking to access the target complexes directly, the reactions between sources of $[(NON)E]^-$ (E = Al, Ga, In) and $Fe(CO)_5$ were targeted, via substitution of a single CO ligand. Reaction between $Fe(CO)_5$ and $K_2[(NON)Al]_2$ in toluene occurs immediately, yielding a dark solution, from which colourless crystals suitable for X-ray diffraction could be grown by slow evaporation. Crystallographic studies reveal that, rather proceeding via Fe–Al bond formation, a dimeric species is generated in which two $[Fe(CO)_4]$ units are linked by a pair of [(NON)Al] fragments via isocarbonyl-type ligation at the aluminium centres (Figure 2). The resulting structure features a 12-membered metallo-macrocyclic structure. This dianionic ring is capped above each face by a potassium cation, which is coordinated by the π-systems of both the NON arene groups and the bridging isocarbonyl ligands. This species can also be viewed as a dimeric analogue of Collman's reagent, $K_2Fe(CO)_4$, in which one of the potassium cations per iron has been exchanged for a $[(NON)Al^{III}]^+$ cation.[29] Related heterobimetallic isocarbonyl species are known for aluminium, as well as gallium and the oxophilic lanthanide elements.[30]

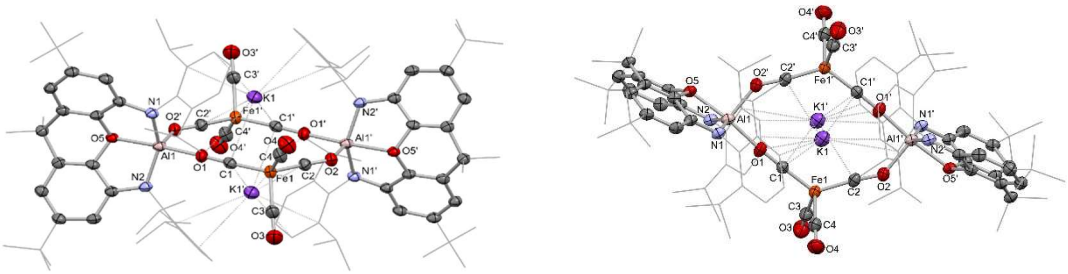

Figure 2. Molecular structure of 1, as determined by single crystal X-ray diffraction. Hydrogen atoms and co-crystallised solvent omitted, and some residues displayed in wireframe format for clarity. Key bond lengths (Å) and bond angles (°): Al1–O1 1.855(2), Al1–O5 1.984(2), Al1–N1 1.878(2), Al1–N2 1.872(2), Al1–O2' 1.830(2), Fe1–C1 1.711(3), Fe1–C2 1.705(3), Fe1–C3 1.799(3), Fe1–C4 1.784(3), C1–O1 1.211(3), C2–O2 1.227(3), C3–O3 1.149(4), C4–O4 1.157(4), K1–O1 3.350(2), K1–C1 3.140(3), K1–C1' 3.215(3), K1–C2' 3.357(3), O1–Al1–O5 173.39(9), O1–Al1–O2' 94.12(9), O5–Al1–O2' 92.49(9), N1–Al1–N2 140.2(1), N1–Al1–O2' 107.6(1), N2–Al1–O2' 109.0(1), C1–Fe1–C2 126.0(1), C3–Fe1–C4 98.3(1), angle of intersection of the least squares planes corresponding to the two xanthene C6 rings 136.58.

The crystallographically equivalent aluminium centres adopt a significantly distorted trigonal bipyramidal (TBP) geometry (τ_5 = 0.55), in which one isocarbonyl O atom and the xanthene O atom are aligned approximately linearly (173.39(9)°), but feature disparate Al–O distances (1.855(2) and 1.984(2) Å, respectively). Distortion from an idealised TBP geometry reflects the wider angle defined by the N-donors (N–Al–N 140.2(1)°) which also lie marginally out of the equatorial plane, as a result of the constraints of the chelating xanthene framework. The iron centres each adopt a distorted tetrahedral geometry (τ_4 = 0.89), with a wider angle between the two isocarbonyl ligands (C–Fe–C 126.0(1)°), and a narrower angle between the two conventional carbonyl ligands (C–Fe–C 98.3(1) °). A significant extension of the C–O bond is seen for the bridging isocarbonyl ligands as compared to the 'conventional' terminal CO ligands (isocarbonyl 1.211(3) and 1.227(3) Å cf. 1.149(4) and 1.157(4) Å).

The description of this species as a Collman's reagent analogue is supported by computational analysis. Bader (QT-AIM) charge analysis assigns a charge of -1.78 e to the $[Fe(CO)_4]$ fragment, +0.88 e to the K atoms, and +0.90 e to the (NON)Al unit. The aluminium atom itself is assigned a charge of +2.55 e, and this highly polarising cation is presumably responsible from the non-uniform distribution of negative charge in the anionic iron carbonyl unit. This polarisation can be seen in the individual CO charge contributions, which become more negative from the terminal carbonyls (-0.30 and -0.28 e) to the bridging isocarbonyls (-0.89 and -0.89 e).

A Mössbauer spectrum collected on a solid state sample of **1** supports the DFT based on the negative shift δ = -0.23 mm/s and quadrupole splitting $|\Delta E_Q|$ = 0.33 mm/s, consistent with a reduced iron species.[31] The minor impurity of the spectra characterized as δ = 0.39 mm/s and $|\Delta E_Q|$ = 0.80 mm/s resembles the reported parameters for $Fe_3(CO)_{12}$ (δ = 0.30 mm/s and $|\Delta E_Q|$ = 0.98 mm/s).[32]

Infrared measurements yield CO stretching frequencies of 1906 and 1970 cm^{-1}, which align closely with the stretching frequency of Collman's reagent (1972 cm^{-1}).

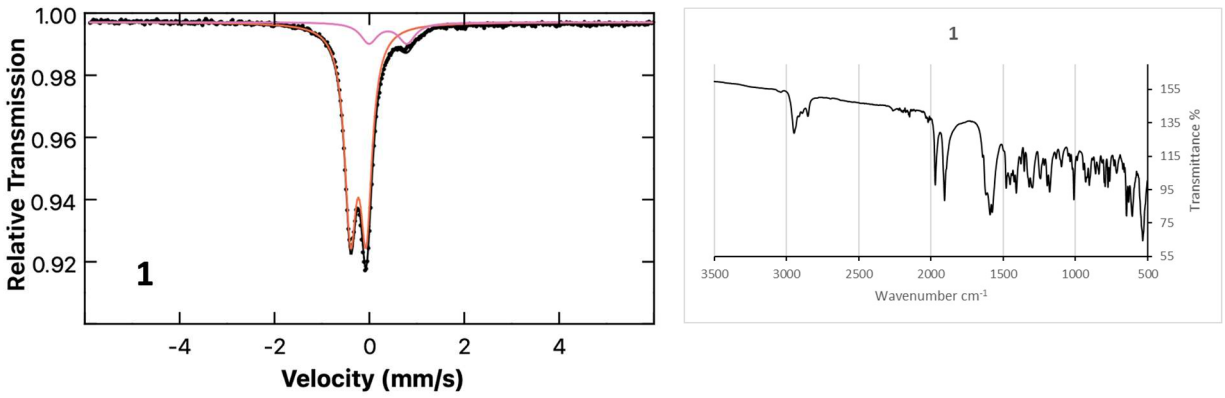

Figure 3. (left) Zero field 80 K 57Fe Mössbauer spectrum of 1 (orange, 87%): δ = -0.23 mm/s, |ΔEQ| = 0.3 mm/s 3; (pink, 13%): δ = 0.39 mm/s, |ΔEQ| = 0.80 mm/s and (right) IR spectrum of 1.

At a broader level, the solid-state structure of **1** raises the question of whether the capping potassium ions are significant in stabilizing this product, and if sequestration before addition of $Fe(CO)_5$ might influence the outcome of the reaction. Literature precedent for this type of reactivity tuning based on the identity/availability of the alkali metal counterion is well established, but has yet to be investigated in the context of bimetallic compounds.[17, 33, 34] With this in mind, the reaction between the [K(2.2.2-crypt][(NON)Al] and $Fe(CO)_5$ was investigated. Here too, reaction occurs instantaneously and yields a dark solution, from which a small quantity of single crystals suitable for diffraction experiments could be obtained.

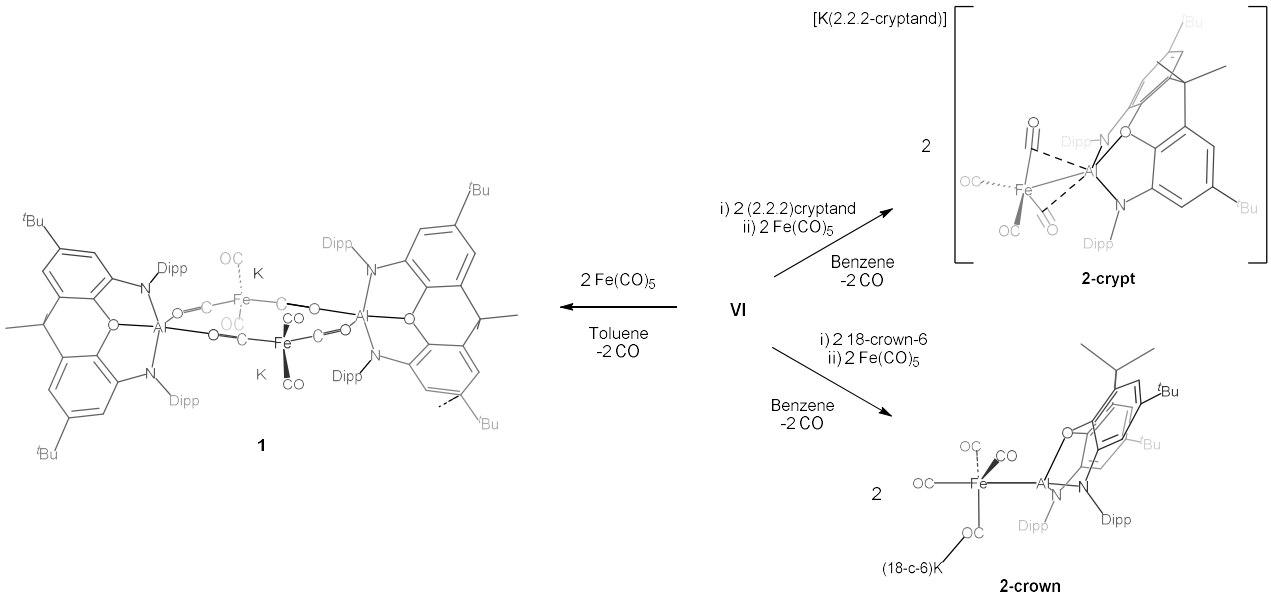

*Scheme 1; Reactivity of **VI** with $Fe(CO)_5$ in the presence of absence of potassium sequestering agents.*

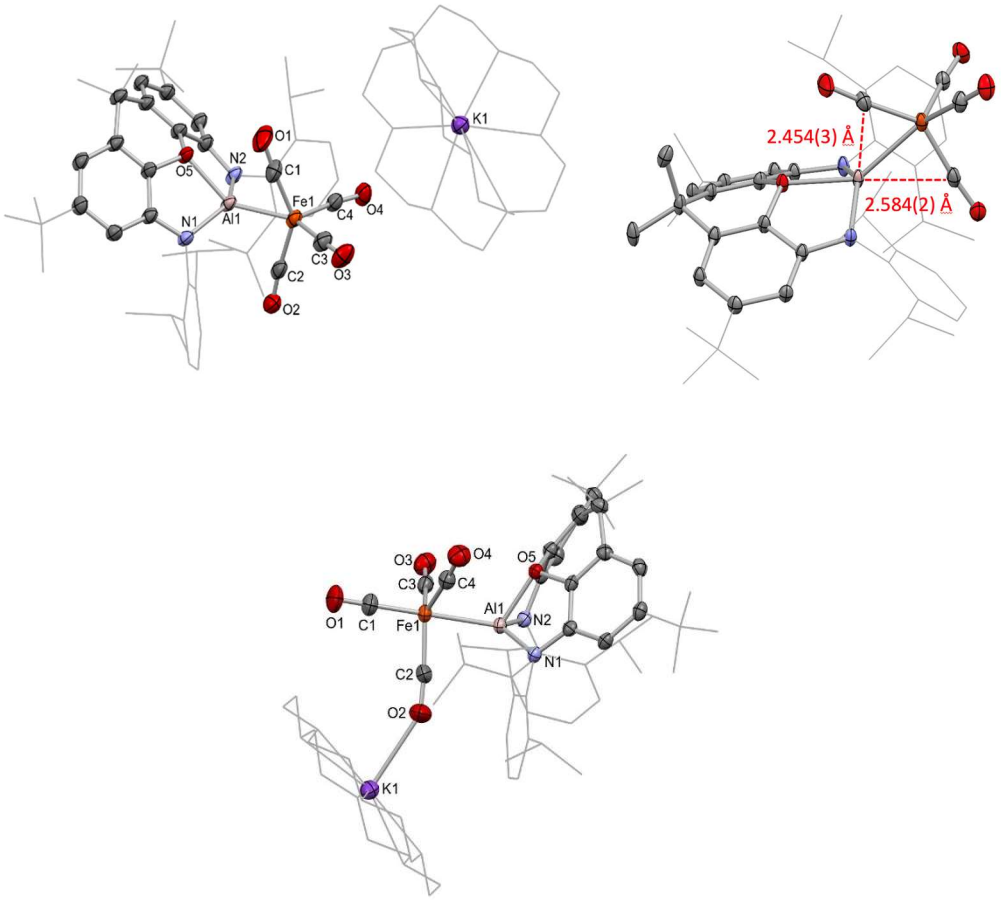

Figure 4. Molecular structures of 2-crypt (upper left and right) and 2-crown (lower), as determined by single crystal X-ray diffraction. Hydrogen atoms and co-crystallised solvent omitted, and some residues displayed in wireframe format for clarity. Key bond lengths (Å) and bond angles (°): (for 2-crypt) Al1–Fe1 2.3938(7), Al1–O5 2.029(1), Al1–N1 1.920(2), Al1–N2 1.901(2), Al1–C1 2.454(3), Al1–C2 2.584(2), Fe1–C1 1.754(2), Fe1–C2 1.764(3), Fe1–C3 1.769(2), Fe1–C4 1.777(2), C1–O1 1.174(3), C2–O2 1.168(3), C3–O3 1.159(5), C4–O4 1.154(3), Al1–Fe1–C1 70.63(9), Al1–Fe1–C2 75.15(8), Al1–Fe1–C3 147.30(8), Al1–Fe1–C4 113.69(7), C1–Fe1–C2 141.2(1), C3–Fe1–C4 99.0(1), angle of intersection of the least squares planes corresponding to the two xanthene C6 rings 130.46. (for 2-crown) Al1–Fe1 2.374(1), Al1–O5 1.973(2), Al1–N1 1.888(3), Al1–N2 1.904(3), Fe1–C1 1.778(4), Fe1–C2 1.759(4), Fe1–C3 1.781(4), Fe1–C4 1.767(4), C1–O1 1.146(6), C2–O2 1.160(5), C3–O3 1.152(5), C4–O4 1.151(5), O2–K1 2.731(4), Al1–Fe1–C1 174.2(1), Al1–Fe1–C2 82.8(2), C1–Fe1–C2 96.8(2), C2–Fe1–C3 121.3(2), C2–Fe1–C4 121.5(2), C3–Fe1–C4 112.2(2), angle of intersection of the least squares planes corresponding to the two xanthene C6 rings 122.45.

Crystallographic analysis reveals that sequestration of the potassium cation by the cryptand does indeed change the course of the reaction, yielding a metal-metal bonded species in this case (albeit in low yield). The monoanionic fragment $[(NON)AlFe(CO)_4]^-$ (Figure 4) features an Fe–Al bond length (2.3938(7) Å) that is well within the sum of the respective covalent radii of (2.53 Å).[35, 36] The geometry at the iron centre, however, is significantly distorted from the TBP expected for an $Fe(CO)_4X$ system, most obviously in the position of two CO ligands (C1O1 and C2O2). These are aligned such

that the carbon atoms sit close to the axial and equatorial sites within the *TBP coordination sphere of Al(1)* commonly seen for $[(NON)AlX_2]^-$ systems (*d*(Al1–C1) = 2.454(3) Å; *d*(Al1–C2) 2.584(2) Å). This distortion presumably results from the highly polarizing nature of the aluminium centre, which has offloaded a significant portion of its electron density to the iron carbonyl fragment (*vide infra*), as well as the lack of an available potassium counterion to provide partial charge neutralization through isocarbonyl coordination. Returning to the coordination at iron, the geometry defined by the carbonyl ligands alone is reasonably close to tetrahedral (τ_4 = 0.78), with one expanded angle (C1–Fe1–C2 141.2(1)°) and one contracted angle (C3–Fe1–C4 99.0(1)°), indicating that, here too, an overall reduction to a Collman's reagent like species has taken place, at least insofar as formal oxidation states are concerned. In this formalism, the $[(NON)Al]^+$ moiety acts as a Z-type ligand at a dianionic iron fragment, being bound through Fe→Al and C→Al donor/acceptor interactions. A Bader charge analysis support this description, returning charges of -1.62 e for the $Fe(CO)_4$ unit, and +0.62 e for the (NON)Al fragment. The Al centre is again highly polarizing, with the proximal CO ligands bearing significantly more negative charge (-0.62 and -0.51 e) compared to the remote carbonyls (-0.32 and -0.31 e).

DFT calculations for the free $[(NON)AlFe(CO)_4]^-$ anion return an optimised geometry which matches the crystallographic data well (see ESI). The HOMO of this species is an iron centred lone pair, which is significantly delocalised into the (π-acceptor) carbonyl manifold; the LUMO is xanthene ligand based. A significant Al–Fe σ-bonding contribution is seen in the HOMO-1, with clear involvement of the CO π* manifold of a proximal CO ligand. Further interactions between the aluminium centre and the occupied π* orbitals of the other carbonyl ligands (including one of the more distal carbonyls) are seen in the HOMO-5 and HOMO-6 (Figure 5). A Quantum Theory of Atoms In Molecules (QTAIM) topological analysis of $[(NON)AlFe(CO)_4]^-$ returns a Bond Critical Point (BCP) between iron and aluminium, with associated parameters that indicate metallic-type bonding. No bond paths are detected between aluminium and the two nearest carbonyl ligands, despite Wiberg Bond Indices (WBIs) for these atom pairs being of similar magnitude to that of the Fe–Al bond (Fe–Al 0.34; Al–C1

0.37; Al–C2 0.33). However, inspection of the Non-Covalent Interactions (NCI) plot for this species locates these interactions, with significant attractive density between these carbon atoms and the aluminium centre (Figure 5).

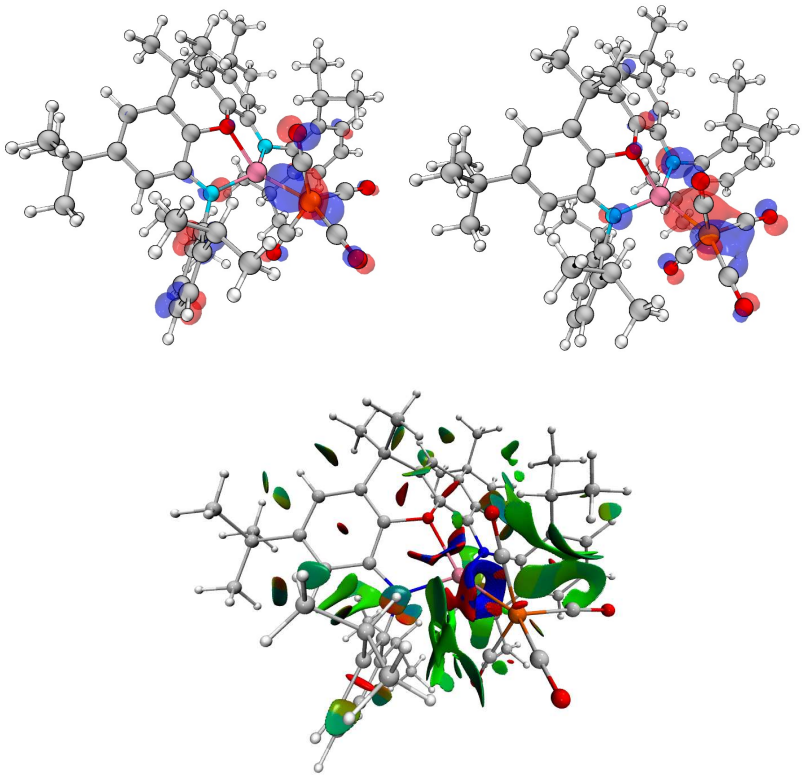

Figure 5. HOMO-1 (upper left) and HOMO-6 (upper right) of 2-crypt, showing the Al–Fe bonding interaction as well as involvement of CO π density. (lower) NCI plot of 2-crypt, showing strong attractive regions (blue) between the aluminium centre and the proximal carbonyl carbon atoms C1 and C2.*

With a view to accessing an Fe–Al bonded species in higher yield, and to further explore the effects of counterion availability, the corresponding reaction utilising 18-crown-6 was attempted (Scheme 1). The reaction is again very rapid and yields a substantial crop of colourless rod-shaped crystals suitable for X-ray diffraction. The crystal structure of this species, **2-crown**, again features a direct Fe–Al bond, but this time within a more conventional TBP iron coordination sphere (τ_5 = 0.88), with the strongly σ-donating aluminyl ligand occupying the expected axial position (Figure 4). The angle between the two axial ligands at iron (∠Al1–Fe1–C1 174.2(1)°) is approximately linear, and the equatorial ligands sit relatively close to the ideal plane (∠Al1–Fe1–C2 82.8(2)°; ∠C1–Fe1–C2 96.8(2)°;

sum of angles in the equatorial plane 355.0°). The more open nature of the crown ether ligand (cf. 2.2.2-cryptand) allows access to the potassium cation by the oxygen atom of an equatorial CO ligand (in the solid state at least). This cation effect is structurally significant, insofar as it appears to prevent the secondary carbonyl-aluminium interactions seen in 'naked' $[(NON)AlFe(CO)_4]^-$ (i.e. in **2-crypt**) presumably by polarizing electron density in the iron carbonyl manifold. In the absence of these weak C→Al donor/acceptor interactions, increased bending of the NON xanthene framework in observed (angle between the two xanthene aromatic rings 122.5°, cf. 130.5° for **2-crypt**), thereby allowing closer proximity of the xanthene O-donor to Al1 (1.973(2) Å, cf. 2.029(1) Å for **2-crypt**) to quench its higher Lewis acidity.

Quantum chemical analysis of **2-crown** indicates that the major Fe–Al bonding orbital is the HOMO-4; a WBI of 0.33 is calculated for the metal-metal bond, *i.e.* similar to that for **2-crypt** (0.34), but no significant values are generated involving aluminium and any of the equatorial carbonyl ligand atoms. A Bader charge analysis reveal no significant differences in the charge distributions of the $Fe(CO)_4$ (-1.62 e), (NON)Al (+0.68 e) or potassium-containing fragments (0.94 e) as compared to **2-crypt**, although the iron centre itself possesses a lower partial positive charge (+0.09 e compared to +0.16 e), potentially due to the closer approach of the strongly sigma donating aluminyl ligand (crystallographically: 2.374(1) vs. 2.3938(7) Å) .

2-crypt and **2-crown** represent the first examples of complexes featuring an aluminyl ligand bound to a binary iron carbonyl, with previously reported iron aluminyl systems relying on the availability of the nucleophilic iron centred anion $CpFe(CO)_2^-$. The possibility of filling this available chemical space through tuning of the aluminyl reactivity by counterion sequestration opens up a wide range of other potential transition metal substrates to which aluminyl ligands could be bound, with diverse onward chemistry. Such investigations are currently underway in our laboratory. However, preliminary experiments with the binary carbonyl $Ni(CO)_4$, for example, yield only the reduced nickel carbonyl cluster $[K(2.2.2\text{-cryptand})]_2[Ni_8(CO)_{18}]$ (see ESI), indicating that this approach may not

necessarily be readily generalizable to other 3d metal carbonyl species, given the very strongly reducing nature of the NON-supported aluminyl ligand. In similar fashion, **2-crown** is found to be unstable in solution, with prolonged storage of a THF solution yielding red single crystals of the potassium-crown salt of known iron motif $[K(18\text{-crown-}6]_2[Fe_2(CO)_8]$, i.e. the formal product of the reductive coupling of two $[Fe(CO)_4]$ units; the fate of the aluminium-containing component in this reaction is unclear.

Syntheses and structures of gallyl and indyl complexes of iron

With a convenient route to Fe–Al bonds in hand, we sought to extend these studies down group 13, in order to identify trends in the properties of the metallo-ligands $[(NON)E]^-$ as a function of E (E = Al, Ga, In). In contrast to the aluminium case, reaction of the potassium gallyl species $K_2[(NON)Ga]_2$ with $Fe(CO)_5$ in the absence of any potassium sequestration agent directly yields the Fe–Ga bonded species **3**. The solid-state structure of **3** determined crystallographically (Figure 6) reveals an Fe–Ga bond length (2.375(1) Å) which is very similar to the Fe–Al separation in **2-crown** (2.374(1) Å), albeit as part of a coordination-polymeric structure that brings about significant distortion of the coordination geometry at iron (∠Ga1–Fe1–C4 = 160.3(1)°; ∠Ga1–Fe1–C3 = 102.1(1)°; ∠Ga1–Fe1–C2 = 78.1(1)°). Potassium ions bridge adjacent $[(NON)GaFe(CO)_4]^-$ units via the Dipp group and O1 of one unit, and O3 and the other Dipp group of the second, and additionally show short contacts to a single bound molecule of benzene. The shortest Ga–C distance (Ga1–C2) however, is 2.657(3) Å, suggesting that carbonyl ligand interactions with the group 13 metal centre are not significant in this species, likely due to the lower Lewis acidity at gallium. Together with the lower magnitude of the reduction potential of gallium (and its reduced oxophilicity compared to aluminium) this likely underpins why no gallium isocarbonyl species (akin to **1**) is observed.[6]

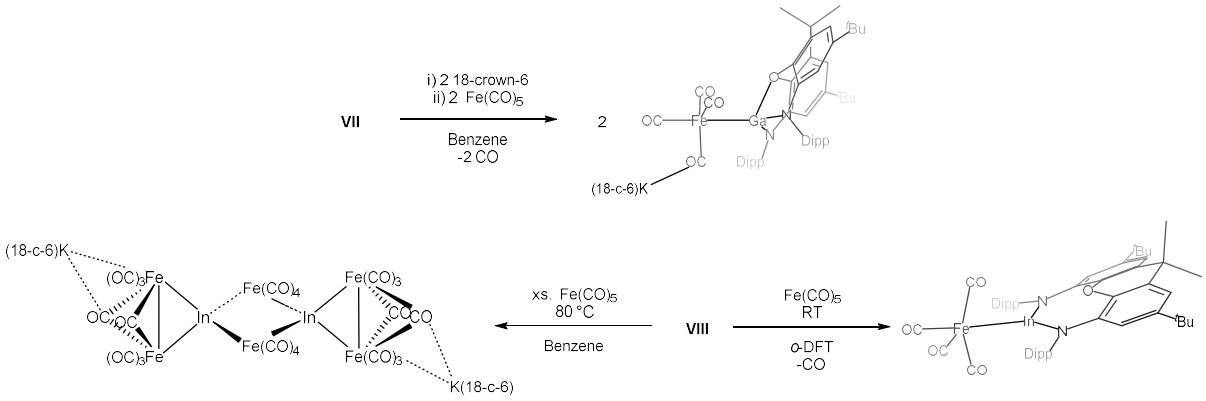

*Scheme 2: Synthesis of **3-crown**, **4** and **5**.*

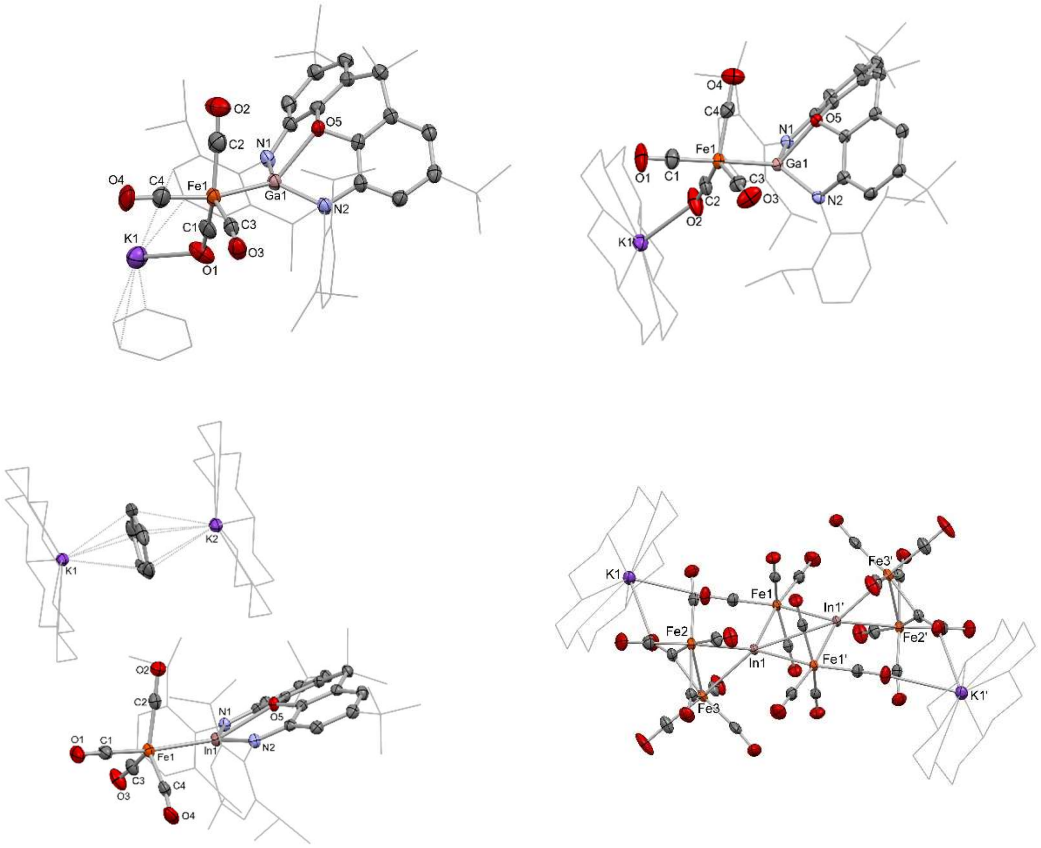

Figure 6. Molecular structures of 3 (upper left), 3-crown (upper right), 4 (lower left) and 5 (lower right), as determined by single crystal X-ray diffraction. Hydrogen atoms and co-crystallised solvent omitted, and some residues displayed in wireframe format for clarity. Key bond lengths (Å) and bond angles (°): (for 3) Ga –Fe1 2.376(1), Ga1–O5 2.244(2), Ga1–N1 1.979(2), Ga1–N2 1.947(2), Fe1–C1 1.732(4), Fe1–C2 1.779(4), Fe1–C3 1.770(4), Fe1–C4 1.767(4), C1 –O1 1.188(4), C2–O2 1.158(5), C3–O3 1.162(5), C4–O4 1.159(5), K1–O1 2.653(3), K1–O3 2.674(2), Ga –Fe1–C1 79.8(1), Ga1–Fe1–C2 78.1(1), Ga1–Fe1–C3 102.1(1), Ga –Fe1–C4 140.3(1), C1–Fe1–C2 134.3(2), C1–Fe1–C3 108.8(2), C2–Fe1–C3 114.7(2), C2–Fe1–C4 92.5(2), angle of intersection of the least squares planes corresponding to the two xanthene C6 rings 124.45. (for 3-crown): Ga1–Fe1 2.3518(7), Ga1–O5 2.125(2), Ga1–N1 1.951(3), Ga1–N2 1.970(3), Fe1–C1 1.763(4), Fe1–C2 1.751(4), Fe1–C3 1.778(3), Fe1–C4 1.773(4), C1–O1 1.163(5), C2–O2 1.172(5), C3–O3 1.149(5), C4–O4 1.159(5), K1–O2 2.677(3), Ga1–Fe1–C1 173.8(1), Ga1–Fe1–C2 81.1(1), C1–Fe1–C2 93.1(2), C2–Fe1–C3 124.5(2), C2–Fe1–C4 122.5(2), C3–Fe1–C4 110.2(2), angle of intersection of the least squares planes corresponding to the two xanthene C6 rings 125.98. (for 4) (°): In1–Fe1 2.5232(5), In1–O5 2.438(1), In1–N1 2.186(2), In1–N2 2.200(2), Fe1–C1 1.762(2), Fe1–C2 1.775(2), Fe1–C3 1.789(2), Fe1–C4 1.780(2), C1–O1 1.157(3), C2–O2 1.167(3), C3–O3 1.151(3), C4–O4 1.157(3), In1–Fe1–C1 165.51(8), In1–Fe1–C2 75.91(7), C1–Fe1–C2 95.6(1), C2–Fe1–C3 117.6(1), C2–Fe1–C4 131.3(1), C3–Fe1–C4 109.6(1), angle of intersection of the least squares planes corresponding to the two xanthene C6 rings 160.17.

Addition of 18-crown-6 to a solution of $K_2[(NON)Ga]_2$ prior to the addition of $Fe(CO)_5$ leads to the formation of **3-crown**, a Fe–Ga bonded species essentially isostructural with its aluminium congener (Figure 6). A similar TBP structure (τ_5 = 0.82, ∠Ga1–Fe1–C1 = 171.4(1)°; ∠Ga1–Fe1–C2 = 81.1(1)°; ∠C1–Fe1–C2 = 93.1(2)°; sum of angles in equatorial plane, 357.2°) features a Fe–Ga bond of

2.3513(7) Å, which is both well within the sum of covalent radii (2.54 Å) and shorter than the Fe–Al bond in **2-crown** (2.374(1) Å). The xanthene backbone is more planar than for **2-crown**, allowing for a longer Ga–O bond (2.125(2) vs 1.973(2) Å), consistent with the more weakly Lewis acidic nature of the gallium metal centre.

DFT calculations (on the full contact ion pair) show that the HOMO-4 is again the dominant metal-metal bonding contribution, and the Fe–Ga bond returns a WBI of 0.44, i.e. larger than in either of the aluminium cases (0.33 and 0.34 for **2-crown** and **2-crypt**, respectively). A Bader charge analysis allocates significantly less negative charge to the $Fe(CO)_4$ moiety as compared with the aluminium congener **3-crown** (-0.99 vs. -1.62 e), and the (NON)Ga fragment is significantly less oxidised with an overall charge of +0.003 e. These parameters are consistent with the idea that the gallyl metallo-ligand donates significantly less electron density into the iron carbonyl manifold. This decreased extent of electron release is also borne out by the spectroscopic data (see below).

Moving finally to indyl-ligated systems, it was found necessary to use the crown-sequestered separated-ion-pair form of the potassium indyl precursor, i.e. $[K_2(18\text{-crown-}6)_2Cp][In(NON)]$, for reasons of solubility.[25] The Fe–In bonded product $[K_2(18\text{-crown-}6)_2Cp][(NON)InFe(CO)_4]$ (**4**) is formed in high yield when the reaction with $Fe(CO)_5$ is carried out at room temperature in *ortho*-difluorobenzene. However, when the reaction is instead carried out in benzene, significant heating is required, which results in onward reaction with additional equivalents of $Fe(CO)_5$ and subsequent isolation of large red crystals of the mixed-metal carbonyl cluster **5** $[K(18\text{-crown-}6)]_2[(CO)_4FeInFe_2(CO)_8]_2$. The fate of the NON ligand and the cation-bound Cp are unknown.

Despite bearing no carbonyl-potassium contacts due to their encapsulation within the $[K_2(18\text{-crown-}6)_2Cp]^+$ cation, the indium-iron fragment is otherwise isostructural with **2-crown** and **3-crown**, featuring an approximately TBP geometry at iron (τ_5 = 0.57) with the group 13 metallo-ligand binding in the axial position and no In–C close contacts present (∠In1–Fe1–C1 = 165.51(8)°; ∠In1–Fe1–C2 = 75.91(7)°; ∠C1–Fe1–C2 95.6(1)°; sum of angles in the equatorial plane, 358.8°). The metal-metal

linkage is again found to be well within the sum of the respective covalent radii (*d*(In–Fe) = 2.5232(5) Å, cf. 2.74 Å). Moreover, the larger (and more weakly Lewis acidic) indium centre leads to a significantly more planar xanthene backbone than for the lighter congeners, with the angle between the two xanthene aromatic rings being 160.2°.

In line with **2-crown** and **3-crown**, the major Fe–In bonding orbital is again the HOMO-4, and the WBI (0.47) is higher than for either the aluminium (0.33) or gallium congeners (0.44). Analysis of the Bader charges defines a trend down group 13, with a less electron rich [$Fe(CO)_4$] manifold (-0.84 e) and a more electron rich (NON)In metallo-ligand (-0.16 e). Consistent with a diminished donor strength down the group, it seems that overall, the bonding is becoming less negatively polarised towards iron, despite the maximum in electronegativity at gallium.[37] In order to probe these trends more fully, further computational analysis was undertaken by QT-AIM methods. First, QTAIM analysis was carried out on all three trigonal-bipyramidal adducts. All three species feature a BCP between the two metals, with associated parameters which indicate metallic bonding in each case (low ρ, positive $\nabla^2\rho$) with very small differences between the three species.[38] However, the greater electron density at the BCP in the gallium case does indicate greater covalency in this species, consistent with results previously reported for an isostructural series of compounds bearing E–Hg bonds (E = Al, Ga, In). Full table of parameters and contour plots available in the ESI.

	2-crown	**3-crown**	**4**
ρ	0.057864	0.067969	0.057687
$\nabla^2\rho$	0.015386	0.020251	0.062144

Table 1: Key QTAIM parameters for E-Fe BCPs

Infrared and Mossbauer spectroscopic probes of [Fe(CO)$_4$] trielyl complexes

With examples of NON-supported trielyl complexes of the type [(NON)EFe(CO)$_4$]$^-$ in hand, we wished to interrogate their electronic structures spectroscopically, making use of two convenient probes available to the [Fe(CO)$_4$] fragment, namely IR and Mössbauer spectroscopies. The infrared spectra of **2-crown**, **3-crown** and **4** (Figure 7) each feature four bands in the carbonyl region, with one (the A_1 mode) well separated from the other three. These show the now established trend (**2-crown**, 1967 cm^{-1}; **3-crown**, 1979 cm^{-1}; **4**, 1981 cm^{-1}), being found at higher energy/wavenumber for E = Ga and In (vs. Al), as a result of reduced back-bonding from a less electron rich iron centre. This in turn reflects the more weakly σ-donating nature of the gallyl and indyl ligands compared to their aluminyl counterpart.[25] The difference in the position of the A_1 band is significantly smaller between the gallyl and indyl complexes (compared to aluminyl/gallyl), which aligns with the more similar (and less polarized towards iron) charge distributions for these two complexes. This finding in turn is also consistent with the lower electronegativity differences between these elements (χ = 1.61 (Al), 1.81 (Ga), 1.78 (In)).

Comparison to other iron carbonyl complexes of comparable geometry is also possible. By this measure, all three complexes studied here yield an A_1 mode at lower energy thank that of the isoelectronic carbene complex I^{iPr}Fe(CO)$_4$ (2036 cm^{-1}),[39] as well as the neutral aluminylene complexes Cp*AlFe(CO)$_4$ [40] (2024 cm^{-1}) and (Nacnac^{Dipp})AlFe(CO)$_4$ [41] (2007 cm^{-1}), presumably due to the anionic nature of these trielyl systems. Looking to other anionic systems, the isostructural complex of a diazabutadiene supported gallyl anion is also known, with an A_1 stretching mode at 1988 cm^{-1}.[42] This indicates that the NON ligand framework yields a more strongly σ-donating gallyl metalloligand than the DAB framework, consistent with the results of previous studies. Indeed, here we see that even the NON-supported indyl anion outperforms the DAB-supported gallyl in terms of donor strength by this metric.

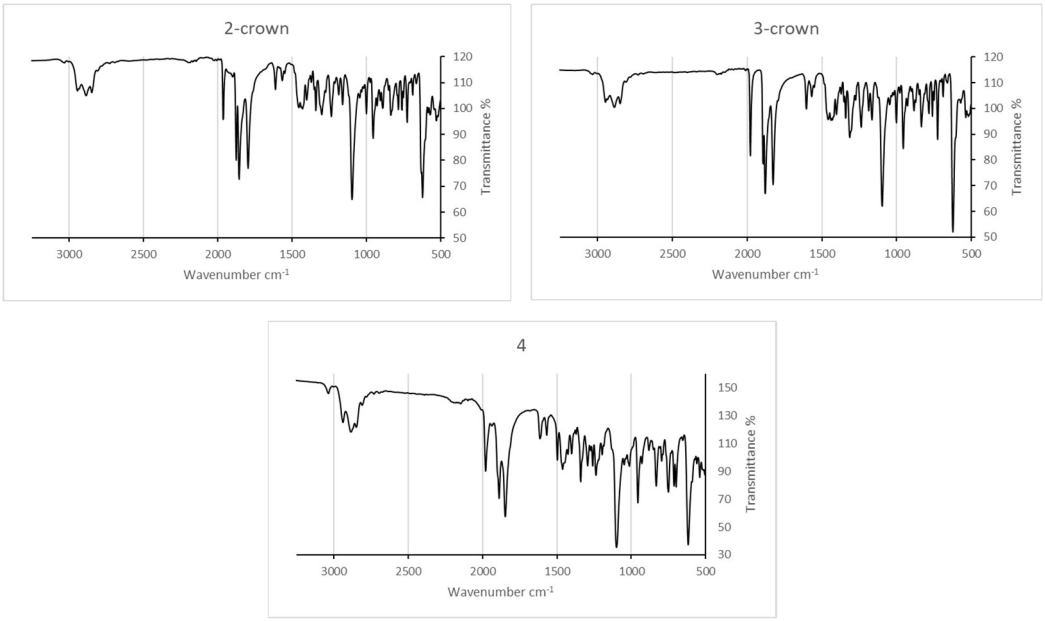

Figure 7: IR spectra for 2-crown (upper left), 3-crown (upper right) and 4 (lower).

For further analysis, solid state 80 K Mössbauer spectra was recorded for each of the three complexes (Figure 8). In the Mössbauer spectrum of **2-crown**, the major species was identified as a doublet with parameters of δ = -0.24 mm/s and $|\Delta E_Q|$ = 2.08 mm/s with a minor component (red, δ = 0.50 mm/s, $|\Delta E_Q|$ = 0.61 mm/s). The minor impurity can be identified as an oxidised iron-carbonyl cluster based on the similarity of the parameters to those reported for $Fe(CO)_4I_2$ (possibly resembling the cluster complex **5**.[43] The major component of the Mössbauer spectrum of **3-crown** was characterized with doublet parameters of δ = -0.13 mm/s and $|\Delta E_Q|$ = 1.53 mm/s. The parameters of **3-crown** resemble those of **2-crown** with a slightly more positive isomer shift and larger quadrupole splitting, as expected for a species in which a larger main group metal is coordinated to the Fe centre, resulting in a larger distortion of electronic distribution around the Fe centre. The minor impurity is the same in both complexes **2-crown** and **3-crown**. The Mössbauer parameters of Complex **4** continued the above trend with an increase in both the shift and the quadrupole splitting to δ = -0.08 mm/s and $|\Delta E_Q|$ = 1.97 mm/s. The minor species (yellow) was characterized as δ = 0.28 mm/s and $|\Delta E_Q|$ = 0.54 mm/s, matching literature parameters for $Fe_2(CO)_9$.[43]

Notably, the complexes followed a consistent trend, with an increase of the isomer shift as the group is descended. The increase of quadrupole splitting from increased distortion in the electric field gradient was in good agreement with the idea of an increased electronic interaction in the case of larger group 13 elements. Few Mössbauer examples appear in literature with iron(0) carbonyls bearing iron-main group metal bonds, making these complexes novel in their characterization and providing valuable insight into the effect of trielyl coordination.

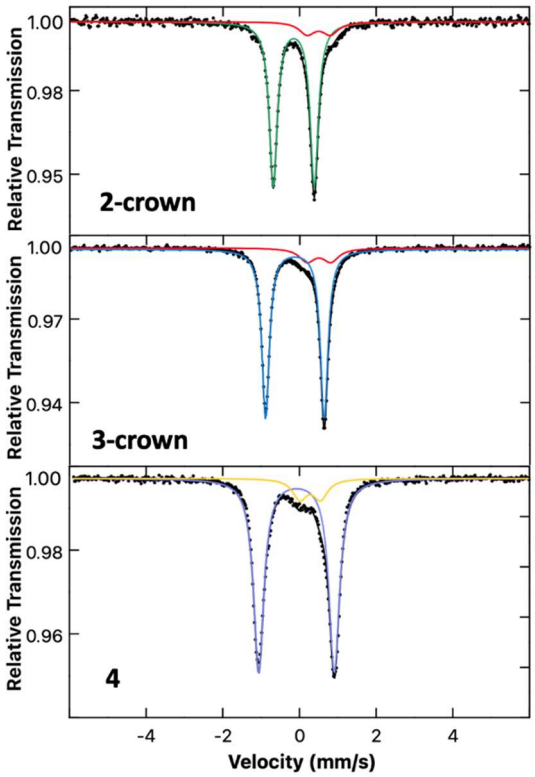

Figure 8. Zero field 80 K 57Fe Mössbauer spectrum of 2-crown (green, 88%): δ = -0.24 mm/s, |ΔEQ| = 2.08 mm/s, (red, 12%): δ = 0.50 mm/s, |ΔEQ| = 0.61 mm/s; 3-crown (blue, 88%): δ = -0.13 mm/s, |ΔEQ| = 1.53 mm/s, (red, 12%): δ = 0.50 mm/s, |ΔEQ| = 0.61 mm/s; 4 (purple, 88%): δ = -0.08 mm/s, |ΔEQ| = 1.97 mm/s, (yellow, 12%): δ = 0.28 mm/s, |ΔEQ| = 0.54 mm/s.

Conclusion and outlook

We have reported an investigation into the synthesis of trielyl–$Fe(CO)_4$ complexes, including a discussion in the case of aluminium of how the reactivity may be tuned by cation sequestration to yield the desired metal-metal bonded product. With the exception of **2-crown**, the iron-aluminium heterobimetallic species generated most closely resemble analogues of Collman's reagent, where one alkali metal cation is exchanged for $[(NON)Al]^+$, bound in various modes. For a series of isostructural complexes bearing direct bonds between iron and the aluminyl, gallyl and indyl metallo-ligands, a thorough experimental and computational comparison has been conducted, revealing significant differences in electronic structure as the group is descended, most notably in terms of the polarisation of the Fe–E bond, which is highly negative at iron for the aluminium ligated species **2-crown**, trending towards polarization in the opposite sense for indium species **4**. These conclusions are supported by IR measurements. Mössbauer spectroscopy indicates an increased perturbation of the iron centred electric field gradient as group 13 is descended, consistent with interactions with increasingly large ligand donor atoms.

Acknowledgements

We thank the EPSRC Centre for Doctoral Training in Inorganic Chemistry for Future Manufacturing (OxICFM, EP/S023828/1, studentships to L.P.G. and A.E.C.), the Leverhulme Trust (studentship to A.H.) and the Alexander von Humboldt Foundation for funding (Feodor Lynen postdoctoral research fellowship to M. A. E.). We also thank Oxford Arc Research Computing for computational resources, and Dr. M Malishewski for supply and advice on the use of $Ni(CO)_4$.

References

[1] Y. Segawa, M. Yamashita, K. Nozaki, *Science* **2006**, *314*, 113-115.
[2] M. Asay, C. Jones, M. Driess, *Chem. Rev.* **2011**, *111*, 354-396.
[3] M. P. Coles, M. J. Evans, *Chemical Communications* **2023**, *59*, 503-519.
[4] J. Hicks, P. Vasko, J. M. Goicoechea, S. Aldridge, *Angewandte Chemie International Edition* **2021**, *60*, 1702-1713.
[5] I. A. I. Mkhalid, J. H. Barnard, T. B. Marder, J. M. Murphy, J. F. Hartwig, *Chem. Rev.* **2010**, *110*, 890-931.
[6] A. J. Downs, *Chemistry of aluminium, gallium, indium and thallium*, Springer Science & Business Media, **1993**.
[7] J. Hicks, A. Mansikkamäki, P. Vasko, J. M. Goicoechea, S. Aldridge, *Nature Chemistry* **2019**, *11*, 237-241.
[8] J. Hicks, P. Vasko, J. M. Goicoechea, S. Aldridge, *Nature* **2018**, *557*, 92-95.
[9] E. S. Schmidt, A. Jockisch, H. Schmidbaur, *Journal of the American Chemical Society* **1999**, *121*, 9758-9759.
[10] R. J. Schwamm, M. D. Anker, M. Lein, M. P. Coles, C. M. Fitchett, *Angewandte Chemie International Edition* **2018**, *57*, 5885-5887.
[11] A. V. Protchenko, D. Dange, J. R. Harmer, C. Y. Tang, A. D. Schwarz, M. J. Kelly, N. Phillips, R. Tirfoin, K. H. Birjkumar, C. Jones, N. Kaltsoyannis, P. Mountford, S. Aldridge, *Nature Chemistry* **2014**, *6*, 315-319.
[12] I. M. Riddlestone, J. Urbano, N. Phillips, M. J. Kelly, D. Vidovic, J. I. Bates, R. Taylor, S. Aldridge, *Dalton Transactions* **2013**, *42*, 249-258.
[13] B. N. Anand, I. Krossing, H. Nöth, *Inorganic Chemistry* **1997**, *36*, 1979-1981.
[14] F. Kallmeier, A. J. R. Matthews, G. R. Nelmes, N. R. Lawson, J. Hicks, *Dalton Transactions* **2024**, *53*, 12450-12454.
[15] T. Chu, I. Korobkov, G. I. Nikonov, *Journal of the American Chemical Society* **2014**, *136*, 9195-9202.
[16] X. Zhang, L. L. Liu, *Angewandte Chemie International Edition* **2021**, *60*, 27062-27069.
[17] M. J. Evans, M. D. Anker, M. G. Gardiner, C. L. McMullin, M. P. Coles, *Inorganic Chemistry* **2021**, *60*, 18423-18431.
[18] J. T. Boronski, L. P. Griffin, C. Conder, A. E. Crumpton, L. L. Wales, S. Aldridge, *Chemical Science* **2024**.
[19] L. P. Griffin, M. A. Ellwanger, J. Clark, W. K. Myers, A. F. Roper, A. Heilmann, S. Aldridge, *Angewandte Chemie International Edition* **2024**, *63*, e202405053.
[20] R. J. Schwamm, M. P. Coles, M. S. Hill, M. F. Mahon, C. L. McMullin, N. A. Rajabi, A. S. S. Wilson, *Angewandte Chemie International Edition* **2020**, *59*, 3928-3932.
[21] G. Feng, K. L. Chan, Z. Lin, M. Yamashita, *Journal of the American Chemical Society* **2022**, *144*, 22662-22668.
[22] K. Sugita, M. Yamashita, *Chemistry – A European Journal* **2020**, *26*, 4520-4523.
[23] P. Zatsepin, T. Moriyama, C. Chen, S. Muratsugu, M. Tada, M. Yamashita, *Journal of the American Chemical Society* **2024**, *146*, 3492-3497.
[24] C. McManus, J. Hicks, X. Cui, L. Zhao, G. Frenking, J. M. Goicoechea, S. Aldridge, *Chemical Science* **2021**, *12*, 13458-13468.
[25] L. P. Griffin, M. A. Ellwanger, A. E. Crumpton, M. M. D. Roy, A. Heilmann, S. Aldridge, *Angewandte Chemie International Edition* **2024**, *63*, e202404527.
[26] H.-Y. Liu, R. J. Schwamm, M. S. Hill, M. F. Mahon, C. L. McMullin, N. A. Rajabi, *Angewandte Chemie International Edition* **2021**, *60*, 14390-14393.
[27] M. M. D. Roy, J. Hicks, P. Vasko, A. Heilmann, A.-M. Baston, J. M. Goicoechea, S. Aldridge, *Angewandte Chemie International Edition* **2021**, *60*, 22301-22306.
[28] G. Feng, K. L. Chan, Z. Lin, M. Yamashita, *Journal of the American Chemical Society* **2024**, *146*, 7204-7209.

[29] H. Strong, P. J. Krusic, J. S. Filippo Jr, S. Keenan, R. G. Finke, in *Inorganic Syntheses*, **1990**, pp. 203-207.
[30] D. Dange, C. P. Sindlinger, S. Aldridge, C. Jones, *Chemical Communications* **2017**, *53*, 149-152.
[31] E. Bill, in *Practical Approaches to Biological Inorganic Chemistry (Second Edition)* (Eds.: R. R. Crichton, R. O. Louro), Elsevier, **2020**, pp. 201-228.
[32] R. P. Brint, M. P. Collins, T. R. Spalding, F. A. Deeney, *Journal of Organometallic Chemistry* **1983**, *258*, C57-C60.
[33] J. Hicks, P. Vasko, J. M. Goicoechea, S. Aldridge, *Journal of the American Chemical Society* **2019**, *141*, 11000-11003.
[34] T. X. Gentner, M. J. Evans, A. R. Kennedy, S. E. Neale, C. L. McMullin, M. P. Coles, R. E. Mulvey, *Chemical Communications* **2022**, *58*, 1390-1393.
[35] B. Cordero, V. Gómez, A. E. Platero-Prats, M. Revés, J. Echeverría, E. Cremades, F. Barragán, S. Alvarez, *Dalton Transactions* **2008**, 2832-2838.
[36] P. Pyykkö, *The Journal of Physical Chemistry A* **2015**, *119*, 2326-2337.
[37] L. Pauling, *Journal of the American Chemical Society* **1932**, *54*, 3570-3582.
[38] R. Bianchi, G. Gervasio, D. Marabello, *Inorganic Chemistry* **2000**, *39*, 2360-2366.
[39] S. Warratz, L. Postigo, B. Royo, *Organometallics* **2013**, *32*, 893-897.
[40] J. Weiss, D. Stetzkamp, B. Nuber, R. A. Fischer, C. Boehme, G. Frenking, *Angewandte Chemie International Edition in English* **1997**, *36*, 70-72.
[41] R. Y. Kong, M. R. Crimmin, *Dalton Transactions* **2021**, *50*, 7810-7817.
[42] R. J. Baker, C. Jones, J. A. Platts, *Dalton Transactions* **2003**, 3673-3674.
[43] R. H. Herber, W. R. Kingston, G. K. Wertheim, *Inorganic Chemistry* **1963**, *2*, 153-158.

Supporting information

General considerations

All manipulations were carried out using standard Schlenk line or dry-box techniques under an atmosphere of argon or dinitrogen. Solvents were degassed by sparging with argon and dried by passing through a column of the appropriate drying agent. Toluene was purified using an MBraun SPS-800 and stored over a potassium mirror. *o*-DFB was dried by storage over molecular sieves before degassing by three freeze pump thaw cycles. NMR spectra were measured in benzene-d_6 (which was dried over potassium, with the solvent then being distilled under reduced pressure), or THF-d_8 (dried by storing over activated molecular sieves and degassed by three freeze pump thaw cycles). NMR samples were prepared under argon in 5 mm Wilmad 507-PP tubes fitted with J. Young Teflon valves. ^{1}H and ^{13}C{^{1}H} NMR spectra were recorded on Bruker Avance III HD nanobay 400 MHz or Bruker Avance III 500 MHz spectrometer at ambient temperature and referenced internally to residual protio-solvent (^{1}H) or solvent (^{13}C) resonances and are reported relative to tetramethylsilane (δ = 0 ppm). Assignments were confirmed using two-dimensional ^{1}H-^{1}H and ^{13}C-^{1}H NMR correlation experiments. Chemical shifts are quoted in δ (ppm) and coupling constants in Hz. Elemental analyses were carried out by London Metropolitan University or Elemental Microanalysis Ltd. $Fe(CO)_5$ was stored over molecular sieves in a freezer in a glovebox and thawed immediately before each use. [2.2.2.]-cryptand was purified by sublimation under vacuum. 18-crown-6 was recrystallised from hot acetonitrile and dried under vacuum. $Ni(CO)_4$ was used as received. **[K{Al(NON)}]$_2$**, **[K{Ga(NON)}]$_2$**, and **[K$_2$(18-crown-6)$_2$Cp][In(NON)]** were prepared according to literature procedures.[s1, s2]

X-ray crystallographic details

Single-crystal X-ray diffraction data for compounds **1**, **2-crypt**, **2-crown**, **3**, **3-crown**, **4**, **5** and **6** were collected on an Oxford Diffraction/Agilent SuperNova diffractometer equipped with a 135 mm Atlas CCD area detector or a Rigaku XtaLAB Synergy-DW VHF equip with a PhotonJet-R dual wavelength rotating anode and HyPix-Arc 150° detector. Crystals were selected under Paratone-N oil, mounted on MiTeGen Micromount loops and quench-cooled using an Oxford Cryosystems open flow N2 cooling device.[s3] Data were collected at 150 K using mirror monochromated Cu Kα radiation (λ = 1.5418 Å; Oxford Diffraction Supernova) or Mo Kα radiation (λ = 0.71073 Å; Oxford Diffraction Supernova). Data collected were processed using the CrysAlisPro package, including unit cell parameter refinement and inter-frame scaling (which was carried out using SCALE3 ABSPACK within CrysAlisPro).[s4] Equivalent reflections were merged and diffraction patterns processed with the CrysAlisPro suite.[s4] Structures were solved ab initio from the integrated intensities using SHELXT[s5] and refined on F2 using SHELXL[s6] with the graphical interface OLEX2.[s7] Selected crystallographic data are summarised in Table s1.

	1 - IsoCO	2-crypt	2-crown	3	3-crown	4	5	6
Formula	$C_{102}H_{124}Al_2Fe_2K_2N_4O_{10}$, $4(C_7H_8)$	$C_{87}H_{116}AlFeKN_4O_{11}$	$C_{63}H_{86}AlFeKN_2O_{11}$, $4(C_6H_6)$	$C_{57}H_{68}FeGaKN_2O_5$, $2.5(C_6H_6)$	$C_{63}H_{86}FeGaKN_2O_{11}$, $1.5(C_6H_6)$	$C_{51}H_{62}FeInN_2O_5$, $C_{35}H_{59}K_2O_{12}$, $0.5(C_6H_6)$, $0.5(C_6H_{14})$	$C_{48}H_{48}Fe_6In_2K_2O_{36}$	$C_{54}H_{72}K_2N_4Ni_8O_{30}$
Fw (g mol^{-1})	2178.44	1515.76	1481.69	1221.07	1329.16	1785.85	1843.80	1805.03
Crystal system	Monoclinic	Triclinic	Monoclinic	Monoclinic	Triclinic	Monoclinic	Triclinic	Triclinic
Space group	I 1 2/a 1	P -1	P 1 c 1	I 1 2/a 1	P -1	P 1 2_1/c 1	P -1	P -1
a (Å)	24.2358(5)	13.0235(2)	25.0904(3)	21.9032(2)	12.7340(2)	12.63069(4)	9.5811(3)	11.2851(10)
b (Å)	18.6924(4)	13.8732(2)	12.4623(2)	13.86540(10)	23.0469(3)	31.79286(9)	13.0624(3)	13.3656(14)
c (Å)	26.7388(7)	23.1100(4)	26.4474(3)	43.2338(4)	24.7089(4)	23.60319(7)	14.1928(3)	24.497(2)
α (°)	90	95.0460(10)	90	90	89.0350(10)	90	87.307(2)	82.483(7)
β (°)	104.412(3)	93.8940(10)	96.0360(10)	90.3340(10)	78.4690(10)	98.2952(3)	89.670(2)	87.949(7)
γ (°)	90	91.1300(10)	90	90	89.3030(10)	90	72.843(2)	79.684(7)
V (Å^{-3})	11732.2(5)	4148.29(11)	8223.83(19)	13129.7(2)	7103.90(19)	9379.07(5)	1695.28(8)	3603.6(6)
Z	4	2	4	8	4	4	1	2
ρ_{calc} (g cm^{-3})	1.233	1.214	1.197	1.235	1.243	1.265	1.806	1.664
Radiation, λ (Å)	1.54184	1.54184	1.54184	1.54184	1.54184	1.54184	1.54184	1.54184
Absorption	Multi-scan	Gaussian	Gaussian	Gaussian	Analytical	Multi-scan	Multi-scan	Multi-scan
μ (mm^{-1})	3.231	2.486	2.490	3.228	3.086	4.507	17.230	3.973
Reflections collected	86175	65512	84967	94154	42712	257953	33594	63026
Independent reflections	12214	17106	27505	13376	42712	19375	7010	13003
$R_{(int)}$	0.0681	0.0362	0.0532	0.0626	N/A, Twin integration performed	0.0356	0.0492	0.1293
Parameters	694	993	1895	863	1741	1071	587	1353
R_1 (all data/I>2σ(I))	0.0642	0.0505	0.0409	0.0519	0.0482	0.0346	0.0291	0.0892
ωR_2 (all data/I >2σ(I))	0.1830	0.1455	0.0979	0.1385	0.1290	0.0906	0.0771	0.2294
GooF	1.042	1.037	1.016	1.049	0.940	1.071	1.029	1.029
T (K)	150.00(10)	150.01(10)	150.00(10)	100.00(10)	150.01(10)	100.00(10)	150.00(10)	150.00

Table s1: X-ray crystallographic details

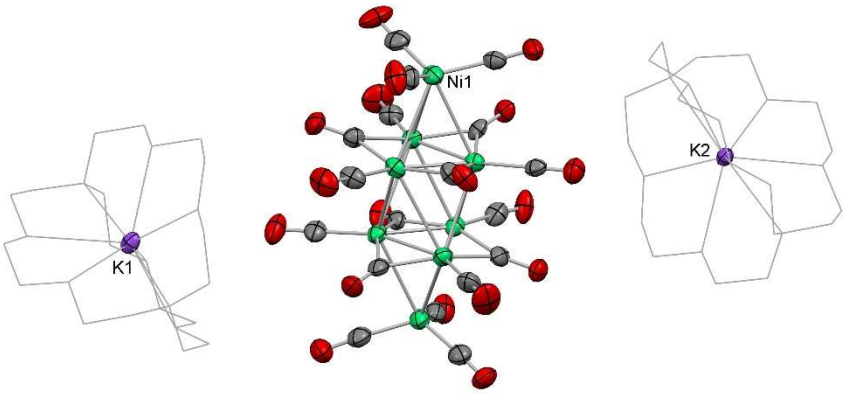

Figure s1: X-ray structure of **6**

Synthesis of novel compounds

Synthesis of **1**

To a toluene (20 mL) solution of $[K\{Al(NON)\}]_2$ (300 mg, 0.41 mmol) was added $Fe(CO)_5$ (0.067 mL, 0.5 mmol), at which point the solution immediately darkened. The solution was filtered into a lambda-shaped J-Youngs tube, which was stored under a partial internal vacuum with the sidearm cooled by a water bath overnight. Large, colourless single crystals were subsequently obtained from the concentrated supernatant solution. This solution was decanted, and the crystals washed with a minimum amount of cold hexane before drying *in vacuo*. Single crystal diffraction allowed identification of the crystals as $K_2[\{(NON)Al\}(OC)_2Fe(CO)_2]_2$ (**1**). Yield 148 mg, 40%.

Calc. for $C_{102}H_{124}Al_2Fe_2K_2N_4O_{10}$: C 67.69%, H 6.91%, N 3.10%. Measured: 68.72%, 7.16%, 2.74%

^{1}H NMR (500 MHz, THF-d_8, 298 K): δ_H 0.94 (d, $^3J_{HH}$ = 6.7 Hz, 6H, CH(CH_3)$_2$), 1.04 (d, $^3J_{HH}$ = 6.7 Hz, 6H, CH(CH_3)$_2$), 1.10 (d, $^3J_{HH}$ = 6.7 Hz, 6H, CH(CH_3)$_2$), 1.14 (s, 18H, C(CH_3)$_3$), 1.45 (d, $^3J_{HH}$ = 6.7 Hz, 6H, CH(CH_3)$_2$), 1.66 (s, 3H, C(CH_3)$_2$), 1.83 (s, 3H, C(CH_3)$_2$), 3.17 (sept, $^3J_{HH}$ = 6.7 Hz, 2H, C*H*(CH$_3$)$_2$), 3.87 (sept, $^3J_{HH}$ = 6.7 Hz, 2H, C*H*(CH$_3$)$_2$), 5.88 (d, $^4J_{HH}$ = 1.7 Hz, 2H, XA-*o*-C*H*), 6.68 (d, $^4J_{HH}$ = 1.7 Hz, 2H, XA-*p*-C*H*), and 7.13-7.29 (m, 6H, Ar*H*) ppm.

^{13}C{^{1}H} NMR (101 MHz, THF-d_8, 298 K): δ_C 150.5, 148.0, 147.5, 143.8, 143.0, 138.7, 131.4, 126.9, 125.7, 124.6, 124.5, 111.2, 107.7, 37.6, 35.8, 34.3, 32.2, 29.1, 28.9, 27.4, 27.2, 24.8 and 23.7 ppm.

Synthesis of **2-cryptand**

To an NMR tube fitted with a J-Young valve containing $[K\{Al(NON)\}]_2$ (0.02g, 0.027 mmol) and [2.2.2]-cryptand (0.01 g, 0.02 mmol) was added benzene (0.3 mL) before brief sonication to yield a red suspension. To this was added $Fe(CO)_5$ (0.04 mL 0.030 mmol), at which point the solution immediately darkened. Storage of this solution for 1 week yielded a small quantity of pale yellow crystals suitable for diffraction measurements, which identified the product as $[K(2.2.2\text{-cryptand})][(NON)AlFe(CO)_4]$.

Attempts to crystallize the material by other methods or at larger scale did not significantly increase the yield of material beyond the small amounts of crystals isolated by this procedure. These crystals were found to be highly insoluble in compatible solvents, so only *in situ* NMR data of the non-selective reaction could be collected.

Synthesis of **2-crown**

To a Schlenk flask containing $[K\{Al(NON)\}]_2$ (0.300 g, 0.41 mmol) and 18-crown-6 (0.108 g, 0.41 mmol) was added benzene (15 mL) before brief sonication to yield an orange suspension. To this was added $Fe(CO)_5$ (0.067 mL, 0.5 mmol), at which point the solution immediately darkened. Storage of the solution for one hour led to the formation of large colourless single crystals suitable for diffraction measurements. Decanting the supernatant and washing with the minimum volume of hexane before drying *in vacuo* allowed isolation of clean material of $[K(18\text{-crown-6})][(NON)AlFe(CO)_5]$. Yield 0.263 g, 55%.

Calc for $C_{63}H_{86}AlFeKN_2O_{11}$: C 64.71%, H 7.41%, N 2.40%. Found: C 64.80%, H 7.52%, N 2.08%

^{1}H NMR (500 MHz, THF-d_8, 298 K): δ_H 0.80 (br. s, 6H, CH(CH_3)$_2$), 0.95 (d, $^3J_{HH}$ = 7.1 Hz, 6H, CH(CH_3)$_2$), 1.05 (d, $^3J_{HH}$ = 7.1 Hz, 6H, CH(CH_3)$_2$), 1.14 (s, 18H, C(*CH*$_3$)$_3$), 1.47 (d, $^3J_{HH}$ = 7.1 Hz, 6H, CH(CH_3)$_2$), 1.68 (s, 3H, C(CH_3)$_2$), 1.81 (s, 3H, C(CH_3)$_2$), 3.16 (sept, $^3J_{HH}$ = 6.6 Hz, 2H, C*H*(CH$_3$)$_2$), 3.61 (s, 24H, OCH_2CH_2O), 3.95 (sept, $^3J_{HH}$ = 6.6 Hz, 2H, C*H*(CH$_3$)$_2$), 5.86 (s, 1H, XA-*o*-C*H*), 5.90 (s, 1H, XA-*o*-C*H*), 6.50 (s, 1H, XA-*p*-C*H*), 6.65 (s, 1H, XA-*p*-C*H*), 7.00 (m, 4H, Ar-*m*-C*H*) and 7.15 (m, 2H, Ar-*p*-C*H*) ppm.

^{13}C{^{1}H} NMR (101 MHz, THF-d_8, 298 K): δ_C 149.7, 147.1, 146.5, 146.3, 145.6, 144.0, 143.8, 142.9, 142.3, 128.0, 125.6, 124.5, 124.1, 123.1, 111.2, 109.9, 106.2, 105.3, 70.1, 34.6, 34.5, 31.1, 31.0, 28.0, 27.8, 26.1, 26.0 and 22.5 ppm.

Synthesis of **3**

To a Schlenk flask containing $[K\{Ga(NON)\}]_2$ (0.1 g, 0.128 mmol) and benzene (10 mL) was added $Fe(CO)_5$ (0.018 mL, 0.13 mmol), at which point the solution immediately darkened. Storage of the solution for 12 hours led to the formation of large needle-shaped colourless single crystals suitable for diffraction measurements. Decanting the supernatant and washing with the minimum volume of hexane before drying *in vacuo* allowed isolation of clean material of $K[(NON)GaFe(CO)_5]$. Yield 0.061g, 50%.

Calc. for $C_{51}H_{62}FeGaKN_2O_5$: C 66.74%, H 6.68%, N 2.73%. Measured: C 66.41%, 6.74%, 2.51%

^{1}H NMR (500 MHz, THF-d_8, 298 K): δ_H 0.85 (br. s, 12H, CH(C*H*$_3$)$_2$), 1.08 (s, 18H, C(*CH*$_3$)$_3$), 1.16 (m, 12H, CH(C*H*$_3$)$_2$), 1.71 (overlapping with residual solvent peak, 3H, C(C*H*$_3$)$_2$), 2.31 (s, 3H, C(C*H*$_3$)$_2$), 3.41 (br. m, 4H, C*H*(CH$_3$)$_2$), 5.85 (s, 2H, XA-*o*-C*H*), 6.44 (s, 2H, XA-*p*-C*H*), 7.00 (m, 4H, Ar-*m*-C*H*) and 7.19 (m, 2H, Ar-*p*-C*H*) ppm.

^{13}C{^{1}H} NMR (101 MHz, THF-d_8, 298 K): δ_C 217.3, 143.8, 143.1, 142.6, 135.6, 134.3, 126.8, 126.1, 123.2, 122.3, 109.4, 103.0, 36.4, 32.5, 29.2, 26.1 and 18.7 ppm.

Synthesis of **3-crown**

To a Schlenk flask containing $[K\{Ga(NON)\}]_2$ (0.2 g, 0.256 mmol) and 18-crown-6 (0.068 g, 0.256 mmol) was added benzene (20 mL) before brief sonication to yield a pale yellow suspension. To this was added $Fe(CO)_5$ (0.036 mL, 0.26 mmol), at which point the solution immediately darkened slightly. Storage of the solution for one hour led to the formation of large colourless single crystals suitable for diffraction measurements. Decanting the supernatant and washing with the minimum volume of hexane before drying *in vacuo* allowed isolation of clean material of [K(18-crown-6)][(NON)GaIFe(CO)$_5$]. Yield 0.132g, 43%

Calc. for $C_{63}H_{86}FeGaKN_2O_{11}$: C 63.49%, H 5.58%, N 2.35%. Measured: C 63.42%, H 6.75%, N 1.87%

^{1}H NMR (500 MHz, THF-d_8, 298 K): δ_H 0.85 (br. s, 12H, CH(CH_3)$_2$), 1.08 (s, 18H, C(*CH$_3$*)$_3$), 1.19 (d, $^{3}J_{HH}$ = 6.9 Hz, 12H, CH(CH_3)$_2$), 1.67 (s, 3H, C(CH_3)$_2$), 2.31 (s, 3H, C(CH_3)$_2$), 3.38 (sept, $^{3}J_{HH}$ = 6.5 Hz, 4H, C*H*(CH$_3$)$_2$), 3.58 (s, 24H, OCH_2CH_2O), 5.86 (s, 2H, XA-*o*-C*H*), 6.43 (s, 2H, XA-*p*-C*H*), 7.08 (m, 2H, Ar-*p*-C*H*) and 7.16 (m, 4H, Ar-*m*-C*H*) ppm.

^{13}C{^{1}H} NMR (101 MHz, THF-d_8, 298 K): δ_C 217.1, 146.1, 143.8, 143.3, 143.2, 142.7, 134.3, 126.8, 126.1, 123.2, 122.2, 121.6, 109.3, 102.8, 68.4, 36.4, 32.5, 29.3, 29.0, 26.0, 21.8, 21.6 and 18.6 ppm.

Synthesis of **4**

To a Schlenk flask containing [K_2(18-crown-6)$_2$Cp][In(NON)] (0.2 g, 0.137 mmol) was added *o*-DFB (20 mL), yielding a yellow suspension. To this was added Fe(CO)$_5$ (0.019 mL, 0.14 mmol) before sonication at room temperature for 1 h, until the suspension clarified. Filtration and layering with hexane yielded large pale orange single crystals of (K_2(18-crown-6)$_2$Cp][(NON)InFe(CO)$_4$] suitable for diffraction measurements. Yield 0.173 g, 87%.

Calc. for $C_{80}H_{115}FeInK_2N_2O_{17}$: C 59.37%, H 6.89%, N 1.61%. Measured: C 59.20%, H 6.92%, N 1.34%

^{1}H NMR (500 MHz, benzene-d_6, 298 K): δ_H 1.34 (d, $^{3}J_{HH}$ = 6.7 Hz, 12H, CH(CH_3)$_2$), 1.35 (s, 18H, C(*CH$_3$*)$_3$), 1.71 (d, $^{3}J_{HH}$ = 6.7 Hz, 12H, CH(CH_3)$_2$), 1.79 (s, 6H, C(CH_3)$_2$), 3.20 (s, 48H, OCH_2CH_2O), 4.09 (sept., 4H, C*H*(CH$_3$)$_2$), 6.14 (s, 5H, C$_5$*H*$_5$), 6.41 (d, $^{4}J_{HH}$ = 2.1 Hz, 2H, XA-o-C*H*), 6.75 (d, $^{4}J_{HH}$ = 2.1 Hz, 2H, XA-*p*-C*H*), 7.39 (m, 2H, Ar-*p*-C*H*) and 7.48 (d, 4H, Ar-*m*-C*H*) ppm.

^{13}C{^{1}H} NMR (101 MHz, benzene-d_6, 298 K): δ_C 219.01, 147.92, 146.20, 145.21, 142.94, 134.66, 125.29, 124.21, 110.44, 104.91, 104.36, 37.34, 35.08, 32.19, 28.84, 27.89, 26.15 and 25.18 ppm.

Synthesis of **5**

To a Schlenk flask containing $[K_2(18\text{-crown-}6)_2Cp][In(NON)]$ (0.1 g, 0.067 mmol) was added benzene (10 mL), yielding a yellow suspension. To this was added $Fe(CO)_5$ (0.012 mL, 0.1 mmol) before heating to 80 °C for 2 h. Filtration and layering with hexane yielded a mixture of crystals of **4** and the mixed metal cluster compound **5**, which was characterised crystallographically. The fate of the NON containing component is unknown.

Synthesis of **6**

To a J-Young flask containing $[K\{Al(NON)\}]_2$ (0.02g, 0.027 mmol) and [2.2.2]-cryptand (0.01 g, 0.027 mmol) was added benzene (0.3 mL) before brief sonication and degassing with three freeze pump thaw cycles. A small excess (as judged by weighing of the tube) of $Ni(CO)_4$ was then vacuum transferred onto the frozen solution before allowing it to thaw. The solution turned dark red, and storage for 6 h yielded small quantities of red crystals of **6**, which was characterised crystallographically. The fate of the aluminium containing component is unknown.

NMR of novel compounds

1

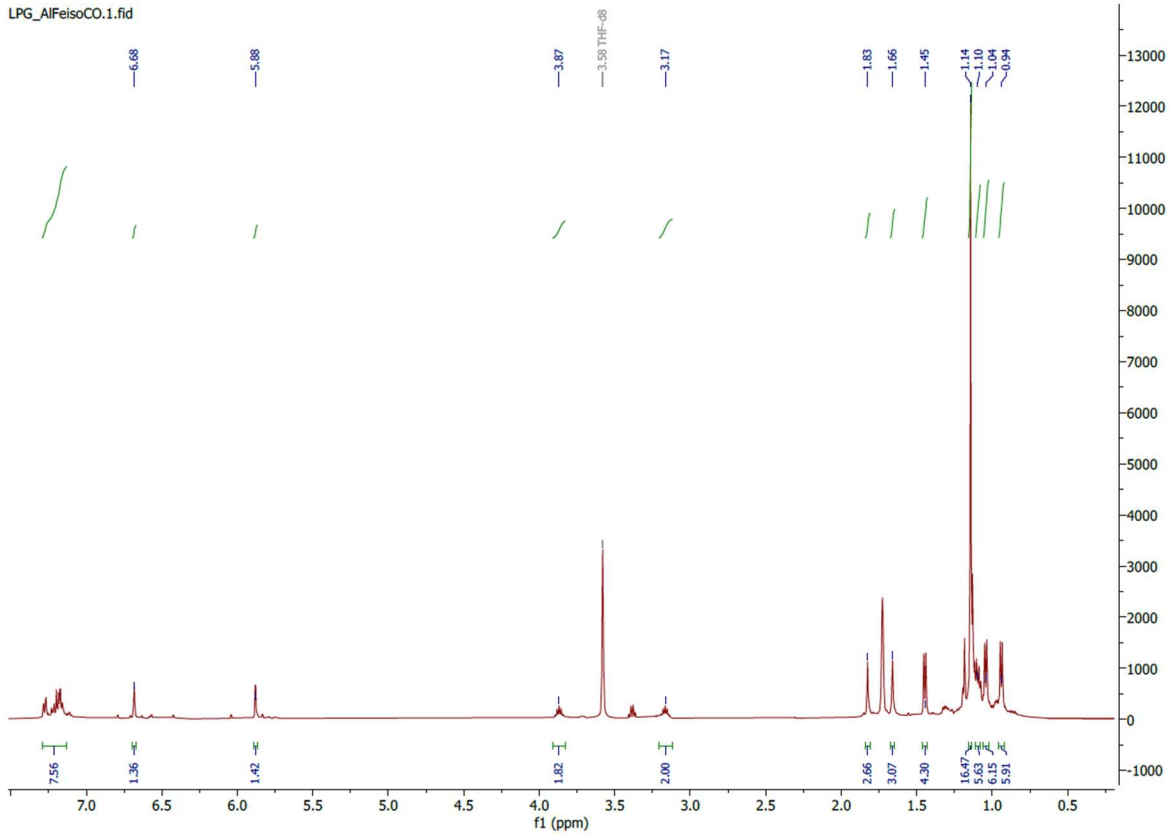

Figure s2: ^{1}H NMR spectrum of **1**

2-crypt

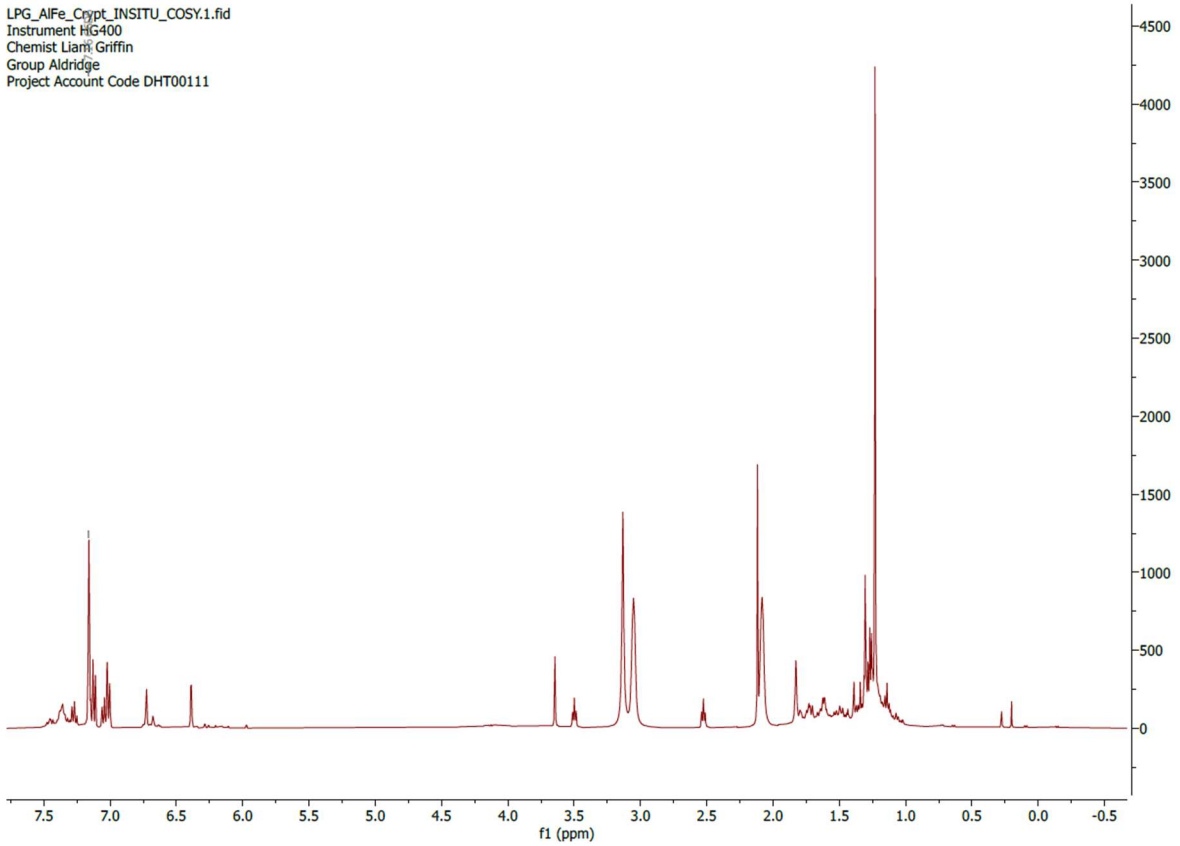

Figure s3: *In situ* ^{1}H NMR spectrum of **2-crypt**, which indicates that an unselective reaction has occurred

2-crown

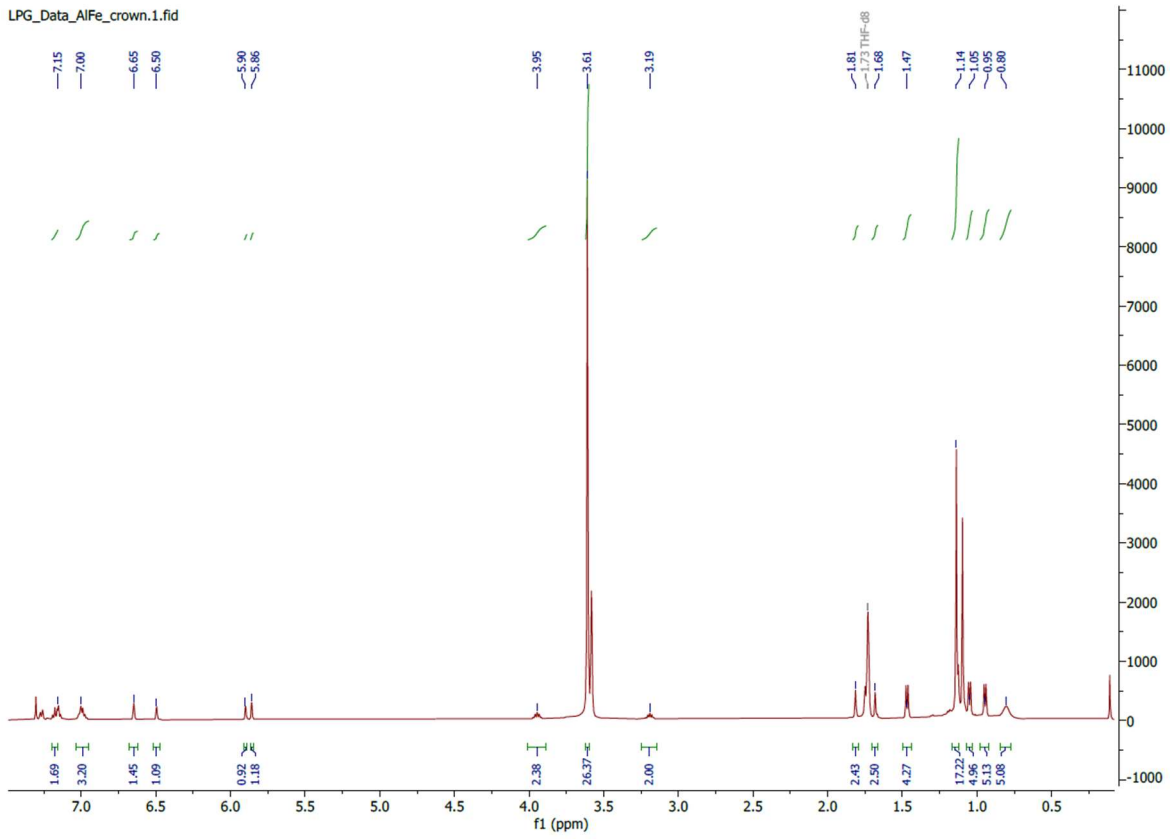

Figure s4: ^{1}H NMR spectrum of **2-crown**

3

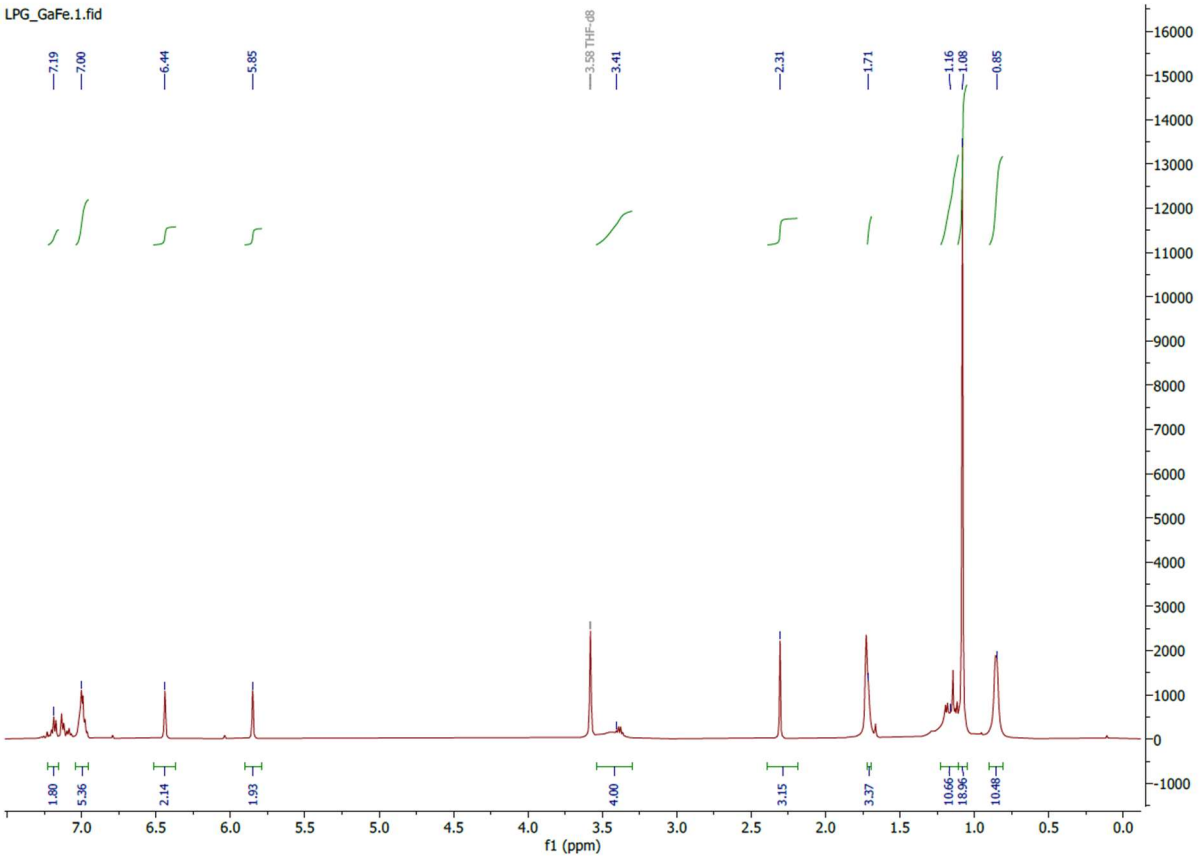

Figure s5: ^{1}H NMR spectrum of **3**

3-crown

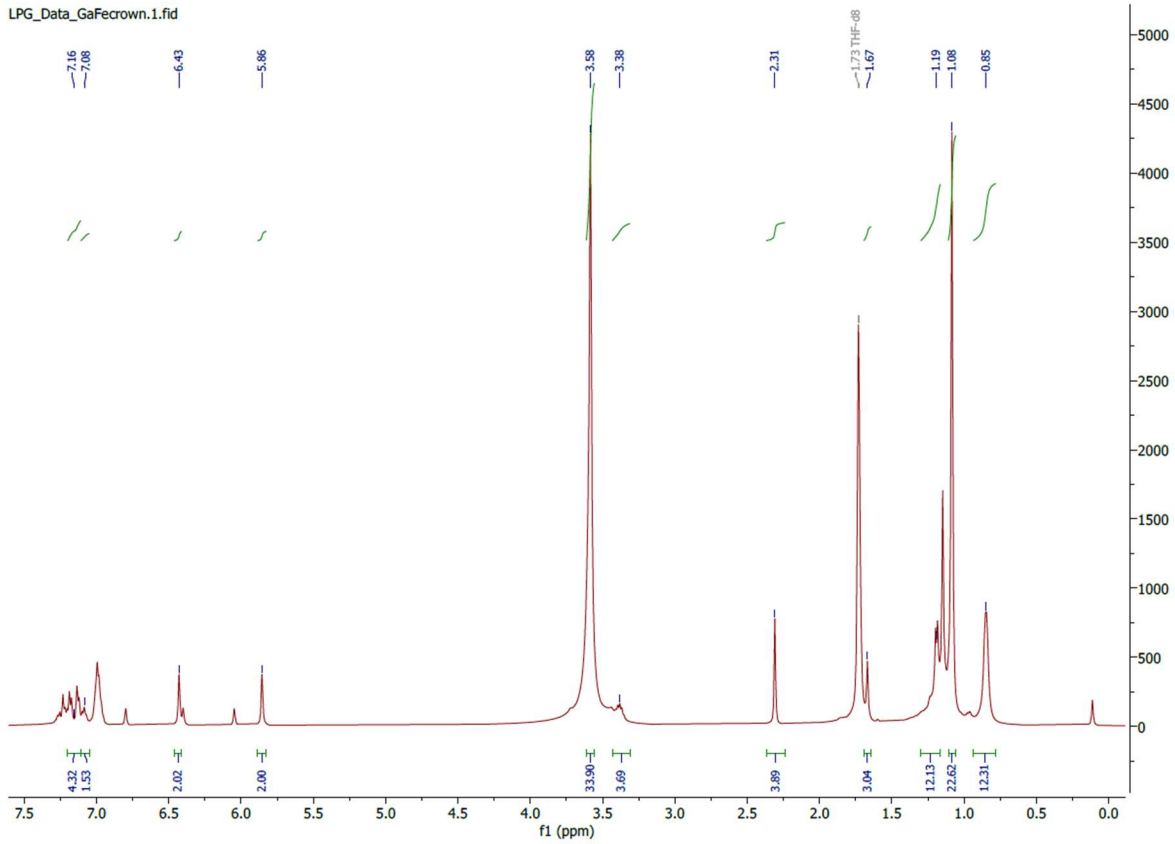

Figure s6: ^{1}H NMR spectrum of **3-crown**

4

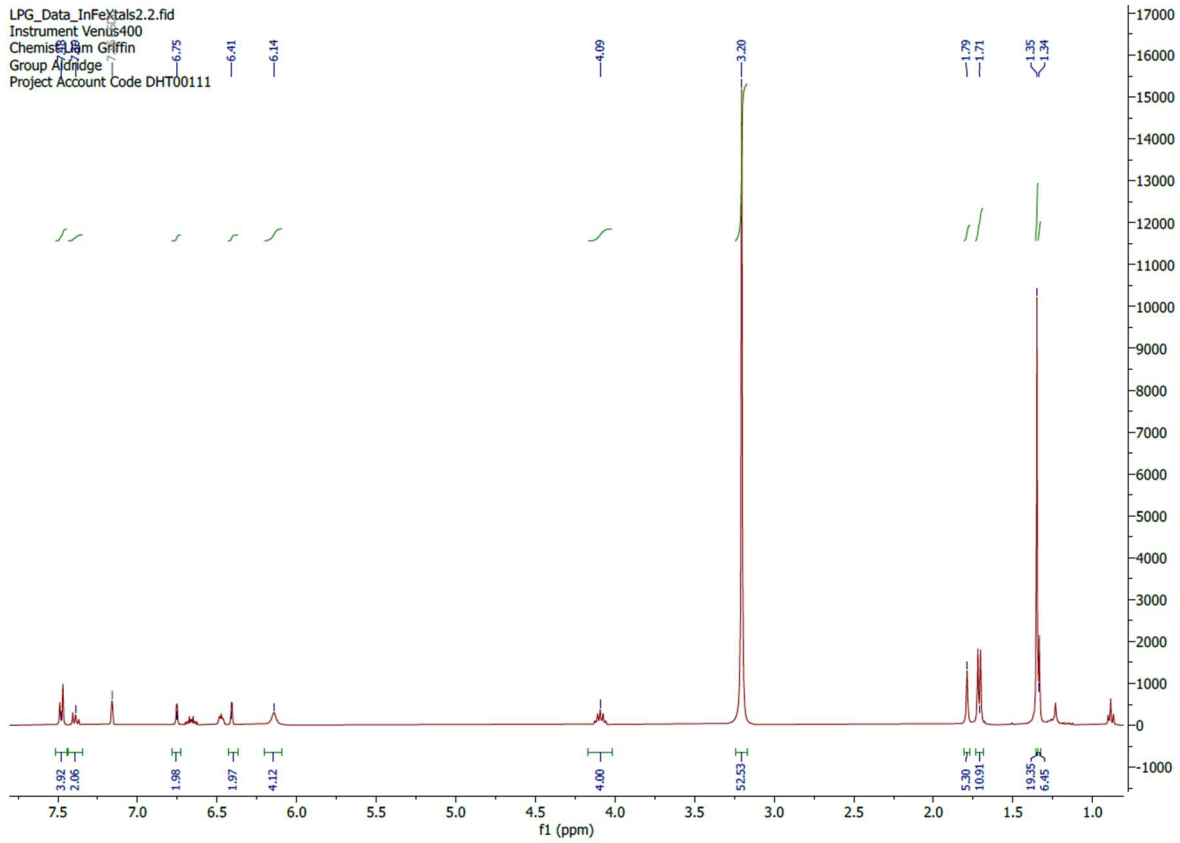

Figure s7: ^{1}H NMR spectrum of **4**

IR spectra of novel compounds

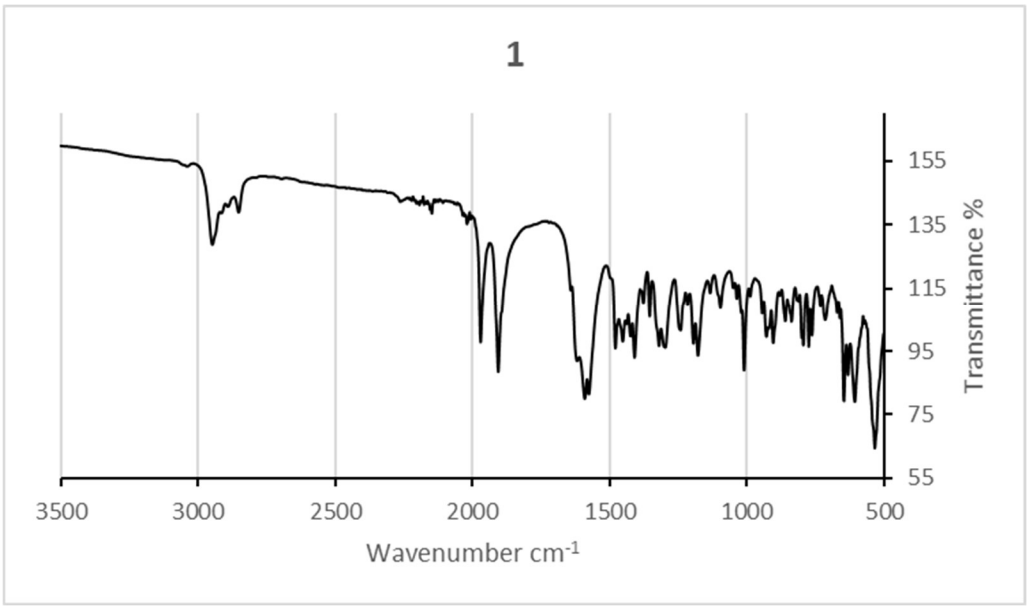

Figure s8: IR spectrum of **1**

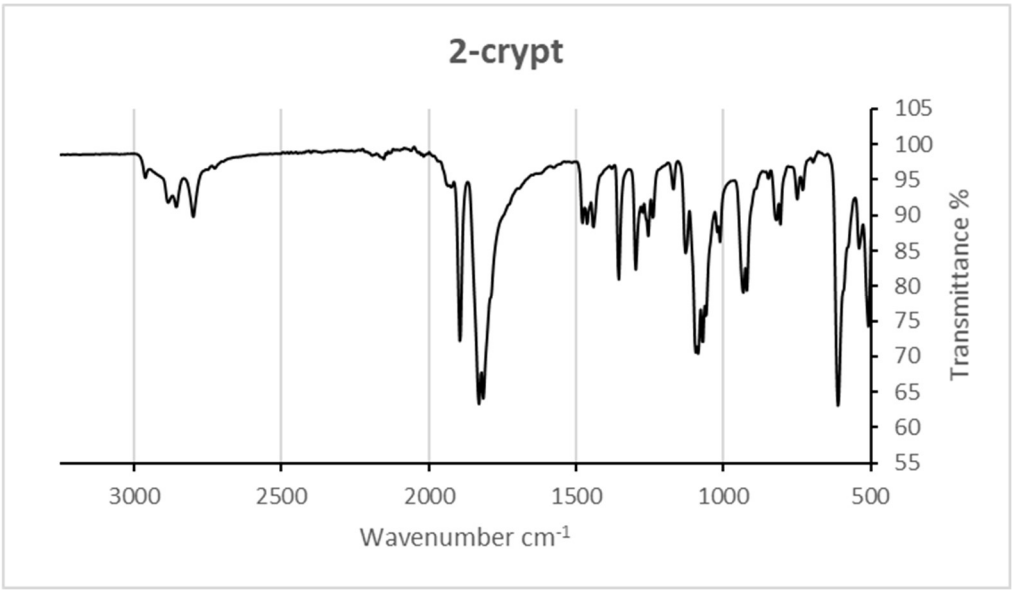

Figure s9: IR spectrum of **2-crypt**

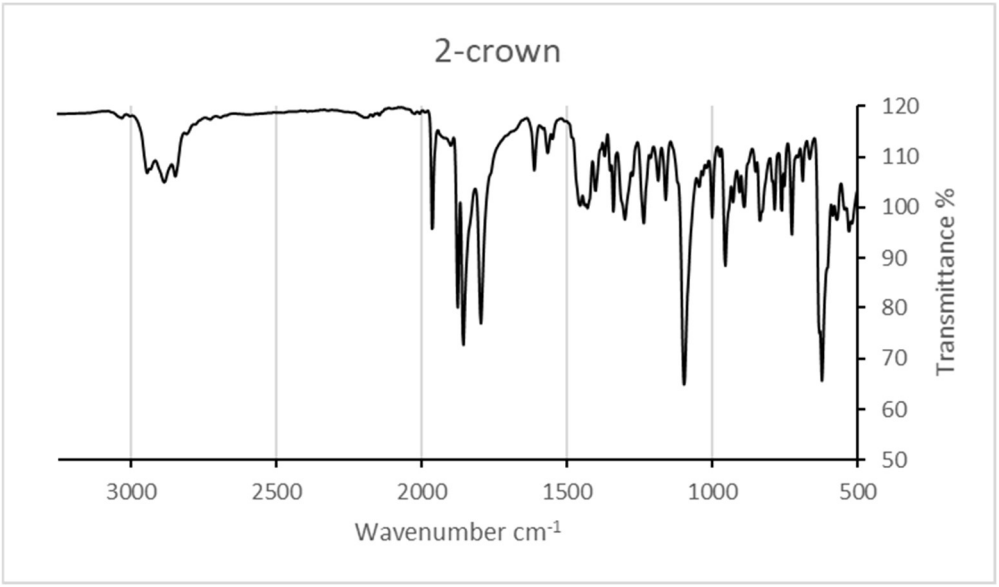

Figure s10: IR spectrum of **2-crown**

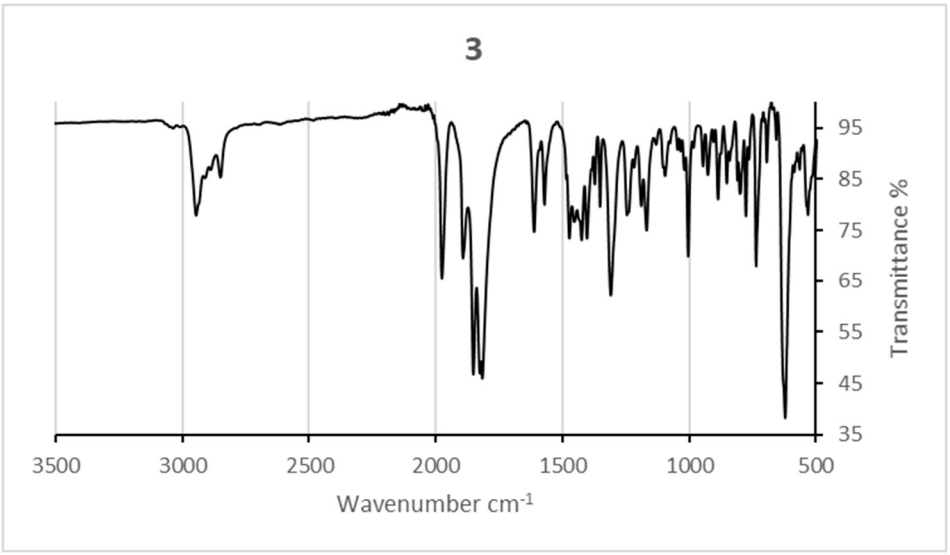

Figure s11: IR spectrum of **3**

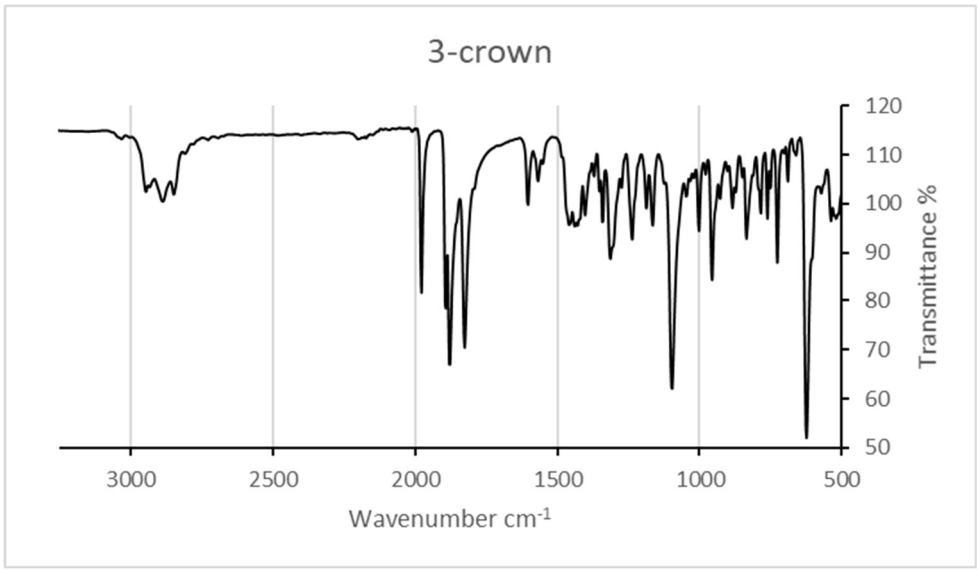

Figure s12: IR spectrum of **3-crown**

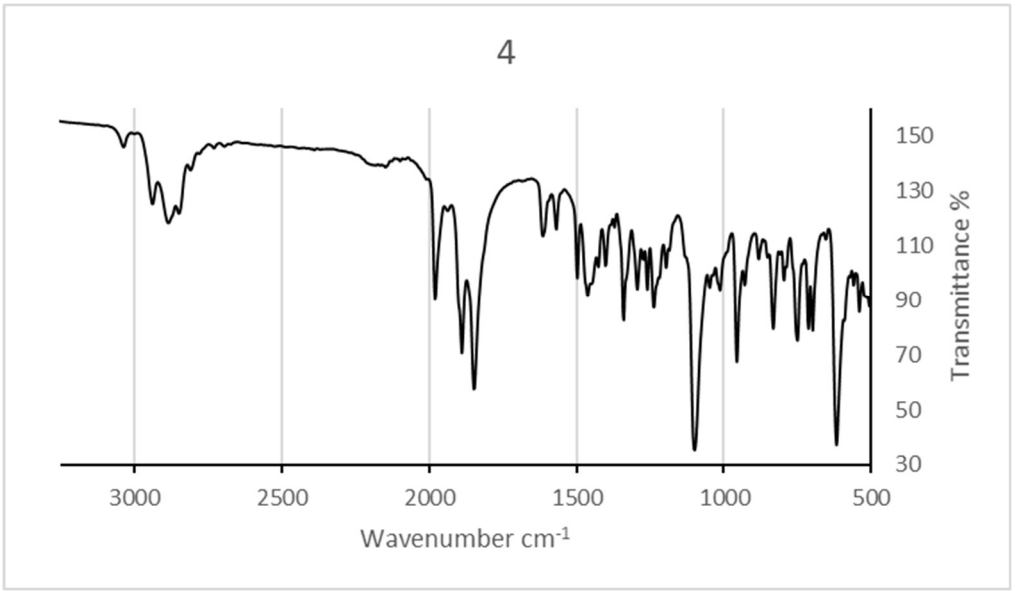

Figure s13: IR spectrum of **4**

Mössbauer spectra of novel compounds

All samples were prepared in a Delrin Mössbauer cup in a glovebox under nitrogen-atmosphere and were frozen under nitrogen to 77K within the glovebox. Each sample was then loaded into the Mössbauer sample compartment under liquid nitrogen. 57Fe Mössbauer measurements were performed using a SEE Co. MS4Mössbauer spectrometer integrated with a Janis SVT-400T cryostat for measurements at 80 K. The Mössbauer spectra were fit using WMoss See Co. Errors of the fit analysis were as follows: δ ± 0.02 mm/s, ΔEQ ± 3%, and quantitation ±3% (e.g., 50 ± 3%).

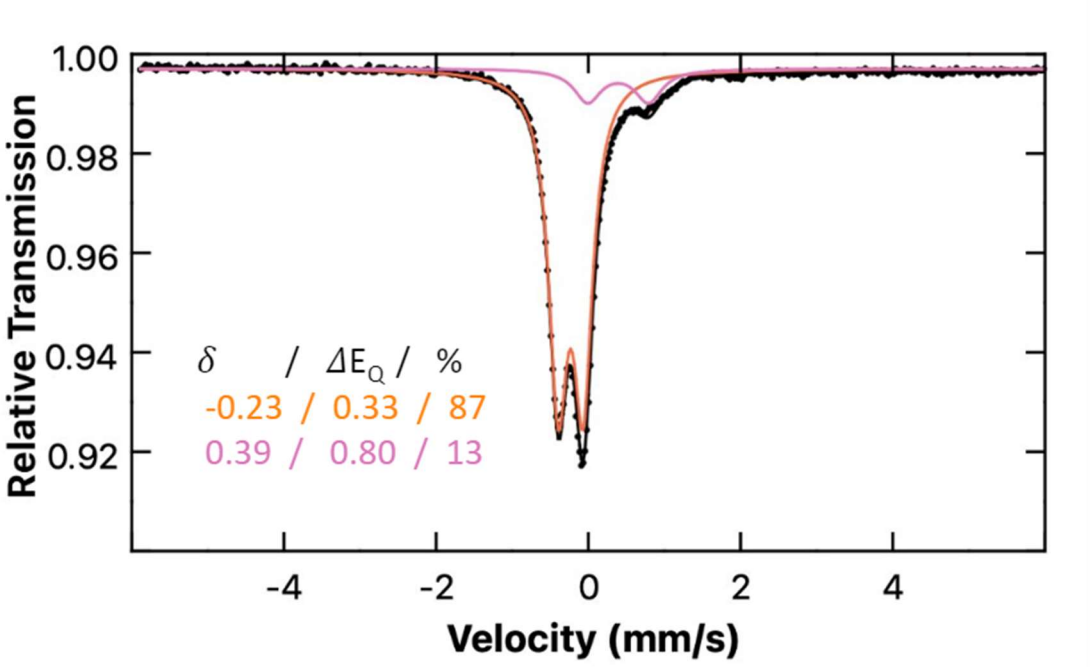

Figure s14: Zero field 80 K ^{57}Fe Mössbauer spectrum of **1** (orange, 87%): δ = -0.23 mm/s, |ΔEQ| = 0.3 mm/s 3; (pink, 13%): δ = 0.39 mm/s, |ΔEQ| = 0.80 mm/s.

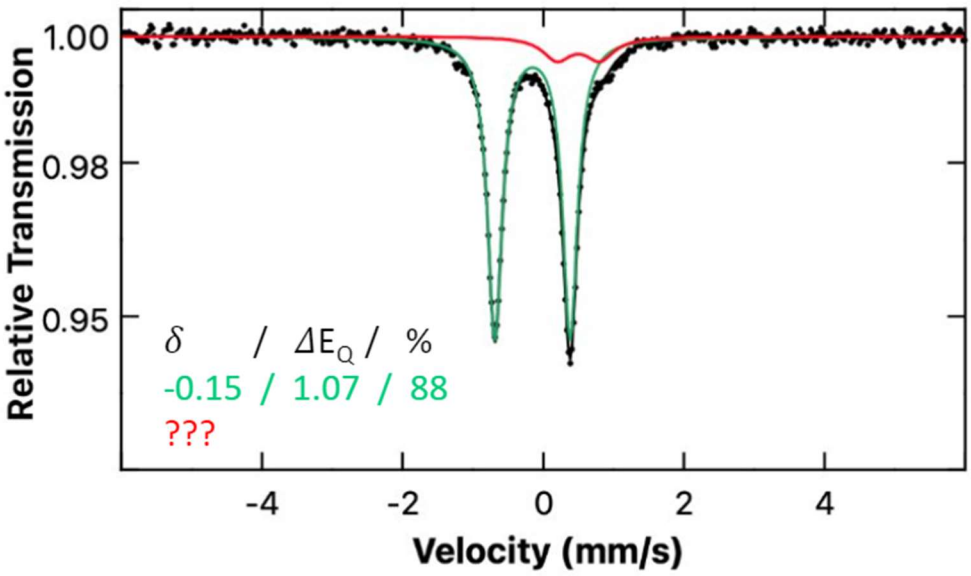

Figure s15: Zero field 80 K ^{57}Fe Mössbauer spectrum of **2-crown** (green, 88%): δ = -0.24 mm/s, |ΔEQ| = 2.08 mm/s, (red, 12%): δ = 0.50 mm/s, |ΔEQ| = 0.61 mm/s

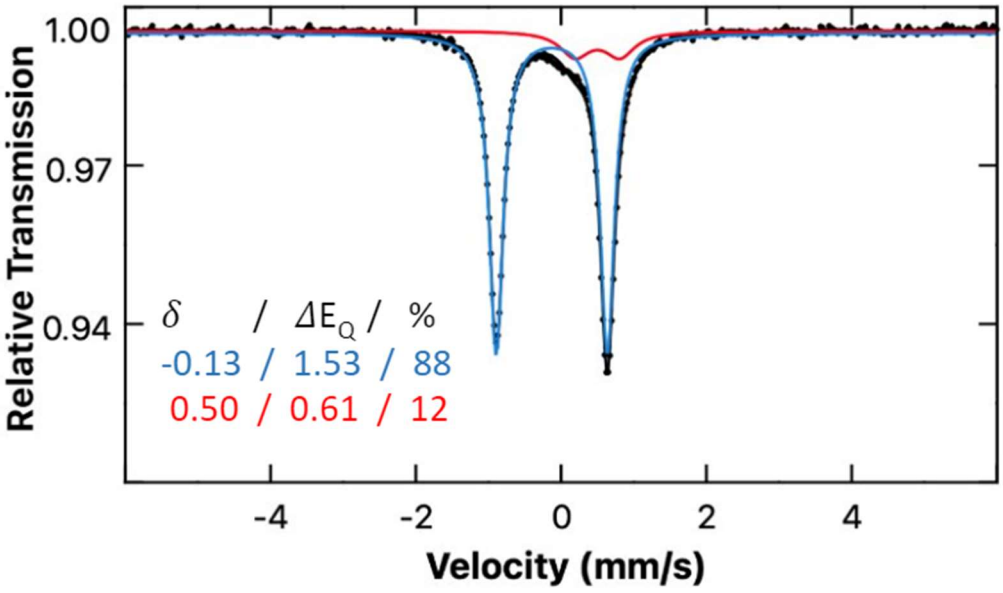

Figure s16: Zero field 80 K ^{57}Fe Mössbauer spectrum of **3-crown** (blue, 88%): δ = -0.13 mm/s, |ΔEQ| = 1.53 mm/s, (red, 12%): δ = 0.50 mm/s, |ΔEQ| = 0.61 mm/s

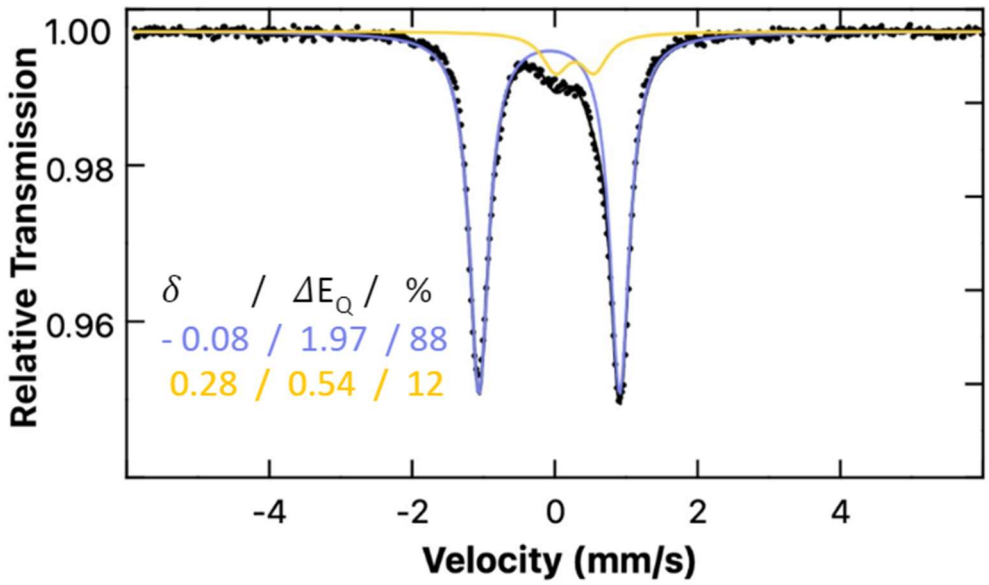

Figure s17: Zero field 80 K ^{57}Fe Mössbauer spectrum of **4** (purple, 88%): δ = -0.08 mm/s, |ΔEQ| = 1.97 mm/s, (yellow, 12%): δ = 0.28 mm/s, |ΔEQ| = 0.54 mm/s

Computational details

Gas phase geometry optimizations and frequency analyses were carried out using the ORCA (5.0.4) software package,[s8, s9] using the R2-Scan-3C method.[s10] The optimized structures were confirmed to be minima on the potential energy surface by the absence of imaginary frequencies. Single point calculations were performed using the ωB97X-D4 functional and Def2-TZVP basis set.[s11-s13] Natural bonding orbital (NBO) analyses were carried out using the NBO 7.0 program.[s14, s15] Atoms in molecules (AIM) and Non-Covalent Interactions (NCI) analyses were conducted using Multiwfn software package.[s16] AIM bonding classifications have been made in accordance with the literature precedent.[s17] All iso-surfaces have been rendered at 0.05, unless otherwise stated.

1

HOMO

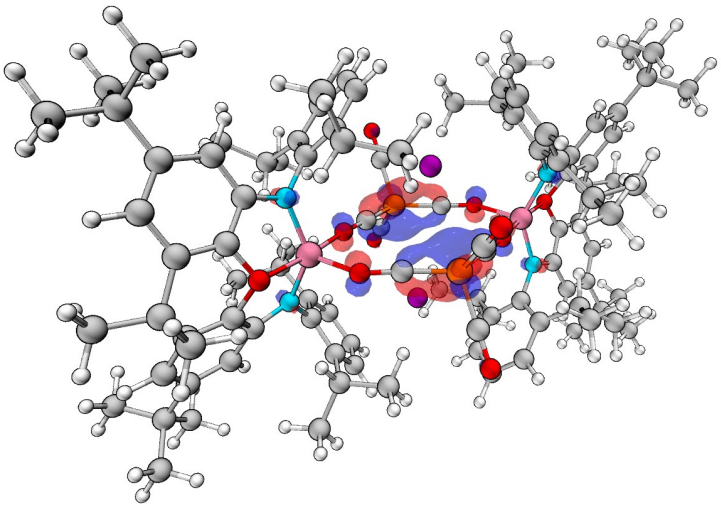

Figure s18: HOMO of **1**

LUMO

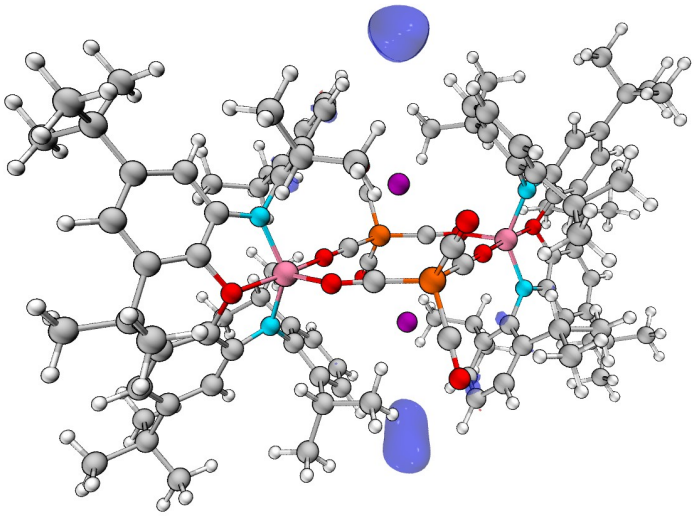

Figure s19: LUMO of **1**. Isosurfaces rendered at 0.02

2-crypt

HOMO

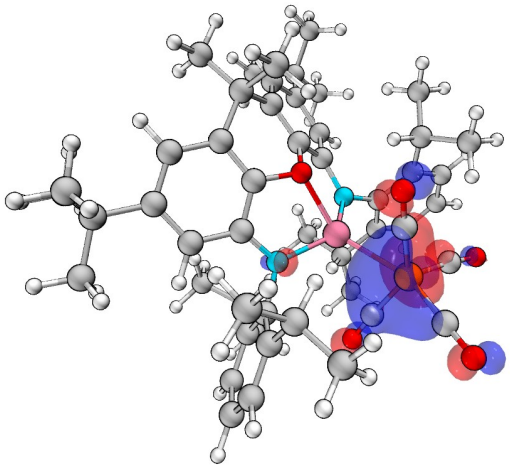

Figure s20: HOMO of **2-crypt**

LUMO

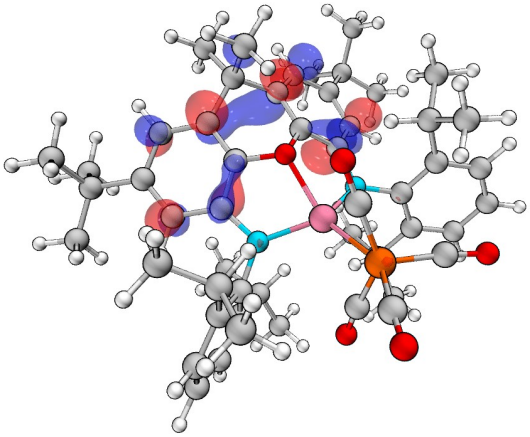

Figure s21: LUMO of **2-crypt**

HOMO-1

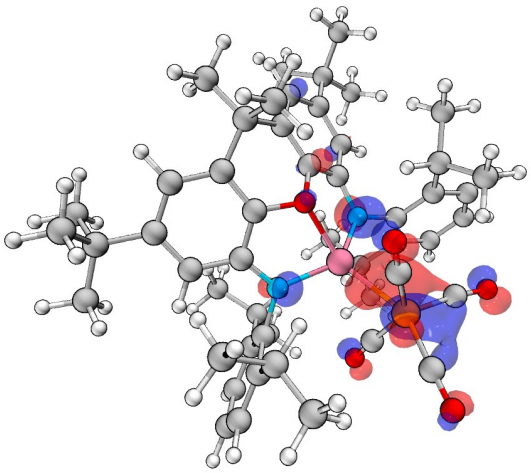

Figure s22: HOMO-1 of **2-crypt**

HOMO-6

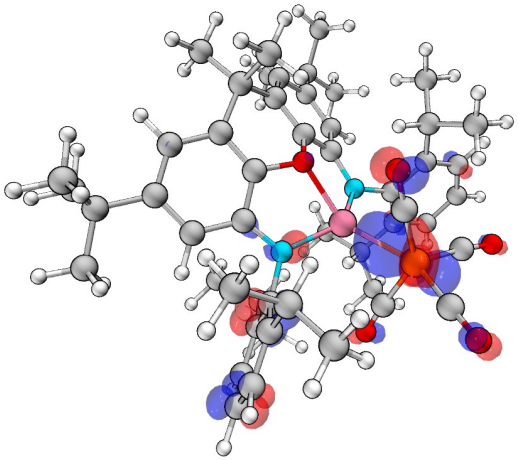

Figure s23: HOMO-6 of **2-crypt**

NCI-plot

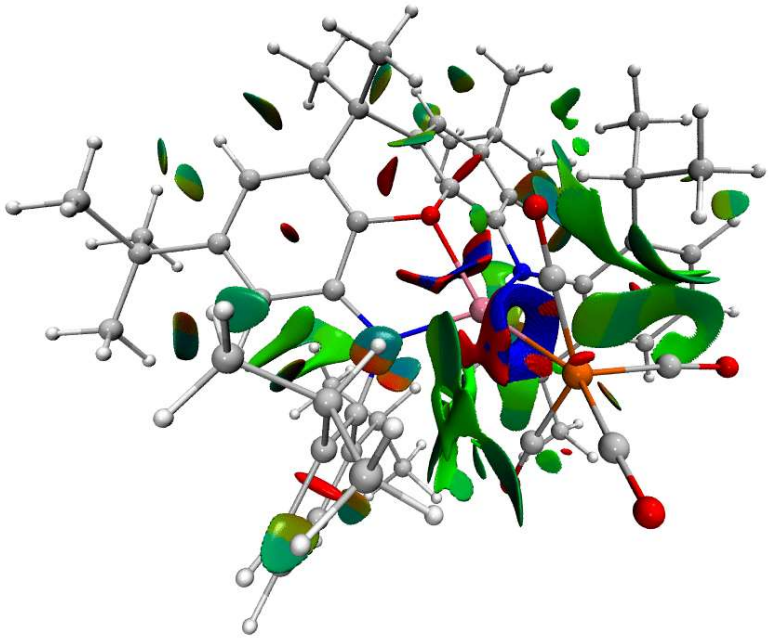

Figure s24: NCI plot of **2-crypt**. Blue regions indicate strongly attractive interactions, red regions indicate strongly repulsive interactions

2-crown

HOMO

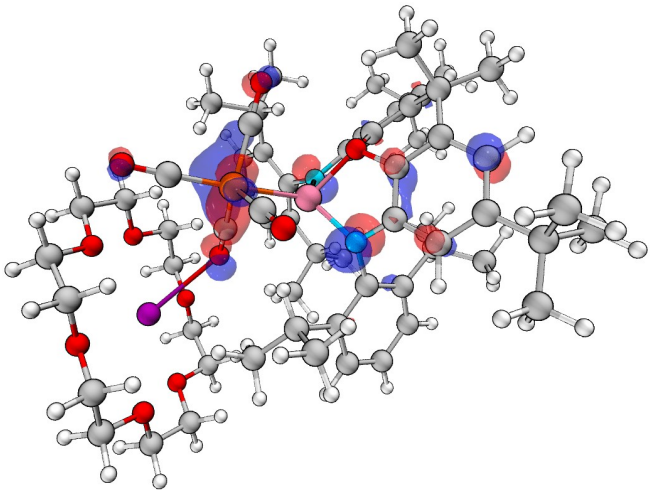

Figure s25: HOMO of **2-crown**

LUMO

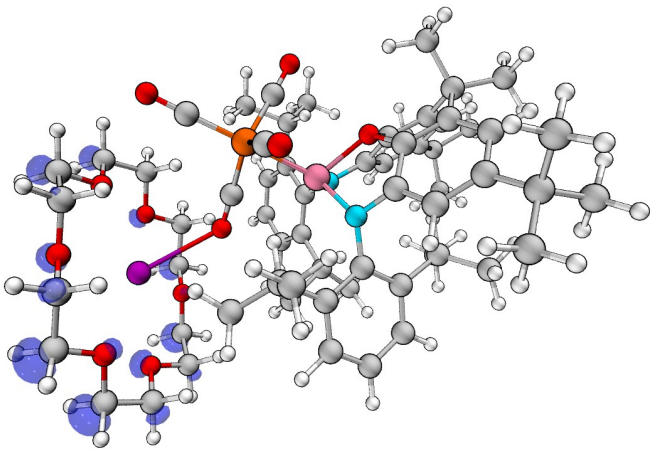

Figure s26: LUMO of **2-crown**. Isosurfaces rendered at 0.02.

HOMO-4

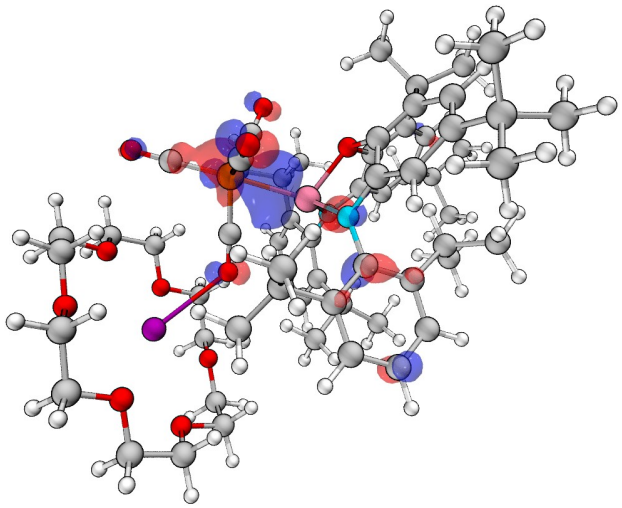

Figure s27: HOMO-4 of **2-crown**

3-crown

HOMO

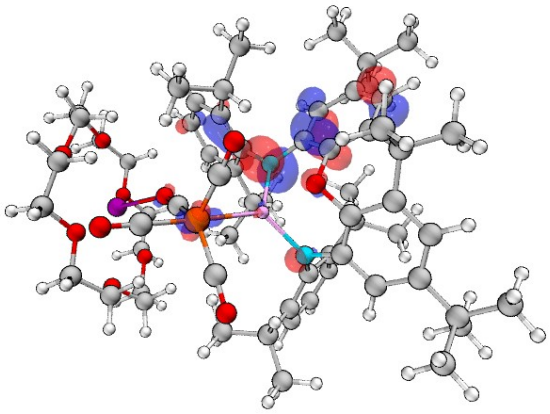

Figure s28: HOMO of **3-crown**

LUMO

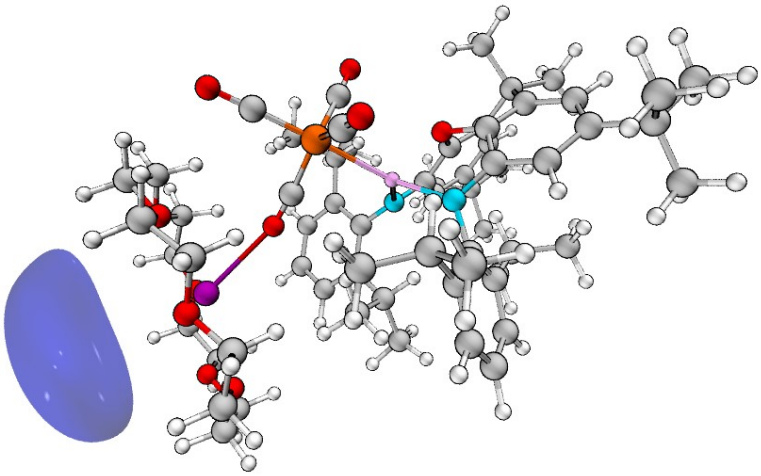

Figure s29: LUMO of **3-crown**. Isosurfaces rendered at 0.025

HOMO-4

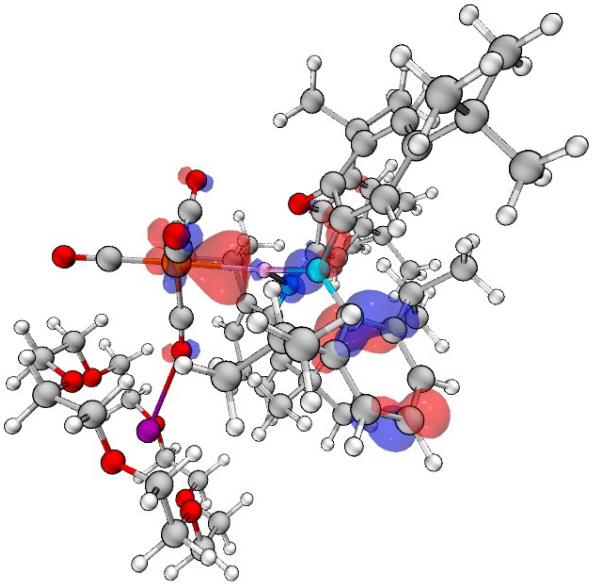

Figure s30: HOMO-4 of **3-crown**

4

HOMO

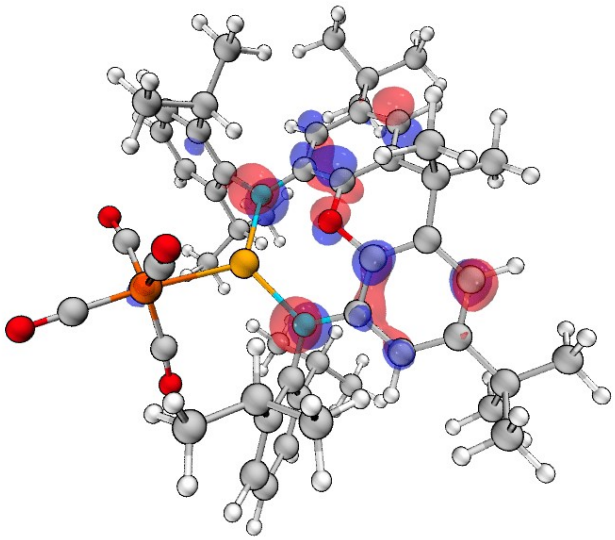

Figure s31: HOMO of **4**

LUMO

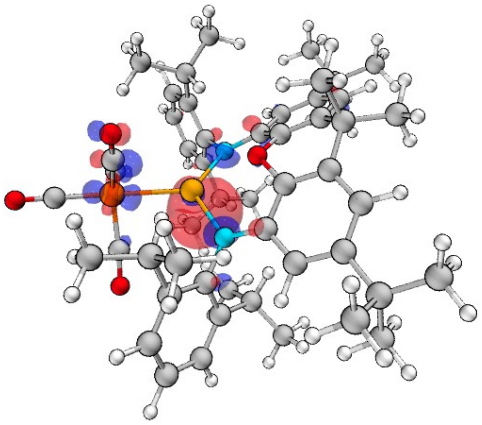

Figure s32: LUMO of **4**

HOMO-4

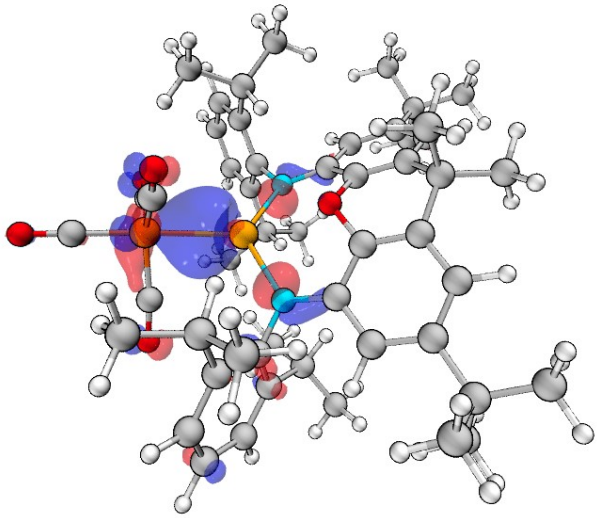

Figure s33: HOMO-4 of **4**

QT-AIM

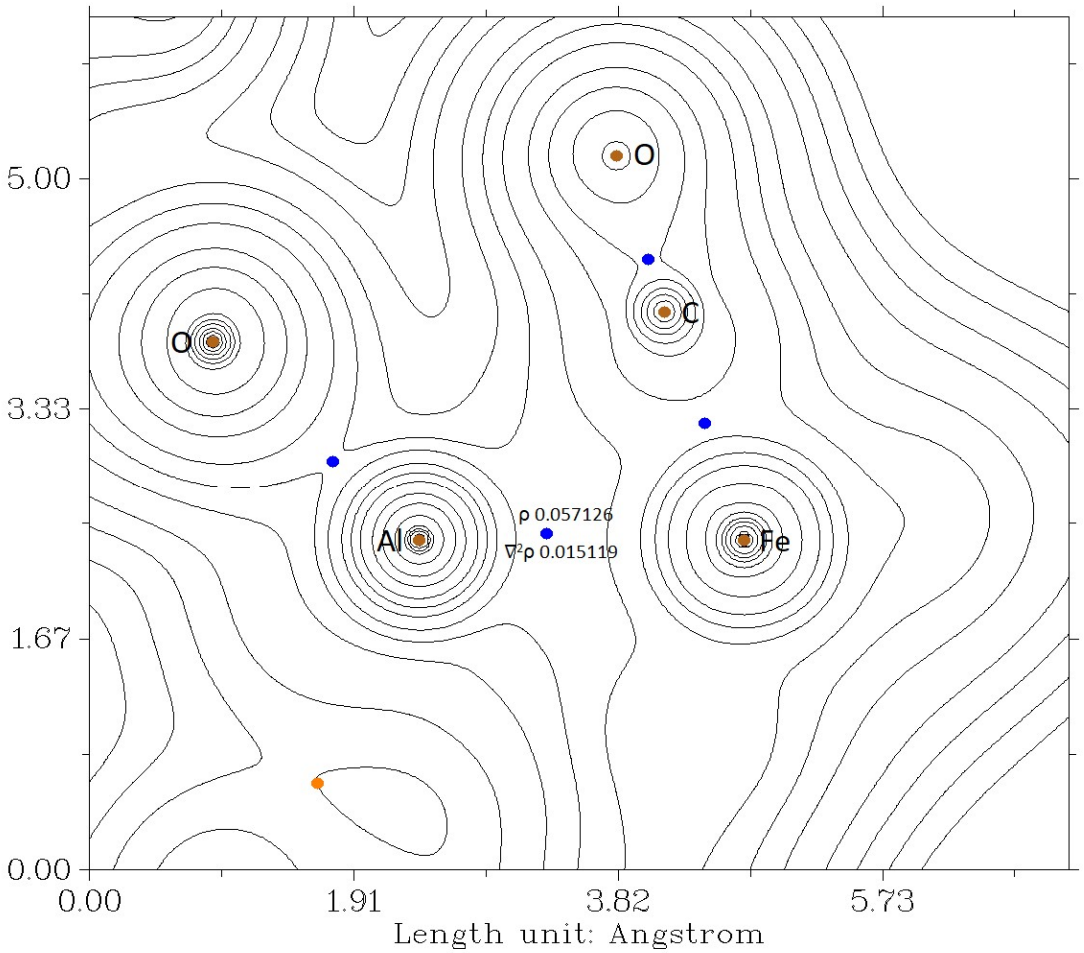

Figure s34: QT-AIM contour map of electron density in the Al–Fe region of **2-crypt**

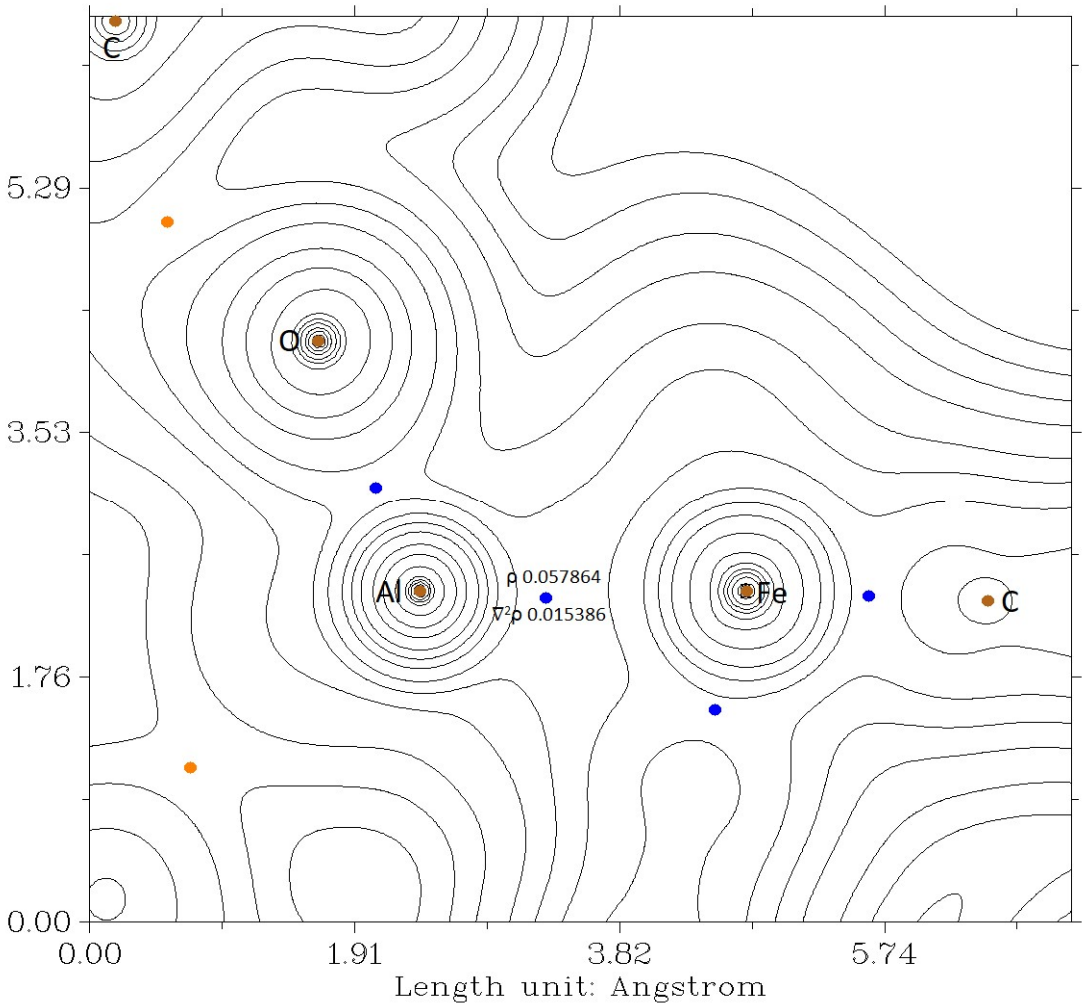

Figure s35: QT-AIM contour map of electron density in the Al–Fe region of **2-crown**

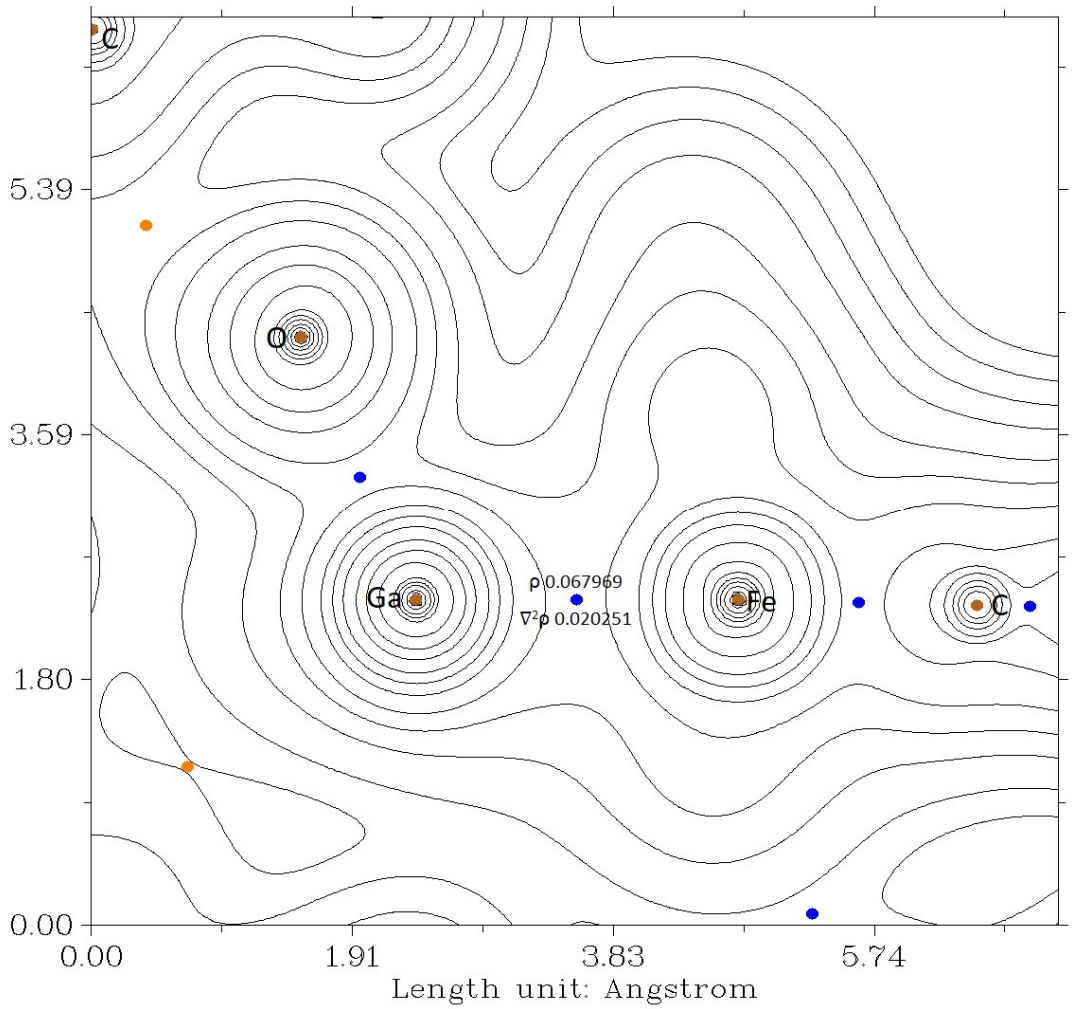

Figure s36: QT-AIM contour map of electron density in the Ga–Fe region of **3-crown**

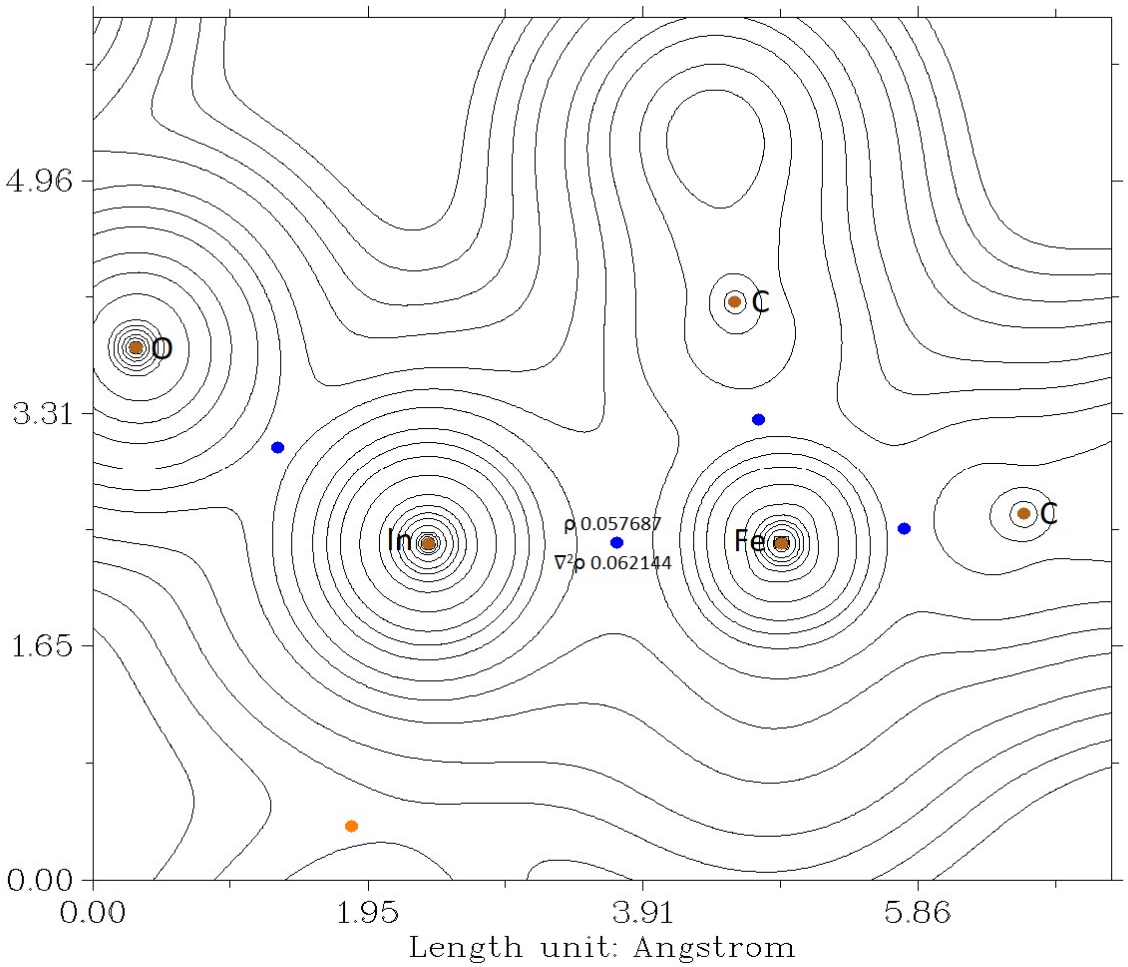

Figure s37: QT-AIM contour map of electron density in the In–Fe region of **4**

QTAIM parameters and WBIs

	2-crypt	**2-crown**	**3-crown**	**4**
ρ	**0.057126**	**0.057864**	**0.067969**	**0.057687**
$\nabla^2\rho$	**0.015119**	**0.015386**	**0.020251**	**0.062144**
V	-0.052513	-0.053231	-0.057701	-0.050277
G	0.028143	0.028539	0.031382	0.032906
E	-0.024367	-0.024692	-0.023190	-0.017370
ε	0.967191	0.413192	0.071881	0.117847
ELF	0.427464	0.431169	0.517386	0.360771
WBI	Al–Fe 0.3368, Al–C1 0.3342, Al–C2 0.3752	0.3315	0.4428	0.4690

Table s2: QTAIM parameters associated with E–Fe bonds

XYZ coordinates of calculated structures

1: -9149.842087326791 E_h				**2-cryptand: -3974.980414229571 E_h**			
Fe	14.523483	4.408251	8.101838	Fe	9.266396	4.078529	3.396226
K	15.119176	4.015754	4.671837	Al	10.377921	4.592930	5.400925
Al	15.425897	8.387874	6.119628	O	12.229864	5.363161	5.924707
O	14.204811	9.914186	6.582684	O	7.260260	6.059679	2.626510
O	14.539229	7.201452	7.229694	O	7.719580	2.611881	5.404047
O	16.374142	2.249200	7.398644	N	11.138447	3.086886	6.336153
N	16.628127	9.400483	7.168407	O	8.936520	2.235031	1.150816
N	14.495828	8.535484	4.483766	N	9.851770	6.292560	6.120591
O	11.757382	3.630957	7.548988	O	11.980458	4.985403	2.740897
O	14.409974	4.540539	11.024246	C	13.034959	4.451100	6.626720
C	14.853039	10.947348	7.277657	C	12.417851	3.224933	6.833778
C	13.616622	9.601205	4.352470	C	12.129705	6.568927	6.637384
C	14.236467	12.165351	7.456383	C	13.167980	2.284690	7.568349
C	12.774569	11.572899	5.571448	H	12.736601	1.304712	7.728898
C	13.454954	10.383641	5.491989	C	10.632591	1.750277	6.417639
C	13.527587	6.663585	3.223067	C	10.831779	7.047168	6.738420
C	16.162012	10.634672	7.611257	C	8.705232	7.034055	5.699632
C	17.828608	8.924092	7.777981	C	10.675295	8.244863	7.458752
C	14.567183	7.602337	3.407857	H	9.678448	8.662943	7.533430
C	12.917489	10.025719	3.217362	C	14.209701	4.873309	7.208971
H	13.010476	9.445985	2.304041	C	13.049838	8.293218	7.952006
C	15.599610	3.153450	7.684133	H	13.894488	8.763359	8.443006
C	14.985861	13.135996	8.123663	C	14.916735	3.922348	7.947312
H	14.551121	14.112728	8.299739	H	15.852667	4.200642	8.418282
C	12.114616	11.982965	4.405063	C	7.440056	6.742040	6.245803
H	11.567668	12.915712	4.414171	C	14.409998	2.621103	8.106561
C	16.296680	12.872990	8.554394	C	11.059486	0.781398	5.486436
C	19.031339	8.848305	7.030782	C	9.773709	1.398093	7.477088
C	16.878005	11.629896	8.292237	C	8.852218	8.063170	4.741746
H	17.905434	11.424892	8.567371	C	8.091071	5.323437	2.973189
C	12.817110	12.326752	6.904376	C	11.771598	8.868443	8.057068
C	17.067131	13.972732	9.294459	C	8.385260	3.183790	4.624376
C	12.174276	11.216323	3.235482	C	13.246130	7.112731	7.232181
C	17.806887	8.547893	9.143708	C	11.613968	10.176672	8.841609
C	14.597754	6.013742	7.555727	C	11.947159	1.124143	4.303947
C	19.126330	9.414850	5.619328	H	11.947569	2.213528	4.196397
H	18.311722	8.975303	5.031176	C	9.391123	0.064115	7.616376
C	15.684011	7.619071	2.541837	H	8.731367	-0.224168	8.429176
C	12.436915	13.797412	6.741686	C	10.651548	-0.541871	5.667188
H	11.414510	13.889612	6.363757	H	10.974990	-1.298289	4.956952
H	13.114107	14.314753	6.054684	C	9.082879	2.953322	2.054460
H	12.465291	14.305193	7.710131	C	10.168508	8.361543	4.038176
C	14.808736	5.653513	1.423544	H	10.916528	7.640910	4.381168
H	14.914206	4.886332	0.661130	C	14.563840	6.353878	7.049585
C	11.498507	11.678987	1.938199	C	7.731869	8.820468	4.402359
C	13.673913	5.694377	2.223534	H	7.831069	9.612395	3.664047
H	12.879207	4.968003	2.062268	C	15.235131	1.598097	8.896627
C	18.976275	8.037498	9.719442	C	6.344445	7.511425	5.855705

H	18.974335	7.757788	10.770728	H	5.361306	7.291065	6.258919
C	16.576344	8.687544	10.029120	C	15.089087	6.602062	5.615088
H	15.746216	9.054289	9.418612	H	14.359737	6.288951	4.863113
C	11.826445	11.653042	7.884121	H	16.012957	6.035506	5.453734
H	11.864057	12.153631	8.857638	H	15.295434	7.668833	5.473102
H	12.070968	10.597039	8.030564	C	9.835237	-0.904909	6.727276
H	10.807097	11.718790	7.489062	H	9.528915	-1.940446	6.851821
C	20.134892	7.883793	8.971843	C	10.057632	8.192280	2.515980
H	21.032524	7.474587	9.428067	H	9.758820	7.175107	2.254939
C	20.156891	8.289582	7.642158	H	11.030241	8.392916	2.051651
H	21.075080	8.178347	7.077715	H	9.326336	8.886560	2.086606
C	15.795514	6.620355	1.574452	C	9.288981	2.436392	8.471680
H	16.663913	6.592482	0.925539	H	9.301436	3.408060	7.963512
C	12.243491	6.694590	4.036683	C	6.487871	8.555546	4.952297
H	12.310164	7.520321	4.751604	H	5.623030	9.143968	4.657762
C	16.349474	14.279797	10.622595	C	10.165048	10.679290	8.858338
H	15.324486	14.624589	10.454306	H	9.791597	10.875034	7.847214
H	16.884533	15.062398	11.173534	H	10.111266	11.616536	9.423686
H	16.302982	13.384725	11.252814	H	9.493059	9.959683	9.338236
C	18.511843	13.567152	9.610826	C	7.291075	5.637211	7.274518
H	18.559841	12.688517	10.263602	H	7.932826	4.806565	6.956395
H	19.013732	14.389893	10.130682	C	15.624202	6.800193	8.053250
H	19.080445	13.353318	8.699011	H	15.854793	7.861243	7.914678
C	16.690894	8.753288	2.595106	H	16.553609	6.243711	7.896349
H	16.707949	9.137363	3.621717	H	15.292500	6.644332	9.085012
C	12.863019	3.914342	7.761690	C	13.395307	0.654847	4.517082
C	18.939394	10.942444	5.614465	H	13.430346	-0.434044	4.651640
H	17.964663	11.250228	5.992245	H	13.848531	1.124294	5.394609
H	19.043515	11.321463	4.591472	H	14.003897	0.907113	3.640597
H	19.712011	11.419317	6.229666	C	11.396695	0.536260	2.998479
C	16.143484	7.341972	10.619885	H	11.910961	0.984052	2.141128
H	15.249542	7.463866	11.239971	H	10.329878	0.741890	2.893535
H	16.921995	6.902378	11.255095	H	11.550403	-0.548836	2.948757
H	15.880886	6.624192	9.837207	C	10.896342	4.623125	3.028909
C	14.467976	4.481159	9.867441	C	12.489257	11.267790	8.195394
C	17.113203	15.246660	8.429282	H	13.549312	10.996521	8.212512
H	17.594007	15.041700	7.466754	H	12.372766	12.217709	8.731955
H	17.684210	16.029712	8.941432	H	12.200705	11.422755	7.149960
H	16.113085	15.641732	8.228845	C	7.786804	6.116743	8.647182
C	16.817260	9.704020	11.155662	H	7.187875	6.971799	8.985007
H	17.603627	9.360138	11.837619	H	8.834182	6.428426	8.603307
H	15.901371	9.837989	11.741335	H	7.697338	5.319877	9.394914
H	17.110100	10.678236	10.756168	C	10.680167	9.771137	4.373790
C	20.440052	9.087633	4.908329	H	9.994475	10.536192	3.989722
H	21.293724	9.551239	5.416798	H	11.661492	9.938709	3.914279
H	20.413145	9.495833	3.894593	H	10.780167	9.910689	5.454107
H	20.620321	8.014931	4.829824	C	7.855333	2.176035	8.942189
C	18.115453	8.349392	2.218748	H	7.792199	1.289449	9.583840
H	18.488933	7.537682	2.849381	H	7.185207	2.036881	8.088418
H	18.776686	9.212796	2.341346	H	7.496805	3.024786	9.534449
H	18.191608	8.035940	1.172151	C	5.871674	5.078165	7.375032

C	12.035920	5.410323	4.842383	H	5.867227	4.195534	8.021826
H	12.822945	5.273343	5.590018	H	5.495532	4.777284	6.392176
H	11.997366	4.524192	4.195541	H	5.176784	5.807373	7.809122
H	11.092094	5.447004	5.395132	C	12.060715	9.960403	10.300108
C	11.029132	6.954608	3.133935	H	11.456097	9.179190	10.773327
H	11.159706	7.867669	2.548973	H	11.943591	10.887007	10.875792
H	10.125671	7.067680	3.742862	H	13.109740	9.654707	10.361182
H	10.863105	6.122659	2.439721	C	10.239319	2.545150	9.673870
C	16.215427	9.909162	1.696611	H	9.884758	3.311679	10.373926
H	16.129264	9.573120	0.656297	H	11.253093	2.810469	9.359972
H	16.936533	10.733642	1.730901	H	10.288026	1.587472	10.207783
H	15.244136	10.295235	2.016825	C	15.473355	2.117431	10.326988
C	12.584515	11.958259	0.880815	H	16.055412	1.388983	10.905287
H	13.279240	12.728806	1.232518	H	14.518261	2.281972	10.837795
H	12.125461	12.306138	-0.052153	H	16.021250	3.064729	10.329415
H	13.165972	11.058995	0.655093	C	14.540876	0.234088	8.996286
C	10.554061	10.581605	1.414498	H	15.177249	-0.458167	9.559188
H	11.099414	9.673487	1.141125	H	14.362213	-0.202206	8.007429
H	10.029939	10.932911	0.518290	H	13.579819	0.304995	9.517176
H	9.807093	10.316407	2.170472	C	16.589384	1.391877	8.192084
C	10.676241	12.959434	2.129445	H	17.161552	2.323349	8.139360
H	9.878503	12.822030	2.867844	H	16.435232	1.035498	7.167547
H	10.207002	13.233813	1.178851	H	17.192697	0.650053	8.730438
H	11.300972	13.802707	2.442691				
Fe	18.503398	4.938146	4.847479				
K	17.907585	5.330227	8.277643				
Al	17.600645	0.958407	6.829014				
O	18.821514	-0.568041	6.365971				
O	18.487765	2.144796	5.719233				
O	16.652541	7.097351	5.549765				
N	16.398323	-0.053888	5.780099				
N	18.530381	0.810480	8.465052				
O	21.269418	5.715489	5.400665				
O	18.617177	4.806075	1.925091				
C	18.173155	-1.601050	5.670888				
C	19.409424	-0.255373	8.596317				
C	18.789568	-2.819127	5.492111				
C	20.251348	-2.227072	7.377257				
C	19.571144	-1.037711	7.456745				
C	19.498728	2.682221	9.725925				
C	16.864258	-1.288146	5.337211				
C	15.197923	0.422654	5.170464				
C	18.459079	1.743539	9.541039				
C	20.108291	-0.680158	9.731495				
H	20.015203	-0.100544	10.644880				
C	17.427108	6.192963	5.264812				
C	18.040059	-3.789622	4.824743				
H	18.474651	-4.766418	4.648663				
C	20.911066	-2.637377	8.543689				
H	21.457866	-3.570207	8.534549				
C	16.729277	-3.526419	4.394019				

C	13.995172	0.498626	5.917621	
C	16.148130	-2.283243	4.656187	
H	15.120704	-2.078128	4.381131	
C	20.208838	-2.980793	6.044253	
C	15.958693	-4.626022	3.653884	
C	20.851328	-1.870863	9.713356	
C	15.219731	0.798759	3.804713	
C	18.429235	3.332599	5.393489	
C	13.900064	-0.067842	7.329092	
H	14.714370	0.372078	7.917390	
C	17.342263	1.726783	10.407081	
C	20.588784	-4.451527	6.206850	
H	21.611139	-4.543932	6.584868	
H	19.911441	-4.968824	6.893736	
H	20.560428	-4.959216	5.238356	
C	18.217758	3.692018	11.525747	
H	18.112401	4.459023	12.288354	
C	21.526806	-2.333769	11.010710	
C	19.352542	3.651202	10.725706	
H	20.147354	4.377430	10.887113	
C	14.050394	1.309156	3.228867	
H	14.052337	1.588737	2.177549	
C	16.450337	0.659048	2.919398	
H	17.280240	0.291677	3.529827	
C	21.199714	-2.307149	5.064678	
H	21.162142	-2.807649	4.091113	
H	20.955374	-1.251095	4.918294	
H	22.219006	-2.373086	5.459850	
C	12.891774	1.463042	3.976419	
H	11.994180	1.872244	3.520116	
C	12.869694	1.057394	5.306147	
H	11.951502	1.168793	5.870553	
C	17.230866	2.725334	11.374644	
H	16.362526	2.753112	12.023641	
C	20.782870	2.651165	8.912357	
H	20.716372	1.825150	8.197743	
C	16.676413	-4.933205	2.325809	
H	17.701335	-5.278152	2.494188	
H	16.141284	-5.715729	1.774830	
H	16.723094	-4.038142	1.695591	
C	14.514082	-4.220177	3.337389	
H	14.466305	-3.341608	2.684510	
H	14.012054	-5.042872	2.817595	
H	13.945473	-4.006117	4.249146	
C	16.335022	0.592917	10.353409	
H	16.317656	0.209338	9.326616	
C	20.163798	5.432148	5.187803	
C	14.087518	-1.595369	7.334151	
H	15.062399	-1.902933	6.956576	
H	13.983317	-1.974284	8.357173	
H	13.315146	-2.072550	6.718880	

C	16.883743	2.004774	2.329388	
H	17.777554	1.882869	1.709114	
H	16.105320	2.445086	1.694568	
H	17.146728	2.721968	3.112475	
C	18.559031	4.865287	3.081897	
C	15.912297	-5.899950	4.519044	
H	15.431471	-5.694898	5.481542	
H	15.341155	-6.682875	4.006851	
H	16.912314	-6.295242	4.719543	
C	16.209269	-0.356814	1.792348	
H	15.423230	-0.012354	1.110305	
H	17.125246	-0.490893	1.206840	
H	15.915939	-1.331098	2.191324	
C	12.586035	0.258938	8.039747	
H	11.732675	-0.205040	7.531094	
H	12.612853	-0.149190	9.053514	
H	12.405318	1.331568	8.118152	
C	14.910671	0.997098	10.730273	
H	14.537395	1.809390	10.100261	
H	14.249100	0.134022	10.607211	
H	14.834832	1.309851	11.777105	
C	20.990249	3.935141	8.106139	
H	20.203493	4.071495	7.358102	
H	21.028277	4.821598	8.752564	
H	21.934298	3.898563	7.553756	
C	21.997257	2.391720	9.815230	
H	21.866839	1.478840	10.400503	
H	22.900762	2.278619	9.206373	
H	22.163104	3.223937	10.509172	
C	16.810292	-0.563546	11.251251	
H	16.896726	-0.228032	12.291714	
H	16.088951	-1.387810	11.216699	
H	17.781421	-0.949745	10.930698	
C	20.440556	-2.612991	12.067858	
H	19.745787	-3.383400	11.715939	
H	20.899373	-2.961028	13.000883	
H	19.859192	-1.713656	12.293538	
C	22.471308	-1.236579	11.534702	
H	21.926046	-0.328397	11.808053	
H	22.995192	-1.588046	12.430986	
H	23.218474	-0.971428	10.778909	
C	22.348934	-3.614311	10.819496	
H	23.146792	-3.476961	10.081219	
H	22.817992	-3.888825	11.770141	
H	21.724143	-4.457484	10.506102	
2-crown: -5498.661744725587 E_h				**3-crown : -7180.985061094257 E_h**
Fe	5.080323	4.122431	14.419651	Ga 9.171422 18.260465 20.754403
K	5.848076	8.806730	15.942223	Fe 9.125540 16.392534 19.311073
Al	2.824683	4.252903	13.753761	K 14.421586 15.785270 19.100205
O	2.172307	2.557518	13.044721	O 7.533088 19.561274 20.507784
O	6.824930	8.863691	13.249790	O 13.928336 15.466917 16.277506

O	5.185519	2.333395	12.104419	N	8.519296	18.319238	22.619266
O	4.223424	2.551394	16.736264	O	12.561788	13.909436	18.179221
O	7.999820	7.260195	15.243795	O	7.455617	18.144161	17.663850
O	4.501538	10.318728	14.039666	N	10.148140	19.889698	20.208321
N	2.272559	4.979744	12.087049	O	15.883932	17.281159	17.262773
O	4.177670	11.020904	16.759665	O	15.424702	15.517687	21.703140
N	1.445609	4.007265	15.057056	O	17.058389	16.777167	19.765275
O	7.619219	7.809743	17.972130	O	7.548345	14.940769	21.312806
O	5.358584	9.335725	18.717394	C	9.790776	22.339054	19.889111
O	4.447784	6.969097	14.518211	H	10.857241	22.510280	19.772891
O	7.969146	4.159360	14.887002	C	6.427687	18.798771	23.879728
C	5.132849	3.067387	13.007973	H	6.778937	18.231019	24.736874
C	1.560817	4.054825	11.328439	O	12.003965	16.820698	19.145200
C	2.655074	6.184593	11.420088	C	8.892769	23.414702	19.896142
C	-0.665229	3.565202	8.255355	C	6.714368	19.537045	21.649023
C	-1.376952	4.212537	14.081827	C	7.045352	21.882570	20.296470
H	-0.652329	3.444598	13.810889	C	7.234839	18.828309	22.734165
C	1.017319	2.685289	15.085031	C	7.974572	20.869222	20.245970
C	0.861405	4.269320	10.134208	C	4.906374	20.406410	22.898080
H	0.877626	5.265222	9.701340	H	4.057798	21.071387	22.988062
C	0.116763	3.241713	9.535764	O	9.204193	14.136020	17.460389
C	1.349621	1.898932	13.984350	C	5.676877	20.435367	21.728367
C	0.064309	1.971996	10.127717	O	13.461748	13.651354	20.812880
H	-0.530826	1.187098	9.680871	C	9.355671	21.019833	20.088162
C	-0.752643	5.135799	15.120836	C	7.526398	23.183379	20.107424
C	3.966476	7.309977	9.720897	H	6.833461	24.012985	20.145156
H	4.718178	7.272715	8.936328	C	5.591973	21.471619	20.597454
C	0.766999	1.707328	11.311116	C	5.245223	19.547264	23.951787
C	3.646010	6.139312	10.408775	C	12.580532	19.696533	20.434115
C	-1.280951	0.127474	16.812554	C	4.378127	19.431410	25.212161
C	1.493624	2.751803	11.823709	C	12.462553	19.447091	21.923506
C	0.573216	4.990099	15.607737	H	11.457645	19.751952	22.226605
C	-1.400715	2.343478	7.691352	C	11.438739	19.898944	19.624061
H	-0.705625	1.533751	7.443780	C	4.739641	22.672291	21.002440
H	-1.924590	2.626411	6.772047	H	5.133951	23.161882	21.898809
H	-2.148587	1.958372	8.393064	H	3.709982	22.358839	21.200165
C	2.030410	7.411585	11.732540	H	4.704861	23.403299	20.188930
C	3.346103	8.515793	10.015401	C	9.449607	24.835510	19.725874
H	3.600196	9.414438	9.458278	C	10.408546	20.103562	17.269734
C	4.385653	4.865843	10.043952	H	9.491300	19.988501	17.852404
H	4.006758	4.055744	10.669325	C	5.181807	19.867324	26.451852
C	0.798459	0.385406	12.102116	H	6.088064	19.267933	26.581363
C	-1.068932	7.033503	16.607919	H	4.571409	19.753537	27.355673
H	-1.705178	7.826548	16.991533	H	5.481044	20.917980	26.370842
C	-1.750167	4.929876	12.780282	C	8.192438	15.545604	20.559975
H	-2.441423	5.762089	12.954791	C	9.342350	18.379841	23.782281
H	-2.233127	4.222033	12.096721	C	9.809251	19.632120	24.266804
H	-0.862658	5.316656	12.275524	C	11.590235	20.048763	18.222662
C	0.174095	2.079330	16.031083	C	4.981292	20.821780	19.333131
H	-0.082241	2.642905	16.920948	H	4.953935	21.551280	18.516433
C	-0.403676	0.834042	15.772547	H	3.959232	20.489543	19.544848

C	2.397797	8.559742	11.024764	H	5.563895	19.958441	19.002806
H	1.906091	9.501734	11.256444	C	8.115539	17.467778	18.339612
C	-1.711166	4.654382	8.562308	C	10.704212	19.637529	25.337137
H	-2.407343	4.314111	9.336575	H	11.071472	20.588265	25.715075
H	-2.286842	4.893868	7.660132	C	8.346675	25.901173	19.706347
H	-1.240227	5.576204	8.917518	H	7.785960	25.923764	20.646992
C	0.665467	0.774140	13.582955	H	7.641219	25.738829	18.884061
C	-1.543101	6.165156	15.635082	H	8.799049	26.889226	19.568359
H	-2.556147	6.288202	15.259711	C	11.126459	18.459259	25.940867
C	4.549480	3.175492	15.811917	H	11.830414	18.492053	26.768294
C	1.055334	5.865461	16.606866	C	13.843631	19.695483	19.840132
C	0.301314	4.078919	7.171699	H	14.721112	19.561723	20.469866
H	0.807777	4.997881	7.481691	C	8.301619	21.567965	24.740982
H	-0.247350	4.294844	6.247279	H	8.814357	21.844453	25.670493
H	1.068014	3.328425	6.950276	H	7.508351	20.858580	24.981961
C	7.441967	7.608637	12.958006	H	7.840344	22.469611	24.321372
H	7.854880	7.613859	11.934962	C	10.397532	25.155264	20.897603
H	6.704763	6.794290	13.028953	H	10.815296	26.163068	20.784454
C	-2.662522	-0.205920	16.218045	H	11.229920	24.446522	20.950071
H	-3.174481	0.702703	15.884666	H	9.860046	25.111432	21.851062
H	-3.286852	-0.695488	16.974706	C	9.104042	15.860094	24.043018
H	-2.588149	-0.883766	15.362692	H	8.295537	16.074839	23.340248
C	-0.202023	0.216226	14.524516	C	10.459038	18.936019	16.271828
H	-0.740672	-0.691728	14.280171	H	11.311804	19.031591	15.587774
C	3.120012	6.958889	17.626030	H	9.544605	18.919655	15.669204
H	2.688220	7.394365	18.535646	H	10.533266	17.978020	16.796030
H	3.065047	7.705954	16.825322	C	10.615496	17.246962	25.503415
H	4.176180	6.758348	17.839525	H	10.908807	16.328022	26.005548
C	5.724778	9.118107	12.374959	C	9.708373	17.189301	24.442862
H	4.977868	8.313677	12.443836	C	12.438177	13.669246	16.783304
H	6.070387	9.173324	11.329093	H	11.443098	13.262930	16.548808
C	-2.608961	3.501098	14.662567	H	13.206791	12.954502	16.442228
H	-2.380960	3.045373	15.629601	C	12.594728	17.955733	22.258938
H	-2.942681	2.709522	13.982008	H	11.825598	17.360905	21.754326
H	-3.441835	4.200497	14.801502	H	12.485417	17.800349	23.338595
C	8.559884	7.369695	13.937919	H	13.573694	17.570836	21.942663
H	9.070760	6.432601	13.666105	C	10.384949	22.001074	23.431131
H	9.289849	8.196674	13.905785	H	10.992963	22.232162	24.313147
C	4.689217	5.807763	14.448282	H	9.907053	22.929805	23.103166
C	2.160877	-0.307093	11.861527	H	11.050470	21.682502	22.626560
H	2.996822	0.332386	12.155742	C	9.298216	20.964602	23.735394
H	2.272063	-0.549042	10.799149	H	8.759060	20.783159	22.802606
H	2.212070	-1.233573	12.443410	C	16.788964	15.832245	21.944884
C	2.428461	5.658771	17.211064	H	17.437074	14.989930	21.649367
H	3.063591	5.184087	16.459180	H	16.955100	16.037436	23.015971
C	0.943105	7.536135	12.780595	C	17.424480	17.898903	18.965704
H	0.754477	6.541252	13.196360	H	18.476695	18.174289	19.150054
C	-0.324507	-0.554157	11.669097	H	16.790211	18.764910	19.216203
H	-0.278480	-1.488809	12.236472	C	9.162761	15.032215	18.199837
H	-0.215048	-0.813000	10.611543	C	12.875877	20.074238	17.683042
H	-1.310229	-0.102241	11.819877	H	12.995672	20.214227	16.610849

C	6.818199	4.160012	14.709834	C	17.148169	17.066454	21.158333
C	0.222276	6.873977	17.090931	H	16.461847	17.889580	21.421019
H	0.586901	7.542864	17.866251	H	18.174085	17.374135	21.421450
C	3.166738	11.246337	15.775248	C	12.593299	14.991377	16.077127
H	2.560645	12.126867	16.046947	H	12.396283	14.859911	15.000385
H	2.500398	10.371328	15.707817	H	11.866229	15.712123	16.483522
C	4.149921	4.466381	8.581297	C	10.325234	21.438996	16.519996
H	4.553439	5.214608	7.888909	H	10.234216	22.275244	17.216781
H	3.082237	4.347641	8.375724	H	9.449674	21.447562	15.861247
H	4.645296	3.512206	8.370354	H	11.214717	21.601689	15.899264
C	6.393239	8.990395	19.633738	C	3.942910	17.962639	25.379779
H	5.988706	8.911911	20.656710	H	3.379688	17.624806	24.503263
H	7.180740	9.762622	19.628976	H	3.306412	17.852786	26.266075
C	5.886137	5.004763	10.336246	H	4.805940	17.300442	25.496627
H	6.403437	4.067099	10.107510	C	10.229220	24.938669	18.402290
H	6.049816	5.227280	11.395439	H	9.580150	24.705217	17.551221
H	6.337686	5.802088	9.733285	H	11.080950	24.251991	18.376033
C	4.738490	10.575754	19.036194	H	10.616212	25.956224	18.270526
H	5.474877	11.396036	18.991908	C	17.256594	17.546196	17.508819
H	4.316843	10.544471	20.055101	H	17.604392	18.399522	16.901791
C	-0.367622	8.050685	12.169252	H	17.872300	16.667352	17.252358
H	-1.163802	8.030889	12.921587	C	10.844383	16.668453	19.264594
H	-0.683866	7.438803	11.318359	C	14.001187	19.905892	18.477942
H	-0.260623	9.083752	11.818335	H	14.991828	19.930321	18.031955
C	-1.496897	0.975627	18.071742	C	12.145448	12.826032	18.999383
H	-0.549400	1.212411	18.567192	H	12.832943	11.969518	18.890599
H	-2.114807	0.417953	18.783649	H	11.129079	12.503328	18.723009
H	-2.014624	1.915008	17.847545	C	14.118126	16.773860	15.744837
C	5.101184	10.436371	12.748950	H	13.492207	17.505915	16.283324
H	5.862742	11.234754	12.759707	H	13.842471	16.801184	14.676898
H	4.334940	10.687442	11.998270	C	13.468945	20.255062	22.750324
C	3.824839	11.497019	14.442454	H	14.490730	19.874414	22.628968
H	3.044157	11.765806	13.709860	H	13.213727	20.181031	23.813181
H	4.528589	12.344158	14.520561	H	13.466880	21.312422	22.466716
C	1.373108	8.448845	13.936504	C	15.574847	17.139230	15.878400
H	1.525439	9.476195	13.580445	H	16.203344	16.355075	15.424723
H	2.311366	8.104812	14.378989	H	15.761124	18.088720	15.348957
H	0.599685	8.458779	14.712275	C	8.497344	15.119999	25.241972
C	-0.579093	-1.180648	17.228815	H	9.264691	14.785424	25.949616
H	-0.444291	-1.848649	16.372461	H	7.954159	14.234154	24.895081
H	-1.172974	-1.708327	17.984961	H	7.795394	15.760004	25.786912
H	0.410216	-0.969688	17.648606	C	3.114652	20.296960	25.137597
C	2.338087	4.690910	18.400112	H	3.356794	21.362956	25.065435
H	1.686639	5.103276	19.180844	H	2.521664	20.152879	26.047143
H	3.330915	4.509874	18.827449	H	2.487523	20.023474	24.282149
H	1.935283	3.724138	18.084414	C	12.124596	13.313580	20.424956
C	8.945369	6.861996	16.226447	H	11.464282	14.192419	20.502800
H	9.698392	7.654063	16.382218	H	11.728576	12.519357	21.078999
H	9.456830	5.939302	15.914442	C	10.126713	14.976098	23.320797
C	3.621977	10.829656	18.056671	H	10.472475	15.464670	22.403832
H	2.923402	9.976610	18.053566	H	9.678552	14.016184	23.039374

H	3.068042	11.729703	18.373551	H	10.994266	14.782732	23.965164
C	6.976938	7.660269	19.231032	C	13.522326	14.144179	22.146391
H	7.701230	7.341996	20.000130	H	13.123567	13.397569	22.853972
H	6.181528	6.898421	19.174943	H	12.921192	15.061612	22.250038
C	8.203215	6.587036	17.507619	C	14.960822	14.424024	22.494995
H	7.420465	5.831725	17.329350	H	15.030053	14.677156	23.565772
H	8.908420	6.194257	18.258042	H	15.576996	13.529808	22.304341

4: -3922.687438121882 E_h

In	6.483577	12.681516	6.127059
Fe	8.487142	13.945666	6.963889
O	4.162628	12.841888	5.209244
O	6.880518	16.199545	5.987056
O	10.744638	15.699682	7.509997
N	4.999116	11.925804	7.556815
O	8.344497	13.118845	9.771921
O	10.193366	12.112153	5.435334
N	6.427476	12.280871	3.957579
C	3.203378	12.238501	6.012979
C	1.912248	12.089440	5.554302
C	5.171578	11.849056	1.871541
H	6.092134	11.630561	1.339441
C	1.377142	11.011772	7.666411
C	4.054295	12.497247	3.866981
C	0.988639	11.460812	6.400367
H	-0.028420	11.322041	6.059700
C	5.271141	12.210899	3.228118
C	2.703197	11.174046	8.078717
H	3.025310	10.817561	9.052529
C	2.759788	11.994564	1.933920
H	1.796842	11.888901	1.453403
C	2.812888	12.369419	3.283901
C	3.669447	11.774183	7.251629
C	0.394766	10.321348	8.621262
C	10.027020	11.549875	1.899299
H	10.964730	11.362138	1.382790
C	3.937417	11.749429	1.222181
C	1.599134	12.657197	4.168897
C	9.563265	12.848886	2.047888
H	10.145136	13.672056	1.642608
C	9.295752	10.491236	2.421411
H	9.668642	9.476625	2.307926
C	5.334006	11.833029	8.931444
C	6.270513	10.620342	10.799200
H	6.785772	9.747275	11.192813
C	7.486112	15.273284	6.361230
C	8.371779	13.119922	2.722390
C	5.264217	12.766734	11.159902
H	5.003030	13.578353	11.834925
C	7.638217	12.039305	3.255449
C	4.983226	12.892081	9.801764
C	9.845889	14.998320	7.297007

C	8.096092	10.715153	3.094355
C	0.313152	12.070738	3.586983
H	-0.539518	12.305297	4.231678
H	0.381944	10.983489	3.477426
H	0.103724	12.508883	2.606328
C	6.001017	10.698085	9.431864
C	9.460111	12.823897	5.989513
C	5.895950	11.637207	11.663428
H	6.115576	11.561229	12.725037
C	7.101802	14.952976	1.571266
H	7.762692	14.917943	0.695584
H	6.716933	15.975054	1.670089
H	6.256600	14.282138	1.389003
C	5.658784	8.271912	8.845489
H	5.868461	7.930365	9.866260
H	5.946138	7.469912	8.154770
H	4.578832	8.431883	8.755787
C	6.428063	9.561010	8.525463
H	6.168518	9.845337	7.499229
C	4.341840	14.170592	9.292284
H	4.259165	14.093081	8.203255
C	0.895968	8.898169	8.933493
H	0.995763	8.314788	8.011492
H	0.192099	8.381482	9.598268
H	1.873254	8.916016	9.425075
C	2.925375	14.357105	9.852821
H	2.290387	13.502613	9.599268
H	2.466700	15.262156	9.437173
H	2.944218	14.460540	10.944764
C	7.869492	14.545500	2.839946
H	7.162184	14.572017	3.674713
C	8.311172	13.403485	8.647355
C	5.220239	15.391997	9.597748
H	5.318998	15.553646	10.677481
H	4.777219	16.294224	9.159953
H	6.223231	15.265780	9.178513
C	-1.016514	10.208581	8.031866
H	-1.440519	11.194538	7.811886
H	-1.675851	9.713919	8.754213
H	-1.024040	9.615245	7.110786
C	8.983001	15.552082	3.143122
H	9.580864	15.228172	4.000734
H	8.543213	16.525197	3.386706
H	9.648473	15.695093	2.283334
C	1.432021	14.191263	4.295620
H	2.337756	14.651158	4.700653
H	0.596566	14.422904	4.966211
H	1.233721	14.629200	3.310640
C	7.943887	9.335247	8.595003
H	8.488351	10.251175	8.340631
H	8.248997	8.547607	7.896925

H	8.254079	9.031510	9.601212
C	7.320618	9.557207	3.691255
H	6.296253	9.902624	3.866771
C	3.926309	11.366467	-0.262958
C	0.300447	11.123941	9.932791
H	1.272454	11.199153	10.429597
H	-0.399350	10.641447	10.626830
H	-0.054478	12.141625	9.735386
C	4.622122	10.005607	-0.454065
H	5.668190	10.042628	-0.136636
H	4.599635	9.709851	-1.510559
H	4.119622	9.230611	0.135283
C	7.922805	9.172257	5.048843
H	7.323631	8.394608	5.537957
H	7.974892	10.037845	5.719528
H	8.948582	8.803315	4.929802
C	7.241953	8.340150	2.765025
H	8.221935	7.871818	2.618333
H	6.846813	8.619814	1.782671
H	6.578235	7.582275	3.196765
C	4.683115	12.440742	-1.067683
H	4.213984	13.421749	-0.933416
H	4.676716	12.194929	-2.137306
H	5.724949	12.523811	-0.743766
C	2.505790	11.258903	-0.830930
H	2.555442	10.985317	-1.891029
H	1.969957	12.211389	-0.755683
H	1.920967	10.490658	-0.312914

References for supporting information

s1 J. Hicks, P. Vasko, J. M. Goicoechea, S. Aldridge, *Nature* **2018**, *557*, 92-95.

s2 L. P. Griffin, M. A. Ellwanger, A. E. Crumpton, M. M. D. Roy, A. Heilmann, S. Aldridge, *Angewandte Chemie International Edition* **2024**, *63*, e202404527.

s3 J. Cosier, A. M. Glazer, *Journal of Applied Crystallography* **1986**, *19*, 105-107.

s4 A. Technologies, **2011**.

s5 G. Sheldrick, *Acta Crystallographica Section A* **2015**, *71*, 3-8.

s6 G. Sheldrick, *Acta Crystallographica Section C* **2015**, *71*, 3-8.

s7 O. V. Dolomanov, L. J. Bourhis, R. J. Gildea, J. A. K. Howard, H. Puschmann, *Journal of Applied Crystallography* **2009**, *42*, 339-341.

s8 F. Neese, *WIREs Computational Molecular Science* **2012**, *2*, 73-78.

s9 F. Neese, *WIREs Computational Molecular Science* **2022**, *12*, e1606.

s10 S. Grimme, A. Hansen, S. Ehlert, J.-M. Mewes, *The Journal of Chemical Physics* **2021**, *154*, 064103.

s11 J.-D. Chai, M. Head-Gordon, *Physical Chemistry Chemical Physics* **2008**, *10*, 6615-6620.

s12 E. Caldeweyher, C. Bannwarth, S. Grimme, *The Journal of Chemical Physics* **2017**, *147*, 034112.

s13 F. Weigend, R. Ahlrichs, *Physical Chemistry Chemical Physics* **2005**, *7*, 3297-3305.

s14 J. K. B. E. D. Glendening, A. E. Reed, J. E. Carpenter, J. A. Bohmann, C. M. Morales, P. Karafiloglou, C. R. Landis, F. Weinhold, **2018**.

s15 E. D. Glendening, C. R. Landis, F. Weinhold, *Journal of Computational Chemistry* **2019**, *40*, 2234-2241.

s16 T. Lu, F. Chen, *Journal of Computational Chemistry* **2012**, *33*, 580-592.

s17 R. Bianchi, G. Gervasio, D. Marabello, *Inorganic Chemistry* **2000**, *39*, 2360-2366.

Conclusions and Outlook

With the reported complexes in hand, onward reactivity studies should be pursued, in particular those which make use of the high electron density at the iron centre. Photolytic or chemical removal of one or more ancillary carbonyl ligand to permit the coordination and onward activation of small molecule substrates would be of particular interest, as the field looks to utilize these ligand complexes as catalysts based on sustainable metals.

Additional computational studies on the reported compounds could also be undertaken in order to probe how the nature of the Fe–E interaction is affected as group 13 is descended. These could include an analysis of the Electron Localisation Function (ELF), to probe how the metal-metal bond is polarised in each case. EDA-NOCV could also be performed, providing information on the most suitable bonding description for these species (E -> Fe dative bond, Fe -> E dative bond, covalent Fe–E bond).

The use of these complexes as single source precursors could also be investigated, with a view to synthesising group 13-iron alloys with potentially different composition or structure to those accessed by conventional methodologies. Prior work has indicated that such main group-transition metal intermetallic phases have great potential as functional materials, such as electrocatalyst coatings for water electrolysis with low overpotentials.

Additionally, as for the previous chapter, and particularly in light of the methodological insights this study has revealed, the synthesis of analogous complexes of other trielyl species or alternative anionic ligand systems would facilitate further comparisons between such fragments, and a library of data might help to inform design and selection of electron donating moieties for future applications.

Statement of Authorship for joint/multi-authored papers for PGR thesis

To appear at the end of each thesis chapter submitted as an article/paper

The statement shall describe the candidate's and co-authors' independent research contributions in the thesis publications. For each publication there should exist a complete statement that is to be filled out and signed by the candidate and supervisor **(only required where there isn't already a statement of contribution within the paper itself).**

Title of Paper	Synthesis and analysis of iron-trielyl complexes
Publication Status	□Published □ Accepted for Publication □Submitted for Publication √Unpublished and unsubmitted work written in a manuscript style
Publication Details	Liam P. Griffin, Alexis Bauer, Dr Agamemnon E. Crumpton, Dr. Mathias A. Ellwanger, Dr. Anja Wiesner, Dr. Andreas Heilmann, Prof. Dr. Michael L. Neidig, Prof. Simon Aldridge

Student Confirmation

Student Name:	Liam P. Griffin		
Contribution to the Paper	Performed all synthetic work, as well as some crystallographic work. Performed all spectroscopic measurements excluding Mössbauer measurements. Prepared samples for Mössbauer spectroscopy. Performed all quantum chemical calculations. Analysed and interpreted all data. Wrote the manuscript and prepared the SI.		
Signature	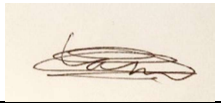	Date	19 September 2024

Supervisor Confirmation

By signing the Statement of Authorship, you are certifying that the candidate made a substantial contribution to the publication, and that the description described above is accurate.

Supervisor name and title: Professor Simon Aldridge		
Supervisor comments: I can confirm that Mr Griffin made a substantial contribution to the work described in this chapter, and that the above description is accurate.		
Signature 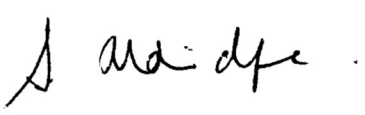	Date	20 September 2024

Synthesis and reactivity of a bis-aluminyl magnesium species

Introduction

In this final chapter, a magnesium species bearing an all-aluminyl ligand set is reported. Initially, uses of this species as a more covalent (and therefore potentially less reactive and less reducing) source of nucleophilic aluminium(I) were investigated, by analogy with Grignard chemistry commonly applied in organic synthesis. However, it was found that this species was still highly reducing, and would yield aluminium halides in reactions with a diverse range of electrophilic metal halide substrates. Therefore, given the unusual trimetallic structure of this species, and the potential subtleties presented by the similar electronegativities of aluminium and magnesium, small molecule reactivity was explored. Whilst this species was indeed shown to be less reactive than its potassium analogue (being unable to activate H_2 and benzene even under forcing conditions), facile reactivity with a number of substrates was nonetheless demonstrated. These included methyl iodide, which confirmed a nucleophilic mode of reactivity for the aluminium centre, and the kinetically inert gas SF_6, for which reductive defluorination yielded an unusual bridging tetrafluoride moiety containing a solubilized MgF_2 unit. However, most interestingly, photolytic activation of bis(aluminyl) magnesium yielded an altogether different and novel mode of reactivity, in which magnesium metal was eliminated and radical-type behaviour was observed for the aluminium fragments. EPR studies confirmed the presence of electron-unpaired intermediates in this reaction.

Bis(Aluminyl)Magnesium: a Source of Nucleophilic or Radical Aluminium-Centred Reactivity

Liam P. Griffin,[a] Mathias A. Ellwanger,[a] Jonathon Clark,[a] William K. Myers,[a] Aisling F. Roper,[a] Andreas Heilmann,[a] Simon Aldridge*[a]

[a] Mr. L. P. Griffin, Dr. M. A. Ellwanger, Mr. J. Clark, Dr. W. K. Myers, Ms. A. F. Roper, Dr. A. Heilmann, Prof. S. Aldridge
Inorganic Chemistry Laboratory, Department of Chemistry
University of Oxford
South Parks Road, Oxford, OX1 3QR (UK)
E-mail: simon.aldridge@chem.ox.ac.uk

Abstract

The homoleptic magnesium bis(aluminyl) compound $Mg[Al(NON)]_2$ (NON = 4,5-bis(2,6-diisopropylanilido)-2,7-di-tert-butyl -9,9-dimethylxanthene) can be accessed from $K_2[Al(NON)]_2$ and MgI_2 and shown to possess a non-linear geometry (∠Al–Mg–Al = 164.8(1)°) primarily due to the influence of dispersion interactions. This compound acts a four-electron reservoir in the reductive de-fluorination of SF_6, and reacts thermally with polar substrates such as MeI via nucleophilic attack through aluminium, consistent with the QT-AIM charges calculated for the metal centres, and a *formal* description as a Al(I)–Mg(II)–Al(I) trimetallic. On the other hand, under photolytic activation, the reaction with 1,5-cyclooctadiene leads to the stereo-selective generation of transannular cycloaddition products consistent with radical based chemistry, emphasizing the covalent nature of the Mg–Al bonds and a description as a Al(II)–Mg(0)–Al(II) *synthon*. Consistently, photolysis of $Mg[Al(NON)]_2$ in hexane in the absence of COD generates $[Al(NON)]_2$ together with magnesium metal.

Introduction

Metal-metal bonded systems have played a central role in the recent development of main group chemistry,[1] both from a fundamental perspective in providing the driver for new models of electronic structure/bonding,[2] and from the viewpoint of defining new patterns of reactivity towards small molecules.[3] Landmark examples include Power's digermyne, $Ar^{Dipp}GeGeAr^{Dipp}$ (Ar^{Dipp} = 2,6-$Dipp_2C_6H_3$; Dipp = 2,6-$^{i}Pr_2C_6H_3$) and related tin compounds which enabled unprecedented main group activation of H_2,[4] together with Carmona's (η^5-C_5Me_5)ZnZn(η^5-C_5Me_5) and Jones' ($Nacnac^{Dipp}$)MgMg($Nacnac^{Dipp}$) ($Nacnac^{Dipp}$ = $HC(MeCDippN)_2$) which accessed previously ill-defined oxidation states for these pre- and post-transition elements.[5,6]

Within this field, a number of systems have recently been reported which take the assembly of covalent metal-metal bonds of this sort one step further by defining trimetallic 'chains' in which a (two-coordinate) central metal atom can be viewed as possessing a formal oxidation state of zero (Figure 1). These include both homo- and hetero-trimetallic compounds (**I** - **III**),[7,8] each of which has been described in terms of a M(I)–M'(0)–M(I) formalism. Beyond the divalent metals of groups 2 and 12, related *s*/*p* block examples are rare - MAl_2 and MGa_2 systems **IV** and **V** have been synthesized by Fischer by insertion of neutral Al(I) or Ga(I) moieties into M–X bonds (M = Zn, Hg; X = CH_3, SC_6F_5, $N(SiMe_3)_2$),[9-11] and systems featuring additional Lewis bases coordinated at the central metal also have literature precedent.[12]

Within this sphere, we perceived that the recent synthesis of nucleophilic Al(I) ('aluminyl') anions might offer an alternative route to access M–Al bonds featuring a wide range of metals.[13,14] While this has proved to be synthetically viable, the only trimetallic bis(aluminyl) systems reported to date via this approach (to our knowledge) are the potassium bis(aluminyl)-cuprate **VI**, synthesized from $K_2[Al(NON)]_2$ and Ph_3PCuI, and a very recently reported bis(aluminyl) samarium complex reported by Yamashita and co-workers.[11,14d] With a view to extending this approach, to allow for systematic exploration of the electronic structure and reactivity of Al–M–Al containing systems, we

report here on the synthesis of the bis(aluminyl) magnesium complex Mg[Al(NON)]$_2$. This compound provides an interesting counterpoint to existing aluminyl chemistry by offering experimental evidence for radical chemistry in addition to nucleophilic behaviour at aluminium.

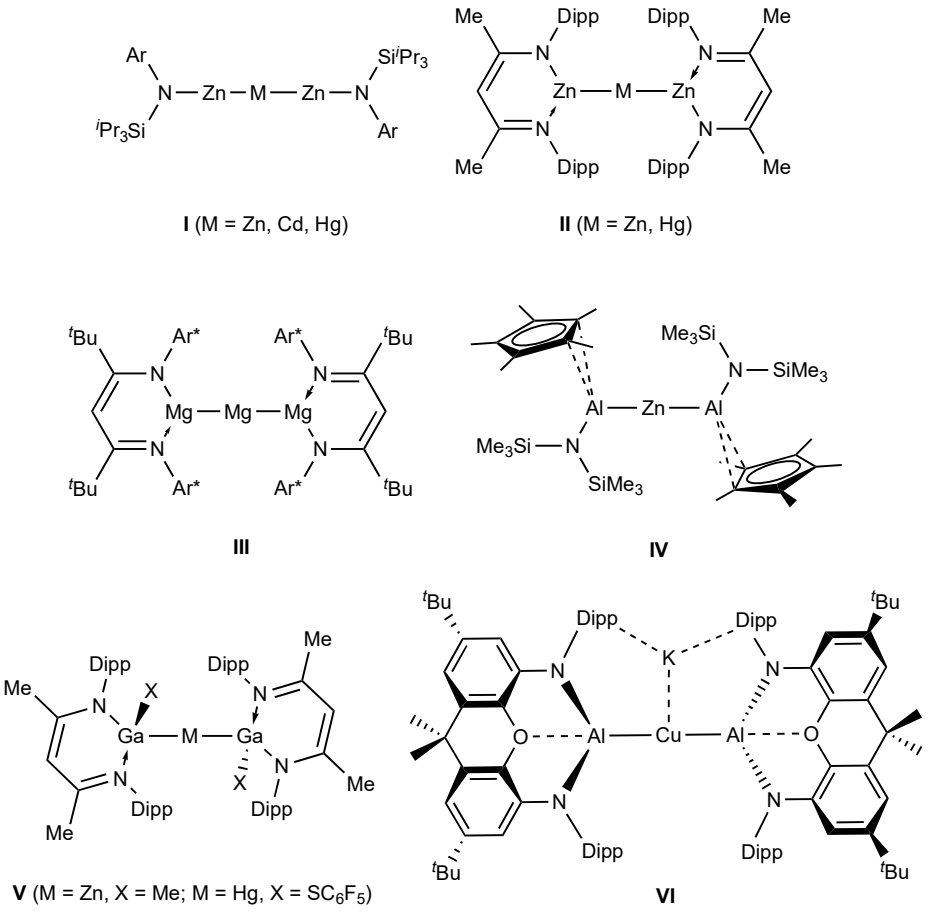

Figure 1; Selected covalently bonded trimetallic compounds of relevance to the current study. (Ar = C_6H_2-Me-4-$(CHPh_2)_2$-2,6; Ar = $C_6H_3(CHEt_2)_2$-2,6)*

Results and Discussion

Reaction of a toluene solution of potassium aluminyl compound **1**[13a] with a slurry containing ca. 0.6 equiv. (by metal) of MgI_2 over a period of 14 h leads to the formation of a new pale-yellow species, characterized by two Dipp CH_3 and one CH signal in its ^1H NMR spectrum in C_6D_6. Recrystallization from pentane gives a yellow crystalline product in ca. 80 % yield (0.15 g scale), which has been characterized by multinuclear NMR, IR and elemental microanalysis. X-ray diffraction studies on single crystals obtained from pentane or benzene solution reveal it to be the magnesium bis(aluminyl) complex $Mg[Al(NON)]_2$ (**2**; Scheme 1 and Figure 2). As such, **2** represents a very rare example of complex featuring a wholly aluminyl supporting ligand set.[10,14d]

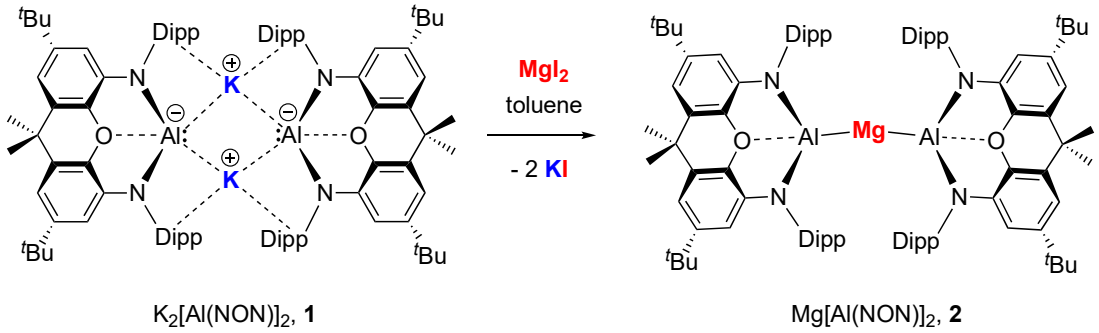

*Scheme 1; Synthesis of bis(aluminyl) magnesium complex **2** from potassium aluminyl dimer **1** via metathesis.*

From a geometric perspective, the molecular structure of **2** is defined by a bent coordination geometry at magnesium (∠Al–Mg–Al = 164.8(1)°; Figure 2). The corresponding angles at the central metal atom in the other two known homoleptic bis(aluminyl) complexes are closer to linear: bis(aluminyl)zinc system **IV** has a *crystallographically imposed* linear geometry at zinc, while the bis(aluminyl)cuprate $K[Cu\{Al(NON)_2\}]$ (**VI**), features an angle of 174.9(1)° at copper, albeit with the positioning of the K^+ counterion between the flanking Dipp groups presumably contributing to the alignment of the ligand scaffold.[14d]

In the case of **2**, the bending at magnesium away from linearity, while reminiscent of the bent structures observed for the heavier alkaline earth dihalides in the gas phase,[15] is thought primarily

result from dispersion interactions involving the flanking Dipp groups of the NON supporting ligands. As such (i) close contacts are observed between ^{i}Pr groups associated with the two different Al(NON) metallo-ligands in the 'pocket' formed by bending the Al–Mg–Al unit (closest H···H contacts: 2.35, 2.37 Å; closest C···C contacts: 3.792(3), 3.857(3) Å); (ii) the molecular structure of **2** is modelled well by quantum chemical calculations employing Grimme's empirical dispersion correction (along with PBE1PBE hybrid exchange functional and Def2-SVP basis set):[16] ∠Al–Mg–Al = 158.9°; *d*(Al–Mg) = 2.682, 2.694 Å (cf. 2.695(1) and 2.689(1) Å); and (iii) the corresponding minimum energy structure optimized without accounting for dispersion (but using an otherwise identical method) involves a significantly wider Al–Mg–Al angle (172.0°).

The Mg–Al bond lengths determined for **2** (2.695(1) and 2.689(1) Å) are comparable to the sum of the respective covalent radii (1.41 + 1.21 Å),[17] but very short compared to those reported for other Mg–Al systems (six examples in the range 2.727(2) - 2.7980(6) Å).[18] The only system featuring a comparable metal-metal separation is (Nacnac^{Mes})Mg–Al(NON) (2.696(1) Å; Nacnac^{Mes} = HC(MeCMesN)$_2$),[13a] which features the same aluminyl 'metallo-ligand'. Compared to this system, **2** might be expected to feature a shorter Mg–Al bond on account of the reduced coordination number at magnesium (i.e. two *vs.* three); on the other hand the mutually *trans* disposition of the two aluminyl units in **2**, and the strong σ-donor capabilities of the Al(NON) fragment,[14d] might be expected to influence the Mg–Al separation in the opposite sense.

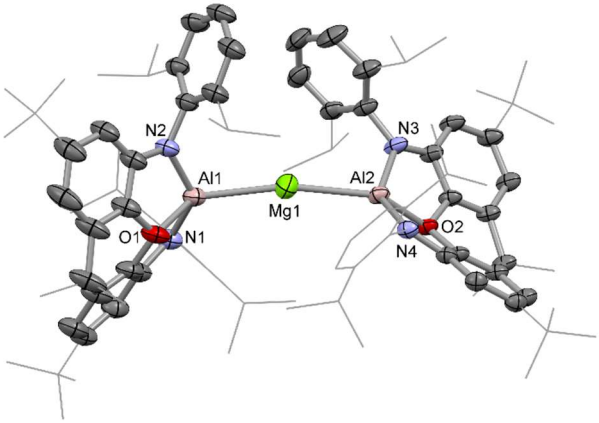

*Figure 2; Molecular structure of **2** in the solid state as determined by X-ray crystallography. Thermal ellipsoids set at 50% probability; H atoms and solvent molecules omitted, and selected substituents shown in wireframe format for clarity. Key bond lengths (Å) and angles (°): Mg–Al 2.695(1), 2.689(1); Al–N 1.900(1), 1.901(1), 1.902(1), 1.904(1); Al–O 2.001(1), 2.014(1); Al–Mg–Al 164.8(1).*

Quantum chemical calculations also show that the HOMO and LUMO for **2** are best described, respectively, as a Mg–Al σ-bonding orbital and an (unoccupied) in-phase π orbital which is delocalized over all three metal atoms (Figures 3 and s10). The associated HOMO energy (-6.44 eV) is significantly lower than determined, for example, for $(Et_2O)_2$Li–Al(NON) (-4.12 eV), reflecting a higher degree of covalency in the Al-M bonds. Consistently, QT-AIM calculations reveal bond critical points between Mg and each Al centre, with associated electron densities (ρ(r) = 0.037, 0.038 e $Å^{-3}$) that are similar to that determined for (Nacnac^{Mes})Mg–Al(NON) (0.036 e $Å^{-3}$), and intermediate between those calculated for $(Et_2O)_2$Li–Al(NON) (0.019 e $Å^{-3}$) and (Nacnac^{Mes})Zn–Al(NON) (0.060 e $Å^{-3}$).[19] The NAO orbital occupancy determined for the Mg 3s orbital is 0.815 e (together with 0.023 e for Mg 3p), which can be compared to 0.46 e for the Mg 3s orbital in (Nacnac^{Mes})Mg–Al(NON), which features a single aluminyl 'metallo-ligand'. ELF calculations reveal the presence of two metal-metal bonding basins for **2** (Figure 3) containing 1.948 and 1.965 electrons.

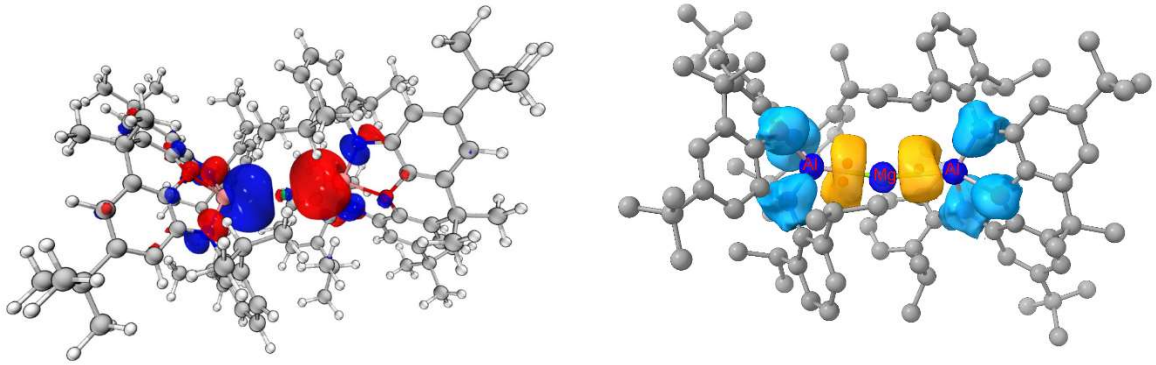

*Figure 3; (left) DFT calculated HOMO (-6.44 eV) for **2**. (Iso-value = 0.03; PBE1PBE hybrid exchange functional, Def2-SVP basis set, Grimme empirical dispersion correction). (right) ELF iso-surface for compound **2** (0.6 a.u.) Key: Yellow = metal-metal bond basins, Blue = ligand-based basins.*

Trimagnesium compound **III** (Figure 1) has been described in terms of a Mg(I)–Mg(0)–Mg(I) formalism, reflecting the essentially non-polar nature of Mg–Mg bonds, and QT-AIM calculated charges of +0.90/+0.36/+0.90 (when allowance is made for the presence of two non-nuclear attractors).[8] By means of comparison, **2** features a significantly higher charge at the central Mg atom (+1.36 vs. +0.36; Al charges: +1.08/+1.10), and, as a consequence, Mg–Al bonds which are polarized in the sense Mg(δ+)–Al(δ-), consistent with the respective Pauling electro-negativities (Al: +1.61; Mg: +1.31). Insofar as formal oxidation states can be assigned with any reliability, a formalism as Al(I)-Mg(II)-Al(I) would therefore seem most appropriate in the case of **2**. Further attempts to probe the electronic structure of **2** experimentally were carried out by examining its patterns of reactivity with respect to polar, oxidizing or unsaturated substrates.

2 is found to be intrinsically less reactive than **1** towards non-polar (or weakly polar) substrates, showing no propensity to activate H_2 or arenes such as benzene under thermal conditions. The more covalent nature of the metal aluminium interaction and accompanying stabilization of the HOMO are presumably of key importance. The capabilities of **2** as a four-electron reductant are,

however, signalled by its reactivity towards the kinetically inert substrate SF_6, with which it reacts at 80 °C over a period of 48 h to give $Mg[(\mu\text{-}F)_2Al(NON)]_2$ (**3**; Scheme 2).

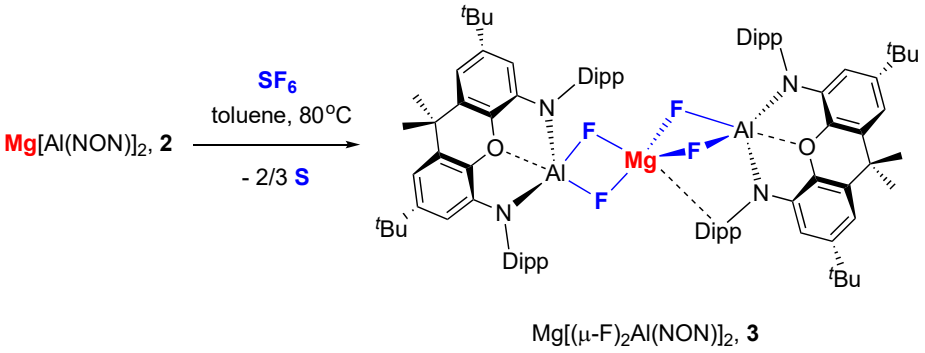

*Scheme 2; Reaction of bis(aluminyl)magnesium complex **2** with SF_6 to generate mixed aluminium/magnesium fluoride complex $Mg[(\mu\text{-}F)_2Al(NON)]_2$, **3**.*

At room temperature **3** gives rise to broad resonances in the ^1H NMR spectrum, and to two broad signals in the ^{19}F NMR spectrum at ca. -170 ppm, *i.e.* in the expected range for aluminium-bound fluorides. X-ray diffraction studies on single crystals obtained from benzene confirm the presence of Al–F bonds (Figure 4), and show that **3** is derived from the formal addition of F_2 across both of the Al–Mg bonds in **2**, via the reductive defluorination of SF_6. No (NON)Al/S containing species could be detected spectroscopically in solution, and the fate of the sulphur component under these conditions is thought to be as amorphous sulphur precipitate observed in the reaction mixture. Consistently, carrying out the reaction in the presence of PPh_3 leads to the formation of PPh_3S.

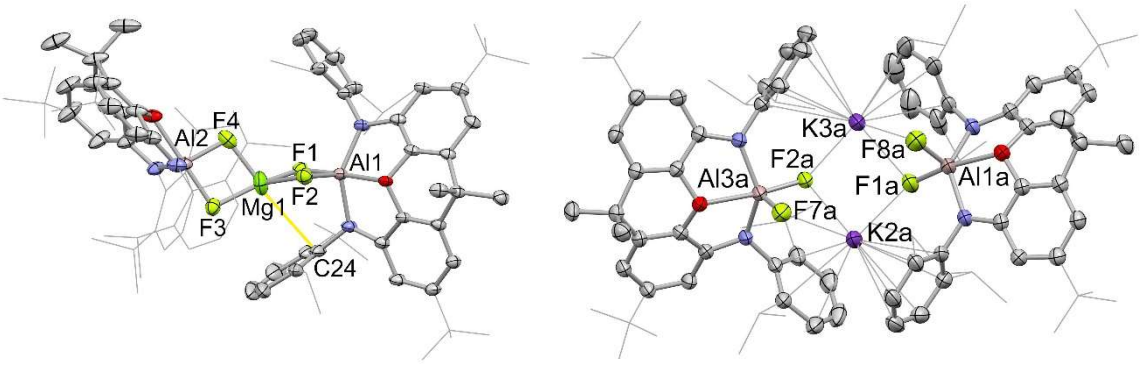

*Figure 4; Molecular structures of Mg[(μ-F)$_2$Al(NON)]$_2$ (**3**, upper) and K$_2$[(NON)AlF$_2$] (**4**, lower) in the solid state as determined by X-ray crystallography. Thermal ellipsoids set at 50% probability; H atoms and solvent molecules omitted, and selected substituents shown in wireframe format for clarity. Key bond lengths (Å): (for **3**) Al–F 1.796(1), 1.821(1), 1.769(1), 1.773(1); Mg–F 1.894(1), 1.902(1), 1.920(2), 1.919(2); Mg···C24 3.197(3); (for **4**) Al–F 1.753(1), 1.709(1), 1.756(1), 1.755(1), K···F 2.875(1), 2.723(1), 2.625(1), 2.652(1), 2.681(1), 3.160(1).*

The structure of **3** is unusual in containing an MgF_2 fragment, formally encapsulated between two [(NON)AlF] units. Despite the high lattice enthalpy of MgF_2 (ca. 2960 kJ mol^{-1}),[20] the presence of strong Al–F interactions presumably serves to prevent further aggregation. The coordination environment at the aluminium centres lies between trigonal bipyramidal and square pyramidal (τ_5 = 0.66, 0.59 for Al1/Al2) with the Al–F distances associated with the axial sites (F1, F3) being somewhat longer than those involving the equatorial fluorides (1.796(1)/1.821(1) vs. 1.769(1)/1.773(1) Å). The coordination environment at magnesium is significantly distorted from tetrahedral; the Mg–F bond lengths are grouped into two sets (1.894(1)/1.902(1) and 1.920(2)/1.919(2) Å), with the shorter bonds being associated with the fluoride ligands which are more weakly bound at aluminium (i.e. F1 and F3, the axial fluorides). Moreover, the Dipp group of one NON ligand interacts weakly with Mg1 (*d*(Mg-C_{ipso}) = 3.197(3) Å) - in an orientation roughly *trans* to F4. The remaining three fluorides (F1-F3) and Mg1 lie in an approximately planar arrangement, with the mean deviation from the least squares plane being 0.059 Å. As such, the coordination geometry at Mg1 could be viewed as tending towards trigonal bipyramidal, with F4 and the C24 formally constituting the axial ligands. In solution, the fluoride ligands undergo fluxional exchange, being rendered equivalent on the NMR timescale at 343 K, and being resolved into an AB multiplet below 273 K (ESI, Figure s8).

This mode of reactivity of **2** is also common to potassium aluminyl compound **1**, which reductively defluorinates SF_6 in similar fashion generating the potassium difluoroaluminate dimer $K_2[(NON)AlF_2]$ (**4**), albeit under somewhat milder conditions (room temperature, 5 min). **4** is isostructural with the corresponding dihydride $K_2[(NON)AlH_2]$, with the K^+ cations held in place by a combination of K···F (2.625(1) - 3.160(1) Å) and K···arene interactions (3.177(2) - 3.392(2) Å; Figure 4). Crimmin and co-workers have previously reported SF_6 activation by $\{HC(MeCDippN)_2\}Al$.[20]

The reduction chemistry observed with **2** reflects the availability of a four-electron reservoir constituted by the two Mg-Al bonds. Furthermore, the polarity of these bonds (and a formalism for **2** as Al(I)-Mg(II)-Al(I)) implied by the QT-AIM charge distribution is supported by reactions with electrophiles such as methyl iodide. The reaction of **2** with MeI in benzene-d_6 solution selectively generates (NON)AlMe, in a manner analogous to the reaction of potassium system **1** with methyl iodide,[13a] and implies that the aluminium centres in each case behave in a nucleophilic manner.

By contrast, the reactivity of **2** towards 1,5-cyclooctadiene (COD) implies that other factors can also be important in driving product formation *under photolytic conditions*. While **1** reacts with alkenes rapidly at room temperature via [2+1] cycloaddition chemistry to generate the corresponding metallacyclo-propanes,[13c] **2** does not react with COD even under more forcing thermal conditions (72 h at 80 °C). On the other hand, broadband UV photolysis of a solution in C_6D_6 (Hg arc lamp, 191-360 nm, 125 W) leads to generation of a single major NON-containing species, as judged by *in situ* ^{1}H NMR monitoring, together with magnesium metal (Scheme 3). Single crystals of the (extremely sensitive) aluminium-containing product suitable for X-ray crystallography were grown from a concentrated benzene solution, and shown to contain a racemic mixture of (*R*,*R*,*R*,*R*) and (*S*,*S*,*S*,*S*) 2,6-dimetallated *cis*-bicyclo[3.3.0]octanes (Figure 5). Structurally, the product **5** features a *cis*-bicyclo[3.3.0]octane core with chemically equivalent [Al(NON)] fragments bound in the 2- and 6-positions, each adopting pseudo-equatorial positions with respect to the C_8 skeleton, in line with steric considerations. The Al–

C and C–C bonds within the organometallic core conform to the expected distances for the respective single bonds.[17]

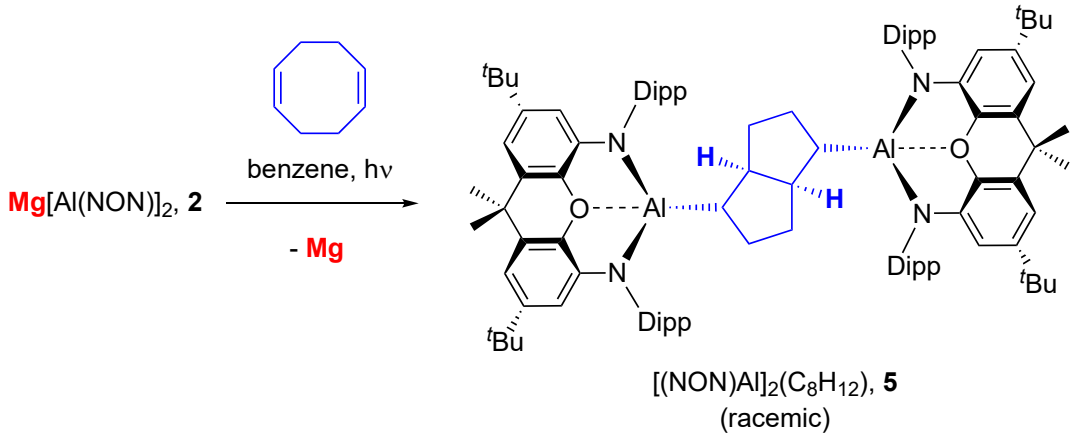

*Scheme 3; Reaction of bis(aluminyl) magnesium complex **2** with 1,5-cyclooctadiene under UV photolysis to generate the racemic (R,R,R,R) and (S,S,S,S) 2,6-dimetallated cis-bicyclo[3.3.0]octane, [(NON)Al]$_2$(C_8H_{12}) (**5**).*

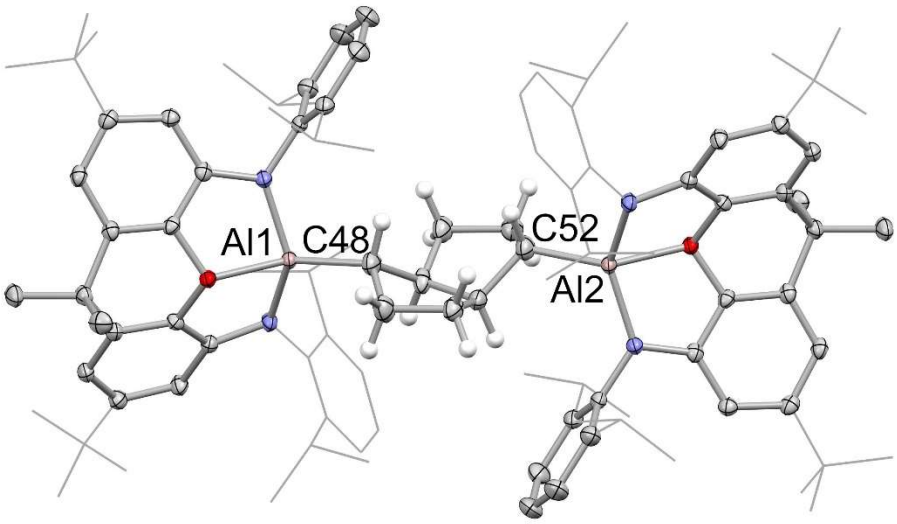

*Figure 5; Molecular structure of [(NON)Al]$_2$(C_8H_{12}) (**5**) in the solid state as determined by X-ray crystallography. Thermal ellipsoids set at 50% probability; most H atoms omitted and selected substituents shown in wireframe format for clarity. Key bond lengths (Å): Al–C 1.948(5), 1.952(5); C–C (within bicyclooctane unit) 1.51(1), 1.531(8), 1.532(9), 1.550(4), 1.518(8), 1.531(8), 1.52(1), 1.542(7).*

Mechanistically, the formation of **5** from **2** and 1,5-cyclooctadiene constitutes a transannular 1,5-cycloaddition reaction involving the creation of four contiguous stereocentres in one step; the crystalline product features a racemic mixture of (*R*,*R*,*R*,*R*) and (*S*,*S*,*S*,*S*) forms.[22] This mode of reactivity (and selectivity) is strongly characteristic of free radical transannular cyclization processes

of 1,5-cyclooctadiene, being widely precedented for classical organic radical systems derived from peroxides, chlorocarbons or carbonyl compounds.[23] Thus, for example, the reaction of COD with CCl_4 under UV photolysis generates the analogous cycloaddition product 2-trichloromethyl-6-chloro-*cis*-bicyclo-[3.3.0]octane. Indeed, related studies have invoked the formation of bicyclic systems of this type from cyclooctene precursors as a mechanistic probe for radical-based chemistry.[24] The stereo-selective formation of **5** from **2** is therefore consistent with the transient formation of Al(II) radical species under photolytic conditions, and with the concurrent generation of magnesium metal.[25]

Consistent with this assertion: (i) photolysis of **2** in the absence of COD in hexane solution generates the (known) Al(II) dimer (NON)Al–Al(NON),[13a] together with metallic magnesium; (ii) radical species featuring well-defined ^{27}Al hyperfine couplings are generated from **2** when it is photolyzed in benzene in the absence of COD (Figure s16); (iii) these radicals react onwards in the presence of COD to generate different radical species (Figure s17); and (iv) under these conditions **5** is ultimately produced.

Moreover, the key role of magnesium complex **2** in giving rise to the radical species from which **5** is produced is emphasized by the fact that independently prepared samples of (NON)Al–Al(NON) neither generate detectable radical species (as shown by EPR spectroscopy) nor react with COD under comparable photolysis conditions in benzene. Attempts to capture the radical species photolytically generated from **2** via the use of other radical traps are currently ongoing.

Conclusions

In conclusion, we report on the synthesis of a homoleptic magnesium bis(aluminyl) compound, which acts a four electron reservoir in the reductive defluorination of SF_6, and which reacts thermally with polar substrates such as methyl iodide via nucleophilic attack through aluminium, consistent with the QT-AIM charges calculated for the metal centres and a *formal* description as a Al(I)–Mg(II)–Al(I) trimetallic. By contrast, under photolytic activation, the reaction with 1,5-cyclooctadiene leads to the stereoselective generation of transannular cycloaddition products consistent with radical based chemistry, emphasizing the covalent nature of the Mg–Al bonds and a description as a Al(II)–Mg(0)–Al(II) synthon.[26]

Acknowledgements

We thank the EPSRC Centre for Doctoral Training in Inorganic Chemistry for Future Manufacturing (OxICFM; EP/S023828/1) and the Leverhulme Trust (RP-2018-246) for funding. ME thanks the Alexander for Humboldt Stiftung for a Feodor Lynen Fellowship. The authors would like to acknowledge the use of the University of Oxford Advanced Research Computing (ARC) facility in carrying out this work.

References

[1] *Molecular Metal-Metal Bonds: Compounds, Synthesis, Properties*, ed. S. T. Liddle, Wiley-VCH, Weinheim, 2015, chps 2, 12-15.

[2] Selected reviews: (a) P. P. Power, *Organometallics* **2007**, *26*, 4362–4372; (b) F. Hanusch, L. Groll, S. Inoue, *Chem. Sci.* **2021**, *12*, 2001–2015.

[3] (a) P. P. Power, *Nature* **2010**, *463*, 171–177; (b) C. Weetman, S. Inoue, *ChemCatChem* **2018**, *10*, 4213-4228.

[4] (a) M. Stender, A. D. Phillips, R. J. Wright, P. P. Power, *Angew. Chem. Int. Ed.* **2002**, *41*, 1785–1787; (b) A. D. Phillips, R. J. Wright, M. M. Olmstead, P. P. Power, *J. Am. Chem. Soc.* **2002**, *124*, 5930–5931; (c) G. H. Spikes, J. C. Fettinger, P. P. Power, *J. Am. Chem. Soc.* **2005**, *127*, 12232–12233; (d) Y. Peng, M. Brynda, B. D. Ellis, J. C. Fettinger, E. Rivard, P. P. Power, *Chem. Commun.* **2008**, 6042-6044.

[5] I. Resa, E. Carmona, E. Gutierrez-Puebla, A. Monge, *Science* **2004**, *305*, 1136-1138.

[6] (a) S. P. Green, C. Jones, A. Stasch, *Science* **2007**, *318*, 1754–1757; (b) C. Jones, *Nat. Rev. Chem.* **2017**, *1*, 0059.

[7] Zn_3 and MZn_2 (M = Cd, Hg) systems: (a) M. P. Blake, N. Kaltsoyannis, P. Mountford, *Chem. Commun.* **2015**, *51*, 5743-5746; (b) J. Hicks, E. J. Underhill, C. E. Kefalidis, L. Maron, C. Jones, *Angew. Chem. Int. Ed.* **2015**, *54*, 10000-1004; (c) C. Bakewell, B. J. Ward, A. J. P. White, M. R. Crimmin, *Chem. Sci.* **2018**, *9*, 2348-2356.

[8] Mg_3 system: B. Rösch, T. X. Gentner, J. Eyselein, J. Langer, H. Elsen, S. Harder, *Nature* **2021**, *592*, 717-721.

[9] MGa_2 systems: (a) A. Kempter, C. Gemel, T. Cadenbach, R. A. Fischer, *Inorg. Chem.* **2007**, *46*, 9481-9487; (b) G. Prabusankar, C. Gemel, M. Winter, R. W. Seidel, R. A. Fischer, *Chem.-Eur. J.*, **2010**, *16*, 6041-6047.

[10] $ZnAl_2$ system: J. Weßing, C. Göbel, B. Weber, C. Gemel, R. A. Fischer, *Inorg. Chem.* **2017**, *56*, 3517-3525.

[11] For a recent *f*-block example, see: G. Feng, F. L. Chan, Z. Lin, M. Yamashita, *J. Am. Chem. Soc.* **2024**, ASAP (DOI: 10.1021/ jacs.4c01193).

[12] See, for example C. Jones, D. P.Mills, J. A. Platts, R. P. Rose, *Inorg. Chem.* **2006**, *45*, 3146-3148.

[13] (a) J. Hicks, P.Vasko, J. M. Goicoechea, S. Aldridge, *Nature* **2018**, *557*, 92-95; (b) J. J. Schwamm, M. D. Anker, M. Lein, M. P. Coles, *Angew. Chem. Int. Ed.* **2019**, *58*, 1489-1493; (c) J. Hicks, P. Vasko, J. M. Goicoechea, S. Aldridge, *J. Am. Chem. Soc.* **2019**, *141*, 11000-11003; (d) S. Kurumada, S. Takamori, M. Yamashita, *Nature Chem.* **2020**, *12*, 36-39; (e) K. Koshino, R. Kinjo, *J. Am. Chem. Soc.* **2020**, 142, 9057-9062; (f) R. J. Schwamm, M. P. Coles, M. S. Hill, M. F. Mahon, C. L. McMullin, N. A. Rajabi, A. S. S. Wilson, *Angew. Chem. Int. Ed.* **2020**, *59*, 3928-3932; (g) S. Grams, J. Eyselein, J. Langer, C. Färber, S. Harder, *Angew. Chem. Int. Ed.* **2020**, *59*, 15982-15986; (h) S. Grams, J. Mai, J. Langer, S. Harder, *Organometallics* **2022**, *41*, 2862–2867; (i) G. Feng, K. L. Chan, Z. Lin, M. Yamashita, *J. Am. Chem. Soc*. **2022**, *144*, 22662–22668; (j) C. Yan, R. Kinjo, *Angew. Chem. Int. Ed*. **2022**, *61*, e202211800; (k) R. A. Jackson, A. J. R. Matthews, P. Vasko, M. F. Mahon, J. Hicks, D. Liptrot, *Chem. Commun*. **2023**, *59*, 5277-5280; (l) D. Sarkar, P. Vasko, A. F. Roper, M. M. D. Roy, A. E. Crumpton, L. P. Griffin, C. Bogle, S. Aldridge, submitted manuscript (copy supplied for reviewing purposes).

[14] (a) J. Hicks, A. Mansikkamäki, P. Vasko, J. M. Goicoechea, S. Aldridge, *Nat. Chem.* **2019**, *11*, 237-241; (b) K. Sugita, M. Yamashita, *Chem.-Eur. J.* **2020**, *26*, 4520-4523; (c) H. Y. Liu, R. J. Schwamm, M. S. Hill, M. F. Mahon, C. F. McMullin, N. A. Rajabi, *Angew. Chem. Int. Ed.* **2021**, 60, 14390-14393; (d) C. McManus, J Hicks, X. Cui, L. Zhao, G. Frenking, J. M. Goicoechea, S. Aldridge, *Chem. Sci.* **2021**, *12*, 13458-13468; (e) M. M. D. Roy, J. Hicks, P. Vasko, A. Heilmann, A.-M. Baston, J. M. Goicoechea, S. Aldridge, *Angew. Chem. Int. Ed.* **2021**, *60*, 22301-22306; (f) M. J. Evans, G. H. Iliffe, S. E. Neale, C. L. McMullin, J. R. Fulton, M. D. Anker, M. P. Coles, *Chem. Commun.* **2022**, 58, 10091-10094.

[15] *Molecules and Models: The Molecular Structures of Main Group Element Compounds*, A. Haaland, OUP, Oxford, 2008, chp 10.

[16] T. Schwabe, S. Grimme, *Phys. Chem. Chem. Phys.* **2007**, *9*, 3397-3406.

[17] B. Cordero, V. Gómez, A. E. Platero-Prats, M. Revés, J. Echeverría, E. Cremades, F. Barragán, S. Alvarez, *Dalton Trans.* **2008**, 2832-2838.

[18] For previous examples of Mg–Al covalent bonds see refs 7c, 13a, 13f, 14e and 14f, plus: (a) A. Paparo, C. D. Smith, C. Jones, *Angew. Chem. Int. Ed.* **2019**, *58*, 11459-11463; (b) S. Brand, H. Elsen, J. Langer, S. Grams, S. Harder, *Angew. Chem. Int. Ed.* **2019**, *58*, 15496-15503; (c) A. Friedrich, J. Eyselein, J. Langer, C. Färber, S. Harder, *Angew. Chem. Int. Ed.* **2021**, *60*, 16492-16499.

[19] *Atoms in Molecules: A Quantum Theory*, R. Bader, OUP, Oxford, 1994.

[20] See also: D. J. Sheldon, M. R. Crimmin, *Chem. Commun.* **2021**, *7*, 7096-7099.

[21] *Chemistry of the Elements*, N. N. Greenwood, A. Earnshaw, 2nd edition, Elsevier, Amsterdam, 1997.

[22] Hydrolysis of **5** with weak acids generates the parent hydrocarbon *cis*bicyclo[3.3.0]octane: W. B. Moniz, J. A. Dixon, *J. Am. Chem. Soc.* **1961**, *83*, 7, 1671–1675.

[23] Early reports of the stereoselective transannular radical cyclization of 1,5-cyclooctadiene to *cis*bicyclo[3.3.0]octanes: (a) R. Dowbenko, *J. Am. Chem. Soc*. **1964**, *86*, 946-947; (b) L. Friedman, *J. Am. Chem. Soc.* **1964**, *86*, 1885-1886; (c) R. Dowbenko, *Tetrahedron* **1964**, *20*, 1843; (d) J. D. Winkler, V. Sridar, *J. Am. Chem. Soc.* **1986**, *108*, 1708-1709.

[24] E. C. Ashby, T. N. Pham, *J. Org. Chem.* **1986**, *51*, 3598-3602.

[25] For a previous report of potential Al(II) radical species see: D. Mandal, T. I. Demirer, T. Sergeieva, B. Morgenstern, H. T. A. Wiedemann, C. W. M. Kay, D. M. Andrada, *Angew. Chem. Int. Ed.* **2023**, *62*, e202217184.

[26] Details of the X-ray crystal structures described in this paper are available from the CCDC, deposition numbers 2219353, 2219355-2219358 and 2221942.

Supporting information

General considerations

All manipulations were carried out using standard Schlenk line or dry-box techniques under an atmosphere of argon or dinitrogen. Solvents were degassed by sparging with argon and dried by passing through a column of the appropriate drying agent. Toluene was purified using an MBraun SPS-800 and stored over a potassium mirror. NMR spectra were measured in benzene-d_6 (which was dried over potassium) with the solvent then being distilled under reduced pressure and stored under argon in Teflon valve ampoules. NMR samples were prepared under argon in 5 mm Wilmad 507-PP tubes fitted with J. Young Teflon valves. ^{1}H, $^{13}C\{^{1}H\}$, ^{19}F and $^{19}F\{^{1}H\}$ NMR spectra were recorded on Bruker Avance III HD nanobay 400 MHz or Bruker Avance III 500 MHz spectrometer at ambient temperature and referenced internally to residual protio-solvent (^{1}H) or solvent (^{13}C) resonances and are reported relative to tetramethylsilane and $CFCl_3$ (δ = 0 ppm). Assignments were confirmed using two-dimensional ^{1}H-^{1}H and ^{13}C-^{1}H NMR correlation experiments. Chemical shifts are quoted in □ (ppm) and coupling constants in Hz. Elemental analyses were carried out by London Metropolitan University or Elemental Microanalysis Ltd. $K_2[Al(NON)]_2$ (**1**) was synthesized according to the literature procedure.[s1] 1,5-Cyclooctadiene and iodomethane were dried over 2 Å molecular sieves. All other reagents were used as received.

Syntheses of novel compounds

Mg[(NON)Al]$_2$ (2): To a Schlenk tube containing MgI_2 (0.41 g, 1.46 mmol) was added a solution of $K_2[Al(NON)]_2$ (1.80 g, 1.22 mmol) in toluene at room temperature, before stirring for 14 h. The resulting solution was filtered and volatiles removed *in vacuo*. The resulting oily residue was dissolved in pentane and filtered. Volatiles were removed from the filtrate *in vacuo* to yield crude $Mg[Al(NON)]_2$ as a pale yellow powder. This residue was redissolved in pentane, filtered, and crystallised by slow evaporation, yielding 1.44 g of compound **2** (83 %).

^{1}H NMR (400 MHz, benzene-d_6, 298 K): δ_H 1.09 (d, $^3J_{HH}$ = 6.7 Hz, 24 H, CH(C*H*$_3$)$_2$), 1.18 (s, 36 H, C(C*H*$_3$)$_3$), 1.23 (d, $^3J_{HH}$ = 6.9 Hz, 24 H, CH(C*H*$_3$)$_2$), 1.64 (s, 12 H, XA-C(C*H*$_3$)$_2$), 3.50 (sept., $^3J_{HH}$ = 6.8 Hz, 8 H, C*H*(CH$_3$)$_2$), 6.23 (d, $^4J_{HH}$ = 1.9 Hz, 4 H, XA-*o*-C*H*), 6.71 (d, $^4J_{HH}$ = 2.0 Hz, 4 H, XA-*p*-C*H*), 7.08–7.20 (m, 12 H, Ar*H*).

^{13}C{^{1}H} NMR (101 MHz, benzene-d_6): δ_C 25.5, 25.6 (CH(*C*H$_3$)$_2$), 27.3 (*C*H(CH$_3$)$_2$), 29.5 (XA-C(*C*H$_3$)$_2$), 31.8 (C(*C*H$_3$)$_3$), 35.1 (*C*(CH$_3$)$_3$), 37.5 (XA-*C*(CH$_3$)$_2$), 107.1, 110.7, 124.5, 126.5, 127.9, 133.7, 140.7, 142.5, 142.8, 147.5, 149.0 (Ar-*C*).

Anal. calc. for $C_{94}H_{124}Al_2MgN_4O_2$: C 79.49%, H 8.80%, N 3.94%, found: C 79.33%, H 8.95%, N 3.73%.

Attempted reaction of 2 with benzene: An NMR tube fitted with a J Youngs valve and containing a benzene-d_6 (0.4 mL) solution of **2** (0.02 g, 0.014 mmol) was heated to 80 °C for 48 h. No change was observed by *in-situ* ^{1}H NMR spectroscopy.

Attempted reaction of 2 with dihydrogen: An NMR tube fitted with a J Youngs valve and containing a benzene-d_6 (0.4 mL) solution of **2** (0.02 g, 0.014 mmol) was degassed by three freeze pump thaw cycles before addition of an atmosphere of H_2. The solution was heated to 80 °C for 48 h. No change was observed by *in-situ* ^{1}H NMR spectroscopy.

Reaction of 2 with MeI: To a benzene-d_6 (0.4 mL) solution of **2** (0.02 g, 0.014 mmol) in an NMR tube fitted with a J Youngs valve was added 0.02 mL (0.32 mmol) of MeI. The resulting solution decolourised immediately and a white precipitate was observed. Formation of the known species (NON)AlMe was confirmed by *in situ* ^{1}H NMR spectroscopy.[s1]

Mg[(NON)AlF$_2$]$_2$ (3): A J Youngs ampoule containing a toluene solution of **2** (0.2 g, 0.14 mmol in 10 mL) was degassed by three freeze pump thaw cycles before being exposed to an atmosphere of SF_6. The ampoule was sealed and heated to 80 °C for 48 h. The resulting (darkened) solution was dried *in vacuo* and the residue dissolved in benzene (10 mL). The solution was filtered and concentrated *in vacuo*; storage at room temperature yielded crystals suitable for X-ray crystallography. This material was washed with minimal hexane, yielding 84 mg (40 %) of **3** as a white solid.

^{1}H NMR (400 MHz, toluene-d_8, 298 K): δ_H 1.04 (br s, 24 H, CH(C*H*$_3$)$_2$), 1.16 (br s, 36 H, C(C*H*$_3$)$_3$), 1.31 (br s, 24 H, CH(C*H*$_3$)$_2$), 1.49 (br s, 12 H, XA-C(C*H*$_3$)$_2$), 3.39 (br s, 8 H, C*H*(CH$_3$)$_2$), 6.05 (br s, 4 H, XA-*o*-C*H*), 6.67 (br s, 4 H, XA-*p*-C*H*), 6.91–7.25 ppm (br m, 12 H, Ar*H*).

^{19}F NMR (376 MHz, toluene-d_8, 298 K): δ_F -171.9, -171.2 (br s, 2 F, AlF).

^{13}C{^{1}H} NMR (101 MHz, benzene-d_6, 298 K): δ_C 27.5 (CH(*C*H$_3$)$_2$), 27.9 (CH(*C*H$_3$)$_2$), 30.3 (*C*H(CH$_3$)$_2$), 25.1 (XA-C(*C*H$_3$)$_2$), 31.1 (XA-C(*C*H$_3$)$_2$), 33.1 (XA-C(*C*H$_3$)$_3$), 109.3 (XA-*p*-*C*H), 112.8 (XA-*o*-*C*H), 125.3 (Ar$_{DIPP}$-*C*), 126.0 (Ar$_{DIPP}$-*C*), 132.7 (Ar$_{XA}$-*C*), 139.7 (Ar$_{XA}$-*C*), 140.9 (Ar$_{XA}$-*C*), 143.4 (Ar$_{DIPP}$-*C*), 147.3 (Ar$_{DIPP}$-*C*), 148.3 (Ar$_{XA}$-*C*).

K$_2$[(NON)AlF$_2$]$_2$ (4): To solid K$_2$[Al(NON)]$_2$ (0.200 g, 0.136 mmol) in a Schlenk tube was added benzene (20 mL) and the solution degassed by three freeze pump thaw cycles. To the resulting clear yellow solution at room temperature was added one atmosphere of SF_6 gas (>10 equiv.). The decolourised solution was stirred for 5 min, after which all volatiles were removed *in vacuo*, and the residue extracted with hexane, filtered and concentrated (ca. 5 mL). After 24 h clear colourless crystals of

$K_2[(NON)AlF_2]_2$ were isolated by filtration yielding 130 mg of product (65%). These crystals were suitable for single X-ray diffraction.

^{1}H NMR (400 MHz, benzene-d_6, 298 K): δ_H 1.09 (d, $^3J_{HH}$ = 6.7 Hz, 24H, CH(CH_3)$_2$), 1.18 (d, $^3J_{HH}$ = 6.7 Hz, 24H, CH(CH_3)$_2$), 1.25 (s, 36H, C(CH_3)$_3$), 1.58 (s, 2x CH_3, 12H, XA-C(CH_3)$_2$), 3.69 (sept, $^3J_{HH}$ = 6.7 Hz, 8H, C*H*(CH$_3$)$_2$), 6.13 (d, $^3J_{HH}$ = 1.5 Hz, 4H, XA-*o*-C*H*), 6.73 (d, $^3J_{HH}$ = 1.5 Hz, 4H, XA-*p*-C*H*), 7.00-7.29 (br m, 12H, Ar*H*).

^{19}F NMR (376 MHz, benzene-d_6, 298 K): δ_F –165.8 (s, 4F, AlF).

^{13}C{^{1}H} NMR (101 MHz, benzene-d_6, 298 K): δ_C 24.6 (CH(*C*H$_3$)$_2$), 25.0 (CH(*C*H$_3$)$_2$), 27.5 (CH(*C*H$_3$)$_2$), 27.8 (XA-C(*C*H$_3$)$_2$), 31.7 (XA-C(*C*H$_3$)$_3$), 106.2 (XA-*p*-*C*H), 109.0 (XA-*o*-*C*H), 124.2 (Ar$_{DIPP}$-*C*), 128.9 (Ar$_{DIPP}$-*C*), 131.4 (Ar$_{XA}$-*C*), 139.4 (Ar$_{XA}$-*C*), 144.2 (Ar$_{XA}$-*C*), 144.8 (Ar$_{DIPP}$-*C*), 147.4 (Ar$_{XA}$-*C*), 148.0 (Ar$_{DIPP}$-*C*).

[(NON)Al]$_2$(C$_8$H$_{12}$) (5): 1,5-cyclooctadiene (0.1 mL, 0.82 mmol) was added to an NMR tube containing a solution of **2** (30 mg, 0.021 mmol) in benzene-d_6 (0.3 mL) and was subsequently irradiated using a broad-band Hg arc lamp (191-360 nm, 125 W) for 6 h. The solution was concentrated *in-vacuo* to the point of incipient crystallisation. Colourless blocks were grown overnight which were suitable for single crystal X-ray crystallography. These crystals could be isolated, yielding 10 mg of product (32 %). **5** is extremely air sensitive and repeatedly gave elemental microanalysis results (even with single crystals) consistent with partial decomposition/hydrolysis under analysis conditions.

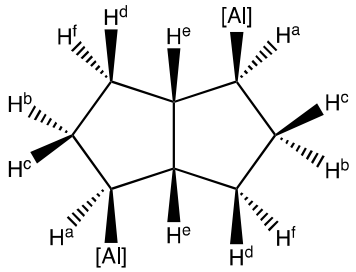

^{1}H NMR (500 MHz, benzene-d_6, 328 K): δ_H 0.20 (m, 2H, H^a), 0.56 (m, 2 H,H^b), 1.02, 1.07, 1.13 (48 H, CH(CH_3)$_2$), 1.16 (s, 18 H, C(CH_3)$_3$), 1.51 (m, 2 H, H^c), 1.59 (s, 12H, XA-C(CH_3)$_2$), 1.76 (m, 2H, H^d), 1.82 (m,

2H, H^e), 2.08 (m, 2 H, H^f), 3.38 (br m, 4H, C*H*$(CH_3)_2$), 3.47 (sept, $^3J_{HH}$ = 6.90 Hz, 4H, C*H*$(CH_3)_2$), 6.22 (d, $^4J_{HH}$ = 1.54 Hz, 4H, XA-*o*-C*H*), 6.71 (d, $^4J_{HH}$ = 1.54 Hz, 4H, XA-*p*-C*H*), 7.22 (br, 4H, Dipp-*p*-C*H*), 7.25 (br, 8 H, Dipp-*o*-C*H*).

$^{13}C\{^1H\}$ NMR (126 MHz, benzene-d_6, 328 K): δ_C 24.1 ($CH(CH_3)_2$), 25.4 ($CH(CH_3)_2$), 28.3, 29.0 ($CH(CH_3)_2$), 30.6 (*C*(Al)(H^a)), 31.2 (XA-C($CH_3)_2$), 34.1 (*C*(H^d)(H^f)), 34.5 (XA-*C*$(CH_3)_3$), 35.4 (*C*(H^b)(H^c)), 49.7 (*C*(H^e)), 107.5 (XA-*p*-*C*H), 112.2 (XA-*o*-*C*H), 124.0 (Ar_{DIPP}-*C*), 126.2 (Ar_{DIPP}-*C*), 134.8 (Ar_{XA}-*C*), 139.3 (Ar_{XA}-*C*), 142.0 (Ar_{DIPP}-*C*), 143.0 (Ar_{XA}-*C*), 145.8 (Ar_{XA}-*C*), 146.0 (Ar_{DIPP}-*C*).

^{1}H NMR spectra of novel compounds

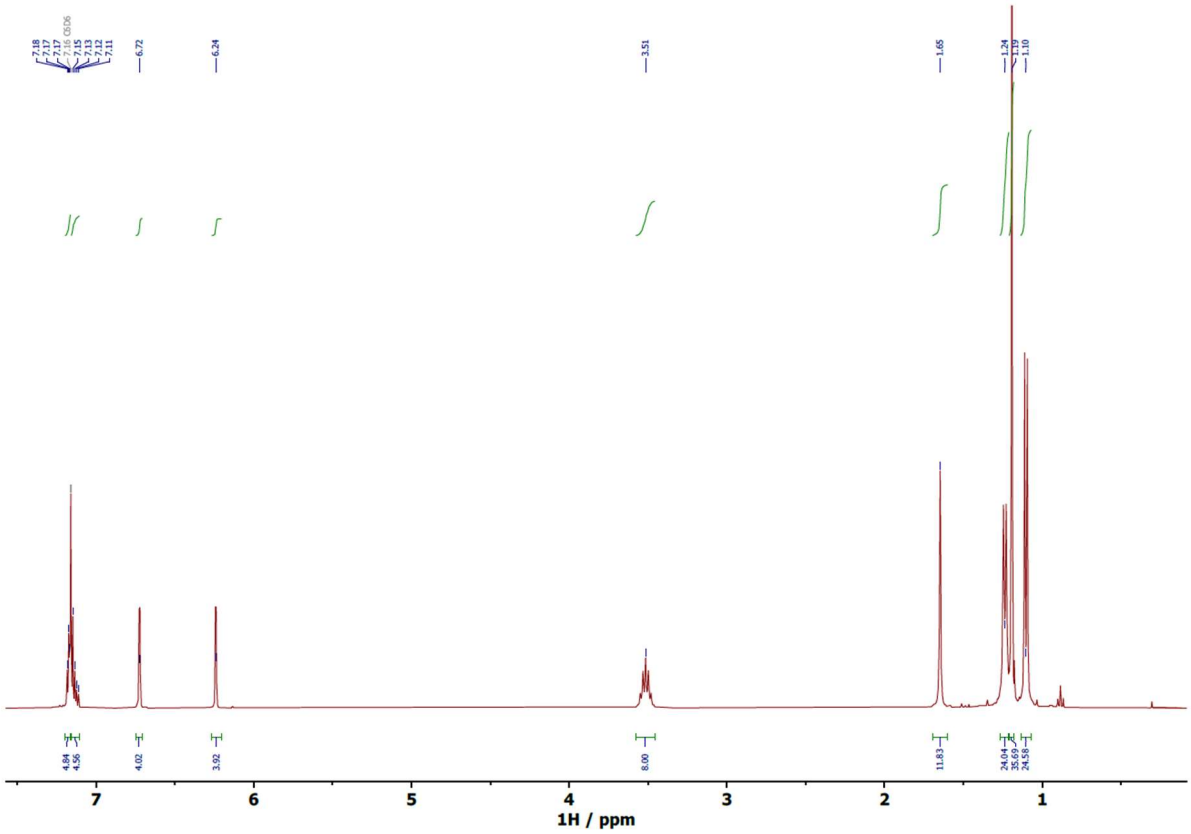

Figure s1: ^{1}H NMR spectrum of **2** in benzene-d_6 at 298 K.

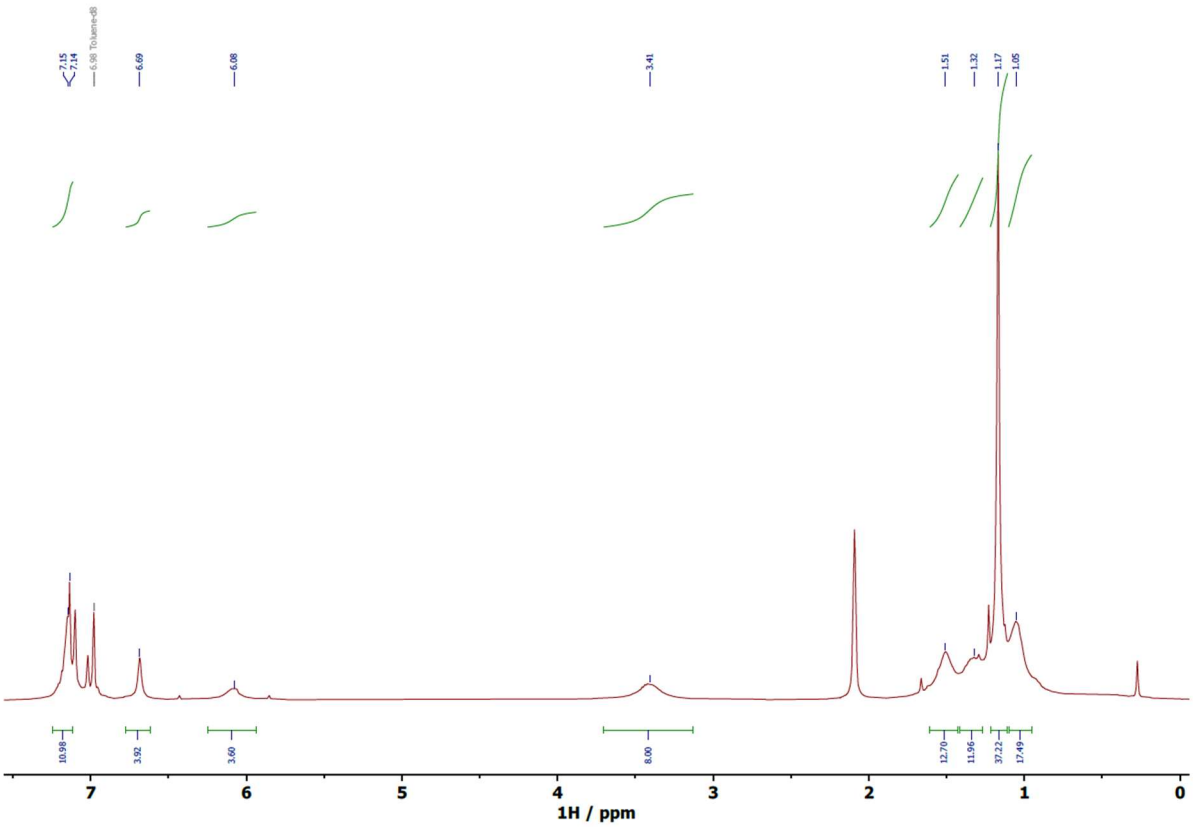

Figure s2: ^{1}H NMR spectrum of **3** in toluene-d_8 at 298 K.

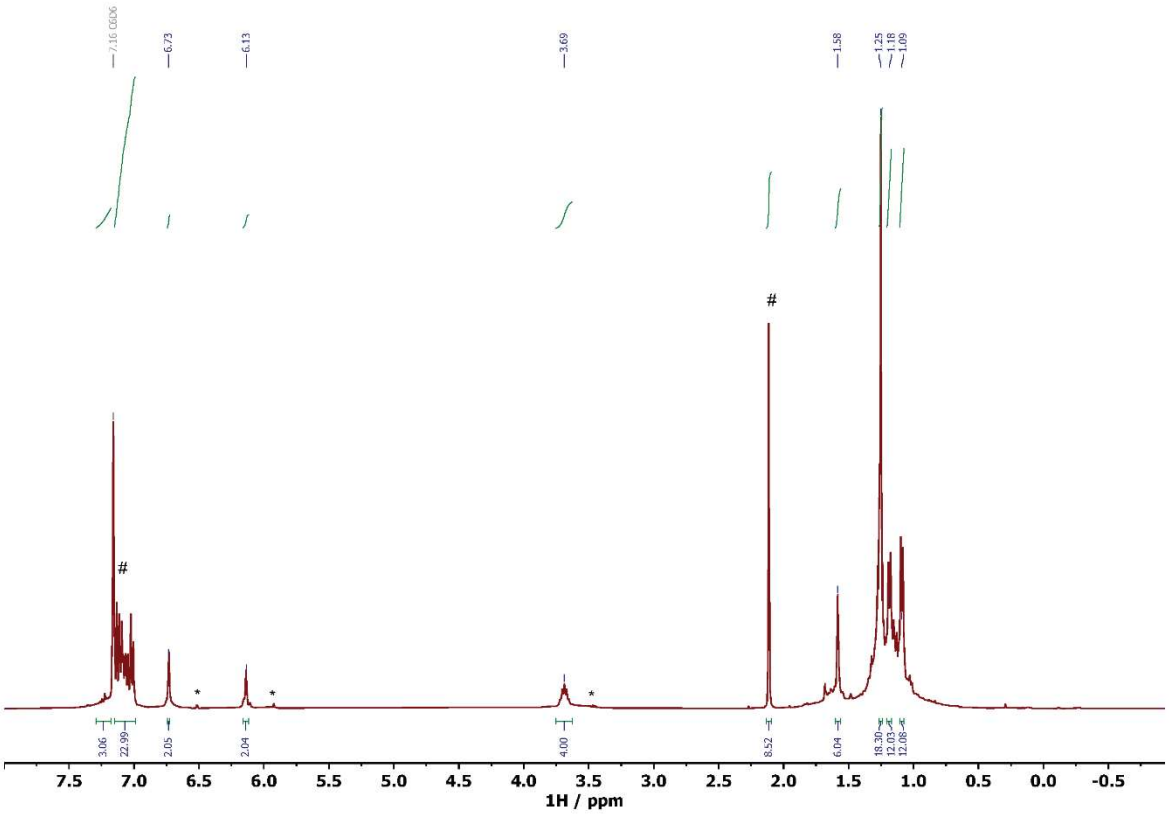

Figure s3: ^{1}H NMR spectrum of **4** in benzene-d_6 at 298 K.

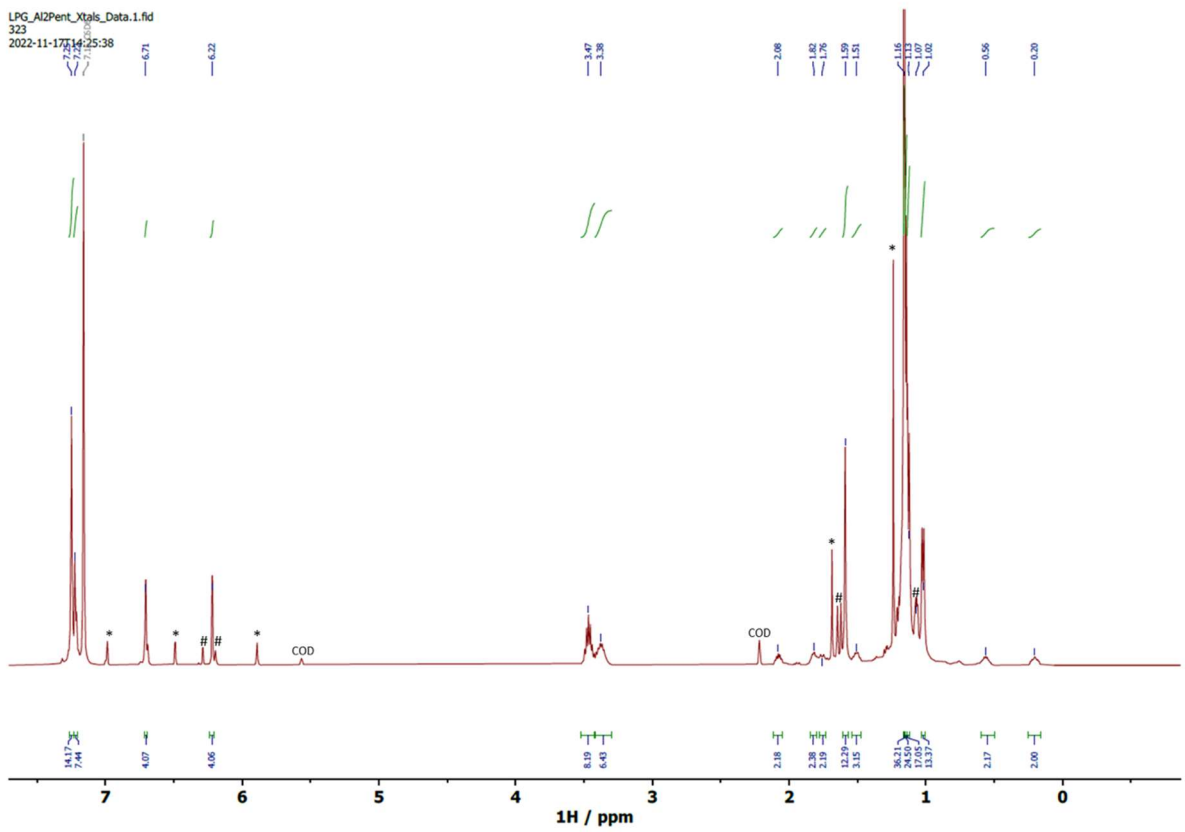

Due to the highly sensitive nature of this compound, some proteo-ligand is present, marked *

Figure s4: ^{1}H NMR spectrum of **5** in benzene-d_6 at 328 K.

^{19}F NMR spectra of novel compounds

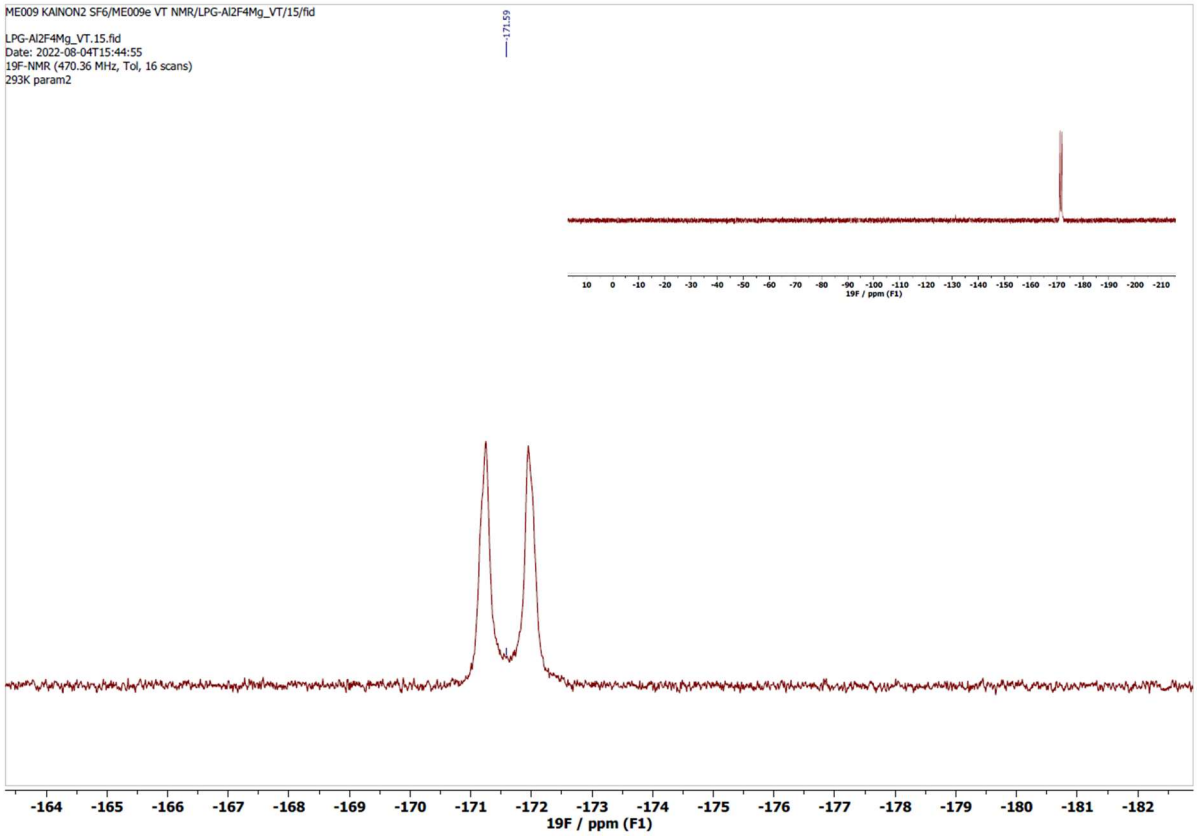

Figure s5: ^{19}F NMR spectrum of **3** in toluene-d_8 at 298 K.

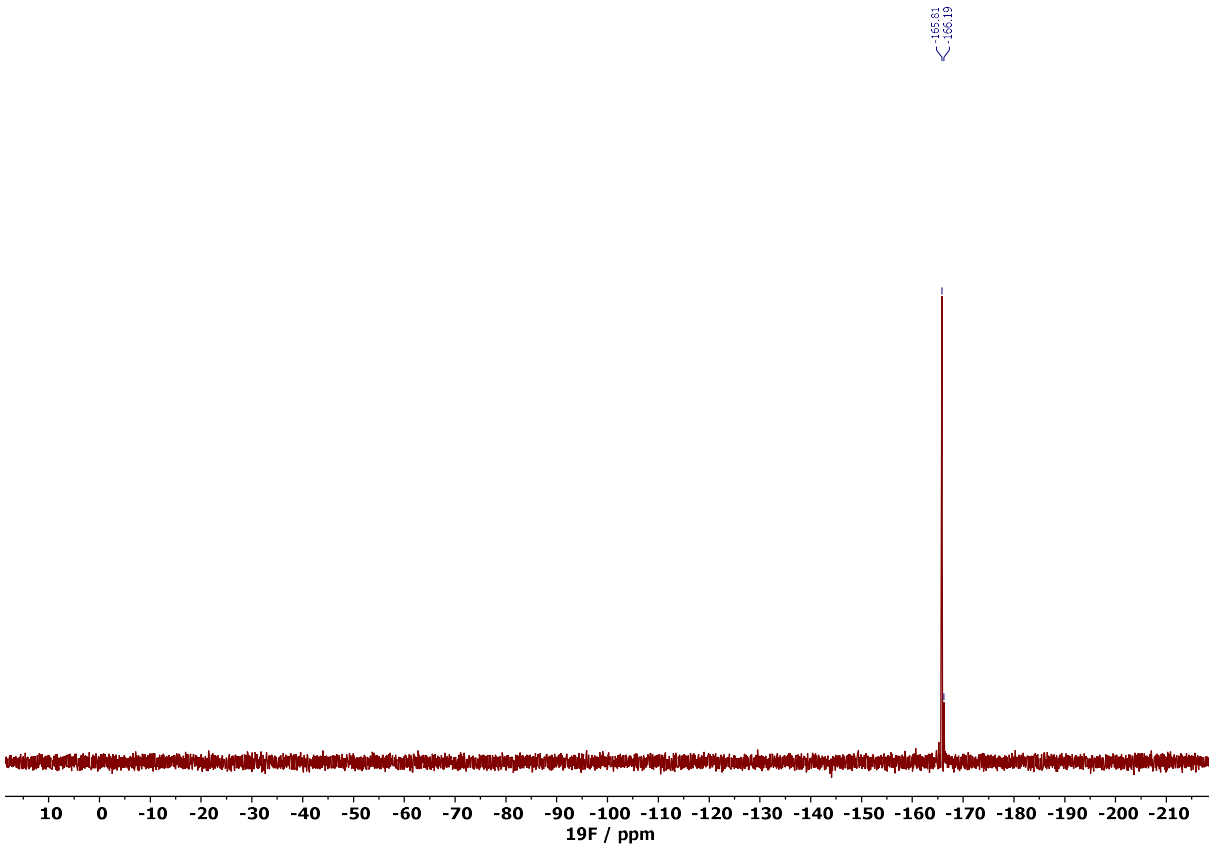

Figure s6: ^{19}F NMR spectrum of **4** in benzene-d_6 at 298 K.

VT-NMR spectra of compound 3

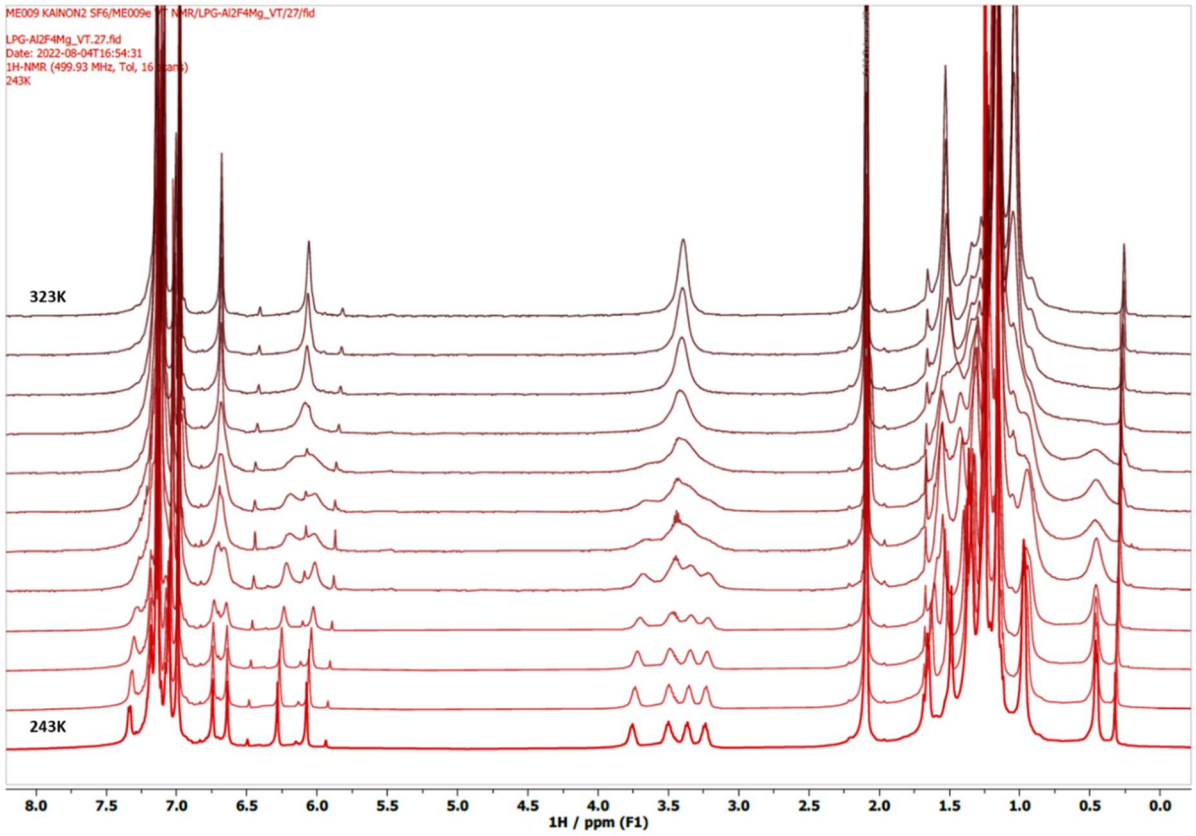

Figure s7: ^{1}H NMR spectra of compound **3** in toluene-d_8 in the temperature range 243-323 K.

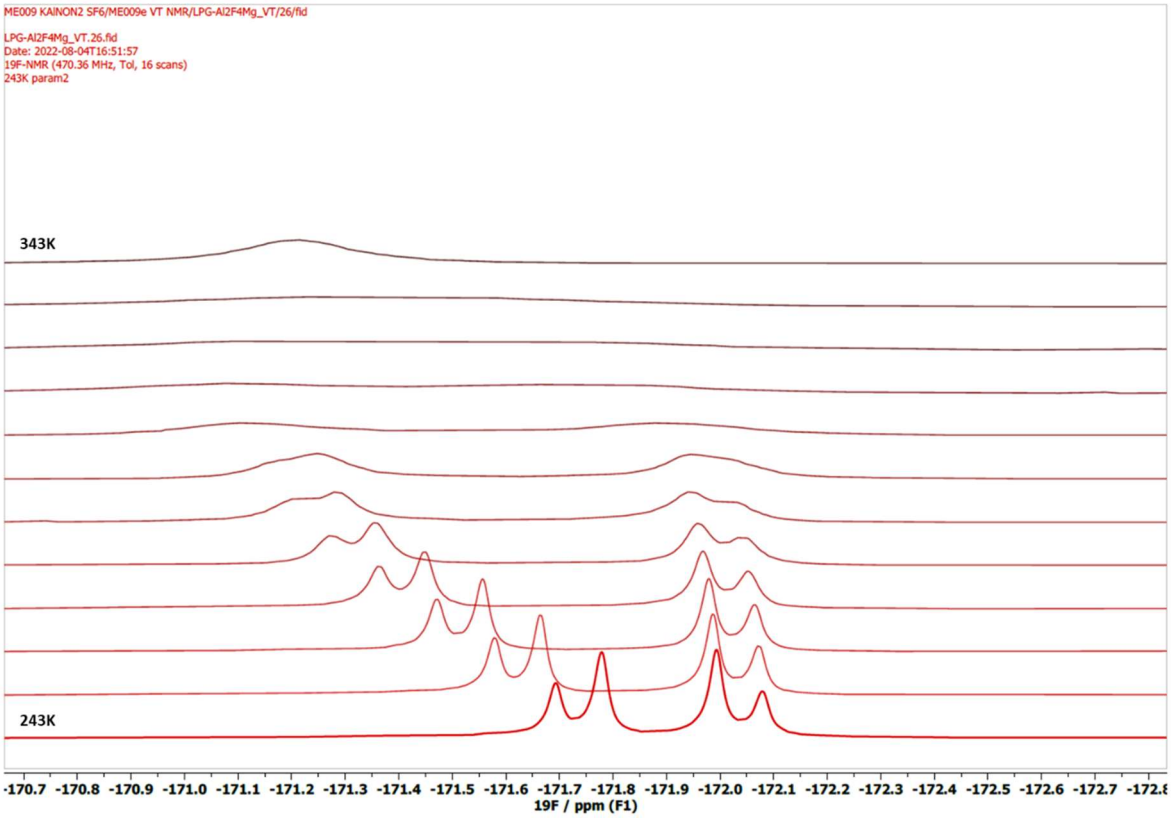

Figure s8: ^{19}F NMR spectra of compound **3** in toluene-d_8 in the temperature range 243-323 K.

UV-Vis Measurements

The UV-visible spectrum of **2** was measured at room temperature in a 10 mm quartz cuvette fitted with a J Youngs valve, in hexane under a nitrogen atmosphere. Measurements were recorded on a Jasco V-770 UV-Visible/NIR spectrophotometer operated under Spectra Manager™ suite. Measurements were made at 0.2 nm intervals with a UV/Vis bandwidth of 1 nm, UV/Vis response of 0.06 sec in continuous scan mode at a rate of 400 nm/min.

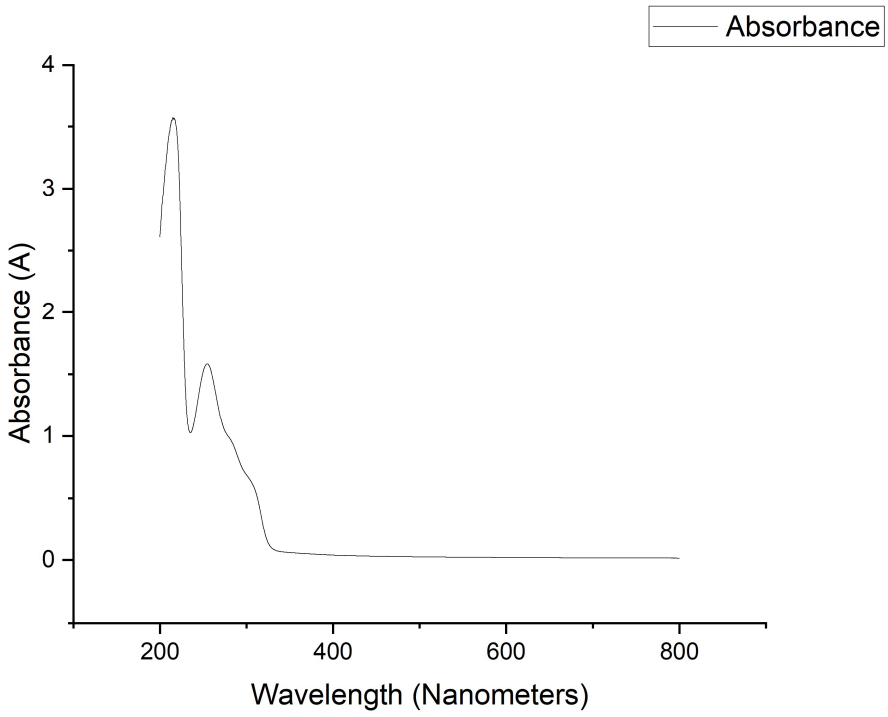

Figure s9: UV-vis spectrum of **2** in hexane solution at 1 mM concentration.

X-ray crystallographic details

Single-crystal X-ray diffraction data for compounds **2, 3, 4, 4-Crypt** and **5** were collected on an Oxford Diffraction/Agilent SuperNova diffractometer equipped with a 135 mm Atlas CCD area detector. Crystals were selected under Paratone-N oil, mounted on MiTeGen Micromount loops and quench-cooled using an Oxford Cryosystems open flow N2 cooling device.[s2] Data were collected at 150 K using mirror mono-chromated Cu Kα radiation (λ = 1.5418 Å; Oxford Diffraction Supernova) or Mo Kα radiation (λ = 0.71073 Å; Oxford Diffraction Supernova). Data collected were processed using the CrysAlisPro package, including unit cell parameter refinement and inter-frame scaling (which was carried out using SCALE3 ABSPACK within CrysAlisPro).[s3] Equivalent reflections were merged and diffraction patterns processed with the CrysAlisPro suite.[s3] Structures were solved ab initio from the integrated intensities using SHELXT[s4] and refined on F2 using SHELXL[s5] with the graphical interface OLEX2.[s6] Selected crystallographic data are summarised in Table s1 and full details are given in the supplementary deposited CIF files (CCDC 2219353, 2219355-2219358 and 2221942). These data can be obtained free of charge from the Cambridge Crystallographic Data Centre via http://www.ccdc.cam.ac.uk/ data_request/cif.

Table s1: Crystallographic details for compounds **2**-**5**

	2	**2** (benzene solvate)	**3**	**4**	**4-Crypt**	**5**
Formula	$C_{94}H_{124}Al_2MgN_4O_2$	$C_{94}H_{124}Al_2MgN_4O_2$, $2(C_6H_6)$	$C_{94}H_{124}Al_2F_4MgN_4O_2$, $2(C_6H_6)$	$C_{94}H_{124}Al_2F_4K_2N_4O_2$, $2(C_5H_{12})$	$C_{18}H_{36}KN_2O_6$, $C_{47}H_{62}AlF_2N_2O$, $3.5(C_6H_6)$	$C_{102}H_{136}Al_2N_4O_2$, $6(C_6H_6)$
Fw (g mol^{-1})	1420.23	1576.45	1652.45	1694.42	1424.92	1972.75
Cell setting	triclinic	triclinic	triclinic	triclinic	monoclinic	triclinic
Space group	$P\bar{1}$	$P\bar{1}$	$P\bar{1}$	$P\bar{1}$	$P2_1/n$	$P\bar{1}$
a (Å)	12.8192(2)	12.5309(3)	12.9111(2)	15.8244(3)	16.5037(2)	14.5163(3)
b (Å)	16.5733(2)	17.1329(4)	16.8041(3)	15.9715(3)	19.7916(2)	15.1146(4)
c (Å)	23.0557(3)	22.6705(5)	22.7512(4)	20.8117(3)	25.2040(3)	15.8736(5)
α (°)	83.2070(10)	84.516(2)	82.675(2)	87.7530(10)	90	109.864(3)
β (°)	88.1180(10)	89.851(2)	88.7830(10)	73.3950(10)	97.3040(10)	112.079(2)
γ (°)	88.0520(10)	88.262(2)	87.045(2)	85.8620(10)	90	92.765(2)
V (Å^{-3})	4859.08(12)	4842.64(19)	4888.76(15)	5026.50(15)	8165.70(16)	2972.85(15)
Z	2	2	2	2	4	1
ρ_{calc} (g cm^{-3})	0.971	1.081	1.123	1.120	1.159	1.102
Radiation, λ (Å)	1.54184	1.54184	1.54184	1.54184	1.54184	0.71073
Absorption	Gaussian	Gaussian	Multi-scan	Gaussian	Gaussian	Multi-scan
μ (mm^{-1})	0.654	0.701	0.776	1.432	1.139	0.077
Reflections collected	98626	69685	128113	186929	105797	60017
Indep. reflections	20050	20039	20314	20852	17034	16270
$R_{(int)}$	0.0280	0.0426	0.0435	0.0547	0.0426	0.0453
Parameters	1175	1240	1268	1280	981	717
R_1 (all data/ I >2σ(I))	0.0450	0.0461	0.0574	0.0494	0.0429	0.0605
ωR_2 (all data/ I >2σ(I))	0.1346	0.1333	0.1699	0.1498	0.1282	0.1595
GooF	1.042	1.012	1.046	1.022	1.018	1.008
T (K)	150.01(12)	150.00(10)	150.01(10)	150.01(10)	150.01(10)	150.01(10)
CCDC No.	2221942	2219353	2219357	2219358	2219355	2219356

EPR details

Under illumination from a 280 nm LED source, a multi-step radical pathway is present to the end of the formation of the pentalene product, in which we observe three or more component radicals. At most this process contains a radical concentration at up to 60 uM for a starting molecular concentration of 3 mM of **1**. In the absence of the cyclooctadiene (COD), simulation in the limit of two components features first a g-value of 2.0028 and hyperfine splittings to ^{27}Al of 12 MHz, with a large second splitting consistent with a proton hyperfine, and second a feature with close to half the ^{27}Al hyperfine splitting, having a significant shift in the g-value to 2.005 (Figure s16), which has consequently been modelled as containing a Mg ion,[s16] although large aluminyl character also leads to a positive isotropic g-shift.[s17] Upon the addition of COD these two radicals diminish and a third (or more) radical species are formed with as shown in Figure s17, beginning clearly at 1.5 hours and more obvious at 10 hours in the light activated time course. In the first minutes of the reaction however, the light induced radical state is independent of COD. Whether this is a photolytic process or intramolecular redox state is unknown, but triplet character as indicated by a half-field signal is absent (not shown) in the low-temperature EPR measurement of sample frozen at peak radical concentrations, figure s16b. The maximum radical concentrations are lower in the presence of COD due to the formation of the diamagnetic product **2**.

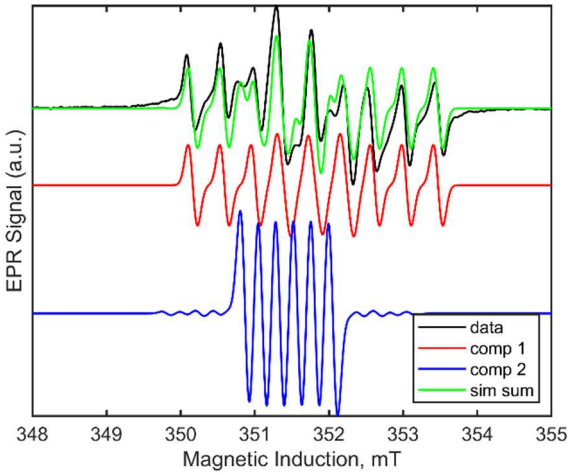

Figure s10: EPR simulation of **1** at one hour of photolysis. A total simulation in green of two components overlays the black data trace. The first component (red) consists of a g-value of 2.0028 with a ^{27}Al with hyperfine value of 12 MHz a ^{1}H hyperfine of 33 MHz. A second component (blue) consists of g = 2.005, including a Mg hyperfine at natural abundance given a value of 12 MHz, while the ^{27}Al hyperfine of is 6.6 MHz.

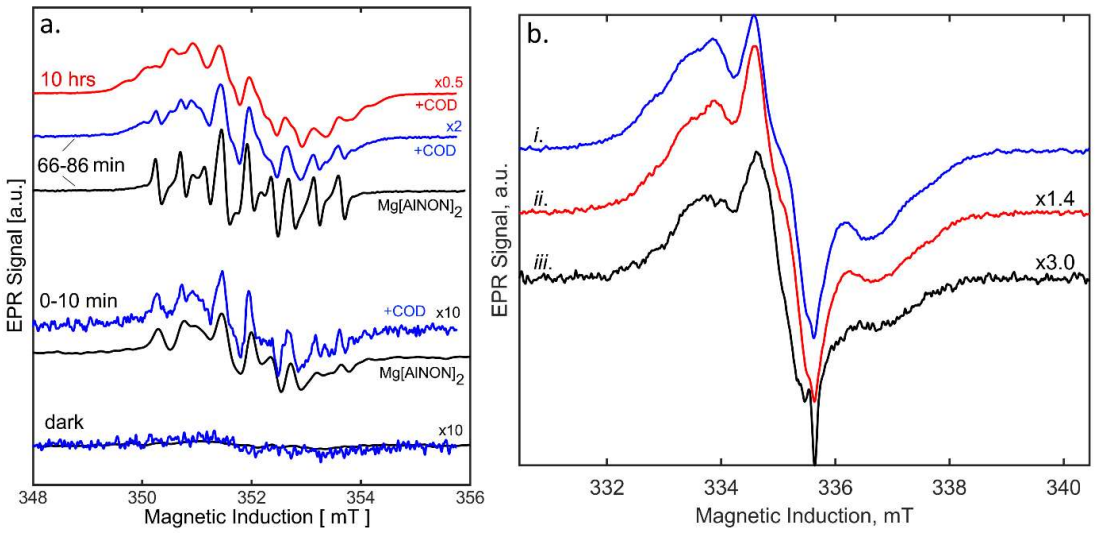

Figure s11: X-band CW-EPR for the (panel a.) room temperature UV-irradiation (280 nm, 10 mW) of **1** as a 0.25 mM solution in benzene, alone (black) and with added COD reactant (blue). The 100 kHz field modulation was 200 uT for the black traces and 30 uT for the blue and red traces. Three time periods are as shown, with a final 10 h time point in red with COD. The black traces used a microwave frequency of 9.8627 GHz with data shifted by 16 uT to match blue traces with a frequency of 9.8668 GHz. Under frozen conditions (panel b), solvent dependence of **1** in benzene (i) and hexane (ii) are shown, while trace (iii) shows the frozen reaction with COD. The measurement had a microwave frequency of 9.3880 GHz, field modulation of 100 uT, microwave power of 2 uW, and temperature of 100 K.

EPR METHODS

Electron paramagnetic resonance (EPR) data was collected in the Centre for Advanced ESR (CAESR) of the Department of Chemistry, University of Oxford. The continuous wave EPR (CW-EPR) spectrometer operating at X-band (9.1-9.9 GHz) was a Bruker Biospin EMXmicro with a Premium bridge and a ER4122-SHQE-W1 resonator, which gives a Q-value of approximately 10500 with a benzene solvent and 3.8 mm OD x 2.8 mm ID clear fused quartz tubes featuring an anaerobic J Young seal adapted at their top. The sample was illuminated with a custom four-LED arrangement to shine into the resonator is light access slots. Simulations were performed with EasySpin routines in the Matlab environment (The Mathworks, Natick, NJ).[s18]

Computational details

The geometry optimizations were performed with the Gaussian16 (Revision C.01) programme[s7] using the PBE1PBE hybrid exchange functional,[s8] and Def2-SVP basis set.[s9] In addition empirical dispersion correction with Becke-Johnson damping (GD3BJ)[s10] was used where indicated. Full analytical frequency calculations were performed for the optimized structures to ensure the nature of the stationary points found (minima, no imaginary frequencies). Single point energies were calculated using the ωB97X-D range separated hybrid functional[s11] in conjunction with the Def2QZVP basis set.[S9] The bonding was examined by using Natural Atomic Orbital and Natural Bond orbital analyses[s12] as implemented in NBO7. QT-AIM analysis performed using AIMALL.[s13] ELF analysis was performed using the programme Multiwfn, isovalue = 0.6,[s14] with images were made using the ChimeraX programme.[s15]

Compound 2 – Bond angles comparison

AlMgAl angles comparison

	With dispersion	without
Angle	158.88	171.99

Compound 2 – With dispersion correction

HOMO-LUMO gap = 7.296016 eV

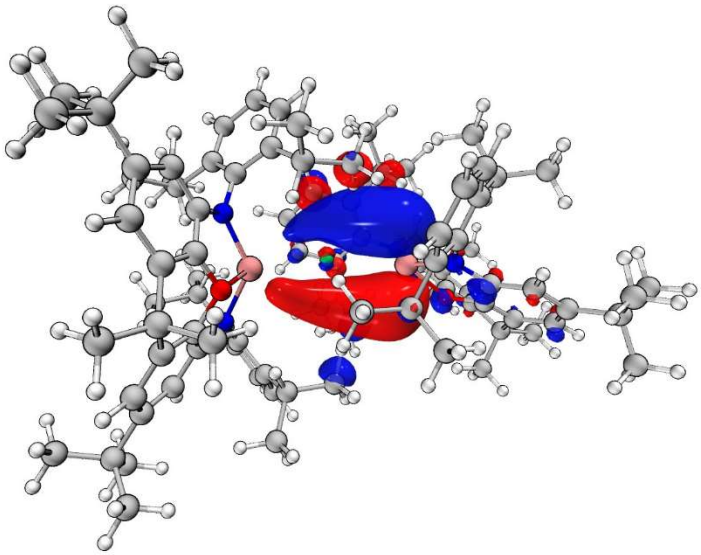

Figure s12: LUMO of compound **2** (E = 0.850483 eV). Orbitals plotted with isovalue 0.03

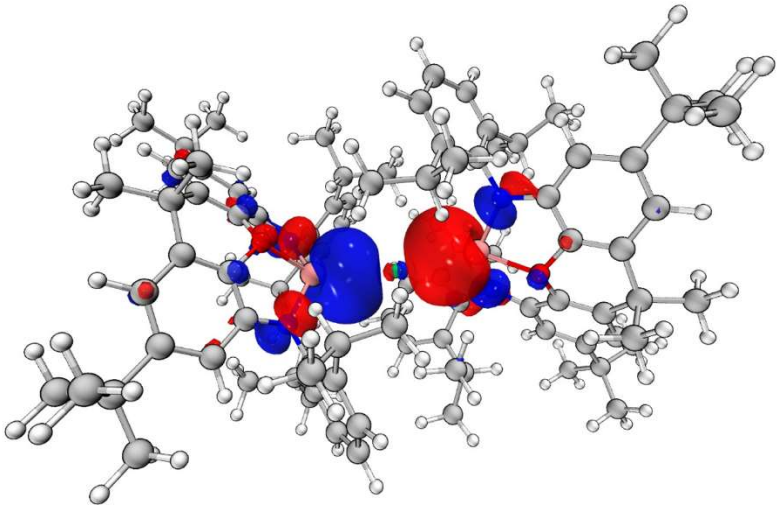

Figure s13: HOMO of compound **2** (E = -6.445533 eV). Orbitals plotted with isovalue 0.03

NBO

NPA charges (e)
Al 1.01032
Al 1.15487
Mg 0.98309

WBI

	Al	Mg	Al
Al	0	0.4220	0.2126
Mg		0	0.5665
Al			0

QTAIM

BCP	398	596
rho	0.037874	0.036625
g	0.019183	0.018511
k	0.009033	0.008534
v	-0.028216	-0.027045
e	-0.009033	-0.008534
delsqrho	0.040599	0.039907
elf	0.289945	0.281662
lol	0.390002	0.385190

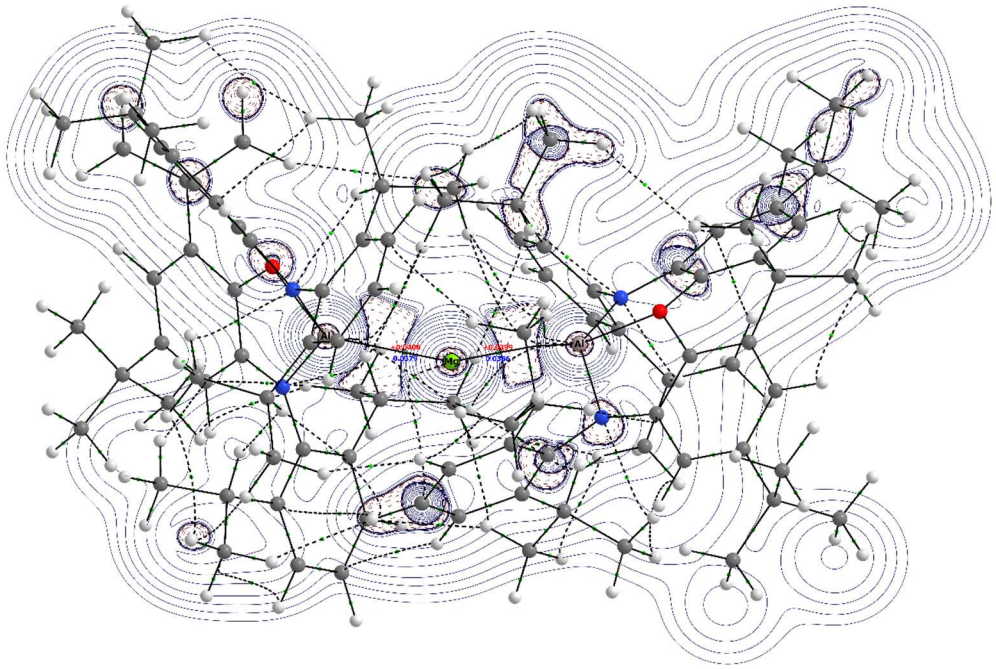

Figure s14: QTAIM plot for compound **2**. Key: Red = Laplacian of electron density, Blue = electron density.

ELF

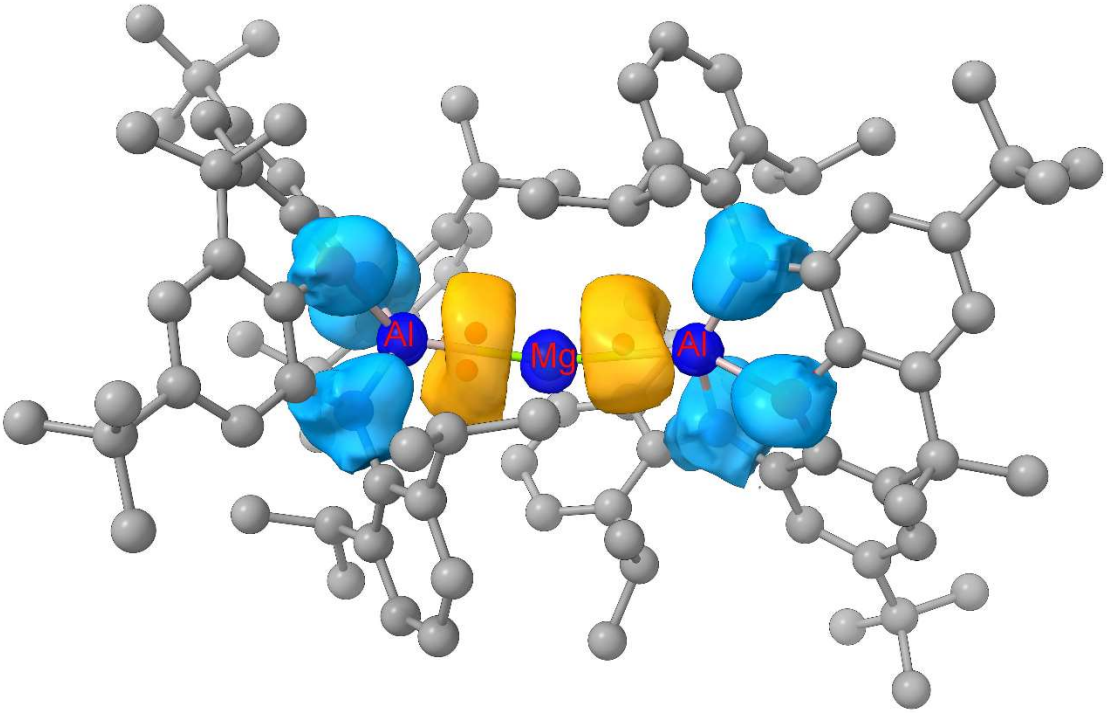

Figure s15: ELF isosurface for compound **2** (0.6 a.u.) Key: Yellow = metal-metal bond basins, Blue = ligand-based basins.

Basin	ELF	pop	vol
118	0.996	1.073	15.096
175	0.995	0.892	12.017
141	0.996	1.948	23.336
sum(halfs)		1.965	27.113
sum(tot)		3.9132	50.449

	Al	Mg	Al	2_check
118	0.8586	0.1631		1.0217
175	0.7306	0.1146		0.8452
sum of above	1.5892	0.27769		1.8669
141		0.24049	1.5943	1.8348

Nacnac^{DiEPE}MgMgMgNacnac^{DiEPE}

NBO

NPA charges (e)
Mg 0.80489
Mg 0.38884
Mg 0.80490

WBI

	Mg	Mg	Mg
Mg	0	0.4731	0.2919
Mg		0	0.4731
Mg			0

QTAIM

BCP	441	444	458	463
rho	0.031289	0.030983	0.030984	0.031290
g	0.006278	0.006988	0.006989	0.006278
k	0.009161	0.009012	0.009013	0.009161
v	-0.015439	-0.016001	-0.016001	-0.015440
e	-0.009161	-0.009012	-0.009013	-0.009161
delsqrho	-0.011533	-0.008097	-0.008097	-0.011532
elf	0.668081	0.611260	0.611254	0.668064
lol	0.586945	0.556689	0.556686	0.586936

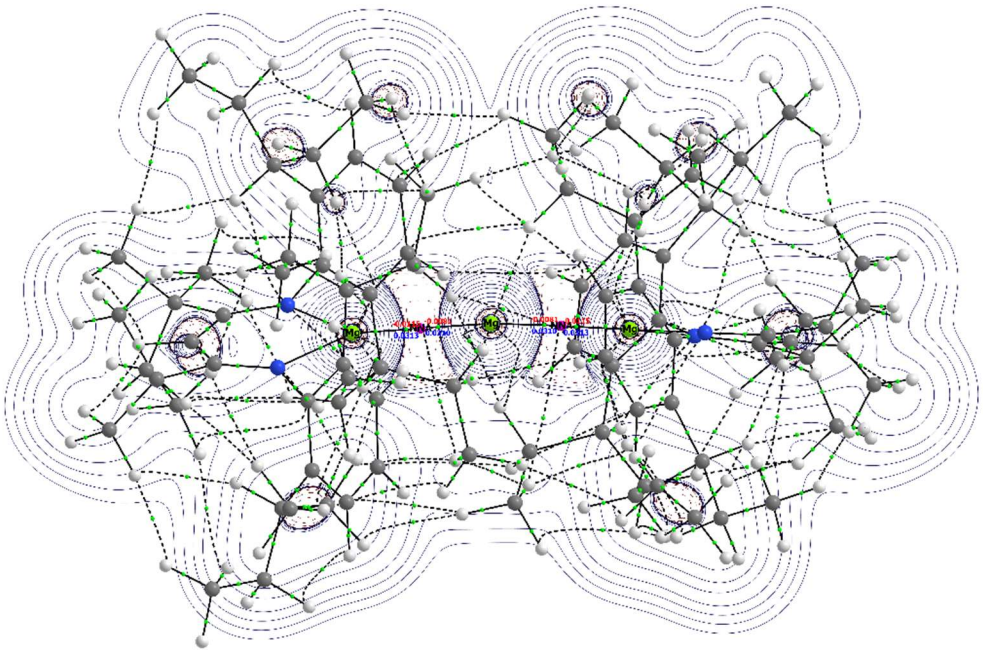

Figure s16: QTAIM plot for Nacnac^{DiEPE}MgMgMgNacnac^{DiEPE}. Key: Red = Laplacian of electron density, Blue = electron density.

ELF

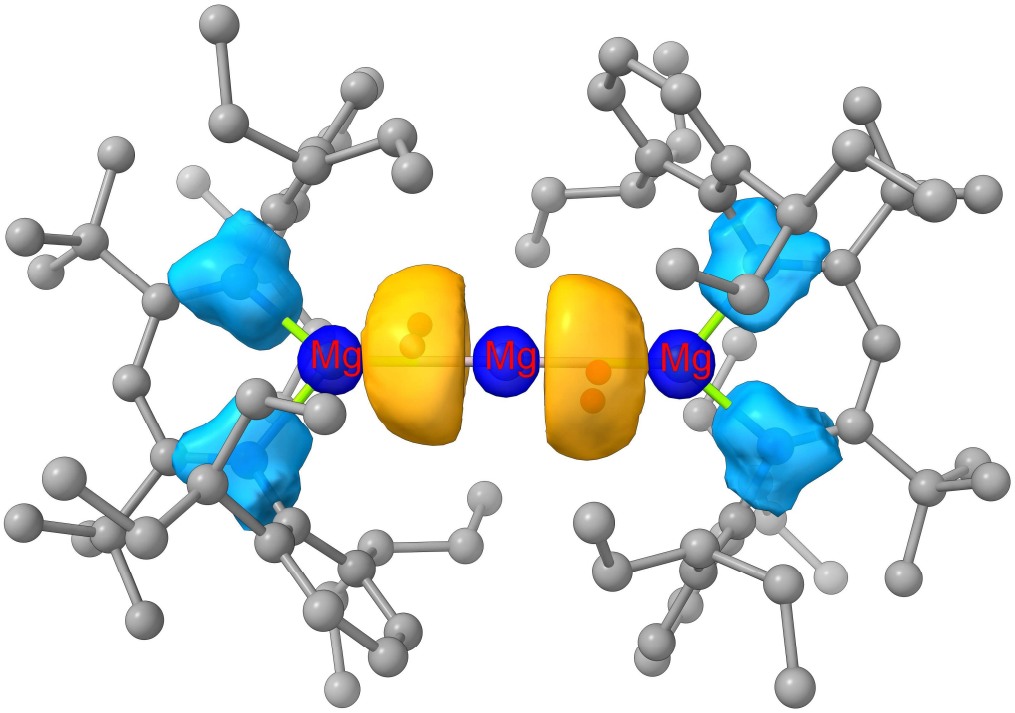

Figure s17: ELF isosurface for Nacnac^{DiEPE}MgMgMgNacnac^{DiEPE} (0.6 a.u.) Key: Yellow = metal-metal bond basins, Blue = ligand-based basins.

Basin	ELF	pop	vol
181	0.994	1.1077	22.607
104	0.994	0.7662	13.403
sumhalf		1.8739	36.01
185	0.994	1.1075	22.6
106	0.994	0.76659	13.4
sumhalf		1.87409	36
sum		3.74799	72.01

	Mg	nna	Mg	nna	Mg	
181	0.25436	0.49261	0.29562			1.04259
104	0.20726	0.33667	0.17176			0.71569
sum of above	0.46162	0.82928	0.46738	0	0	1.75828
185			0.29557	0.49252	0.25125	1.03934
106			0.17185	0.33678	0.20731	0.71594
sum of above	0	0	0.46742	0.8293	0.45856	1.75528

Nacnac^{Dipp}MgAlNON

NBO

NPA
Al 1.00852
Mg 1.43684

WBI

0.5995

XYZ coordinates of optimised structures

(Nacnac^{Dipp})MgAl(NON)			
E = -3459.629480 Eh			
Al	-0.07780000	-0.09608000	-0.28509000
O	-1.89740000	0.26045000	0.52856000
N	-0.45748000	1.58100000	-1.12632000
N	-0.94893000	-1.77741000	-0.67668000
C	-2.51890000	1.38555000	-0.00413000
C	-2.73300000	-0.85306000	0.54191000
C	-1.72484000	2.09333000	-0.90967000
C	-2.18192000	-1.96594000	-0.09358000
C	-2.32010000	3.22764000	-1.47397000
H	-1.73339000	3.82101000	-2.17789000
C	-3.82893000	1.65536000	0.32510000
C	-3.64650000	3.57880000	-1.16801000
C	-0.34628000	-2.87286000	-1.34458000
C	-2.99371000	-3.11549000	-0.11074000
H	-2.59748000	-4.01517000	-0.57868000
C	0.57820000	2.47985000	-1.48302000
C	-4.39231000	2.78774000	-0.28074000
H	-5.42637000	3.04447000	-0.06121000
C	0.96658000	3.50790000	-0.58869000
C	-4.04972000	-0.71409000	0.93327000
C	-4.30593000	-3.07584000	0.37581000
C	-4.50511000	0.69854000	1.31746000
C	0.37462000	-3.84355000	-0.61239000
C	1.26217000	2.31501000	-2.70780000
C	-5.20329000	-4.31818000	0.34142000
C	-0.47132000	-2.98466000	-2.75264000
C	-4.25057000	4.81188000	-1.85108000
C	-4.83739000	-1.86731000	0.86355000
H	-5.88168000	-1.82232000	1.17276000
C	0.33375000	3.67353000	0.78073000
H	-0.43976000	2.90254000	0.89285000
C	2.00535000	4.36677000	-0.95900000
H	2.30614000	5.16486000	-0.27467000
C	0.48600000	-3.77654000	0.89766000
H	0.02006000	-2.83017000	1.20202000
C	0.90260000	1.16882000	-3.62691000
H	-0.15801000	0.93769000	-3.43649000
C	-3.99152000	1.02351000	2.73491000
H	-4.27117000	2.05072000	3.01502000
H	-2.89657000	0.94042000	2.79347000
H	-4.42896000	0.32624000	3.46615000
C	0.97350000	-4.90460000	-1.30014000
H	1.53266000	-5.65857000	-0.73961000
C	-1.29107000	-1.97824000	-3.54252000
H	-1.11129000	-0.99338000	-3.08053000
C	2.31158000	3.18154000	-3.02484000
H	2.84940000	3.05050000	-3.96586000
C	0.15111000	-4.05821000	-3.39502000
H	0.07069000	-4.15645000	-4.47888000
C	-6.02232000	0.82917000	1.28276000
H	-6.42442000	0.60373000	0.28437000
H	-6.32885000	1.84813000	1.55984000
H	-6.48614000	0.14426000	2.00720000

2 with dispersion correction			
E = -4711.912762 Eh			
Al	2.653559	0.257660	-0.070565
O	4.370243	-0.408354	0.838874
N	3.261242	1.857877	0.773147
N	3.378616	-0.977387	-1.406919
C	5.066084	0.569379	1.533056
C	6.316033	0.309435	2.057362
C	4.426780	1.809065	1.509681
C	6.306412	2.630020	2.826902
C	5.060210	2.839899	2.221920
H	4.570672	3.811539	2.264300
C	6.424447	-1.609878	0.501498
C	5.163296	-1.247183	0.069809
C	2.556824	3.087870	0.717788
C	6.879406	-1.103471	1.874867
C	6.935524	1.377249	2.716506
H	7.924908	1.232848	3.150679
C	4.588001	-1.580451	-1.157773
C	7.145124	-2.445592	-0.358155
H	8.145527	-2.768117	-0.069216
C	6.606399	-2.880499	-1.582925
C	6.257262	-2.015645	2.951212
H	6.531454	-1.661281	3.956604
H	6.614113	-3.049756	2.828470
H	5.159898	-2.021420	2.878414
C	1.421890	3.288416	1.537859
C	5.337704	-2.439169	-1.979180
H	4.908487	-2.739387	-2.934656
C	8.398088	-1.123108	2.006066
H	8.876243	-0.481977	1.251323
H	8.784643	-2.145786	1.891101
H	8.705341	-0.776648	3.003026
C	1.218821	5.548087	0.664827
H	0.701403	6.510378	0.651533
C	2.360056	-1.502067	-2.219269
C	0.772294	4.526167	1.495893
H	-0.101045	4.694760	2.129916
C	2.993403	4.108877	-0.157377
C	2.316327	5.332016	-0.160106
H	2.652802	6.128880	-0.828594
C	0.929250	2.208773	2.480580
H	1.336965	1.255119	2.109844
C	1.733176	-2.738543	-1.909815
C	1.779970	-0.634775	-3.188014
C	4.156387	3.897807	-1.107641
H	4.482824	2.853637	-0.989854
C	1.484499	2.424306	3.888823
H	2.584291	2.457092	3.879067
H	1.172493	1.610542	4.563075
H	1.121826	3.374772	4.313310
C	2.325934	-3.698713	-0.892088
H	3.418556	-3.602972	-0.947583
C	-0.591566	2.074002	2.484477
H	-1.090655	2.954911	2.918340

C	-3.40949000	6.05038000	-1.51155000	H	-0.900322	1.201362	3.079991
H	-3.82993000	6.94568000	-1.99693000	H	-0.984282	1.936973	1.463880
H	-2.36881000	5.94491000	-1.85154000	C	-0.122719	-2.138723	-3.372607
H	-3.39165000	6.22677000	-0.42507000	H	-1.111871	-2.359323	-3.777848
C	-5.64984000	-4.65391000	1.77153000	C	5.347990	4.796262	-0.776935
H	-6.21219000	-3.82584000	2.22761000	H	6.182799	4.600837	-1.468253
H	-4.77965000	-4.86084000	2.41345000	H	5.710220	4.619143	0.245434
H	-6.29859000	-5.54469000	1.77486000	H	5.082178	5.862013	-0.867376
C	1.93474000	-3.75496000	1.37915000	C	0.496693	-3.029185	-2.501262
H	2.45982000	-4.69368000	1.14158000	H	-0.009749	-3.957345	-2.234380
H	1.98563000	-3.61782000	2.46969000	C	1.996125	-5.160090	-1.183606
H	2.51538000	-2.94533000	0.91159000	H	0.933305	-5.386489	-1.007328
C	2.67762000	4.21125000	-2.16583000	H	2.577124	-5.813117	-0.514751
H	3.49252000	4.88832000	-2.43382000	H	2.241061	-5.432079	-2.221771
C	-5.68928000	5.07540000	-1.40469000	C	2.536410	0.607923	-3.626536
H	-6.07751000	5.97102000	-1.91331000	H	2.722545	1.214807	-2.719276
H	-5.75397000	5.25419000	-0.32051000	C	3.715723	4.085847	-2.559322
H	-6.35630000	4.23699000	-1.65646000	H	3.452657	5.134722	-2.769841
C	0.86942000	-5.01267000	-2.68004000	H	2.834012	3.471511	-2.789795
H	1.34577000	-5.84478000	-3.20425000	H	4.523672	3.801393	-3.251918
C	-0.35017000	5.02926000	0.94365000	C	0.526598	-0.958278	-3.727951
H	0.37281000	5.85769000	0.87125000	H	0.037199	-0.277583	-4.425791
H	-0.83893000	5.09840000	1.92817000	C	1.903820	-3.324785	0.526692
H	-1.11867000	5.17902000	0.17293000	H	2.217047	-2.301504	0.786157
C	-2.79360000	-2.25516000	-3.43302000	H	2.353510	-4.006255	1.265610
H	-3.03086000	-3.25373000	-3.83531000	H	0.810688	-3.384568	0.641679
H	-3.36103000	-1.51179000	-4.01487000	C	1.769925	1.473610	-4.615147
H	-3.15108000	-2.21547000	-2.39738000	H	1.597381	0.937720	-5.562295
C	1.35422000	3.43323000	1.88903000	H	2.349913	2.377870	-4.850991
H	1.80437000	2.43238000	1.79741000	H	0.793451	1.788496	-4.227447
H	0.87934000	3.48099000	2.87999000	C	3.903780	0.242873	-4.210148
H	2.17356000	4.16914000	1.86416000	H	4.524503	-0.306645	-3.491860
C	-4.48220000	-5.53785000	-0.23432000	H	4.448033	1.155230	-4.499799
H	-5.15788000	-6.40676000	-0.22586000	H	3.781655	-0.378715	-5.111669
H	-3.59190000	-5.80307000	0.35592000	Al	-2.579904	-0.444896	-0.267635
H	-4.16551000	-5.37327000	-1.27530000	O	-3.907538	0.516462	0.972049
C	-0.90819000	-1.89174000	-5.01690000	N	-3.536009	0.637640	-1.537379
H	0.17438000	-1.77380000	-5.16729000	N	-3.158869	-1.910339	0.830149
H	-1.41043000	-1.03095000	-5.48368000	C	-3.042571	0.907144	-2.837626
H	-1.22768000	-2.78895000	-5.57089000	C	-4.156805	-1.658306	1.753778
C	1.05469000	1.49658000	-5.10836000	C	-4.574390	-0.333681	1.845231
H	0.51394000	2.41696000	-5.37618000	C	-2.200998	2.025070	-3.047899
H	0.65612000	0.67524000	-5.72227000	C	-4.763362	1.393640	0.317056
H	2.11056000	1.62883000	-5.39436000	C	-3.399647	0.065422	-3.917016
C	-6.43377000	-4.03273000	-0.53167000	C	-2.405911	-3.095732	1.006712
H	-7.08850000	-4.91795000	-0.57599000	C	-4.531933	1.463818	-1.057734
H	-6.13161000	-3.77711000	-1.55896000	C	-4.813032	-2.568494	2.598529
H	-7.02953000	-3.19525000	-0.14007000	H	-4.503251	-3.611921	2.567318
C	-4.25111000	4.59350000	-3.37135000	C	-5.621550	0.140632	2.611155
H	-4.84501000	3.70584000	-3.63807000	C	-6.256776	-0.800222	3.426920
H	-3.23365000	4.44444000	-3.76144000	H	-7.086641	-0.482978	4.058689
H	-4.68508000	5.46571000	-3.88641000	C	-2.921481	0.371212	-5.194535
C	-0.29036000	-4.90778000	1.57268000	H	-3.185908	-0.269198	-6.037735
H	-1.34906000	-4.89643000	1.27813000	C	-5.850113	-2.147024	3.439782
H	-0.24435000	-4.80748000	2.66883000	C	-4.327865	-1.113411	-3.692438
H	0.12819000	-5.89253000	1.30856000	H	-4.073869	-1.530762	-2.704892
C	1.73906000	-0.05286000	-3.25202000	C	-1.777934	2.311020	-4.349993

H	1.51364000	-0.92564000	-3.88067000	H	-1.152301	3.189550	-4.527631
H	1.58067000	-0.35619000	-2.20099000	C	-2.129637	1.494085	-5.417230
H	2.81101000	0.17182000	-3.33904000	H	-1.782549	1.728585	-6.426483
Mg	2.20445000	-0.32105000	1.07309000	C	-5.361769	2.341848	-1.767349
N	4.13712000	-0.77836000	0.58220000	H	-5.199216	2.456272	-2.840370
N	2.55448000	-0.41674000	3.08851000	C	-6.409176	3.024860	-1.127421
C	4.58810000	-0.45650000	-0.72657000	C	-5.810502	1.979413	0.994726
C	1.71462000	0.30316000	3.97499000	C	-1.605979	-3.255050	2.164401
C	4.92985000	0.87753000	-1.01685000	C	-6.640746	2.821852	0.240576
C	3.56992000	-1.13087000	3.57182000	H	-7.479724	3.312185	0.729246
C	4.62745000	-1.43494000	-1.73941000	C	-5.962744	1.628803	2.478451
C	4.97721000	-1.32033000	1.45547000	C	-2.457707	-4.120184	0.031307
C	4.64957000	-1.59945000	2.80142000	C	-1.419108	-2.141285	3.180556
H	5.40524000	-2.15567000	3.35523000	H	-2.037112	-1.290392	2.861995
C	0.38120000	-0.09702000	4.19220000	C	-7.365001	1.934154	2.990141
C	2.19512000	1.49287000	4.55980000	H	-7.586883	3.006700	2.894520
C	5.08445000	-1.06822000	-3.00705000	H	-7.450707	1.682333	4.056973
H	5.12248000	-1.83255000	-3.78927000	H	-8.129064	1.369652	2.436191
C	5.45606000	0.24287000	-3.31490000	C	-4.931336	2.441568	3.286638
C	5.35912000	1.20205000	-2.30598000	H	-3.906872	2.242469	2.939828
H	5.61951000	2.24162000	-2.52487000	H	-4.989164	2.177350	4.353640
C	6.38661000	-1.63179000	1.02437000	H	-5.126218	3.519366	3.177216
H	6.40561000	-2.28457000	0.14002000	C	-1.751194	-5.304373	0.260381
H	6.95849000	-2.10238000	1.83271000	H	-1.789149	-6.106483	-0.478285
H	6.89485000	-0.70098000	0.72697000	C	-0.940052	-4.468671	2.361892
C	3.59190000	-1.45629000	5.04385000	H	-0.331217	-4.603960	3.259764
H	3.73691000	-0.55098000	5.65164000	C	-3.299276	-3.938296	-1.217919
H	4.39086000	-2.16825000	5.28370000	H	-3.081697	-2.921659	-1.594026
H	2.62444000	-1.88116000	5.35185000	C	0.031910	-1.658343	3.205752
C	3.58670000	1.97593000	4.27245000	H	0.727782	-2.468855	3.473767
H	3.73167000	2.99848000	4.64660000	H	0.160596	-0.850429	3.943212
H	3.79140000	1.96804000	3.19076000	H	0.346120	-1.265101	2.225553
H	4.35878000	1.33833000	4.73243000	C	-1.014334	-5.491724	1.426140
C	4.12326000	-2.82592000	-1.49418000	H	-0.482165	-6.431143	1.593024
H	3.02345000	-2.83091000	-1.41068000	C	-2.961444	-4.913624	-2.338545
H	4.50985000	-3.26502000	-0.56315000	H	-1.891244	-4.905106	-2.592708
H	4.38650000	-3.49303000	-2.32613000	H	-3.522676	-4.653483	-3.246714
C	1.33966000	2.24406000	5.36945000	H	-3.236165	-5.946954	-2.073670
H	1.71741000	3.17057000	5.81284000	C	-1.886056	-2.548608	4.577612
C	-0.44139000	0.69377000	4.99718000	H	-2.938201	-2.867079	4.565840
H	-1.47643000	0.37628000	5.15714000	H	-1.797211	-1.701837	5.276027
C	4.80074000	1.93991000	0.03464000	H	-1.280998	-3.376181	4.981268
H	5.27288000	2.87661000	-0.28982000	C	-4.171235	-2.222980	-4.725167
H	5.24641000	1.63203000	0.99235000	H	-4.782734	-3.092109	-4.439822
H	3.73868000	2.17522000	0.22531000	H	-3.127371	-2.558417	-4.821499
C	-0.15355000	-1.34605000	3.56197000	H	-4.515507	-1.906163	-5.722281
H	-1.16959000	-1.57049000	3.91282000	C	-5.789115	-0.664520	-3.617007
H	0.48873000	-2.21618000	3.76432000	H	-6.101433	-0.201564	-4.567364
H	-0.20310000	-1.24228000	2.46486000	H	-5.949949	0.066716	-2.814335
C	5.87480000	0.62005000	-4.70622000	H	-6.448350	-1.526298	-3.426311
H	6.51087000	1.51696000	-4.70868000	C	-4.794844	-3.997690	-0.900758
H	4.99450000	0.84067000	-5.33453000	H	-5.065407	-4.996364	-0.521943
H	6.42739000	-0.19388000	-5.19823000	H	-5.391620	-3.805981	-1.806869
C	0.01591000	1.86701000	5.60187000	H	-5.079587	-3.256562	-0.142920
C	-0.88704000	2.68332000	6.48083000	C	-2.388577	4.298218	-1.951972
H	-1.90406000	2.74472000	6.06489000	H	-2.048183	4.906280	-1.099173
H	-0.50836000	3.70768000	6.60741000	H	-3.484347	4.232603	-1.910286

H -0.97427000 2.23749000 7.48587000	H -2.110811 4.832405 -2.875276 C -1.742418 2.913327 -1.906127 H -2.062044 2.428705 -0.970533 C -0.221511 3.038398 -1.858034 H 0.172437 3.592068 -2.724445 H 0.275356 2.053517 -1.851501 H 0.099184 3.573366 -0.953412 Mg 0.080099 -0.351237 -0.586817 C -7.294555 3.948155 -1.971896 C -6.564069 -3.127315 4.377435 C 7.023930 3.755794 3.580840 C 7.435823 -3.823196 -2.462268 C -6.355846 -2.669791 5.828654 H -6.764216 -1.662969 6.000609 H -6.855103 -3.360345 6.527350 H -5.284205 -2.643116 6.079999 C -8.064206 -3.148162 4.052119 H -8.592207 -3.850732 4.716685 H -8.525861 -2.157969 4.178818 H -8.233867 -3.466013 3.011962 C -6.025486 -4.552407 4.242201 H -6.162755 -4.946232 3.223793 H -4.954796 -4.611884 4.490085 H -6.563377 -5.219560 4.932913 C -8.379459 4.631171 -1.138589 H -8.982037 5.290649 -1.781636 H -9.063799 3.901193 -0.680184 H -7.948456 5.250397 -0.337128 C -6.423287 5.037303 -2.613838 H -5.913124 5.636194 -1.843656 H -5.651593 4.609383 -3.270405 H -7.041617 5.716316 -3.222577 C -7.978894 3.122655 -3.071596 H -7.246532 2.639669 -3.735052 H -8.604913 2.330512 -2.632786 H -8.622986 3.765791 -3.692667 C 6.183907 5.032187 3.650338 H 5.972464 5.441068 2.650782 H 5.223382 4.861188 4.159601 H 6.728746 5.804645 4.214238 C 7.321534 3.300673 5.016517 H 7.965410 2.409289 5.039115 H 7.835587 4.099492 5.574830 H 6.390130 3.054667 5.549334 C 8.339197 4.082639 2.858567 H 8.145999 4.406692 1.824216 H 8.874537 4.893570 3.378320 H 9.008561 3.210753 2.815828 C 7.717947 -5.117230 -1.685037 H 8.310342 -5.814819 -2.298726 H 8.280151 -4.923349 -0.759750 H 6.778050 -5.618541 -1.406759 C 8.761593 -3.141639 -2.829848 H 9.355126 -2.891912 -1.938176 H 9.372200 -3.804134 -3.464133 H 8.580243 -2.207633 -3.383390 C 6.711396 -4.191986 -3.757584

	H 5.758994 -4.707445 -3.560780 H 6.501242 -3.305881 -4.375503 H 7.339558 -4.871237 -4.353832
(Nacnac^{DiPEP})MgMgMg(Nacnac^{DiPEP}) E = -4180.212639	**2** without dispersion correction E = -4232.379354 Eh
Mg 2.824115 0.031073 -0.017822 N 4.079502 1.672704 0.209940 N 4.403225 -1.267255 -0.409653 C 5.392552 1.641012 0.025733 C 6.083591 0.437456 -0.235484 H 7.156131 0.570785 -0.309327 C 5.680615 -0.907783 -0.392041 C 6.324470 2.894441 0.011456 C 5.657585 4.240269 0.311778 H 4.804163 4.448071 -0.343225 H 6.403261 5.034049 0.148423 H 5.307065 4.321169 1.347156 C 7.471394 2.731165 1.021951 H 7.087381 2.619283 2.046370 H 8.107894 3.629608 1.001168 H 8.114261 1.866797 0.807222 C 6.912774 2.998086 -1.409100 H 7.498400 2.111436 -1.686746 H 7.571259 3.878585 -1.475969 H 6.114265 3.116371 -2.157347 C 6.890353 -1.892559 -0.469685 C 7.847172 -1.487985 -1.603993 H 7.332188 -1.453542 -2.574844 H 8.657534 -2.229595 -1.681272 H 8.314249 -0.507499 -1.439616 C 7.645364 -1.792320 0.870204 H 8.021624 -0.778577 1.062209 H 8.504253 -2.482081 0.864245 H 6.995862 -2.070023 1.713593 C 6.540677 -3.369102 -0.673888 H 5.854484 -3.751715 0.090242 H 7.471293 -3.954118 -0.607666 H 6.092818 -3.569408 -1.653021 C 3.314441 2.706145 0.789044 C 3.402890 2.939481 2.185822 C 2.586949 3.919672 2.754006 H 2.666886 4.130347 3.822160 C 1.663508 4.626126 1.988846 H 1.033910 5.388816 2.452755 C 1.524423 4.329174 0.639171 H 0.767321 4.849784 0.049766 C 2.329545 3.368115 0.017909 C 4.314755 2.089464 3.049277 H 5.122951 1.712081 2.406666 C 3.569048 0.832172 3.540257 H 3.128908 0.330140 2.658819 H 4.304855 0.116992 3.944668 C 2.468796 1.075016 4.558317 H 2.854090 1.542205 5.478211 H 1.989851 0.128816 4.849817	Al 2.76506 -0.17810 -0.02694 O 4.42495 0.63741 -0.91377 N 3.47508 -1.70994 -0.96044 N 3.41581 0.98732 1.37385 C 5.16475 -0.24414 -1.68955 C 6.37858 0.13928 -2.22258 C 4.61231 -1.52931 -1.72439 C 6.50657 -2.11274 -3.14518 C 5.30060 -2.46102 -2.51720 H 4.90684 -3.47497 -2.61788 C 6.42219 1.90952 -0.50509 C 5.19430 1.44183 -0.08227 C 2.86883 -2.99690 -1.00679 C 6.86368 1.56377 -1.93239 C 7.05306 -0.83431 -2.97415 H 8.01689 -0.60417 -3.43088 C 4.62167 1.62912 1.18106 C 7.13103 2.68685 0.42302 H 8.11183 3.08883 0.16381 C 6.59904 2.95917 1.69086 C 6.16396 2.53322 -2.90811 H 6.43414 2.29024 -3.94743 H 6.46572 3.57116 -2.69869 H 5.06971 2.47074 -2.81700 C 1.83119 -3.25928 -1.93553 C 5.35523 2.43094 2.06860 H 4.95214 2.63451 3.06385 C 8.37578 1.68695 -2.09905 H 8.91576 1.01089 -1.42007 H 8.70521 2.71679 -1.89930 H 8.67270 1.45266 -3.13145 C 1.74686 -5.56629 -1.17047 H 1.31569 -6.56816 -1.23995 C 2.51235 1.42691 2.37423 C 1.28841 -4.54761 -1.99738 H 0.49396 -4.76033 -2.71703 C 3.32732 -4.02703 -0.14861 C 2.75500 -5.29931 -0.25237 H 3.11028 -6.10036 0.40108 C 1.32499 -2.19769 -2.89574 H 1.68058 -1.22725 -2.51403 C 1.91512 2.71351 2.28748 C 2.13933 0.53987 3.41768 C 4.43009 -3.79788 0.87057 H 4.61546 -2.71316 0.90615 C 1.91804 -2.38659 -4.29473 H 3.01736 -2.37100 -4.26881 H 1.58257 -1.58539 -4.97301 H 1.60288 -3.34943 -4.72956 C 2.26491 3.68942 1.17295

H	1.684365	1.730075	4.150744	H 3.30125 3.49113 0.86862
C	4.994749	2.872830	4.176165	C -0.20131 -2.13837 -2.95448
H	5.473707	3.763037	3.733773	H -0.63653 -3.04854 -3.39659
H	4.247635	3.264245	4.885806	H -0.53197 -1.28998 -3.57316
C	6.031068	2.065291	4.942275	H -0.64632 -2.01747 -1.95262
H	6.564653	2.692879	5.671935	C 0.55109 2.19052 4.23268
H	6.783071	1.630911	4.263274	H -0.22063 2.48188 4.94943
H	5.574399	1.232732	5.499002	C 5.73972 -4.47703 0.46048
C	2.135140	3.054507	-1.451759	H 6.52809 -4.27536 1.20317
H	2.542354	2.041129	-1.615723	H 6.09566 -4.11479 -0.51409
C	2.957757	3.972699	-2.374535	H 5.61444 -5.57042 0.39466
H	4.026052	3.764008	-2.206112	C 0.94669 3.06995 3.23243
H	2.764248	3.672345	-3.417726	H 0.48202 4.05647 3.17575
C	2.704287	5.463943	-2.224766	C 2.21707 5.15300 1.60914
H	2.968860	5.822345	-1.218261	H 1.18883 5.49968 1.79871
H	1.647324	5.720765	-2.398278	H 2.62774 5.79437 0.81413
H	3.302264	6.035448	-2.950922	H 2.80818 5.32429 2.52180
C	0.652471	2.999102	-1.842424	C 2.84913 -0.79366 3.59152
H	0.075264	2.560983	-1.007804	H 2.90353 -1.26916 2.59407
H	0.240658	4.014118	-1.957950	C 4.01100 -4.24863 2.27017
C	0.376123	2.194132	-3.099913	H 3.90862 -5.34382 2.33282
H	0.900178	2.599342	-3.979709	H 3.04768 -3.80744 2.56405
H	-0.700075	2.188566	-3.325719	H 4.76682 -3.95083 3.01401
H	0.699023	1.146346	-2.975325	C 1.14711 0.93826 4.32085
C	3.834868	-2.488411	-0.830583	H 0.83326 0.25900 5.11397
C	3.141590	-3.295929	0.102272	C 1.38273 3.46595 -0.05521
C	2.514670	-4.460684	-0.355106	H 1.50765 2.44245 -0.44775
H	2.003089	-5.105804	0.361222	H 1.64984 4.15832 -0.86862
C	2.516435	-4.804580	-1.700067	H 0.31637 3.62183 0.17413
H	2.024780	-5.720722	-2.035532	C 2.12298 -1.76126 4.51941
C	3.120690	-3.955185	-2.622691	H 2.11738 -1.39619 5.55896
H	3.077698	-4.204578	-3.684637	H 2.63680 -2.73366 4.52665
C	3.774966	-2.792196	-2.217166	H 1.07928 -1.92722 4.21416
C	3.055225	-2.911349	1.566811	C 4.28922 -0.58558 4.07036
H	3.122140	-1.808567	1.610536	H 4.86451 0.04348 3.37792
C	4.253236	-3.411637	2.390251	H 4.80991 -1.55185 4.16434
H	5.161616	-2.941831	1.983482	H 4.29712 -0.10069 5.06010
H	4.157014	-3.021251	3.417324	Al -2.69607 0.23090 -0.00574
C	4.436432	-4.919876	2.429711	O -4.11680 -0.64467 -1.18607
H	5.317773	-5.192210	3.030157	N -3.56655 -0.92318 1.27855
H	4.578663	-5.336020	1.420172	N -3.31690 1.76537 -1.00576
H	3.567630	-5.428524	2.875999	C -3.06043 -1.23524 2.57127
C	1.697892	-3.275744	2.177923	C -4.36716 1.55977 -1.88414
H	0.912073	-3.047766	1.439518	C -4.81637 0.24119 -1.99745
H	1.631409	-4.363171	2.349311	C -2.17376 -2.33017 2.73339
C	1.379425	-2.539871	3.466942	C -4.94055 -1.55057 -0.52616
H	1.345752	-1.452185	3.293900	C -3.47113 -0.48389 3.69885
H	2.121767	-2.729801	4.257793	C -2.60720 2.98867 -1.15823
H	0.395486	-2.843719	3.854216	C -4.61687 -1.69847 0.82565
C	4.354908	-1.819554	-3.225968	C -5.05248 2.50026 -2.66956
H	5.269065	-1.394776	-2.783676	H -4.74487 3.54810 -2.64068
C	4.750542	-2.441770	-4.567289	C -5.90574 -0.19692 -2.72431
H	3.853845	-2.865941	-5.051848	C -6.57302 0.77962 -3.47667
H	5.071302	-1.622940	-5.232649	H -7.44409 0.50950 -4.07578
C	5.851582	-3.488303	-4.504621	C -2.99807 -0.84904 4.96382
H	6.781903	-3.067382	-4.093777	H -3.31636 -0.27959 5.84016
H	6.082147	-3.881573	-5.506373	C -6.14228 2.11303 -3.46369

H	5.569223	-4.341585	-3.869386
C	3.392416	-0.636686	-3.451386
H	2.661998	-0.917795	-4.229909
H	2.779696	-0.474794	-2.545492
C	4.097446	0.657493	-3.819324
H	3.377194	1.458507	-4.039193
H	4.736632	0.536649	-4.708049
H	4.739424	0.997202	-2.990739
Mg	0.000025	-0.000109	0.145424
Mg	-2.824103	-0.031023	-0.017594
N	-4.079542	-1.672705	0.209814
N	-4.403152	1.267264	-0.409669
C	-5.392564	-1.641003	0.025434
C	-6.083566	-0.437433	-0.235838
H	-7.156096	-0.570751	-0.309837
C	-5.680553	0.907799	-0.392304
C	-6.324475	-2.894427	0.010978
C	-5.657629	-4.240240	0.311455
H	-4.804087	-4.448065	-0.343379
H	-6.403270	-5.034033	0.148005
H	-5.307293	-4.321084	1.346901
C	-7.471607	-2.731185	1.021237
H	-7.087815	-2.619359	2.045743
H	-8.108103	-3.629627	1.000274
H	-8.114432	-1.866811	0.806412
C	-6.912504	-2.998043	-1.409695
H	-7.498089	-2.111386	-1.687405
H	-7.570963	-3.878548	-1.476719
H	-6.113862	-3.116281	-2.157808
C	-6.890255	1.892605	-0.470079
C	-7.846971	1.488086	-1.604491
H	-7.331886	1.453595	-2.575288
H	-8.657275	2.229748	-1.681865
H	-8.314131	0.507634	-1.440153
C	-7.645412	1.792337	0.869729
H	-8.021695	0.778588	1.061664
H	-8.504295	2.482105	0.863695
H	-6.995997	2.070016	1.713191
C	-6.540507	3.369140	-0.674191
H	-5.854408	3.751701	0.090054
H	-7.471111	3.954187	-0.608084
H	-6.092498	3.569465	-1.653252
C	-3.314547	-2.706152	0.789006
C	-3.403215	-2.939526	2.185757
C	-2.587297	-3.919675	2.754053
H	-2.667366	-4.130356	3.822195
C	-1.663710	-4.626070	1.989022
H	-1.034123	-5.388716	2.453019
C	-1.524452	-4.329110	0.639363
H	-0.767232	-4.849684	0.050080
C	-2.329523	-3.368086	0.017988
C	-4.315281	-2.089595	3.049084
H	-5.123407	-1.712275	2.406351
C	-3.569812	-0.832233	3.540235
H	-3.129694	-0.330044	2.658876
H	-4.305786	-0.117206	3.944610
C	-2.469633	-1.074989	4.558391

C	-4.45461	0.66575	3.57262
H	-4.44599	0.97964	2.51699
C	-1.73753	-2.66114	4.02067
H	-1.06730	-3.51433	4.15487
C	-2.14428	-1.93251	5.13170
H	-1.79600	-2.20974	6.12996
C	-5.41426	-2.60752	1.54008
H	-5.19954	-2.79520	2.59456
C	-6.49934	-3.24748	0.92271
C	-6.02871	-2.10007	-1.17416
C	-1.78896	3.18994	-2.29962
C	-6.81693	-2.97619	-0.41506
H	-7.69318	-3.45084	-0.85945
C	-6.26625	-1.68379	-2.62971
C	-2.74121	4.02013	-0.19552
C	-1.54286	2.10450	-3.33595
H	-2.06390	1.19677	-2.99667
C	-7.70602	-1.94399	-3.06255
H	-7.94218	-3.01594	-2.99740
H	-7.85500	-1.64754	-4.11093
H	-8.42426	-1.39142	-2.43932
C	-5.31037	-2.48411	-3.53911
H	-4.25967	-2.32290	-3.25699
H	-5.43360	-2.17525	-4.58869
H	-5.52303	-3.56157	-3.46172
C	-2.09946	5.24254	-0.42204
H	-2.20411	6.04781	0.30679
C	-1.17975	4.43551	-2.48557
H	-0.56195	4.60110	-3.37248
C	-3.60300	3.83000	1.04119
H	-3.47681	2.78100	1.35997
C	-0.05487	1.76420	-3.44539
H	0.53987	2.63055	-3.77528
H	0.10815	0.95640	-4.17623
H	0.36325	1.43212	-2.48070
C	-1.33890	5.46199	-1.56507
H	-0.85892	6.43012	-1.72838
C	-3.18497	4.71597	2.21127
H	-2.11568	4.60276	2.44790
H	-3.75951	4.45318	3.11038
H	-3.37856	5.78153	2.01010
C	-2.10878	2.47731	-4.70846
H	-3.18585	2.68968	-4.65239
H	-1.96338	1.65230	-5.42387
H	-1.60571	3.36664	-5.12162
C	-4.06758	1.87104	4.42656
H	-4.75111	2.71123	4.22951
H	-3.04066	2.20597	4.21541
H	-4.13670	1.65224	5.50394
C	-5.88206	0.21362	3.89583
H	-5.95481	-0.13869	4.93808
H	-6.20580	-0.60469	3.23729
H	-6.59140	1.04767	3.77164
C	-5.08755	4.02733	0.72230
H	-5.27663	5.06062	0.38811
H	-5.70571	3.84337	1.61587
H	-5.42758	3.34747	-0.07101

H	-2.854954	-1.542451	5.478137
H	-1.990957	-0.128739	4.850167
H	-1.684992	-1.729773	4.150793
C	-4.995398	-2.873086	4.175824
H	-5.474255	-3.763271	3.733277
H	-4.248365	-3.264541	4.885529
C	-6.031870	-2.065701	4.941885
H	-6.565490	-2.693421	5.671405
H	-6.783828	-1.631303	4.262848
H	-5.575343	-1.233174	5.498773
C	-2.134928	-3.054454	-1.451662
H	-2.542073	-2.041055	-1.615643
C	-2.957494	-3.972601	-2.374522
H	-4.025793	-3.763900	-2.206152
H	-2.763939	-3.672221	-3.417695
C	-2.704046	-5.463852	-2.224786
H	-2.968697	-5.822289	-1.218314
H	-1.647072	-5.720675	-2.398230
H	-3.301974	-6.035324	-2.951008
C	-0.652222	-2.999106	-1.842157
H	-0.075127	-2.560965	-1.007469
H	-0.240393	-4.014124	-1.957574
C	-0.375680	-2.194207	-3.099643
H	-0.899699	-2.599406	-3.979464
H	0.700539	-2.188762	-3.325356
H	-0.698500	-1.146385	-2.975147
C	-3.834680	2.488385	-0.830546
C	-3.141452	3.295866	0.102385
C	-2.514467	4.460616	-0.354912
H	-2.002957	5.105730	0.361469
C	-2.516096	4.804537	-1.699866
H	-2.024394	5.720680	-2.035260
C	-3.120278	3.955170	-2.622559
H	-3.077170	4.204569	-3.684498
C	-3.774633	2.792197	-2.217121
C	-3.055252	2.911285	1.566937
H	-3.122085	1.808490	1.610648
C	-4.253409	3.411467	2.390213
H	-5.161692	2.941594	1.983304
H	-4.157308	3.021086	3.417299
C	-4.436709	4.919695	2.429632
H	-5.318045	5.192001	3.030097
H	-4.578990	5.335795	1.420081
H	-3.567920	5.428407	2.875873
C	-1.698014	3.275771	2.178215
H	-0.912088	3.047683	1.439962
H	-1.631563	4.363221	2.349458
C	-1.379751	2.540132	3.467418
H	-1.346184	1.452401	3.294624
H	-2.122125	2.730341	4.258165
H	-0.395805	2.843952	3.854705
C	-4.354533	1.819623	-3.226017
H	-5.268755	1.394871	-2.783837
C	-4.750020	2.441931	-4.567341
H	-3.853258	2.866083	-5.051798
H	-5.070760	1.623151	-5.232773
C	-5.851015	3.488514	-4.504709

C -2.34506 -4.55928 1.55231
H -2.00591 -5.13653 0.67749
H -3.44162 -4.49330 1.51356
H -2.06845 -5.12807 2.45523
C -1.69864 -3.17122 1.56087
H -2.01566 -2.65217 0.64231
C -0.17558 -3.29617 1.52054
H 0.20930 -3.89342 2.36238
H 0.32290 -2.31316 1.57625
H 0.15796 -3.78737 0.59371
Mg 0.04328 0.10550 0.15816
C -7.32225 -4.22894 1.71159
H -7.53798 -3.85313 2.72337
H -8.28012 -4.44366 1.21675
H -6.78886 -5.18688 1.83071
C -6.84459 3.14423 -4.30401
H -6.23182 3.43019 -5.17527
H -7.80581 2.77022 -4.68411
H -7.03939 4.06454 -3.73239
C 7.21306 -3.13089 -3.99785
H 8.23783 -2.81506 -4.23952
H 7.26815 -4.10900 -3.49536
H 6.68049 -3.28839 -4.95041
C 7.35666 3.82557 2.65954
H 8.38741 4.00401 2.32198
H 6.87026 4.80799 2.77779
H 7.40136 3.36666 3.65924

H -6.781374 3.067622 -4.093920 H -6.081512 3.881817 -5.506464 H -5.568651 4.341769 -3.869440 C -3.392079 0.636721 -3.451440 H -2.661510 0.917897 -4.229796 H -2.779536 0.474634 -2.545465 C -4.097150 -0.657343 -3.819714 H -3.376935 -1.458360 -4.039692 H -4.736252 -0.536266 -4.708470 H -4.739226 -0.997176 -2.991259	

References for supporting information

s1. J. Hicks, P. Vasko, J. M. Goicoechea, S. Aldridge, *Nature* 2018, 557, 92–95.

s2. J. Cosier, A.M. Glazer, *J. Appl. Cryst*. 1986, 19, 105–107.

s3. CrysAlisPro v.1.171.42.70a, Agilent Technologies, 2011.

s4. G.M. Sheldrick, *Acta Crystallogr.* 2015, A71, 3–8.

s5. G.M. Sheldrick, *Acta Crystallogr.* 2015, C71, 3–8.

s6. O. V. Dolomanov, L. J. Bourhis, R. J. Gildea, J. A. K. Howard, H. Puschmann, *J. Appl. Cryst*. 2009, 42, 339–341.

s7. Gaussian 16, Revision C.01, M. J. Frisch, G. W. Trucks, H. B. Schlegel, G. E. Scuseria, M. A. Robb, J. R. Cheeseman, G. Scalmani, V. Barone, G. A. Petersson, H. Nakatsuji, X. Li, M. Caricato, A. V. Marenich, J. Bloino, B. G. Janesko, R. Gomperts, B. Mennucci, H. P. Hratchian, J. V. Ortiz, A. F. Izmaylov, J. L. Sonnenberg, D. WilliamsYoung, F. Ding, F. Lipparini, F. Egidi, J. Goings, B. Peng, A. Petrone, T. Henderson, D. Ranasinghe, V. G. Zakrzewski, J. Gao, N. Rega, G. Zheng, W. Liang, M. Hada, M. Ehara, K. Toyota, R. Fukuda, J. Hasegawa, M. Ishida, T. Nakajima, Y. Honda, O. Kitao, H. Nakai, T. Vreven, K. Throssell, J. A. Montgomery, Jr., J. E. Peralta, F. Ogliaro, M. J. Bearpark, J. J. Heyd, E. N. Brothers, K. N. Kudin, V. N. Staroverov, T. A. Keith, R. Kobayashi, J. Normand, K. Raghavachari, A. P. Rendell, J. C. Burant, S. S. Iyengar, J. Tomasi, M. Cossi, J. M. Millam, M. Klene, C. Adamo, R. Cammi, J. W. Ochterski, R. L. Martin, K. Morokuma, O. Farkas, J. B. Foresman, and D. J. Fox, Gaussian, Inc., Wallingford CT, 2019.

s8. (a) J. P. Perdew, K. Burke, M. Ernzerhof, *Phys. Rev. Lett*. 1996, 77, 3865-3868. (b) J. P. Perdew, K. Burke, M. Ernzerhof, *Phys. Rev. Lett*. 1996, 78, 1396. (c) C. Adamo, V. Barone, *J. Chem. Phys*. 1999, 110, 6158-6170.

s9. (a) F. Weigend and R. Ahlrichs, *Phys. Chem. Chem. Phys.* 2005, 7, 3297-3305. (b) F. Weigend, *Phys. Chem. Chem. Phys*. 2006, 8, 1057-1065. (b) J.-D. Chai and M. Head-Gordon, J. Chem. Phys. 2008, 128, 084106.

s11. (a) J.-D. Chai and M. Head-Gordon, Phys. Chem. Chem. Phys. 2008, 10, 6615-6620. (b) S. Grimme, S. Ehrlich, L. Goerigk, *J. Comp. Chem*. 2011, 32, 1456-1465.

s12. NBO 7.0. E. D. Glendening, J. K. Badenhoop, A. E. Reed, J. E. Carpenter, J. A. Bohmann, C. M. Morales, P. Karafiloglou, C. R. Landis, F. Weinhold, Theoretical Chemistry Institute, University of Wisconsin, Madison, WI 2018.

s13. AIMAll (Version 19.10.12), Todd A. Keith, TK Gristmill Software, Overland Park KS, USA, 2019

s14. T. Lu, F. Chen, J. Comput. Chem. 2012, 33, 580-592.

s15. Meng EC, Goddard TD, Pettersen EF, Couch GS, Pearson ZJ, Morris JH, Ferrin TE. Protein Sci. 2023, 32(11)

s16. Murphy DM, McDyre LE, Carter E, Stasch A, Jones C. A CW-EPR, ENDOR and special TRIPLE resonance study of a novel magnesium ketyl radical. Magnetic Resonance in Chemistry. 2011 Apr; 49(4): 159-63.

S17. Mandal D, Demirer TI, Sergeieva T, Morgenstern B, Wiedemann HT, Kay CW, Andrada DM. Evidence of AlII Radical Addition to Benzene. Angewandte Chemie. 2023 Mar 20; 135(13): e202217184.

S18. Stoll S, Schweiger A. J. Mag. Res. 2006, 178, 42–55

Conclusions and Outlook

This investigation gives an insight into the significant impact a powerful donor ligand can have on the chemistry of a metal centre, here inducing reactivity consistent with the magnesium(0) oxidation state from a compound which (formally) bears a magnesium(II) centre. Such studies support the argument that, for electropositive metal-metal bonded systems such as these, tight formalisms of oxidation state can become unsuitable as a means of describing the true electronic structure and reactive character of a compound. Observations such as this drive the development of increasingly advanced models, improving our ability to interpret (and predict) chemical behaviour.

Future studies in this area should focus on more finely probing the behaviour in the ground state, and investigating whether judicious selection of substrate can induce thermal (rather than photolytic) behaviour in which the electron richness of the magnesium centre plays a more significant role. Additionally, further reactivity studies under photolytic conditions would be highly informative, potentially revealing more details about the mechanism of such reactions, as well as uncovering additional onward pathways for the exotic intermediates so-generated.

Additionally, efforts to extend this chemistry to the heavier group 2 elements, where more ionic character might see an intermediate extent of reactivity between the potassium aluminyl and bis-aluminyl magnesium reagents should be explored, in order to uncover further examples of unusual small molecule activation reactions.

Statement of Authorship for joint/multi-authored papers for PGR thesis

To appear at the end of each thesis chapter submitted as an article/paper

The statement shall describe the candidate's and co-authors' independent research contributions in the thesis publications. For each publication there should exist a complete statement that is to be filled out and signed by the candidate and supervisor **(only required where there isn't already a statement of contribution within the paper itself).**

Title of Paper	**Bis(Aluminyl)Magnesium: A Source of Nucleophilic or Radical Aluminium-Centred Reactivity**
Publication Status	√ Published □ Accepted for Publication □Submitted for Publication □Unpublished and unsubmitted work written in a manuscript style
Publication Details	Liam P. Griffin, Dr. Mathias A. Ellwanger, Jonathon Clark, Dr. William K. Myers, Aisling F. Roper, Dr. Andreas Heilmann, Prof. Simon Aldridge; Bis(Aluminyl)Magnesium: A Source of Nucleophilic or Radical Aluminium-Centred Reactivity; *Angew. Chem. Int. Ed.*, 2024, 63, e202405053, doi.org/10.1002/anie.202405053

Student Confirmation

Student Name:	Liam P. Griffin		
Contribution to the Paper	Performed a high majority of the synthetic work. Performed spectroscopic analysis on all reported compounds. Performed quantum chemical calculations. Analysed and interpreted all data. Wrote the manuscript and prepared the supporting information. Supervised the experimental work of one co-author.		
Signature	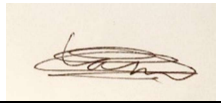	Date	19/09/2024

Supervisor Confirmation

By signing the Statement of Authorship, you are certifying that the candidate made a substantial contribution to the publication, and that the description described above is accurate.

Supervisor name and title: Professor Simon Aldridge		
Supervisor comments: I can confirm that Mr Griffin made a substantial contribution to the work described in this chapter, and that the above description is accurate.		
Signature 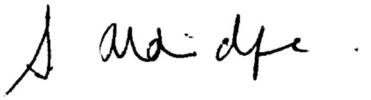	Date	20 September 2024

Conclusions and areas for future work

This thesis describes a range of attempts to better understand the installation and properties of group 13 X-type ligand fragments, with a particular focus on the most electron donating congener, the aluminyl metallo-ligand.

Chapter 2 describes the synthesis of a Nacnac-stabilized zinc boryl complex via diborane(4) disproportionation, using B–O bond formation as a driving force. This approach successfully yielded the targeted species (Nacnac^{Mes})ZnBpin, which was fully characterised, and its onward chemistry (also dominated by B–O bond formation) explored. Given the strength of Al–O bonds (the effects of which have also appeared elsewhere in this thesis) and the increasing prevalence of dialane(4) species in the literature, attempts to access metal aluminyl species by analogous routes, avoiding the need for alkali metal reductions, could be considered as an avenue for future investigations. Additionally, this may allow for a more diverse range of aluminyl fragments with less sterically demanding supporting ligand frameworks to be accessed, since kinetic stabilization of the anion is less crucial in this procedure (as indicated by the small pinacolate ligand utilized in the boryl chemistry discussed).

This chapter also underlined the need for consistency in the supporting ligand used to stabilize the trielyl moiety when wishing to compare reactivity behaviour down the group 13 series, since without this, steric effects on product identities cannot be ruled out. This principle was diligently applied throughout the synthetic investigations of the later chapters (4 and 5).

Chapter 3 utilized the powerful spectroscopic technique of XAS to probe the electronic structure of a series of compounds of the form (Nacnac^{Mes})ZnX, where X = Al(NON), BeCp, Si(TMS)$_3$, Zn(Nacnac^{Mes}), Bpin, Me and OB{(NDippCH)$_2$}. These data have been interpreted in terms of the ability of the X-ligand to donate or withdraw electron density from the zinc centre, therefore providing experimental quantification of ligand properties. Additionally, these data were used to benchmark the parameters derived from a selection of common computational techniques, which broadly aligned with the measured trends.

This investigation allowed for properties of the aluminyl ligand to be put into context alongside other strongly donating ligands. The data suggest that its donor strength is greater than that of the Zn(Nacnac^{Mes}) 'zincyl' fragment (indicating a zinc oxidation state of less than 1 in the aluminyl complex) but less than that of the BeCp 'berylyl' unit (as is to be expected based on the lower electronegativity and more electron donating Cp supporting ligand of beryllium). Indeed, the parameters showed strong similarity to those measured for the Si(TMS)$_3$ 'hypersilyl' ligand.

Future work using XAS to better understand the electronic structure of metal aluminyl complexes is already underway in our laboratory, in collaboration with the Lovelock group at the University of Reading. Aluminium XAS measurements have been performed on a selection of metal aluminyl complexes featuring a wide range of main group and transition metals, with the subsequent data analysis and computational investigation currently underway. We hope that these studies will give further insight into how the aluminyl fragment behaves when ligated to different metal centres, and on the electronic structure it induces. Future work generalizing such approaches to other classes of compound, such as the transition metal complexes of the L-type ligand (Nacnac)Al would also help to further our understanding of metal-metal and metallo-ligand bonding.

Chapter 4 showcases the utility of linear d^{10} complexes bearing suitable 'probe' moieties (Ag–P bonds, boron centres, trans-disposed linkages for structural analysis) for informing on ligand properties, in this case on a series of group 13 E(I) anions. These studies confirm the superior σ-donor strength of the aluminyl metallo-ligand as compared to its heavier congeners, further motivating the synthesis of new metal-aluminyl complexes due to the unusual reactivity these remarkable ligand properties might induce.

A result of this high donor strength is an inherent instability of the resulting very electron rich complexes. This chapter also therefore highlights the importance of a suitable ancillary ligand set when targeting stable metal-aluminyl complexes, and indicates that strongly bound ligands capable of accepting electron density offloaded by the metal centre would be desirable.

Given the unprecedented reactivity reported between coinage metal-aluminyl complexes and C–C multiple bonds such as alkynes, investigation of the analogous reactivity exhibited by the heavier group 13 congeners should be investigated. These species (which bear significantly less polarised metal-metal bonds) may display additional new carbon-functionalization reaction pathways, or provide insights into the reasons for those observed in the aluminium case.

This chapter also details a methodology for accessing an indyl anion via the reaction of a (readily available) indium(I) precursor and a potassiated dianionic ligand, removing the need for alkali metal reduction. This methodology could be readily applied to the heavier group 13 element thallium, allowing the range of thallyl anions to be extended beyond one. Additionally, an equivalent methodology utilizing aluminium, gallium and indium(I) precursors has been successfully applied to the synthesis of the acyclic bis-boryloxy trielyl anions recently reported by our group. Wider adoption of this synthetic route may allow for access to an increased diversity of trielyl species, with highly tuned ligand frameworks for particular applications, some of which may not be synthetically accessible via reductive pathways.

Chapter 5 builds upon the principles established in chapter 3, with aluminyl complexes of iron carbonyl fragments targeted. In practice, tuning of the reaction conditions based upon the potassium cation availability was required to access the desired target motifs, *i.e.* complexes of the form $[Fe(CO)_4EX_2]^-$ (E = Al, Ga, In). This is the first example of such tunability (which has been observed previously in the activation of small molecules such as H_2 and benzene) being applied to the installation of aluminyl ligands at a metal centre. Knowledge of when this phenomenon applies and how in general it operates has the potential to open up a broad range of metal-centred electrophiles to productive installation of an aluminyl ligand, expanding the range of known examples of such species, potentially leading to new onward reactivity. That the synthesis of the heavier congeners is comparably facile demonstrates the significant challenges that are still present in metal-aluminyl chemistry, as compared to the analogous chemistry (primarily of gallium) that preceded it.

Additionally, the wealth of data provided by the iron carbonyl complexes of this trielyl series provides insight into the differing ligand properties of each congener, meaning that the ligand species with desired donor strength and covalency can be selected when designing a target complex with certain properties for a particular application.

Exploration of the onward chemistry of these reported compounds, particularly processes at iron-centred vacant sites generated by photolytic or oxidative removal of a carbonyl ligand, offers the possibility of investigating the reactivity of a low valent transition metal compound which bears an aluminyl (or heavier trielyl) ligand, and how this differs from alternatively ligated iron complexes. The use of these compounds and other future transition metal analogues as single source precursors for intermetallic phases should also be explored.

Chapter 6 discusses the synthesis of a more covalent aluminyl source, namely a bisaluminyl magnesium reagent. Despite the reduction in reactivity (no activation of H_2 or benzene) as compared to the potassium salt, this analogue did not lead to more productive reactivity with metal halide substrates, and reductive chemistry was still observed. This suggests that tuning of aluminyl anion transfer via the protocol described in chapter 5 is a more powerful methodology for such reactions. However, taking advantage of this halophilic reactivity profile, onward defluorination chemistry was realised with SF_6, yielding a species containing an MgF_2 fragment. The solubilization of this motif is unusual due to its high lattice enthalpy, and is likely driven by the competing affinity of aluminium for fluoride. This chemistry can potentially inform on current studies investigating the use of calcium fluoride as a nucleophilic fluorinating reagent, which suffers similar solution-availability issues. The addition of a solubilising aluminium additive in a heterobimetallic type approach may potentially be a fruitful line of investigation in this area.

In terms of the observed photolytic chemistry, isotope labelling experiments may facilitate an improved understanding of the precise intermediate species involved, through their effect on the form of the *in-situ* measure EPR spectra. More information in this area would be valuable in facilitating

more targeted screening of substrate molecules, so that this remarkable chemistry can be more fully exploited in small molecule activation and functionalisation reactions.

Finally, the use of heavier group 2 cations to increase the ionic component of the metal-metal bonding may lead to a more intermediate reactivity profile, between that of potassium and magnesium aluminyl species. Such species may exhibit divergent reactivity, as has been demonstrated already for Nacnac stabilized mono-aluminyl species in the literature.

In general, a number of lessons can be taken from this thesis as a whole. A variety of known and novel means of probing ligand donor strength are used to compare the aluminyl ligand to congeners, as well as other ligand fragments from across the Periodic Table. That these methods can be applied to such a reactive and extremely donating ligand as an aluminyl, as well as more common or gentle fragments (methyl, gallyl), demonstrates both their robustness as methods, and their broad utility in the evaluation and comparison of known and novel ligands. Such quantitative analysis helps to inform ligand selection and design as chemists seek to ever more finely tune the electronic structure at a metal centre.

Additionally, this thesis has led to a number of design principles when it comes to the synthesis of metal aluminyl complexes in terms of the ancillary ligand requirements, as well as methodologies for the tuning of aluminyl reactivity in order to avoid or minimise reactivity with these ancillary ligand sets. Such lessons can easily be applied in future synthetic chemistry in order to access a wider library of metal aluminyl species for investigation of their own structure and reactivity.

Finally, it has explored the possibility of avoiding alkali metal reductions in the synthetic routes towards these trielyl metal compounds, namely accessing an indyl anion via indium(I) precursors, or the generation of boryl species via diborane(4) disproportionation reactions. This has already been applied to aluminium in the synthesis (via $[AlCp^*]_4$) of the aforementioned bis-boryloxy aluminyl anion, and work in this area should continue to permit the isolation of aluminyl species with increasingly diverse ligand sets. Additionally, synthetic routes involving dialane(4) compounds should

be considered in future chemistry as a potential source of an aluminyl anion, given the success this route has brought for the lighter boron congeners.

Such approaches have great potential, and may give access to as yet facilitate access to aluminyl complexes of the group 4, 6 or 7 metals, open shell transition metal centres, or actinide elements, all of which have yet to be realised in the literature.